



The Application of Knowledge Modelling as A Decision Support Tool to Optimise the Design and Performance of Seawater Reverse Osmosis Desalination Plants

By

Bashayar Al Mukhaini B.Eng.

A Thesis Submitted in Fulfilment of the Requirements of the Degree
of Doctor of Philosophy (PhD)

Supervised by

Dr. Lorna Fitzsimons & Prof. Suzanne Little

School of Mechanical and Manufacturing Engineering

School of Computing

Dublin City University

January 2024

ACKNOWLEDGMENT

I would like to express my deepest gratitude to those who supported me throughout my PhD journey.

First and foremost, I extend my heartfelt thanks to my supervisors, Dr. Lorna Fitzsimons and Prof. Suzanne Little, for their invaluable guidance, unwavering support, and constant encouragement. Their expertise and insights have been pivotal in shaping my research and ensuring its success. I am profoundly grateful for their patience and the many stimulating discussions that greatly enriched my work.

I would also like to acknowledge the financial support provided by Science Foundation Ireland (SFI) and the ML-Labs Centre (*Grant number 18/CRT/6183*) for Doctoral Training. Their funding was crucial in enabling this research and providing the resources necessary for its completion.

To my colleagues and fellow researchers at Dublin City University, thank you for creating a collaborative and stimulating environment. Your camaraderie and intellectual exchange have been integral to my academic growth.

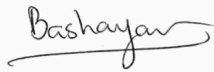
To my friends and family, your unwavering faith in me and your emotional support have been my anchor throughout this journey. Thank you for your patience, understanding, and love. Your sacrifices and encouragement have been the cornerstone of my achievements. This accomplishment is as much yours as it is mine.

Thank you all

DECLARATION

I hereby certify that this material, which I now submit for assessment on the programme of study leading to the award PhD is entirely my own work, and that I have exercised reasonable care to ensure that the work is original, and does not to the best of my knowledge breach any law of copyright, and has not been taken from the work of others save and to the extent that such work has been cited and acknowledged within the text of my work.

Signed: _____



ID No.: 19214009

Date: 31/01/2024

Table of Contents

CHAPTER 1 INTRODUCTION	1
1.1 WATER SCARCITY	1
1.2 CAUSES OF WATER SCARCITY	3
1.2.1 <i>Climate Change</i>	3
1.2.2 <i>Industrial Demand and Urbanisation</i>	7
1.2.3 <i>Agriculture</i>	8
CHAPTER 2 LITERATURE REVIEW: NEW DIRECTIONS OF REVERSE OSMOSIS	12
2.1 WATER TREATMENT TECHNOLOGIES	12
2.1.1 <i>Conventional Water Treatment</i>	12
2.1.2 <i>Desalination</i>	12
2.2 DESALINATION TECHNOLOGIES	14
2.2.1 <i>Multi-Stage Flash (MSF)</i>	15
2.2.2 <i>Multi-Effect Distillation (MED)</i>	18
2.2.3 <i>Reverse Osmosis</i>	20
2.3 NEW DIRECTIONS OF REVERSE OSMOSIS	21
2.3.1 <i>RO Transport Models</i>	21
2.3.2 <i>RO Membrane</i>	24
2.3.3 <i>Auxiliary RO Equipment</i>	25
2.3.4 <i>Fouling</i>	30
2.3.5 <i>New configurations of RO</i>	33
CHAPTER 3 LITERATURE REVIEW: ARTIFICIAL INTELLIGENCE & MACHINE LEARNING.....	50
3.1 ARTIFICIAL INTELLIGENCE & MACHINE LEARNING.....	50
3.2 APPLICATION OF AI & ML IN WATER TREATMENT TECHNOLOGIES	52
3.2.1 <i>Reverse Osmosis</i>	53
3.2.2 <i>Energy</i>	60
3.2.3 <i>Fouling</i>	61
3.2.4 <i>Membrane Design</i>	62
3.2.5 <i>Fault Detection & Equipment Failure</i>	65
3.2.6 <i>Algae Detection</i>	68
3.3 EFFECTIVENESS OF ARTIFICIAL INTELLIGENCE VS CONVENTIONAL MODELLING	77
3.4 CHALLENGES OF ADAPTING AI IN WATER TECHNOLOGIES	80
3.5 RESEARCH GAP AND PROBLEM	85
3.6 PROPOSED SOLUTION	87
CHAPTER 4 ONTOSWRO	89

4.1 ONTOLOGY.....	89
4.2 KNOWLEDGE MODELLING AND ONTOLOGY DEVELOPMENT.....	91
4.3 VOCABULARY DEVELOPMENT AND DATA STRUCTURING	93
4.3.1 <i>Scale of Desalination Plant</i>	94
4.3.2 <i>Intake and Discharge Sub-systems</i>	94
4.3.3 <i>Pretreatment System</i>	96
4.3.4 <i>RO System</i>	97
4.3.5 <i>Posttreatment System</i>	97
4.4 ONTOLOGY SPECIFICATION AND VERIFICATION	99
4.5 CASE STUDIES	100
4.5.1 <i>Case Study 1</i>	101
4.5.2 <i>Case Study 2</i>	104
4.5.3 <i>Case Study 3</i>	107
4.6 SUMMARY.....	112
CHAPTER 5 SWRO DESALINATION PROCESS DESIGN	114
5.1 WATER DENSITY AND VISCOSITY.....	114
5.2 INTAKE SYSTEM	116
5.2.1 <i>Intake Capacity</i>	116
5.2.2 <i>Intake Structure</i>	117
5.3 CHEMICAL SYSTEM AND POSTTREATMENT	120
5.4 PRETREATMENT SYSTEM	124
5.4.1 <i>Clarifiers</i>	124
5.4.2 <i>Granular Media Filtration</i>	133
5.4.3 <i>Membrane Filtration</i>	137
5.5 CARTRIDGE FILTER	139
5.6 REVERSE OSMOSIS SYSTEM	139
5.6.1 <i>Identify Initial Plant Parameters</i>	142
5.6.2 <i>Design RO Membrane System</i>	142
5.6.3 <i>Water and Salt Membrane Permeability Coefficient</i>	144
5.6.4 <i>Determination of Feed Pressure</i>	147
5.6.5 <i>Parameters Determination for Each Element</i>	148
5.6.6 <i>Concentration Polarisation Factor</i>	149
5.6.7 <i>Salt Rejection for Permeate</i>	150
5.6.8 <i>Crossflow Velocity Calculation</i>	151
5.6.9 <i>Specific Energy Consumption</i>	152
5.7 DISCHARGE SYSTEM	152
5.8 POWER CALCULATION	157

5.9 RO MODEL EVALUATION	163
5.10 SUMMARY.....	172
CHAPTER 6 ECONOMIC COST ASSESSMENT.....	174
6.1 FINANCIAL ASPECT OF DESALINATION	174
6.2 LIFE CYCLE COST ANALYSIS	176
6.3 LCC CONCEPT.....	176
6.4 LCC PROCEDURE	177
6.5 LCC METHODOLOGY.....	178
6.5.1 Present Value	179
6.5.2 Discounting	180
6.5.3 Sensitivity Analysis	181
6.6 LIFE CYCLE COSTING AND SWRO	181
6.6.1 System Lifetime and Availability	181
6.6.2 Capital Expenditure	182
6.6.3 Operational Expenditure	183
6.6.4 Factors Influencing Desalination Cost	184
6.6.5 Life Cycle Cost Model	186
6.7 METHODOLOGY	190
6.7.1 Capital Expenditure.....	191
6.7.2 Operational Expenditure	194
6.7.3 Unit Product Cost	207
6.8 SUMMARY.....	207
CHAPTER 7 EVALUATION OF ONTOSWRO AND LCCA TOOL.....	209
7.1 MODEL DEVELOPMENT AND IMPLEMENTATION	209
7.2 MODEL ANALYSIS AND EVALUATION.....	221
7.2.1 Analysis and Evaluation for Case 1.....	221
7.2.2 Analysis and Evaluation for Case 2.....	227
7.2.3 Analysis and Evaluation for Case 3.....	234
7.2.4 Benefit of SWRO Design and LCCA TOOL	238
7.3 INTEGRATION BETWEEN ONTOSWRO, SWRO DESIGN AND LCCA TOOL.....	240
CHAPTER 8 CONCLUSION AND FUTURE WORK.....	242
8.1 CONCLUSION	242
8.2 THESIS CONTRIBUTION	245
8.3 LIMITATION	246
8.4 FUTURE WORK	246
REFERENCE.....	248

List of Figures

FIGURE 1–1: (A) TOP 10 GLOBAL RISK IN TERMS OF LIKELIHOOD AND IMPACT [5], (B) ESTIMATED PEOPLE IN WATER SCARCITY OR STRESS [7]	2
FIGURE 1–2: NUMBER OF PEOPLE SEVER FROM WATER SCARCITY DURING N MONTH PER YEAR. PERIOD 1996 – 2005 [4].....	3
FIGURE 1–3: CLIMATE CHANGE RELATED PROBLEMS IN CERTAIN REGIONS [9].....	4
FIGURE 1–4: GLOBAL AVERAGE TEMPERATURE IN JULY 2020 [12]	5
FIGURE 1–5: NUMBER OF FIRES AND ACRES BURNED BETWEEN 2000 AND 2019 IN THE WORLD [13]	6
FIGURE 1–6: THE WORLD POPULATION PROJECTION BY THE UNITED NATIONS FROM 1950 TO 2100 [15]	7
FIGURE 1–7: IMPACT OF WATER ON ENERGY PRODUCTION, ADAPTED FROM [19].....	7
FIGURE 1–8: THESIS CHAPTERS STRUCTURE FLOWCHART	11
FIGURE 2–1: TIMELINE OF DESALINATION TECHNOLOGY ADAPTED FROM [35]. MULTI-EFFECT DISTILLATION(MED) MULTISTAGE FLASH (MSF), MEMBRANE DISTILLATION (MD), REVERSE OSMOSIS (RO), ENERGY RECOVERY DEVICE (ERD)	13
FIGURE 2–2: TOTAL GLOBAL INSTALLED DESALINATION CAPACITY BY TYPE OF USE, ADAPTED FROM[37]	14
FIGURE 2–3: SCHEMATIC CLASSIFICATION OF DESALINATION TECHNOLOGIES	15
FIGURE 2–4: SCHEMATIC OF MULTI STAGE FLASH [42]	18
FIGURE 2–5: SCHEMATIC OF MULTI EFFECT DISTILLATION [42].....	19
FIGURE 2–6: PROS AND CONS OF THE THREE MOST POPULAR DESALINATION TECHNOLOGIES	20
FIGURE 2–7 : SCHEMATIC DIAGRAM OF RO DESALINATION PLANT AND RO MEMBRANE	20
FIGURE 2–8: RO DEVELOPMENT TIMELINE, ADAPTED FROM [46]	21
FIGURE 2–9: SCHEMATIC OF MASS TRANSPORT MODEL FOR REVERSE OSMOSIS, C_f IS FEED CONCENTRATION, C_p PERMEATE CONCENTRATION, J_w WATER FLUX, J_s SALT FLUX, A IS THE WATER PERMEABILITY COEFFICIENT OF THE MEMBRANE, B IS THE SALT PERMEABILITY COEFFICIENT OF THE MEMBRANE, $C_{D,B}$ AND $C_{F,B}$ ARE THE SOLUTE CONCENTRATIONS IN THE BULKS, $\Delta\pi$ IS THE OSMOTIC PRESSURE DIFFERENCE BETWEEN THE BULKS, AND ΔP IS THE HYDRAULIC PRESSURE APPLIED ON THE DRAW WATER SIDE	22
FIGURE 2–10: SCHEMATIC DIAGRAM FOR SCALING FORMATION STEPS ON MEMBRANE SURFACE, ADAPTED FROM [105]	31
FIGURE 2–11:SCHEMATIC DIAGRAM OF SEMI-BATCH REVERSE OSMOSIS.....	33
FIGURE 2–12: THE BEHAVIOUR OF BRO AND RO IN TERMS OF TDS OVER TIME [100].....	39
FIGURE 2–13: A CONTOUR MAP FOR (A) - CALCITE ($CaCO_3$) NUCLEATION, (B) GYPSUM ($CaSO_4$) NUCLEATION OVERLAID WITH CURVES FOR RESIDENCES TIMES OF CONTINUOUS RO AND BATCH RO [100].....	40
FIGURE 2–14: MODELLED SEC FOR CONVENTIONAL AND TIME-VARIANT RO CONFIGURATIONS AGAINST RECOVERY RATIOS WITH 3 G/KG NaCl FEED AND PUMP EFFICIENCY 80% [112]	42
FIGURE 2–15:WATER PERMEABILITY TREND OVER TIME AT SALINITY = 25 G/L FOR BATCH RO [127]	43
FIGURE 3–1:MACHINE LEARNING MODEL WORKFLOW AND ALGORITHM CLASSIFICATION HIERARCHY.....	52
FIGURE 3–2: NF-RO HYBRID PILOT PLANT SCHEMATIC DIAGRAM: 1.RAW WATER PUMP, 2.BAG FILTER, 3.MICRON FILTER, 4.HP PUMP, 5.PRESSURE GAUGE, 6.FLOW METER, 7.RO MEMBRANE MODULE, 8.NF MEMBRANE MODULE, 9.PERMEATE STREAM, 10.CONCENTRATE STREAM, 11.FEED TANK, 12.PRESSURE CONTROL VALVE, 13.HYBRID NF-RO PARALLEL CONFIGURATION, 14.HYBRID NF-RO SERIES CONFIGURATION, 15.TEMPERATURE INDICATOR, 16.TEMPERATURE REGULATOR [159]	54

FIGURE 3–3 : HYBRID AI MODEL TO PREDICT LEAD IN TWO STATION IN AUSTRALIA [162]	56
FIGURE 3–4: PROPOSED AI AND ML APPROACH TO CONTROL MEMBRANE FOULING, ADAPTED FROM [184]	62
FIGURE 3–5: FACTOR THAT IMPACT THE DETERIORATION OF PIPELINES BASED ON PHYSICAL, ENVIRONMENTAL, AND OPERATIONAL FACTORS	66
FIGURE 3–6 : INFLUENCING FACTORS OF ALGAL BLOOM	71
FIGURE 3–7: AI MODEL BASED ON TIME SERIES DATA TO FORECAST ALGAL BLOOM, (A)[214], (B) [217]	74
FIGURE 3–8: SAMPLES OF THE OBTAINED ALGAL DETECTION WHERE THE FIRST TWO ROWS REPRESENT ACCURATE CLASSIFICATION AND DETECTION OUTCOMES. THE LAST ROW DEPICTS THREE DIFFERENT SORTS OF INACCURATE FORECASTS. FROM LEFT TO RIGHT, UNIDENTIFIED ALGAE, ALGAL BLOCKAGE, AND MISCLASSIFICATION ARE THE THREE TYPES OF INACCURACY [219].....	75
FIGURE 3–9: WATER SAMPLE, MULTI-BAND FLUORESCENCE IMAGE MICROSCOPY DATA PROCESSING, IMAGE SEGMENTATION, FEATURE EXTRACTION, AND NEURAL NETWORK MODELS ARE THE FIVE BASIC COMPONENTS OF THE PROPOSED TECHNIQUE OF AUTOMATIC IDENTIFICATION OF DIFFERENT TYPES OF ALGAE SPECIE [220].....	77
FIGURE 3–10: COMPARISON OF 3D SIMULATED AND OBSERVED FOULING IMAGES REGARDING THICKNESS ESTIMATION FOR NF MEMBRANE (NE 90, TORAY, JAPAN) AND AN RO MEMBRANE (RE SHF, TORAY)[169]	80
FIGURE 3–11: EXAMPLES OF DIFFERENT POSSIBLE CONFIGURATIONS OF SWRO DESALINATION PLANT	86
FIGURE 4–1: PHASES INVOLVED IN DATA STRUCTURING PROCESSES. 1. DATA GATHERING, 2. BRAIN STORMING 3. STRUCTURING THE DATA INTO TABLE AND 4. ORGANISING THE DATA INTO NODE AND RELATIONSHIP.....	92
FIGURE 4–2: INTAKE SYSTEM STRUCTURE	95
FIGURE 4–3: DISCHARGE MANAGEMENT SYSTEM.....	96
FIGURE 4–4: PRETREATMENT SYSTEM STRUCTURE	96
FIGURE 4–5: RO SYSTEM STRUCTURE	97
FIGURE 4–6: POSTTREATMENT SYSTEM STRUCTURE	98
FIGURE 4–7: REPRESENTATION OF CLASSES AND RELATIONSHIPS USED TO BUILD UP SWRO DESALINATION ONTOLOGY.	98
FIGURE 4–8: RECOMMENDED CLASSES FOR CASE 1.....	102
FIGURE 4–9: DEFINING SPECIFIC ALGAL BLOOM CLASS FROM CONNECTION AND DATA PROPERTIES	102
FIGURE 4–10: RECOMMENDED FULL DESIGN FOR CASE 1.....	103
FIGURE 4–11: ONTOLOGY’S FEATURES IN CAPTURING CLASS EXPRESSION	104
FIGURE 4–12: EQUIPMENT RECOMMENDATION FROM ONTOSWRO BASED ON DESALINATION CAPACITY	105
FIGURE 4–13:ASSESSING APPROACH FOLLOWED IN CASE 2	106
FIGURE 4–14: EXAMPLE OF STEPS FOR OWLREADY2 QUERYING APPROACH FOLLOWED IN THIS SCENARIO	106
FIGURE 4–15: ALL CLASSES WITH PHRASE “SMALL”	108
FIGURE 4–16: ONTOGRAF LIMITATION	108
FIGURE 4–17: OFFSHORE VISUALISATION.....	109
FIGURE 4–18: EQUIPMENT THAT HAS LOW ENVIRONMENTAL IMPACT	109
FIGURE 4–19: MEMBRANE PRETREATMENT VISUALISATION.....	110
FIGURE 4–20: VISUAL REPRESENTATION OF DAF WITH FURTHER DETAILS ABOUT THE DATA PROPERTIES ASSOCIATED WITH DAF..	110
FIGURE 4–21: SANITARY SEWER DISCHARGE VISUALISATION.....	111
FIGURE 5–1: VELOCITY CAP INLET OFFSHORE INTAKE STRUCTURE	118

FIGURE 5–2: FLOW PATTERN AND PARAMETERS FOR LAMELLA SEDIMENTATION, ADAPTED FROM[301][310]	130
FIGURE 5–3: FLOW CHART FOR DESIGNING A. CONVENTIONAL SEDIMENTATION TANKS, B. LAMELLA SEDIMENTATION TANK	132
FIGURE 5–4: FLOWCHART OF GRANULAR MEDIA FILTER DESIGN	137
FIGURE 5–5: CLEANING STEPS FOR UF PROCESS	139
FIGURE 5–6: SELECTED MEMBRANE TYPE FOR THIS RESEARCH	140
FIGURE 5–7: THE STEPS FOLLOWED IN DESIGNING RO SYSTEM.	141
FIGURE 5–8: ILLUSTRATION OF THE FLOW STREAM INSIDE PRESSURE VESSELS WITH 8 ELEMENTS IN SERIES.....	148
FIGURE 5–9: FLOWCHART FOR DETERMINING PARAMETERS FOR EACH ELEMENT IN PRESSURE VESSEL	149
FIGURE 5–10: A FLOWCHART OF THE DISCHARGE SOURCES IN THE SWRO FACILITY.....	153
FIGURE 5–11: SUGGESTED DILUTION TANK.....	155
FIGURE 5–12: IMPACT OF TEMPERATURE VARIATION ON APPLIED PRESSURE AND PERMEATE CONCENTRATION FOR THE THREE MODELS.	165
FIGURE 5–13: IMPACT OF TEMPERATURE ON PERMEABILITY FOR WAVE AND DESIGNED MODEL.....	166
FIGURE 5–14: IMPACT OF WATER MEMBRANE PERMEABILITY COEFFICIENT ON SEC, WHERE ENERGY MODEL IS VALUE OF SEC AT DIFFERENT TEMPERATURE, A IS WATER PERMEABILITY.	168
FIGURE 5–15: IMPACT OF VARYING SALINITY ON SEC.....	169
FIGURE 5–16: BEHAVIOUR OF CROSS VELOCITY ALONG THE PRESSURE VESSEL.....	170
FIGURE 5–17: BEHAVIOUR OF FLUX INSIDE THE PRESSURE VESSEL	171
FIGURE 5–18: BEHAVIOUR OF CPF ALONG THE MEMBRANE ELEMENTS.....	172
FIGURE 6–1: CAPEX AND OPEX BASED ON DESALINATION TECHNOLOGIES	175
FIGURE 6–2:WHOLE LIFE CYCLE COST ACCORDING TO ISO15686 [345].....	177
FIGURE 6–3:TEN STEPS OF LIFE CYCLE COST DEVELOPED BY GREENE AND SHAW [348].....	178
FIGURE 6–4: DISCOUNT RATE FOR DIFFERENT COUNTRIES ACCORDING TO CENTRAL BANK [362]	181
FIGURE 6–5: HISTOGRAM REPRESENTATION OF LIFETIME OF 1640 SWRO DESALINATION THAT STILL OPERATING	182
FIGURE 6–6: INFLATION ANALYSIS OF ENERGY SOURCES IN EU [367]	184
FIGURE 6–7: FLOW CHART FOR THE PROCESS OF SELECTING SITE [277].....	186
FIGURE 6–8: CAPITAL COST COMPARISON BETWEEN REAL CASES AND OBTAINED RESULTS BY THE EMPIRICAL MODEL, DEEP, AND WTCOST [379]	189
FIGURE 6–9: STRUCTURE OF CAPEX AND OPEX USED IN THIS RESEARCH.....	191
FIGURE 6–10: RECOMMENDED LABOUR STRUCTURE FOR SWRO DESALINATION PLANT	202
FIGURE 6–11: ELECTRICITY PRICES ACROSS A SELECTION OF COUNTRIES UTILISING SWRO DESALINATION	204
FIGURE 7–1: DASH PLOTLY FRAMEWORKS FOR SWRO DESIGN AND LCCA TOOL.....	210
FIGURE 7–2: SCREENSHOT FROM THE MODEL INTERFACE	211
FIGURE 7–3: INTAKE SYSTEM FRAMEWORK FOR SUPPORT DECISION TOOL	213
FIGURE 7–4: PRETREATMENT SYSTEM FRAMEWORK FOR SUPPORT DECISION TOOL.....	214
FIGURE 7–5:PRETREATMENT SYSTEM FRAMEWORK FOR SUPPORT DECISION TOOL	215
FIGURE 7–6: RO SYSTEM FRAMEWORK FOR SUPPORT DECISION TOOL.....	216
FIGURE 7–7: DISCHARGE SYSTEM FRAMEWORK FOR SUPPORT DECISION TOOL	217

FIGURE 7–8: CHEMICAL CALCULATION FRAMEWORK FOR SUPPORT DECISION TOOL.....	218
FIGURE 7–9: SEC FRAMEWORK FOR SUPPORT DECISION TOOL.....	218
FIGURE 7–10: CAPEX FRAMEWORK FOR SUPPORT DECISION TOOL.....	219
FIGURE 7–11: OPEX FRAMEWORK FOR SUPPORT DECISION TOOL.....	220
FIGURE 7–12: CAPEX BREAKDOWN FOR CASE 1.....	226
FIGURE 7–13: OPEX BREAKDOWN FOR CASE 1.....	226
FIGURE 7–14: CAPEX BREAKDOWN FOR SOLUTION 1.....	231
FIGURE 7–15: OPEX BREAKDOWN FOR SOLUTION 1.....	232
FIGURE 7–16: CAPEX BREAKDOWN FOR SOLUTION 2.....	232
FIGURE 7–17: OPEX BREAKDOWN FOR SOLUTION 2.....	233
FIGURE 7–18: CAPEX BREAKDOWN FOR CASE 3.....	237
FIGURE 7–19: OPEX BREAKDOWN FOR CASE 3.....	237

List of Tables

TABLE 2-1: TYPE OF DESALINATION TECHNOLOGIES IN TERMS OF THEIR DRIVING FORCE, STATUS AND APPLICATION [36], [41]	16
TABLE 2-2: COMPARISON BETWEEN SOLUTION-DIFFUSION MODEL AND SOLUTION-FRICTION MODEL [54]	23
TABLE 2-3: COMPARISON BETWEEN FOUR TYPE OF RO MEMBRANE MODULES [64][46][65].....	25
TABLE 2-4: CURRENT RANGES OF ENERGY CONSUMPTION FOR MEDIUM – LARGE SWRO SYSTEMS [28]	26
TABLE 2-5: SUMMARY OF MEDIUM AND LARGE DESALINATION’S ERD [74], [76], [81], [82], [83].....	28
TABLE 2-6: SUMMARY OF THE AVAILABLE ERD OPTIONS FOR SMALL DESALINATION PLANTS [92], [93], [94], [95], [96], [97], [98], [99].....	30
TABLE 2-7: EFFECTS OF FOULING CATEGORY ON THE MEMBRANE PROCESS, DATA FROM [102], [103], [104].....	31
TABLE 2-8: SUMMARY OF ALL BRO CONFIGURATIONS [112], [114]	35
TABLE 2-9: COMPARISON BETWEEN CONTINUOUS RO, SEMI-BATCH AND BATCH RO	38
TABLE 2-10: FACTOR IMPACTING SEC OF RO PROCESS [42].....	41
TABLE 2-11: OBTAINED PERMEATE QUALITY FROM BATCH RO CYCLES [132]	49
TABLE 3-1: DEFINITIONS OF THE MAIN GROUP CLASSES OF ML	51
TABLE 3-2: ANN MODEL PREDICTIONS [21]	55
TABLE 3-3: EXAMPLES OF APPLYING NEURAL NETWORKS IN RO AND NF TECHNOLOGIE	58
TABLE 3-4: EXAMPLES OF APPLYING AI AND ML TO ESTIMATE PIPE FAILURE AND CONDITIONS	69
TABLE 3-5: EXAMPLES OF APPLYING AI AND ML PAPERS TO DETECT ALGAL BASED ON TIME INTERVAL LAG.....	73
TABLE 5-1: CAPACITY OF DIFFERENT SUBSURFACE INTAKE SYSTEMS [305][281]	119
TABLE 5-2: CHEMICAL USED IN SWRO PLANT [306].....	122
TABLE 5-3: SETTLING TIME FOR DIFFERENT TYPE OF PARTICLES [308]	125
TABLE 5-4: SETTLING VELOCITY EQUATION IN TERMS OF PARTICLES DIAMETER AND TYPE OF FLOW [310][311]. C_d IS DRAG COEFFICIENT WHICH IS OBTAINED BY DETERMINING THE REYNOLDS NUMBER	126
TABLE 5-5: SUPPLEMENTARY INFORMATION FOR CONVENTIONAL AND LAMELLA SEDIMENTATION [245], [301], [314]	128
TABLE 5-6: OVERVIEW OF DAF CHAMBERS AND CORRESPONDING AVAILABLE VALUES [30].....	133
TABLE 5-7: COMPARISON BETWEEN GRAVITY AND PRESSURE GRANULAR MEDIA FILTRATION [317][318][245].....	134
TABLE 5-8: FEATURES OF MATERIAL THAT APPLIED IN GRANULAR MEDIA FILTRATION [319], [320]	136
TABLE 5-9: SUPPLEMENTARY INFORMATION FOR MEMBRANE FILTRATION [301]	138
TABLE 5-10: STEPS FOR DESIGNING MEMBRANE FILTRATION SYSTEM [301]	138
TABLE 5-11: EQUATIONS FOR IDENTIFY INITIAL PLANT PARAMETERS [323]	142
TABLE 5-12: DESIGN GUIDELINES FOR 8-INCH FILMTECH ELEMENTS IN WATER TREATMENT APPLICATIONS [321]	143
TABLE 5-13: EQUATIONS AND STEPS FOR DESIGN RO MEMBRANE [323]	144
TABLE 5-14: STEPS FOR OBTAINING THE COEFFICIENT FACTOR OF WATER AND SALT PERMEABILITY [323].....	146
TABLE 5-15: EQUATIONS FOR CALCULATING DIFFUSER SYSTEM DESIGN CHARACTERISTICS [301], [330], [333], [334]	156
TABLE 5-16: RECOMMENDED VALUE FOR DESIGNING DIFFUSER SYSTEM [301], [330], [333], [334].....	156
TABLE 5-17: DESIGN C-FACTOR VALUES FOR DIMENSIONS AND POTENTIAL DILUTION RATE OF SINGLE-JET DIFFUSERS IN STAGNANT CONDITIONS [4], [331], [332], [333], [334], [335].....	157

TABLE 5-18: SEC CONSUMPTION FOR PRETREATMENT CONFIGURATIONS [30], [301]	158
TABLE 5-19: MINIMUM EFFICIENCIES H_M FOR IE3 EFFICIENCY LEVEL AT 50 Hz (%)	160
TABLE 5-20: MINIMUM EFFICIENCIES H_M FOR IE4 EFFICIENCY LEVEL 50 Hz (%)	161
TABLE 5-21: INTERPOLATION COEFFICIENTS FOR MOTORS WITH RATED POWER OUTPUT P FROM 0.12 kW UP TO 0.55 kW	162
TABLE 5-22: INTERPOLATION COEFFICIENTS FOR MOTORS WITH RATED POWER OUTPUT P FROM 0,75 kW UP TO 200 kW	163
TABLE 6-1 : FORECAST OF ENERGY USE AND COST FOR MEDIUM AND LARGE RO DESALINATION PLANT [243]	183
TABLE 6-2: BREAKDOWN FOR THE FACTORS INCLUDED IN DIRECT AND INDIRECT CAPEX IN TERMS COST RANGES AND ASSOCIATED PARAMETERS FOR EACH FACTOR [49], [366], [383], [384]	195
TABLE 6-3: BREAKDOWN FOR OPERATIONAL EXPENDITURE [49], [384], [385], [386]	199
TABLE 6-4: THE STAFFING REQUIREMENTS FOR A SWRO DESALINATION PLANT, CATEGORISED BY PLANT CAPACITY AND SKILL LEVEL [381]	201
TABLE 6-5: LABOUR CATEGORIES, ROLES, AND ASSOCIATED COSTS	202
TABLE 6-6: COST COMPARISON OF MEDIA CLEANING AND FULL MEDIA REPLACEMENT [400]	206
TABLE 7-1: SUMMARY OF SWRO DESIGN SPECIFICATIONS FOR CASE 1	221
TABLE 7-2: SUMMARY OF CAPEX AND OPEX FOR CASE 1	223
TABLE 7-3: SUMMARY OF SWRO DESIGN SPECIFICATIONS FOR CASE 2	227
TABLE 7-4: SUMMARY OF CAPEX AND OPEX FOR CASE 2	229
TABLE 7-5: SUMMARY OF SWRO DESIGN SPECIFICATIONS FOR CASE 3	234
TABLE 7-6: SUMMARY OF CAPEX AND OPEX FOR CASE 3	235
TABLE 7-7: COMPARISON BETWEEN THE LITERATURE AND RESULT OBTAINED FROM THE THESIS	238

Nomenclature

Δ_{ss}	Amount of Solids Removed by Process
A_d	Aquifer Drawdown
B_{th}, k	Salt Permeability
C_d	Drag Coefficient
$d_{ch,\theta}$	Distance between Inclined plates of lamella
f_{loss}	Capacity Loss Factor of Wells
K_c	Advective Hindrance Factor
K_d	Diffusional Hindrance Factor
L_j	Lifespan, j refer to plant, SWRO or equipment
m_j	Sum of Molarity
p^t	Total Pressure
PO_{days}	Total Duration of Plant Operation in Days
Q_c	Flow Rate per Tank
Q_{fwell}	Flow Rate of Well
R_o	Observed Membrane Recovery Rate
T_d	Aquifer Transmissivity
v_c	Hazen Velocity
v_s	Settling Velocity
\emptyset	Diameter
A	Area
A, K_w	Water Permeability
AEC	Annual Equivalent Cost
AMTA	American Membrane Technology Association
ANN	Artificial Neural Networks
aw	Percentage of Additional Water
BOD	Biological Oxygen Demand
BRO	Batch Reverse Osmosis
bw	Percentage of Backwash
C	Cost
C	Molar Concentration of Solute

<i>CAPEX</i>	Capital Expenditure
<i>CNN</i>	Convolutional Neural Networks
<i>CP</i>	Concentration Polarisation
<i>CPF</i>	Concentration Polarisation Factor
<i>D</i>	Bulk Diffusivity
<i>d</i>	Depth
<i>DEEP</i>	Desalination Economic Evaluation Programme
<i>dr</i>	Discount Rate
<i>DWEER</i>	Dual Work Exchanger Energy Recovery
<i>eff</i>	Efficiency of device
<i>ERD</i>	Energy Recovery Device
<i>f</i>	Frictional Coefficient
<i>FT</i>	Francis Turbine
<i>FV</i>	Future Value
<i>GA</i>	Genetic Algorithms
<i>GBT</i>	Gradient Boosted Tree
<i>GCC</i>	Gulf Cooperation Council
<i>h</i>	Hight
<i>HAB</i>	Harmful Algal Bloom
<i>HPD</i>	Working Hour per Day
<i>i</i>	Van't Hoff Factor
<i>IRR</i>	Internal Rate of Return
<i>J</i>	Flux
<i>k</i>	Mass Transfer Coefficient
<i>l</i>	Length
<i>LCA</i>	Life Cycle Analysis
<i>LCC</i>	Life Cycle Cost
<i>LCCA</i>	Life Cycle Cost Analysis
<i>LR</i>	Loading Rate
<i>MED</i>	Multi-Effect Distillation
<i>ML</i>	Machine Learning
<i>MLR</i>	Multiple Linear Regression
<i>MSF</i>	Multi-Stage Flash

<i>N</i>	Number
<i>NF</i>	Nanofiltration
<i>NOM</i>	Natural Organic Matter
<i>NPV</i>	Net Present Value
<i>NS</i>	Net Savings
<i>OPEX</i>	Operational Expenditure
<i>P</i>	Pressure
<i>PB</i>	Payback Period
<i>PI</i>	Profitability Index
<i>PO</i>	Plant Operation
<i>PoM</i>	Post-Monsoon
<i>PrM</i>	Pre-Monsoon
<i>PT</i>	Pelton Wheel
<i>PV</i>	Present Value
<i>PX</i>	Pressure Exchanger
<i>Q</i>	Flow Rate
<i>R</i>	Gas Constant
<i>R</i>	Recovery Rate
<i>r</i>	Radius
<i>RBF</i>	Radial Basis Function
<i>Re</i>	Reynolds Number
<i>RF</i>	Random Forest
<i>RO</i>	Reverse Osmosis
<i>RSM</i>	Response Surface Methodology
<i>SBRO</i>	Semi-Batch Reverse Osmosis
<i>Sc</i>	Schmidt Number
<i>SD</i>	Solution Diffusion
<i>SE</i>	Membrane Surface Area
<i>SEC</i>	Specific Energy Consumption
<i>SHEC</i>	Specific Heat Energy Consumption
<i>SIR</i>	Savings To Investment Ratio
<i>SPV</i>	Single Present Value
<i>SS</i>	Suspended Solid Content

<i>SVM</i>	Support Vector Machines
<i>SWRO</i>	Seawater Reverse Osmosis
<i>t</i>	Detention period or time
<i>T</i>	Temperature
<i>TCF</i>	Temperature Correction Factor
<i>TDS</i>	Total Dissolved Solids
<i>TFC</i>	Thin Film Composite
<i>TSS</i>	Total Suspended Solids
<i>UPV</i>	Uniform Present Value
<i>v</i>	Velocity
<i>V</i>	Volume
<i>w</i>	Width
<i>WAVE</i>	Water Application Value Engine
<i>WHO</i>	World Health Organisation
<i>WTCost</i>	Water Treatment Cost Estimation Programme

Greek Symbol

η_M	Efficiency of Motor
η_P	Efficiency of Pump
η_{VSD}	Efficiency of Variable Speeds Drive
ρ_s	Density of Removed Particles
\emptyset	Diameter
x	Dimensionless Coordinate Through Membrane
z	Ion Charge
ε	Effective Membrane Porosity
μ	Dynamic Viscosity
ν	Kinematic Viscosity
π	Osmotic Pressure
ρ	Density of Fluid
ϕ	Dimensionless Electrical Potential Inside Membrane

Subscript

<i>b</i>	Bulk
<i>bs</i>	Bottom Intake Structure
<i>c</i>	Concentrate
<i>ch</i>	Lamella Channel
<i>cp</i>	Conveyance Pipe
<i>e</i>	Elements
<i>EE</i>	Employee
<i>f</i>	Feed
<i>h</i>	Hydraulic
<i>i</i>	Ions
<i>j</i>	Refer to Number or Equipment
<i>lam</i>	Lamella
<i>m</i>	Membrane
<i>o</i>	Initial
<i>p</i>	Permeate
<i>pl</i>	Lamella plates
<i>pv</i>	Pressure Vessel
<i>repl</i>	Replacement
<i>rp</i>	Riser Pipe
<i>s</i>	Salt
<i>vc</i>	Velocity Cap
<i>w</i>	Water
$\$/h$	Cost Rate per Hour
$\$/kg$	Cost Rate per Kg

Note: all nomenclatures are explained in the context and clarified.

Publications resulting from this research

Two papers submitted for review.

Review Paper - Applications of Artificial Intelligence in Desalination and Water Treatment: Opportunities and Challenges

This paper was submitted to Environmental Modelling and Software Journal

OntoSWRO: An Ontology for Holistic Design of Seawater Reverse Osmosis Desalination Plants

This paper was submitted to Desalination Journal

Abstract

The Application of Knowledge Modelling as a Decision Support Tool to Optimise the Design and Performance of Desalination Plants

By

Bashayar Al Mukhaini

Addressing the global demand for fresh water in communities and industries is a pressing concern. Over the years, several investigations and advancements have been conducted in the field of desalination, aiming to establish highly efficient and economically viable systems. Seawater reverse osmosis desalination (SWRO) is well recognised as the predominant technology because of its relatively low energy consumption. Nevertheless, the design and execution of SWRO is complicated, and several factors contribute to optimising its effectiveness and mitigating the associated issues. Each process and subprocess in a SWRO desalination plant relies on the output of the previous system to deliver high-quality results, efficiently, and with minimal environmental impact. There is a lack of a holistic approach to the design process of SWRO desalination that take all design factors into considerations. This thesis presents a methodology for assessing system design and selection under changing conditions, elucidating trade-offs between capital and operational costs, environmental impact, geographical features, and the associated limitations of each process. In addition, it assesses the suitability of a design according to these specific criteria. To achieve this, a suitable methodology for SWRO system evaluation is necessary.

To address this challenge, this research proposes an ontology for complex and holistic analysis by assimilating data from all subcomponents and representing their interconnectedness within a desalination system. The ontology represents standardised knowledge (terms, relationships and rules) related to all the major components and processes of SWRO desalination. Thus, the developed ontology facilitates and encourages reusability of data for a multitude of alternative configurations within the SWRO domain. Three case studies were used to demonstrate the capabilities of the ontology to effectively model complex relationships and constraints.

However, a review of the literature has shown that integrating the life cycle cost approach offers a greater understanding of the actual cost of system implementation and significantly influences the decision-making process for plant design selection. A SWRO design and LCCA tool was developed to simplify system analysis in user-defined, site-specific scenarios. The included life cycle cost data were gathered from a diverse range of academic and industry sources, facilitating the development of a cost database that is both user-friendly and accessible for regular updates. The methodology was assessed by evaluating the design derived from the three case studies. This demonstrates the tool's ability to capture the engineering principles of these processes and to perform life cycle cost analysis. Furthermore, it demonstrates the influence of different pretreatment methods, water characteristics, and specific process choices on the total capital expenditure (CAPEX) and operational expenditure (OPEX) resulting in a more holistic and comprehensive understanding of SWRO as a highly complex and interdependent solution to water availability.

Chapter 1

Introduction

1.1 Water Scarcity

Water is a substance essential to all known forms of life on earth. Water is used for drinking, cleaning, agriculture, power generation, and much more. In other words, water is a crucial element of life for human beings, animals and the planet they live on. Approximately 97% of earth's water is saline and just under 3% is not easily accessible. The remaining percentage of approximately 0.014% constitutes easily accessible freshwater. This supply of freshwater is enough to serve our global demand and need. According to the United Nations, 200,000 cubic kilometres of freshwater are available for human use; this is out of a total 1.4 billion cubic kilometres of freshwater [1]. Although there seems to be an abundance of water on earth, according to the United Nations Development Programme, only an estimated one percent of this supply is available for use by human beings [2]. This percentage must be shared by the entire population on this planet, resulting in significant challenges to ensure sufficient and equitable global water supply.

As a result of increased water demand for potable water, agriculture, and industrial uses, fresh water withdrawals have increased resulting in water stress and water shortages in many areas of the world [3]. Water scarcity can be defined in two ways: water shortages and water stress. The low availability of water per capita is what defines water shortage while stress is defined as the result of excessive water use (either consumption or withdrawal) in comparison to available water [3].

Climate change, along with the unequal global distribution of freshwater, results in some geographical areas being increasingly wet or dry. Additionally, the increased demand for freshwater as result of continuous population growth and increased industrialisation has resulted in significant water scarcity in some regions [4]. In 2015 the World Economic Forum stated that the water crisis is one of the top ten risk factors that will hugely impact life over the next decade, both in terms of impact and likelihood as shown in Figure 1–1 (a) [5]. Also, a 2024 report from the World Economic Forum [6] indicated that environmental risk will

dominate in the next 10 which included extreme weather events, critical change to earth systems, biodiversity loss and ecosystem collapse and natural resource shortages.

Top 10 risks in terms of Impact	Top 10 risks in terms of Likelihood
1 Water Crises	1 Interstate conflict
2 Spread of infectious diseases	2 Extreme weather events
3 Weapons of mass destruction	3 Failure of national governance
4 Interstate conflict	4 State collapse or crisis
5 Failure of climate change adaption	5 Unemployment or underemployment
6 Energy price shock	6 Natural catastrophes
7 Critical information infrastructure breakdown	7 Failure of climate change adaption
8 Fiscal crises	8 Water crises
9 Unemployment or underemployment	9 Data fraud or theft
10 Biodiversity loss and ecosystem collapse	10 Cyber attacks

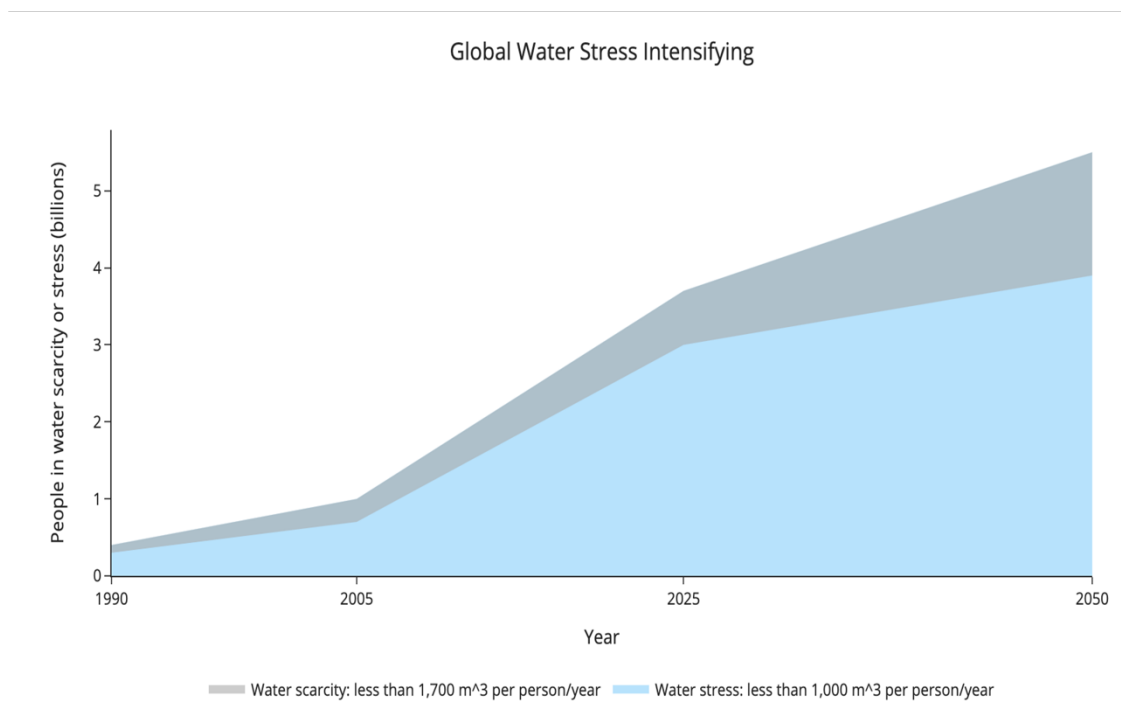


Figure 1-1: (a) Top 10 global risk in terms of likelihood and impact [5], (b) Estimated people in water scarcity or stress [7]

Water stress is experienced by a region when less than 1700 m³ of water supply is available per person per annum in that region. A limited or periodic shortage of water is a possible result seen when the level of supply per person per year is between 1000 and 1700 m³. As the supply of water drops to that of less than 1000 m³ per person per year, the region or county is said to

face water scarcity [7]. Previous studies have estimated that around 1.7 to 3.1 billion people are experiencing water scarcity, and this is shown in Figure 1–1(b). However, a more recent study (2016) conducted by Mekonnen and Hoekstra, stated that two-thirds of the world’s population are facing water scarcity which indicates a more significant figure than in that of Figure 1–1(b). This study was carried out by analysing water scarcity on a monthly basis to provide an accurate estimate of the problem. The data in Figure 1–2 indicates that half a billion people suffer from water crises all year, and around 1.8 to 2.9 billion people face critical water scarcity for a period that last between 4 to 6 months per annum [4].

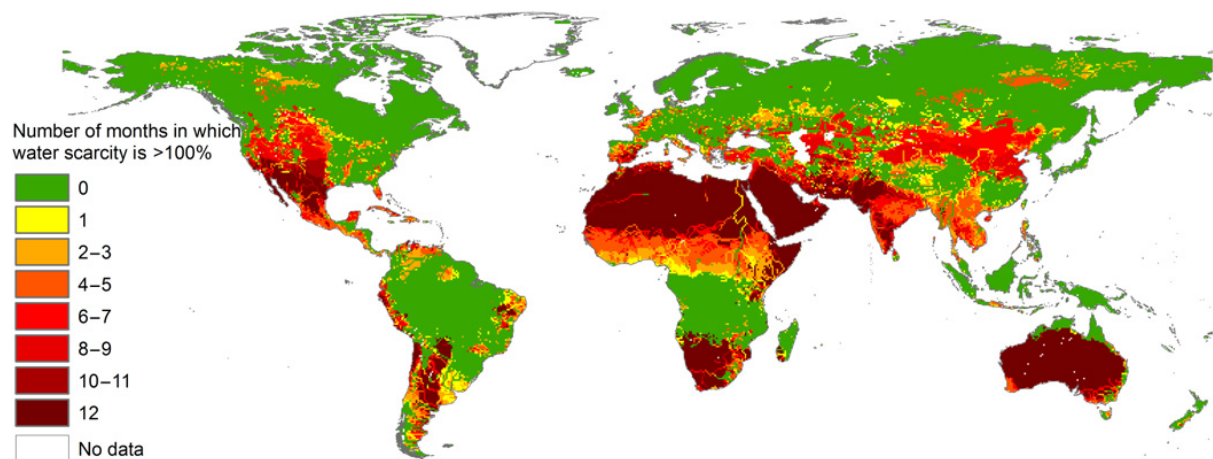


Figure 1–2: Number of people sever from water scarcity during n month per year. Period 1996 – 2005 [4]

1.2 Causes of Water Scarcity

Various reasons contribute to higher freshwater usage, including climate change, population growth, economic growth, water shortages, and insufficient infrastructure. Since 1900, there has been a significant rise, approximately six-fold, in the freshwater abstraction for industry, power generation and agriculture [8].

1.2.1 Climate Change

Climate change has significant repercussions for water resources, inducing more drought, diminished water quality and fluctuating weather conditions. Different regions of the globe have endured multiple adverse effects due to climate change. Figure 1–3 briefly outlines some of the main climate change-related issues faced by certain regions [9].

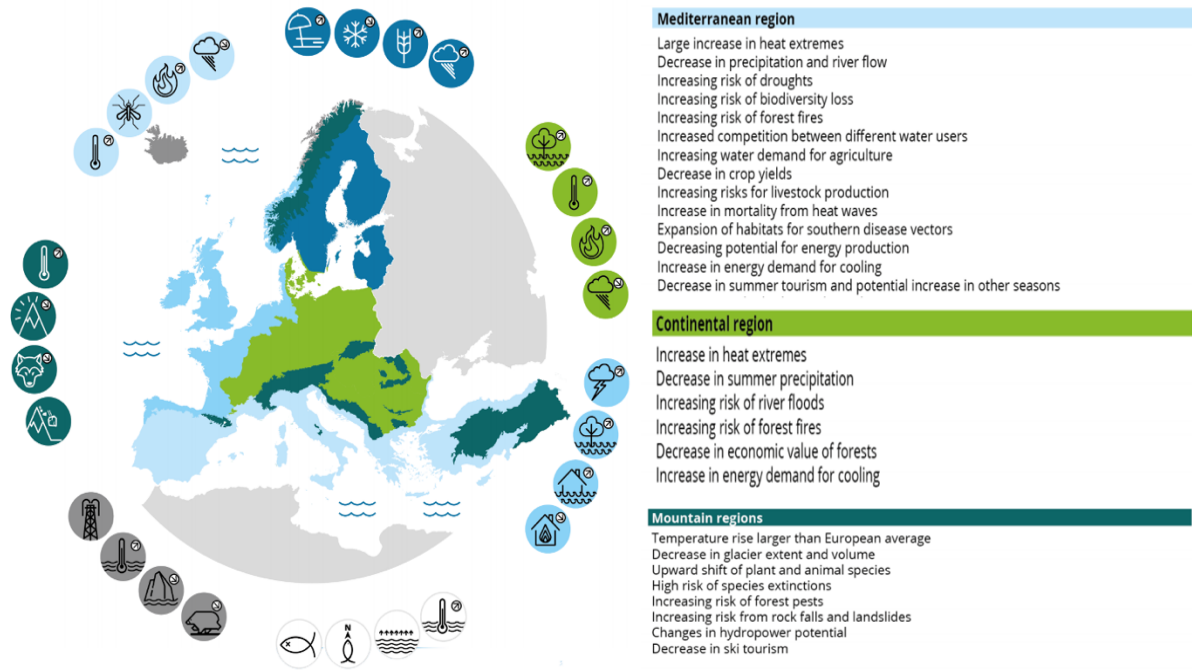


Figure 1-3: Climate change related problems in certain regions [9]

Drought is another cause of water shortage experienced by some regions in the world. It is believed that approximately 11 million people have lost their lives due to drought since 1900, with than one billion people impacted [10]. Drought in some regions of the world has significantly impacted water supply in the affected area. Mexico City has 40% of its water supply imported although the city is built on an ancient lakebed; the increased withdrawal of water has resulted in the sinking of parts of the city by centimetres every year. The water system director in the city, Ramón Aguirre Díaz, believes heavier rainfall with increased flooding and prolonged and more frequent droughts are to blame [11]. Similarly, the state of California in the United States experienced extreme droughts between 2011 and 2016. In this period, the state suffered its worst droughts which resulted in the drying up of approximately 1900 wells. In the middle east, Syria recorded its worst droughts in history between 2007 and 2010 [11]. This resulted in hundreds of thousands of people in the affected rural communities leaving the land and moving to the main cities in the country.

Climate change has resulted in a noticeable rise in temperature across the world at a worrying rate. The National Oceanic and Atmospheric Administration (NOAA) states in their Global Climate Summary report for 2019 that an average increase rate of temperature of 0.07°C per decade was observed since 1880. However, the average rate of temperature rise has more than

doubled to approximately 0.18°C [12]. Figure 1–4 is a geographical representation of the global average temperature in July 2020.

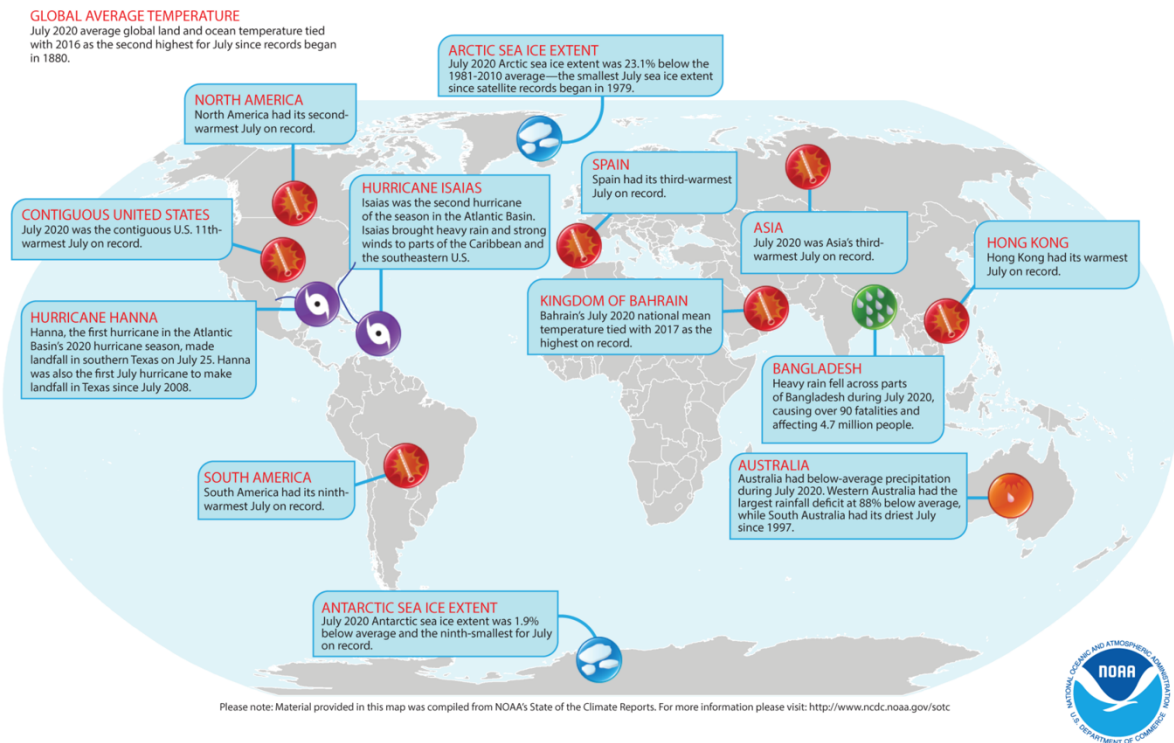


Figure 1–4: Global average temperature in July 2020 [12]

As a consequence of a rise in the incidence of heatwaves and drop in the rainfall level, the occurrence of wildfires increased significantly in the 20th century. For instance, 49,786 global fires had been recorded in 2019, which resulted in the burning and destruction of approximately 18.74 billion m^2 of land [13]. The National Interagency Fire Center reported 41,051 fires in 2020, which is 5,665 more fires when compared to the same period of 2019. Although the number of fires has decreased in the last couple of years, the area of scorched lands is considered significantly higher [13], as shown in Figure 1–5.

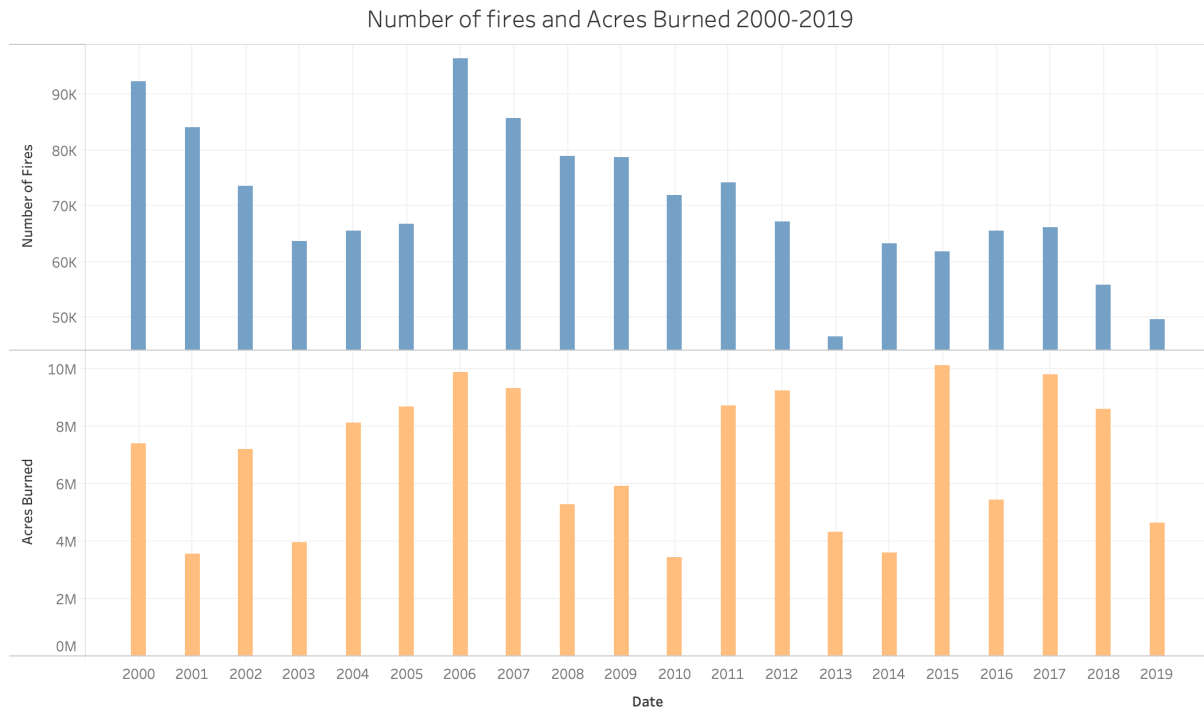


Figure 1–5: Number of fires and acres burned between 2000 and 2019 in the world [13]

Rises in sea level, stronger and more frequent tornadoes and hurricanes have been recorded across the world due to the effects of the ongoing climate change. The sea level has risen by 20.32 cm since 1880 and climate models predict that a further increase between 30 cm and 243 cm will occur by the year 2100 [14]. This increase will have an important impact on the ground water as well as posing a serious threat to life in low-lying coastal areas as a result of possible disastrous flooding.

Population

The current world population is around 7.8 billion, predicted to reach 8.6 billion in 2030 and 9.5 billion around 2050, as seen in Figure 1–6. UNICEF estimated approximately 140 million are born and 58 million people die each year, meaning around an 82 million increase in world population every year [15]. It is apparent from Figure 1–6 that in the 20th century, the population increased more than fourfold. Water consumption in agriculture, municipal use and industrial has risen by 5, 10 and 18 percent respectively [16] resulting in increased pressure on water resources. For instance, the largest total freshwater withdrawal of 760 billion m³ per annum was recorded in India in 2014, followed by the figures of 600 billion m³ in China and between 480 and 490 billion m³ in the United States for that year [17].

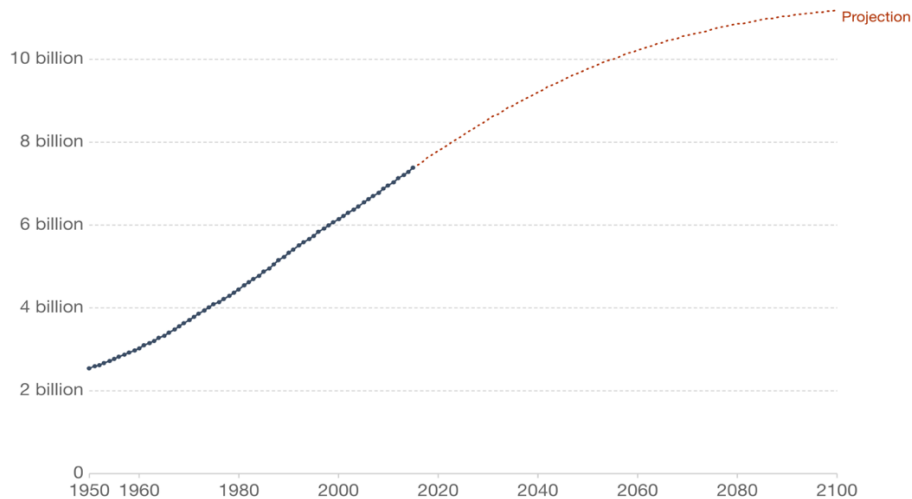


Figure 1–6: The world population projection by the United Nations from 1950 to 2100 [15]

1.2.2 Industrial Demand and Urbanisation

Industrialisation and increased urbanisation in the 1700s and 1800s led to a greater need for freshwater. The first noticeable water shortage was seen in the 1800s, which led to the development of the first water storage facility.

Water is a critical resource for nations throughout the globe in order to satisfy their daily energy demands. However, finding adequate water resources to generate the requisite energy, and then distributing the remaining quantity, is becoming more problematic. Many power utilities and energy corporations have been affected by water-related issues in the last five years. Water poses a significant threat to company activities; according to survey conducted by CDP nearly two-thirds of surveyed companies are reducing or maintaining their freshwater withdrawal [18]. In the year 2035, the International Energy Agency predicts that the world's energy consumption will rise by 35 percent, resulting in an 85 percent increase in water usage [19]. For a few nations, as shown in Figure 1–7, water has a significant influence on energy production [19]

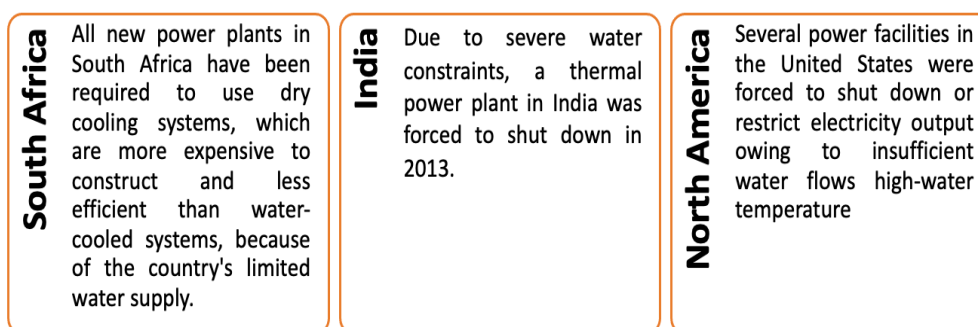


Figure 1–7: Impact of water on energy production, adapted from [19]

Numerous studies have been conducted on the influence of urbanisation on water quality and water demand. The use of water resources in cities is one of the earliest effects of urbanisation. Several researchers have found a linear relationship between urbanisation and the increase in total water usage [20], in contrast to this, other research has suggested that the impact of urbanisation on water resources usage is non-linear [21].

There have been changes in the world's coastlines due to ongoing urbanisation; these changes have been observed in a time frame of years up to decades. Studies demonstrate that urbanisation has a harmful influence on water quality [22][23]. The majority of people live in close proximity to rivers and coastlines. In the United States, between 1970 and 2010, coastal coastline counties rose in population to 125 people per square mile (48 people per km²), over three times the national average of 39 (15 people per km²) [24]. Waterways and aquatic environments generally suffer as coastal and watershed populations rise. Because of their large watersheds, estuaries are particularly vulnerable. Urbanisation has a number of effects on estuaries, including changes in streamflow and salinity, as well as consequences on plankton, marshes, seagrasses, shellfish, and fish present in the estuary [24].

1.2.3 Agriculture

Globally, agriculture is considered the sector most responsible for the stress on freshwater resources. It accounts for 70% of the total water consumption, even though some developed countries get 60% of their agriculture production from rainfed irrigation [17]. Furthermore, agriculture is responsible for an average of 90% of the water use in low-income countries; this figure drops to approximately 79% for middle-income countries [17]. Water consumption in high-income countries is around 41% [25]. As of 2017, agriculture was responsible for 59% of water use in Europe [26]. However, in developed countries, a projected increase of 14% in irrigation water withdrawal is expected, in terms of volume that is an increase from 2130 km³ per annum to 2420 km³ by 2030 [27].

In light of the significant current, and the predicted future, water availability challenges, this project focuses on desalination. Desalination is widely used to extract salts from sea and brackish waters. However, it is a resource intensive process, particularly in terms of energy consumption. There are four primary elements that dictate the energy requirements of the process: the influent water quality, the effluent quality requirements, the technology used, and the scale of the desalination plant. Many desalination technologies are well understood and established, and significant progress has been made to reduce the energy impact of desalination

processes in recent years. However, there remains the opportunity for improvement to design, operate and optimise desalination plants from a holistic systems perspective as opposed to the more common process perspective. Artificial Intelligence (AI) and Machine Learning (ML) technologies can potentially support this system optimisation. With this in mind, the specific objectives of this research are to:

1. Review and evaluate the potential of AI and ML technologies to improve the design, operation and optimisation of seawater desalination plants from a holistic, system perspective
2. Identify, evaluate and compile relevant information and data relating to desalination plant design, technology, characteristics and parameters
3. Integrate the compiled data and information to develop, analyse and implement an ontology and knowledge graph approach for in-depth analysis and understanding of the interrelationships among various complex processes and subprocesses within the seawater reverse osmosis (SWRO) desalination process
4. To develop and implement a life cost analysis tool for modelling an optimised and purpose-fit design of SWRO desalination plants, providing valuable insights to users.

Figure 1–8 gives a visual overview of the chapters in this thesis and how they relate to each other with the aim of fulfilling the objectives above.

A comprehensive examination of the historical background, contemporary advancements, and operational procedures relating to desalination and the new direction of reverse osmosis technology is examined in Chapter 2: “New Directions of Reverse Osmosis”.

Chapter 3: “Artificial Intelligence & Machine Learning” shifts the focus to review the application of AI and ML in water treatment and desalination, while explaining the challenges associated with integrating these two fields. This chapter concludes by highlighting research gaps, defining the research problem, and presenting proposed solutions. Together these chapters address Objective 1 and 2.

Chapters 4, 5 and 6 provide an in-depth exploration of the three main contributions to understanding the requirements, design and cost-analysis for SWRO systems and address Objectives 2, 3 and 4.

Chapter 4: “OntoSWRO” introduces the development of OntoSWRO ontology, offering insights into the design aspects of seawater reverse osmosis desalination plants and three scenarios are developed for evaluating OntoSWRO.

Chapter 5: “SWRO Desalination Process Design” provides a deep analysis of the formulated equations, exploring their significance in the context of SWRO desalination facilities. Additionally, comprehensive equations are presented for system limits and flows that extend beyond the purview of this particular study.

Moving forward to Chapter 6: “Economic Cost Assessment”, the focus is directed towards the life cost analysis component. This section provides further details pertaining to the functional unit, capital expenditure, and operational expense. The assumptions and procedures that are vital to this research are clearly articulated.

The outcomes from Chapters 4, 5 and 6 form the basis of the resulting SWRO design and LCCA tool for holistic design of desalination. Chapter 7: “Evaluation of OntoSWRO and LCCA” outlines the development process of a decision support tool's user interface and programme architecture, presenting results from system analysis. This chapter also explores the integration between ontology and life cost analysis in the context of desalination plant design.

Finally, Chapter 8: “Conclusions and Future Work” summarises the thesis by presenting conclusions, outlining contributions made by the thesis, and proposing potential directions for further work.

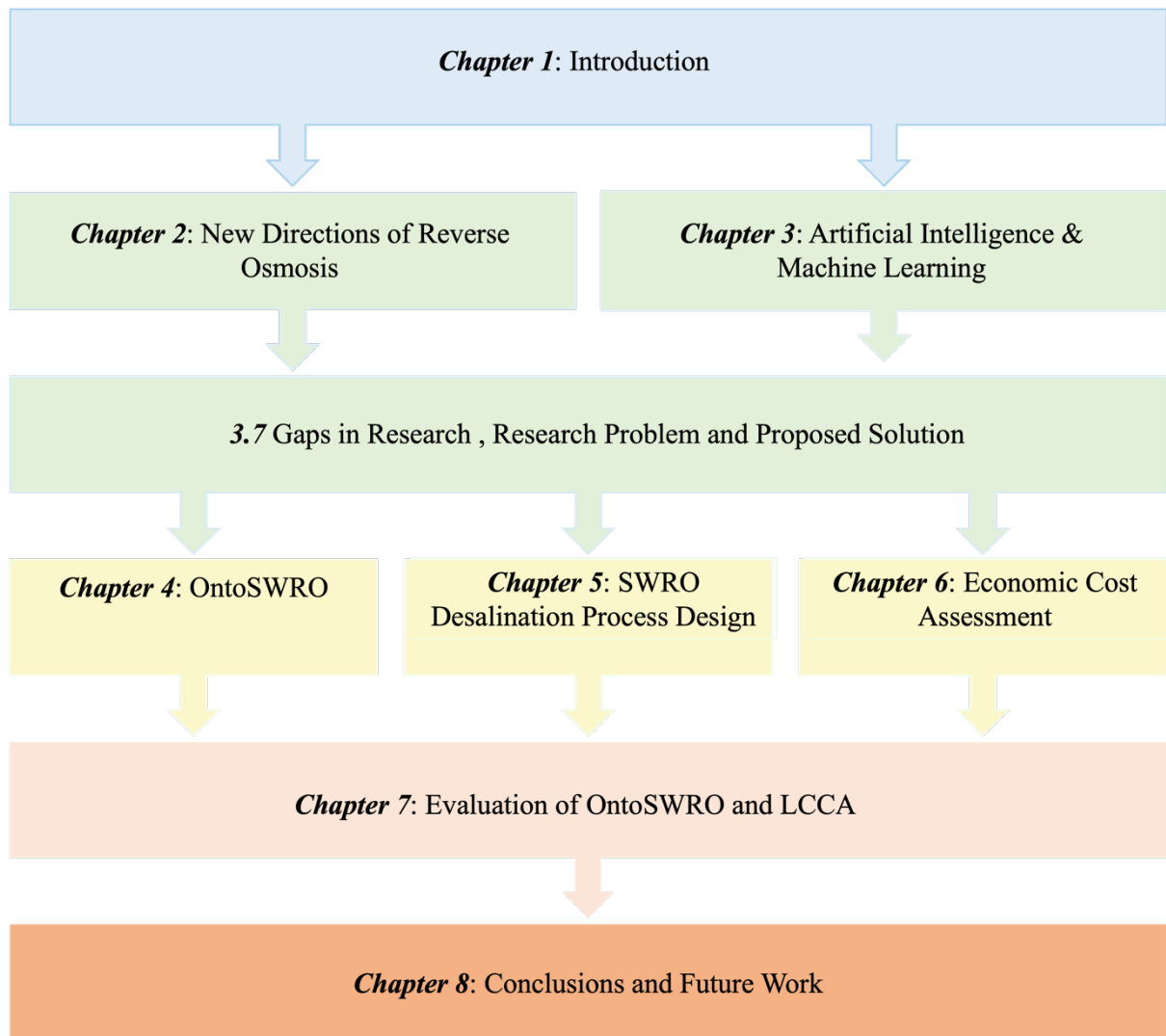


Figure 1–8: Thesis chapters structure flowchart

Chapter 2

Literature Review: New Directions of Reverse

Osmosis

This chapter presents an overview of water treatment methods and offers a comprehensive examination of the historical background, contemporary advancements, and operational procedures pertaining to desalination. The primary emphasis is placed on seawater reverse osmosis desalination. This chapter will examine the emerging trends in reverse osmosis and emphasise the current research focus in the field, specifically in relation to membrane technology, auxiliary components, and system configurations.

2.1 Water Treatment Technologies

Two primary technologies for potable water treatment are available and widely in use; these are conventional water treatment and desalination.

2.1.1 Conventional Water Treatment

Conventional water treatment is an approach that is applied in treating surface water. It removes the turbidity and any harmful bacteria from the water using various processes, including flocculation, sedimentation, filtration, and chlorine disinfection. The specific energy consumption (SEC) of these processes is approximately between 0.2 and 0.4 kWh/m³. The technology is limited to only less than 3% of water resources available around the world [28].

2.1.2 Desalination

Due to the factors that have been addressed in the previous section, it is necessary to establish an alternative solution in which the feed water source will be primarily saline or brackish water. Therefore, desalination technology has emerged as a feasible solution for the future. The term desalination refers to the process of removing total dissolved solids (TDS) from source water. TDS is composed of total inorganic and organic material such as salt and metal ions. The International Standard by World Health Organisation (WHO) outlines that the TDS in

freshwater should be less than 1000 mg/L [29]. In seawater, the amount of TDS is between 35,000 mg/L and 45,000 mg/L while brackish water contains amounts between 3000 mg/L and 20,000 mg/L [30]. Desalinating this raw water will remove the majority of the dissolved solids producing freshwater that can be used industrially, in agriculture and for drinking.

Desalination plants were first established in the year 1881; however, research and development over the years brought about commercial distillation desalination at the beginning of the 1920s prior to the second world war. The goal of this technology was to cope with the water demand for remote areas lacking a water supply. Desalination was further developed over the years by the United States and other countries. The technology became commercially established in the year 1960, with the thermal process as the most commonly applied technology at the time. Membrane technology then came about in the late 1960s and was mainly involved in brackish water treatment. Both technologies became fully commercial by the 1980s [31]. Figure 2–1 illustrates a timeline of the desalination plant development over the years.

As of 2019, over 15,000 desalination plants are active around the world across a total of 177 countries [32]. However, according to the International Desalination Association (IDA), in 2018, the global number of contracted desalination plants was approximated as more than 20,000 [33]. There has been a noticeable increase in the number of desalination plants and the water they produce recently, in the three-year period from 2016 to 2019, there was a 12.4 % and 41.2% increase, respectively [34].

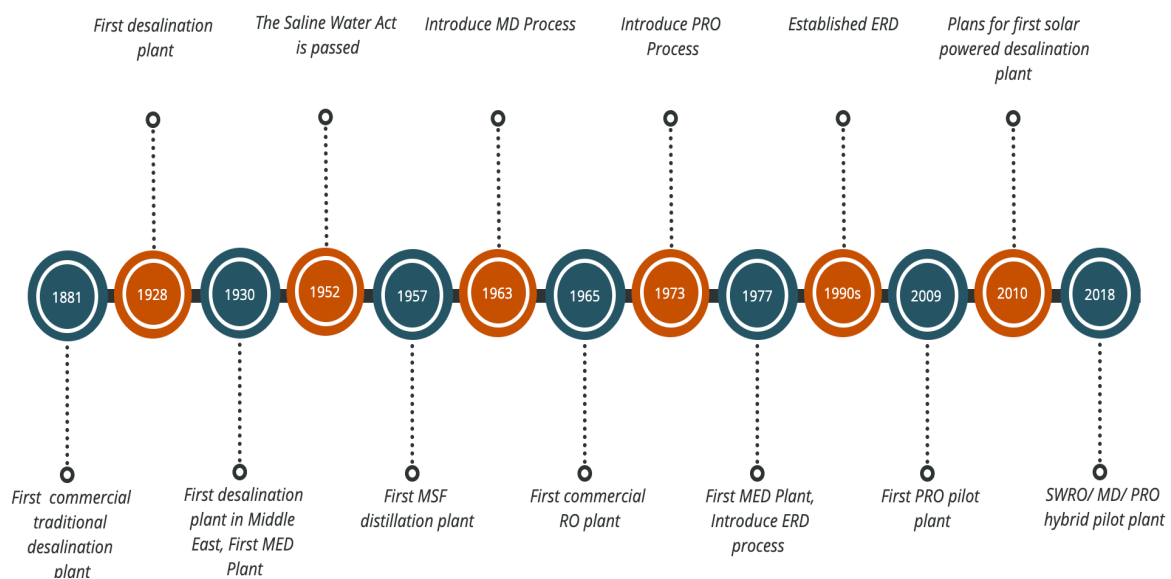


Figure 2–1: Timeline of desalination technology adapted from [35]. Multi-effect distillation (MED) multistage flash (MSF), membrane distillation (MD), reverse osmosis (RO), Energy recovery device (ERD)

The municipal sector is the main utiliser of desalinated water accounting for 60% of the available desalinated water. About 33% is utilised by power and industrial users. The remainder of the desalinated water is utilised for irrigation, military as well as other applications as shown in Figure 2–2 [36][37].

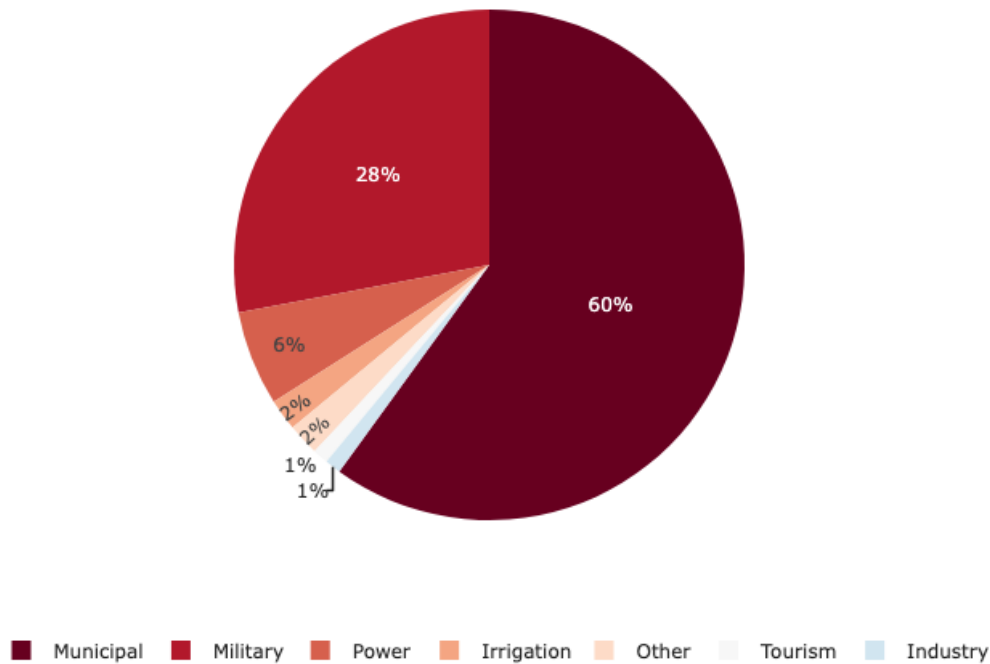


Figure 2–2: Total Global installed desalination capacity by type of use, adapted from[37]

2.2 Desalination Technologies

Membrane and thermal processes are the two main types of technology commonly used. With thermal technology, water is evaporated resulting in any dissolved solids or contaminants being left behind. The vapour is then condensed and clean water is produced. Membrane technology involves filtration of the source water through a semipermeable membrane by means of high pressure resulting in production of freshwater [38]. Examples of several technologies in use are listed in Figure 2–3.

Nowadays, Reverse Osmosis (RO) is the most common method applied in desalination technology, this is followed by Multi-Stage Filtration (MSF) and Multi-Effect Distillation (MED) technologies. Statistics for 2018 showed that total installed capacity worldwide is mainly accounted for by these three technologies. The percentage of the desalination capacity for each of RO, MSF and MED was approximately 68.7%, 17.6% and 6.9% respectively, and the remaining 6.8% is composed of other technologies. The main source of water for

desalination around the globe is seawater at approximately 70.5% of the total capacity [39]. In this section, the three main technologies are discussed along with issues and challenges associated with them. Other technologies have been omitted as they have little application worldwide in comparison to RO, MSF, MED, and will not be of relevance in the next stages of this research. Table 2-1 discusses the available desalination technologies in terms of their classes, type of driving force, status and application.

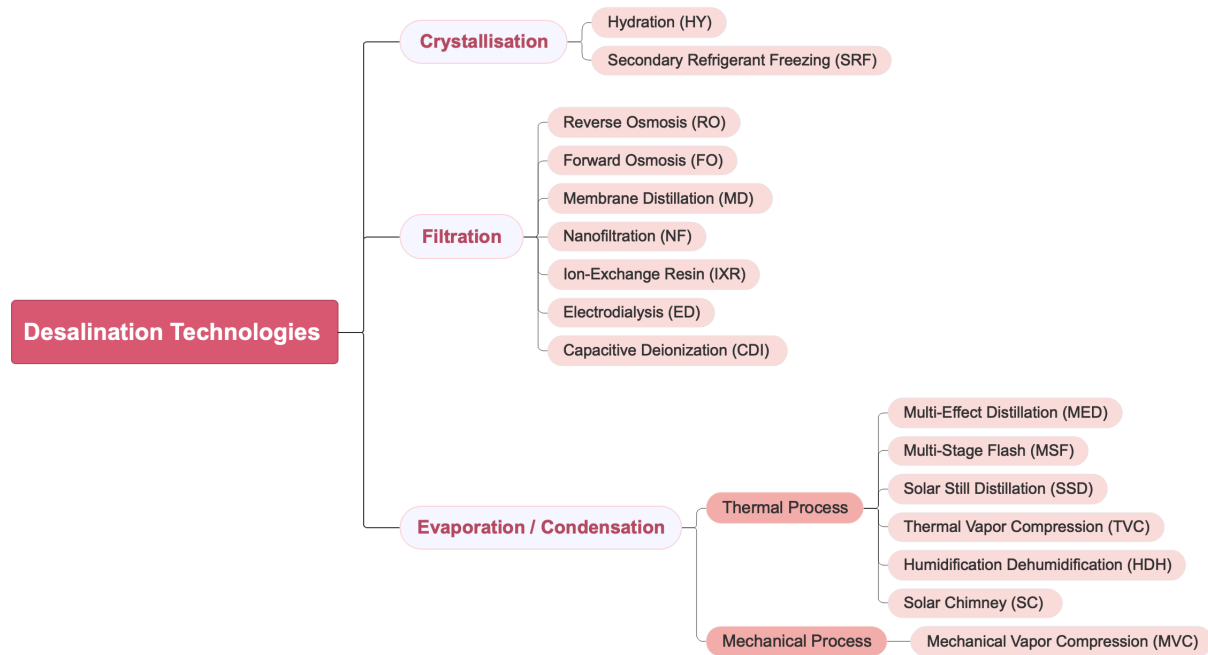


Figure 2–3: Schematic classification of desalination technologies

2.2.1 Multi-Stage Flash (MSF)

In MSF distillation, saline water is heated by means of a brine heater using steam at low pressure. The heated water is passed through a series of stages (flash chambers), each under lower pressure than the previous one. The temperature is always above that of boiling point for each pressure in all flash chambers and a small amount of the brine water turns into steam reducing the temperature to reach a point of equilibrium. [34], [40]. Entrainment separators separate high-salinity mist from low-salinity rising steam which is condensed into distillate. Pure water referred to as the distillate, which had condensed on the heat tubes is collected in distillate trays. This pure water is transferred to the water product tank.

The brine is formed in each stage and is collected at the end to lower the volume of source water collected by the intake for desalination as shown in Figure 2–4. The recirculated brine

Table 2-1: Type of desalination technologies in terms of their driving force, status and application [36], [41]

Technique	Technology	Driving force	Status	Application	Limitations
Membrane	Continuous Electrodeionization (CEDI)	Electric field	Mature	Polishing RO permeate Non - water purification application	Limited to certain feed water conditions Limited electrical resistance of the module
	Electrodialysis	Electric field	Mature		Ongoing research in: Poor economic efficiency for low salinity product water production High energy consumption Membrane fouling
	Forward Osmosis	Osmotic Pressure	Commercial	Desalination application	Requires additional treatment Draw solutes must be designed for high solubility
	Membrane Distillation	Vapour pressure	Ongoing study		High capital cost High energy consumption Flux inconsistency Cannot be applied to large scale operation
	Nanofiltration	Pressure	Mature	Softening Partial demineralisation of saltwater Pretreatment in RO desalination	High capital cost Intensive pretreatment Insufficient rejection of pollutants
	Piezodialysis	Pressure	Limited commercial	Kidney dialysis	Decrease in salt separation as feed salt concentration increases
	Reverse Osmosis	Pressure	Mature	Food processing Pharmaceutical Industrial Agriculture Water for potable use	Intensive pretreatment Ongoing research in: Fouling resistance Chlorine tolerance Energy reduction Maintaining or improving rejection

Technique	Technology	Driving force	Status	Application	Limitations
Thermal	Humidification Dehumidification (HDH)	Temperature	Under development	-	High specific energy consumption
	Freezing Melting (FM)	Temperature	Under development	Food processing	High capital cost Complex process
	Multi-Stage Flash (MSF)	Temperature	Mature	Desalination application	High energy consumption Low level of flexibility in operation High prone to corrosion Slow operation start up Whole plant shutdown for maintenance
	Multi-Effect Distillation (MED)	Temperature	Mature	Desalination application	Scaling Corrosion
	Capacitive Deionization (CDI)	Electric Field	Under development	-	Expensive material Short life span
Other	Ion Exchange	Ion charge	Mature	Low salinity brackish water desalination	Limited in resin capacity Prone to fouling quickly at high salinity may

eliminates the latent heat of condensation. This pre-heating of the recirculated brine helps recover energy from condensing vapour and reduces total heating needs of the source water.

Each flash stage typically yields 1% of the entire desalination plant condensate volume. The overall MSF plant recovery is normally 19 to 28%. Comparatively, RO seawater desalination systems recover 40-45%. A 45-stage MSF unit may function at a 45 percent recovery rate. This characteristic rival RO systems in terms of recovery.

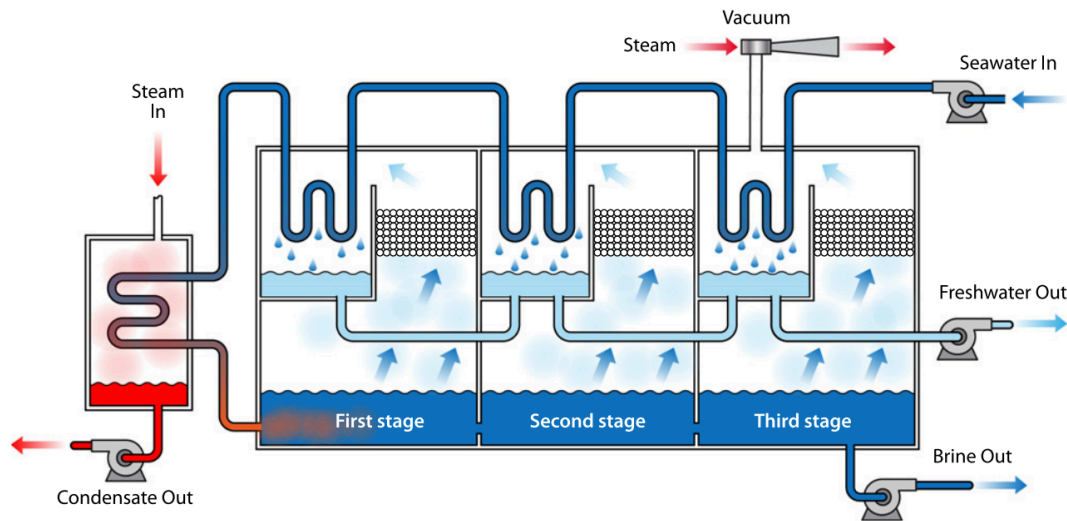


Figure 2–4: Schematic of Multi Stage Flash [42]

2.2.2 Multi-Effect Distillation (MED)

MED functions similarly to MSF in which a series of flash chambers with pressure decreasing along the chambers are utilised. This setup ensures the elimination of the requirement of energy supply for boiling past the first chamber as feed seawater undergoes many boiling phases. Heated steam from the seawater is directed inside a multiple tube connection, heat resulting in the tubes is then transferred to the source water which flows over the heated tube as illustrated in Figure 2–5. The steam running through the tube results in the evaporation of the saline water. In summary, seawater under heat transfers into the first tube and vapour is formed and this process repeats along multiple chambers and in the last chamber condensed fresh water is produced [43][34][31].

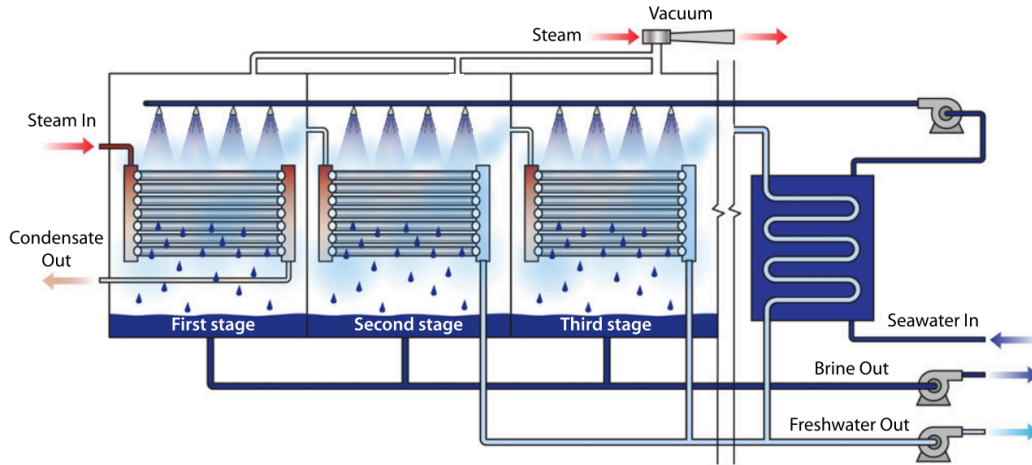
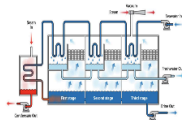


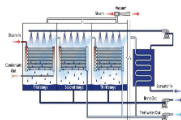
Figure 2–5: Schematic of Multi Effect Distillation [42]

Multiple factors have driven countries towards a membrane system rather than a thermal system, such as reduced capital cost in an RO setup as a result of cheaper construction material, versatility of feed sources, and the fact that RO does not require thermal energy to operate [36]. However, MSF and MED are cost effective in regions where energy is subsidised or in the case where the desalination plant is co-located in conjunction with steam generated power. Hence, thermal processes are common in the middle east region, although with new energy initiatives such as Dubai Clean Energy 2050, there is a drive to move towards membrane technology specifically seawater reverse osmosis (SWRO) [44]. With this in mind, the main desalination focus of this review will be on the RO process. Figure 2–6 specifies the advantages and challenges among the three most popular desalination technologies.



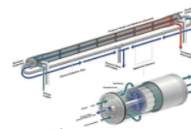
Multi-Stages Flash (MSF)

- **Advantage**
 - Easy to operate and maintain
 - Treat high saline water
 - High water Quality
 - Large capacity design
 - Long operational life
 - Minimal pre-treatment required
- **Disadvantage**
 - High energy consumption
 - Low level of flexibility in operation
 - highly prone to corrosion
 - Slow operation start up
 - Shut the whole plant for maintenance
 - Larger footprint
 - Low recovery ratio
- **Status**
 - Commercially available



Multi-Effect Distillation (MED)

- **Advantage**
 - High water quality
 - Minimal pre-treatment required
 - Tolerate biological problem
 - Low energy consumption compared to other thermal processes
 - Minimum supervision required
- **Disadvantage**
 - Scaling in the pipe
 - High energy consumption
 - Process is susceptible to corrosion
- **Status**
 - Commercially available



Reverse osmosis (RO)

- **Advantage**
 - Lower capital cost
 - Lower energy consumption
 - Well commercialised
 - Quick start up
 - Small footprint
 - High production
 - Could couple with multiple renewable energy sources
- **Disadvantage**
 - Lower water quality
 - Subject to fouling
 - Requires comprehensive pre-treatments to
 - Minimum membrane life expectancy
- **Status**
 - Commercially available

Figure 2–6: Pros and cons of the three most popular desalination technologies

2.2.3 Reverse Osmosis

Reverse osmosis (RO) is a demineralisation process that relies on molecule filtration through semipermeable membranes. Feedwater is pumped through the semipermeable membrane at an applied pressure greater than that of the osmotic pressure of the feedwater as illustrated in Figure 2–7. This results in the separation of molecules as the water passes from a high concentration solution to a low concentration compartment [45][46]. RO is considered to be an energy efficient process compared to thermal desalination processes. This is primarily due to the fact that the process operates at ambient temperatures and requires no heating or cooling during phase changes [47]. The advancement of energy recovery devices, pumps, and membrane technology in the last two decades has led to a significant improvement in the performance and cost-effectiveness of membrane based desalination [48], [49].

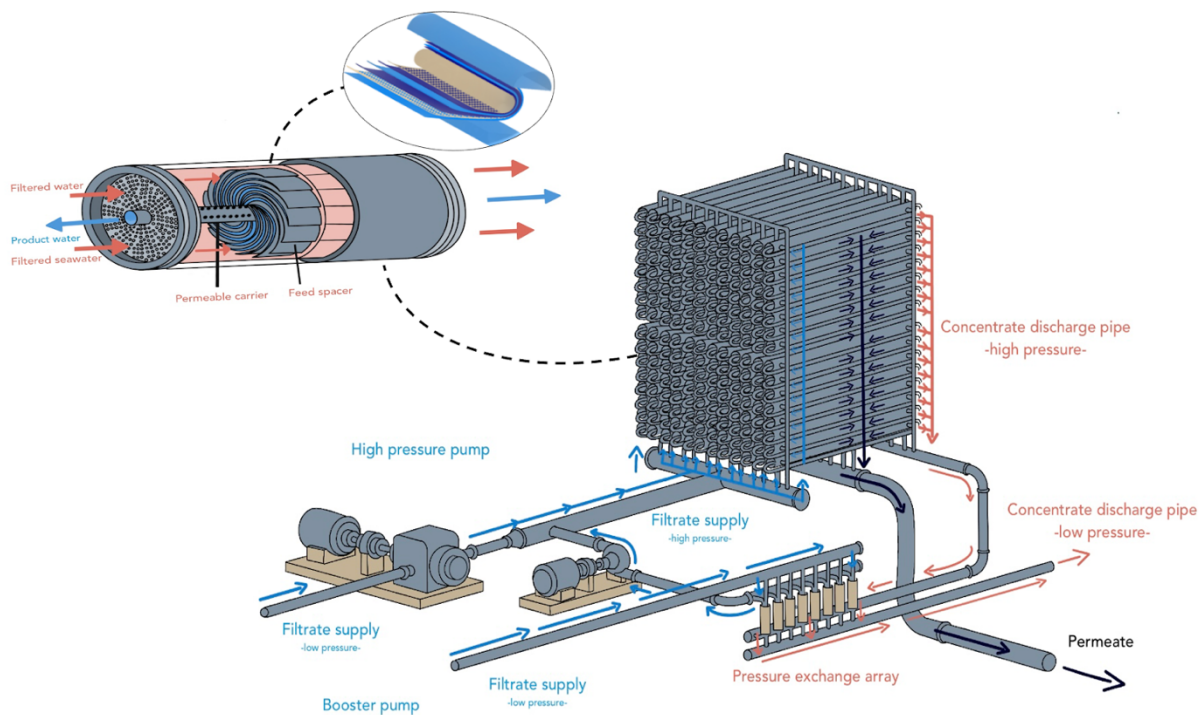


Figure 2–7 : Schematic diagram of RO desalination plant and RO membrane

The phenomenon of osmosis was observed in 1748 by Abbe Nollet; as a result the first documentation of the term semipermeable membrane was recorded that year [50]. However, current technology was studied in 1940s by Dr Gerald Hassler at University of California in Los Angeles (UCLA). Dr Hassler started to investigate the osmotic properties of cellophane membranes. Hasslers’ assumption was that the process of osmosis happened by evaporation

occurring at the membrane's surface and the vapour produced travelled through an air gap followed by condensation on the surface of the opposing membrane. Nowadays, it is known that Hassler assumption is not correct and that the most likely process of osmosis is the solution - diffusion model at the membrane [51]. Sourirajan developed the first asymmetric cellulose acetate membrane the 1960s at UCLA, Figure 2–8 illustrates the timeline of the important development that occurred in the history of RO.

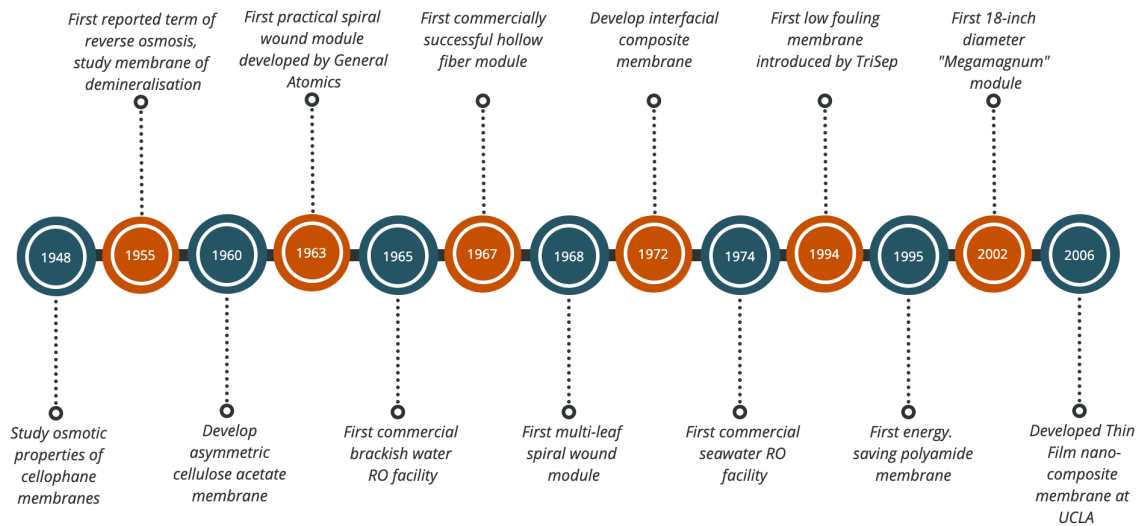


Figure 2–8: RO development timeline, adapted from [46]

2.3 New Directions of Reverse Osmosis

2.3.1 RO Transport Models

Even though RO is inherently a more energy efficient technology than thermal processes, there has been a lot of recent research developments in the area of improved energy performance. An optimal energy RO operation in theory is obtained by having a consistent water flux along the membrane area. Flux of water is the volumetric flow rate of water through a defined membrane area which is proportionally dependent on the net pressure driving force applied to the water, represented in Eq 2.1 [46], [52].

$$J_w = A \left((P_f - P_p) - (\pi_f - \pi_p) \right) \quad \text{Eq 2.1}$$

Where J_w is water flux ($L/m^2/h$), A is the water permeability ($m/min/bar$), P_f feed pressure (bar), P_p permeate pressure (bar), π_f feed osmotic pressure (bar), π_p permeate osmotic pressure (bar). There is a common understanding with the process of membrane separation that the

relationship of solute flux rate through the membrane with that of the effective concentration difference of solute across the membrane is one of direct proportionality. As the concentration gradient increases, the solute flux through the membrane also increases. This concept (Eq 2.1 and Eq 2.2) is fundamental in terms of membrane separation and one which the design and operation of membrane based processes depend on.

$$J_s = K(C_{A2} - C_{A3}) \quad \text{Eq 2.2}$$

Where J_s is flux of solute ($\text{g/m}^2\text{s}$), K salt permeability coefficient ($\text{kg/ m}^2\text{s}$), C_A molar concentration of solute (g/kg), where 2 relates to the boundary layer, and 3 to the permeate. As feedwater flows across the membrane surface, pure water dissolves and diffuses across the membrane at a faster rate than the salt. Along the length of the membrane channel, the applied feed pressure and pressure on the permeate side remain generally constant. The remaining feedwater now has a higher concentration resulting in a higher osmotic pressure while the osmotic pressure of permeate remains close to zero. As a consequence, the driving force for pure water flow across the membrane gets maximised at the inlet of the membrane and starts decreasing gradually as the membrane length increases. This will cause the net pressure driving force to be maximised near the inlet and decrease along the membrane [53]. Figure 2–9 shows a schematic representation of a mass transfer model of RO. As a result of these changes in the water flux, reduction in the energy efficiency occurs. Consequently, to improve performance, process scale up and simulation, an accurate model for flux decline is essential.

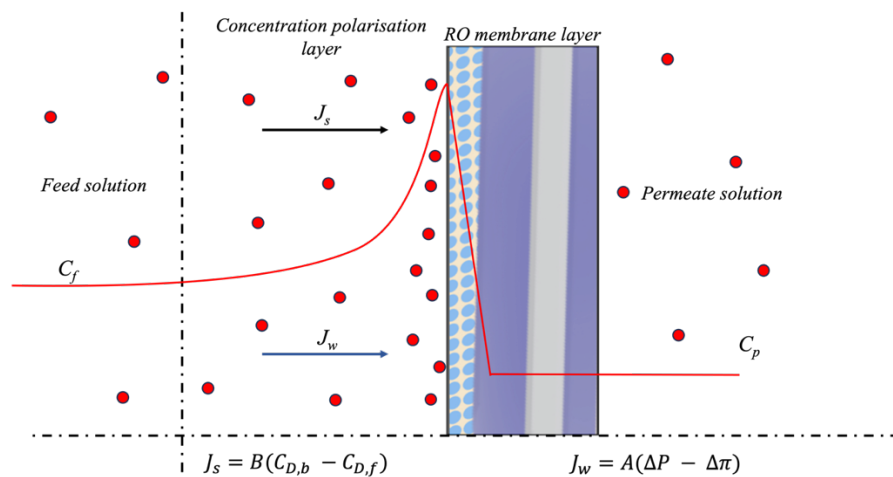


Figure 2–9: Schematic of mass transport model for Reverse osmosis, C_f is feed concentration, C_p permeate concentration, J_w water flux, J_s salt flux, A is the water permeability coefficient of the membrane, B is the salt permeability coefficient of the membrane, $C_{D,b}$ and $C_{F,b}$ are the solute concentrations in the bulks, $\Delta\pi$ is the osmotic pressure difference between the bulks, and ΔP is the hydraulic pressure applied on the draw water side

The widely used solution-diffusion (SD) model lacks the ability to fully describe the intricate transport mechanisms of water molecules and ions through the membrane. In order to address this limitation, Wang *et al.* [54] proposed a novel ion transport model for RO, termed the solution-friction model. This approach involves a rigorous consideration of the partitioning mechanisms and the interactions among water, salt ions, and the membrane, leading to a more accurate description of ion transport through the membrane. Specifically, the author employed the extended Nernst-Planck equation to describe ion transport which is known as ion flux (Eq 2.3), while accounting for the relative frictions between different species (i.e., ion, water, and membrane matrix). Meanwhile, water flow was modelled through the membrane using the hydraulic pressure gradient (Eq 2.4) and the relative frictions between water and both the membrane matrix and ions.

$$J_i = K_{c,i}c_i v_f - K_{d,i}\varepsilon D_i \left(\frac{dc_i}{dx} - z_i c_i \frac{d\phi}{dx} \right) \quad \text{Eq 2.3}$$

Where J_i is the flux of ion i , $K_{c,i}$ the advective hindrance factor, $K_{d,i}$ the diffusional hindrance factors, c_i the concentration of ion, v_f the permeate water velocity, ε the effective membrane porosity, D_i the bulk ion diffusivity, ϕ the dimensionless electrical potential inside the membrane, z_i the ion charge and x the dimensionless coordinate through the membrane.

$$\frac{dP^t}{dx} = RT f_{f-m}(v_m - v_f) + RT \sum_i f_{i-f} c_i (v_i - v_f) \quad \text{Eq 2.4}$$

Where P^t is total pressure, R is the gas constant, T is the absolute temperature, v_m , v_i , v_f are the velocities of the membrane, ions and fluid (water) respectively, f_{f-m} is the frictional coefficient between the fluid and membrane, and f_{i-f} is a parameter related to the friction between the ions and the fluid.

Table 2-2 shows a comparison between the two diffusion models and provides the equations for water and salt permeability coefficients.

Table 2-2: Comparison between Solution-Diffusion Model and Solution-Friction Model [54]

Parameter	Solution-Diffusion model	Solution-Friction model
Salt permeability	Constant	Varies with salt concentration and applied pressure
Hydraulic pressure across the membrane	Constant	Linear decrease

Parameter	Solution-Diffusion model	Solution-Friction model
Mechanism of water transport	Diffusion	Hydraulic pressure gradient
Mechanism of salt transport	Diffusion	Diffusion ,Advection , electromigration
Water permeability coefficient equation	$A = \frac{J_w}{\Delta P - \Delta \pi}$	$A = \frac{J_w}{P - 2RT(c_{i,w} - c_{i,p})}$
Salt permeability coefficient Equation (B_{th})	$K = \frac{J_s}{C_{A2} - C_{A3}}$	$B_{th} = \frac{c_{i,p} J_w}{c_{i,w} - c_{i,p}}$

2.3.2 RO Membrane

Over the past three decades, significant improvements have been made in RO membrane technology, including advancements in membrane material, module design, process design, flux, permeability, salt passage, energy reduction, and water recovery. For example, membrane permeability and salt rejection have improved significantly in recent years, largely due to advancements in membrane material and design [55], [56], [57], [58], [59], [60]. The use of highly productive membranes can reduce energy consumption by approximately 5% to 15% [28].

Membrane permeability has improved through the development of thin film composite (TFC) membranes, which consist of a thin, selective layer of polymer on top of a support layer. The TFC membranes have a higher permeability than previous generations of membranes, allowing for higher flux rates and lower energy consumption which is due to their highly crosslinked and ultra-thin polyamide skin layer. Salt rejection has also improved through the use of improved membrane materials and design. TFC membranes have a high degree of selectivity, which allows them to reject salt more effectively than earlier membrane technologies. Additionally, improvements in module design have led to increased turbulence and shear rates within the membrane module, which enhances the membrane's ability to reject salt. Nevertheless, there are restricted trade-offs between water permeability and salt rejection, as well as challenges related to membrane scaling and fouling, which must be addressed to ensure the sustainable implementation of polymeric membranes in desalination methods.

In industrial applications, the RO membrane modules must have a high packing density to achieve a compact process, easy installation, and maintenance, as well as low capital costs. Among the available membrane types, TFC polyamide (PA) membrane is the most widely used, exhibiting a salt rejection rate of up to 99.8% in conventional seawater RO test settings [61]. In the past, tubular or plate and frame configurations were used in RO membranes.

However, these membrane modules have been removed due to undesirable low packing density, equipment space requirements, and high capital cost [62] [46]. These two membrane types are now confined to the food and dairy sectors. Nowadays, spiral wound and hollow fibre is the most popular membrane module. Hollow fibre membranes are more prone to particle and biofouling fouling compared to other configurations. To tackle this issue, either an intensive pretreatment must be applied to remove particle foulants from the source water or apply this element to a source water with low turbidity and SDI, such as water received from well intakes [63]. Table 2-3 is a comparison between the four modules membrane [64][46][65].

Table 2-3: Comparison between four type of RO membrane modules [64][46][65]

Type of membrane	Packing density (m ² /m ³)	Fouling propensity	Ease of Cleaning	Capital Cost
Plate and frame	147 - 492	Moderate	Good	High
Tubular	20 - 394	Low	Excellent	Very high
Spiral wound	392 - 1246	High	Poor	Moderate
Hollow fibre	492 - 4921	Very High	Poor	Low

2.3.3 Auxiliary RO Equipment

The energy efficiency of RO is an essential factor in obtaining a sustainable process. In the 1970s the RO process consumed approximately 20 kWh/m³ (m³ refers to permeate produced) due to several factors: less efficient pumps, lower membrane permeability, lack of energy recovery device (ERDs) [66]. In recent years, a significant reduction has been observed in the total cost of desalinated water [67], [68] due to continuous process improvement. The actual SEC of the whole SWRO desalination plant varies between 2.5 and 4.0 kWh/m³ of treated water depending on the operating conditions [48]. A figure of 1.58 kWh/m³ was claimed by the Affordable Desalination Collaboration (ADC) in the United States in 2006 [69], [70], [71], the lowest SEC recorded for a single pass RO at operating conditions of 42.5% recovery rate, an average temperature of 15.2 °C and flux of 10.2 L/m²h. The SEC of MED ranges approximately between 6.5 and 17 kWh/m³ [72]. MSF consumes more energy than MED as SEC consumption is reported to range from 15 kWh/ m³ and reaches up to 20 kWh/m³ [43] [31]. Table 2-4 summarises the energy consumption ranges observed in medium to large seawater RO systems, which have been obtained from a survey of 30 distinct SWRO facilities constructed between 2010 and 2017. The table reveals that the average energy required for generating one cubic metre of fresh water from a desalination plant is approximately

3.1kWh/m³, with some facilities achieving energy efficiencies as low as 2.4 - 2.8 kWh/m³, which are considered to be the best-in-class energy performance metrics.

Table 2-4: Current Ranges of energy consumption for medium – large SWRO systems [28]

Classification	SEC of SWRO system (kWh/m ³)
Low-end bracket	2.4–2.8
Medium range	2.9–3.2
High-end bracket	3.3–4.0

In recent years, the advancements achieved for RO technologies in terms of membranes, pumps and ERDs have appeared to have reached a limit, resulting in a plateauing of energy reduction trends. This limit has been assessed in terms of the minimum theoretical energy required for desalination [28]. Minimum theoretical energy is the required amount of energy to exceed the osmotic pressure in order to produce desalinated water. For the RO to operate at the minimum theoretical value, the applied pressure for the feed water must not be less than that of the osmotic pressure of the concentrate. This figure is calculated based on the thermodynamic constraints, which was found to be 1.06 kWh/m³ with total dissolved solids of 35,000 mg/L and a 50% recovery rate [69], [70], [71]. Small perturbations in the feed water recovery rate, pump efficiency, or salinity can lead to variations in the theoretical energy required by a RO system. However, in practical settings, the SEC of RO systems tends to exceed the theoretical limit due to the non-reversible nature of the process and the time-varying flux. If an RO system were to operate at the theoretical limit, it would require significantly longer desalination times. This performance gap in continuous RO is attributed to the lack of reversibility associated with high pumping pressures, which arise due to the need to overcome the outlet osmotic pressure, which is higher than the inlet pressure. The non-reversible nature of the process results in additional energy consumption, which must be accounted for when designing and operating RO systems [73].

Traditionally, the rejected brine underwent a throttling process to reduce its relatively high pressure before being discharged. This resulted in significant exergy destruction and a lost opportunity to do useful work as brine was ejected through the pressure control valve. This accounts for up to 60 percent of energy that is dissipated [74]. However, more recently, in seawater desalination the throttling valve has been replaced by centrifugal energy recovery devices, such as Pelton wheel (PT) and Francis Turbine (FT), or isobaric ERD such as PX, and

Dual Work Exchanger Energy Recovery (DWEER), to recover the loss in pressure and reduce the overall energy consumption [74], [75], [76], [77], [78].

Table 2-5 presents a comprehensive summary of the various types of ERDs that are currently available in the market. This table highlights the distinct advantages and disadvantages of each ERD, along with the specific equipment components that are required to operate them effectively. Additionally, this table provides information regarding the desalination scale that each ERD is capable of serving, as well as the SEC of SWRO plants that utilise these ERDs.

The Magtaa SWRO desalination facility in Algeria is a good example of the energy savings possible using ERDs. In 2014, Magtaa was considered the world's largest membrane-based desalination plant, with a capacity of 500,000 m³/day. The plant has 25 AT-7800 turbochargers in operation. Using ERDs, 40 MW of energy can be saved, equating to around \$25 million in financial terms [75]. SEC decreases with increased capacity in desalination plants, as is well-documented. Energy recovery devices also play a major role in reducing energy consumption. Use of PX ERDs instead of standard ERDs has led to a significant reduction of SEC, according to evidence. In ERD Inc.'s estimation, PX can recover up to 98 percent of the concentrated brine's energy [79], [80].

Many desalination facilities have shown that SEC can be improved by using PX ERDs [84], [85], [86]. The SWRO desalination plant in Palmachim, Israel, works at a recovery rate of 46 percent and a flux of 13–14 L/m²h at 25 °C with a RO feed pressure of 63 bar and a high pressure (HP) pump efficiency of roughly 85 percent and capacity of 274,000 m³/day [87]. With no ERD, the total RO energy consumption of the aforementioned plant is 4.476 kWh/m³, of which 2.059 kWh/m³ is for permeate generation and 2.417 kWh/m³ is for brine energy waste. When the ERT-PX HYBRID ERD device was used, the reported energy value of 2.70 kWh/m³ was achieved [88]. PX recovery technique showed a saving of approximately \$12 million in yearly energy costs at the Carlsbad SWRO desalination plant in San Diego, California, according to an independent evaluation [89].

In comparison to isobaric ERD, the efficiency of centrifugal devices is known to be reliant on the applied pressure, which can lead to limitations. In addition, isobaric devices encounter major difficulties due to mixing, leakage, and over flush. The water that is directly drained to

Table 2-5: Summary of medium and large desalination's ERD [74], [76], [81], [82], [83]

Type ERD	Scale desalination	Advantage	Disadvantage	Type	Equipment	Efficiency (%)	SEC (kWh/m ³)
Francis Turbine	Medium, Large	Simple and easy to operate	Low peak efficiency Inability to operate optimally when conditions vary Difficult to maintain Inefficient for low flow ranges There is no power generation until 40% of the design condition is reached	Centrifugal	Reverse running pump	75	6 - 7
Pelton Wheel	Medium, Large	Flexibility: takes advantage of the high-pressure energy Very easy to operate More compact Less costly	Loss of efficiency	Centrifugal	Turbine bucket impeller	65 - 78	3.5–5.9
Turbo-charger	Small, Medium	Suitable for small scale Low equipment cost Small footprint Simple to operate and maintain	Pump efficiency reversely proportional to the delivered pressure Low efficiency for large-plant-size Higher sensitivity of energy-recovery efficiency to actual operating flow and pressure fluctuations	Centrifugal	Turbine, centrifugal pump impeller	50 - 71	
Pressure Exchanger	Small, Medium, Large	Compact design No limit in the flow Multiple parallel modes can be used, Less energy consumption High energy recovery efficiency	Mixing Leakage Over flush High – low pressure differential Noise High CAPEX	Isobaric	Ceramic rotor, rotor chamber	91 - 98	3 – 5.3*
DWEER	Small, Medium, Large	High efficiency Large capacity Simple processing	Complexity of design, operation, maintenance	Isobaric	two cylinders, a LinX valve, a check seat	up to 98	3.5 – 4.6

* note: A SEC of plant with PX is reported to be less than 3

remove any remaining brine from the vessel before filling it with feed is known as over flush. However, this over flush results in increased power consumption by the HPP, leading to decreased efficiency due to the need to supply more feed. In addition, a substantial amount of pre-treated feed water is wasted due to this, which results in additional costs for pre-treatment [77], [90], [91], [92].

The term “mixing” is used to describe the process through which brine contaminates saltwater before it flows through the membranes. A high mixing rate has a knock-on effect of increasing the power consumption of the high-pressure feed pumps due to the increase in salinity [90][91]. In the case of the most advanced currently available isobaric ERD technology, the mixing rate is less than 2.5% by volume, leading to a little over 1% mixing at the membrane input. For Example, at a recovery rate of 45% and a permeate flow rate of 190,000 m³/h, the additional yearly energy cost due to mixing of 1.0 percent over an isobaric ERD is roughly \$84,000. This is based on an assumed price of \$0.142/kWh[92]. Leakage rate, which refers to the direct release of high-pressure brine, is an additional significant issue to consider in isobaric ERD. This can cause an overall decrease in the quantity of high-pressure brine from which energy can be recovered. For instance, isobaric ERDs have leakage rates of about 0.4% of the high-pressure brine flow into the device. In this scenario, the plant incurs an additional yearly operating cost of around \$283,900 for every 1% of leakage from an isobaric ERD [92]. When considering the total cost of ownership over a period of 25 years or more, it becomes evident that even a marginal change in system loss rates across different ERD designs can have a significant impact.

Small desalination plants typically use 9-12 kWh/m³ of electricity [93]. In comparison to the volume of water that is generated, this energy expenditure is considered to be high. For smaller capacity desalination plants (those producing less than 100 m³/day), the number of commercially available ERD units is restricted. This is due to the prevailing approach in small plants, which involves utilising a brine valve to regulate pressure levels. However, due to production inconsistencies of the membranes in small RO plants, the actual production of fresh water can significantly vary, sometimes up to ±10%. [93], [94]. Consequently, standard energy recovery systems pose difficulties in terms of regulation whenever applied to smaller sites (ERDs). By utilising positive displacement pumps and ERDs, small plants can be optimised to attain an ideal operational state with regards to energy consumption. Table 2-6 summarises the available ERD options that currently serve small desalination plants.

Table 2-6: Summary of the available ERD options for small desalination plants [92], [93], [94], [95], [96], [97], [98], [99]

Device	Design	Flow	Recovery rate (%)	Energy (kwh/m ³)	Efficiency	Device characteristics
Axial piston pump (APP) and axial piston motor (APM)	APP and APM connected with double-shafted electric motor	0.4 – 3.5 m ³ /h	32	3 - 5	94%	Long life cycle High efficiency Minimum maintenance required High CAPEX
Pressure amplifier	Energy-recovery pressure-amplification device positive displacement principle (2 piston)	Flow rate up to 10 (m ³ /d)	-	3.7	93 -97	High efficiency No requirement for booster pump
RO-Boost™ from Danfoss	Pressure intensifier (four pistons)	Permeate 0.72–3 m ³ /d	13 %	-	-	Minimum pulsations Small and compact Smooth operation
ISOBARIX	Ceramic rotor inside pressure vessel, operating principle similar to PX	Up to 137 m ³ /h	-	-	-	Higher efficiency 50% less mixing Smaller footprint
iSave	Pressure exchanger, booster pump, motor	Up to 41 m ³ /h	-	2.10	95%	High efficiency Smaller footprint Little maintenance Adequate pre-treatment required Quite noisy
SALINO Pressure	Horizontal, product-lubricated axial piston pump with integrated energy recovery.	7.1 – 20.2 m ³ /h	24 – 45%	-	-	High efficiency Lower CAPEX and OPEX Minimum maintenance required Reduce energy up to 75%

2.3.4 Fouling

RO is a popular technology for water desalination, but membrane fouling is an unavoidable challenge in the membrane industry; it results from the deposition of inorganic, organic, biological or chemical oxidants on the membrane's surface due to residual chlorine oxidation under various conditions [46]. Table 2-7 delineates three categories of membrane fouling, accompanied by comprehensive descriptions of their respective causes and impacts on

membrane processes. The consequences of fouling are significant, as demonstrated in Table 2-7, which includes reduced permeate flux, lower water quality, decreased energy efficiency, and the need for frequent membrane replacements. The RO's operational costs could significantly rise as a result of the previously mentioned factors [100], [101].

Table 2-7: Effects of fouling category on the membrane process, data from [102], [103], [104]

Type of fouling	Description	Causes	Impact
Biofouling	The accumulation of aquatic organisms and their metabolic products (EPS) on the membrane surface	Bacteria, fungi, algae, and protozoa	Increased resistance to water Increased pressure drop Flux decline Possible at all stage element Forms biofilm
Inorganic fouling or scaling	The accumulation of inorganic precipitates on the pore structure of membrane due to exceeding their saturation concentration	Ca, Mg, Ba, Sr, Si, F, SO ₄ , CO ₃ , HCO ₃	Flux decline Loss of solute rejection Increase of salt passage Frequent in last stage tail element
Organic fouling	The formation of natural organic matter on the surface of membrane	Natural organic matter (NOM)	Flux decline Decrease of salt passage Increase feed pressure Possible for all elements

Figure 2–10 depicts the fundamental stages of mineral scale formation in RO membrane systems [105] which can result in fouling over time. The blue stars signify soluble salts or ions that generally exist in a dissolved state in the bulk feed water at the far left side of the

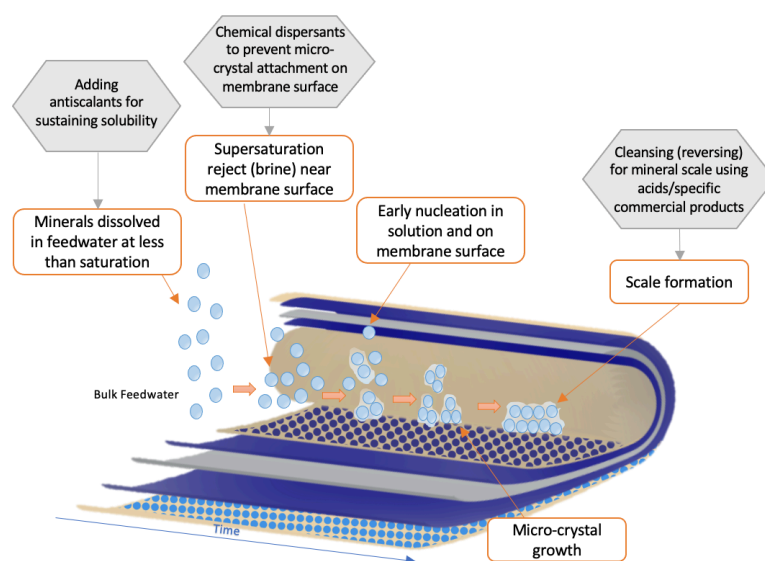


Figure 2–10: Schematic diagram for scaling formation steps on membrane surface, adapted from [105]

illustration. However, as these solutes are rejected by the membrane, they tend to accumulate in the viscous sublayer in the proximity of the membrane surface where they may surpass their solubility limits. This progresses from left to right in membrane elements. Termed supersaturation, this means a condition wherein the concentration of solute in a solution surpasses its equilibrium concentration at a particular temperature and pressure, resulting in a state where the solution contains more solute than it can dissolve. The nucleation and microcrystal formation occurs both in solution, primarily in the viscous sublayer, as well as on the membrane surface. Over time, microcrystals can increase in size and quantity, ultimately resulting in cohesive mineral scaling that can obstruct water transport and deteriorate the active semipermeable layer. RO membrane fouling induced by crystal scaling can be reduced by regulating the nucleation induction time. The nucleation induction time is the time interval between the point at which a solution becomes supersaturated and the initiation of the formation of crystal nuclei. During this period, the solution remains in a metastable state, and crystal formation is delayed due to the lack of sufficient critical nuclei [105], [106], [107].

In continuous RO, inorganic fouling tends to increase near the tail elements of membranes. Cross-flow velocity decreases as water is transferred from the feed to the permeate due to the build-up of concentration polarisation at the membrane surface [108]. Concentration polarisation (CP) occurs when rejected solutes aggregate in a thin boundary layer near the membrane surface, increasing solute concentration and decreasing water flux. As water travels across the membrane, the boundary layer and solute concentration increase, decreasing crossflow velocity. Laminar flow explains this behaviour. As water is flowing across the membrane, frictional forces generated between water and the membrane surface create a boundary layer. This boundary layer where solutes rejected by the membrane have accumulated has a concentration gradient between it and the bulk water. This concentration gradient causes solutes to diffuse from the boundary layer to the bulk water, decreasing the boundary layer solute concentration. The osmotic pressure disparity across the membrane increases as the boundary layer solute concentration increases, decreasing water flux and crossflow velocity [109]. This provides an explanation for the negative consequences that concentration polarisation has on RO membranes. This process is complex, and a number of parameters, including the rate of solute rejection by the membrane, the flow velocity, and the thickness of the boundary layer, all play a part in the way it operates.

2.3.5 New configurations of RO

As previously mentioned, RO is a resource-intensive process, and although economies of scale can somewhat mitigate operating costs for large seawater desalination plants, smaller-scale systems with lower inlet flow rates are becoming more common in the treatment of low salinity water. However, these systems face technical process challenges and require operational cost optimisation. Batch reverse osmosis (BRO) and semi-batch reverse osmosis (SBRO) have emerged with potential for improved energy efficiency to address the aforementioned challenges. These methods depend on time-varying pressure to limit the degree of irreversibility of that of the high-pressure pump.

Semi-batch reverse osmosis (SBRO) is also known as closed-circuit reverse osmosis (CCRO). This process operates by continuously adding feed water over a period of time. A portion of the feedwater is allowed to pass through the membrane, producing permeate, while the concentrate is recirculated and then mixed with new feedwater. The mixed water is then subjected to the membrane, as depicted in Figure 2–11. Consequently, the concentration of brine increases, resulting in a corresponding rise in the pressure required to overcome the osmotic pressure over time [110]. The loop cycle is repeated continually until the desired recovery rate is reached. At the conclusion of the process, the brine is rejected, and the system is flushed before replacing the feed water to initiate a new CCRO cycle.

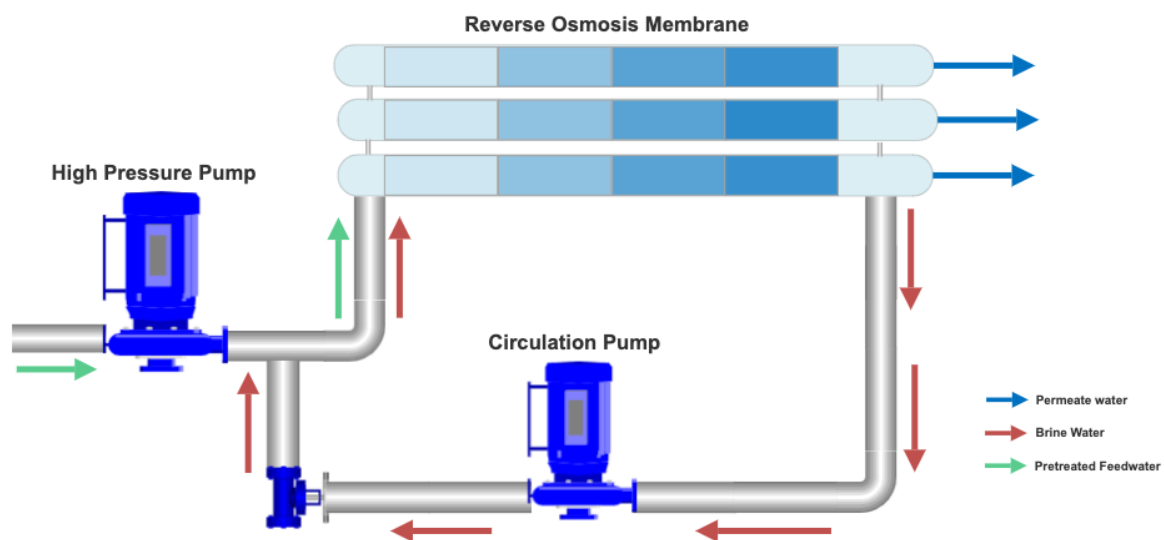


Figure 2–11: Schematic diagram of semi-batch reverse osmosis

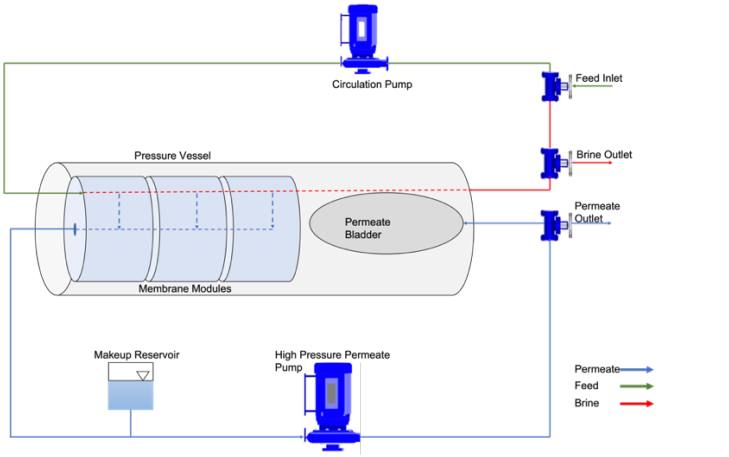
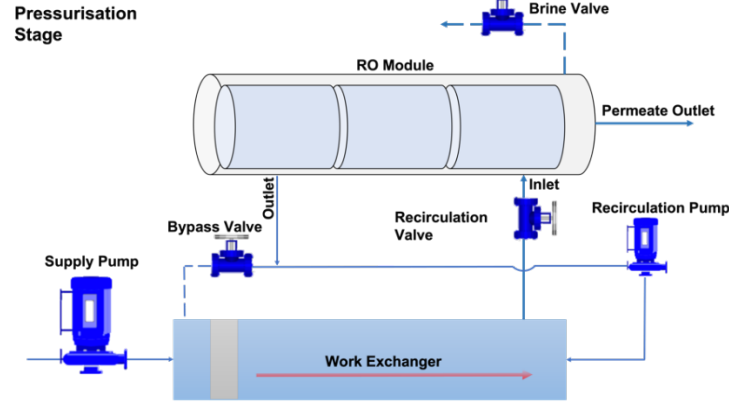
BRO operates on hydrostatic principles where brine is recycled in the process. Upon achieving the required recovery, the system will undergo a quick flush to remove the residual brine

allowing a new feed water batch into the loop cycle and this is a repetitive process [111], [112]. Various configurations for BRO or pressure-driven membrane processes have been developed for a variety of industries, including fine chemicals, food, and mechanical [113]. The standard design is to continuously recycle the brine to an unpressurised feed tank until the required recovery is achieved. However, BRO requires that the recirculation loop system remain completely pressurised, with the pressure in the loop growing as the osmotic pressure of its contents increases. Due to the incompressibility of water and the diminishing volume of retained solution throughout the course of a cycle, it is difficult to meet this requirement. Incorporating a pressurised headspace may overcome this problem, but this would entail significant complexity, cost and safety implications. BRO operates either in two or three stages depending on the design of the process. It is possible to implement the Batch RO in two or three steps, depending on the model used. Currently, four different configurations are being developed and tested, as summarised in Table 2-8, along with their process stages. Table 2-9 compares conventional RO, semi-batch, and batch RO in terms of their advantages, disadvantages, recovery rate, TDS capacity, treated water quality, and SEC.

2.3.5.1 Fouling

Batch and semi-batch methods offer a significant benefit over continuous flow RO, in that they operate transiently, limiting the period of supersaturated conditions. They discharge all of the brine and replenish the system with feed water on a periodic basis. Provided no crystals have formed and the feed is not completely saturated, advancement toward nucleation should be reversed after each cycle when brine rejection from the system occurs. The graphical representation (Figure 2–12) illustrates the influence of alterations in the salinity cycling regime for BRO compared to RO, wherein the duration of exposure of the final membrane element to a highly-supersaturated solution is restricted.

Table 2-8: Summary of all BRO Configurations [112], [114]

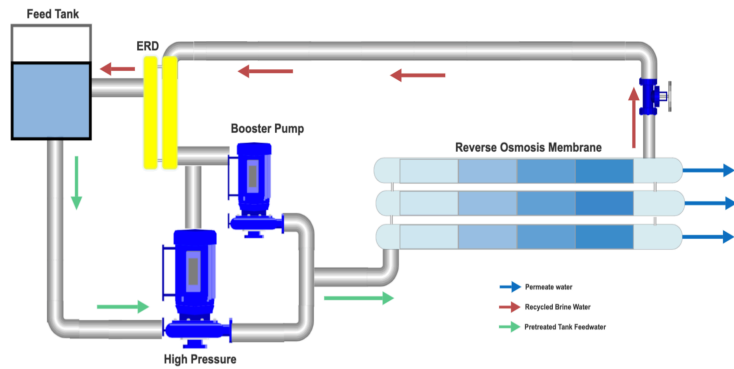
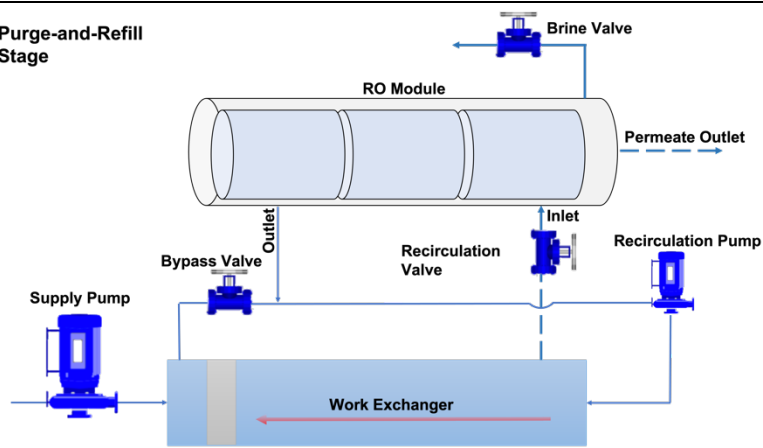
Diagram	Stages	Description
	3	<p>A variable-volume tank is included in the pressure vessel in this model. The permeate is passed into a flexible permeate bladder contained within the pressure pipe as it is produced. The external circulation pump forces flow through the membrane feed channels; the permeate is passed through the membranes while this occurs. The flush and recharge stages restore the system's salinity and empty the bladder, allowing for a restart of the batch cycle.</p>
<p>Pressurisation Stage</p> 	2	<p>The free-piston is located at the work exchanger vessel's left end at the start of the pressurisation phase. Then, high pressure is produced by the supply pump which is delivered via the free piston to the feed water within the work exchanger. Permeate leaves the system once the applied pressure exceeds feed water's osmotic pressure, while the recirculation pump returns the brine to the work exchanger. As the batch RO loop concentration steadily increases, the supply pump's pressure must be adjusted to compensate for the osmotic pressure increase and maintain a consistent permeate flow rate. When the piston reaches the right end of the work exchanger, the pressurisation process is complete.</p> <p>Then, the purge-and-refill phase removes brine from the system and refills the work exchanger's right compartment. The recirculation pump then moves the solution from the left to the right end of the work exchanger in order to shift the piston from right to left. The purging phase is carried out until the volume of brine collected at the brine outlet is equal to that of the volume of brine available inside the RO module. Now the system is ready for the next cycle.</p>

Diagram

Stages

Description

Purge-and-Refill Stage



2

This model uses an atmospheric feed tank and energy recovery devices.

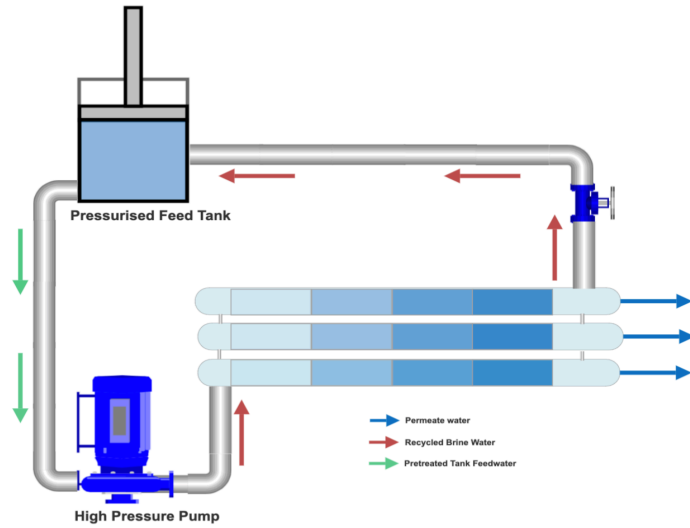
Diagram

Stages

Description

3

This model is called an ideal Batch RO which is considered relatively impractical due to its reliance on a pressurised feed tank, which is only optimal in terms of energetics. The reason for this is the complete retention of the brine's energy.



3 stages: Pressurised stage, Flush stage, Recharge stage, 2 stages: Pressurised stage, Purge-and-Refill stage

Table 2-9: Comparison between continuous RO, semi-batch and batch RO

Technology	Advantages	Disadvantages	Recovery range (%)	TDS (mg/L)	Treated water quality	Energy consumption (kWh/m ³)
Continuous RO	<p>Low energy consumption</p> <p>Membrane can achieve high salt-rejections</p> <p>Well commercialised</p> <p>Quick start up</p> <p>Good water quality</p> <p>Increased permeability while maintaining salt rejection</p> <p>High production</p> <p>Could be coupled with multiple new renewable energy.</p> <p>Reduced footprint (up to 40%)</p>	<p>Expensive membrane elements</p> <p>Membrane performance decrease over time</p> <p>Intensive pretreatment</p> <p>Ongoing research in: fouling resistance</p> <p>chlorine tolerance</p> <p>energy reduction</p>	40–50%	<p>Up to 40,000⁽¹⁾</p> <p>Up to 20,000⁽²⁾</p>	Depends on the type of membrane element	<p>1.73 –2.49⁽¹⁾</p> <p>0.5 – 2.5⁽²⁾</p>
Semi-batch RO	<p>Reduced energy consumption (up to 34%)</p> <p>Energy recovery devices are not required</p> <p>High recovery</p> <p>High operational flux</p> <p>Less susceptibility to fouling</p> <p>Few membrane elements</p>	<p>Only pilot and demonstration scale testing</p> <p>Unknown impact of brine circulation on membrane life</p> <p>Loss energy due to the mixing</p>	<p>Up to 50%⁽¹⁾</p> <p>Up to 97%⁽²⁾</p>	Up to 45,000 mg/L (TDS)	Depends on the type membrane element	<p>1.5 – 1.8⁽¹⁾</p> <p>1.02⁽²⁾</p>
Batch RO	<p>Reduced energy consumption (up to 53%*)</p> <p>Energy recovery devices are not required</p> <p>Operate at high recoveries</p> <p>Few membrane elements</p>	<p>Only experiment, simulation</p> <p>Unpractical design</p> <p>Pressurised system</p> <p>Ongoing research in: Large scale, Applicable Design for batch RO, Fouling for large scale, Cost analysis</p>	<p>Variable Up to 90% *⁽²⁾</p> <p>Up to 80%**⁽²⁾</p>	Up to 5 (experiment brackish water)	<p>Water quality varies in each cycle</p> <p>Further study required for water quality</p>	<p>1.97⁽¹⁾</p> <p>0.14 – 0.84⁽²⁾</p> <p>Under development</p>

⁽¹⁾ Seawater Desalination ⁽²⁾ Brackish water , * Simulation study, ** Experiment study

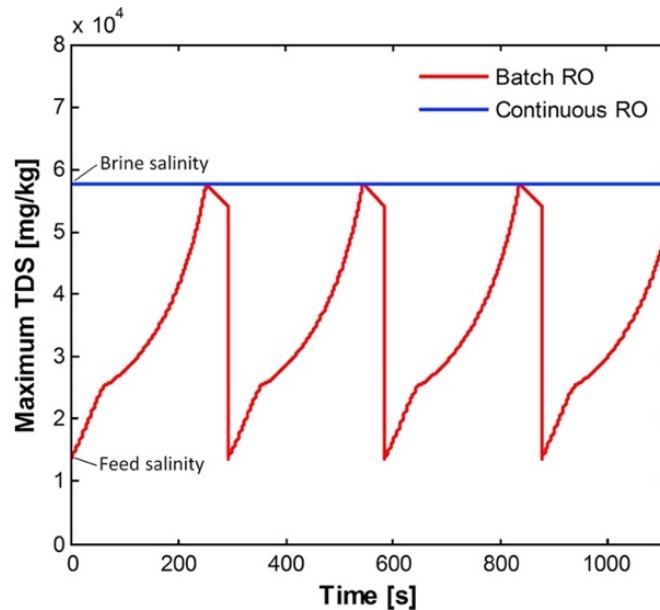


Figure 2-12: the behaviour of BRO and RO in terms of TDS over time [100]

Several studies [59]–[61] illustrated that the time variation processes could perform at a high recovery rate producing a significant level of highly saturated salts that are sparingly soluble without any requirement for scaling inhibitors. However, in contrast a study conducted by Sonera *et al.* [118] demonstrated the viability of closed-circuit desalination in volume reduction applications to achieve a zero liquid discharge, as a CCD pilot used to desalinate feedwater with approximately half-saturation (TDS: 1,304 ppm; SiO₂: 57 ppm) and recovery reaching 93.8% under high silica supersaturation (930 ppm). The results show that no forms of fouling and scaling were observed in the process with the use of antiscalant (FLOCON-260) [118]. In other work by Gal *et al.* [119], a similar outcome was noted where there was no scaling and fouling. However, in this study, feedwater with 32 ppm of SiO₂ was utilised as a first pass for boiler-feed supplies at a recovery rate of 96% with the presence of antiscalant (Hydrex-4192 and 4102). Although it is suggested that the tendency of mineral scaling in SBRO is less than steady-state RO with partial recycle (SBRO-PR), no published experimental data is available to confirm this. It is argued that monitoring the tendency of mineral scaling on the membrane on the bases of induction time of crystallisation on solution is questionable. Studies have shown that crystallisation on the membrane surfaces when seeds are present is much shorter than that of induction time for crystallization in solution [120], [121]. Lee *et al.* [122] demonstrated how to evaluate mineral scaling propensity in semi-batch RO (SBRO) and single-pass steady-state RO with partial recycling, utilising gypsum as the choice for model scalant. When mineral scaling was compared at equal recovery and solution saturation, it was shown that SBRO had a more significant scaling propensity than SSRO-PR. Specifically, SBRO had a faster rate of

emergence of surface crystals and a shorter observed crystallisation induction time when compared to SSRO-PR under the same circumstances. For batch reverse osmosis in terms of fouling, Warsinger *et al.* [100] predicted the nucleation induction time at what value of recovery rate the system can reach before entering the inorganic scaling phase. This was achieved by comparing the time between cleaning processes in continuous RO to that of batch RO cycle time using two popular scalants. Figure 2–13 presents a comparative analysis between BRO and continuous reverse osmosis (CRO) in terms of the recovery rate at which induction time is attained, under conditions where the system scalant is restricted to either calcite or gypsum. The graph clearly indicates that both processes exhibit a greater tendency to foul when gypsum is utilised, as opposed to calcite. Consequently, considering the extended induction periods associated with calcite, it is anticipated that batch systems would confer a lesser benefit over conventional RO as opposed to gypsum.

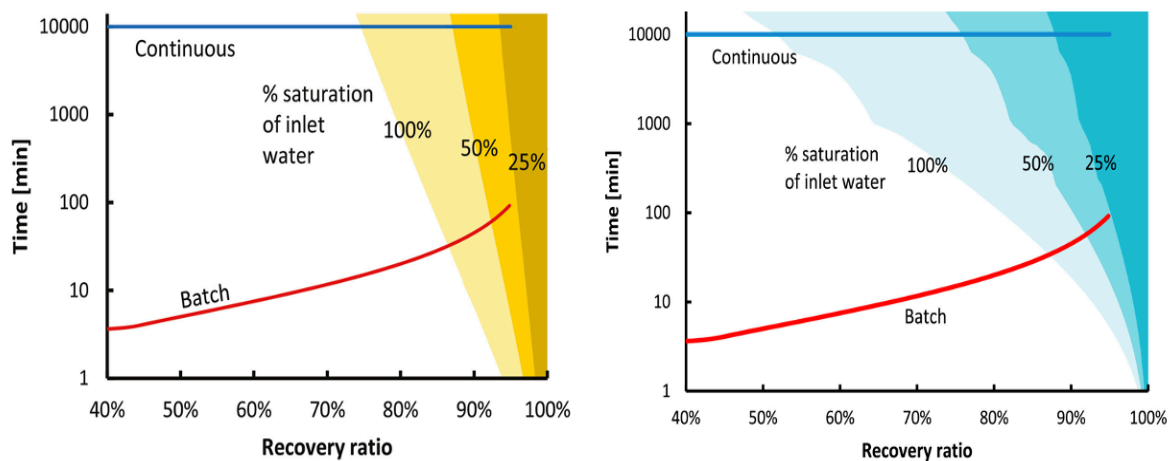


Figure 2–13: A contour map for (a) - calcite (CaCO_3) nucleation, (b) gypsum (CaSO_4) nucleation overlaid with curves for residences times of continuous RO and batch RO [100]

The number of membrane elements has an impact on scaling that occurs on the surface of membranes. The number of elements (N_E) can be obtained by dividing the design permeate flow rate (Q_p) by the product of the design flux and the membrane surface area (SE) for the desired element. Most systems that run on high-quality feed waters have a high flux value when correctly designed and the opposite is the case for poor quality feed water systems. Conventional RO for seawater uses between 6 and 8 elements per vessel [123]. However, batch and semi-batch employ 3 to 4 elements per vessel. Researchers have asserted that using fewer membrane elements reduced the likelihood of fouling in semi-batch RO [124], [125], [126]. The drawback of using a large number of N_E is that the later elements in the vessels are more

susceptible to scaling as discussed earlier. This, however, would impact cost effectiveness, since a lower number of elements per pressure vessel would necessitate a greater number of pressure vessels in the system, leading to an increase in desalination’s capital costs. Thus, determining the primary objective of the desalination plant is critical to optimising either operational expenses or capital costs.

2.3.5.2 Energy

Energy consumption is a key challenge in desalination industries. Several factors can influence the SEC in a RO system as discussed in Table 2-10. Overall, minimising the SEC in an RO system requires a careful balance between these factors, with each influencing the other. An optimised RO system should be designed to maximise recovery rate, and minimise operating pressure and membrane fouling, while also considering feed water quality and temperature. The RO section highlighted the recent ranges of SEC and the theoretically predicted value. This section focuses on recent studies performed on BRO and CCRO to estimate SEC.

Table 2-10: Factor impacting SEC of RO process [42]

Factor	Description
Feed water quality	Determines the amount of pre-treatment required before the water enters the RO system Higher levels of impurities require more pre-treatment, which can increase the SEC
Recovery rate	Higher recovery rates typically result in lower SEC as less energy is required to produce a given volume of permeate
Operating pressure	The operating pressure of the RO system is directly proportional to the SEC Higher pressures require more energy to maintain, resulting in a higher SEC
Membrane performance	If the membrane is fouled or damaged, it may require more energy to maintain the desired flow rate and recovery rate
Temperature	Higher temperatures generally result in lower SEC as the water viscosity decreases, making it easier to pump through the system
System design	including the configuration and number of stages A well-designed system can minimise energy losses and optimise energy recovery

From an energy efficiency perspective, for batch RO systems, Warsinger *et al.* [112], [117] proposed and utilised a numerical model to analyse and compare batch RO against semi-batch and single stage RO to differentiate their energy efficiencies across a range of salinities and recovery ratios. The results illustrate that RO with pressure exchanger (PX), CCRO and BRO performed quite similarly at low recoveries ($\leq 55\%$). However, BRO and CCRO were

considered more energy efficient options compared to conventional RO at high recoveries resulting in an energy reduction by 53% and 34%, respectively. The Batch RO and Batch with PX were reported to be particularly suitable options for high recoveries, as shown in Figure 2–14. The authors reported that when recoveries are low, a greater volume of fluid is irreversibly depressurised per unit permeate than when recovery ratios are high. Time variant systems conserved the energy via pumping the permeate to a raised pressure, and therefore using ERD might not be beneficial for the process. The study compared the energy consumption of various batch and continuous RO systems, while disregarding other important process parameters such as salt retention.

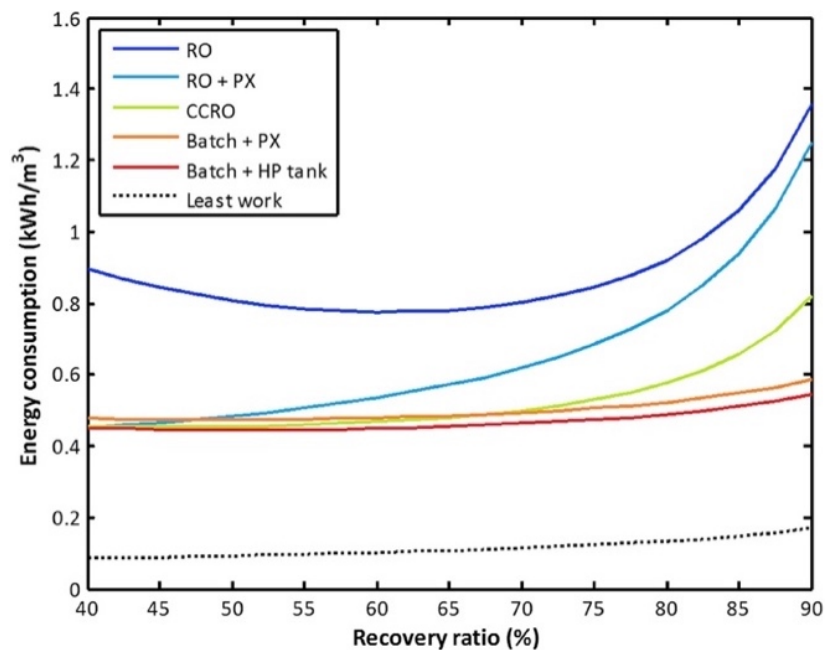


Figure 2–14: Modelled SEC for conventional and time-variant RO configurations against recovery ratios with 3 g/kg NaCl feed and pump efficiency 80% [112]

2.3.5.3 Water Permeability

The coefficient of water permeability is often assumed to remain constant in the batch and semi-batch models [53], [112]. It is important to note, that this assumption may oversimplify the relationship between permeate and salt flux over the membrane and the water and salt permeability coefficients. Research by Barello *et al.* [127] suggests that the coefficient of water permeability is not solely determined by pressure or its decay over time due to fouling. In fact, Barello’s results indicate that the coefficient of water permeability also depends on feed salinity, as demonstrated in Eq 2.5 in BRO. This equation follows the formatting of the original publication in the way it is written.

$$k_w = \frac{M_p}{(\Delta P - \Delta \pi) A C_1} \quad \text{Eq 2.5}$$

Where k_w (m/min/bar) is water permeability, A the membrane area (m²), C_1 conversion factor (=1000 L/m³) and M_p permeate flow rate (L/min). According to Figure 2–15, as the feed salinity of batch keeps increasing, a lower water permeability coefficient would be obtained, indicating that the assumption of constant water permeability may not hold.

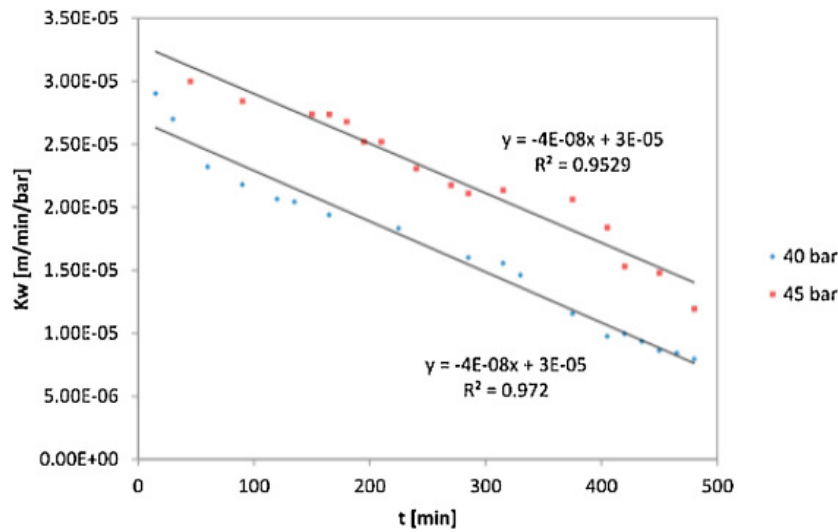


Figure 2–15: Water permeability trend over time at salinity = 25 g/L for batch RO [127]

2.3.5.4 Concentration Polarisation

Concentration polarisation is another intrinsic limitation of RO. When the applied pressure exceeds the osmotic pressure difference in membrane separation, water enters the membrane from the feed to the permeate side. CP degrades the efficacy of membrane separation processes significantly, as the osmotic pressure difference is dependent on the difference in concentration across the membrane, which is the primary determinant of the operating pressure. A model was developed to assess the changes that the concentration polarisation phenomenon can cause in spiral-wound membrane modules for batch RO using both the Kimura–Sourirajan mass-transfer and the Film model [128]. Sherwood correlations were used to reveal the relationship between flow rate and the mass transfer coefficient as part of this study’s goal to systematically investigate mass transfer coefficients and concentration polarisation for various RO elements. Equation 6 is used to calculate the concentration polarisation factor CPF:

$$CPF = \frac{C_m - C_p}{C_b - C_p} = \exp\left(\frac{J_v}{k}\right) \quad \text{Eq 2.6}$$

Where CPF is the concentration polarisation factor, C_m the solute concentrations at membrane surface ($\text{kg}\cdot\text{m}^{-3}$), C_b the concentration of the bulk solution ($\text{kg}\cdot\text{m}^{-3}$), J_v the permeate flux ($\text{m}\cdot\text{s}^{-1}$), k the mass transfer coefficient ($\text{m}\cdot\text{s}^{-1}$). Eq 2.6 can be rearranged as (Eq 2.7) by taking the natural logarithm of both sides of the equation and substituting the concentration terms with both the observed membrane rejection fraction (R_o) and the real membrane rejection fraction (R):

$$\ln\left(\frac{1 - R_o}{R_o}\right) = \frac{J_v}{k} + \ln\left(\frac{1 - R}{R}\right) \quad \text{Eq 2.7}$$

Where R_o is equal to $\frac{C_b - C_p}{C_b}$ and R is $\frac{C_m - C_p}{C_m}$. The film model is a simplified model that assumes a thin, stagnant layer of solute on the membrane surface, known as the concentration polarisation layer. The solute concentration in this layer is assumed to be constant and equal to the bulk concentration of the feed solution. This model assumes that the flux of water through the membrane is directly proportional to the osmotic pressure difference across the membrane and the membrane hydraulic permeability. Kimura-Sourirajan is a mechanistic membrane model in which solute transport through the membrane is purely through diffusion [129]. According to this model, solvent and solute fluxes do not interact and are transported through the membrane separately. Solute concentrations in the concentration polarisation layer vary with distance from the membrane surface, and the concentration gradient of solutes in the concentration polarisation layer influences water flux through the membrane. The KS model helps to eliminate unknown parameters from equation 6 and determines the J_v and k using Eq 2.8, where P_s is the salt permeability coefficient ($\text{m}\cdot\text{s}^{-1}$).

$$\frac{J_v}{k} = \ln\left(\frac{1 - R_o}{R_o}\right) - \ln\left(\frac{P_s}{J_v}\right) \quad \text{Eq 2.8}$$

Qiu [128] derived Sherwood correlations (Sh) to examine the relationship between flow rate and mass transfer coefficient in Equation 9 for unsteady batch operation due to the fact that either laminar or turbulent flow can explain RO membrane flow behaviour. According to the study, the spiral wound membrane RO element has a geometric shape that is similar to that of an unwound flat rectangular membrane channel. The turbulent flow is unlikely to reach full

development due to the narrow feed channel and low mean crossflow velocity. Therefore, laminar flow can be assumed; however, the emergence of recirculation regions indicates that the flow cannot be pure laminar and is undergoing transition. Eq 2.9 showed the derived Sherwood correlations from the obtained experimental data.

$$Sh = \frac{k \cdot d_h}{D} = 2.09 \cdot Re^{0.26} \cdot Sc^{0.38} \cdot \left(\frac{\phi_h}{L}\right)^{0.33} \quad \text{Eq 2.9}$$

Where ϕ_h is hydraulic diameter, D is diffusion coefficient, Re is Reynolds number, Sc is Schmidt number and L is channel length. The results in BRO showed that the increase in concentration polarisation factor over time was primarily driven by a concurrent increase in permeate flow rate and decrease in feed flow rate. Specifically, at any given time point, CPF was observed to be greater for small feed flow rates, which supports the concept that higher flow rates are conducive to minimising CPF, as anticipated by the Sherwood correlation. Similarly, for continuous RO, higher crossflow velocities were found to correspond with reduced CPF values. This can be attributed to the increased back-diffusive transport of salt away from the membrane surface, which, as was covered in the earlier, works to counteract the concentration gradient. The observed decrease in CPF underscores the role of velocity in promoting more efficient salt removal, which has important implications for enhancing the performance and efficacy of continuous RO systems.

Weber *et al.* [130] applied analytical and numerical modelling to investigate the impact of realistic process inefficiencies including frictional pressure loss and concentration polarisation on energy efficiency for continuous, staged continuous, batch and semi-batch ROs. It was discovered that semi-BRO and two-stage RO resulted in equivalent and significant energy reductions 13% (0.29 kWh/m³) and 15% (0.34 kWh/m³), respectively, when compared to single-stage RO at 50% recovery for SWRO.

2.3.5.5 Impact of Dispersion

In BRO, the flushing and filling phases are prone to causing dispersion, which leads to unwelcome mixing of concentrated brine with less concentrated feedwater. This, in turn, results in increased salt concentration and energy consumption during the next pressurisation phase of the cycle. In response to this issue, Qiu and Davies [131] investigated the impact of longitudinal dispersion in spiral wound RO modules in BRO. The experimental work carried out by Wei *et al.* [132] further supports the findings of Qiu and Davies. Wei *et al.* [132] designed and conducted experiments to explore the effects of salt retention on batch RO (bladder batch RO)

energy consumption. The results of the study indicated that batch RO systems consume more energy than that estimated by prior theoretical models, but less than conventional RO systems (1.97 vs. 2.21 kWh/m³, representing an 11% reduction in SEC). Moreover, the study demonstrated that batch RO systems are likely to operate at higher feed salinities than the plant's intake salinity due to insufficient brine flushing between cycles. For example, the feed salinity may be 38 g/kg instead of the intended 35 g/kg at 50% recovery. The findings highlight the importance of adequate brine flushing to prevent salt build-up and minimise energy consumption in batch RO systems. A mathematical model by Li [133] was developed to examine the effect of finite flux and flushing efficacy on normalized specific energy consumptions (NSECs) for both BRO and SBRO and a two-stage RO. The outcomes showed that both semi-batch and batch ROs are not as efficient as a two-stage RO based on a 95% flushing efficacy and typical flux (12.8 L/m²h) that is used in industrial desalination. The findings indicate that an ideal batch RO, which is equivalent to an infinite-stage RO, marginally outperforms a two-stage RO in terms of energy efficiency. However, as the number of stages increased, the benefit of additional stages decreased rapidly until salt retention effects dominate, and batch RO performance became inferior to that of two-stage RO. For typical fluxes used in industry, SBRO with perfect flushing was found to be not as efficient as two-stage RO. Thus, when reduced flushing efficiency is taken into account, its performance is even further inferior. The author reported that this limitation could be overcome if both technologies operated at low flux or an elevated dimensionless membrane area (γ) due to mitigating concentration polarisation.

2.3.5.6 System Design

Due to the impracticality of the ideal batch RO system in terms of implementation in reality, researchers have been investigating the different components of the system in an effort to improve system design. The sizes of tanks and pipelines have an impact on the performance and SEC consumption of BRO. These criteria were explored in a study conducted by Swaminathan *et al.* [53]. The primary purpose of this work was to explore the effect of practical design factors of BRO on SEC. The aim was to assess, compare and reduce the energy consumption of BRO relative to RO (2.06 kWh/m³). The authors suggested that salinity in the membrane elements should not exceed the average brine salinity considerably; tanks and pipelines must be considerably smaller than the membrane components because the small size of the tanks and pipelines ensures that the water in the system is constantly moving, reducing the risk of fouling and scaling. Additionally, this minimises the energy required to pump the

concentrate out of the system which helps to improve the energy efficiency of the batch RO process, reducing operational costs and improving the overall sustainability of the desalination process.

In order to avoid overflowing the tank, the intake pipe volume should be less than the outflow pipe's volume, and the tank should be emptied after each cycle. Theoretically, batch RO has greater SEC efficiency than continuous RO; however, it has the disadvantage of not being productive throughout all three phases of its cyclic operation, as discussed in Table 2-8. Only the pressurisation phase generates output; the purge and refill stages do not. As a result, when batch and continuous RO processes are compared on an equal output per membrane area basis, the batch process's permeate water flow will be greater. This results in a penalty in SEC, lessening the benefit of continuous RO [28]. Therefore, it is critical to minimise downtime related to the inadequate purge and refill stages. The study concluded that the rest period should be shorter than the batch RO operating cycle. However, a shorter cycle may result in the system being under-flushed, increasing the total plant recovery ratio while also raising the system feed salinity. Swaminathan *et al.* [53] also demonstrated that batch RO systems with fewer membrane components in series would potentially consume up to 8% less energy than continuous RO systems.

To this point, there has been no reported experimental studies implementing batch RO with ERDs. However, a few studies have examined the performance of batch processes that incorporate an energy recovery device using theoretical models. For instance, Werber *et al.* [130] discovered that batch combined with ERD is less efficient than other approaches, which agrees with the findings in Swaminathan *et al.* [53] and Warsinger *et al.* [112]. These studies showed that the efficiency of ERD in batch processes needs to be greater than 0.95 and 0.995 to consume less energy than one-stage RO and two-stage RO, respectively. Based on the literature, no existing ERD can achieve such high efficiencies currently.

2.3.5.7 Recovery Ratio

The recovery ratio is an important parameter that impacts the efficiency and performance of the RO desalination process. Currently, SWRO desalination operates at a recovery rate range between 35% to 50% [134], with higher ratios resulting in higher product water output but also higher energy consumption and greater wear and tear on the plant's components, while brackish desalination can be up to 90%. Unlike traditional RO, where recovery is a function of the number of membrane elements in series, CCRO recovery is proportional to the batch time

T, regardless of the number of elements per module [135]. The recovery rate (R_{CCRO}) of semi-batch is calculated based on the following Eq 2.10:

$$R_{CCRO} = \left(\frac{v}{v + V} \right) \times 100 \quad \text{Eq 2.10}$$

Where V (m^3/h) refers to the fixed intrinsic volume of the batch reactor and v (m^3/h) is the volume of permeate produced. In batch RO, recovery (R) is calculated based on cumulative permeate volume (V_P) and the feed tank volume (V_T) as follows $R = V_P / V_T$.

Based on the analysis from the preceding studies, the optimal BRO technique is most effective when the recovery ratio exceeds 75%. Research by Nayar *et al.* [136] investigated the effect of altering the recovery ratio (50–95 percent) on the specific energy required for different types of brackish water desalination technologies, including RO, CCRO, and reverse electrodialysis (EDR). The model was developed using a feed salinity of 3 g/kg and a temperature of 20°C, and a target salinity of 0.2 g/kg. The results indicated that CCRO utilised significantly less energy for recoveries less than 92%, ranging between 0.20 and 0.83 kWh/m³. This finding is consistent with the Stover model, in which the SEC is determined to be 0.41 kWh/m³ for salinity of 1.8 g/kg and 0.67 kWh/m³ for a salinity of 2.9 g/kg, respectively [137], [138].

2.3.5.8 Water Quality

When designing and operating a RO desalination plant, it is crucial to take into account the permeate water quality and its potential uses. Permeate water quality must fulfil strict standards set by regulatory authorities to guarantee its suitability for consumption in specific applications, such as drinking water production. The quality of the permeate water in these applications must be consistently high, free from harmful contaminants, and have a desirable taste and odour. For industrial applications, the quality of permeate varies depending on the specific requirements of each process; some processes favour low levels of dissolved solids or minerals whilst other processes require water of high conductivity and pH. Continuous RO has advantages over other RO processes in that it has the ability to produce a consistent and high-quality water output. Unlike batch RO, which produces water in batches resulting in varying salt passage as feedwater salinity increases, continuous RO operates continuously, ensuring that the water quality is generally consistent over time. Furthermore, continuous RO also offers better control over the water quality. Using a variety of sensors and instruments, the system can be monitored and adjusted to provide the required water quality ensuring consistency in achieving the desired standards.

On the other hand, the quality of water in a BRO system might vary significantly across cycles owing to the quantity of salt that is not properly drained throughout the flush and recharge phases. The study undertaken by Wei *et al.* [132] showed that the quality of permeate is poorest during the start of the permeate production phase due to salt passage prior to the system being turned on and during the flush and recharge phases. As seen in the first two rows of Table 2-11, permeate quality increases with longer permeate production stages, as the salty permeate is diluted with more fresh permeate. The initial batch RO cycle produces poorer quality permeate; however, this improves with future cycles owing to the quicker time between cycles. According to the research carried out by Davies *et al.* [139], the salinity of permeate increased with reduced pressure, and flux in batch RO. It is well-established that flux is a function of pressure; consequently, a reduction in flux results in salt concentration remaining relatively constant, as it is based on the difference in concentration, which leads to an increase in salt concentration. Therefore, for certain industrial uses or to meet potable water requirements, water permeate of high quality may be required. Further research should be conducted to see whether batch RO can meet those requirements.

Table 2-11: Obtained permeate quality from batch RO cycles [132]

Cycle number	Feed salinity (g NaCl/kg)	Recovery ratio (%)	Brine salinity (g NaCl/kg)	T_{pp}/t_{cyc} (%)	Permeate salinity (g NaCl/kg)	Salt rejection (%)
1	2.0	29	2.8	72	0.31	87.0
1	2.0	48	3.8	81	0.19	93.4
1	2.0	52	4.1	86	0.14	95.5
2-5	2.0	52	4.1	81 - 86	0.08	97.5

t_{pp} : permeate production time, t_{cyc} : batch cycle time

Chapter 3

Literature review: Artificial Intelligence & Machine Learning

This chapter delves into the application of AI and ML in desalination technology, highlighting their autonomous learning and problem-solving capabilities. It offers a comprehensive overview of established and recent AI and ML applications in desalination, covering topics such as RO, membrane morphology, salinity control, flux optimisation, energy efficiency, and fouling prevention. It also explores fault detection and pipe failure for desalination plant and water distribution monitoring. Additionally, Section 3.2.6 discusses algal prediction techniques for environmental mitigation. A comparative analysis of AI and ML against conventional engineering methods is provided in Section 3.3 to assess their effectiveness. This chapter addresses current challenges and unexplored research areas in AI and ML for desalination (Section 3.4), offering insights into the field's potential and limitations in tackling water desalination issues. The chapter concludes by identifying the gaps in existing research and proposing potential solutions.

3.1 Artificial Intelligence & Machine Learning

In recent times, many organisations have come to rely upon compiled data as a key determinant in their decision making processes. This data, which is often voluminous, requires a thorough and in-depth analysis before it can be of any use in predicting future trends or informing significant strategic choices. In response to this challenge, the technological advancements of AI, and its subset, ML, have emerged as dynamic tools for efficiently handling large datasets and processing them to support decision-making.

[140]. It is also defined as the process that builds a computational system capable of improving with experience through the implementation of a learning process [141]. In the last two decades, ML has evolved as a viable solution for enhancing practical software in various

applications, such as computer vision, medical diagnostics, robotics, speech recognition, natural language processing, dosage prediction, and risk assessment [142].

ML is considered a branch of AI. It is defined as an automated analytical model that searches and analyses the descriptive features and target features in the dataset to determine their relationship [140]. It can also be defined as the process that builds a computational system capable of improving with experience through the implementation of a learning process [141]. In the last two decades, ML has evolved as a viable solution for enhancing practical software in various applications, such as computer vision, medical diagnostics, robotics, speech recognition, natural language processing, dosage prediction, and risk assessment [142]. ML algorithms have been classified into four main categories, based on the desired outcome, as defined in Table 3-1.

Table 3-1: Definitions of the main group classes of ML

Types of ML	Definitions and main characteristics
Supervised learning	All data is labelled Algorithms learn to predict the target features from the descriptive features [141]
Unsupervised learning	Objective: learn about the unlabelled data using distribution and structure of the dataset Input data is available Note: no output variable corresponding to this data is given [141]
Semi-supervised learning	Combination of supervised and unsupervised learning Algorithm learns from a combination of labelled and unlabelled data [141]
Reinforcement learning	Main features: trial and error search and delayed reward Method: Learning what needs to be done and how to map a situation to an action in order to get the highest numerical reward Learner is not given a specific action to follow but will have to discover the action by trial and observation of highest rewards [143]

A typical workflow for constructing a ML model and identifying viable algorithms is illustrated in Figure 3–1. Typically, a project employing ML or AI can be generally categorised into six distinct steps. The initial two steps include defining the problem and assessing the necessary resources that will be required to address the issue. The subsequent two steps involve dataset selection and data preparation, which are fundamentals for ensuring that any ML model is effective. Prior to training a model, the data must be carefully inspected and prepared. The fifth and sixth steps include model development, training, evaluation, and refinement, all of which are vital components to identify the optimal parameters for the best performance.

Operationalisation is the final step, which entails observing the already-deployed model in its working environment and estimating its impact while quantifying its success [144].

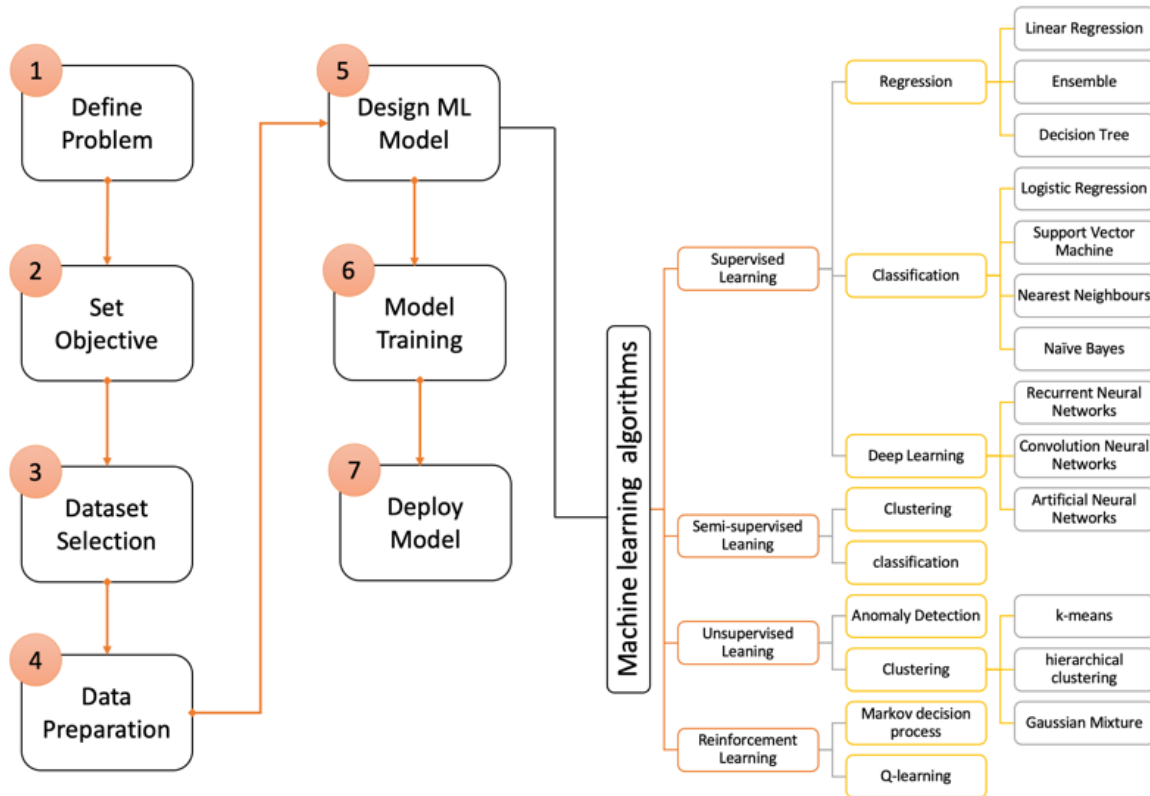


Figure 3-1: Machine learning model workflow and algorithm classification hierarchy

3.2 Application of AI & ML in Water Treatment Technologies

AI and ML have strong potential to address the challenges that face the water treatment and wastewater sector. This is due to their capability in solving complex issues with competing priorities. Several researchers have been actively applying different AI and ML tools in water treatment [145], [146], [147], wastewater treatment [148], [149], [150] and desalination industry [151], [152], [153]. Artificial neural networks (ANNs) were applied to manage the variable operation of a simple SWRO for predicting and optimising processes. ANNs, genetic algorithms (GA) and support vector machines (SVM) have emerged as widely adopted predictive tools capable of predicting the removal of pollutants, flux decline, energy consumption, cost optimisation, water production ratio, and fault detection, and facilitating the dynamic simulation of the fouling process in membranes [154].

3.2.1 Reverse Osmosis

Pilot-scale RO desalination does not accurately reflect the performance of large-scale, long-term RO desalination plants. For example, water quality variation seen during the pilot testing phase may not be representative of that in the future as a result of multiple factors. Factors that could affect the source water quality include climate change, land utilisation and agricultural activity changes, seasonal changes, and increased urbanisation. Moreover, newly introduced contaminants, including emerging pollutants and microplastics may adversely affect the quality of the source water.

Since the industrial revolution, the ocean has absorbed approximately 25 to 30 percent of the carbon dioxide emitted as a result of human activity [155]. A recent assessment of partial ocean pressure of CO₂ (pCO₂) has shown that the acidity level of the ocean has been increasing gradually over the last two to three decades [155]. Due to natural causes and anthropogenic pressures, such as eutrophication, oxygen depletion in coastal and marine waters has increased in terms of both spatial extent and duration over the past few decades, with 9% of sampled sites exhibiting deterioration [156]. The investigation revealed that the elevation of pCO₂ levels led to a concurrent augmentation in the biovolume of bacteria within a brief period of study [157]. Bacterial presence significantly influences the selection of pretreatment and RO systems, as well as the determination of appropriate cleaning protocols and chemical dosages required to mitigate bacterial growth-related concerns. Therefore, it is critical to keep track of the water quality and operational factors as well as data in the RO plant to assess overall performance. Permeate conductivity, which is impacted by pH, temperature, pressure, and other variables, is primarily utilised in RO plants to determine the quality of the generated water. To ensure consistent performance, i.e. acceptable quality and quantity of the product water in a facility of this type, it is essential to monitor the parameters mentioned earlier, and to adapt operationally when required.

Different techniques have been used to analyse the performance of full-scale RO desalination plants. Choi *et al.* [158] conducted a study to assess the long-term performance of a full-scale RO plant by utilising two ML models, namely ANN and M5P Tree Model (TM). The study considered different factors such as feed temperature, feed TDS (total dissolved solids), permeate TDS, operational duration, and cleaning frequency on feed pressure and differential pressure. The results indicated that both models were effective in predicting and capturing the relationship between the input and output variables. During the operation, feed TDS, flow rate, and pressure remained relatively constant, but feed temperature, permeate TDS, and

differential pressure showed significant fluctuations. The authors reported that this was because permeate TDS and differential pressure were highly dependent on feed temperature [46]. It is crucial to note that this is not necessarily a novel insight, and the impact of temperature on feedwater, and consequently RO performance, is already known from science and engineering principles. Elevated temperature enhances salt passage, resulting in an increase in permeate TDS. In contrast, low temperature increases the feed water's viscosity and consequently, the pressure drop in the pressure vessel.

Furthermore, in another study, ANN and Response Surface Methodology (RSM) were employed to analyse and optimise the performance of a pilot-scale Nanofiltration (NF) and RO membrane system [159]. The study determined the optimal configuration for the treatment of brackish water among three hybrid configurations (parallel NF-RO, series RO-Concentrate-NF, series NF-Concentrate-RO). Figure 3–2 depicts the experimental arrangement of the pilot-scale plant for the nanofiltration-reverse osmosis (NF-RO). The parallel NF-RO arrangement was found to be optimal, with recovery and salt rejection of approximately 57.18% and 44.89%, respectively.

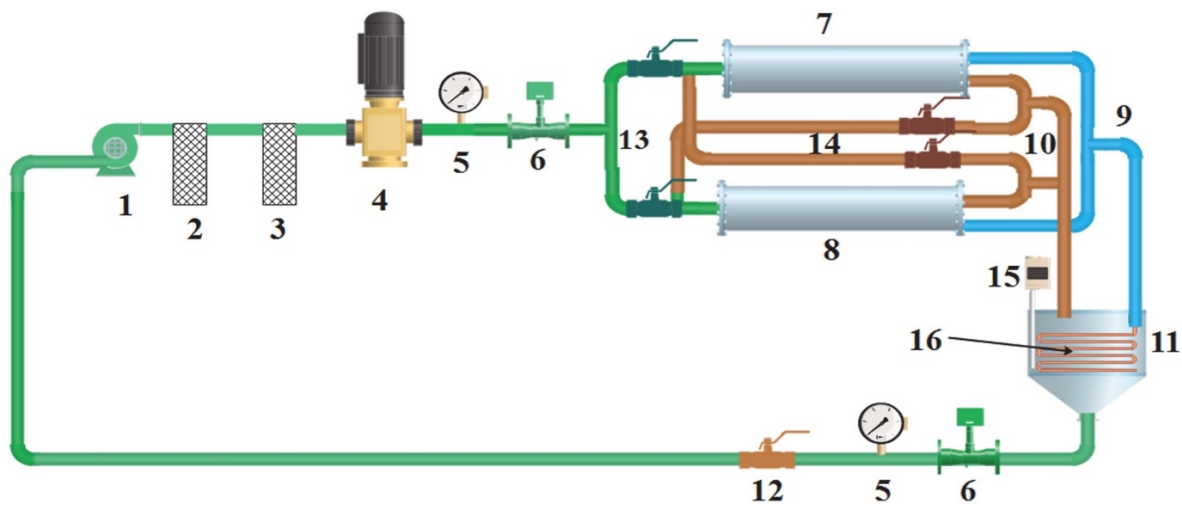


Figure 3–2: NF-RO hybrid pilot plant schematic diagram: 1.raw water pump, 2.bag filter, 3.micron filter, 4.HP pump, 5.pressure gauge, 6.flow meter, 7.RO membrane module, 8.NF membrane module, 9.permeate stream, 10.concentrate stream, 11.feed tank, 12.pressure control valve, 13.hybrid NF-RO parallel configuration, 14.hybrid NF-RO series configuration, 15.temperature indicator, 16.temperature regulator [159]

The presence of certain impurities in the feed water can have significant adverse effects on the treated water quality hindering desalination technology. Suitable pretreatment processes, such as various filtration technologies, are used to mitigate these effects. In work by Jing *et al.* [160],

the removal of sodium chloride using electro dialysis (ED) was investigated. The process was assisted with backpropagation neural networks and improved backpropagation techniques (the adaptive learning rate method and flexible backpropagation algorithm). The separation of NaCl was found to have a non-linear relationship with four influencing parameters: flow rate, feed concentration, reaction temperature, and applied voltage. The percentage separation exhibited a positive correlation with both voltage and temperature, while a negative correlation was observed with flow rate and concentration. Additionally, the improved backpropagation method demonstrated superior performance due to its generalisation ability, ability to manage high values and adapt to constantly changing learning rates and weights.

In a recent investigation, the performance of a RO desalination plant in the Gaza Strip was evaluated by predicting fluctuations in TDS and permeate water flow over the course of a week [161]. To accomplish this, the feed water’s pressure, conductivity, and pH characteristics were utilised to construct and train multilayer perceptron (MLP) and radial basis function (RBF) neural networks. The results demonstrated that both neural networks were capable of accurately ($R = 0.9904$, $R = 0.9853$, respectively) forecasting the TDS level and permeate water output. The ANN models precisely captured the values of permeate water and TDS compared to other methods, as shown in Table 3-2. Nonetheless, the model somewhat underpredicted the permeate results while overpredicting the TDS results. The level of precision achieved in a desalination facility may substantially impact expectations for the subsequent processes. Thus, this level of precision may be acceptable in desalination in some contexts but may not be in others.

Table 3-2: ANN model predictions [21]

Permeate flowrate (m ³ /h)		TDS (mg/L)	
Observed	Predicted	Observed	Predicted
20.0	23.40	147.7	134.45
8.4	9.25	11.74	10.66
8.3	9.27	11.45	10.49
50	49.98	64.7	59.87

Predicting the quantity of material in the source water is crucial for assessing the performance of RO systems and water treatment plants. Bhagat *et al.* [162] conducted research on forecasting lead (Pb) in sediment at two Australian stations, namely Bramble (BB) and Deception (DB), using hybrid AI models. To extract the relevant input parameters for Pb prediction, a feature selection (FS) technique called extreme gradient boosting (XGBoost) was employed and compared to principal component analysis (PCA), recursive feature elimination

(RFE), and the GA for performance (GA). The suggested model focused on data preparation prior to the training phase, as illustrated in Figure 3–3, owing to the possibility that redundant features may introduce more noise than meaningful information when characterising the phenomenon of interest. The primary advantages of this approach include minimising the resources required for data collection and storage, mitigating the reduction in prediction accuracy caused by limited training data, shortening the time required to implement that data, and making it easier to interpret through visualisation and analysis [163], [164].

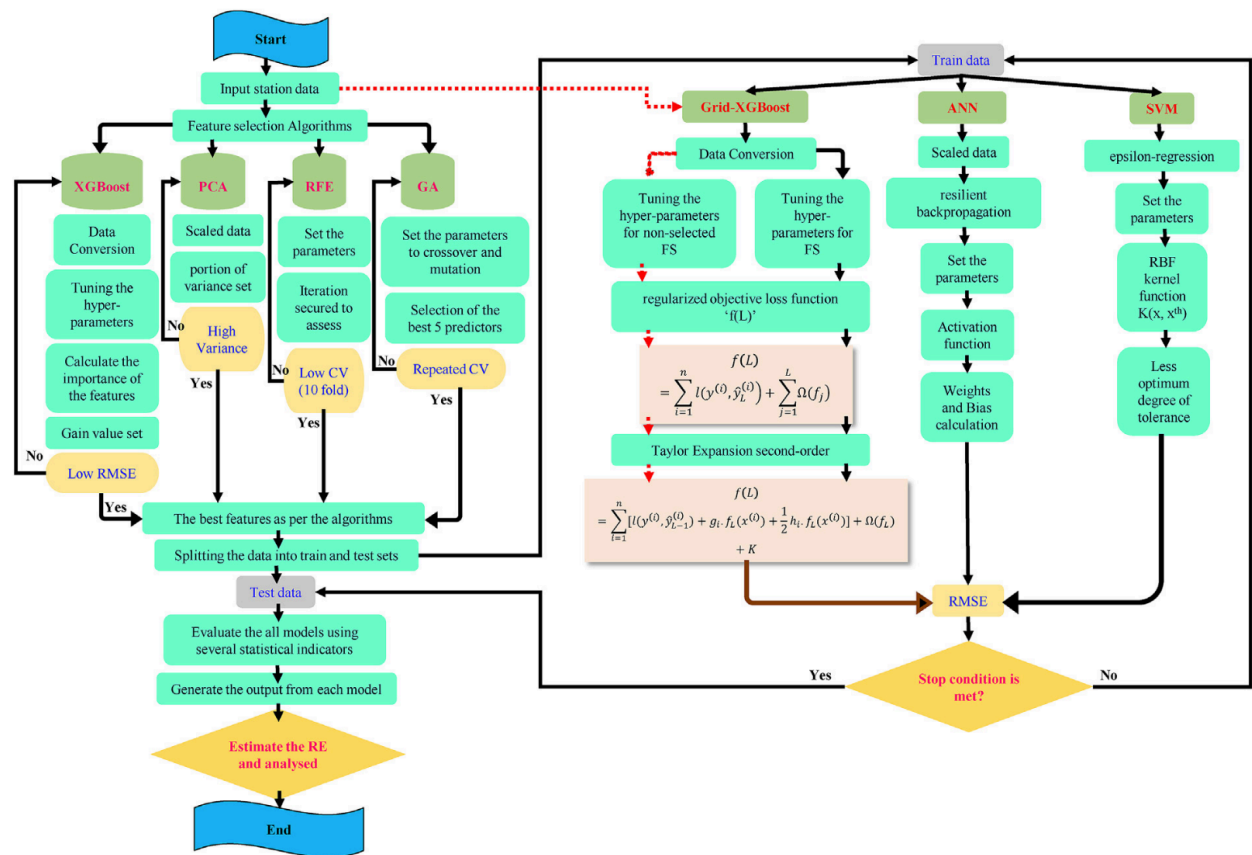


Figure 3–3 : Hybrid AI model to predict lead in two station in Australia [162]

The prediction of flux in various RO systems has become a crucial factor in ensuring proper membrane function, leading to several studies [135]–[138] that have investigated how AI and ML might help in forecasting flux and the aspects that influence its decline. As an example, Jawad *et al.* [170] developed a multi-layered neural network model to predict the permeate flux in forward osmosis (FO). The performance of the proposed model was compared to that of a multiple linear regression (MLR) model. Nine input variables were considered, based on lab-scale experimental the orientation of the membrane, membrane type, solution and draw solution, molarity of feed and draw solution, as well as the crossflow velocity and temperature

of both feed solution and draw solution. The multi-layered neural network achieved an R^2 value of 97.3% for the trained data and 82.1% for the tested and validated data, demonstrating its superior performance over the MLR model, which had an R^2 value of just 51.6%.

In another study, Jawad *et al.* [171] investigated the ability of a combined AI and response surface methodology to predict and optimise the membrane flux of an FO process using osmotic pressure difference, velocity, and temperature of both feed solution and draw solution as inputs. The developed AI and RSM models obtained coefficients of determination of 0.98036 and 0.9408, respectively.

The complexity of equipment networks and operational conditions presents significant challenges in the design and optimisation of site utility systems in process industries. Accurately estimating cogeneration potential is essential for simulating and optimising utility systems. An optimisation method in the ML field has been adapted, for example, Manesh *et al.* [172] used a genetic algorithm to perform a comprehensive site analysis along with an exergoeconomic optimisation to design a site utility steam network combining a Multiple Effect Distillation (MED) & RO desalination facility. This study aimed to minimise the total cost and increase the hybrid system's gain output ratio. Gain output ratio (GOR) refers to the ratio of the amount of freshwater produced to the amount of thermal energy input into the system. In other words, GOR is a measure of the efficiency of a thermal desalination process in converting thermal energy into freshwater. GA were used to identify the Pareto set to determine the global optimum for the resulting multi-objective optimisation problem. The outcome established the benefits of ML and GA specifically, as desalinated water production increased to 126,300 m³/d at a cost of \$0.81/m³, with a gain output ratio of 9.1. These findings demonstrated that the osmotic pressure difference, feed and draw solution velocity were the input values with the highest impact on flux.

Table 3-3 provides additional examples of neural network applications in estimating pollutant removal from RO and NF technologies, including input, output, data size, applied approach, and obtained results.

Table 3-3: Examples of applying neural networks in RO and NF technologie

Input	Output	Technology	Data size	Data source	Method	Results	Ref
Raw water flow, Product water flow, ERD, TDS of source water, TDS of permeate, Pressure, Temp, Inverse recovery	SEC		45	Literature review	Linear regression	Equation 10	[173]
Time, Pressure, feed conductivity, feed flow rate and power	Permeate recovery Permeate flow rate SEC	NF/RO, NF/RO/PV	60	Pilot testing	ANN Projected gradient decent (PGD)	R _{flow rate} : 0.9992 R _{recovery} : 0.999	[174]
Feed inlet temperatures, feed flow rates, and membrane lengths	Permeate flux Specific heat energy consumption	VMD	36	Experiment	Back propagation ANN	R ² _{Flux} :0.9936 R ² _{SHEC} : 0.9645	[175]
Salt concentration, mixture composition, pH	Salt Rejection (NaCl, Na ₂ SO ₄ , MgCl ₂ , MgSO ₄ and their mixture)	NF	Time series	Pilot testing	Single optimised ANN	-	[176]
Inlet flow rate, inlet pressure, inlet temperature, inlet concentration	Chlorophenol rejection	RO	70	Pilot testing	Multi-layered artificial neural network (back propagation) Genetic Algorithm	R ² : 0.990	[177]
Water temperature, pressure, pH and conductivity, Feed pressure, feed pH and feed conductivity	TDS Permeate flow rate	RO	120	Actual desalination	Radial basis function (RBF) neural networks, Multilayer perceptron (MLP)	R : 0.9904 R: 0.9858	[161]

Input	Output	Technology	Data size	Data source	Method	Results	Ref
TMP, pH, cross-flow velocity, concentration of bovine serum albumin (BSA) in feed	Flux declined	MF	-	-	Pore blocking and feed forward ANN models	R^2 : 0.996	[178]
Permeate flux and TMP, concentration of fluorescent nanoparticle, and the mass of permeate particles	Area of the membrane breach	MF	-	-	Genetic programming (GP)		[179]
Membrane type, Membrane orientation, feed solution (FS) concentration, draw solution (DS) concentration, FS crossflow velocity (CFV), DS CFV, FS temperature, DS temperature, Type DS	Permeate flux	FO	709	Laboratory-scale FO experimental data from literature	ANN	R^2_{Training} : 97.3% R^2_{Testing} : 82.1%	[170]
Feed concentration, temperature, pH and pressure	Permeate flux Water recovery Salt rejection SEC	NF/RO	30	Pilot testing	ANN, RSM	Parallel NF-RO had a recovery of 57.18% and rejection of 44.89%	[159]

3.2.2 Energy

Significant challenges associated with desalination technologies are now discussed, including high energy consumption, high energy prices, and expensive infrastructure costs. It is imperative to identify the factors that affect the energy usage of desalination facilities to improve their performance and reduce energy consumption. The energy required for RO is dependent on several factors, such as salinity, temperature, equipment efficiency, quality goals, and permeate volume [48], [180]. These aspects have been studied and analysed using AI techniques and optimisation approaches due to their potential to capture non-linear relationships.

To identify the operational parameters that significantly impact SEC for small-scale membrane-based desalination ($0.7 \text{ m}^3/\text{day} \leq q_{pw} \leq 220 \text{ m}^3/\text{day}$) and municipal-scale desalination ($2500 \text{ m}^3/\text{day} \leq q_{pw} \leq 368,000 \text{ m}^3/\text{day}$) desalination, statistical analyses were conducted, including multiple linear regressions [173]. The linear regression model showed that the utilisation of energy recovery equipment and an increase in pressure, temperature, and product water flow rate all contributed to a reduction in SEC. This is demonstrated by Eq 3.1 and Eq 3.2:

$$SEC = 7.7 + 3.9 \times 10^{-2}q_{rw} - 8.6 \times 10^{-2}q_{pw} + \frac{1.7}{1-R} + 6.2 \times 10^{-4}c_{rw} + 4.2 \times 10^{-3}c_{pw} - 0.34P - 5.4ER - 0.20T \quad \text{Eq 3.1}$$

$$SEC = 260 - 0.13YR + 8.3 \times 10^{-5}c_{rw} - 2.4 \times 10^{-3}c_{pw} \quad \text{Eq 3.2}$$

Where equation parameters represent the following: SEC is estimated specific energy consumption (kWh/m³), rw is raw water, pw is product water, q is flow rate (m³/day), R recovery rate, c is TDS (mg/L), P = pressure (bar), ER is energy recovery system, T is temperature (°C) and YR is the initial year of operations.

The performance of the vacuum membrane distillation (VMD) process, which includes permeate flux and specific heat energy consumption (SHEC), using an ANN for a variety of feed inlet temperatures, feed flow rates, and membrane lengths was estimated by Yang *et al.* [175]. According to the observations, the expected permeate flux increased with the rise in feed

temperature and feed flow rate, while it decreased with the increase in membrane length. Increased length led to declining heat transfer coefficient and more detrimental temperature and concentration polarisation phenomena, which enhanced local transfer resistance and hindered the mass and heat transfer process. As length increased, the hot feed residency time in the module became longer, and the temperature drop along the membrane fibre increased because of the resulting larger proportion of water vapour. Furthermore, the build-up of permeate water vapour on the module shell side had a negative impact on maintaining high level of vacuum, and therefore the actual driving force of VMD process decreased. Conversely, in predicting energy consumption, SHEC increased with increasing membrane length but dropped with increasing feed intake temperature and feed flow rate.

Energy cost models, based on logarithmic, exponential, and linear functions, are currently employed, but may not adequately capture all interactions between complicated parameters. To tackle this, Torregrossa *et al.* [181] utilised two ML models, Neural Networks (NN) and Random Forest (RF), to construct energy cost functions from a database of 317 wastewater treatment plants in northwest Europe. The two models were employed to predict the annual energy consumption of the plants in the study. ML methods were found to provide more accurate predictions than conventional methods. However, RF outperformed NN according to the coefficient of determination (R^2). For the RF model, the R^2 for training test and validation test was 0.95 and 0.82, respectively. More importantly, the study found that the pollutant load (COD) at the intake, total phosphorus, total nitrogen, and influent flow rate were the most elevated influence on the energy cost of the WWTPs, whereas the price of energy had a minimal impact. This means that water had to be treated irrespective of the cost of the energy.

3.2.3 Fouling

Comprehensive review papers on the use of AI and ML for forecasting membrane filtration performance and fouling behaviour were compiled by Viet *et al.* [182], Niu *et al.* [183] and Baghari *et al.* [184]. There was consensus among the reviewed publications that ANN, fuzzy logic, genetic algorithm, support vector machine [185], and search algorithms demonstrated high competence in forecasting membrane fouling, with an R^2 value up to 99%.

The optimisation of parameters that contribute to membrane fouling, such as operational conditions (flow rate and filtering time), particles conditions (concentration of fluorescent nanoparticle, mass of permeate particles, algae) and feed water quality (turbidity, temperature, pH, flux, TMP), has been achieved by the utilisation of a genetic algorithm [179], [186].

Different strategies that were successfully applied in membrane fouling control included clustering analysis [187], image recognition [188], and feature selection. Figure 3–4 illustrates a proposed hybrid AI and ML model that acts as an automated controller system to reduce membrane fouling [184].

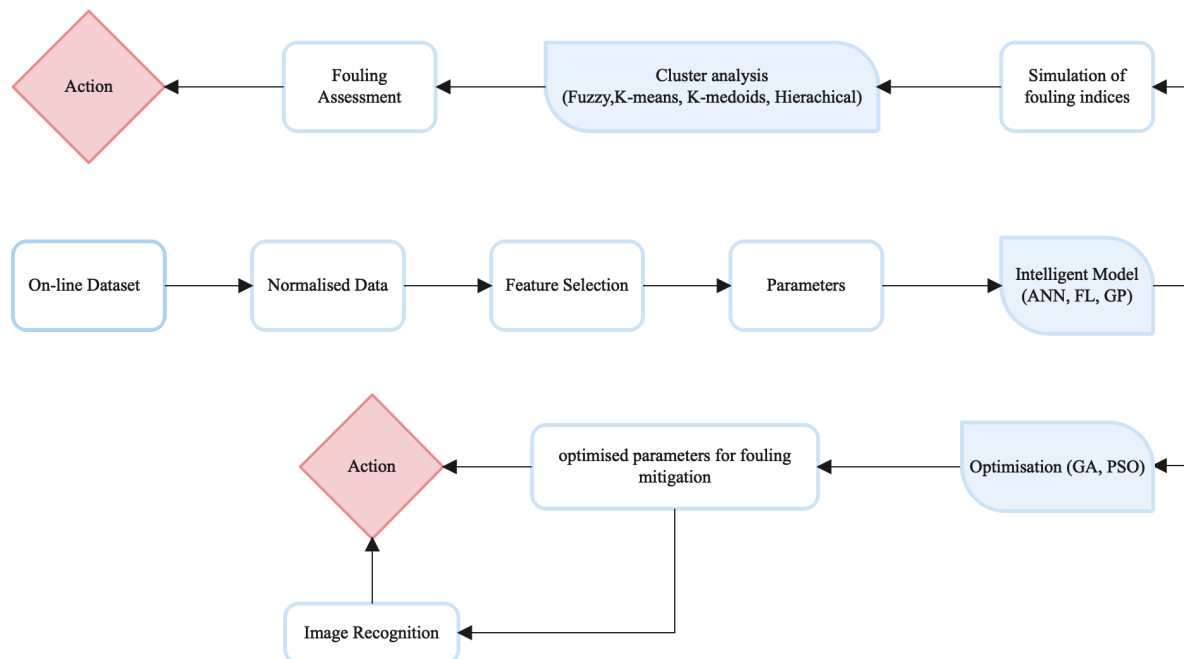


Figure 3–4: proposed AI and ML approach to control membrane fouling, adapted from [184]

3.2.4 Membrane Design

As mentioned previously, AI and ML have been used in several aspects of the RO process, including membrane performance improvement and operational optimisation. Recently, focus has been on determining factors that influence the performance of RO and either predict or optimise the process. AI and ML are powerful tools that can be applied in other areas such as designing membranes or generating novel membranes and processes. This section highlights previous work in the field of membranes, particularly with regards to membrane materials, membrane specifications, and membrane morphology.

The dynamics and morphology of porous membranes drive the flow and transport processes via these structures. Therefore, it is crucial for building new synthetic membranes to be able to accurately predict the velocity and pressure fields, as well as the concentration fields, of the components in a fluid mixture moving through a membrane. To accurately determine the best combinations of unknown monomers and their production circumstances, Gao *et al.* [189] presented a membrane design technique that uses machine learning-based Bayesian

optimisation (BO). To effectively predict water permeability and salt rejection from membrane monomer types (represented by the Morgan fingerprint) and fabrication circumstances, tree-based ML models (XGBoost and CatBoost) were developed. BO was constructed on the built ML model to inversely discover sets of monomer/fabrication condition combinations that had the best chance of exceeding the theoretical maximums for Na₂SO₄ and NaCl selectivity and permeability. The BO algorithm revises its prior knowledge of the design space to account for the results of the latest evaluations of candidate designs. It adjusts its search approach depending on the acquired information, giving greater weight to areas that are more likely to provide enhanced performance. By iterating through these steps, the BO algorithm investigates and improves the monomer/fabrication settings, looking for optimal combinations that result in the target membrane characteristics.

Without relying on any numerical values for training their ML models, Kamrava *et al* [190] employed 2D images as inputs to predict flow parameters. In this study, a deep network using Residual U-Net was developed to predict flow parameters of porous membranes based on their morphology, such as the spatial distributions of fluid pressure and velocity. CFD-obtained, high-resolution pictures of the membranes together with the pressure and velocity distributions in their pore space at discrete times were used to train the model. In this study, since the other two boundaries of the system were assumed to be impermeable and the no-slip condition on the solid surface was established, fluid was injected into the membrane on one side and a fixed pressure was applied on the other. The outcome demonstrated a high accuracy of model prediction that is matched with the CFD images.

Membrane materials used in RO present several difficulties. Thin films made of polymers, rather than cellulose, are increasingly widely used in membrane materials. Although polymer-based semipermeable membranes provide improved fluxes and salt rejection, they still fall short of the optimal performance target of carbon nanotube-based filters' high fluxes and zeolites' high rejection rates [191]. There has been some research on saltwater desalination using nanoporous two-dimensional materials including graphene, graphene oxide, and molybdenum disulfide etc; however, the observed water flows at high salt rejection rates are not adequate for industrial-scale deployment [191]. Therefore, membrane material and design optimisation models are important for determining the optimal performance of desalination. For instance, water flow and salt rejection rates are calculated computationally, and then a ML model establishes relationships between these variables and 44 additional chemical, electrical, and structural membrane and pore properties [192]. The most influential factors on desalination

performance were found to be the pore atomic number, the maximum negative/positive charge of the membrane, and the dielectric constant of the water model used in MD simulations [192]. In all, the model checks 3814 2D items from public databases. Nonmetals like halogens and chalcogens boost the average flux of water, whereas transition metals improve the average salt rejection rates. It has been hypothesised and predicted that complexes of 2D transition metal oxides, carbides, and nitrides (MXenes) would be beneficial in desalination [192].

The ability to analyse ML models and fully understand their inner workings and prediction methods is crucial for engineers, since these models have shown to be useful tools. In addition, it is critical to analyse and explain situations in which a ML model places less importance on a parameter that researchers had previously considered vital. To tackle these issues, Jeong *et al.* [193] utilised explainable artificial intelligence (XAI) methods to analyse in depth the information learned by ML models on the mechanics of ion transport across polyamide membranes in RO and NF processes. A total of 1,585 data points from 26 distinct membrane types were included in the analysis. The accuracy predictions of ML models were low, ranging between R^2 0.55 and R^2 0.72. Shapley additive explanation (SHAP) was employed as the XAI approach to determine how different ion and membrane parameters affected the model's predictions. SHAP uses cooperative game theory to fairly distribute the "credit" or effect of each feature on the model's output [194]. The use of XAI demonstrated that ML models can accurately represent the decisive part that size exclusion and electrostatic interactions play in regulating membrane separation processes. In addition, the XAI study found that cation and anion rejections during RO and NF filtering are accomplished by processes directing ion transport in various ways. Although the solution diffusion model has traditionally been used to describe solvent and solute transport, recent studies have led to other approaches, such as the Solution-Friction model [54], which takes into account the overall interactions between salt ions, water, and the membrane.

The advancement of gas separation membranes, for example, is profoundly affected by the use of polymer materials. However, until recently, engineers had to depend on trial-and-error techniques to create innovative membrane materials, which required a significant amount of time and effort. Yang *et al.* [195] addressed this shortcoming by introducing a dependable and precise ML framework for finding high-performance new polymers. By using experimental data to build multitask ML models, the authors link polymer chemistry to the permeabilities of He, H₂, O₂, N₂, CO₂, and CH₄. To better understand how various chemical moieties affect permeability and selectivity, it is helpful to evaluate ML models such as random forest

regression and deep neural networks (DNNs). The frequency of chemical moieties (substructures) in molecules was captured using Morgan fingerprint with frequency (MFF). Next, feature significance was extracted from ML models using SHAP for interpretation. Using this information, the authors [195] searched through a database of more than 9 million hypothetical polymers, finding several that achieve better performance than what is currently possible. This included the discovery of ultrapermeable polymer membranes with O₂ and CO₂ permeabilities of more than 104×10^{-10} and 105×10^{-10} mol/msPA (104 and 105 Barrers), respectively, which had never been observed previously. High-fidelity molecular dynamics simulations further verified the ML-predicted gas permeabilities, providing additional evidence that these potential candidates may be translated into practical applications.

For further information, Yin *et al.* [196] published a comprehensive review article on ML approaches employed in the membrane discovery cycle, including topics such as membrane material design, membrane application and membrane process design for various membrane systems. AI and ML approaches used to select and improve membrane material design are promising emerging field of research that might significantly advance the membrane sector. Understanding and predicting membrane performance based on morphology is currently limited, but with the use of AI and ML, these techniques can help to improve understanding and applicability of various membrane materials. However, this systematic review and others emphasise several problems, such as the quality, quantity, and absence of well-documented data that restrict the spread of research in this subject, despite the rising body of research in this domain.

3.2.5 Fault Detection & Equipment Failure

Water distribution losses are a challenge that is often encountered in the water management network. In 2017, the average European nation lost 26% of its water due to leaks, with Ireland recording the highest percentage at 47% of distributed water [197]. ML approaches have been applied in the area of pipe and equipment fault detection in the water sector. Zukang *et al.* [198] conducted a comprehensive review of model-based and data-driven approaches for identifying and localising leaks in water distribution systems. The degradation of water network infrastructure is a factor that increases the risk of failure of treated water. These failures exacerbate supply-demand imbalances, reduce dependability and disrupt society. It is critical to identify and prioritise pipes that pose the greatest risk of catastrophic failure before collapsing, and they should be rehabilitated or replaced as soon as possible.

Data-driven models have high potential for forecasting pipe failure due to their ability to consider multiple variables, as pipeline deterioration is dependent on physical, environmental, and operational factors that are summarised and illustrated in Figure 3–5. This section summarises several studies that have applied AI techniques to predict pipe failure in water distribution systems using a variation of factors showed in Figure 3–5.

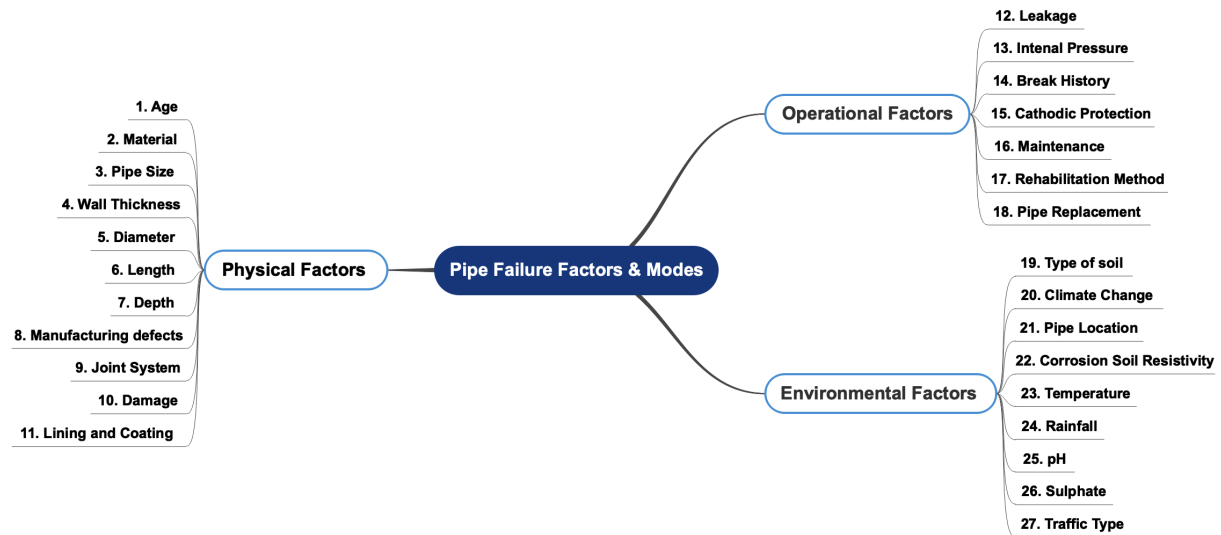


Figure 3–5: Factor that impact the deterioration of pipelines based on physical, environmental, and operational factors

Utilising previous failure patterns, environmental and demographic variables and pipe properties, Yazdekhasti *et al.* [199] applied different AI tools, including decision trees, random forests, SVM, and logistic regression to assess the future probability of water pipe failure. The data used in this paper is an example of the “zero inflation problem”. The zero-inflation problem is a common issue in modelling count data, where a significant proportion of the observations have a value of zero, and it is unclear whether the zeros are due to the absence of an event or a measurement error. In this paper, the zero-inflation problem refers to the fact that some water pipes have never failed in the historical data, leading to a high number of zeros in the dataset. This can cause issues when modelling the data since some traditional statistical models assume a normal distribution, which is not appropriate for count data with a large number of zeros.

Therefore, the study [199] incorporates spatio-temporal features germane to the placement of water pipes, such as proximity to the closest river or soil type, alongside temporal features that relate to the time of data acquisition, including month and year. This study focused on the top 10th percentile which denotes the process of arranging the outcomes from greatest to least

likelihood of failure, as determined by the positive response value of 1. The top one percentile of the pipe's failure could be predicted with an accuracy of 84% by the random forest model.

Winkler *et al.* [200] proposed a novel approach for modelling water distribution pipe degradation by using decision tree learning algorithms. The study addressed the issue of skewed data distribution by employing simple random sampling (SRS) and stratified sampling, while bagging and boosting were used to compensate for the high variance of decision tree classifiers. The highest performing classifier is determined to be boosted decision trees with random under-sampling, which is utilised to create a rehabilitation plan in which the model is used to forecast the pipe network status in five and ten years.

Fang *et al.* [201] conducted an examination to evaluate the performance of water mains to optimise pipeline rehabilitation using soil properties by comparing stacking ensemble ML approaches to four other ML models. Although the ensemble model outperformed the other methods, the dataset for this model was limited and the model was not validated. Robles-Velasco *et al.* [202] examined the possibility of applying ANNs to forecast breakdowns in water supply pipes, taking into account both physical and operational aspects. Over-sampling and under-sampling were used to overcome the inequality in the dataset (619 failures in 2018 out of 89,595 pipe sections).

On the other hand, Giraldo and Rodríguez [203] examined several statistical and ML models for a more complete and accurate prediction of pipe failure to obtain a better knowledge of pipe failure models' performance and constraints. Linear Regression, Poisson Regression, and Evolutionary Polynomial Regressions (EPR) were the statistical models that were employed to forecast pipe failure based on the diameter, age, and length of the pipe as explanatory factors. Individual pipe failure rates were predicted using four ML algorithms, including Gradient-Boosted Tree (GBT), Bayes, SVMs, and ANNs. With the statistical models, poisson regression performed better in predicting failures in pipes R^2 (0.927) and RMSE (22.09). The accuracy test shows that all ML models performed very well; however, the F-measure test identifies that GBT outperformed the other models. This strategy has the benefit of prioritising misclassified pipes in each iteration rather than focusing only on properly categorising pipes that do not fail. In comparison to SVM, GBT results are more readable, transparent, and furthermore accurately identify the explanatory factors' importance. Additionally, the unbalanced dataset greatly affected ANNs' ability to accurately identify failed pipes. Table 3-4 showcases an overview of research that have employed AI techniques for the purpose of predicting pipe failure. The table provides information regarding the scale of the water network and dataset utilised in each

study, as well as the specific AI methodology employed and the corresponding accuracy achieved.

3.2.6 Algae Detection

The intake system is the first system of the desalination plant connecting the source water to the plant. Its main purpose is obtaining water of appropriate quality and quantity in response to the desired quality and volume of product water to be produced by the desalination plant during its lifespan. The intake design significantly influences the presence of foulants in the source water and the complexity of the pre-treatment system required to control membrane fouling in RO. The intake system consists of intakes, screens and pump stations [204]. The design and performance of RO desalination are heavily influenced by the quality of the source and consequently the feed water. Inadequate source water conditions increase the desalination process's complexity, leading to higher capital and operating expenditures. Thus, modelling water quality parameters is essential in examining water systems to effectively manage and predict desalination behaviour, enabling the appropriate precautions to prevent pollution and damage to the RO membrane.

Microscopic algae pose a significant operational challenge in seawater RO systems. Early prediction of algal blooms is necessary to select appropriate mitigation strategies to reduce their impact and prevent algal cells from reaching the RO membrane. The detrimental effect of algae on SWRO gained more attention in 2008-2009 following a catastrophic "red tide" bloom episode in the Gulf of Oman that resulted in a plant shutdown for as long as two months. This "red tide" (hence referred to as harmful algal blooms or HABs) prompted several SWRO facilities in the vicinity to scale back or shut down operations due to clogged pretreatment systems or unacceptably low RO feed water quality. The latter has raised concerns about irreversible fouling of RO membranes, leading to the closure of several plants. To put this problem in context, around 70% of seawater RO plants in the Middle East experience biofouling issues [205]. This 'red tide' occurrence demonstrated the significant problem that algal blooms could create in countries relying heavily on SWRO facilities for water supply, emphasising the critical nature of sufficient pre-treatment in such systems.

Algal blooms occur naturally due to seasonal variations in water temperature, sunlight availability, and nutrient concentrations in the water. Toxic organic pollutants emitted by causative algae species can cause disease or death in humans and aquatic creatures in specific algal blooms due to the bacterial decomposition process of this organic material, leading to a

Table 3-4: Examples of applying AI and ML to estimate pipe failure and conditions

Research Type	Water network size (km)	AI/ML method	Dataset size	Parameters	Accuracy	Recall	Specificity	R ² /RMSE
Pipe failure [199]	2000	RF	600,000	Geographical locations of each pipe segment, length, diameter, material, installation year, hydraulic characteristics, soil properties, land use, and proximity to transportation infrastructures (road and rails), climate change, engineered features.	0.84	-	-	-
Pipe conditions [201]		Ensemble	109	Resistivity, pH value, sulphide, moisture, thickness, soil type, soil corrosivity, pipe wall thickness,	-	-	-	R ² = 0.75 RMSE = 0.14
Pipe failure [203]	1819	GBT	4371	Diameter, age, length, land use, valves hydrants, previous failures, moisture content, soil contraction and expansion potential, precipitation	0.996	0.429	0.999	-
Pipe failure [200]	851	Boosted DT	39,637	Failure, age, type, diameter, pressure, length, material, connection, hydrants, valve on pipe, valve in street section, total failure, new failure.	0.83-0.96	0.702-0.808	0.835-0.989	-
Pipe failure [202]		ANN	89,595	Material, diameter, age, length of the segment, connections, network type, pressure fluctuation, number of previous failures type	0.783	0.817	0.73	-

rapid decrease in dissolved oxygen concentration in the water. Algae organic matter (AOM) and biomass produced by certain hazardous algal blooms (HABs) may not create dangerous substances, but can accumulate in high quantities near or below the water's surface. As a result of the bacterial decomposition process of this organic material, the concentration of dissolving oxygen in water drops rapidly, resulting in the death of aquatic plants and animals [206]. If not properly removed by pre-treatment, particulate debris comprising algal cells, their detritus, and AOM can build up on the surface of SWRO membranes during the filtration of algal bloom-influenced waters, leading to low flux and high feed channel pressure drops, resulting in significant permeability loss.

Bacteria can attach, gather, and grow in RO systems, forming a slimy covering of bacteria and associated extracellular polymeric compounds known as a biofilm [205]. Algal blooms may lead to the formation of biofilms due to the elevated AOM content in seawater. Some AOM components, notably transparent exopolymer particles (TEP), have a tendency to attach and collect on the membranes and spacers due to their tendency to stick. Bacteria can successfully consume biodegradable nutrients from the feed water, which are contained in the accumulated TEP. Additionally, TEP can be partially destroyed and may serve as a substrate for bacterial growth in the future. A significant (> 15%) decline in normalised membrane flux, net driving pressure, or feed channel pressure drop can indicate an operational issue.

Different aspects of algae have been addressed by ML approaches, including the detection of algal bloom occurrence, the quantification of algal cell content, and the classification of algal types. Forecasting and predicting algorithms for cyanobacteria blooms in freshwater lakes were reviewed systematically by Russo [207]. The following section highlights various approaches to forecasting and predicting algal blooms for different water resources and treatments.

Detection

In saline water, there is currently no straightforward approach to preventing HABs. However, the gathering and analysis of various data and parameters may assist in predicting the occurrence of such blooms. The schematic diagram presented in Figure 3–6 depicts the various factors that may potentially contribute to the occurrence of algal blooms. Recently, researchers have deployed ML and AI techniques to predict the early occurrence of algal blooms. Oman has reported that algal blooms are no longer limited to the summer months; the country has experienced such blooms throughout the winter months (December to March) in previous years

[208]. Seawater desalination would benefit significantly from the ability to forecast algal blooms in advance.

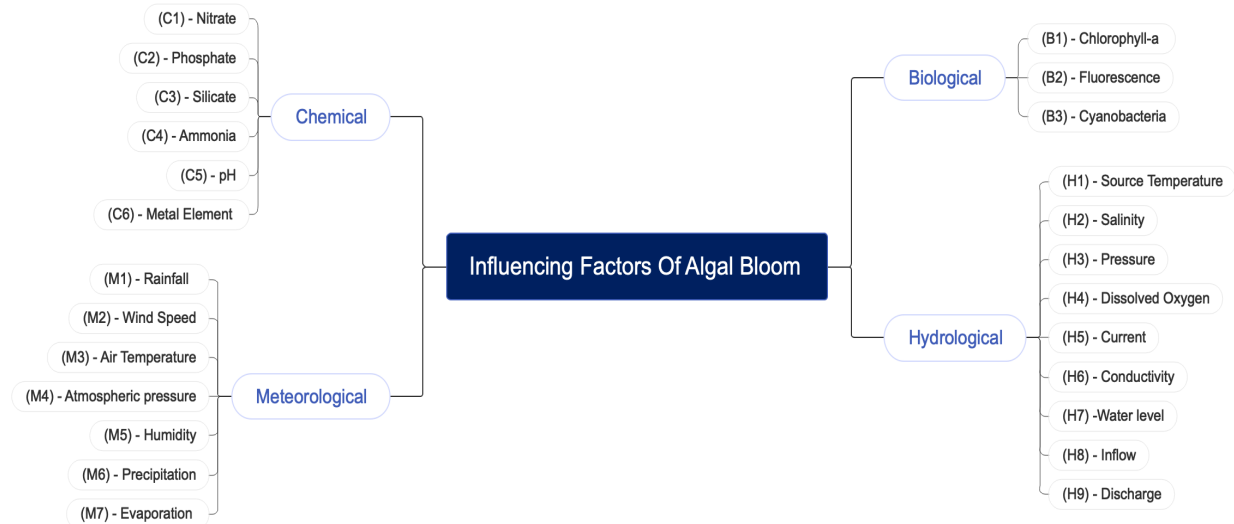


Figure 3–6 : Influencing factors of algal bloom

Several researchers have employed ML techniques to forecast water quantity measurements and quality characteristics using correlated variables from environmental datasets. These methods commonly aim to predict the content of algal biomass, such as chlorophyll-a concentration or algal cell density, which are useful indicators of algal growth dynamics. One particular identification approach was utilised by Deng *et al.* [209] to determine the consequential characteristics that have a substantial impact on algal dynamics using stepwise and weight methods. Both approaches demonstrated that the time-lagged Chlorophyll-a concentration is the most influential factor in algal growth, followed by a 5-day biochemical oxygen demand (BDO₅), total inorganic nitrogen, dissolved oxygen, and pH in the studied area. It was found that after implementing long-term strategies to mitigate biological oxygen demand (BOD) and nutrient load in the studied area, the frequency of HABs occurrences had significantly decreased.

Using M5P and Extreme Machine Learning (ELM), Yi *et al.* [210] constructed a model to predict Chlorophyll-a concentrations in short-term algal blooms (1-7 days). The two models showed high performance in forecasting chlorophyll-a after 1-day; however, the accuracy of the models decreased as the number of days increased. This was a result of the increased complexity of the system and difficulty in the accurate prediction of long-term changes in environmental conditions. Furthermore, other factors not taken into consideration in the

models, including biological interactions and human activities, may have also contributed to the decreasing accuracy of the predictions over time.

Researchers have employed various techniques, including the use of warning levels of algal cells to anticipate blooms. Park *et al.* [211] used a comprehensive approach that leveraged detailed water quality, hydrodynamic, and meteorological data to estimate algal alert levels for the early warning of blooms in a freshwater reservoir using ANN and SVM models. Sensitivity analysis of the input variables was achieved using the Latin-hypercube one-factor-at-a-time (LH-OAT) approach and using pattern search algorithm, the model parameters were optimised. The resulting algal alert system comprised four levels: normal ($L_0 = <1000$ cells mL^{-1}), caution ($L_1 = \geq 1000$ cells mL^{-1}), warning ($L_2 = \geq 10,000$ cells mL^{-1} and $< 1,000,000$ cells mL^{-1}), and bloom ($L_3 = \geq 1,000,000$ cells mL^{-1}). However, there were no bloom incidents in the collected data. The performance of the ANN and SVM models for early-warning prediction of alert levels at various data intervals was satisfactory in some cases and ANN was able to predict level 2 better than SVM. The results also revealed that the 6 and 7 day intervals were appropriate for early-warning periods.

Similarly, Kim *et al.* [212] concentrated on developing a model for early warning of harmful blooms (cyanobacterial blooms) utilising ANN and SVM alongside adaptive synthetic (ADASYN) sampling to produce synthetic data owing to the imbalance in the alert levels of algal bloom (data size for each level: $L_0 = 210, L_1 = 87, L_2 = 93$). The findings demonstrated that ADASYN greatly improved the performance of both models in forecasting level 1 and level 2 despite decreasing the prediction for level zero. Again, ANN outperformed SVM as the optimal model for predicting early warnings. From previous research, SVM performed well in predicting the input parameters; however, the inclusion of nonlinear relations between variables and outputs was found to reduce SVM's computing accuracy and efficiency. Table 3-5 provides additional instances of the utilisation of AI in the domain of algal detection by presenting the employed methodology, duration of time lags, origin of data, as well as the anticipated outcomes for both the training and testing phases. As it can be seen, when the interval time lag was shorter, more accurate prediction for algae was achieved. Also, SVM algorithm shown superior adaptability and predictive performance in comparison to other AI and ML algorithms.

Table 3-5: Examples of applying AI and ML papers to detect algal based on time interval lag

Output	Method	Time interval lags	data	Test result	Ref
Predict Chlo-a	Forward stepwise, simplified weight, SVM, ANN	Short term	Daily 1988 – 2018 (11293)	SVM had the highest R:0.984 compared to ANN (R:0.97) but lower RMSE:0.66.	[213]
Predict Chlo-a	ELM, M5P	Short term	Daily (Jan 2013 - Dec 2016)	ELM had better performance; R ² :0.87, RMSE:10.7	[210]
Alert level	LH-OAT, pattern search algorithm, ANN, SVM	Short term	L ₀ :165, L ₁ : 74, L ₂ : 115	SVM outperformed ANN in testing phase	[211]
Alert level	ADASYN , ANN, SVM	Short term	L ₀ : 210, L ₁ : 87, L ₂ : 93	ANN predicted better than SVM	[212]
Cyanobacterial cell density	WNN	Short term	Online Daily	R ² :0.986, MARE:0.07	[214]
Predict Chlo-a	MLR, SVM, ANN	Long term	Monthly (2000 - 2017)	SVM had better prediction; R ² :0.81, RMSE:1.51.	[215]

Research to date shows that the choice of factors is crucial. Ye *et al.* [216] stated that early warning systems should be based on input variables that are easily and quickly measurable. The classic chemical analysis of nutrients or phosphorus is time-consuming as the process requires several days for on-site sampling, transportation, chemical analysis and data quality control in the laboratory, which can lead to a time lag. Therefore, the following studies have tested the possibility of using real-time online monitoring datasets to predict HAB.

Xiao *et al.* [214] developed and validated an innovative single-parameter technique that integrates wavelet analysis with artificial neural networks (WNN) to forecast algal blooms utilising daily online monitoring datasets of algal density, as shown in Figure 3–7(a). The Wavelet neural network (WNN) model process involves breaking down the dataset into a series of data at n levels, with approximation at the nth level and details at the 1, 2,..., nth level, before feeding those into an ANN and summing the outputs to simulate the original dataset for data decomposition verification. Then, the first three wavelet decomposition series' data were fed into an ANN with two hidden layers. The output was compared to the goal series to achieve an optimistic network, and the network weight (W) was adjusted between layers. The model provided the best forecast, as indicated by the lowest mean absolute error (MAE: 0.103×10^4 cells mL⁻¹) and Mean absolute relative error (MARE: 0.070) values, as well as the most significant correlation coefficient (R²:0.986).

In research conducted by Wen *et al.* [217], a deep learning technique based on a long-short-term layer (LSTM) was utilised to predict future HABs. The first phase of HAB's primary environmental factors extraction model (HMEM) performs dimensionality reduction to eliminate noise and irrelevant variables or features from a maritime station monitoring dataset. The Spatio-Temporal Feature Clustering Model (STFCM) differentiates numerous regional warning levels of HABs on the basis of space, time, and attributes according to the algal growth rate. The continuously obtained time series environmental parameters from Autoregressive Integrated Moving Average (ARIMA) are inputted to LSTM to predict algal bloom. Diagram (b) demonstrates the model's steps in Figure 3–7(b). The model was 82.1% accurate in predicting the development of Alexandrium.

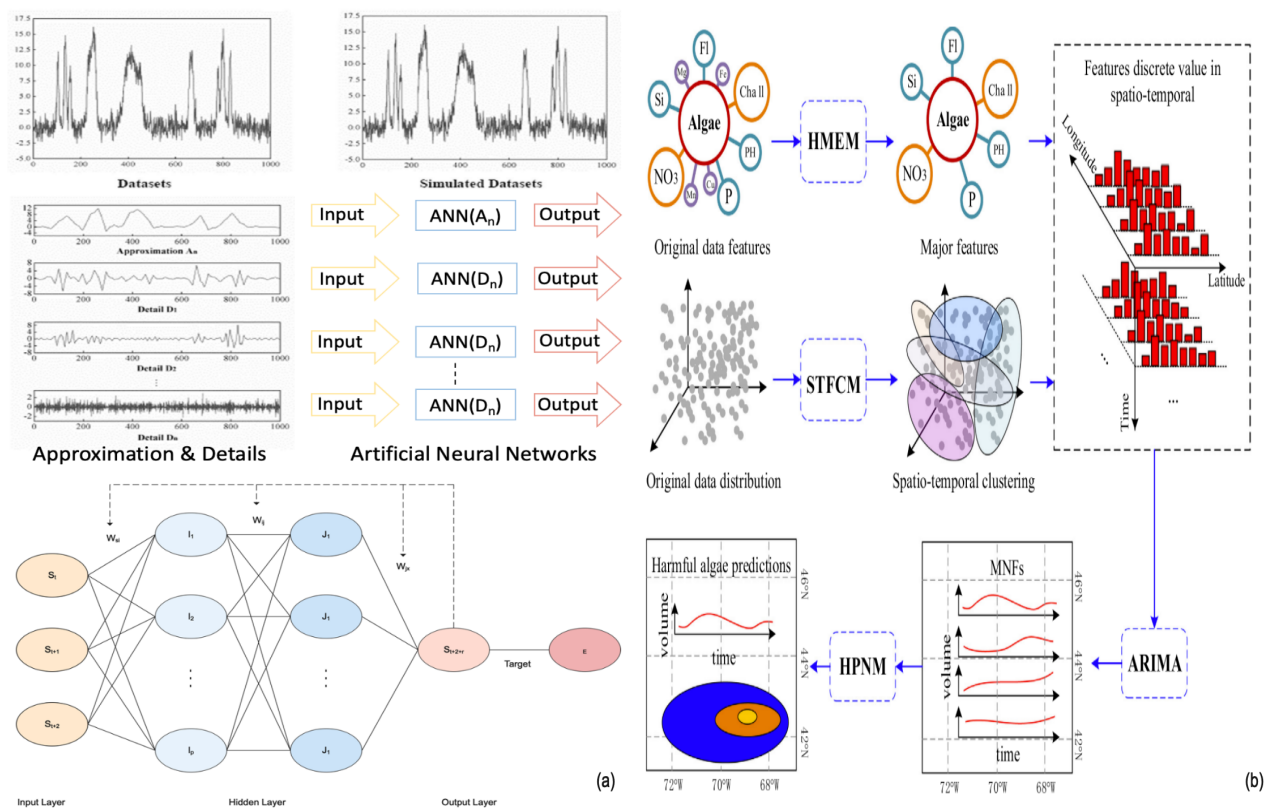


Figure 3–7: AI model based on time series data to forecast algal bloom, (a)[214], (b) [217]

Classification

Microscopic examination of water samples reveals crucial information regarding the presence, abundance, and viability of microorganisms that can aid in selecting the most suitable treatment option in water technology. Convolutional neural networks (CNN) have emerged as a standard method capable of processing high-dimensional image data to extract sophisticated features for classification and regression treatment strategies. This makes this approach ideal for

classification and regression applications. In order to better understand the efficacy of water, treatment strategies and the risks connected with algae, taxonomy or classes or genus identification is essential.

Li *et al.* [218] has demonstrated the effectiveness of a Mueller matrix imaging system coupled with CNN in distinguishing morphologically related algae. The dataset comprised eight algal species and one cyanobacterial species, with each species having 10,463 The integration of Mueller matrix with CNN has yielded excellent accuracy and F1 score (ACC: 97%, F1: 0.968); however, the research has highlighted limitations in correctly classifying *Thalassiosira eccentrica* due to an imbalance in the data, representing only 0.9% of the total data.

The dataset consisted of 37 species of algae belonging to six biological groups. However, due to data imbalance, ten genera were merged into one class. The study achieved a Mean Average Precision (mAP) of 74.64% for algal detection based on genera and 81.17% for algal detection based on class. The study has also identified data quality as a critical challenge in the classification of algae. A significant proportion of undetected algae are transparent and fade into the background, while occlusion due to the overlap of algae with other objects is also a significant issue. Misclassification can occur due to the similarity in shape and class, as evident in Figure 3–8.

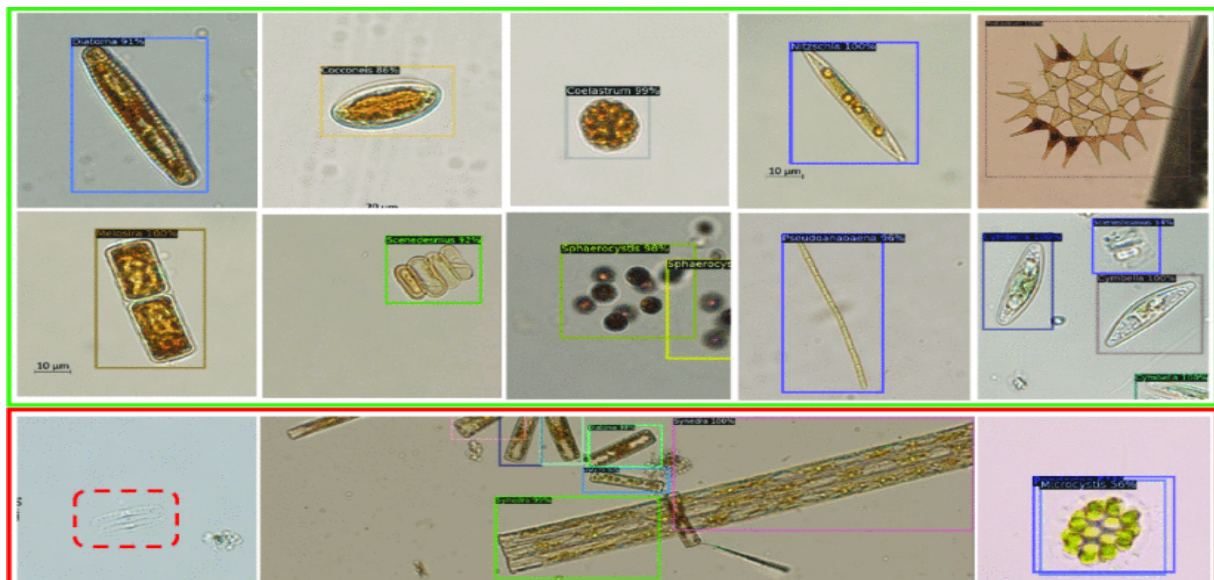


Figure 3–8: Samples of the obtained algal detection where the first two rows represent accurate classification and detection outcomes. The last row depicts three different sorts of inaccurate forecasts. From left to right, unidentified algae, algal blockage, and misclassification are the three types of inaccuracy [219]

Similar challenges were observed in Qian *et al.*'s research [219], in which a Faster R-CNN architecture was utilised to categorise large-scale coloured microscopic pictures. The dataset consisted of 1859 high-resolution microscopic images of 37 species of algae in six biological groups; however, due to an imbalance in the data, ten genera were amalgamated into one class. The Mean average precision of predictions with IoU \geq 50% (mAP) is 74.64 percent for algal detection based on genera and 81.17 percent for algal detection based on class. The quality of data was also identified as a difficulty connected with the classification of algae in this study.

The majority of unaccounted algae after detection would transparent and faded into the background. Additionally, algae can overlap with that of other objects and algae present leading to occlusion. Another issue is misclassification that may occur as a result of similarity in class and shape. These previous issues are shown in the last row of Figure 3–8.

When the deep learning-based ResNeXt CNN model was used to detect and categorise 16 algal families, Yadav *et al.* [221] observed that a few photos were misclassified due to commonalities, including filamentous morphological form and the presence of helical trichomes. Although the model achieved an impressive F1-score of 99.97%, the families considered in this study exhibited relatively fewer commonalities, leading to very low false-positive values compared to true positive values.

Deglint *et al.* [220] studied the viability of employing ML and fluorescence-based spectral-morphological characteristics with Feed-Forward Neural Networks to enable the identification of six distinct species of algae. Initially, an algae-containing water sample was observed with a multi-band fluorescence imaging microscope. The data was subsequently processed using data processing methods to eliminate the background, as shown in Figure 3–9. The processed data was next split into background objects and micro-organism objects, followed by the isolation of individual algae. The isolated microorganism imaging data was then used to extract a variety of morphological and spectral fluorescence features. The retrieved characteristics were then utilised for training three distinct neural network models. The third model, which used morphological-spectral features for its training showed considerably greater average accuracy as well as lower standard deviations equal to $96.1\% \pm 0.8\%$.

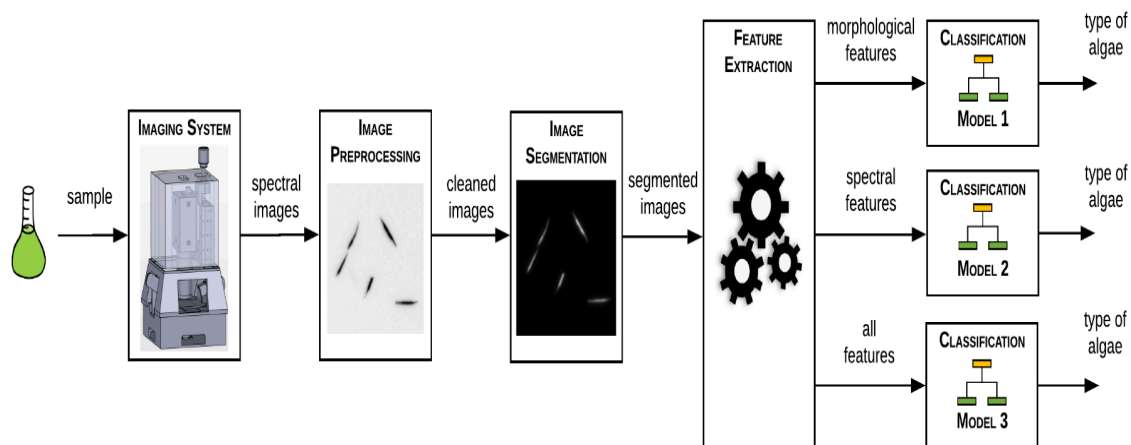


Figure 3–9: Water sample, multi-band fluorescence image microscopy data processing, image segmentation, feature extraction, and neural network models are the five basic components of the proposed technique of automatic identification of different types of algae specie [220]

CNN requires a substantial amount of data to train the systems. Therefore, augmentation methods have been applied to increase the size of data and improve the accuracy of CNN. Park *et al.* [222] conducted research on the morphological identification of algae in the management of drinking water treatment processes using Neural Architecture Search (NAS) for CNN. The Flow Cytometer and Microscope (FlowCAM) were used to acquire 1922 pictures, which were subsequently augmented to 7701 by mirroring, rotating, and top-down flipping. However, the original data in the convolutional neural network constructed by neural architecture search (NAS) outperformed the augmented data. In recent research carried out by Sonmez *et al.* [223], two distinct classification algorithms were employed to determine if the acquired algal picture belonged to the Cyanobacteria or Chlorophyta microalgae categories. Compared to the CNN model, the AlexNet-SVM structure with the cubic kernel function delivers greater generalisation and classification accuracy (Acc:99.66%) for the augmented dataset.

3.3 Effectiveness of Artificial Intelligence VS Conventional Modelling

The conventional engineering modelling approach necessitates the incorporation of several assumptions to simplify the complexity of the system. Such simplifications may lead to discrepancies between theoretical models and experimental observations, resulting from insufficient knowledge of the system’s complexity, thereby impacting model accuracy. Conversely, various AI applications have demonstrated their capacity to address the challenges

of complex modelling scenarios [147]. Furthermore, AI and ML tools eliminate the requirement for in-depth comprehension of the engineering process. They do not depend on detailed assumptions or governing equations for mathematical descriptions of engineering phenomena. By learning from provided dependent inputs and independent outputs, these algorithms can understand and model complex systems [224].

Research work by Khayet *et al.* [225] utilised both conventional modelling and ML. Response surface methodology (RSM) and ANN were applied to predict and optimise the performance index of RO. Operational conditions, including feed concentration, flow rate, feed temperature, and operating pressure, were presented as input variables, while the performance index defined as permeate flux multiplied by salt rejection, was considered as output. The response surface methodology (RSM) approach was not successful in developing a global model that could predict the performance of RO across a wide range of salt concentrations in the feed solution compared to an ANN, which was capable of doing so. In addition, ANN predicted the optimal global solution for the tested RO pilot plant.

Algal blooms are a complex phenomenon caused by more than 180 different species of algae, each with unique environmental requirements. The maritime station monitoring (MSM) approach typically uses nitrogen and phosphorus indicators as measures, rather than other, more pertinent main environmental elements (MEFs). It is possible that some places where HABs are initiated are not being monitored because MSM measurement points are not only spread out over the ocean but also have an extended period [217]. Remarkably, AI and ML have demonstrated the ability to forecast and differentiate between various types of algae using different techniques, as highlighted in the literature review of algal studies. This is a noteworthy accomplishment, considering the intricate interactions between marine environments and their constituent parts.

Continuous monitoring of Transmembrane pressure (TMP) and permeate flux helps prevent membrane fouling. Most model-based control systems compare flow drops to data simulated by mechanistic models like cake filtration and total blocking in an attempt to identify the overall membrane fouling process based on real-time data. Once the primary fouling mechanism for the system has been identified, the optimum control actions can be adopted. On the other hand, there are potential downsides to using online data in this manner, as the membrane permeate flux may be affected by factors other than the mixed liquid filterability, such as membrane history. Given that it is unclear whether the current high fouling propensity

or the cumulative effect of earlier fouling occurrences is responsible for the decrease in membrane permeability, the optimum decision may not be taken [184].

A CNN is a possible approach that can provide the possibility of identifying, using image simulation and segmentation, the causes of fouling and the beginning of particle accumulation on the membrane surface. Using in-situ fouling image data from optical coherence tomography (OCT), Park *et al.* [169] trained a deep neural network (DNN) to simulate membrane fouling and flux decline in NF and RO. OCT is a non-invasive imaging technique that has been recently applied in the field of membrane fouling monitoring. It involves the use of a light beam that is split into a membrane cell and a reference arm. The backscattered beam from the membrane cell is then combined with the reference beam to create an interference spectrum which is subsequently Fourier-transformed to obtain a 3D view of the fouled surface [64]. By providing a high-resolution image of the membrane surface, this method can be utilised to monitor any type of fouling and detect small changes to the membrane's structure. OCT has substantial potential for improving membrane-based processes' efficiency and performance by monitoring and analysing membrane fouling in real time.

The use of OCT to monitor and analyse membrane fouling in real time has great promise for improving the efficacy and performance of membrane-based processes in a wide range of applications. In this study, a comparison was made between the DNN model's results and those of pre-existing mathematical models. Totalling 13,708 photos, high-resolution photographs of the fouling layer were used to train and test the DNN model. The DNN model recreated two-dimensional and three-dimensional representations of organic fouling growth after it was trained to simulate both the development of organic fouling and the reduction of flux, as illustrated in Figure 3–10. The DNN model outperformed the prior mathematical models in terms of the accuracy of predictions. For fouling increase, it achieved an R^2 of 0.99 and RMSE of 2.82 μm ; for flux reduction, it achieved an R^2 of 0.99 and RMSE of 0.30 $\text{Lm}^{-2}\text{h}^{-1}$. According to the model, both cases exhibited a comparable pattern at the initial phase of fouling development, while distinctions in the patterns surfaced in later stages. Therefore, the model has demonstrated its capacity to deliver estimations of fouling growth with reasonable accuracy, at least for short-term projections.

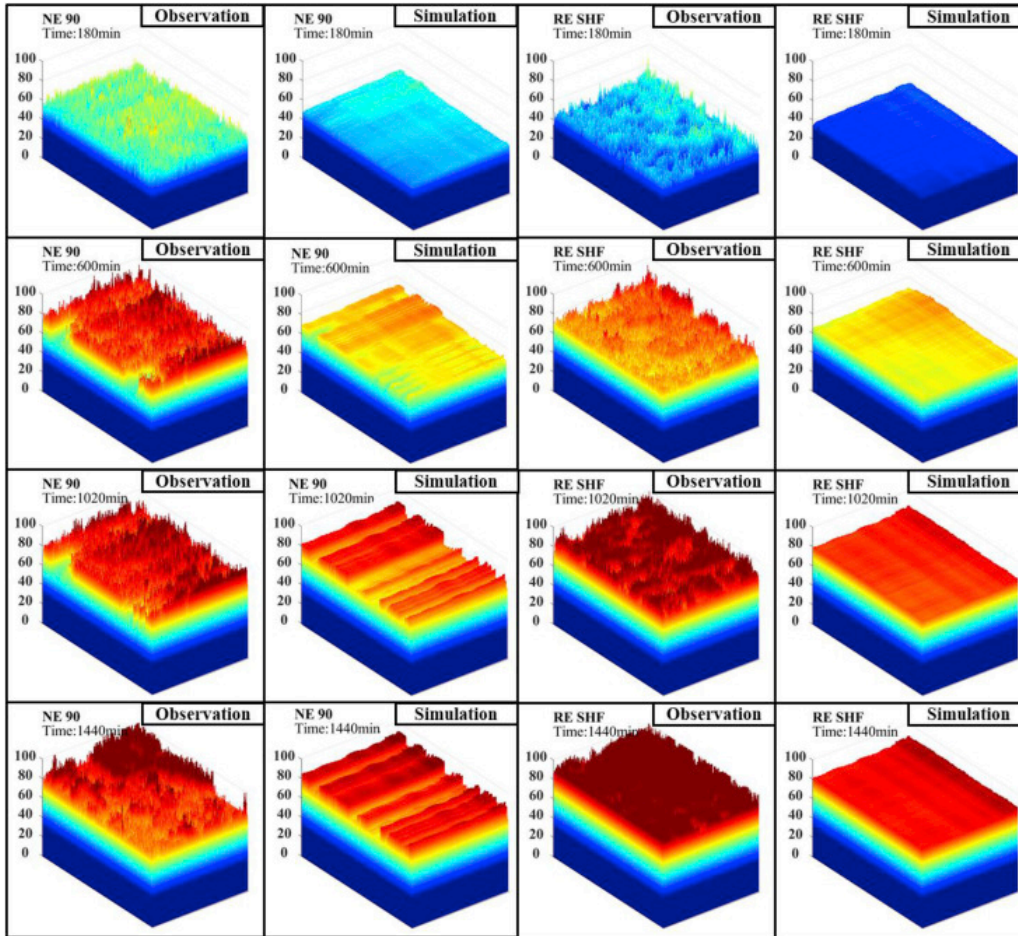


Figure 3–10: Comparison of 3D simulated and observed fouling images regarding thickness estimation for NF membrane (NE 90, Toray, Japan) and an RO membrane (RE SHF, Toray)[169]

The synergistic integration of AI and desalination and water treatment technologies has sparked great interest in recent years, holding significant promise for predictive and classification applications in certain areas of the field. Nonetheless, while initial results in some areas have been encouraging such as algae and membrane morphology, the majority of the aforementioned findings on RO performance could be anticipated by virtue of the well-established and accurately modelled underlying engineering principles, rendering conventional approaches sufficient for this purpose.

3.4 Challenges of Adapting AI in Water Technologies

The integration of AI into water treatment technologies presents substantial obstacles in achieving sustainable operational efficiency. The following discussion explores the limitations between these two sectors based on recent publications and observations.

The adoption of ML algorithms faces limitations attributed to their inclination to deviate from intended outcomes in response to unanticipated changes. For example, the effectiveness of ANNs is contingent upon the quality of input data, which may lead to imperfections in their prediction processes under specific circumstances. Furthermore, the reproducibility of ANNs is unsatisfactory as the weights and biases among neurons tend to converge upon suboptimal solutions arbitrarily [226].

In engineering fields, the abundance of available data obtained from instruments and sensors is a commonality. However, this is not the case for the water treatment industry. The lack of annotated, informative datasets in the water sector presents a challenge for the precise application of AI and ML in optimising water treatment technologies, such as desalination. Many water treatment and desalination plants are operational worldwide and generate large volumes of observed data. Water utilities receive data from supervisory control and data acquisition (SCADA) systems, such as flow statistics, online monitoring, sensor measurements, dissolved oxygen (DO) measurements, and air flows, as well as data from laboratory information management systems (LIMS) and computerised maintenance management systems (CMMS) [227]. Although this data provides significant insights into fundamental operations, it is commercially valuable and not readily available to the public. Consequently, most of the available data originates from small-scale experiments conducted in different studies. This compromises the precision and reliability of any ML models developed. Therefore, having effortless and uniform access to data from existing plants that are operational could significantly improve the application of AI and ML in the sector.

In the field of engineering, data collection involves various methods. Three commonly adopted techniques include retrospective studies, observational studies, and designed experiments. Retrospective studies employ historical data collected from various research studies to examine the relationship between variables [228]. However, such studies may include irrelevant information and overlook critical data, rendering the approach inappropriate for data collection related to a specific problem or relationship. Thus, it is crucial to ensure that retrospectively obtained data is still applicable to the case and that the objectives to be achieved are not significantly different to avoid inaccuracies. Moreover, different experiments, tasks, and businesses may require distinct approaches to data collection, including real-time analysis or the selection of the most accurate data collection and transmission intervals. Setting the appropriate time interval in data collection is crucial, as long intervals might compromise capturing the changes occurring while running the experiments, or shorter intervals can

overload the system with a large amount of data. Sampling frequency should be representative of system and seasonal changes.

In the domain of data collection, sensors have a strong contribution to the quality of data. The type of sensor selected for a given application has a direct impact on the accuracy of data collected and the data cleaning process. Failure to use an appropriate sensor type can result in erroneous data that requires additional cleaning steps. Additionally, sensors are susceptible to malfunction, resulting in the collection of irrelevant or irrational data. Over time, sensors may experience drift, which can lead to a drop in sensitivity and reading capability [229]. Occasionally, sensors may collect incorrect or missing data without an obvious explanation. In such cases, the researcher must use common-sense judgement to determine whether the error is due to sensor issues or other factors related to the experiment setup. The use of appropriate sensors is critical for the smooth operation of desalination facilities. Taweelah, a desalination plant located in the UAE, utilises more than 300 sensors, including specialised sensors designed to function in brine [230]. To ensure reliable data collection, regular cleaning, calibration, and validation of these sensors are necessary. However, this can be a costly process that may hinder the development of advanced AI and ML techniques.

Insufficient data quality is a common issue that manifests through numerous defects such as missing data, inconsistencies, errors, repetitions, and age, which reduces the credibility and reliability of data for decision-making. Despite advancements in computing technologies, many organisations still struggle with data quality issues that have persisted for years. The acquisition and upkeep of precise consumer data require substantial time and labour investments. It is also challenging and costly to combine customer data from different sources, resulting in data silos and duplications. Organisations often overestimate the quality of their data and underestimate the consequences of its shortcomings. Misleading data can have severe repercussions, including project cancellations, revenue loss, strained customer relationships, and customer churn. According to a report by the Data Warehousing Institute (TDWI), inadequate data quality costs American businesses an estimated \$700 billion annually [231], in 2016 IBM estimated that these data cost \$3.1 trillion [232]. Hence, it is imperative to recognise the consequences of planning, implementation, and long-term of AI technologies in operation of desalination and water treatment plants.

The quality of source water can be influenced by the environment surrounding it. Researchers have extensively investigated the seasonal variations in water quality parameters, fouling deposition, and operation costs of desalination plants [233], [234], [235]. Such applications

demand a dataset that captures all changes occurring throughout the year. For example, in an attempt to estimate trihalomethanes (THMs) in drinking water, Mahato and Gupta [236] evaluated the applicability of three different models, namely neural networks, SVM, and multivariate linear regression. Data from five major water utilities situated in distinct states across India was gathered for two seasons: pre-monsoon (PrM) and post-monsoon (PoM). The data were divided into two sets, PrM and PoM, for model development and validation, respectively. However, the results of the study revealed that the models failed to accurately predict the THMs, which necessitated a change in approach. Consequently, separate models were constructed to predict THMs for each of the two seasons, PrM and PoM. This study underscores the significant impact of dataset size, quality, variety, and structure on the performance of ML and AI models.

It is essential, that in the field of ML, model performance should be optimal and maintained to perform well throughout the stages of development, testing and production. This requires a training dataset that accurately represents the actual datasets that the model is expected to encounter. In the context of algae classification, it is estimated that there are anywhere from 30,000 to over a million species, with diatoms alone comprising over 200 thousand species [237]. The classification of these algae species is based on their distinct characteristics and environmental factors. However, the parameters used to differentiate these species can vary depending on the study, including the location of the area analysed or the source from which the data was collected [217]. This introduces the possibility that ML models may not capture the relevant information needed to generalise and accurately predict new data if the training dataset is not comprehensive enough or if important parameters are omitted. Additionally, different governing bodies may have different strategies and specific parameters for collecting data. These strategies may not capture the correct information that can help ML develop a model that can generalise or predict accurately when given new data.

Another limitation is that ML and ANN models are time-consuming and require a large amount of data to be able to give an accurate estimation [226]. Insufficient data may lead to a poorly fitted model, resulting in underfitting or overfitting. Over-constrained and under-constrained models will result in underfitting and overfitting of a small training dataset, respectively. Therefore, both conditions have poor performance. In a study, Zhang *et al.* [238] carried out an investigation on whether the water quality of the source has an influence on the water production capacity of drinking water treatment plants using a hybrid statistical model named HANN that combines ANN and GA algorithms. Four hundred and ninety-eight datasets from

45 DWTPs were used to train the model; however, the result showed that feeding more training datasets significantly increased the model's prediction from 0.71 to 0.93 (R^2) [238].

The processing of an extensive dataset typically necessitates the use of specialised data storage techniques or cloud computing. Nonetheless, large subsets can complicate infrastructure building and lengthen training periods. Processing very large quantities of data or records might likewise take very long periods of time [239]. In another study, Rocchetti *et al.* [239] attempted to predict the failure or replacement of water meters using a recurrent deep neural network. The work involved 15 million readings collected from one million water meters across North Italy to train the model. The comprehensive dataset resulted in nonpositive prediction due to poor attention given to the quality of analysed data [239]. Therefore, a new methodology was established based on new semantics that were enforced on the training data. This allowed only representative samples of the complicated phenomena of faulty water meters to be extracted. By utilising data sets of the appropriate size and diversity, ML models' efficacy in the water domain can be improved.

ML holds great potential for identifying pipe failures, but its accuracy in prediction is currently hindered by challenges associated with the data's nature and complexities linked to imbalanced data, as well as various components associated with the cause of pipe failure. Studies [200], [203] demonstrate that characteristics such as age, material, length, and diameter play a critical role in predicting pipe failure. The other environmental and operational factors utilised for modelling were found to be irrelevant throughout the studies. However, it is important to note that each material has unique properties that contribute to pipe failure and distinguish it from other pipe materials [240], [241]. Fault detection and anomaly detection also involve a significant amount of unbalanced data due to the likelihood of fault occurrence. Consequently, the precision of ML models may be reduced, particularly in comparison to conventional management techniques. Before applying ML algorithms, it is important to consider additional factors to prevent poor fault prediction for pipe failure, detect anomalies, and select input parameters that can capture the correct relationship.

The water treatment process is vulnerable to the risks associated with AI's unexplained aspects. A lack of transparency and explainability in an AI system, for instance, can make it difficult for operators to grasp how the system is generating decisions and spot any faults or biases it may have. There is also the risk associated with data breaches and cyberattacks if the data used by the AI system is not adequately protected. To mitigate risks while maximising advantages,

the desalination and water treatment industries must apply AI in a transparent, explainable, and ethical manner.

In conclusion, despite the significant progress accomplished in applying ML to water treatment and desalination technologies, several challenges still remain to be addressed and overcome before these models can be effectively implemented in real-world settings. One of these challenges concerns the lack of exposure of these models to actual operating conditions. Due to variation in demand by consumers as well as other factors, desalination and water treatment facilities face major impacts, and in turn affect the performance of ML models. It is necessary to test models with real-world scenarios to determine the validity and optimal deployment of such models. Furthermore, it is important to consider user-friendliness of the model; researchers must aim to develop easily accessible tools for their utilisation by operators of water treatment systems. To this end, the ACCIONA [242] company's AI initiative in the Umm Al Houl desalination plant provides a promising example of how ML models can be implemented in a practical context. The Maestro AI platform processes operational data in real-time, allowing for predictive, autonomous, and continuous optimisation at scale, which in turn lowers operational costs while simultaneously improving output, plant dependability, and water quality. However, there is no clear documentation regarding the followed approach and the advancement of the model in the desalination plant. At this stage, it remains unclear how the operators of treatment systems can utilise these introduced models to improve the performance of treatment systems.

3.5 Research Gap and Problem

Desalination technology is a continuously growing approach in coping with water supply shortages in many regions of the world [36], [243]. The establishment of a desalination plant is a complex and extensive process in selecting the most suitable system configuration given the environmental and economic conditions to deliver both a sufficient and a sustainable supply of clean water [40], [204], [244]. There is a lack of a standardised approach in this selection and design process. Consequently, there is a need to develop a standardised approach with user-friendly tool support to enable system design that takes account of site-specific conditions and that is flexible with regard to data availability limitations commonly seen in the sector. AI and ML tools have not been utilised to their greatest capability to potentially create an algorithm that would factor in multiple aspects and parameters in the design of a desalination

plant employing the most appropriate and cost-effective technology suited to the region and its needs.

Several academic publications [30], [36], [46], [245], [246], [247] have researched the theoretical and practical aspects of the key stages in the SWRO process: the intake system, pretreatment, RO, and posttreatment stages. However, there is an absence of tools that can effectively establish connections and dependencies between these sub-systems and other influential factors, including water quality, geographical features, environmental considerations, technical constraints, and the other potential challenges faced by the available technologies. . Figure 3–11 shows some examples of possible configurations of these sub-systems. It is not currently possible to represent, and interrogate, the entire desalination system with all its inherent interdependencies and complexities; this research seeks to address that gap.

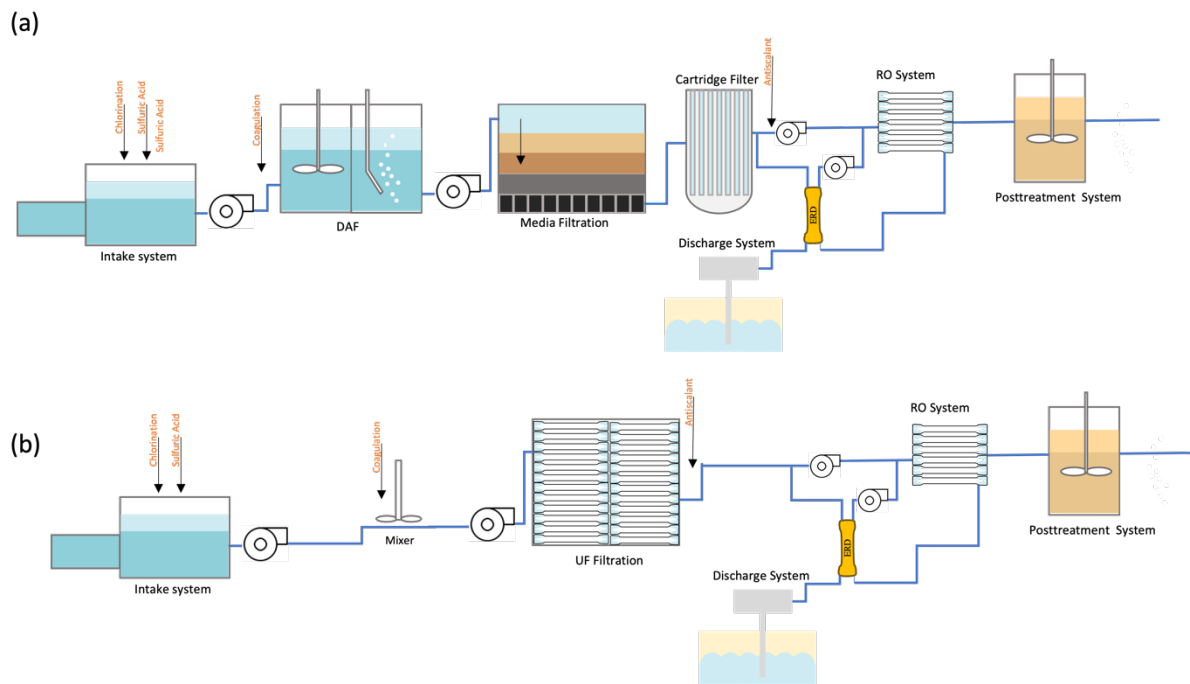


Figure 3–11: Examples of different possible configurations of SWRO desalination plant

The literature research (Chapter 2) indicates a gap in the field of life cost analysis for SWRO desalination plants. The current tools exhibit several constraints, which can be attributed to either their outdated structure or their reliance on empirical data. Outdated tools may not accurately reflect the current technological landscape and advancements in SWRO desalination. On the other hand, tools based on empirical data may lack the capability to provide a detailed and comprehensive understanding of the various cost factors involved in SWRO desalination plant design and operation. There is an opportunity to enhance the current

life cost analysis tools that can effectively handle the complexities of SWRO desalination processes. This tool should take into account many elements like advancing technologies, operational parameters, and emerging cost considerations.

3.6 Proposed Solution

A data-driven approach can provide a holistic, analytical perspective to desalination plant design. By utilising real-time sensor data, historical operational datasets, and standard rules and principles identified by previous studies, algorithms can be developed to advise on each step of the desalination design process. The inputs of water quality, location attributes, regulations, costs, and technical specifications can be used to tailor configuration process and operational parameters. As the plant operates, continuous measurement, monitoring, and optimisation guided by models further improves performance and reliability. This data-centric approach combines both domain expertise and data analytics to standardise desalination process selection and operation. It enables customisation to unique project conditions while maintaining consistency and efficiency.

In this research, a data-driven approach is proposed, using an ontology – a formal representation of concepts and relationships within one particular domain. While traditional relational data models have proven useful for capturing and organising operational data from desalination facilities, an ontological approach provides additional advantages for a comprehensive process selection and optimisation system. An ontology represents knowledge of the desalination domain as a graph of interconnected entities and rules, mirroring how human experts conceptualise information. With an ontology, the interdependent relationships between intake methods, pre-treatment steps, membrane types, post-treatment needs, and the multitude of influencing factors can be encoded, enabling more complex analytical reasoning to be performed. Therefore, a knowledge representation can be developed that ensures a common understanding of information and unified domain assumptions within the SWRO desalination plant. The main objective is to produce a standard knowledge base for modelling within the SWRO desalination domain that could be further reused for other use cases.

This research also demonstrates an intuitive life cost analysis model, implemented in Python, for designing each process and subprocess within the SWRO desalination plant. The tool will allow users to select specific parameters for the process, generating detailed designs encompassing structural aspects, operational parameters, and a comprehensive breakdown of

costs, including both capital and operational expenditures. Additionally, the tool conducts a sensitivity analysis tailored to the user's case, enhancing its functionality and adaptability.

This chapter has reviewed the relevant literature utilising AI and ML techniques to address related issues in the water treatment and desalination domains. It is clear that such technologies have great potential to improve our ability to understand, assimilate and model desalination processes with the outcome of improving the holistic design of such systems and ultimately their effectiveness and economic viability. The next chapter presents the ontology created to model the complex systems, ontoSWRO.

Chapter 4

OntoSWRO

This chapter describes the process of developing OntoSWRO and evaluates its potential utility using two distinct case studies. Section 4.1 outlines the specific advantages that knowledge modelling using ontologies offers and summarises previous work in domains related to desalination. Section 4.2 outlines the methodology used to develop OntoSWRO including the use of the Protégé tool, Section 4.3 presents the approach followed in building the vocabulary, while Section 4.4 provides an overview of the ontology, which can also be accessed online. Case studies are used to demonstrate the utility of the proposed ontology in understanding design decisions for a holistic view of SWRO (Section 4.5). The graphs presented in the cases will not cover all the detail and information that are captured by the ontology due to the limitation of size of picture and clarity. OntoSWRO is available at <http://github.com/suzannelittle/ontoswro>

4.1 Ontology

Ontologies offer a systematic and standardised vocabulary for defining concepts, relationships, and properties in a particular field. More than a controlled vocabulary, ontologies are intended to enable intelligent web-based agents to comprehend and process information [248]. This is achieved using standards to create a shared framework for expressing and capturing knowledge that is accessible to both machines (software agents) and humans [249]. An ontology is, therefore, a formal and explicit description of a domain of knowledge that enables better integration, richer search and reasoning capabilities using data.

Ontologies are typically coded using a formal language like the Web Ontology Language (OWL) and recorded in a syntax like the Resource Description Framework (RDF) [250]. This enables the description of resources (concepts) using subject-predicate-object triples to capture the relationships (predicate)[251]. OWL therefore enables the formal and structured definition of classes, properties, individuals and relationships, and supports different levels of expressivity from basic taxonomies to advanced logical reasoning. Ontologies can either be

integrated with software, e.g., for decision support and reasoning, using APIs (e.g., Owlready2) or the RDF representation can be queried directly using a query language like SPARQL (SPARQL Protocol and RDF Query Language [252]) to retrieve matching patterns [253]. Additionally, inference engines and reasoning systems employ logical rules to deduce new information from existing data, relying on the axioms of the ontology [254]. This enables the automated deduction and discovery of implicit relationships.

Ontologies provide additional functionality that enables the capturing of more expressive semantic relations, better integration by using unified concepts, rich inferencing and reasoning capabilities and the flexibility to grow and adapt data models. These advantages have been exploited in various domains related to water treatment, including water [255], [256], [257], wastewater treatment [258], [259], [260] and environmental evaluation [261], [262], [263]. Cabezut-Boo and Sánchez-Aguilar [264] constructed a knowledge base with the purpose of generating a domain ontology for waste water treatment plants (WWTP). Their attention was specifically on two technologies: an activated sludge facility and a stabilisation lagoon. Sottara [265] conducted an examination of WWTP and developed a tailored framework for the WWTP field, aiming to offer a coherent depiction of the instrumentation (including sensors and probes), actuators, and data gathering systems [265]. The objective of this study was to develop an ontology that could provide the necessary concepts and terminology for the formalisation of a domain expert's expertise in the field of plants and their management strategies. Furthermore, this technology enables the expression of knowledge in a standardised format that can be easily exchanged and utilised across various industrial facilities and their automated control systems.

In other research, a semantic framework was devised to enhance the management of water quality [266] by improving data integration options. This study involved the integration of three distinct ontologies, namely the ontology for real-time observational water quality data, the regulations ontology, and the polluters ontology, along with the incorporation of water expert rules. These individual ontologies were merged into a unified ontology, another key advantage of ontologies. Xiaomin *et al.* [267] developed an ontology model specifically tailored for the purpose of monitoring river water quality. This model aimed to describe river water quality data using semantic features, thereby establishing semantic connections among various concepts within the area of river water quality monitoring. Similarly, Grimaldi [268] proposed a data model that employs an ontological approach to cater to the distinct requirements of the Integrated Water Service (Italian Ministry of Infrastructures and

Transport). The purpose of this model is to facilitate the assessment of key macro-indicators and the creation of compatible datasets, in accordance with the specifications outlined in the ARERA resolution. This model also supports the overarching objective of the Sistema Informativo Nazionale Federato delle Infrastrutture (SINFI) to effectively oversee and supervise all infrastructure and underground utilities interventions through a unified dashboard.

4.2 Knowledge Modelling and Ontology Development

An approach was applied to utilise linked data and graph database technologies to capture the knowledge and relationships related to SWRO desalination facilities. The employment of ontologies is anticipated to yield the creation of a standardised and user-friendly model of the terminology and relationships that can be used for more complex applications. Figure 4–1 presents a graphical illustration of the phases involved in the process of constructing the ontology, highlighting the data structuring processes. Subsequently, the last step involved the translation of data to software capable of facilitating the creation of the ontology structure. Section 4.3 explained in detail the type of information that were gathered to develop OntoSWRO.

The initial phase (1) of developing the SWRO ontology was the gathering of a substantial and diverse array of pertinent material from reputable sources. Thorough research was conducted on each sub-system and process of the desalination plant, encompassing a comprehensive examination of all relevant aspects, including scientific and engineering first principles models. Following this, a preliminary brainstorming session was conducted to capture specific details related to these processes (2).

Subsequently, the data was systematically arranged into numerous tables to combine relevant parameters (3). However, the utilisation of tables as the primary form of visualisation presented difficulties in comprehending the interconnections and integration between these processes. Additionally, it was challenging to establish the necessary data properties, relationships, and categories.

As a result, a diagrammatic approach was employed, wherein each class was represented as nodes and their interconnections were indicated by arrows Figure 4–1 (4). The meaning of each arrow and the arrangement of information beneath these nodes were carefully established. By following these steps, a thorough examination of the existing data, its interconnections, and any gaps in the connection between data and processes was conducted. This approach

facilitated the identification of further data that required collection. During this phase, the vocabulary and taxonomy of the SWRO ontology were systematically organised and structured. The process encompassed the establishment, grouping, and optimising of relations and data properties and determining which elements should be classed as classes and which should be designated as data properties.

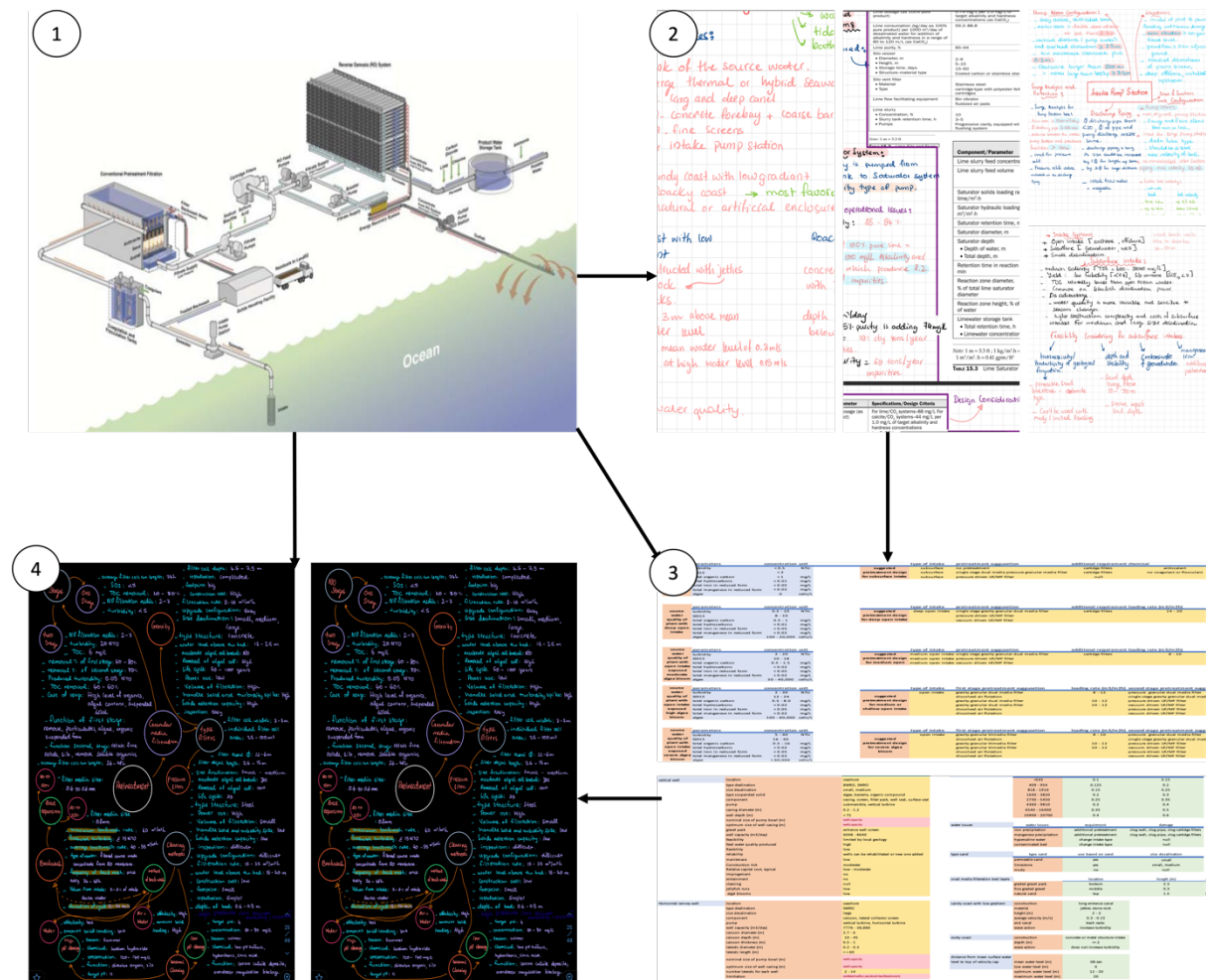


Figure 4-1: Phases involved in data structuring processes. 1. Data gathering, 2. Brain storming 3. Structuring the data into table and 4. Organising the data into node and relationship.

Protégé (version 5.5.0) is an ontology editor and framework that is freely available and open-source. The purpose of this tool is to facilitate the development and administration of knowledge frameworks [269]. This feature is particularly advantageous for tasks related to semantic web development, knowledge representation, and ontology modelling. The software offers a comprehensive platform that enables users to establish definitions for concepts, entities, relationships, and constraints within a structured framework. Protégé is equipped with the capability to accommodate a range of ontology languages, one of which is OWL [270].

Protégé was used to create nodes and relationships, where each node represents an entire sub-system or process of the desalination process, and within each sub-system are multiple nodes representing the parameters and factors associated with those. The classes generated in Protégé were structured in a manner similar to Figure 4–2 and up to Figure 4–6. The various colours in these diagrams indicate the distinct categories of parents and children within the hierarchical structure of the desalination ontology. This structure facilitates understanding of the ontology, ensuring that users from diverse backgrounds may easily grasp the logical progression.

In this research, the ontology structure developed, referred to as OntoSWRO, was rigorously validated and assessed within Protégé. Due to challenges in acquiring detailed design information for large-scale implementations, real-world desalination cases at a smaller scale were utilised as the basis for evaluation. To thoroughly test the capabilities of OntoSWRO, three specific cases were constructed. These cases were designed to reflect complex scenarios that a desalination plant might encounter, allowing observation of how the ontology could handle these challenges and offer feasible solutions.

To carry out the evaluations, various features and tools available in Protégé were employed. These tools enabled effective simulation of the scenarios and analysis of the ontology's response to each situation. The specific tools and methods used in these evaluations are detailed in Section 4.4, where it is explained how each feature contributed to the assessment process and helped validate the functionality and applicability of OntoSWRO in practical settings.

4.3 Vocabulary Development and Data Structuring

This section will provide an overview of the steps involved in the development of the ontology, with a specific emphasis on the vocabulary and knowledge that were examined and acquired. The data collection procedure started by aggregating data from many sources, including a variety of relevant books, papers, and other scholarly works. The primary emphasis was placed on the examination of water quality and the many equipment choices available for each step of SWRO desalination. These sub-systems and processes include the intake system/discharge, pretreatment, chemicals, RO, and posttreatment as illustrated in Figure 3–11.

4.3.1 Scale of Desalination Plant

The size of a SWRO desalination plant can be categorised into one of three scales: small, medium and large. Studies and books have varied in their classifications of desalination plants in terms of their scale (i.e. providing different range definitions for the terms small, medium or large). Based on an extensive survey of existing research [87], [271], [272], [273], [274], a small-scale desalination plant is defined as a capacity under 5000 m³/day, medium scale capacity ranges between 5000 and 80,000 m³/day and any capacity above 80,000 m³/day is regarded as large scale.

4.3.2 Intake and Discharge Sub-systems

The design of the intake system plays a crucial role in determining both the quantity and quality of the feed water. It is essential for this design to strike a balance between the requirements and priorities of the local community and the surrounding ecology. The factors considered are: site circumstances, technology options, permit requirements, environmental implications, stakeholder values, and utility limitations and interests [204]. This research was placed on examining the factors of site circumstances, technology alternatives, and environmental implications. This choice was motivated by the recognition that regulations and contractual agreements pertaining to desalination may vary across different countries [275], [276], [277]. The same approach was implemented for the discharge process. The permissible maximum of salinity concentration that can be discharged into the sea differs across different countries, resulting in varying regulations and permitting processes.

Constructing the ontology for the intake system entailed the collection of an extensive array of data points, including several facets of the system's design and operational as depicted in Figure 4–2. The information encompasses several aspects linked to water intake, including water quality, geographical coordinates, desalination scale and type, TDS levels, depth, performance metrics, environmental effect evaluations, and accessibility for cleaning and maintenance [204], [272], [273], [278], [279], [280], [281].

Furthermore, comprehensive data was gathered pertaining to the screen component of the desalination plant [282], [283], [284]. This data encompassed the scale of the plant, the type of screen utilised, the type of intake employed, the precise location and orientation of the screen, its installation position, its function within the system, the specifications of its mesh (including opening, width, and length), its head loss characteristics, the accessibility for cleaning purposes, the flow rate it can accommodate, and any distinctive properties that set it apart from

alternative screen options. In addition, the pump station [278] [30] entails other significant aspects, including the type of intake, its position, the depth of the well, the layout of the intake pump, the advantages it offers, the dangers associated with corrosion, the maintenance requirements, the types of pumps utilised, and the provisions for accessing maintenance. Within the domain of chemical systems, pertinent details comprise chemical dosage and concentration, duration and frequency of administration, as well as the desired aim of the chemical treatment.

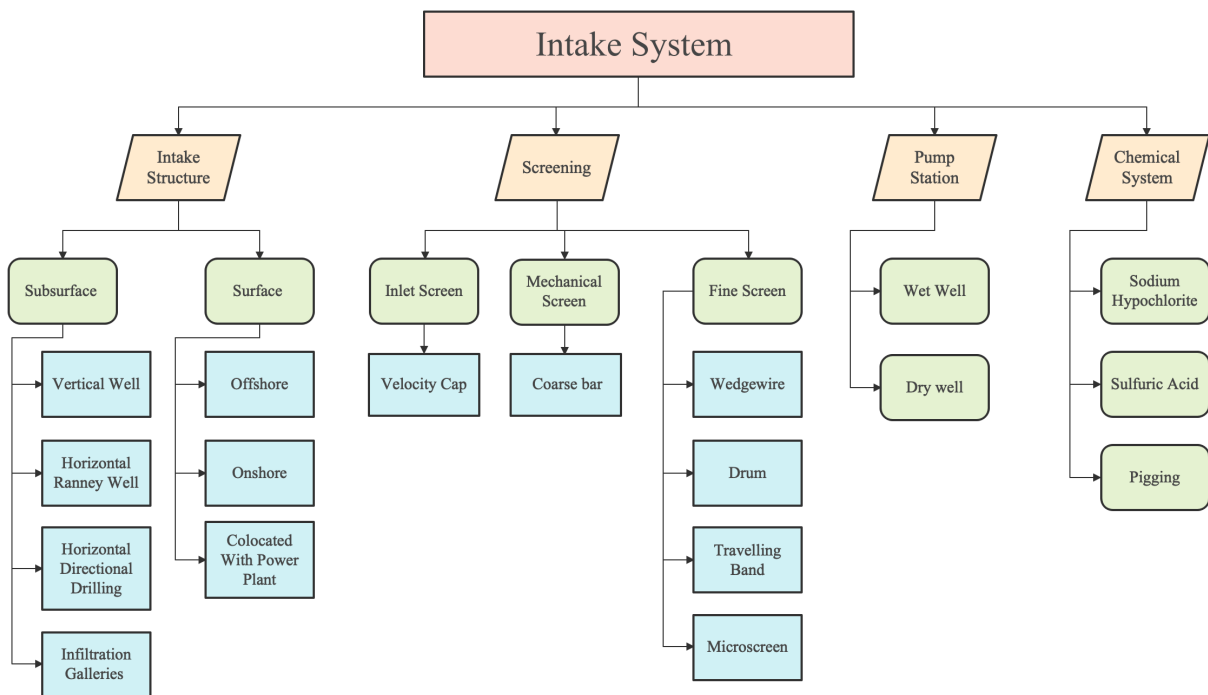


Figure 4–2: Intake system structure

A discharge system may use various methods for the disposal of brine. However, the selection of these methods (shown in Figure 4–3) has been restricted to three prevalent processes that manage the salinity levels of brine. The ontology related to the discharge management system was developed through the compilation and organisation of a dataset. The dataset included important data such as the discharge system type, brine concentrate characteristics, brine quality parameters, desalination operation scale, environmental impact assessments, geographical locations, design criteria, outfall pipe specifications, outfall diffuser features, maintenance requirements, dilution processes, water quality considerations, and TDS measurements [285][286][30].

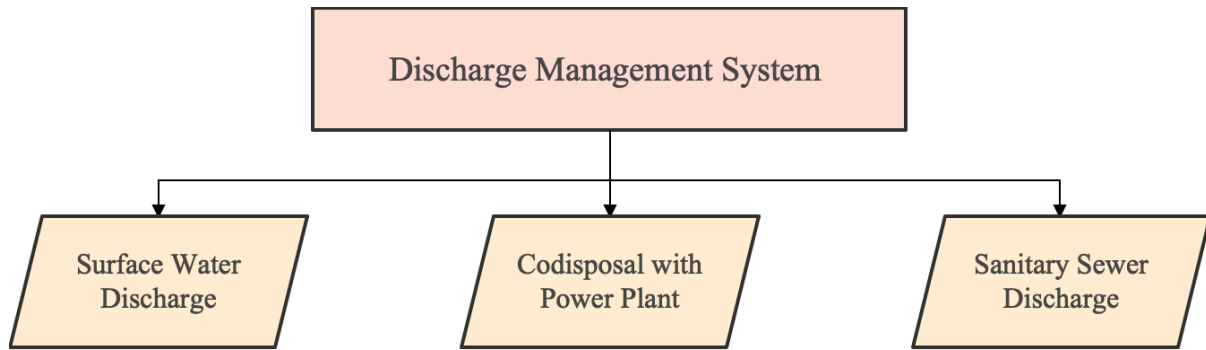


Figure 4-3: Discharge management system

4.3.3 Pretreatment System

The process of constructing the ontology for pretreatment involved the systematic collection and arrangement of a comprehensive set of essential data points. The aforementioned factors encompassed various critical parameters pertaining to water quality, the influence of intake type on pretreatment processes, the scale of desalination, functional aspects, design specifications, chemical classifications, maintenance procedures, cleaning protocols, surface loading rates, performance metrics, the number of filter cells, flux characteristics, supplementary prerequisites, and other criteria. In addition, these criteria included considerations such as the composition of the filtration media layer, its dimensions, thickness, elevation, and the effective size for filtration media. The provided information encompassed many aspects such as flow rates, loading rates, diameters, and backwash procedures, among other relevant characteristics [40], [245], [271], [287], [288], [289], [290], [291], [292]

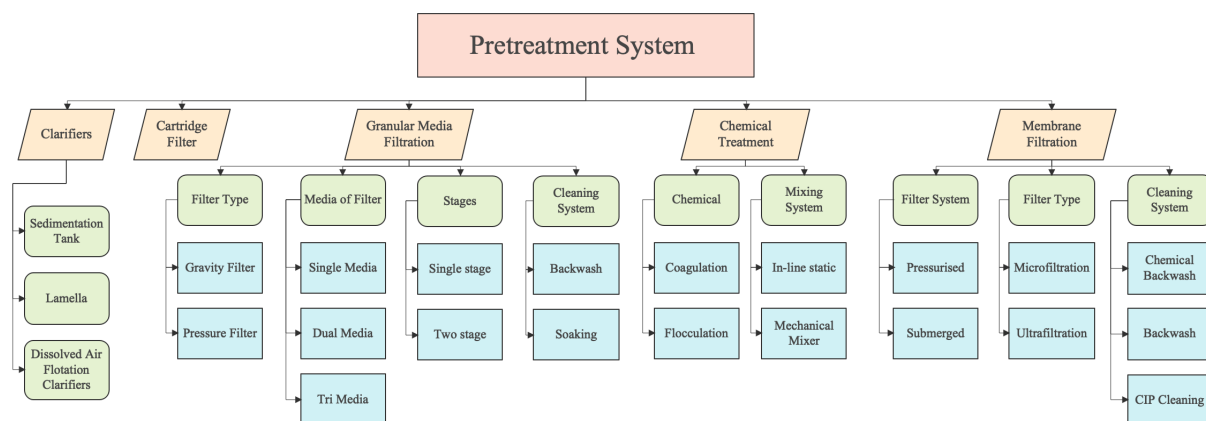


Figure 4-4: Pretreatment system structure

4.3.4 RO System

To develop the ontology for RO, a comprehensive set of data points was gathered and organised. These data points encompassed various aspects of the RO system, including information on the filtered transfer pump (such as its type, location, operating pressure, and performance), the high-pressure pumps (covering details such as type, capacity, efficiency, location, and other relevant factors), the RO elements (including configuration, flow rate, rejection, water quality, and various membrane specifications), the pressure vessels (including information on pressure and material type), the RO system piping (with considerations for quality, salinity, and other relevant factors), and the energy recovery devices (ERD) (encompassing details such as type, efficiency, coupling position, working mechanism, and footprint).

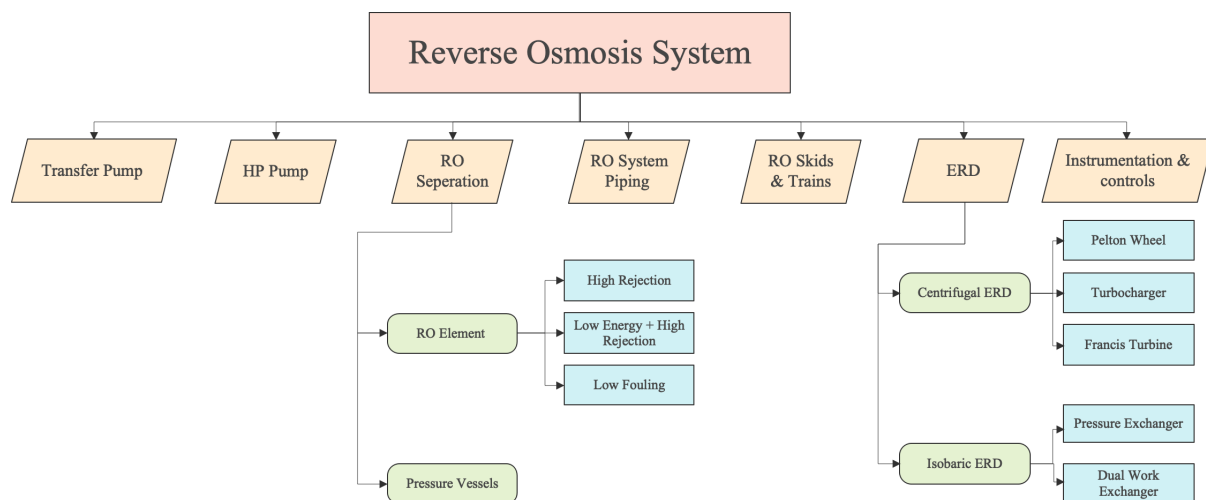


Figure 4–5: RO system structure

4.3.5 Posttreatment System

The posttreatment sub-system consists of two distinct steps, namely remineralisation and disinfection. This system took into account and examined various factors to acquire a comprehensive understanding of the underlying processes. These factors encompassed the type of consumable, the percentage concentration and the quantity of chemical involved at each process stage, relevant chemical equations for dosing, methods to enhance solubility, cost considerations, the system's footprint, pH levels, maintenance requirements, and specific design criteria for the system [30], [293], [294].

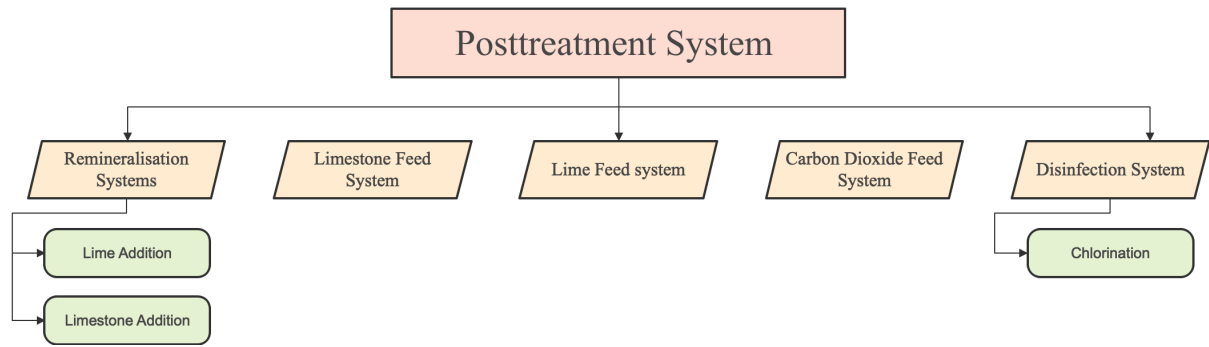


Figure 4-6: Posttreatment system structure

To augment the level of detail associated with individual classes in the ontology, data properties and object properties are employed. Figure 4-7 shows examples of object properties establishing connections between classes. Additionally, the accompanying table (APPENDIX A) give a comprehensive description of each object property, including the potential classes with which it may link. This ontology does not include specification of the domain and range for these object properties to avoid imposing additional constraints and adding unnecessary complexity to the model [295].

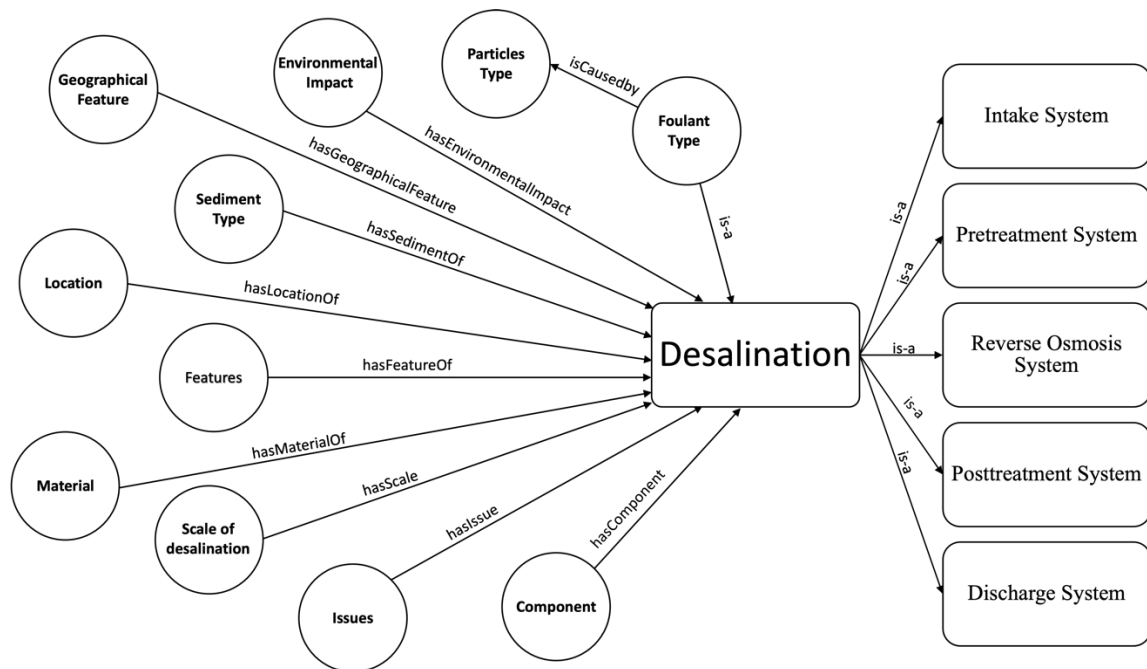


Figure 4-7: Representation of classes and relationships used to build up SWRO desalination ontology.

In the SWRO process, any vocabulary that has numerical value (float or integer numbers) and is susceptible to changes in each process or technology has been designated as a data property. The ontology encompasses a total of 120 data properties, which serve as representations for

various parameters including turbidity, temperature, depth, and so on. The logical axioms were formulated based on the data and object properties and classes.

4.4 Ontology Specification and Verification

To capture the knowledge modelled in the previous section, a formal ontology was constructed using the Protégé tool [269] and defined using OWL. The resulting ontology contains 1,991 axioms that define the relationships between entities and concepts previously identified. Of these, 1,403 axioms are specifically allocated for logical reasoning, which serves to maintain the consistency and coherence of the ontology's conceptual structure. There are 452 declaration axioms that explicitly introduce and define classes, properties, and individuals, including 306 classes that represent different concepts or categories related to SWRO desalination (such as classes shown in images in Section 4.3). The ontology includes 131 data properties (such as depth, detention time, temperature, etc) that describe attributes and characteristics of classes. There are 16 object properties that describe relationships and connections between entities or classes in the ontology (such as hasScale). This represents the highly complex interdependencies and interactions in the SWRO desalination domain. The OntoSWRO ontology is available for public access at <https://github.com/suzannelittle/ontoswro>

To examine and verify the coherence of the ontology the Pellet reasoner was used. This step was key for the ontology engineering process to guarantee the logical coherence of the defined OntoSWRO model. The Pellet reasoner performs an automatic analysis of the ontology, detecting and highlighting any inconsistencies, contradictions, or errors present in the axioms, classes, properties, and relationships of the ontology. The aforementioned procedure improved the correctness of the ontology in terms of representing knowledge, making inferences, and facilitating compatibility across different applications and domains.

The OntoGraf plugin in Protégé was utilised to visually explore the ontology, improving comprehension of its structure and relationships and aiming to improve the correctness and completeness of the knowledge capture. OntoGraf's graphical visualisation and search feature is highly valuable for understanding ontologies. By utilising the search feature, efficient retrieval of a comprehensive list of classes whilst exploring their interconnectedness within the ontology was achieved. This facilitated a thorough analysis of the relationships between classes, shedding light on the semantic connections among different entities in the ontology leading to a deeper comprehension of its knowledge structure.

OntoGraf is primarily used for visualising classes and relationships to understand data properties. Therefore, to obtain additional information about constraints and data properties associated with classes, simple queries were performed using the Owlready2 library for ontology-oriented programming in Python [296].

To verify the validity of OntoSWRO, various small cases were employed during the development of each system component. Given the challenge of finding detailed, real-world desalination scenarios that encompass all necessary data for plant design, these small cases were crucial. They ensured that the input data accurately reflected desalination knowledge and that the tool was capable of capturing this information to suggest appropriate designs.

For example, one specific scenario tested the intake system design. The test involved a plant with a capacity of 85,000 and design specifications matching those of a vertical well intake system, as detailed in APPENDIX F. Despite the expectation of a vertical well being the suggested outcome, OntoSWRO recommended an open intake system instead. This discrepancy prompted further investigation, revealing that selecting a vertical well for this capacity would likely lead to significant environmental impacts and require extensive land for the construction of the necessary wells.

Further research was conducted to understand why vertical wells are uncommon in desalination plants with capacities exceeding 80,000, as this contradicted the information found in published research [87], [271], [272], [273], [278], [279], [281]. However, no relevant studies provided details on the reasons for this choice or any operational implications it might entail. This investigation demonstrated that OntoSWRO was successful in capturing the design specifications and highlighting potential consequences of selecting a vertical well under such conditions.

4.5 Case Studies

To evaluate the utility of OntoSWRO and demonstrate the viability of the knowledge modelling to assist in holistic design of SWRO plants, three hypothetical cases studies with increasing complexity are presented that show scenarios that would be challenging to capture and evaluate without the concepts and relationships defined in OntoSWRO. This approach was necessitated by the absence of comprehensive, real-world desalination plant scenarios suitable for use in this study. As a result, these hypothetical scenarios designed to reflect realistic conditions.

The first scenario relied solely on OntoGraf, utilising the “expand” feature to establish and link relationships between classes. In contrast, the second and third scenarios involved a more intricate approach, combining simple querying and graphical representation.

4.5.1 Case Study 1

Case 1 Information:

The first scenario of a SWRO desalination system design requires a production scale of **25,000m³/day** and a recovery rate of 45%. The water quality characteristics include an **algal count** of 30,000 cell/L, a **total organic carbon** level of 0.8 mg/L, and **Silt Density Index** value of 18, **turbidity** at 20 NTU, a **TDS** concentration of 35,000 mg/L, **temperature** of 25°C and an **iron** content of 5 mg/L.

Location-specific features further constrain the design: plant site has a maximum construction depth of 40 m and is in proximity to possible ship traffic, approximately 500 meters away from the seawater source, with no nearby power plant. The geographical area is characterised by a ground transmissivity of **2000 m³/day/m**, **no space limitation**, **non-muddy terrain**, **natural wave flushing** dynamics, and the presence of **limestone** while not experiencing **beach erosion**. These essential objectives should be considered while **minimising construction costs**, ensuring a plant **lifecycle of 20** years, **low energy consumption**, **minimising solid handling** requirements, and **mitigating environmental impacts**.

Case 1 Analysis:

The initial design step involves assessing the equipment options for desalination based on the scale required. A desalination capacity of 25,000 m³/day falls within the medium scale range. Figure 4–8 displays the equipment suitable for medium-scale operations. While some of these equipment options may also be suitable for other scales, the focus of the figure is on the medium class, thus excluding other scales from the illustration. In the case of the discharge system, surface discharge is the only viable option due to the absence of a nearby power plant in the surrounding of the desalination plant.

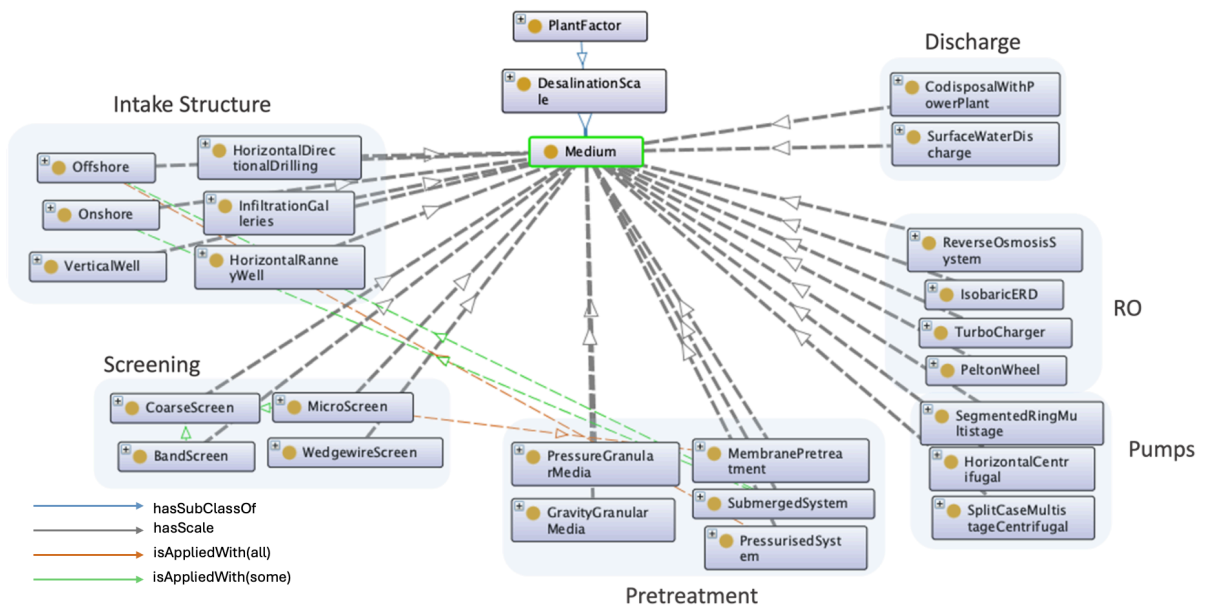


Figure 4–8: Recommended classes for Case 1

The water quality assessment indicates the presence of an algal bloom based on the turbidity, SDI and higher algal counts compared to standard seawater conditions. These values were used to identify the specific classes that exhibit these characteristics. Figure 4–9 shows how the class ModerateAlgalBloom is defined and relates to other classes (Algae, ParticlesType).

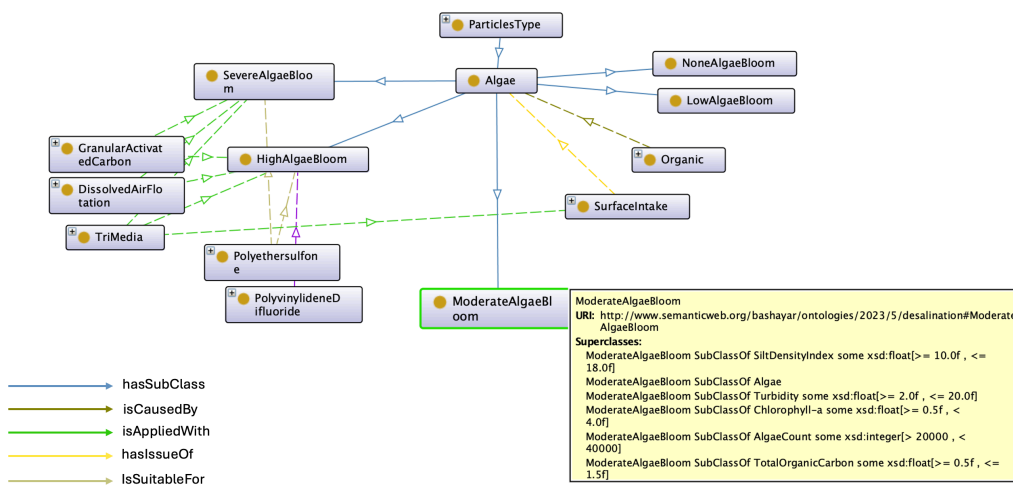


Figure 4–9: Defining specific algal bloom class from connection and data properties

The ontology analysis (Figure 4–10) suggests that the subsurface intake method, particularly the vertical well, is suitable based on the relevant geographical criteria. The high transmissivity of the land makes this approach the preferred solution, as supported by the accompanying graphical representation that highlights the challenges of this design [272]. It is important to acknowledge that the long-term sustainability of vertical well design poses inherent risks, particularly related to increased contamination risks from algae and bacteria [297].

In this scenario, chemical intake systems and screening mechanisms is considered unnecessary, resulting in decreased construction expenses (as observed in Figure 4–10). The cost-saving attribute of the vertical well mechanism is due to its inherent filtration capabilities [298]. However, it is crucial to acknowledge the elevated iron levels in the water source; therefore direct pumping of source water to the RO system can present a significant risk of membrane fouling. Pre-treatment measures are crucial for ensuring the effectiveness and durability of desalination plants [299]. The OntoSWRO proposed single media filter and cartridge filter that can be utilised for this purpose (Figure 4–10).

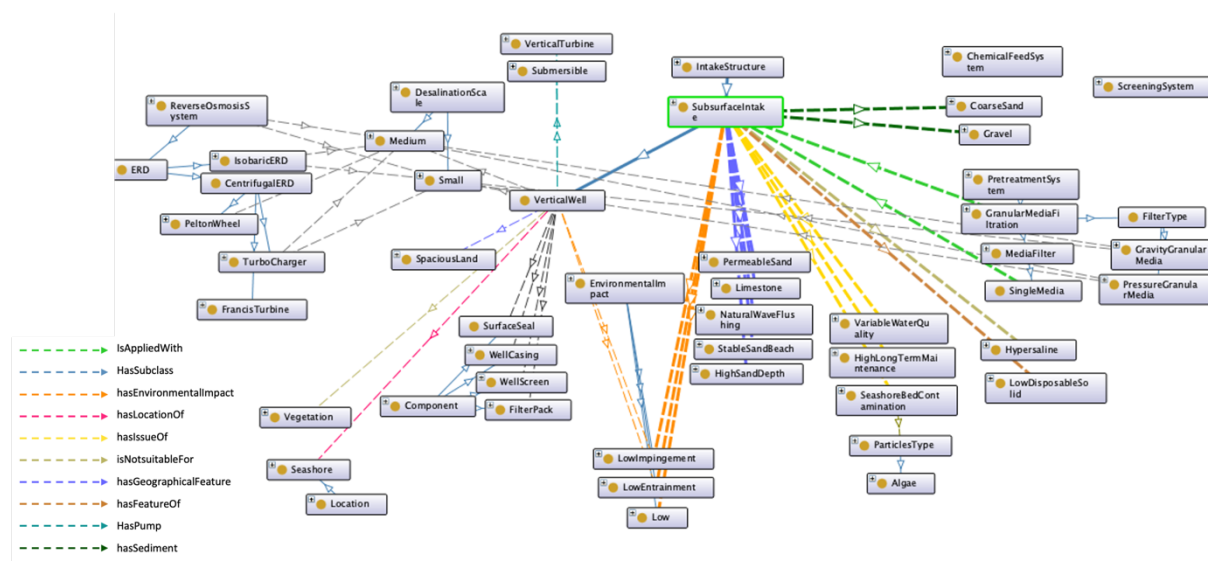


Figure 4–10: Recommended full design for Case 1

The selection of the filter type for granular media filtration and posttreatment was based on two key factors: low energy consumption and effective solids handling. This inquiry also identified two types of RO membrane elements that can be effectively used in the system. The graphical representation establishes a relationship between these elements and the low energy consumption class, denoted as “hasFeatureOf”. However, the colour of this relationship is different due to the particular class expression that was used as shown in Figure 4–11. The ‘SW30XL400’ membrane element is used for low energy consumption, while the

‘SW30HRLE400’ element has both low energy consumption and high rejection rates features. This demonstrates the advantages of using class expressions such as “some” and “only” in an ontology to specify constraints on relationships between classes. Existential quantification (Some), represented as “someValuesFrom” states that there exists at least one individual that fulfils a specific condition. The concept of universal quantification (Only), denoted by allValuesFrom, asserts that all individuals must satisfy a certain condition.

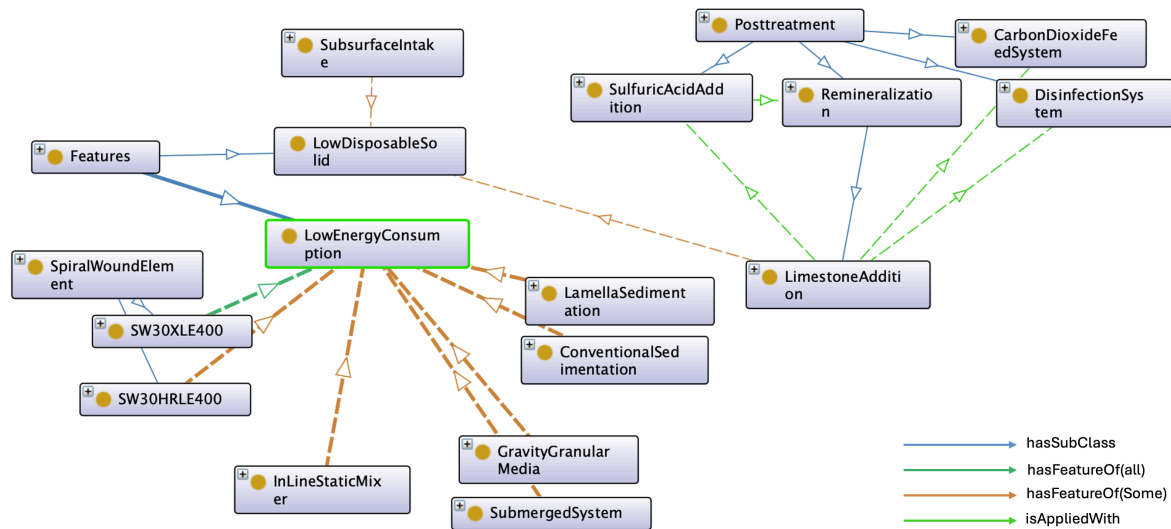


Figure 4–11: Ontology’s features in capturing class expression

4.5.2 Case Study 2

The water quality was historically studied and assessed over many varying seasons. This was carried out to capture and understand the behaviour of the water characteristics to predict any feature occurrences. This water quality in this scenario indicates an occurrences of **high algal bloom**, with an **algal count** of 48,000 cell/L, **Chlorophyll-a** concentration of $4.8 \mu\text{g}$, and particle **size** $90 \mu\text{m}$. Other water quality parameters include **turbidity** levels, which have an average value of 32 NTU and reached 100 NTU on specific occasions. The **TOC** is measured at 4 ppm, the **SDI** is 13, the **TDS** is 38,000 mg/L, the **iron content** is 0.8 mg/L, and the **temperature** ranges from 28 to 32°C . The plant is situated on a **32,000 m²** plot of land and is about **800 m** away from the **shoreline**. The plant site is an **abandoned commercial** property with an elevation of 12 m **above sea level**. The location includes **seasonal rain patterns** that contribute to water flowing from a **valley** into the sea. The desalination plant is located in a

Middle East North Africa (MENA) country. The geographical attributes include a ground **transmissivity** of 800 m³/day/m, shallow sand depth, and limited availability of land.

The desalination plant has a daily **production capacity** of 120,000 m³. Its main goals are to provide **consistent water quality**, be **easy** to maintain and operate, use corrosion-resistant materials, have a **lifespan** of at least 20 years, consume **low energy**, and achieve **high rejection** rates.

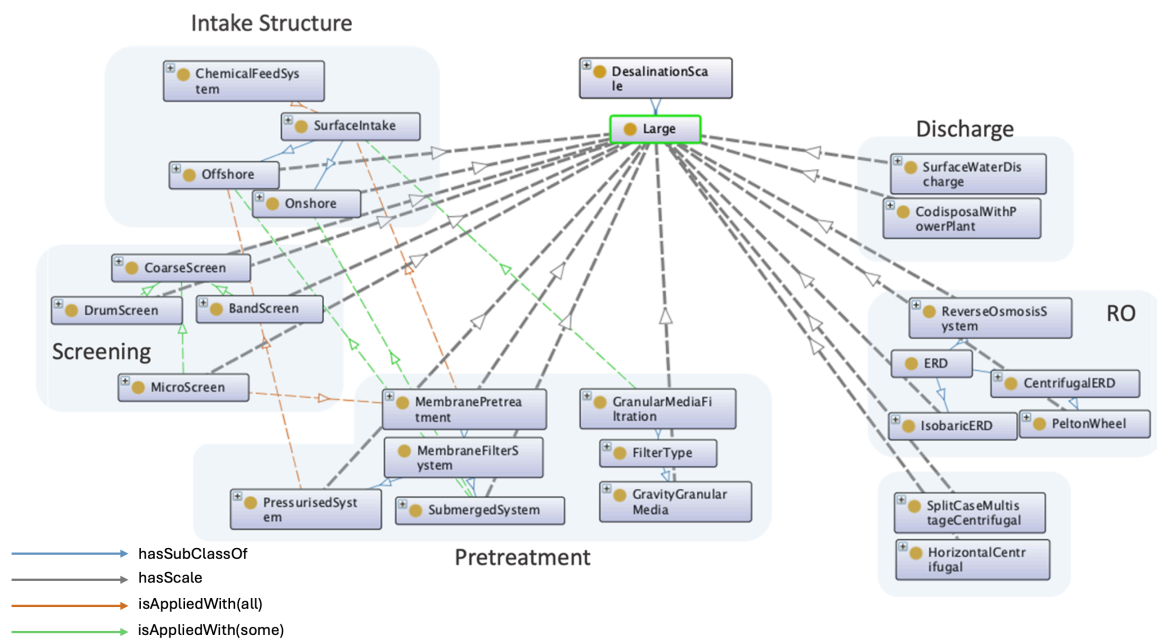


Figure 4-12: Equipment recommendation from OntoSWRO based on desalination capacity

Figure 4-12 presents a suitable equipment recommendation that is specifically designed for the scale of this particular scenario. The equipment selection approach in this context followed matrix decision-making as seen in Figure 4-13. The method entails assessing each equipment option based on specific criteria derived from the scenario's information. This evaluation determines the extent to which the options align with the requirements and their potential outcomes. The process involves systematically identifying the optimal equipment configurations based on specified parameters and desired outcomes. The matrix for this scenario is provided in APPENDIX B.

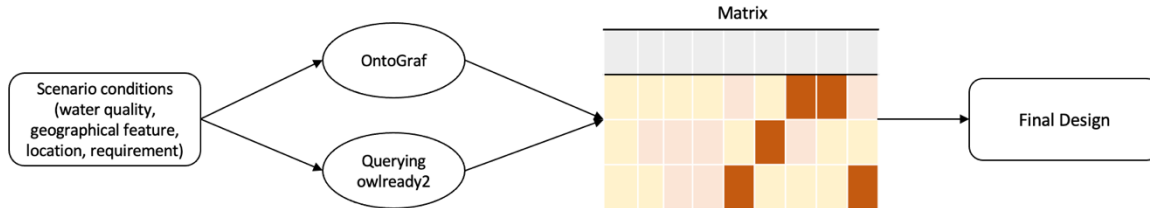


Figure 4–13: Assessing approach followed in Case 2

A visualisation of an example of the Owlready2 querying approach is shown in Figure 4–14.

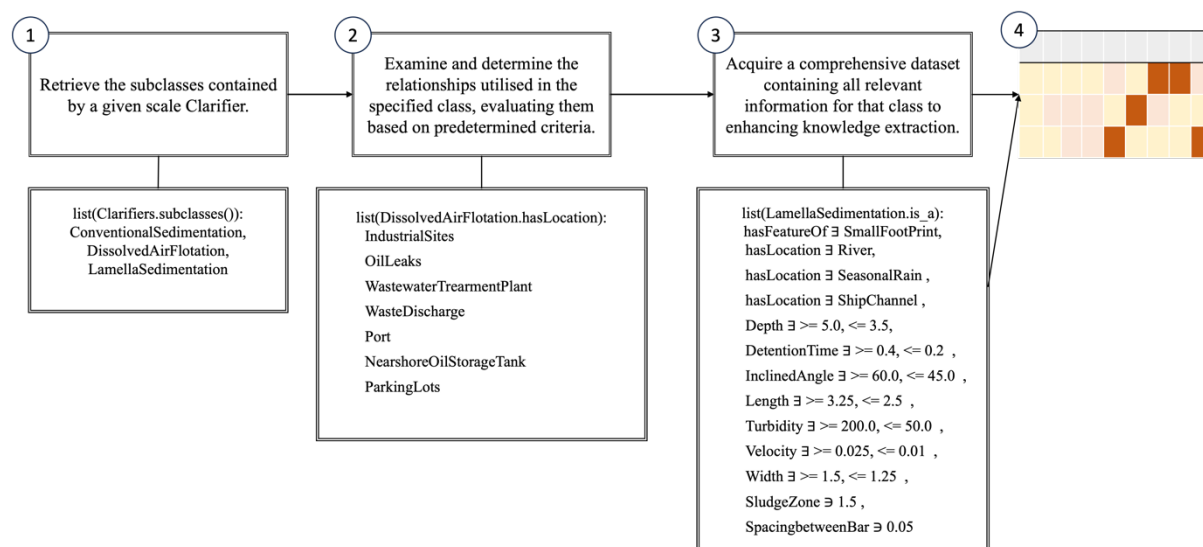


Figure 4–14: Example of steps for Owlready2 querying approach followed in this scenario

The final result showed that there are two feasible designs:

1. First suggestion: Offshore – coarse screen – band screen – dry well pump station – Sodium Hypochlorite and Sulfuric Acid – Coagulation – Lamella – gravity dual media filtration – Cartridge Membrane –Scale Inhibitors - RO system – Calcium Addition – CO₂-Chlorination – Sulfuric Acid
2. Second suggestion: Offshore – coarse screen – microscreen screen – dry well pump station – Sodium Hypochlorite and Sulfuric Acid – Coagulation – Lamella – UF –Scale Inhibitors - RO system – Calcium Addition – CO₂-Chlorination – Sulfuric Acid

Both of these designs demonstrate the capability to operate effectively, as evidenced by the knowledge captured in the OntoSWRO. When considering these scenarios, designers should

take into account the prioritisation and sustainability of the design, potential long-term concerns, and the impact of capital and operational cost to make an informed decision.

4.5.3 Case Study 3

This scenario differs from the previous two scenarios in several aspects. In this case, the process design is in its preliminary stages with limited information available regarding water quality, which is described qualitatively rather than quantitatively. The proposed design involves an **offshore intake facility**, including **membrane pretreatment, RO, and sewer discharge**, as a sewage treatment plant is located near the desalination plant. The desalination plant has a daily **capacity of 5000 m³/day** and is situated in an **industrial area**. The **TDS** of seawater is 35,000mg/L.

The **intake structure** is estimated to be approximately **1200 m** away from the sea, and there are **space constraints** that necessitate a solution with a **small footprint**. The primary objectives for this scenario are to identify the features and potential issues associated with this design and develop a comprehensive design that aligns with these considerations while providing practical suggestions.

One noteworthy aspect is the need to **minimise environmental impact** and ensure **resistance to fouling**. Although the overall water quality is good, there is a recurring issue with **oil leaks** that require special attention in the design process.

According to OntoSWRO, a daily capacity of 5000 m³ is categorised as small-scale. When the phrase “small” is queried using OntoGraf, all classes that include the term “small” are presented. Considering the requirement for a small footprint, equipment with small footprint features is shown on the right side of the figure, while equipment suitable for small scale is presented on the left side. When the figure is examined, it is apparent that all intake structures are suitable for this design. However, in Figure 4–15, it can be observed that vertical wells and horizontal directional drilling require more spacious land.

OntoGraf has limitations when it comes to visualising complex OWL restrictions, particularly those involving the “not” keyword, which represents the opposite in OWL ontologies, as shown in Figure 4–16. Visualising opposites within constraints can be challenging because it involves representing the absence of something. For instance, “hasGeographicalFeature some (not (SpaciousLand))” signifies that the class should have geographical features that do not include "SpaciousLand". The visualisation of opposites using graphical tools such as OntoGraf may

not always offer an easy or obvious approach, particularly when dealing with complex class expressions that contain embedded opposites.

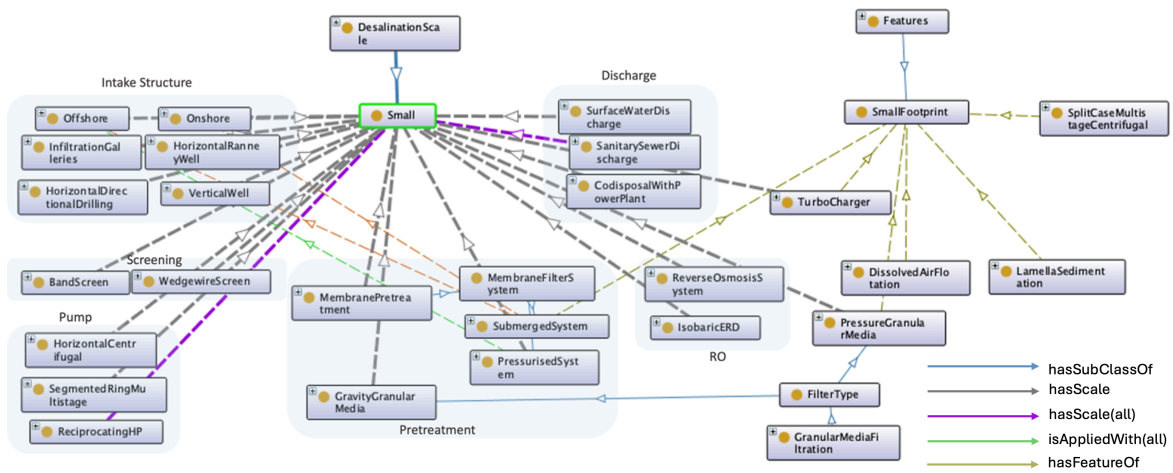


Figure 4–15: All classes with phrase “small”

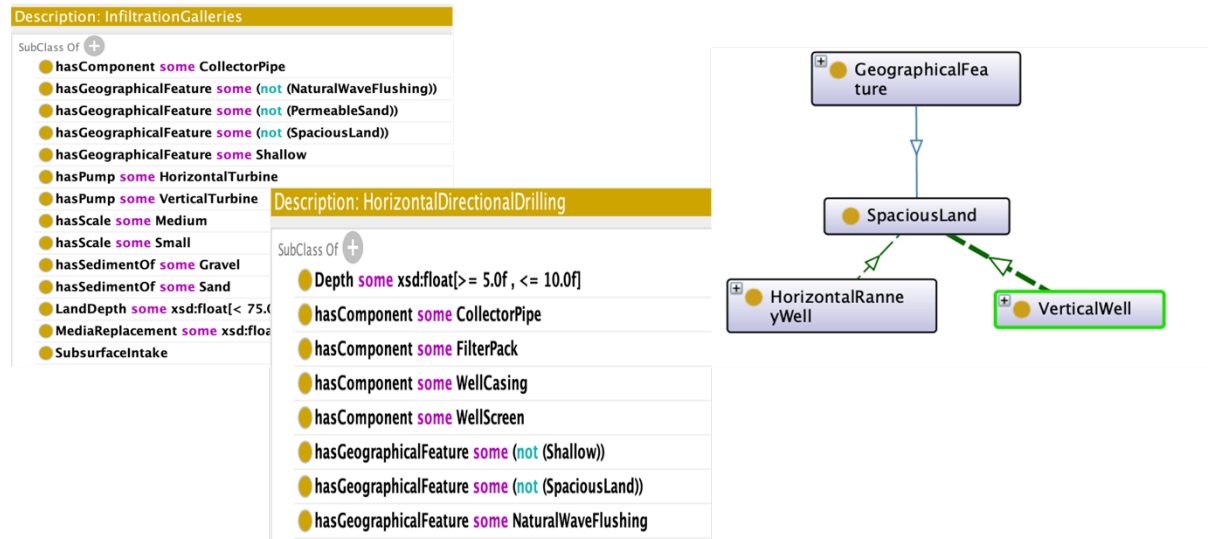


Figure 4–16: OntoGraf limitation

In the ontology “OffshoreStructure” is a subclass of “SubsurfaceIntake”, meaning the constraints associated with subsurface intakes are inherited by it. This relationship is visually represented in the Figure 4–17. The implementation of a screen system is required for an “OffshoreStructure”, including a velocity cap and a fine screen to minimise impingement and entrainment. In the context of low environmental impact, a suitable choice that meets the specified criteria is represented by the “WedgewireScreen” (Figure 4–18). Additionally, equipment such as cleaning systems, chemical systems, and mixers should be incorporated

with this structure. However, it's important to note that the lack of water quality information poses challenges related to algae. Consequently, special consideration should be given to the depth at which the intake is installed to minimise the impact of algae on the system [206].

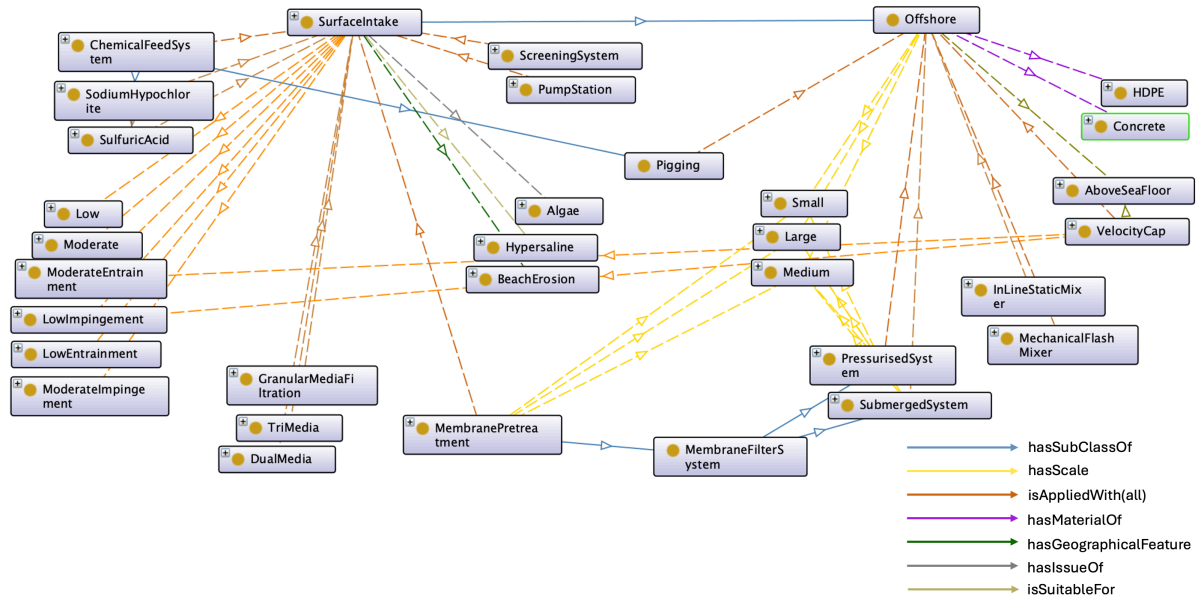


Figure 4-17: Offshore visualisation

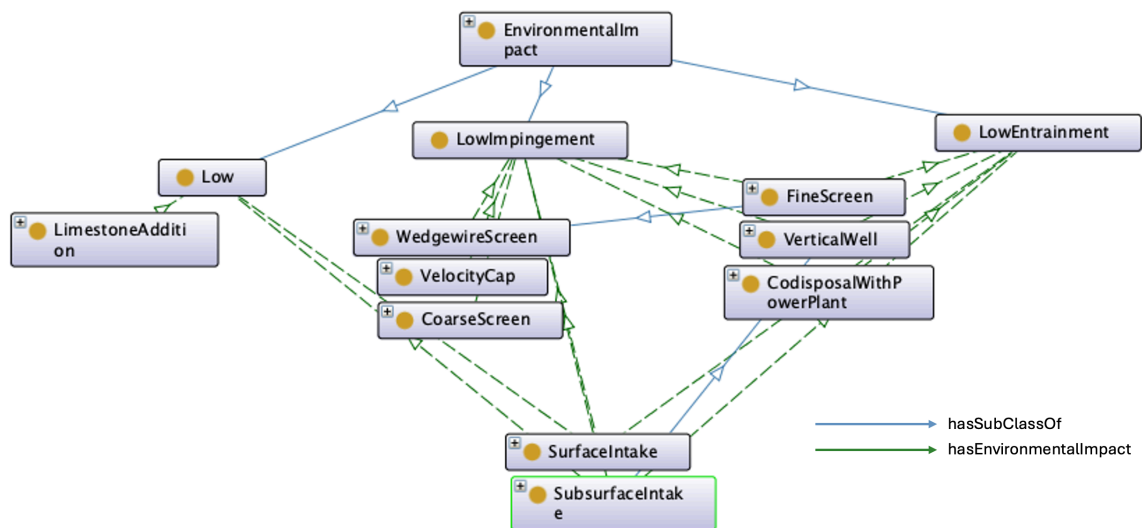


Figure 4-18: Equipment that has low environmental impact

Membrane pretreatment is one of the systems that was selected and it is an option that is suitable for this scale that can deliver good quality and high rejection. Something to be noted in that these systems must be equipped with microscreen as a fine screen (Figure 4-20) therefore the previous screening system must be updated. Membrane pretreatment have two

disadvantaged high construction cost and high energy consumption and require an extensive cleaning process. Since, there is a limitation in spaces, submerged system is more compatible with small land site, easy to inspect and consume less energy compare to the other system. However, pretreatment system cannot handle the presence of oil in water therefore it must be removed and the only process that capable for that is DAF as shown in Figure 4–20.

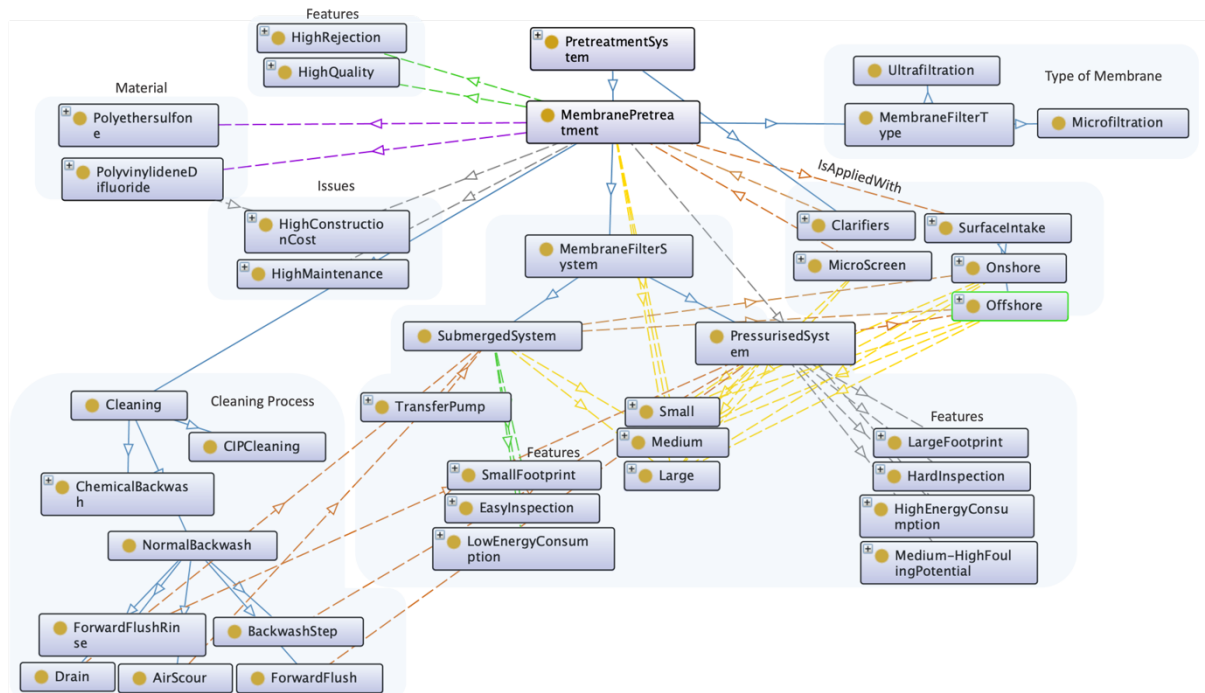


Figure 4–19: Membrane pretreatment visualisation

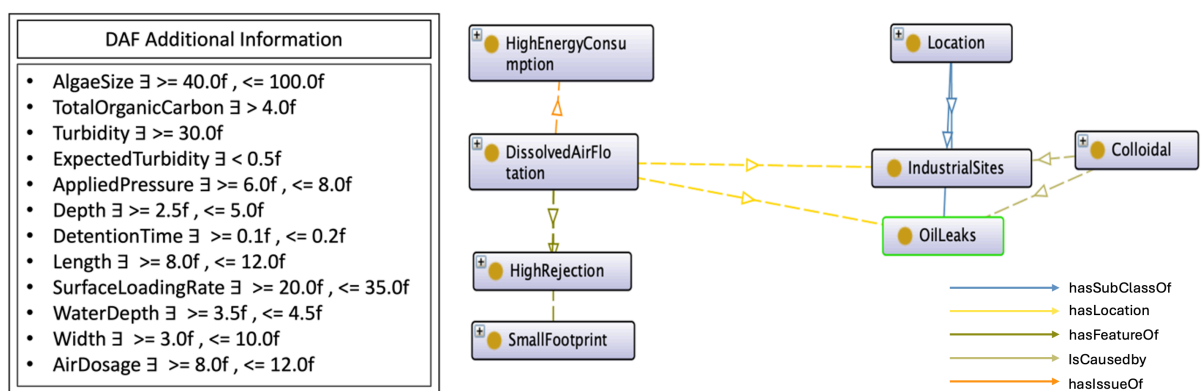


Figure 4–20: Visual representation of DAF with further details about the data properties associated with DAF

In terms of the discharge system, utilising a sanitary sewer discharge proves advantageous if the desalination plant is located in close proximity to a wastewater treatment facility, thereby

saving construction costs associated with building a new discharge system. However, this solution presents challenges, as seawater with high salinity can adversely affect anaerobic bacteria and the wastewater treatment plant. Additionally, this method is capable of handling only TDS with a maximum value of 3000 mg/l (Figure 4–21). Given that the feed seawater has a salinity of 35,000 mg/l and assuming a recovery rate of 45%, the salinity of the brine would reach around 63,000 mg/l. also, both the chlorine and sodium must be at specific threshold. Consequently, a critical consideration arises: whether the wastewater treatment plant has sufficient water to dilute this salinity or if the desalination plant needs to establish a dilution system before directing it to the wastewater plant.

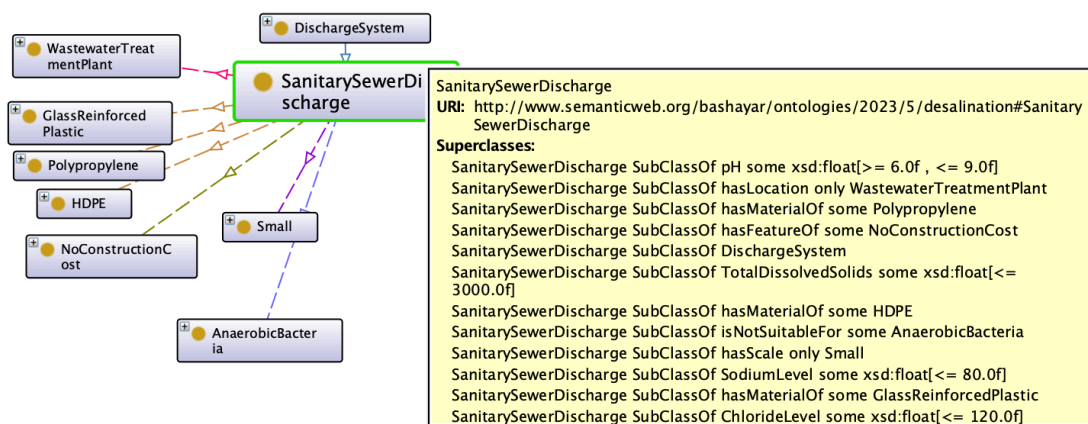


Figure 4–21: Sanitary sewer discharge visualisation

Regarding the proposed design, membrane pretreatment appears as a viable option, although its suitability for this small capacity may be influenced by the associated construction and operational expenses. The ontology facilitates integration between various processes and subprocesses, highlighting both the benefits and limitations of the solution; however, the ultimate decision rests with the user. Notably, membrane pretreatment is more prevalent in large desalination plants, with limited implementation in SWRO desalination plants. Some ontology classes feature annotations providing additional information, such as the annotation for DissolvedAirFlotation, indicating its potential coupling with GranularMediaFiltration, contingent on supplier verification for specific scenarios. Consequently, granular media filtration and DAF present an alternative solution, addressing concerns about space constraints. Notably, granular media filtration offers advantages, including low construction costs, ease of operation, and minimal energy consumption, making it a viable consideration for pretreatment in this plant design.

Based on this Case, the following conclusions should be taken into consideration:

1. The offshore design proves to be suitable for this case, yet two other subsurface intake options could also be explored if additional criteria are met. The user is advised to delve deeper into these alternatives, considering the limitations of the current scenario.
2. Membrane pretreatment is a potential implementation; however, a thorough cost analysis of construction and operation is necessary to evaluate its impact on the overall water cost. Additionally, DAF and granular media present viable alternative solutions worth considering.
3. The sewer discharge option comes with various challenges that require careful consideration by the user. It is essential to assess how these challenges can be addressed and whether this solution offers advantages or falls on the disadvantageous side.

4.6 Summary

The case studies presented here help to verify and validate the proposed OntoSWRO as a critical requirement for developing a full understanding of the design and deployment of seawater desalination plants that can take into account key considerations including geographic constraints, energy efficiency, cost mitigation and effective production of potable water. As an aid to identifying key decision points, unrealised constraints or unrecognised solutions the ontology model provides a suitable formal structure to integrate into future decision support or design systems. A challenge encountered during the construction of this ontology was the limited access to actual raw data, which necessitated reliance on literature reviews. High and low were occasionally employed to elucidate the influence of particular features or issues. The issue lies in the subjectivity of relative terms such as “high” and “low” It would be more preferable to have quantifiable definitions for these terms. For example, the sedimentation classes is characterised by low energy consumption, while another sibling class, DAF, consumes a higher amount of energy. Although this statement holds true in reality, various factors affecting power consumption make it difficult to provide a specific quantification of the energy or power consumed by DAF. The statement would vary depending on these factors, and in some cases, DAF would not be considered a high energy consumer, relatively speaking. Multiple factors should be taken into account when making the final decision, rather than relying on only one or two features.

The forthcoming chapters explore the engineering components and life cycle costs of the SWRO desalination plant in depth. By integrating insights gained from the ontology with the detailed analyses provided in these chapters, a SWRO design and LCCA tool is being

developed to facilitate the holistic design of desalination systems. This tool aims to tackle the interaction of ontology, SWRO design process and life cost analysis, enabling the determination of the most effective SWRO desalination design tailored to user-specific requirements.

Chapter 5

SWRO Desalination Process Design

Chapter 5 presents a thorough analysis of the design process for the SWRO desalination plant. It starts by establishing the fundamental principles, such as water density and viscosity, in Section 5.1 . It then proceeds to examine the essential processes and subprocesses of the SWRO plant. The intake system design is outlined in Section 5.2 , followed by a discussion on the chemical and posttreatment systems in Section 5.3 . In Section 5.4 , the chapter provides more detailed information about the pretreatment system, specifically focusing on each subprocess from clarifiers to membrane filtration. In Section 5.6 , the RO system is thoroughly examined which includes a detailed evaluation of the basic plant parameters, membrane system design, and the important factors that determine its performance. The chapter ends by providing information on the discharge system in Section 5.7 5.8 , power calculations in Section 5.8 , and an in-depth evaluation of the RO model in Section 5.9 . This leads to a complete grasp of SWRO plant design and its operating dynamics.

The equations utilised for SWRO desalination plant design were primarily derived from the literature sources mentioned earlier [30], [40], [245], [278], [281], [283], [292], [300], [301], and additional references will be cited within the respective chapters.

5.1 Water Density and Viscosity

The consideration of density as a significant thermodynamic property of water is crucial, as it directly affects various aspects of plant operation, as well as the processes of mixing and dispersion. The density of seawater is a function of salinity, temperature, and pressure. However, it is assumed in this model that the pressure is at atmospheric levels, and therefore it is neglected in the determination of density. The seawater density (Eq 5.1) model utilised in this study was formulated by El-Dessouky and Ettouney [302].

$$\rho = (A_1F_1 + A_2F_2 + A_3F_3 + A_4F_4) \times 10^3 \quad \text{Eq 5.1}$$

The variable ρ represents the density of seawater, measured in kg/m^3 . The parameters outlined below are utilised in the calculation of seawater density based on temperature and salinity.

- $A_1 = 4.032219G_1 + 0.115313G_2 + 3.26 \times 10^{-4}G_3$
- $A_2 = -0.108199G_1 + 1.571 \times 10^{-3}G_2 - 4.23 \times 10^{-4}G_3$
- $A_3 = -0.012247G_1 + 1.74 \times 10^{-3}G_2 - 9 \times 10^{-6}G_3$
- $A_4 = 6.92 \times 10^{-4}G_1 - 8.7 \times 10^{-5}G_2 - 5.3 \times 10^{-5}G_3$
- $F_1 = 0.5$
- $F_2 = A$
- $F_3 = 2A^2 - 1$
- $F_4 = 4A^3 - 3A$
- $A = (2T - 200)/160$
- $G_1 = 0.5$
- $G_2 = B$
- $G_3 = 2B^2 - 1$
- $B = \frac{(2X/1000)-150}{150}$

Where the variable X denotes the salinity of seawater, expressed in parts per million (ppm), and T is temperature of seawater ($^{\circ}C$). The validity of this correlation extends to the specified ranges: X is constrained to a range between 0 and 160,000 ppm, while the T is limited to a range between 10 and 180 $^{\circ}C$. The dynamic viscosity and kinematic viscosity of seawater is calculated as follows using Eq 5.2 and Eq 5.3 respectively:

$$\mu = \frac{\mu_x \mu_y}{1000} \quad \text{Eq 5.2}$$

$$\nu = \frac{\mu}{\rho} \quad \text{Eq 5.3}$$

Where μ is dynamic viscosity of fluid is measured in (kg/ms), ν is kinematic viscosity of fluid in (m^2/s), T ranges between $10^{\circ}C$ and $180^{\circ}C$ and X ranges between 0 and 130,000 ppm.

- $\ln \mu_y = -3.79418 + \frac{604.129}{139.18+T}$
- $\mu_x = 1 + AX + BX^2$

- *where*
- $A = 1.474 \times 10^{-3} + 1.5 \times 10^{-5}T - 3.927 \times 10^{-8}T^2$
- $B = 1.0734 \times 10^{-5} - 8.5 \times 10^{-8}T - 2.23 \times 10^{-10}T^2$

5.2 Intake System

The performance of seawater desalination facilities depends on reliable and consistent seawater intake. Despite this, the dynamic nature of the ocean, which is constantly changing due to a variety of factors like strong waves, shifting currents, fluctuating water depths, and varying water quality, makes this objective more challenging. Further, seawater is highly corrosive, and marine organisms can foul equipment and systems, resulting in additional problems. To overcome these challenges, intake systems must be designed to be robust and reliable, accounting for ocean changes. Establishing the plant's capacity is the first step in the design of the intake system for desalination plants, followed by choosing the intake system that optimally suits the plant's structure. It is recommended to employ screens of various sizes to reduce impingement and entrainment. In addition, a pump station with sufficient capacity must be installed to ensure required water flow. Chemical treatment is also ultimately required to prevent further bacterial development in the intake system. The following section presents the relevant equations for each sub-system and process used in desalination plant design.

5.2.1 Intake Capacity

The determination of the intake capacity for desalination processes requires computation at the required maximum capacity. One commonly employed equation for estimating intake capacity is, $\frac{Q_p}{1-R}$, where Q_p is permeate flow rate (m^3/day), and R is recovery rate (%), defined as the ratio of permeate flow rate to influent seawater. Nevertheless, it is essential to consider the influence of backwash and additional water for the plant on the capacity of intake. The relationship between the variables is established by the equation provided below:

$$Q_{f_{SWRO}} = \frac{Q_p}{1-R} \times \frac{1 + bw + aw}{100} \quad \text{Eq 5.4}$$

In the equation, bw is volume of backwash (%), and aw is additional water (%). The volume of backwash can exhibit variability based on the particular pretreatment system utilised. For instance, media filtration typically results in lower backwash volumes, typically falling within the range of 3% to 6%. In contrast, membrane filtration systems generally necessitate backwash

volumes ranging from 5% to 10% [30]. The equation takes into account an additional volume of water equal to 1% [30].

5.2.2 Intake Structure

Three necessary components must be installed to ensure the effective functioning of an intake structure: inlet structure, pump station and screening. The first is the inlet structure, responsible for delivering the fluid to the desalination plant. The subsurface intake is situated along the shoreline, while the offshore intake is located at a considerable distance from the facility. The use of screens is necessary in the design of offshore intakes to minimise impingement and entrainment. The initial screen, known as the velocity cap, is positioned at the bottom of the sea and serves as the inlet for the intake structure. To design the velocity cap, it is necessary to determine the number of intake structures.

The dimensions of a cylindrical velocity cap and the calculation of its extraction flow can be achieved by utilising Eq 5.5. However, it is necessary to determine the feed water approached velocity (v_f) upon which the design intake relies. This velocity is determined based on the maximum through-velocity ($v_{through}$) passing through the intake screen, typically ranging between 0.1 and 0.15 m/s [278]. The velocity can be determined by use Eq 5.7.

$$A_{vc} = \frac{Q_{f_{SWRO}}}{86.4 \times 10^3 N_{pipe} * v_f} \quad \text{Eq 5.5}$$

$$\phi_{vc} = \frac{Q_{f_{SWRO}}}{86.4 \times 10^3 N_{pipe} * v_f * \pi * h_{vc}} \quad \text{Eq 5.6}$$

$$v_f = v_{through} * \left[1 - \left(\frac{w_b}{s_b + w_b} + f_{mg} \right) \right] \quad \text{Eq 5.7}$$

Where A_{vc} is the intake head structure in (m^2), N_{pipe} is number of intake pipes, ϕ_{vc} is the inner diameter of velocity cap in m, h_{vc} is height of velocity cap in m, w_b is the width of screen bars (mm) is assumed to be 25 mm, s_b is space between the bars in mm and f_{mg} is a correction factor for reduction of area due to marine growth which ranges from 0.3 to 0.5. The internal diameter of the bottom of intake structure (ϕ_{bs_j}), the internal diameter of the riser pipe (ϕ_{rp_j}) and the internal diameter of the conveyance pipe (ϕ_{cp_j}) can be calculated using Eq 5.8, Eq 5.9, Eq 5.10 respectively:

$$\phi_{bsj} = \sqrt{\frac{4 * Q_{fj}}{86.4 \times 10^3 v_{bs} * \pi}} \quad \text{Eq 5.8}$$

$$\phi_{rpi} = \sqrt{\frac{4 * Q_{fj}}{86.4 \times 10^3 v_{rp} * \pi}} \quad \text{Eq 5.9}$$

$$\phi_{cpi} = \sqrt{\frac{4 * Q_{f_{SWRO}}}{86.4 \times 10^3 v_{cp} * \pi}} \quad \text{Eq 5.10}$$

Where, Q_{fj} is the flow per intake structure (m^3/day), v_{bs} is flow velocity in the bottom structure (0.8 m/s), v_{rp} , v_{cp} are flow velocities in the riser pipe and conveyance pipe, respectively and their values ranges between 2.0 and 2.5 m/s. Figure 5–1 illustrates the configuration of the velocity cap located at the inlet of the intake structure, along with the suggested dimensions.

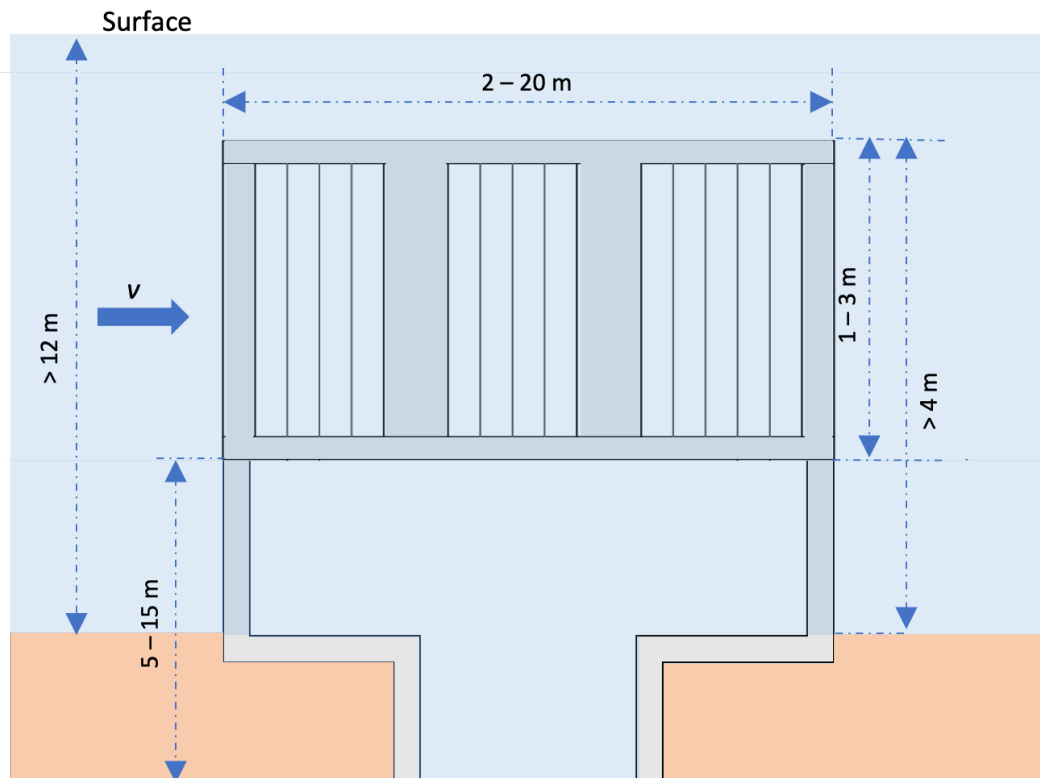


Figure 5–1: Velocity cap inlet offshore intake structure

The design of subsurface intake systems is challenging due to the complex relationship between ground filtration and various geological and hydrogeological parameters [303]. Developing an engineering model for subsurface intake is particularly difficult because parameters such as hydraulic conductivity and transmissivity etc, cannot be assumed or readily

obtained from existing literature. Hence, only the number of wells will be considered in this study, excluding other calculations. For further information, Ludwig [301] has provided detailed calculations for designing vertical wells only based on known information and detailed design knowledge, Bennett [304] discussed the infiltration galleries.

The number of wells or subsurface intake structures needed is determined by dividing the required plant intake capacity by the combined capacity of a single well ($Q_{f_{well}}$) and its reduction capacity (f_{loss}) which typically falls between 0.2 and 0.4. The factor in question is dependent on the quality of the effluent water, the age of the well, and the frequency of maintenance. Table 5-1 provide the ranges of $Q_{f_{well}}$ for different configurations of subsurface intake. The equation for calculating $Q_{f_{well}}$, which is dependent on aquifer drawdown and transmissivity, can be expressed as follows in Eq 5.12.

$$N_{well} = \frac{Q_{f_{SWRO}}}{Q_{f_{well}} * (1 - f_{loss})} \quad \text{Eq 5.11}$$

$$Q_{f_{well}} = \frac{T_d \times A_d}{4.4} \quad \text{Eq 5.12}$$

where T_d is transmissivity (m^2/s) which is calculated as the product of aquifer permeability (k) in m/s and thickness of the aquifer (h) in m. Aquifer drawdown (A_d), measured in m, is observed in a vertical well when water is pumped from the well, resulting in a decrease in the groundwater level in the adjacent aquifer which results a formation of a cone of depression in the surrounding aquifer. The cone visually represents the water level's reduction caused by pumping. Aquifer drawdown is the result of a decrease in hydraulic head within a well due to water extraction. This reduction in hydraulic head causes groundwater to flow towards the well to replenish the extracted water [275].

Table 5-1: Capacity of different subsurface intake systems [305][281]

	Capacity (m ³ /day)
Vertical Well	6048 – 8640
Horizontal Ranney Well	7776 – 38,880
Horizontal Directionally Drilled	4320 – 12,960
Infiltration Galleries	Up to 19,000

5.3 Chemical System and Posttreatment

The desalination process relies on the use of chemicals to, either enhance the process or introduce supplementary minerals to the desalinated water during the post-treatment process. Table 5-2 comprehensively presents an overview of the chemicals employed in a SWRO desalination plant. The table provides information on the purpose of each chemical, its application location, dosage, and concentration.

The determination of chemical requirements in desalination entails a series of essential procedures, which vary based on the particular stage or process of the overall desalination system. Two methodologies are employed, one for the initial processes encompassing intake to RO process, and another for the subsequent post-treatment process.

The quantity of chemical (kg/day) required in the desalination process is determined by a formula (Eq 5.13) that takes into account the dose, which refers to the amount of chemical to be added, as well as the flow rate of plant (m^3/day).

$$Chemical\ use = \frac{dosage \times Q_f}{1000} \quad Eq\ 5.13$$

Eq 5.14 presented below serves to determine the requisite quantity of chemical substance that must be stored within the facility (A_{st}) in kg. The analysis considers both the utilisation of chemicals and the concentration of the product, in addition to the duration of storage. The typical duration for storing chemicals is from 14 to 28 days. However, in challenging circumstances or when facing extended and highly variable ordering and delivery timelines, the storage period may exceed three to four weeks [300]. Hence, it is assumed in this study that the storage duration for all compounds is 30 days.

$$A_{st} = \frac{Chemical\ use}{Product\ Concentration} \times storage\ time \quad Eq\ 5.14$$

After determining the value of A_{st} , the following formula (Eq 5.15) is utilised to calculate the actual storage volume (V_{st}) in m^3 , taking into account the chemical's bulk density.

$$V_{st} = \frac{A_{st}}{bulk\ density} \quad Eq\ 5.15$$

To guarantee a sufficient supply, it is common practise to augment the storage volume by a range of 10% to 15% to accommodate any unanticipated fluctuations or surges in demand as indicated in Eq 5.16.

$$V_{st} = V_{st} \times 1.15 \quad \text{Eq 5.16}$$

The depth of the storage tank (d) in m can be determined using the following formula (Eq 5.17), which takes into account the intended volume (V_{st}), the number of tanks (n), and the radius of the tank (r).

$$d = \frac{V_{st}/n}{\pi r} \quad \text{Eq 5.17}$$

In the context of a SWRO desalination plant, it is essential to implement a dilution process for specific chemicals before their utilisation (Eq 5.18)

$$\begin{aligned} & \text{average dilution flow} \\ & = \frac{\text{chemcial use} \times \left[\frac{\text{Product Concentration}}{\text{Application Concentration}} - \frac{1}{\text{bulk density}} \right]}{24} \end{aligned} \quad \text{Eq 5.18}$$

Eq 5.19 calculates the optimal rate at which a chemical metering pump should operate, hence guaranteeing accurate and consistent dosing of chemicals during a 24-hour timeframe. The analysis considers both the chemical utilisation and the bulk density.

$$\text{chemical metering pump} = \frac{\text{chemcial use}}{\text{bulk density} \times 24} \quad \text{Eq 5.19}$$

During posttreatment process, the main goal is to adjust the alkalinity of the water to fulfil particular criteria according to WHO standard or the state's regulations. The chemical employed for post-treatment (Eq 5.20) is contingent upon the desired level of alkalinity, the dosage required, and the degree of chemical purity.

$$\text{chemcial use} = \frac{\text{alkalinity} \times \text{dosage}}{\text{purity}} \quad \text{Eq 5.20}$$

The aforementioned calculations collectively contribute to the optimisation of chemical usage in the desalination process, hence enhancing the efficiency and effectiveness of the process and ultimately resulting in the production of desalinated water of superior quality.

Table 5-2: Chemical used in SWRO plant [306]

Chemical	Purpose	Location	Typical product concentration (%)	Bulk density (kg/L)	Application concentration (%)	Dosage (mg/L)	Storage time (days)	Cost (US\$/kg)
Sodium hypochlorite	Suppress bio-logical growth	Open intake structure Offshore pipeline	13	1.23	5	4* - 6**	30	2.2 - 3.5
Sulfuric Acid (93% h ₂ so ₄)	Suppress bio-logical growth pH adjustment	Open intake structure Offshore pipeline	98	1.83	20	100* - 140**	30	0.06 - 0.1
Ferric sulfate	Coagulant Reduces colloidal fouling and natural organic matter	Pretreatment Sedimentation tanks Dissolved air flotation units or filters	40	1.55	5	5 - 30	30	0.4 - 1.2
Ferric chloride	Coagulant Reduces colloidal fouling and natural organic matter	Pretreatment Sedimentation tanks Dissolved air flotation units, or filters	40	1.42	5	15 - 50	30	1.67
Flocculation (polymer)	Improve seawater pretreatment	Pretreatment				0.2 - 0.5	30	
Sodium hexametaphosphate	Scale inhibitors Prevent scaling fouling	Prior to RO system	99	1	20	0.25 - 4	30	1.6 - 4.0
Chlorine dioxide	Suppress the growth of aquatic organisms, disinfection	Intake pipes Equipment Tanks Distribution channels Other structures in contact with the source seawater		1.5	30	0.18-0.2	30	3.0 - 5.5
Sulfuric acid	Adjust pH	Posttreatment Chemical backwash				1.02*		0.06 - 0.1

Chemical	Purpose	Location	Typical product concentration (%)	Bulk density (kg/L)	Application concentration (%)	Dosage (mg/L)	Storage time (days)	Cost (US\$/kg)
Sodium hydroxide	Adjust the pH of the feed seawater Backwash	Prior to RO system Pretreatment backwash	50	1.525	20	5 - 8	24 months	0.65 - 0.85
Sodium bisulfite	Reduce membrane degradation Dichlorination Removal of oxidant residual	After cartridge filter	99	1.48	20	3		0.35 - 0.55
Hydrated lime	Remineralisation Add alkalinity	Posttreatment	50	1.44	-	0.74	48 months	0.3 - 0.4
Calcite	Remineralisation Add alkalinity	Posttreatment	50	1.493	-	1	12 months	0.05 - 0.08
Carbon dioxide	Adjust pH	Posttreatment	40	1.87	-	0.88, 0.44	28	0.08 - 0.12
Other cleaning chemicals (US\$/m ³ of permeate)								0.005 - 0.008

5.4 Pretreatment System

5.4.1 Clarifiers

Clarifiers are generally used for the continuous removal of solid particulates or suspended solids from source water prior to the granular media filtration or ultrafiltration. In SWRO desalination, sand removal, conventional sedimentation tanks, lamellar sedimentation settlers, and dissolved air flotation (DAF) are used to apply additional pretreatment depending on the source water quality. Sand removal devices are not commonly used in desalination plant as a well-designed intake systems should help the sand and silt content to settle and be removed. However, in cases where the water quality is good and turbidity is low, but the sand content is high due to the plant location, then sand removal devices would be a viable option instead of other clarifier systems. These devices are applicable only in small and medium desalination plants where the capacity is equal or less than 20,000 m³/day [30]. Due to their declining use in the desalination area and subsequent replacement by other clarifier technologies, these devices will not be incorporated into the study.

5.4.1.1 Sedimentation Tank

In sedimentation tanks, which are also referred to as settling tanks, solids are collected and disposed of as they settled to the bottom of the basin due to the density differences and gravity. The technique is predicated on slowing the velocity of water, to a settling velocity that allows suspended particles to settle and be removed. The settling velocity is typically between 0.3 and 1.1 m/min [307]. It is possible to use standard sedimentation tanks if the turbidity of the source water is above 20 NTU and below 50 NTU [40]. The addition of lamella plates to these tanks increases their turbidity-treating capacity fourfold, to 200 NTU [291]. In addition to their various benefits, lamella settlers have found widespread use in the desalination industry because of their small footprint due to the inclined plates. A CFD study was conducted by Tarpagkou and Pantokratoras [291] to simulate the dynamics and flow structure of a rectangular sedimentation tank and lamella tank for potable water through a multiphase approach. Based on the findings, it was observed that particles were concentrated at the bottom of lamella settlers as opposed to conventional settlers. As a result of the lamella plate configuration, unsettled particles are redirected so that they can be collected in the sludge hopper located at the base of the system, resulting in 93% efficiency compared to 75% for conventional designs [291]. Sedimentation tanks can be either rectangular or circular in shape.

While circular shapes are commonly used for wastewater treatment, rectangular shapes are more common in water treatment. Consequently, a rectangular regular and lamellar sedimentation tank were chosen for this research.

Principle of Sedimentation:

The effectiveness of a clarifier system in collecting suspended solids is influenced by several factors, including the particle size (as seen in Table 5-3.), temperature, viscosity, and the size and shape of the tanks.

Table 5-3: Settling Time for different type of particles [308]

Diameter of particles	Type of particles	Settling time
10 mm	Gravel	1 s
1 mm	Sand	10 s
0.1 mm	Fine sand	2 min
10 micron	Protozoa, Algae, Clay	2 h
1 micron	Bacteria, Algae	8 days
0.1 micron	Viruses, colloids	2 years
10 nm	Viruses, colloids	20 years
1 nm	Viruses, colloids	200 years

Stokes' law [309] provides insights into the settling velocity (v_s) of particles, stating that it is directly proportional to the density difference between the solid phase and the liquid phase, inversely proportional to the viscosity of the liquid, and directly proportional to the square of the particle diameter as shown in Eq 5.21

$$v_s = \frac{g(\rho_s - \rho)\phi_p^2}{18\mu_w} \tag{Eq 5.21}$$

Where ρ is density of fluid which is dependent on temperature; ρ_s density of particles removed (2650 kg/m³), g gravitational acceleration (m/s), ϕ_p particle's diameter (m) and μ_w kinematic viscosity of water. Table 5-4 demonstrates the settling velocity based on particles diameter and type of flow and Reynolds number. Calculating the settling velocity aids in determining the threshold of sedimentation tank overflow velocity.

Table 5-4: Settling Velocity equation in terms of particles diameter and type of flow [310][311]. C_d is drag coefficient which is obtained by determining the Reynolds number

Type of flow	d_p (mm)	Settling velocity	Drag coefficient	Re
Turbulent	> 1	$v_s = \sqrt{\frac{3.33g(\rho_s - \rho)\Phi_p}{\rho}}$	$C_d = 0.44$	$500 < Re \leq 2 \times 10^5$
Transitional	$0.1 - 1$	$v_s = \sqrt{\frac{4g(\rho_s - \rho)\Phi_p}{3C_d\rho}}$	$C_d = \frac{24}{Re} + \frac{3}{\sqrt{Re}} + 0.34$	$2 \leq Re \leq 500$
Laminar	< 0.1	$v_s = \frac{g(\rho_s - \rho)\Phi_p^2}{18\mu_w}$	$C_d = \frac{24}{Re}$	$Re < 1$

In the sedimentation tank, the critical particle-settling velocity, or surface overflow rate, refers to the velocity at which the clarified effluent is discharged which aids in determining hydraulic loading on the sedimentation tank. In the presence of too high overflow velocity, suspended particles can be carried over, causing turbulence while low overflow velocity may lead to short-circuiting. As a consequence, it is essential that the overflow velocity is lower than the settling velocity to avoid both conditions. The overflow rate of a sedimentation tank is influenced by the basin's depth (Eq 5.22). In the case of a continuous flow basin, it is essential to ensure that the length and duration for which a unit volume of water remains within the basin, are such that, particles traveling at the prescribed velocity settle completely to the tank's bottom. Consequently, the following equation can be used to calculate the overflow velocity [312]:

$$v_c = \frac{Q_c}{A} = \frac{d}{t} \quad \text{Eq 5.22}$$

Where v_c is the overflow velocity ($\text{m}^3/\text{m}^2\text{h}$), Q_c the flow rate per tank (m^3/h), A the surface area (m^2), d is depth (m) and t is the detention period (h). Detention period, residence time, or settling time is the typical amount of time it takes for water to settle in the sedimentation tank which help to determines the time available for sedimentation to occur. Usually settling time ranges from 1 to 4 h [312] in sedimentation while lamella have shorter settling times, ranging between 0.2 to 0.4 h [245], [281]. Assuming the number of tanks at the start of the process helps in the determination of the flow rate per the Eq 5.23.

$$Q_c = \frac{Q_f}{n} \quad \text{Eq 5.23}$$

Subsequently, the surface area of the sedimentation tank can be calculated based on the relationship between the flowrate per tank and the surface loading rate. The surface loading (LR) rate typically falls within the range of 1 to 2 m³/m²h, as indicated by Eq 5.24.

$$A = \frac{Q_c}{LR} \quad \text{Eq 5.24}$$

Then the volume of a tank (m³) is obtained by multiplying the flow rate per tank by the detention time since it is assumed that sludge is automatically removed [310] which is calculated using Eq 5.25.

$$V = Q_c t \quad \text{Eq 5.25}$$

The dimensions of the tank, including depth (*d*), width (*w*), and length (*l*), can be determined using the following equations: Eq 5.26, Eq 5.27, Eq 5.28. It is worth noting that the length-to-width ratio is maintained at a minimum value of 4:1 [245], and the depth of the tank must fall within the range of 2 to 4.9 m [245], [281]. The total depth would be the sum of the calculated depth, 1 m for sludge and 0.5 m for a free board or venting space [313]. Free board is known as the vertical distance between the top of tank and water level. if the calculated depth is less than 2, it implies that the number of tanks should be decreased, whereas if the calculated depth exceeds the maximum value, the number of tanks should be increased.

$$d = \frac{V}{A} \quad \text{Eq 5.26}$$

$$w = \sqrt{\frac{V}{4d}} \quad \text{Eq 5.27}$$

$$l = 4w \quad \text{Eq 5.28}$$

The overflow velocity can be calculated using Eq 5.22, the acceptable value is below or equal to 0.3 m/min [58]. Figure 5–3 illustrates the flow chart for designing the sedimentation tank in this research.

Table 5-5: Supplementary information for conventional and lamella sedimentation [245], [301], [314]

	Sedimentation	Lamella Sedimentation
Overflow velocity (m/min)	≤ 0.3	0.01 – 0.025
Detention time (h)	1 - 4	0.2 – 0.4, ≤ 0.2
Length (m)	Length to width ratio	2.5 – 3.25
Width (m)	Length to width ratio	1.25 – 1.5
Depth (m)	2 – 4.9	3.5 - 5
Sludge zone (m)	1	1.5
Min number of tanks	4	2
Lamella surface loading rate ($\text{m}^3/\text{m}^2\text{h}$)	-	1 - 2
Clarifier surface loading rate ($\text{m}^3/\text{m}^2\text{h}$)	1 - 2	7.5 - 25

Due to the presence of inclined lamella plates, the design approach for a lamellar tank differs slightly. These plates are inclined to facilitate the sedimentation procedure. There are three different arrangements in which the untreated water can pass through the separation units of lamella in relation to the sludge discharge direction resulting from solids separation, including counter-current, co-current, and cross-flow configurations. The counter-current design is widely employed in practical applications; therefore, the design calculation is based on this [310].

The optimal angle of inclination for lamella plates lies between 45 and 60 degrees [310]. If the angle is below this threshold, particulates have a tendency to accumulate on the plates, which may impede the settling process. In contrast, angles exceeding the maximum recommended limit may reduce sedimentation efficiency. In practical applications, it is common to add multiple rows of lamella plates to the sedimentation basin to increase the settling capacity. The number of lamella rows is typically between 2 and 8, with 3 or 4 rows being the norm [315]. This arrangement enhances particle separation and sedimentation within the tank. Nominal spacing between plates (d_{ch}) is 40 – 100 mm, with an inclined length of 1 to 2 m [310] [315]. Eq 5.29 is utilised to compute the allowable velocity (v_{ch}) within the plate channel, which is dependent on the supplied plate parameters and the chosen Hazen velocity (v_c). The Hazen velocity frequently varies between 0.6 and 1.5 m/h, with the utilisation of greater rates (>1.0 m/h) primarily in cases when the water exhibits elevated levels of turbidity [314].

$$v_{ch} = \frac{v_c l_{p,active} \cos \theta}{3600 d_{ch}} \quad \text{Eq 5.29}$$

Where v_{ch} is allowable velocity in lamella channel (m/s), θ is inclination angel of plates ($^\circ$), d_{ch} is the depth of the lamella channel (m), l_p the plate length (m), and $l_{p,active}$ is the active plate length (m) which is determined by $= l_p * f_p$ where f_p is factor of active plate length which ranges between 0.75 and 0.85 [301].

The calculation of the maximum flow rate (Q_{lam}) across the plate channel, which is determined by the allowable flow rate v_{ch} , is performed by utilising Eq 5.30 in relation to the cross-sectional areas A_{ch} of the channel.

$$Q_{lam} = 3600 v_{ch} w_{pl} d_{ch} \quad \text{Eq 5.30}$$

The variables Q_{lam} represent the feed flow to the channel of the lamella unit in m^3/h and w_{pl} is the width of the plates in m. The estimation of the total number of lamella units, denoted as N_{lam} , is determined by two factors (Eq 5.31): the flow rate of the raw water (Q_{SWRO}) that needs to be treated by the reactor, and the allowable flow rate (Q_{lam}), via each individual lamella channel.

$$N_{lam} = \frac{Q_{SWRO}}{Q_{lam}} \quad \text{Eq 5.31}$$

The surface area of the lamella packs in a solids separator is determined by the pack depth (d_{lam}) and the lamella width (w_{pl}) according to Eq 5.32.

$$A_{lam} = d_{lam} w_{pl} \quad \text{Eq 5.32}$$

The dimensions of the pack depth (Eq 5.33) are influenced by various factors including the distance between the inclined plates ($d_{ch,\theta}$), calculated using Eq 5.34, the thickness of the plates (t_{pl}), the number of lamella units in the pack (N_{lam}), and an additional length. Figure 5–2 is an illustration of the counter-current flow pattern and parameters for lamella sedimentation tank.

$$d_{lam} = (d_{ch,\theta} + t_{pl}) \times N_{lam} + (l_p \times \cos \theta) \quad \text{Eq 5.33}$$

$$d_{ch,\theta} = \frac{d_{ch}}{\sin \theta} \quad \text{Eq 5.34}$$

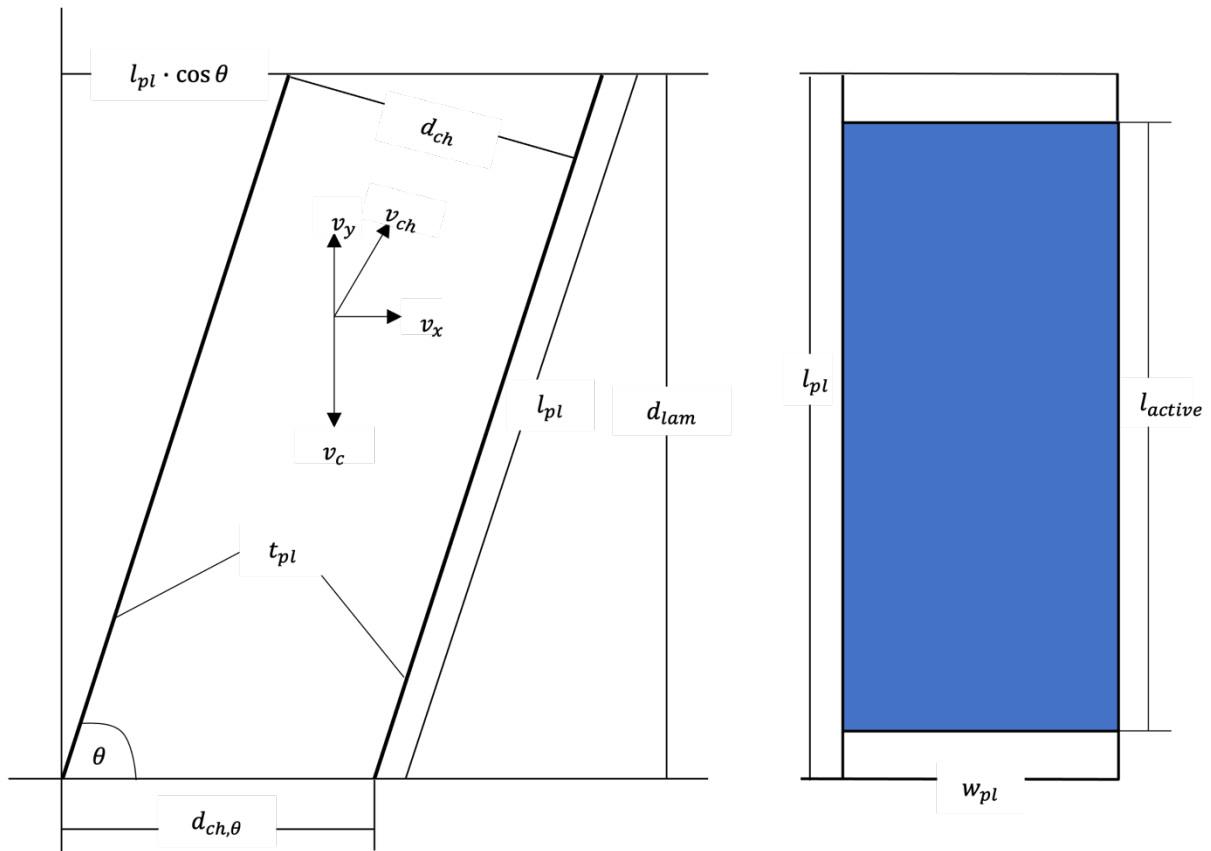


Figure 5-2: Flow pattern and parameters for lamella sedimentation, adapted from [301][310]

Finally, the surface loading rate of the lamella process can be determined using the following equation (Eq 5.35):

$$LR_{lam} = \frac{Q_{SWRO}}{A_{lam}} \quad \text{Eq 5.35}$$

The efficiency of the lamella sedimentation process (eff_{lam}) is determined by Eq 5.36. This efficiency is measured in terms of the suspended solid content in seawater (SS_{SW}), with a targeted range of 2-10 mg/L [310] for the suspended solids in the lamella (SS_{lam}). Additionally, Metcalf and Eddy [316] proposed an equation that evaluates the performance data for removing of biological oxygen demand (BOD) and TSS in sedimentation tanks. This equation takes into account the detention time and constituent concentration and is generated from observations of the actual performance of sedimentation processes.

$$eff_{lam} = \frac{SS_{sw} - SS_{lam}}{SS_{sw}} \times 100 \quad \text{Eq 5.36}$$

$$eff_{lam} = \frac{t}{a + b} \quad \text{Eq 5.37}$$

Where, t is detention time (h), a and b are empirical constants: a for TSS = 0.0075, and BOD = 0.018; b: for TSS = 0.014, and BOD = 0.02. Eq 5.38 is employed to ascertain the quantity of solids separated during the sedimentation process (Δ_{ss}), whilst Eq 5.39 is utilised to compute the quantity of sludge generated within the sludge chamber of the reactor (Δ_{sludge}).

$$\Delta_{ss} = \frac{Q_{f,swro} SS_{sw} eff_{lam}}{100,000} \quad \text{Eq 5.38}$$

$$\Delta_{sludge} = \frac{\Delta_{ss} \times 100}{SC_{sludge}} \quad \text{Eq 5.39}$$

Where Δ_{ss} is the amount of solids removed by lamella sedimentation in kg/h, SS_{sw} is suspended solid content in seawater (mg/L), Δ_{sludge} is amount of sludge produced in kg/h and SC_{sludge} is the solids content of sludge which ranges between 1 and 2 %. Eq 5.55. to Eq 5.39 can be applied as well to determine the sludge removal by the conventional sedimentation process. Figure 5–3 illustrate the process that can be followed to design the two types of sedimentation tanks.

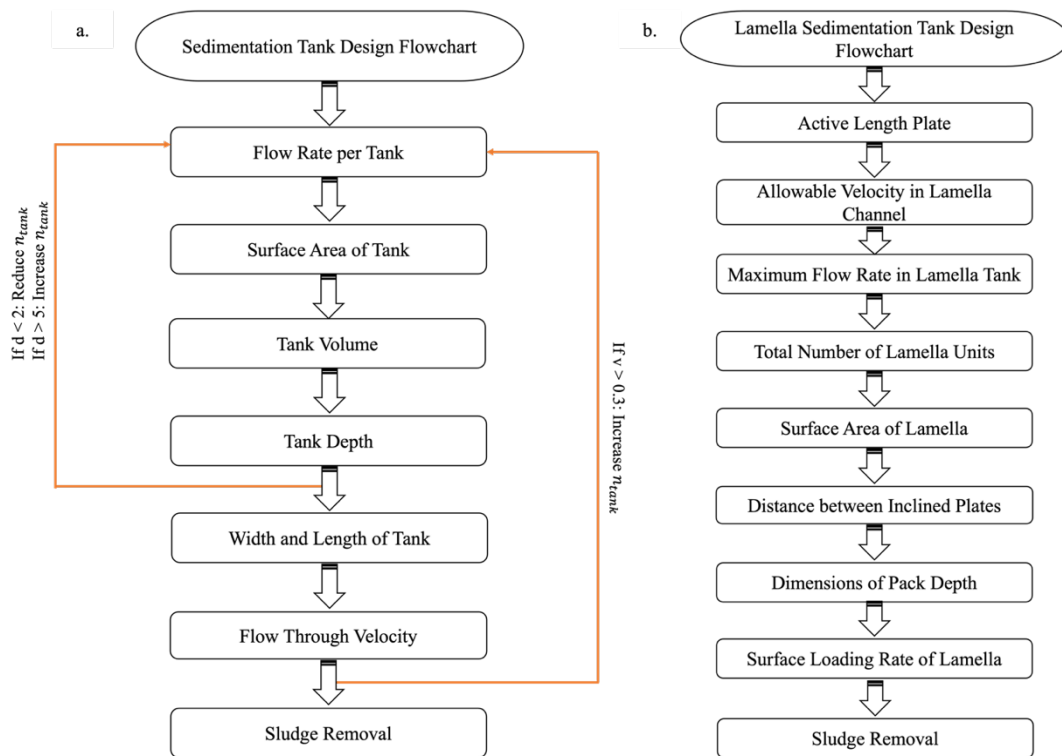


Figure 5-3: Flow chart for designing a. conventional sedimentation tanks, b. lamella sedimentation tank

5.4.1.2 Dissolved Air Flotation

The efficiency of the flotation process is heavily influenced by factors such as the surface characteristics of the particles, the air system, the quantity of air, and the velocity at which the particles rise [ref]. The DAF design process is one that is complex and involves variable equations depending on the various shapes of particles in seawater, hence it falls beyond the scope of this study's focus. Ludwig [300], [301] has presented a set of equations and accompanying explanations, along with a required graph. However, to effectively utilise these equations, it is necessary to gather specific information regarding the plant case, such as air density, particle shape, and other relevant factors. Table 5-6 provides an overview of the design criteria for DAF system components.

To determine the quantity of sludge that can be eliminated using DAF, equations Eq 5.36 to Eq 5.39 can be employed. It should be noted that the concentration of solids in the flotation effluent typically falls between the range of 1 to 10 mg/l, with an average of 5 mg/l. The solids percentage of the SC_{sludge} might reach a maximum of 3 - 4% [301].

Table 5-6: Overview of DAF chambers and corresponding available values [30]

DAF	Parameters	Values
Mixer or coagulation chamber	Velocity gradient	500 - 1600
Flocculation chamber	Contact time	10 – 20 min
	Number of flocculation chamber	2 - 4
	Water depth	3.5 – 4.5 m
	Blade area as percentage of tank	0.1 to 0.2 percent
	Shaft speed	40 to 60 r/min
DAF chamber	Min number of tank	2
	Tank width	3 – 10 m
	Tank length	8 – 12 m
	Tank depth	2.5 – 5 m
	Surface loading rate	10 – 40 m ³ / m ² L
	Hydraulic detention time	10 – 20 min
	Area	120 – 180 m ²
Treated water recycle system	Recycle rate	8 – 15 % of intake flow
	Maximum air loading	10 g/ m ³
	Saturator loading rate	60 - 65
	Operating pressure	6 – 8 bar

5.4.2 Granular Media Filtration

Granular media filtration involves filtering water at its source through a series of layers of filter mediums. Commonly employed granular media include: anthracite coal, silica sand, and garnet. During the filtration process, water is treated by traversing through a filter medium, which effectively retains coagulated particles and impurities present in the water, resulting in clarified water. Passes through the filter to remove particles but can only pass through the filter once the particles are removed.

The conventional filters utilised for pretreating saline water typically consist of rapid single-stage, dual media units, incorporating both anthracite and sand layers. However, there are circumstances in which the implementation of a two-stage filtration system is required, particularly when the source water exhibits elevated levels of organic compounds (with a total organic carbon concentration exceeding 6 mg/L) and suspended solids (with a monthly average turbidity surpassing 20 NTU) [40], [245], [271].

The selection of the appropriate filtration system, whether single-stage or two-stage, depends on various factors, such as the quality of the source water, the specific requirements of the treatment process, the desired effluent quality, size, type, depth and uniformity of the filter bed.

This filtration is only suitable for removing particulates larger than 50 μm from source water. Media filtration provides a SDI_{15} less than 5 [245]. Based on extensive field observations conducted at various full-scale granular media pretreatment filter installations, source-water turbidity has been consistently reduced to levels below 0.1 NTU [245].

There are two main types of granular media filters, distinguished by the force used to filter the water: gravity and pressure. These two varieties of filters are distinguished from one another by the filtering rate at which they operate, the type of vessel used to house the media, and the required head to assist the flow of water through the media bed. Small and medium-capacity RO plants frequently use pressure filters due to the high costs associated with creating large pressure vessels with sufficient corrosion-resistant surfaces. However, gravity pretreatment filters are useful in small, medium, and large RO-desalination systems. Table 5-7 illustrates the differences between gravity and pressure media filtration in terms of dimensions, applications and materials.

Table 5-7: Comparison between gravity and pressure granular media filtration [317][318][245]

	Gravity Cell	Pressure Cell
Material	Reinforced concrete	Steel or plastic
Size of desalination plant	Small, medium, large	Small - medium
Surface loading rate	8 – 15 $\text{m}^3/\text{m}^2\text{h}$	24 – 45 $\text{m}^3/\text{m}^2\text{h}$
Life span	50 – 100 years	≤ 25 years
Depth	4.5 – 7.5	0.6 – 1.5
Width/ Diameter	3 - 8	1.2 - 6
Max surface area	25 - 100	25 - 100
Length	-	2.5 - 15
Length-to-width ratio	2:1 – 4:1	1:1 - 4:1
Water level	1.8 – 2.5	15 – 30 m

*Length-to-diameter ration

The number of filter cells is primarily determined by the total flow that these filters are designed to handle. There are several crucial factors to consider when determining the minimum number of filters to employ. There are practical limits to the size of each individual filter bed, which makes it difficult to use larger area filters as they are prone to uneven backwashing. The second factor is that if one or two filters are in the backwash mode, the remaining filters in operation have a higher filtration rate. Lastly, how the RO system is configured, including the number of individual trains and the intended operational mode, plays an important role in deciding how many filters are needed [245].

Calculating the surface area of filtration system (Eq 5.40) with a projected value from the surface loading rate range is the first step in determining how many filters are needed for each request.

$$A = \frac{Q_f}{LR} \quad \text{Eq 5.40}$$

This amount can be used in Eq 5.41 to calculate the optimal number of tanks by dividing the required area for the specified plant capacity by the maximum surface area per filter.

$$n = \frac{A}{\text{max } A_{\text{per filter}}} \quad \text{Eq 5.41}$$

The total filter count is determined by Eq 5.41, with the addition of a standby filter unit. This assumption simplifies calculations and accounts for scenarios where filters may be undergoing backwashing or are temporarily offline for maintenance. In these situations, the number of operational filters decreases, requiring higher surface loading rate for the remaining units. The standby unit serves as a contingency, ensuring the system's continuous and normal operation. Then, the surface area per filter is recalculated to double check that the user selected the right value in the previous step, and the Eq 5.42 can be used:

$$A_{\text{per filter}} = \frac{A}{n} \quad \text{Eq 5.42}$$

After that the width and length are calculated using the length-to-width ratio using Eq 5.43.

$$w = \sqrt{\frac{A}{l - \text{to} - w \text{ ratio}}} \quad \text{Eq 5.43}$$

The overall depth of the filter bed is determined by the cumulative depth of its many layers, which include the supporting layer and the filter layer in the case of single-medium filters. In the case of multi-media filters, the total depth is influenced by several filter layers, in addition to the water level as seen in Eq 5.44:

$$d_{\text{total}} = d_{\text{layers}} + d_w + d_{\text{support layer}} \quad \text{Eq 5.44}$$

The depth of each layer in this study is determined using a commonly accepted guideline that assumes a ratio between 1000 and 1500 [319] multiplied by the effective size of the material in

each layer, as presented in Table 5-8. The depth of the support layer includes both the supporting layer and the underdrain system, with a range typically between 0.3 to 0.5 m [245].

Table 5-8: Features of material that applied in granular media filtration [319], [320]

Material	Position of layer	Effective size (mm)	Specific density (tons/ m ³)	Uniformity coefficient
Pumice	First layer	0.8 – 2	1.2	1.3 – 1.8
Anthracite	First layer	0.8 – 2	1.4 – 1.7	1.3 – 1.8
Silica sand	Second layer	0.4 – 0.8	2.6 – 2.65	1.2 – 1.6
Garnet	Third layer	0.2 – 0.6	3.5 – 4.3	1.5 – 1.8
GAC	Top layer	0.8 – 2	1.43 – 1.87	1.3 – 2.4

To eliminate the suspended solids that have accumulated between the layers, the filters have to go through a backwash process. The backwash method employed in this study is a hybrid system that utilises both air and water. To determine the necessary backwash flow rate (in m³/min) and the required volume per filter (in m³), the following two equations (Eq 5.45 and Eq 5.46) are employed:

$$Q_{bw} = \frac{LR_{bw} \times A}{60} \quad \text{Eq 5.45}$$

$$V_{bw/filter} = Q_{bw} \times (t + t_{drain}) \quad \text{Eq 5.46}$$

The LR_{bw} typically ranges from 45 to 60 m³/m²h, with a process length (t) of 10 to 15 min [30]. The period for draining the water down (t_{drain}) for each cycle falls between 5 to 10 min [30]. Figure 5–4 shows the steps for designing granular media filtration.

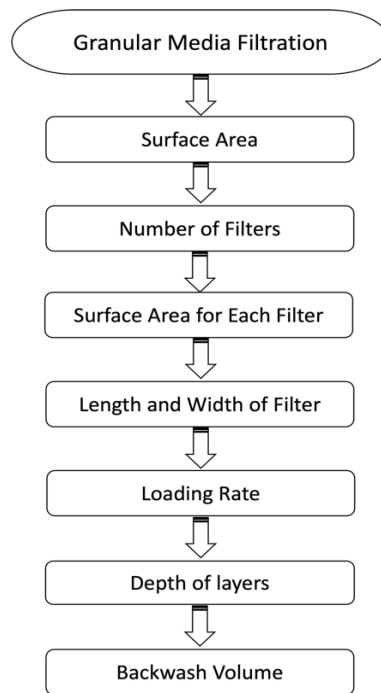


Figure 5-4: Flowchart of granular media filter design

5.4.3 Membrane Filtration

When designing a membrane filter plant for a specific membrane type, it is necessary to calculate the system membrane area, determine the appropriate number of membrane modules of the selected module type, and establish the required feed pressure. This process involves considering the specific properties and operating parameters of the module type, including:

- The surface area of the membrane per module
- The maximum allowable system feed pressure
- The maximum allowable transmembrane pressure (TMP)
- Membrane Flux
- The duration of the filtration cycle.
- The frequency at which chemically enhanced backwash (CEB) and cleaning-in-place (CIP) processes are conducted.

Table 5-9 presents a comprehensive range of values pertaining to the principal parameters involved in membrane filtration. In this research, it is not possible to recommend a single UF membrane due to the existence of several alternatives that are suitable for specific instances. Therefore, it is advised that the user carefully selects the membrane that best suits their individual case and utilises its corresponding values for performing the calculation.

Table 5-9: Supplementary information for membrane filtration [301]

Parameter	Unit	Values
Membrane surface area per module	m ²	30 - 105
Feed pressure	bar	3 - 6
TMP	bar	Submerged system = 1.5 - 3 pressurised system = 0.2 - 0.8
Backwash pressure	bar	1.4 - 3
Strainer mesh size	μm	100-500
Recommended Flux	Lmh	Submerged system = 30 - 60 pressurised system = 45 - 100
Filtration cycle length for SWRO Plant	min	20 - 90

The procedures involved in designing the membrane filtration system, specifically in relation to the membrane filtration area, number of membrane modules, and membrane flow, are presented in Table 5-10.

Table 5-10: Steps for designing membrane filtration system [301]

Steps	Unit	Equation	
Filtration surface area of membrane system	m ²	$A = \frac{Q_f \times 1000}{J_e \times 24}$	Eq 5.47
Number of elements of membrane system		$N_e = \frac{A}{A_e}$	Eq 5.48
Number of vessels of membrane system		$N_{pv} = \frac{N_e}{N_{e/pv}}$	Eq 5.49
Number of trains of membrane system		$N_T = \frac{N_{pv}}{N_{pv/T}}$	Eq 5.50
Area of train		$A_T = A_e \times N_{e/pv} \times N_{pv/T}$	Eq 5.51
Flow rate per train	m ³ /h	$Q_{f/T} = \frac{A_T \times J_e}{1000}$	Eq 5.52

Where A_T is filtration surface area of a train, the subscript e is element, pv is vessel and T is train. Another crucial aspect that must be taken into consideration while constructing UF systems is the cleaning process, which encompasses the following sequential steps (Figure 5-5):

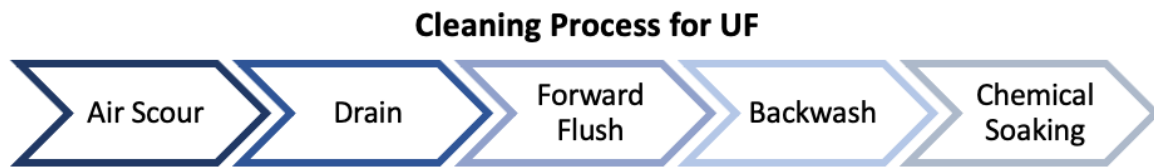


Figure 5–5: Cleaning steps for UF process

The OntoSWRO framework would offer guidance regarding the appropriate duration and frequency for implementing each cleaning step.

5.5 Cartridge Filter

Cartridge filters are commonly positioned in the downstream section of the granular media filtering system and their primary function is to effectively capture and retain fine sand, particles, and silt that may be present in the water after undergoing pretreatment and protect RO’s pump. The cartridge filtering systems have been specifically engineered to accommodate hydraulic loading rates ranging from 0.2 to 0.3 L/s per 250 mm of length [30], [40], [245], [271]. The normal length of standard cartridge filters used in desalination plants ranges from 101.6 to 1524 cm. These filters are commonly mounted in pressure vessels, either horizontally or vertically. Cartridges are assigned ratings for the filtration of particles measuring 1, 2, 5, 10, or 25 μm [30], [40], [245], [271], with the size most commonly employed being 5 μm . therefore, number of cartridge filter ($N_{cartridge}$) and number of cartridge filter per vessel ($N_{cartridge/PV}$) can be determined using Eq 5.53 and Eq 5.54, respectively.

$$N_{cartridge} = \frac{1000 \times Q_f}{86400 \times \left(LR \times \frac{L}{250} \right)} \quad \text{Eq 5.53}$$

$$N_{cartridge/PV} = \frac{N_{cartridge}}{N_{PV}} \quad \text{Eq 5.54}$$

5.6 Reverse Osmosis System

The methodical design of a RO system is substantially aided by having a firm understanding of the system’s core function. There are three primary objectives that have been identified when it comes to membrane selection: achieving high rejection rates, decreasing the potential of

fouling, and energy efficient while achieving an acceptable flux as well as the salinity of the water. The optimal selection of one of these objectives enables the determination of a RO membrane type that corresponds to the desired result. This research followed the recommendations of DUPONT membranes [321] and employed four distinct varieties of membrane, which are the preferred membranes for the three aforementioned objectives: FILMTEC SW30HR-320 for applications with high potential of fouling; FILMTEC SW30XLE-400i for reducing energy consumption; FILMTEC SW30HRLE-400i for establishing an appropriate compromise between low energy consumption and high rejection; and FILMTEC SW30HR-380, chosen for its rejection capabilities. However, FILMTEC SW30HR-320 is being discontinued therefore, and therefore FILMTEC SW30XFR-400 is used instead [322]. Figure 5–6 provides the performance and geometrical information for the RO membranes that are employed in this research.

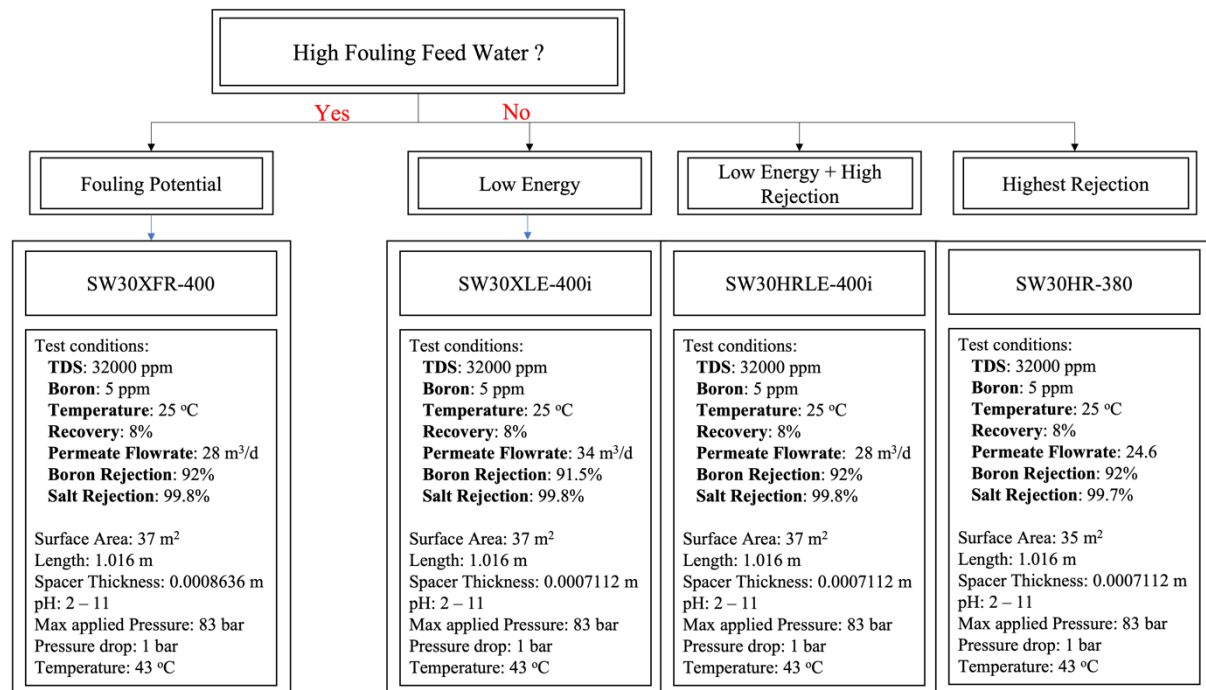


Figure 5–6: Selected membrane type for this research

The initial objective was to develop an RO system and conduct a number of experiments in the Wave software, and collect data under different operating conditions. A possible limitation of this method is that it is only applicable to the tested scenarios, limiting its usefulness to a subset of use cases. The reliability of the model could be impacted as a result, especially in regards to the RO system which is the foundation of the desalination plant. Furthermore, the first principles engineering of the WAVE software (further information, Section 6.6.5.4) was

challenging to reverse due to the lack of clarity in the documentation pertaining to the equations utilised throughout the development of this model.

Therefore, as depicted in Figure 5–7, this study adapted the mathematical model developed by Salini-Rodriguez *et al.* [323]. However, it was necessary to make several changes to enhance the overall accuracy and the principle of this model. Several equations in the published steps [323] utilised the rule of thumb for the equivalence of osmotic pressure; therefore, to improve the model from a theoretical engineering perspective, the Van't Hoff equation (Eq 5.55) was utilised instead.

$$\pi = iRT \sum m_j \quad \text{Eq 5.55}$$

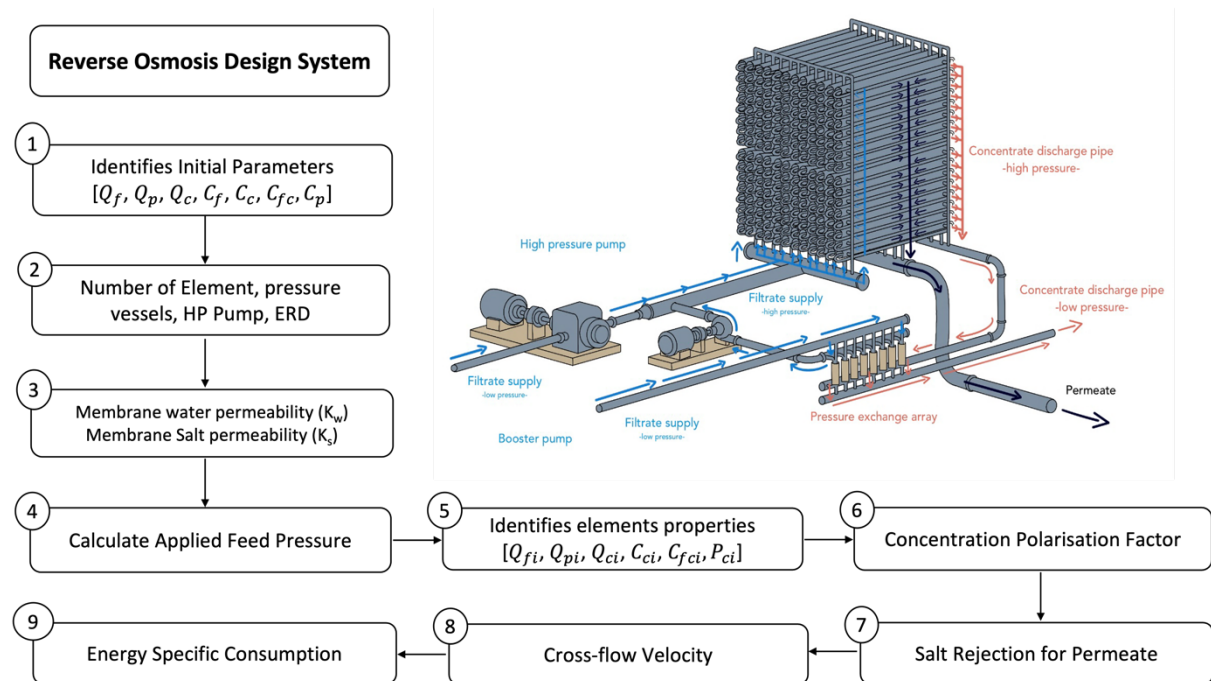


Figure 5–7: The steps followed in designing RO system.

where, π is osmotic pressure in Pa, R is the ideal gas constant ($8.303 \text{ J}/(\text{mol} \cdot \text{K})$), T is the absolute temperature in K, m_j is the sum of molarity of all ionic and non-ionic constituents in water which is in mol/m^3 and i is the Van't Hoff factor that accounts for both the stoichiometric dissociation and the degree of dissociation of a single electrolyte in solution.

5.6.1 Identify Initial Plant Parameters

The initial step in the design of a RO system involves the determination of the characteristics and quantities of the influent and effluent streams of a desalination facility. Equations that were employed in the process of completing this step are shown in the Table 5-11.

Typically, the formula $C_c = C_f / (1 - R)$ is utilised for determining the salinity of brine, assuming perfect salt rejection of 100 percent. However, in practise, complete salt rejection (SR) is not feasible for single pass RO, resulting in salt ion passage into the permeate. Therefore Eq 5.58 is utilised instead; this formula's derivation is presented in the APPENDIX C. The variation in salinity between the feed and brine boundaries is taken into consideration when determining the salinity of the permeate using Eq 5.59 and Eq 5.60.

Table 5-11: Equations for identify initial plant parameters [323]

Parameters	Unit	Equations	
Feed flowrate	m ³ /h	$Q_f = \frac{Q_p}{R}$	Eq 5.56
Concentrate flowrate	m ³ /h	$Q_c = Q_f - Q_p$	Eq 5.57
Concentration of concentrate	mg/l	$C_c = \frac{C_f(1 - R(1 - SR))}{1 - R}$	Eq 5.58
Average feed-concentrate concentration	mg/l	$C_{fc} = \frac{C_f + C_c}{2}$	Eq 5.59
Permeate concentration	mg/l	$C_p = C_{fc}(1 - SR)$	Eq 5.60

5.6.2 Design RO Membrane System

The average flux of a system relates the permeate flow rate of the system to the active membrane area of the system. System flux is useful for estimating the number of required elements for a project. The majority of systems that operate on high-quality feed water tend to have a high flux value, while the converse is true for low-quality feed water systems. Systems utilising the same category of input water can be designed with higher or lower flux values, depending on whether the objective is to minimise initial investment costs or long-term operating costs. To determine the appropriate average flux, for different types of intake systems using an 8-inch FILMTEC element, Table 5-12 serves as a useful reference.

Table 5-12: Design guidelines for 8-inch FilmTech elements in water treatment applications [321]

	Well or open intake with UF	Open intake with advanced pretreatment*	Open intake generic conventional pretreatment
SDI	SDI < 2.5	SDI < 3	SDI < 5
Average flux (Lmh)	15 -19	14 - 17	12 - 17
Maximum element flux	36	34	32
Maximum element recovery	15	14	13
Max Q_f for 34.4m ² element	14	13.5	13
Max Q_f for 35.3m ² element	16	15	14
Max Q_f for 37.2m ² element	16	15	14

*advanced pretreatment: this means membrane filtration or advanced conventional pretreatment.

As shown in Eq 5.62, the number of elements (N_e) in a system can be determined by dividing the design permeate flow rate (Q_p) by the input flow rate per element. To compute the feed flow rate per element, the selected flux value from Table 5-12 is multiplied by the membrane surface area (A_e) corresponding to the element of interest (options shown in Figure 5–6). After obtaining the necessary number of elements, the number of pressure vessels (N_{pv}) is computed. As shown in Eq 5.63, this calculation entails dividing N_e by the number of elements per pressure vessel ($N_{e/pv}$). It is essential to determine the number of elements per pressure vessel which range between 6 and 8. N_{pv} must be rounded to the nearest integer, and N_e must be recalculated using the amended N_{pv} value.

In addition, it is necessary to recalculate the flux and flow per element to evaluate the alterations caused by the preceding step. Notably, the difference between the calculated flux and the presumed flux should not exceed 0.5 LMH during the calculation procedure. If this threshold is exceeded, the calculation must be repeated with a different presumed flux. Finally, it is viable to ascertain the feed, permeate, and concentrate flow rates per pressure vessel. Step 2 can be carried out by following Table 5-13’s outlined sequence. The final evaluation consists of determining whether the feed flow per pressure vessel is less than the maximum feed flow per element (as shown in Table 5-12). In the event that this is not the case, the calculation must be repeated using a different flux value.

Table 5-13: Equations and steps for design RO membrane [323]

Steps	Unit	Equations	
Flow per element	m^3/h	$Q_e = \frac{J_{assumed} A_e}{1000}$	Eq 5.61
Number of elements required in the plant		$N_e = \frac{Q_p}{Q_e}$	Eq 5.62
Number of pressure vessels required in the plant		$N_{pv} = \frac{N_e}{N_{e/pv}}$	Eq 5.63
Recalculate number of elements		$N_e = N_{pv} N_{e/pv}$	
Recalculate new flux	l/m^2h	$J_{avg} = \frac{Q_e}{N_e A_e}$ If: $J_{avg} - J_{assumed} < 0.5$, 'ok', 'Not ok'	Eq 5.64
Check the flow per element		Eq 5.61	
Feed flow per pressure vessel	m^3/h	$Q_{fpv} = \frac{Q_f}{N_{pv}}$	Eq 5.65
Permeate flow per pressure vessel	m^3/h	$Q_{ppv} = R Q_{fpv}$	Eq 5.66
Brine flow per pressure vessel	m^3/h	$Q_{cpv} = Q_{fpv} - Q_{ppv}$	Eq 5.67
Number of trains		$N_T = \frac{N_{pv}}{N_{pv/T}}$	Eq 5.68

5.6.3 Water and Salt Membrane Permeability Coefficient

The water permeability (K_w) is not available directly from the manufacturer; however, it can be calculated using the membrane test results under standard conditions. Figure 5–6 provides information regarding the parameters and value used in the standard test conditions. K_w is defined as follows:

$$K_w = \frac{Q_s}{NDP_s A_e} \quad \text{Eq 5.69}$$

Where, K_w is water permeability (L/bar m^2h), NDP_s is net driving pressure (bar), A_e is element surface area (m^2) and s indicates that these parameters are at standard test conditions for the membrane element.

The NDP (bar) of a membrane system is the difference between the feed pressure and the osmotic pressure. It provides a numerical representation of the actual driving force that forces water through a membrane. The determination of net driving pressure involves the

measurement of the feed pressure itself, pressure drop, osmotic pressure, and permeate pressure which presented as follows:

$$NDP = P_{f_s} - \left[\frac{\Delta P_e}{2} + \Delta\pi_{f_c-p} + P_{p_s} \right] \quad \text{Eq 5.70}$$

Where P_{f_s} is feed pressure, ΔP_e is pressure drop, $\Delta\pi_{f_c-p}$ is equal to the difference between the feed-concentrate osmotic pressure (π_{f_c}) and the permeate osmotic pressure (π_p). The pressure drop term represents the decrease in pressure that occurs along the direction from the feed end to the concentration end within the housing pressure vessel. Typically, this value falls within or below the threshold of 0.35 bar for a given membrane element while the maximum permissible pressure loss per pressure vessel should not exceed 3.5 bar [324], [325]; according to another reference, the range is reported to be between 1.2 and 2 bar [323] which can be determined using the following equation (Eq 5.71):

$$\Delta P_e = 0.01n \left(\frac{Q_f + Q_c}{2} \right)^{1.7} \quad \text{Eq 5.71}$$

Where, Q is feed flow rate (m^3/h) for feed (f) and brine (c), L_{pv} is the length of pressure vessels (m) which calculated by number of elements within the pressure vessels by the length of element (nL_e), μ water viscosity ($\text{Pa} \cdot \text{s}$), w is membrane width (m) and d is thickness of spacer (m).

The determination of the osmotic pressure of the feed-concentrate entails a sequential process. The calculation of osmotic feed pressure and brine feed pressure is performed Eq 5.55. Subsequently, the mean value of these two pressures is determined. The permeate osmotic pressure is also calculated using Eq 5.55. After determining the aforementioned values, the flux is computed using Eq 5.76. However, in this case, the nominal capacity for permeate (Q_{w_s}) is utilised, which denotes the permeate flow rate of the element divided by a period of 24 hours. At this step, all parameters have been determined, thereby enabling the calculation of water permeability and permeability productivity (Eq 5.77, Eq 5.78 respectively). Table 5-14 presents a guideline that should be followed to achieve step 3. The DuPont technical report [326] states that the membrane permeability (\bar{A}) was determined based on the average concentration-side osmotic pressure, $\Delta\pi_{f_c}$, which can be computed using the following equations (Eq 5.74). The water permeability, K_w , typically exhibits a range of 1 to 2 Lmh/bar

[66]; however, in the event that the osmotic pressure exceeds the upper limit, the resulting equation will yield a negative value for permeability.

$$\bar{A}(\bar{\pi}) = 0.125; \bar{\pi} \leq 25 \text{ psi}$$

$$\bar{A}(\bar{\pi}) = 0.125 - 0.011 \left(\frac{\bar{\pi} - 25}{35} \right); 25 \leq \bar{\pi} \leq 200 \text{ psi} \quad \text{Eq 5.72}$$

$$\bar{A}(\bar{\pi}) = 0.07 - 0.0001(\bar{\pi} - 200); 200 \leq \bar{\pi} \leq 400 \text{ psi}$$

The calculation of salt permeability can be determined utilising Eq 5.79. It is important to recognise that the calculations regarding water and salt permeability are performed under standardised conditions, specifically at a temperature of 25°C. Nevertheless, it is crucial to acknowledge that these analyses may necessitate execution at varying temperatures, which can be either lower or higher than the standard. To accommodate variations in temperature, it is possible to employ a temperature correction factor (TCF) by multiplying the membrane permeability by the correction factor. In order to ascertain the suitable temperature correction, one can employ the following equations; in Eq 5.73, T is the temperature in degrees Celsius.

$$TCF = e^{\left(2640 \left(\frac{1}{298} - \frac{1}{273+T} \right) \right)}; T \geq 25^\circ\text{C} \quad \text{Eq 5.73}$$

$$TCF = e^{\left(3020 \left(\frac{1}{298} - \frac{1}{273+T} \right) \right)}; T \leq 25^\circ\text{C}$$

Table 5-14: Steps for obtaining the coefficient factor of water and salt permeability [323]

Steps	Unit	Equation
Brine concentration	mg/L	$C_{c_s} = \frac{C_{f_s}(1 - R_e(1 - SR))}{1 - R_e}$
Permeate concentration	mg/L	$C_{p_s} = C_{f_s}(1 - SR)$
Osmotic feed pressure, Osmotic concentrate pressure, Osmotic Permeate Pressure	bar	Eq 5.55, assume that seawater consist of NaCl
Osmotic feed/concentration average	bar	$\pi_{f_{c_s}} = \frac{\pi_{f_s} + \pi_{c_s}}{2}$ Eq 5.74
Osmotic pressure difference	bar	$\Delta\pi_{f_{c_s}-f_{p_s}} = \pi_{f_{c_s}} - \pi_{p_s}$ Eq 5.75

Steps	Unit	Equation	
Permeate pressure	bar	$P_{ps} = 0$	
Net driving Pressure	bar	Eq 5.70	
Flux under standard conditions	L/m ² h	$J_{ws} = \frac{Q_{ws}}{A_e} \times 1000$	Eq 5.76
Water permeability	L/bar m ² h	$K_w = \frac{J_{ws}}{NDP_s}$	Eq 5.77
Permeability Productivity	m ³ /h/bar	$K_w A_e$	Eq 5.78
Salt permeability	L/m ² h	$K_s = J_s \left(\frac{C_{ps}}{C_{fc_s}} \right)$	Eq 5.79
Permeability correction		$K_s, K_w \times TFC$	Eq 5.80

5.6.4 Determination of Feed Pressure

This step involves evaluating the feed pressure applied in the RO system. It is imperative to recognise a constraint of this model, specifically the underlying assumption that the composition of seawater is exclusively comprised of sodium chloride. Seawater, in actuality, comprises a diverse array of ions and solutes. Consequently, this assumption has the potential to undermine the precision of the computed feed pressure. The calculated flux from step 2 and water permeability from step 3 are used to determine the NDP:

$$NDP = \frac{J_{avg}}{K_w} \quad \text{Eq 5.81}$$

Then step 3 to 6 in Table 5-14 should be repeated to determine the average side-concentrate osmotic pressure using the value for the study case. After that, the headloss per pressure vessel should be calculated by multiplying the obtained value from Eq 5.71 by the number of elements per pressure vessels.

$$\Delta P_{pv} = \Delta P_e N_{e/pv} \quad \text{Eq 5.82}$$

The estimated feed pressure can be calculated using the following equation and the value should be rounded to the nearest number.

$$P_f = NDP + \left[\frac{\Delta P_e}{2} + \Delta \pi_{fc-p} + P_{ps} \right] \quad \text{Eq 5.83}$$

5.6.5 Parameters Determination for Each Element

Throughout this specific step, the determination of the recovery, feed flow rate, and permeate flow rate is conducted for each individual element. The schematic diagram in Figure 5–8 shows the flow pattern of the feed water within the pressure vessels, encompassing the configuration of a maximum number of elements interconnected in series.

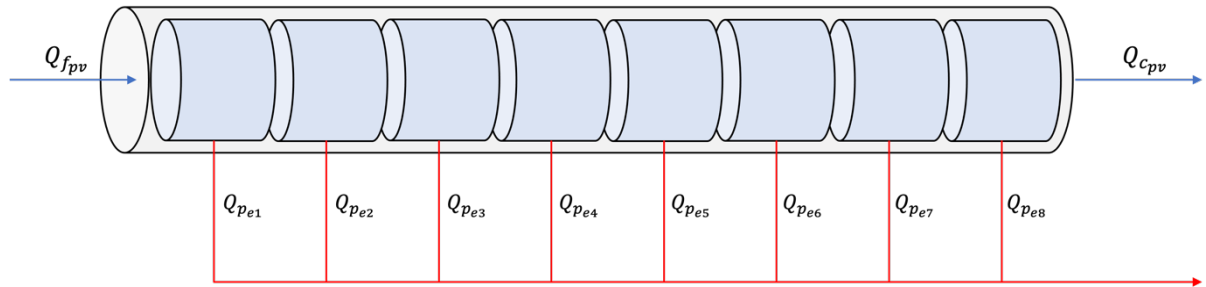


Figure 5–8: Illustration of the flow stream inside pressure vessels with 8 elements in series

Figure 5–9 depicts a series of sequential steps that are executed for every individual component within the pressure vessels. The majority of information and equations regarding water feed flow rate, concentration, and applied feed pressure for each pressure vessel have already been determined. As a result, it is recommended that steps 1 to 8 follow the similar procedure and calculations employed in step 4. In the ninth step, a newly equation is utilised to calculate the permeate flow rate for the element, which is represented as (Q_{pi}). This equation is expressed as:

$$Q_{pi} = NDP_i K_w A_e \quad \text{Eq 5.84}$$

The calculation of the recovery rate for the element involves the division of the permeate flow rate by the feed flow rate of the element. If the recovery rate that has been calculated is consistent with the assumed recovery rate, then the subsequent step can be carried out. In the event of a disagreement the calculated recovery rate is adopted as the new assumed recovery rate, necessitating a repetition of the process starting from step 5 in the diagram. The iterative loop continues until the assumed recovery rate is equivalent to the calculated recovery rate. Step 12 involves the assessment of various parameters, including the brine flow rate (Q_{ci}), the

average flow rate between the concentrate and feed sides (Q_{fc_i}), the concentration of the brine, and the brine pressure of the first element (P_{c_i}). This objective is achieved by employing the subsequent equations:

$$\begin{aligned}
 Q_{c_i} &= Q_{f_i} - Q_{p_i} \\
 Q_{fc_i} &= \frac{Q_{f_i} + Q_{c_i}}{2} \\
 C_{fc_i} &= \frac{C_{f_i} + C_{c_i}}{2} \\
 P_{c_i} &= P_{f_i} - \Delta P_{e_i}
 \end{aligned}
 \tag{Eq 5.85}$$

In the context of a sequential process, the output of the preceding element is utilised as the input for the subsequent element. Consequently, the acquired information in step 12 is employed as the input for the next element, necessitating the repetition of the procedure from step 5 onwards. The aforementioned procedure is implemented for all elements integrated within the design of the RO system.

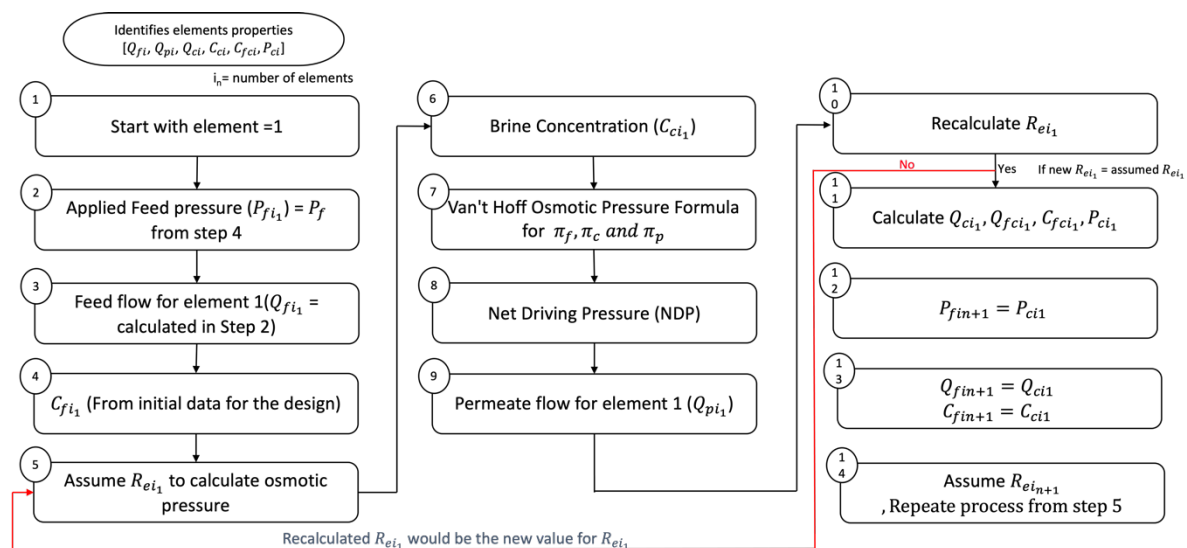


Figure 5–9: Flowchart for determining parameters for each element in pressure vessel

5.6.6 Concentration Polarisation Factor

The concentration polarisation factor (CPF) can be determined for each element by utilising the obtained results per element, employing the following formula:

$$CPF = e^{0.7R}
 \tag{Eq 5.86}$$

It is important to note that the formula provided is specifically applicable to Dow membranes. If a different type of membrane is utilised, it is necessary to verify the validity of this equation for the specific case and element being considered. For instance, the calculation of concentration polarisation using Hydranautics membranes is performed using a different equation ($\beta = 0.99e^{(Q_{pi}/Q_{fi})}$), as opposed to DOW's equation. To prevent the occurrence of membrane fouling, it is advisable to ensure that the CPF does not exceed the recommended upper limit of 1.2 [327].

5.6.7 Salt Rejection for Permeate

From Figure 5–9, the final permeate concentration per pressure vessel can be found by determining the product of the permeate concentration and the permeate flowrate for each element. The product is then divided by the sum of the element flow rates. This means that the permeate concentration of each element (C_{p_i}) is dependent on the salt rejection of element ($C_{p_i} = C_{fc_i}(1 - SR)$).

$$C_{product} = \frac{\sum_i^n C_{p_i} Q_i}{\sum_i^n Q_i} \quad \text{Eq 5.87}$$

However, other factors such as flux and concentration polarisation will hinder salt rejection along the membrane which means some salt will pass to the permeate. Therefore, a more suitable approach should be used to take account of these parameters. The methods used to determine the permeate concentration of each pressure vessel in Salini-Rodriguez *et al.* [323] model are represented below in Eq 5.89:

$$J_i = \frac{Q_{p_i}}{A_e}$$

$$C_{p_i} = \frac{K_s C_{fc_i}}{J_i} \quad \text{Eq 5.88}$$

$$C_{product} = \frac{\sum_i^n C_{p_i} J_i}{\sum_i^n J_i}$$

However, these equations do not consider the impact of concentration polarisation, and therefore Eq 5.89, which takes this into account, is proposed and recommended.

$$C_{p_i} = K_s C_{f_{c_i}} \overline{CPF} \frac{A_e}{Q_i} \quad \text{Eq 5.89}$$

5.6.8 Crossflow Velocity Calculation

In the context of maintaining system functionality, crossflow velocity emerges as a significant determinant. The utilisation of crossflow operation is employed within the field of external membrane systems to induce a high shear environment on the surface layer of the membrane. The reduction of concentration polarisation and cake layer resistance can be significantly mitigated through the utilisation of a high crossflow velocity that is oriented perpendicular to the surface of membrane [109]. Based on the results of a prior investigation [109], the examined cross-flow velocity values were documented to range between 0.35 and 0.65 m/s. In contrast, Salini-Rodriguez *et al.* [323] suggested that it is advisable to maintain the cross-flow velocity within the range of 0.1 to 0.2 m/s.

$$v_{f_{c_i}} = \frac{Q_{f_{c_i}}}{A_{effective} \times 3600} \quad \text{Eq 5.90}$$

Where $v_{f_{c_i}}$ is crossflow velocity (m/s), $A_{effective}$ is the effective surface area (m^2) which can be found using the following equations:

$$A_{effective} = \varepsilon w h_e$$

$$w = \frac{A_e}{l_e} \quad \text{Eq 5.91}$$

Where ε is the porosity (0.85 m), w is total spacer width and h_e is height of feed spacer. Porosity is an intrinsic characteristic that delineates the existence of empty spaces within a substance and is commonly measured as the proportion of void volume to the overall volume of the substance. In the context of spiral-wound membrane systems, the porosity of the feed channel pertains to the proportion of void volume within the channel relative to the overall volume of the spacer. The porosity value in question exhibits a range between 0 and 1 [328], with 0 denoting the complete absence of voids and 1 indicating a structure that is entirely porous. In practical applications, feed spacer porosity values of 0.8 or 0.85 [329] are frequently employed.

5.6.9 Specific Energy Consumption

The literature review examines and emphasises the issue related to the SEC associated with RO systems, as well as the projected energy rate. The calculation of SEC can be theoretically determined using Eq 5.92. However, it is important to note that this equation does not incorporate the ERD equation.

$$SEC = \frac{0.0275P_f}{\eta_P\eta_M R} \quad \text{Eq 5.92}$$

Where 0.0275 is the required energy to raise the pressure of 1 m^3 water to 1 bar, and P_f is the applied feed pressure for the RO process, $\eta_P\eta_M$ is the efficiency of pump and motor respectively. R is recovery rate since in RO and NF, the recovery is less than 100%. To integrate the effectiveness of ERD and minimise the impact of high SEC, the following equation can be employed:

$$SEC = \frac{0.0275P_f}{\eta_P R} - \frac{0.0275(1 - R)P_c\eta_{ERD}}{R} \quad \text{Eq 5.93}$$

Where, P_c is the brine pressure of the last element in the pressure vessel, η_{ERD} is the efficiency of ERD.

5.7 Discharge System

Three important factors that should be considered when designing the discharge system, including:

1. Quality and quantity of effluent
2. Diffuser system design characteristics
3. Jet and dilution properties

The overall discharge volume encompasses the combined discharges originating from the pretreatment system and the RO system, including both the brine and the membrane cleaning solution. Figure 5–10 illustrates the various sources of effluent within a plant. This section provides a discussion on the formulas used to determine the quantity derived from various sources.

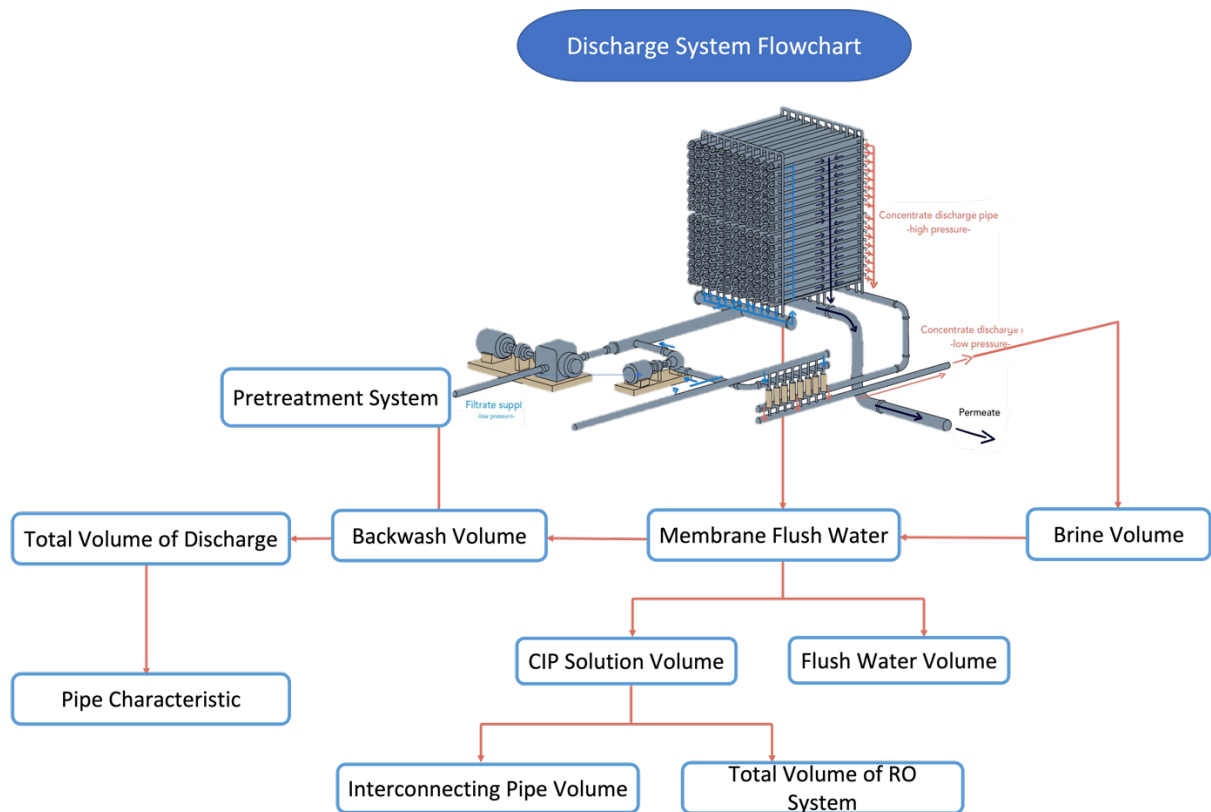


Figure 5–10: A flowchart of the discharge sources in the SWRO facility

The volume of the brine obtained from RO system is determined by Eq 5.94.

$$Q_c = Q_p \times \frac{1 - R}{R} \quad \text{Eq 5.94}$$

To eliminate accumulated foulants on the surface of membranes during ordinary plant operations, it is necessary to routinely clean the membranes used RO separation using chemical agents. Therefore, the RO sub-system must undergo a cleaning process that includes cleaning-in-place (CIP) and flush water.

The estimation of the typical volume of a cleaning solution (V_{CIP}) involves the summation of the volume of the RO system ($V_{RO-system}$) and the volume of the interconnecting pipes (V_{pipe}). In general, the quantities of cleaning solution ($V_{unit-cleaning}$) produced during a CIP procedure for RO membranes range from 1.0 to 1.8 L/m² of membrane surface area [30], a value of 1.50 L/m² is assumed in this research. Hence, the overall volume of cleaning solution required for the RO system can be determined using Eq 5.95, whereas the volume of the interconnecting

pipes can be computed using Eq 5.96, where the diameter, ϕ , is assumed to be 0.2 m and the length, L, is 1500 m [30].

It is worth mentioning that these equations solely illustrate the theoretical logic underlying the process and may not be applicable to all membrane elements from different manufacturers, as their membranes are specifically developed to address specific membrane fouling. Hence, it is advisable to verify the prescribed methodology for CIP.

$$V_{RO-system} = \frac{N_{pv}N_{e/pv}A_E V_{unit-cleaning}}{1000} \quad \text{Eq 5.95}$$

$$V_{pipe} = 1000\pi \frac{\phi^2}{4} L \quad \text{Eq 5.96}$$

$$V_{CIP} = V_{RO-system} + V_{pipe} \quad \text{Eq 5.97}$$

The quantity of flushing water (V_{flush_water}) in required for the cleaning of RO is contingent upon the dimensions of the RO system, as a general guideline, the volume of flushing water should be approximately 5 to 10 times greater than the volume of the cleaning chemicals utilised; this is accounted for by using a factor c in Eq 5.98 .

$$V_{flush_water} = V_{RO-system}(1 + c) \quad \text{Eq 5.98}$$

The backwash water (Q_{bw}) obtained from pretreatment is calculated using the following equation (Eq 5.99):

$$Q_{bw} = Q_p \times \frac{bw}{R} \quad \text{Eq 5.99}$$

This study proposes the inclusion of an additional step, namely the installation of a Dilution Tank into the discharge system as shown in Figure 5–11. In certain geographical areas, there may exist regulations regarding the permissible concentration of dissolved solids that can be released into seawater. Consequently, the incorporation of a dilution tank can serve as a means to adjust the TDS content of the effluent, which is calculated using Eq 5.100. This step requires obtaining TDS values for both the input and output to determine the necessary flow rate (Q_d) for achieving the desired target TDS (TDS_b).

$$Q_d = \frac{(Q_c + Q_{bw})TDS_b - (Q_cTDS_c + Q_{bw}TDS_{bw})}{TDS_d - TDS_b} \quad \text{Eq 5.100}$$

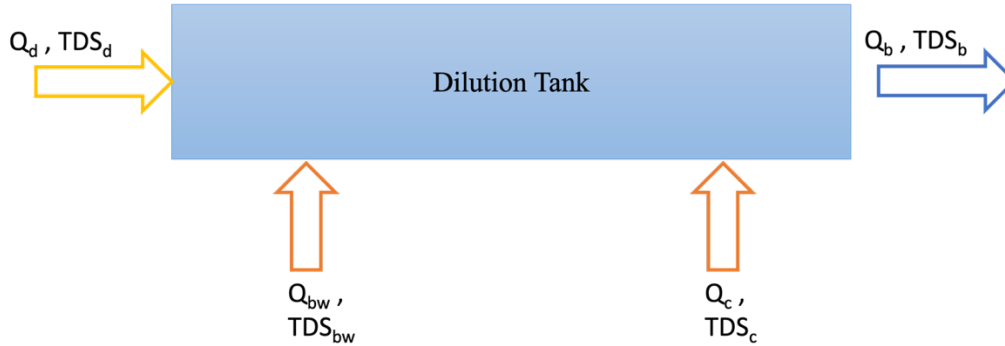


Figure 5-11: Suggested dilution tank

The total flow rate of the discharge system comprises the combined quantities of backwash water, brine, CIP, and dilution, if the last option was chosen.

$$Q_{discharge} = Q_d + Q_c + Q_{bw} + Q_{CIP} + Q_{flush_water} \quad \text{Eq 5.101}$$

The diffuser system design characteristics are developed from the following papers [301], [330], [331], [332]. The sequence of computational steps is presented in Table 5-15, accompanied by a separate

Table 5-16 containing suggested initial values for doing these calculations.

First, the discharge angle, offshore slope angle, number of diffuser openings, port diameter and port height and diffuser offshore location should be selected. The effluent from the SWRO systems descends and settles on the seabed, where the magnitude of the sinking phenomenon can be described by the buoyant acceleration (\acute{g}_o), as represented in Eq 5.102. The formation of the liquid jet from the diffuser's nozzle is influenced by the exit speed (v_{diff}) and the diameter (\emptyset_{diff}) of the nozzle. The densimetric Froude number Fr_o , as defined in Eq 5.103, characterises both parameters. Q_{port} (m^3/s) is flow at the port of the nozzle which can be calculated by dividing brine flow rate by number of ports. The Reynolds number of jet is calculated to check that the discharge jet achieves a good mixing with the seawater and its Reynolds number of jet to be in the turbulent range of > 4000 ; $\nu_{discharge}$ is the kinematic viscosity of the discharge in (m^2/s).

Table 5-15: Equations for calculating diffuser system design characteristics [301], [330], [333], [334]

Steps	Unit	Equations	
Buoyant acceleration	m^2/s	$\dot{g}_o = g \frac{\rho_{discharge} - \rho_{sw}}{\rho_{discharge}}$	Eq 5.102
Velocity at diffuser port	m/s	$v_{diff} = \frac{4Q_{port}}{\pi\Phi_{diff}^2}$	Eq 5.103
Froude number		$Fr_o = \frac{v_{diff}}{\sqrt{\Phi_{diff} \times \dot{g}_o }}$	Eq 5.104
Reynold's number of jet		$R_o = \frac{v_{diff}\Phi_{diff}}{v_{discharge}}$	Eq 5.105
Buoyancy flux	m^4/s^3	$J_o = \dot{g}_o Q_{port}$	Eq 5.106
Momentum flux	m^4/s^3	$M_o = v_{diff} Q_{port}$	Eq 5.107
Discharge length	m	$L_o = \sqrt{\frac{\pi D^2}{4}}$	Eq 5.108
Momentum length scale	m	$L_M = \frac{(M_o)^{\frac{3}{4}}}{\sqrt{J_o}}$	Eq 5.109

Table 5-16: Recommended value for designing diffuser system [301], [330], [333], [334]

Parameters	unit	Recommended value
Froude number (Fr_o)		≥ 10 , recommended 20–25
Velocity at diffuser port (v_{diff})	m/s	4–6
Nozzle exit diameter (Φ_{diff})	m	0.1–1, recommended ≥ 0.25
Reynolds number of jet (R_o)		> 4000
Discharge angle (Θ_o)	degrees	30–60, for deep water 60
Port height (h_{port})	m	0.5 - 1

Extensive laboratory tests were conducted to investigate the geometry of the discharge jet at different Froude numbers, nozzle diameters, and nozzle angles. The tests were performed under defined Froude numbers and flow conditions in the discharge area of diffuser ports. The diffusers were of single-port, multiport, and rosette configurations [331], [332], [333], [334], [335]. The investigations result in equations containing empirical coefficients, which are

presented in Table 5-17[4]. These equations pertain to a diffuser with a single port and stagnant flow conditions at discharge. For complex calculation, there are multiple software such as CORMIX, VISJET software and Delft 3D [4].

Table 5-17: Design C-factor values for dimensions and potential dilution rate of single-jet diffusers in stagnant conditions [4], [331], [332], [333], [334], [335]

Parameter dilution at	Unit	Equation	Nozzle angle/ C factor			
			30°	45°	60°	75°
Impact point (s_i)	-	$Fr_o C_1$	1.2	1.6	1.65	1.5
Near field (s_n)	-	$Fr_o C_2$	1.85	2.5	2.6	2.1
Location of impact point (x_i)	m	$\emptyset_{diff} Fr_o C_3$	3.5	3.6	2.75	1.9
Near – field length (x_n)	m	$\emptyset_{diff} Fr_o C_4$	10.3	11.0	9.5	8.4
Height of jet rise (y_i)	m	$\emptyset_{diff} Fr_o C_5$	1.18	1.8	2.25	2.64

5.8 Power Calculation

The power demand of an intake system utilising direct extraction can be calculated by adding the power demands of the SWRO supply pumps and the intake screening systems. The power demand of active screening equipment is determined by the contributions of:

1. Power for driving the moving screening elements or the rotating drum
2. Power for the pressurised water spray that dislodges solids from the screens' surfaces
3. Power to activate the compressor, which generates compressed air for the purpose of flushing the screen elements of its extraction heads.

Hence, there is no specific equation in the literature that can be utilised to calculate this power. Therefore, only the power requirements of the SWRO supply pumps is considered for the intake system power, which can be determined using Eq 5.110.

$$P_{Intake} = \frac{g\rho Q_{fSWRO} \Delta H}{3.6 \times 10^6 \eta_M \eta_P \eta_{VSD}} \quad \text{Eq 5.110}$$

Where, P_{Intake} is power demand of intake system (kW), ρ is density of seawater (kg/m³), ΔH head of seawater supply pump (m), $\eta_P, \eta_M, \eta_{VSD}$ is efficiency of the pump, motor and variable

speeds drive respectively. In practise, the head of a pump must take into account various factors, including the depth of the intake, and the overall pressure head losses in the feed pipe and suction pipe. These losses encompass both minor losses (such as those caused by valves and bends) and major losses (caused by friction) [336]. This calculation necessitates extensive data and graphs pertaining to the material and shape of the pipe, which pose challenges in their consideration. Hence, the system losses are neglected and the intake power requirement is determined solely by the intake system's depth.

Table 5-18 provides the expected SEC for different configurations of the pretreatment subsystem and Eq 5.93 calculates the SEC for the RO subsystem.

Table 5-18: SEC consumption for pretreatment configurations [30], [301]

Pretreatment process	Pretreatment	
	recovery %	SEC (kWh/m ³)
Mechanical mixer		
Conventional sedimentation	-	0.0012 – 0.0017
Lamella sedimentation	-	-
DAF	-	0.006 – 0.0072
Static mixer and gravity granular media filtration	0.95	0.02
Static mixer and two stage gravity granular filter media	0.94	0.03 – 0.05
Gravity granular media filtration + floc basins	0.95	0.1
Two stage gravity granular media filtration + floc basins	0.94	0.12
Static mixer and pressure granular media filtration	0.95	0.1
Static mixer + two stage pressure granular media filtration	0.95	0.2 – 0.4
Sedimentation and granular media filtration	0.95	0.14
Sedimentation and two stage granular media filtration	0.94	0.15
DAF and granular media filtration	0.95	0.15
DAF and two stage granular media filtration	0.94	0.16
Membrane filtration and static mixer	0.93	0.1 – 0.2
DAF and membrane filtration	0.92	0.25

The posttreatment and product water delivery only contribute approximately 5% of the total SEC of SWRO desalination plant, therefore, in this research the study would assume that the value of SEC is 0.18 kWh per m³ of treated water [28]. The power demand of a discharge system is contingent upon the specific configuration employed. A recent study found that the SEC for discharge systems falls within the range of 0.01 to 0.03 kWh per cubic metre of treated water [337]. However, another research study reported a higher value of approximately 0.27

kWh per cubic metre of treated water, which encompasses the power required for solid handling as well [28].

To determine pump efficiency, a comprehensive dataset was gathered from various sources, encompassing a wide range of pump capacities. This extensive data collection was undertaken to facilitate the selection of the most suitable pump for each unique scenario. The dataset comprises approximately 6,575 individual pumps, each with a flow rate ranging from 46 m³/h to 9791 m³/h. Data for these pumps was collected within an operational range that extends up to $\pm 30\%$ from their respective best efficiency points. The dataset includes crucial information such as flow rate, head, rated power, efficiency, Net Positive Suction Head Required (nsph), diameter, and maximum suction pressure for each pump. This diverse dataset provides valuable insights into the performance characteristics of different pumps and aids in making informed pump selections for various applications. In the future, when coupled with a more complex energy model, this dataset has the potential to provide significant insights into the SEC patterns observed in different sections of the system. These insights can be valuable in identifying areas that require process modifications. It is imperative to acknowledge that within this study, the utilisation of the aforementioned data will be limited to particular system components, namely the intake, RO, and discharge systems.

To assess the motor's efficiency, it is essential to comply with EU Commission Regulation [338], which mandates that all pumps and motors must meet a minimum IE3 efficiency standard. For 50 Hz motors with rated outputs falling between 0.12 and 200 kW [338] and not explicitly listed in Table 5-19 and

Table 5-20, the following equation can be applied:

$$\eta_m = A \left(\log_{10} \left(\frac{P_m}{1kW} \right) \right)^3 + B \left(\log_{10} \left(\frac{P_m}{1kW} \right) \right)^2 + C \left(\log_{10} \left(\frac{P_m}{1kW} \right) \right) + D \quad \text{Eq 5.111}$$

Given the known rated power of the pump, a general guideline is followed, which states that the motor output must be greater than the shaft head work. Consequently, data from Table 5-19 and

Table 5-20, are utilised to select a value that aligns with this guideline. As per the EU Commission Regulation [338], the efficiency of Variable Speed Drives (VSD), denoted as (η_{VSD}) should fall within the range of 79% to 87%. In this study, an assumed average value of 83% is employed to comply with this requirement.

Table 5-19: Minimum efficiencies η_m for IE3 efficiency level at 50 Hz (%)

Rated output power P_m (kW)	Number of poles			
	2	4	6	8
0.12	60.8	64.8	57.7	50.7
0.18	65.9	69.9	63.9	58.7
0.2	67.2	71.1	65.4	60.6
0.25	69.7	73.5	68.6	64.1
0.37	73.8	77.3	73.5	69.3
0.4	74.6	78	74.4	70.1
0.55	77.8	80.8	77.2	73
0.75	80.7	82.5	78.9	75
1.1	82.7	84.1	81	77.7
1.5	84.2	85.3	82.5	79.7
2.2	85.9	86.7	84.3	81.9
3	87.1	87.7	85.6	83.5
4	88.1	88.6	86.8	84.8
5.5	89.2	89.6	88	86.2
7.5	90.1	90.4	89.1	87.3
11	91.2	91.4	90.3	88.6

Rated output power P_m (kW)	Number of poles			
	2	4	6	8
15	91.9	92.1	91.2	89.6
18.5	92.4	92.6	91.7	90.1
22	92.7	93	92.2	90.6
30	93.3	93.6	92.9	91.3
37	93.7	93.9	93.3	91.8
45	94	94.2	93.7	92.2
55	94.3	94.6	94.1	92.5
75	94.7	95	94.6	93.1
90	95	95.2	94.9	93.4
110	95.2	95.4	95.1	93.7
132	95.4	95.6	95.4	94
160	95.6	95.8	95.6	94.3
200 up to 1 000	95.8	96	95.8	94.6

Table 5-20: Minimum efficiencies η_m for IE4 efficiency level 50 Hz (%)

Rated output power P_m (kW)	Number of poles			
	2	4	6	8
0.12	66.5	69.8	64.9	62.3
0.18	70.8	74.7	70.1	67.2
0.2	71.9	75.8	71.4	68.4
0.25	74.3	77.9	74.1	70.8
0.37	78.1	81.1	78	74.3
0.4	78.9	81.7	78.7	74.9
0.55	81.5	83.9	80.9	77
0.75	83.5	85.7	82.7	78.4
1.1	85.2	87.2	84.5	80.8
1.5	86.5	88.2	85.9	82.6
2.2	88	89.5	87.4	84.5

Rated output power P_m (kW)	Number of poles			
	2	4	6	8
3	89.1	90.4	88.6	85.9
4	90	91.1	89.5	87.1
5.5	90.9	91.9	90.5	88.3
7.5	91.7	92.6	91.3	89.3
11	92.6	93.3	92.3	90.4
15	93.3	93.9	92.9	91.2
18.5	93.7	94.2	93.4	91.7
22	94	94.5	93.7	92.1
30	94.5	94.9	94.2	92.7
37	94.8	95.2	94.5	93.1
45	95	95.4	94.8	93.4
55	95.3	95.7	95.1	93.7
75	95.6	96	95.4	94.2
90	95.8	96.1	95.6	94.4
110	96	96.3	95.8	94.7
132	96.2	96.4	96	94.9
160	96.3	96.6	96.2	95.1
200 up to 249	96.5	96.7	96.3	95.4
250 up to 314	96.5	96.7	96.5	95.4
315 up to 1 000	96.5	96.7	96.6	95.4

The interpolation coefficients A, B, C, and D in Eq 5.111 are to be determined based on the information provided in Table 5-21 and Table 5-22.

Table 5-21: Interpolation coefficients for motors with rated power output P from 0.12 kW up to 0.55 kW

IE code	Coefficients				
	2 poles	4 poles	6 poles	8 poles	
IE3	A	6.8532	7.6356	-17.361	-0.5896
	B	6.2006	4.8236	-44.538	-25.526
	C	25.1317	21.0903	-3.0554	4.2884
	D	84.0392	86.0998	79.1318	75.831
IE4	A	-8.8538	8.432	-13.0355	-4.9735

B	-20.3352	2.6888	-36.9497	-21.453
C	8.9002	14.6236	-4.3621	2.6653
D	85.0641	87.6153	82.0009	79.055

Table 5-22: Interpolation coefficients for motors with rated power output P from 0,75 kW up to 200 kW

IE code		Coefficients			
		2 poles	4 poles	6 poles	8 poles
IE3	A	0.3569	0.0773	0.1252	0.7189
	B	-3.3076	-1.8951	-2.613	-5.1678
	C	11.6108	9.2984	11.9963	15.705
	D	82.2503	83.7025	80.4769	77.074
IE4	A	0.34	0.2412	0.3598	0.6556
	B	-3.0479	-2.3608	-3.2107	-4.7229
	C	10.293	8.446	10.7933	13.977
	D	84.8208	86.8321	84.107	80.247

5.9 RO Model Evaluation

The validation of the modified RO system model developed in this research involved a detailed comparative analysis against the model established by Salini-Rodriguez *et al* [323] and the widely used WAVE software as discussed in Section 5.6 . The objective of this validation was to assess the impacts of specific modifications introduced in RO model on key performance metrics. This process is systematically documented through two main analyses, with all relevant data tables provided in APPENDIX D.

Analysis 1: Temperature Variation Impact

The first phase of validation focused on evaluating how temperature variations affect performance indicators such as applied pressure, energy consumption, and permeate salinity. For this analysis, a consistent scenario was maintained across all models: the plant operates at a capacity of 5000 m³/h, with a seawater salinity of 36,045 mg/L, a plant recovery rate of 45%, and temperatures ranging from 15°C to 34°C. This setup allowed for a direct comparison under varying thermal conditions to observe how each model predicts changes in system performance.

Analysis 2: Salinity Level Impact

The second phase examined the impact of varying salinity levels on the Specific Energy Consumption (SEC). In this setup, while the plant capacity and recovery rate remained constant as in the first analysis, the salinity levels were altered. The models were evaluated at three different salinity concentrations: 32,945 mg/L, 36,039 mg/L, and 41,199 mg/L, all at a constant temperature of 25°C. This approach provided insights into the robustness of the models under different ionic stress conditions.

Membrane Specification

Throughout both analytical phases, the SW30XLE-440i membrane was used consistently to ensure that performance variations were attributable to model differences and not membrane characteristics.

Impact of Temperature:

The Salini-Rodriguez *et al.* model proposed in the research [323] demonstrates a capability in computing multiple parameters associated with the RO process. Nevertheless, it has been shown that the values of all relevant parameters stay constant when subjected to different temperatures, as depicted in Figure 5–12c. The Salini-Rodriguez *et al.* model doesn't take into consideration the impact of the temperature on water and salt permeability parameters, as well as the applied pressure. To address this constraint, a modification was implemented as a component of this PhD research, with the objective of integrating the dynamic impacts of temperature, as discussed in the previous section. Additionally, it is essential to acknowledge that the comparative analysis presented in model validation does not incorporate the impact of ERD on SEC values, despite the meticulous consideration of ERD in step 9 of the research, as detailed in section 5.6.9. The reason for this exclusion is due to the limitation of the WAVE software, which only provides SEC values without the inclusion of ERD.

A summary of the results of this comparison are shown Figure 5–12. The finding from the WAVE model and modified model indicates that an elevation in temperature typically results in a corresponding rise in the concentration of permeate (C_p). The underlying cause for this phenomenon is that variations in temperature have an impact on the solubility of solutes in water. In the majority of instances, it can be observed that an increase in temperature leads to an increase in the solubility of salts and other dissolved substances. This means that at higher temperatures, the water can hold more dissolved solids (salts) before reaching the point of saturation, leading to a higher concentration in the permeate [339]. Moreover, the viscosity of

water exhibits a decrease in value as the temperature increases. A decrease in viscosity facilitates the passage of water through the membrane. Consequently, the applied pressure required would decrease due to the previous mentioned phenomenon, resulting in a subsequent drop in the SEC. The captured behaviour is evident in both models, as depicted in Figure 5–12a to Figure 5–12b.

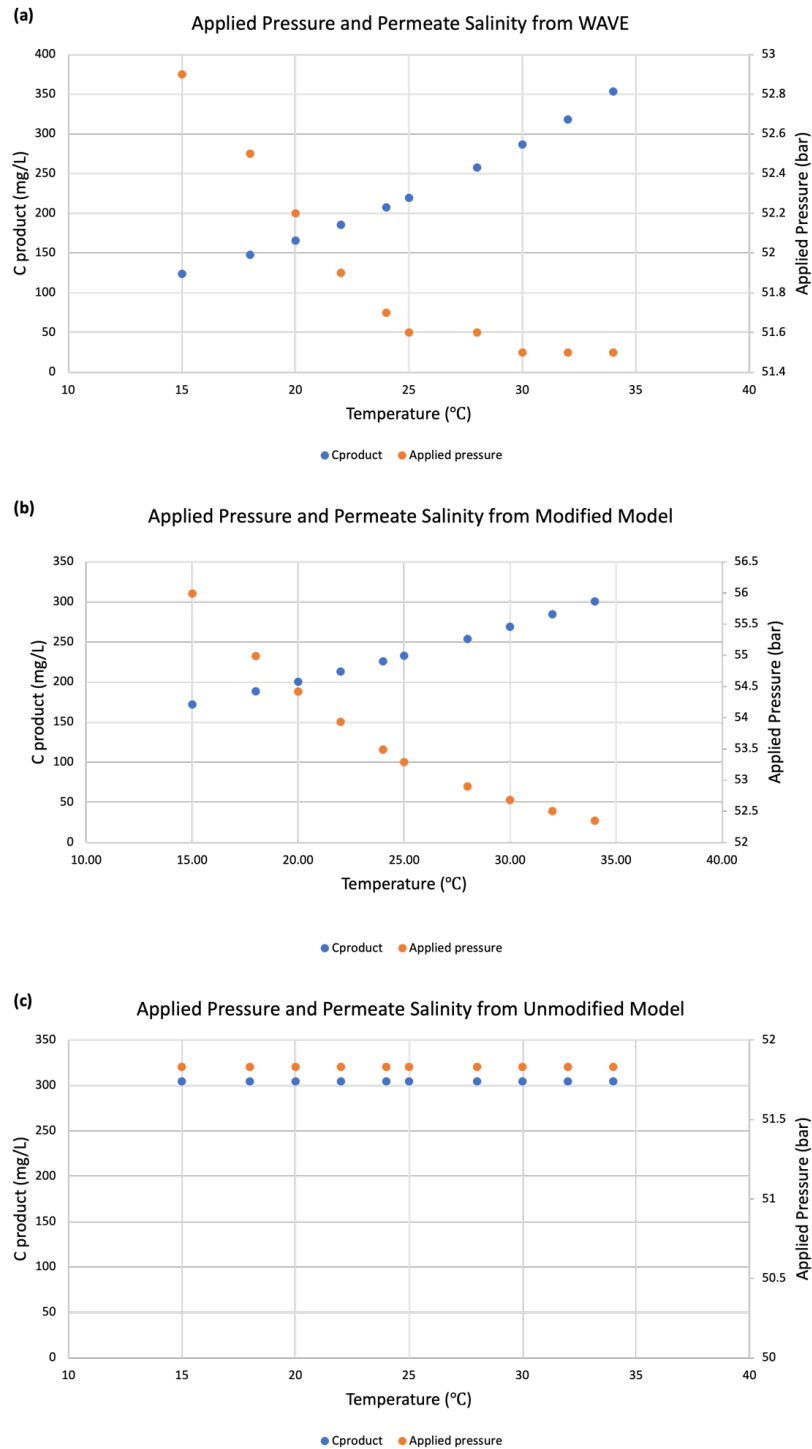


Figure 5–12: Impact of temperature variation on applied pressure and permeate concentration for the three models.

The increase in temperature leads to a gradual increase in the water permeability coefficient. This phenomenon can be attributed to various variables that have been previously explained, including the diffusion rate and thermodynamic effects. Significantly, elevated temperatures result in greater kinetic energy within water molecules, leading to enhanced rates of diffusion. Consequently, this accelerates the movement of water molecules across the membrane. Furthermore, it is imperative to recognise the impact of temperature on the osmotic pressure of the feedwater. Increasing the temperature leads to a simultaneous decrease in osmotic pressure, which in turn reduces the pressure gradient necessary for water to pass through the membrane [51].

Figure 5–13 exhibits a noticeable difference in the values of parameter A obtained from WAVE and the values acquired from the updated model. In the WAVE system, the parameter A exhibits fluctuations between 0.819 and a maximum value of 1.061 LMH/bar as the temperature increases. On the other hand, the modified model’s parameter A shows a range of values from 1.0 to 1.85 LMH/bar as the temperature rises. It is important to acknowledge that the specific method utilised by WAVE to compute coefficient A lacks detailed documentation. The determination of the value of A was carried out using Equation 5.112, as the report provided by WAVE outlines the definitions of flux and NDP values. The calculated value of parameter A obtained from the adjusted model corresponds to the established range of water permeability commonly observed in commercial TFC RO membranes specifically developed for SWRO. This range typically falls between 1 and 2 LMH/bar, as reported in previous studies [340].

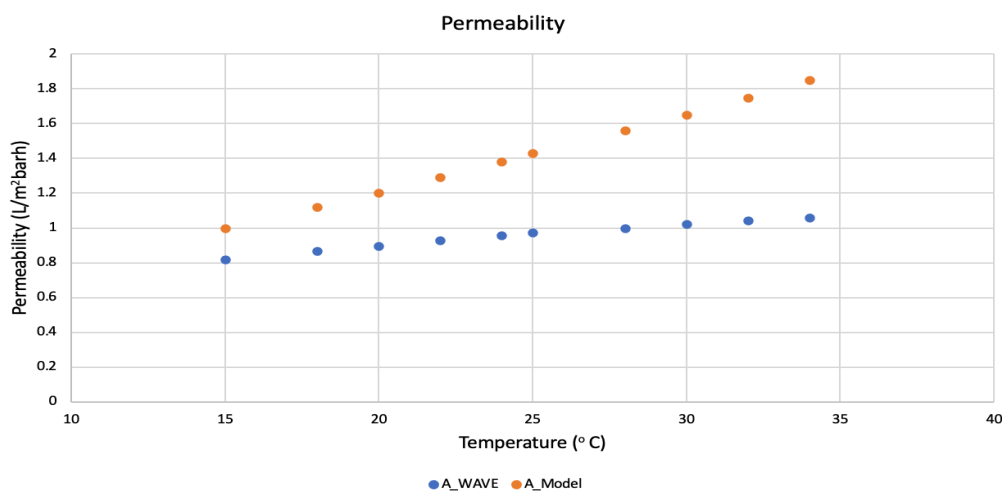


Figure 5–13: Impact of temperature on permeability for wave and designed model

The aforementioned results indicate a significant relationship between the increase in water permeability in a RO membrane component and a decrease in SEC. This phenomenon is supported by the principle that a RO membrane element with greater water permeability can reduce the requirement for extra pressure beyond the osmotic pressure of the brine, particularly when aiming to maintain a consistent average permeate flux. Moreover, it has the potential to enhance the rate at which water permeates through a membrane, leading to an increased recovery rate by raising the average flux of permeate water, while maintaining a constant feed pressure [66]. Nevertheless, in the last ten years, numerous scholars [341], [342], [343] have proposed that the current water permeability of RO membranes has approached a point near the limits imposed by thermodynamics and transport. As a result, additional increases in the permeability of the membrane may only result in minimal decreases in the amount of energy consumed per unit. As stated in the literature TFC has low permeability which may hinder the efficiency of SWRO membrane. However, a lot of studies found that when the water membrane permeability goes above the 3 LMH/bar, there has negligible benefit for the process productivity [341], [342], [343].

Werber *et al.* [341] reviewed module-scale modelling research to determine how membrane water permeability affects process efficiency. The salt mass transfer coefficient at the membrane surface on the feed side path was maintained at 2.77×10^{-5} m/s in their model. Osmotic pressure was computed using the Van't Hoff equation, with a Van't Hoff constant of 2. The model assumed 0% pressure loss in a RO module and 100% pump and ERD efficiency. For SWRO, set input concentration at 35,000 ppm NaCl, recovery rate at 50%, and average system flow at 15 LMH were set. An increase in membrane water permeability from 0.2 to 1 LMH/bar reduced SEC by 45%, or 1.55 kWh/m³ and by 3.7 for permeability between 2 to 10 LMH/bar . The WAVE model demonstrated a 12% reduction in energy consumption, while the modified model exhibited a more significant 28% reduction, as shown in the accompanying Figure 5–14. It is important to note that this analysis accounted for inefficiency variables and maintained the pump efficiency at a constant 80%.

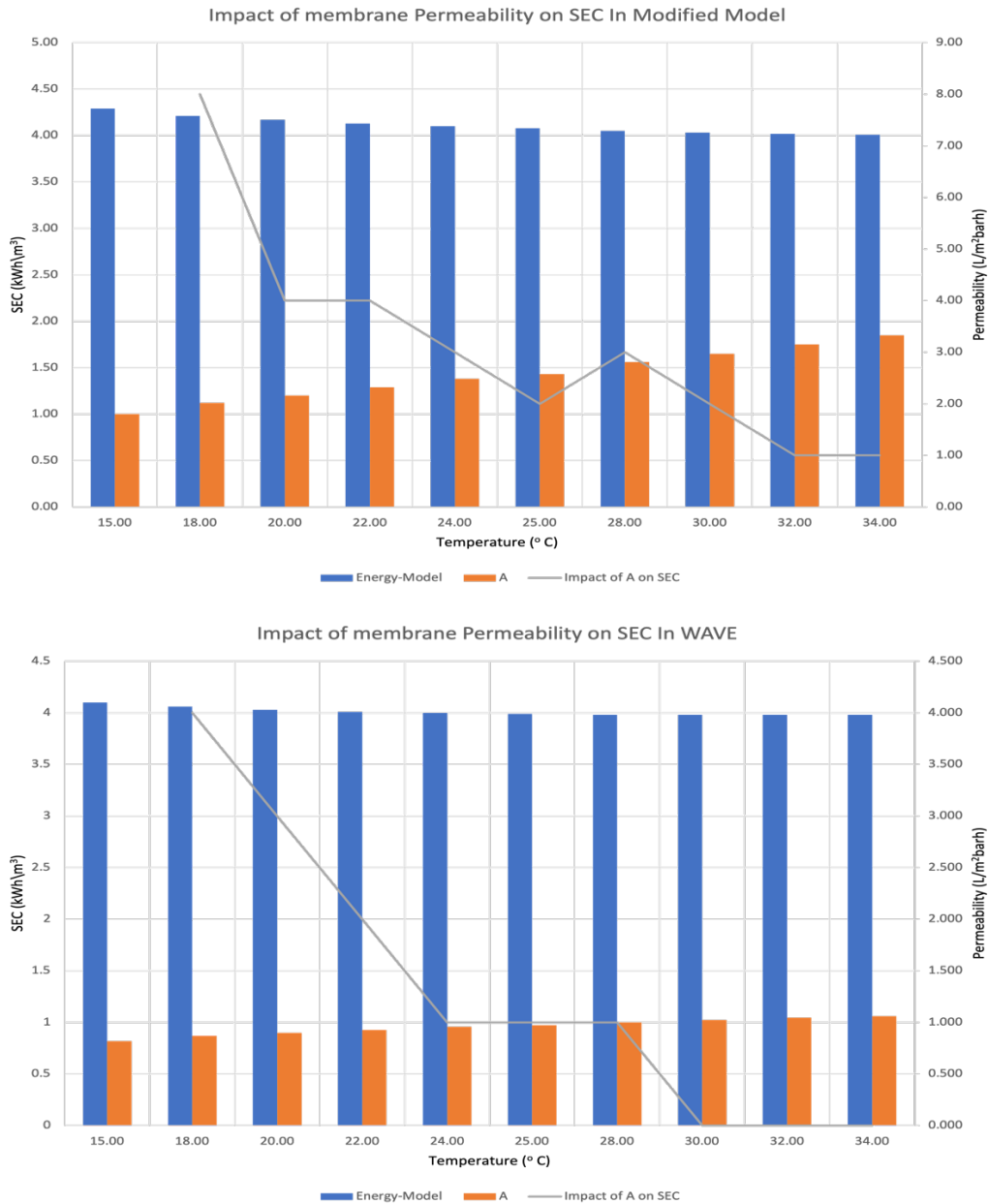


Figure 5–14: Impact of water membrane permeability coefficient on SEC, where energy model is value of SEC at different temperature, A is water permeability.

Impact of varying salinity

The elevation of input water salinity can result in an significant increase in SEC in desalination process as can be seen in Figure 5–15, as a consequence of various interconnected factors:

1. Osmotic pressure has a positive correlation with the salinity of the feed water, whereby an increase in salinity leads to a corresponding elevation in osmotic pressure which

consequently requires a greater amount of energy to facilitate the movement of water across the membrane against this pressure.

2. In the case of feed water with elevated salinity levels, the RO membrane is subjected to increased effort to effectively separate the salts from the water. This necessitates a greater amount of energy input to counteract the heightened driving force resulting from the high salinity.
3. In systems characterised by feed water with elevated salinity levels, the permeate flux tends to decrease. The decrease in permeate flux results in a reduction in the recovery rate, necessitating the allocation of extra energy to sustain a stable production of freshwater.
4. The phenomenon of membrane fouling can be accelerated as the presence of more salinity in the feed water has a negative impact of lowering the permeate flux, hence necessitating increased SEC to compensate for the compromised system performance.

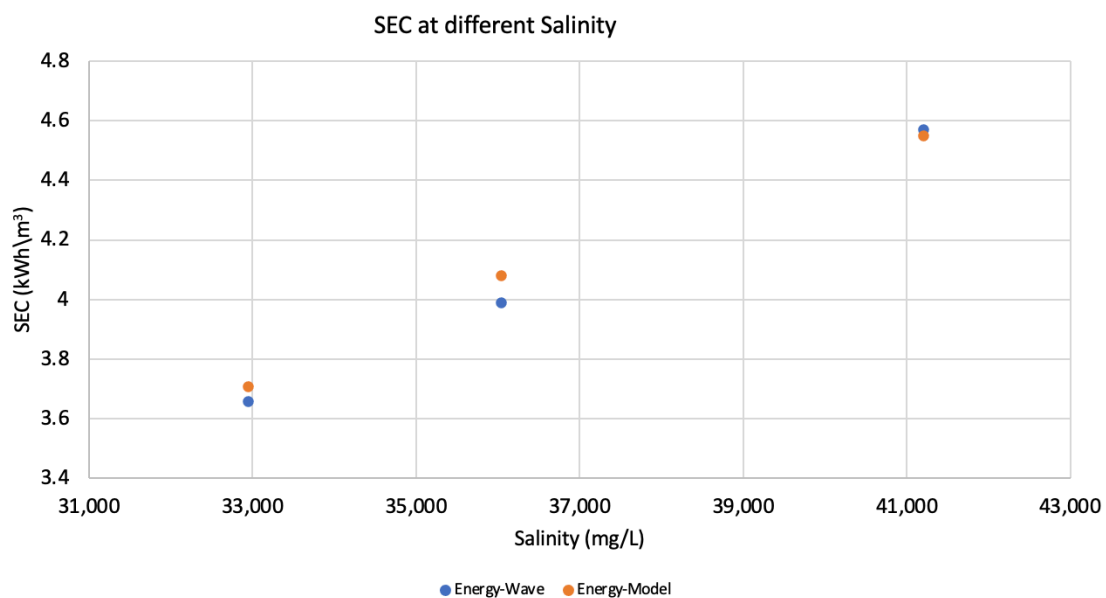


Figure 5-15: Impact of varying salinity on SEC

The results of the investigations demonstrate that both models provide similar outcomes. However, it is important to note that, overall, the WAVE model consistently generated lower values (SEC, C_p , k_w , applied pressure, concentration pressure) compared to the modified model. In addition, as the temperature approached 28 °C and beyond, all the examined parameters exhibited a plateau-like behaviour. In contrast, the adjusted model exhibited a consistent decrease in the examined parameters, with little variations observed from 28 °C

onwards. Koutsou *et al.* [339] conducted a thorough study on the influence of temperature on SEC in SWRO desalination processes. The findings indicate that there was a decrease in the SEC as the temperature increased. However, this decrease reached a plateau state at 35 °C and beyond, which their values remained relatively stable with slight drop. This result align with the result obtained in this study as shown in Figure 5–13.

Behaviour of CPF, Cross Velocity and Flux Through Membrane

The observed data in Figure 5–16, Figure 5–17 and Figure 5–18 indicates a decline in cross velocity, flux, and concentration polarisation factor across the membranes in pressure vessels as the elements advance from the inlet (Element 1) to the outlet (Element 7). The observed phenomena can be ascribed to multiple variables, in accordance with established principles of membrane separation processes.

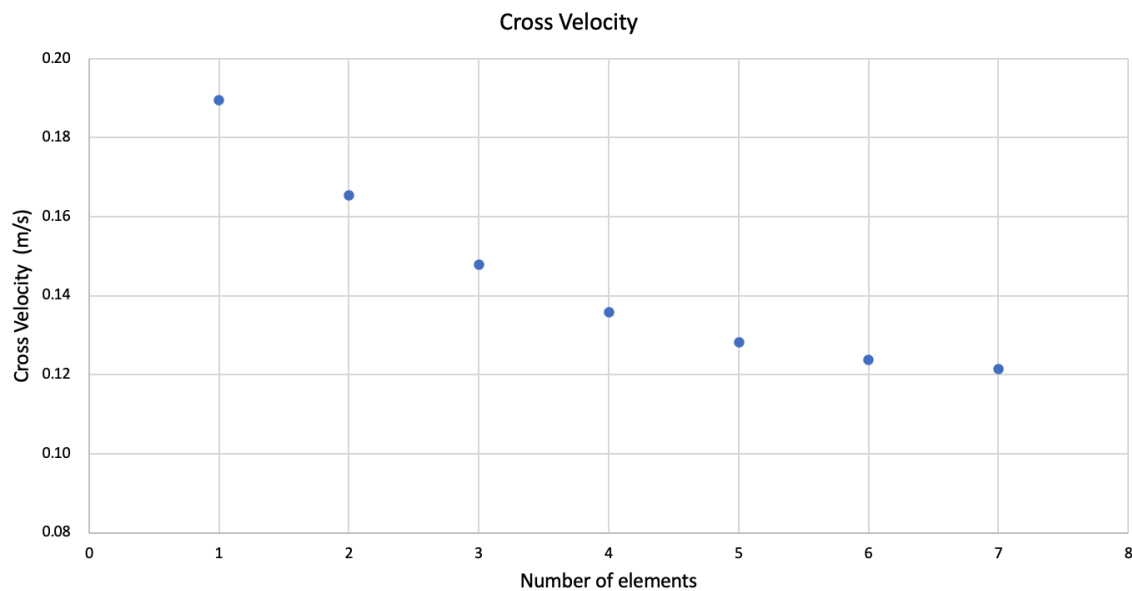


Figure 5–16: Behaviour of cross velocity along the pressure vessel

The reduction in cross velocity is predominantly linked to the presence of non-uniform flow distribution within the pressure vessel. As the feed water flows through the vessel, it experiences different levels of resistance due to many factors, including the vessel's architecture and the arrangement of membrane parts. As a result, it is common for the middle area of the vessel to encounter elevated cross velocities, whereas the outer areas have diminished cross velocities. The presence of non-uniform flow distribution results in a reduction in cross velocity in proximity to the membrane surface.

The drop in cross velocity is intricately linked to the reduction in flux. A decrease in cross velocity in close proximity to the membrane surface leads to an increase in the thickness of the boundary layer that is adjacent to the membrane. The presence of a thicker boundary layer impedes the efficient transportation of solute molecules towards the surface of the membrane, resulting in a reduction in the rate at which solutes flow through the membrane. This phenomenon is consistent with the established principles of mass transfer in membrane-based systems.

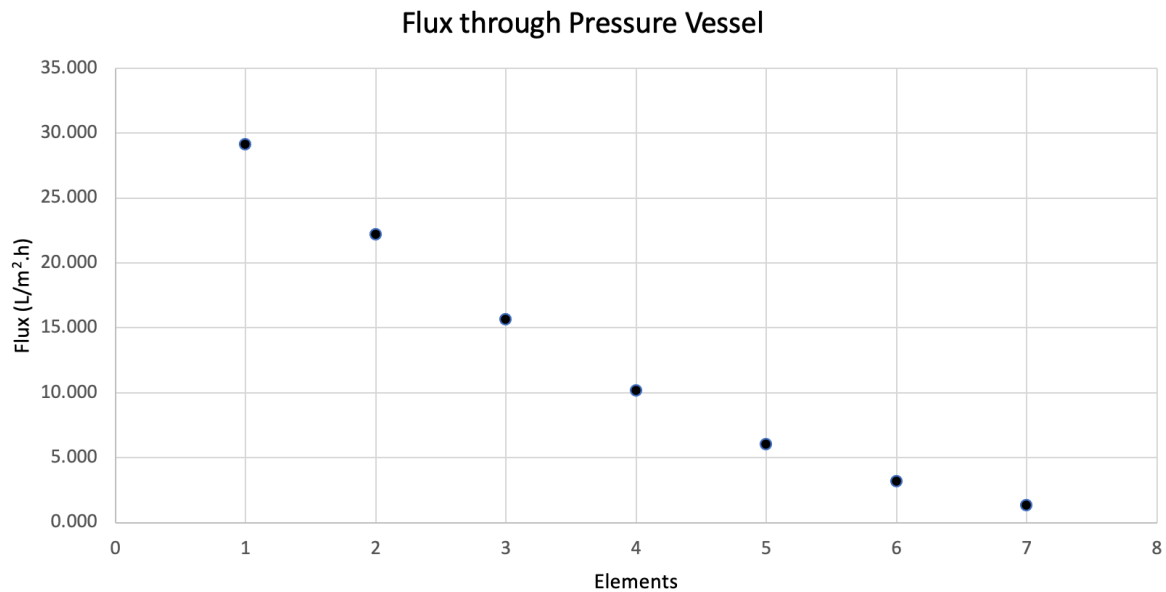


Figure 5–17: Behaviour of flux inside the pressure vessel

Simultaneously, the concentration polarisation factor (CPF) likewise decreases across the membrane elements. Concentration polarisation is a phenomenon characterised by the build-up of solute molecules in close proximity to the surface of a membrane, resulting from disparities in solute concentrations. As the velocity of the flow perpendicular to the membrane surface decreases, the effectiveness of the flow in removing solute molecules decreases. As a result, a high concentration polarisation phenomenon arises, leading to the accumulation of dissolved salts, organic compounds, colloidal materials, and suspended particles on the surface of the membrane. The occurrence of high concentration polarisation can result in several unfavourable outcomes, such as the formation of sparingly soluble compounds, enhanced accumulation of colloidal and suspended particles, heightened salt permeation caused by elevated concentrations at the membrane interface, and a decrease in the overall driving force due to increased osmotic pressure. It is recommended to keep the CPF < 1.2 to minimise the fouling, and the values shown in Figure 5–18 are below the threshold since the recommended

recovery (by DOW membranes) varies with the quality of the feed water, for example membrane used for seawater should have recoveries between 10 and 12 %.

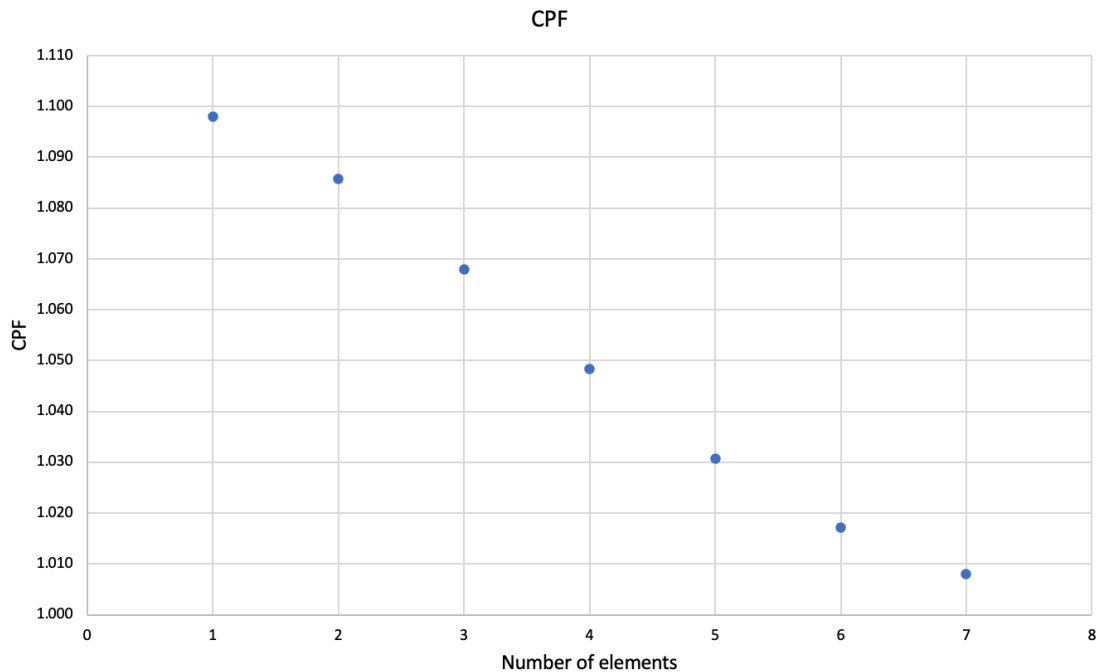


Figure 5-18: Behaviour of CPF along the membrane elements

The non-uniform distribution of cross-flow velocity in a RO pressure vessel is also evident in the non-uniform flux distribution along the vessel. The front elements, which are located closer to the inlet, have a greater production rate as compared to the rear elements situated in proximity to the outlet. The observed disparity in production rates can be attributed to the aforementioned parameters that impact cross velocity and concentration polarisation.

5.10 Summary

This chapter researched the design perspective of SWRO desalination, focusing on engineering the parameters critical to the process. It systematically developed the engineering equations that encompass not only the RO system but also the integral processes such as intake, pretreatment, discharge, and posttreatment. The developed RO system investigated in this research demonstrated behaviour and results that are consistent with established systems like WAVE, as well as aligning with the theoretical frameworks of RO systems. Also, it was noted that, overall, the WAVE model consistently generated lower values (SEC, C_p , k_w , applied pressure, concentration pressure) compared to the modified model. Furthermore, a dataset of pumps was created to increase the efficiency of energy calculations and select proper pumps with the best efficiencies.

The forthcoming chapter explore the life cycle cost analysis of SWRO desalination, outlining the methodologies used to calculate the capital expenditures and operational expenditures. This analysis also details the approaches adopted in this research to provide a comprehensive understanding of the economic aspects associated with SWRO desalination.

Chapter 6

Economic Cost Assessment

This chapter focuses on analysing the economic factors of SWRO desalination plant through a thorough life cost analysis. This explores the several factors that play a crucial role in determining the life cycle expenses of the plant. This chapter explains the methods used in life cycle cost analysis, focusing on SWRO, in an effort to establish the foundation for the development of a user-friendly tool in Chapter 7.

6.1 Financial Aspect of Desalination

As a result of growing demand for freshwater in areas with limited freshwater sources, desalination plants have become an increasingly popular solution to the global water crisis. When designing a desalination technology, it is crucial to evaluate its cost-effectiveness in order to ensure the successful implementation of a well-designed plant within a reasonable budget. The financial aspects of establishing and operating a desalination facility can be divided into two categories: capital expenditure (CAPEX) and operational expenditure (OPEX). The selection of desalination technology type significantly impacts the operational costs of the facility. Figure 6–1 shows a graphical comparison of CAPEX and OPEX across different desalination technologies. The data shown in this graph was sources from DesalData [344] which then utilised to construct the graph.

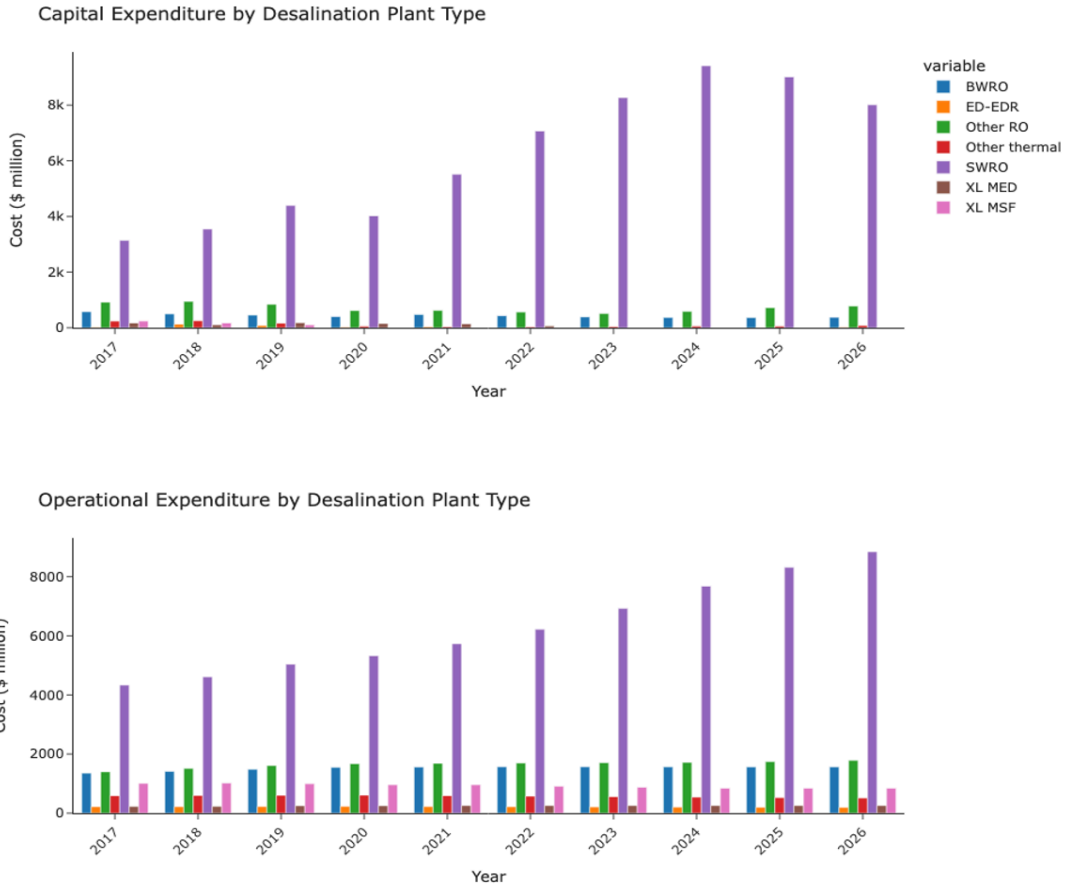


Figure 6–1: CAPEX and OPEX based on desalination technologies

The cost of freshwater production through desalination has decreased over time due to technological advancements and refinements. According to Karagiannis and Soldatos [67], historical data shows a significant decrease in the costs of RO desalination. The 1988 report from the US Congress stated that unit costs ranged from \$1.57/m³ to \$3.55/m³ of produced freshwater. The field has made significant progress, resulting in a substantial decrease in costs. Reported figures in 2004 ranged from \$0.5 to \$0.7/m³[67]. Diverse viewpoints on costs can be observed, as indicated by the American Membrane Technology Association (AMTA), which provides cost estimates ranging from \$0.75/m³ to \$2.0/m³ [67]. Moreover, it is expected that desalination costs will continue to decrease as the technology advances. However, it is difficult to predict whether this trend will continue in the future. As it can be seen in Figure 6–1, a consistent increase trend in both CAPEX and OPEX for RO technologies as the years progress. It is essential to keep in mind that initial performance enhancements frequently involve relatively simple, and cost effective measures. Nonetheless, as these initial gains are realised, the subsequent pursuit of additional improvements may encounter the law of diminishing

returns, wherein attaining additional advancements requires larger economic investments and becomes increasingly difficult to implement.

6.2 Life Cycle Cost Analysis

The concept of Life Cycle Cost (LCC) pertains to the comprehensive expenditure incurred during the whole lifespan of an asset where the approach for assessing LCC is known as life cycle cost analysis (LCCA). This encompasses many elements such as pre-production planning, design, procurement, as well as any related support expenses, in addition to expenditures directly linked to the ownership and utilisation of such asset. According to the International Standard BS ISO 15686-5 [345], LCC is defined as the

“Cost of an asset or its parts throughout its life cycle, while fulfilling the performance requirements”.

This methodology enables the identification of the most economically efficient solution from a variety of options by comprehensively evaluating all monetary inflows and outflows over the lifespan of the system. Moreover, it empowers professionals to recognise potential benefits and compromises between upfront capital and long-term financial expenditures.

6.3 LCC Concept

LCC was initially created by the United States Department of Defence (DOD) in the 1960s and has since been employed as a valuable resource for managing extensive construction endeavours, including military installations, architectural constructions, and petroleum refining plants. During the period spanning from the 1980s to the early 1990s, many cost models were formulated to estimate LCC. One notable model that emerged during this time was Activity-Based Life Cycle Costing, which was introduced in 2001 [346].

The study of LCC has uncovered additional expenses associated with the proposed item during its entire lifespan, indicating that the total cost of ownership might significantly exceed the initial acquisition cost. Therefore, LCC provides a comprehensive assessment of the efficiency, financial viability, and economic implications pertaining to the asset under analysis. The application of LCC analysis facilitates the selection of the most economically efficient technique for the establishment and utilisation of an asset. According to Flanagan and Norman [347], LCC places emphasis on four primary aims:

- To enhance the evaluation of objective options in a more efficient manner

- To consider the comprehensive impact of all expenses, rather than focusing primarily on the original capital cost
- To facilitate the proper management of buildings and projects after their completion.
- To provide the opportunity to choose among competing alternatives.

6.4 LCC Procedure

Since the first introduction of LCC, several aspects of LCC have undergone development and refinement, culminating in the establishment of a standard as outlined in a specific paragraph pertaining to LCC procedures for building and built assets under ISO 15686 (2008) [345]. In line with ISO 15686, Figure 6–2 provides a graphical representation of the expenses that are to be incorporated in life-cycle costing, as well as the broader costs and revenues that are to be referred to as whole-life costs. An externality refers to a measurable cost or benefit that arises when the activities of individuals or organisations impact persons or entities outside those directly involved.

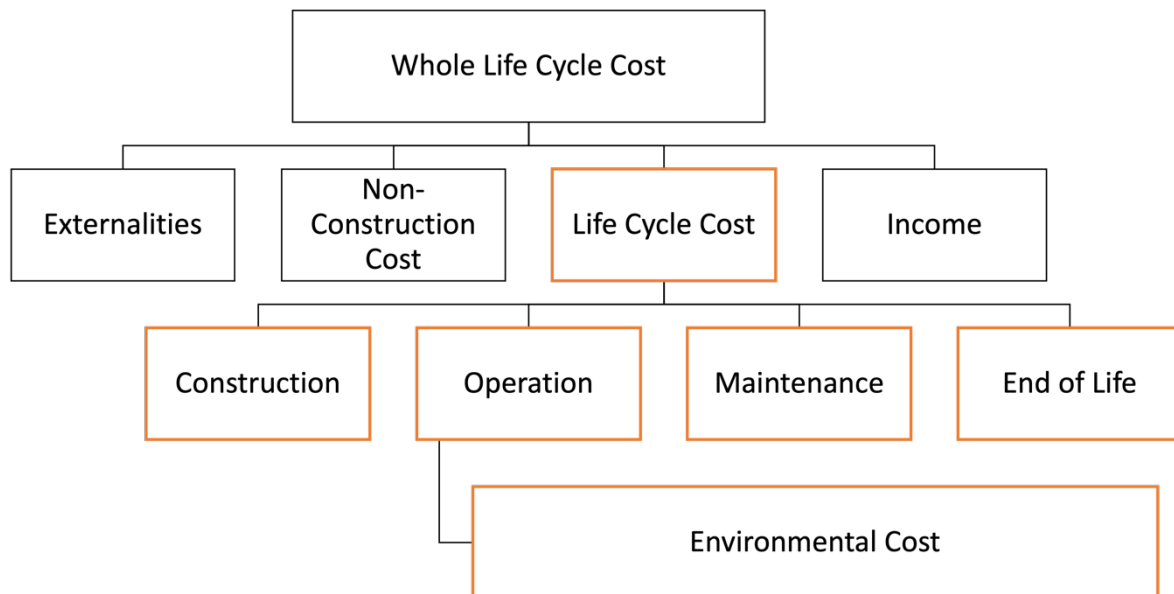


Figure 6–2: Whole life cycle cost according to ISO15686 [345]

Nevertheless, a standard LCC study often consists of a sequence of steps that entail carrying out critical evaluations, e.g. performing essential sensitivity analysis, and assessing potential risks. The significance of these two assessments relates to the presence of uncertainties pertaining to both input and quantities, as well as the corresponding particular costs. Figure 6–3 presents a process to perform Life Cycle Cost (LCC) analysis, as outlined by Greene and Shaw [348].

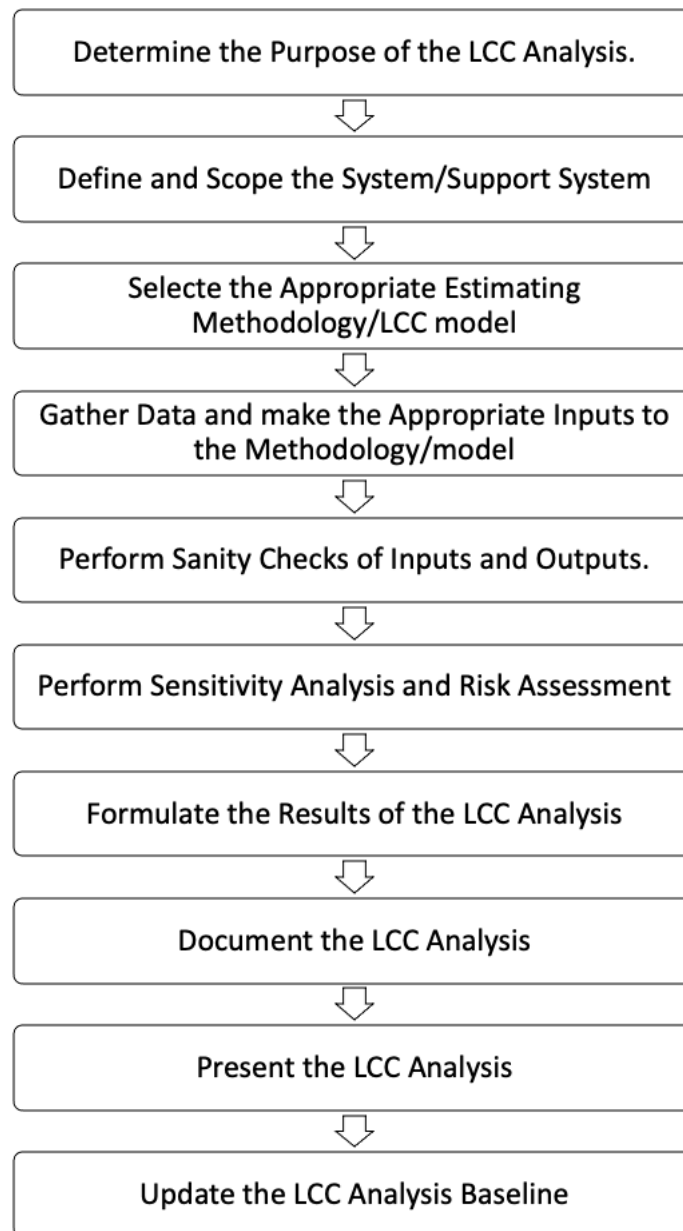


Figure 6–3: Ten steps of life cycle cost developed by Greene and Shaw [348]

6.5 LCC Methodology

Due to the dynamic nature of the time value of money, it becomes challenging to directly compare expenses that occur at various future periods in time. As a consequence of this complexity, it is necessary to compute the expenses in a manner that accurately reflects their worth using a standardised reference date.

Several techniques of life cycle economic evaluation have been defined such as Real Cash-Flow, Net Present Value (NPV), Annual Equivalent Cost (AEC), Payback Period (PB), Net Savings (NS), Savings to Investment Ratio (SIR), and Internal Rate of Return (IRR). The

concept of the AEC is employed to convert all forthcoming expenses into a uniform annual cost. This enables the evaluation of LCC based on a singular value that reflects the average yearly expenditure during a specified duration of analysis. The PB denotes the duration necessary for the anticipated yearly savings to recoup the initial expenditure. The NS is a straightforward method used to quantify the disparity between the earnings derived from an investment and the initial CAPEX associated with that investment. The IRR and the profitability index (PI), also known as the benefit-cost ratio, are conventional financial evaluation methods. These approaches yield a percentage and a ratio, respectively, to assess the performance of an initial investment over a specified timeframe by considering the relationship between income and investment [349].

The NPV technique is often regarded as a robust and preferred approach due to its emphasis on cash flow analysis. This method is advantageous in the assessment of design decisions, as it avoids the limitations of relying just on a single percentage or ratio that may oversimplify the complexities of cash flow [349].

6.5.1 Present Value

The concept of present value (PV) refers to the current monetary worth of a forthcoming quantity of money or a series of cash flows, taking into account a certain rate of return. PV is determined by discounting the future value (*FV*) using a discount rate (*dr*) over a period of *n* years. The formula presented below (Eq 6.1), is commonly referred to as the Single Present Value (SPV) formula which does not allow adjustment to the inflation rate. This method may be utilised to discount the nominal cost, which refers to costs that already incorporate inflation, associated with a certain year to its current value [350].

$$PV = \frac{FV}{(1 + dr)^n} \quad \text{Eq 6.1}$$

In projects pertaining to construction, capital budgeting, and investment planning, a supplementary Eq 6.2 is employed to compute the net present value (NPV). The NPV signifies the cumulative future cost and is determined by the following formula [345], where C_n represents the cash inflow in year *n* and *p* is the period of analysis :

$$NPV = \sum_{i=0}^p \frac{C_n}{(1 + dr)^n} \quad \text{Eq 6.2}$$

In scenarios where the fixed uniform sum increases annually and is discounted proportionately throughout the duration of the building's life cycle, it is appropriate to utilise the uniform present value (UPV), as represented by Eq 6.3.

$$UPV = \frac{(1 + dr)^n - 1}{dr(1 + dr)^n} \quad \text{Eq 6.3}$$

6.5.2 Discounting

The discount rate serves as a measure of the present value of future cash flows, taking into account the time value of money. It is employed in the computation of the NPV. The selection of either a real discount rate or a nominal discount rate for the calculation of NPV is contingent upon the specific objectives of the costing study. In contrast to the real discount rate, the nominal discount rate does not take into account the impact of any deflation or inflation. Therefore, it is recommended to apply a real discount rate [351].

In the context of performing a LCCA to compare competing systems, it is sufficient to employ a real discount rate [352]. At present, the prevailing discount rate employed in Ireland is a nominal rate of 3.96% for projects spanning a duration of 10 to 20 years. The discount rate for cost benefit analysis (CBA) was amended by the department of finance in 2007, decreasing from 5% to 4% [353]. Nonetheless, as indicated by the department of public spending and reform, the discount rate utilised for the assessment and evaluation of projects is at 5% in real terms [354].

Indeed, a significant proportion of the literature on desalination costs has adopted a certain estimate, often ranging from 5% to 8% [355], [356], [357], [358], [359], [360]. The discount rate exhibits significant variability based on numerous criteria, and is subject to variation across different countries, as seen in Figure 6–4. Hermelink and de Jager [361] conducted an assessment to examine the influence of discount rates on the appraisal of various energy and climate policy alternatives within the European Union (EU). The study revealed that there exists an inverse relationship between the discount rate and the attractiveness of high-energy-efficiency investments and supporting policies. It is recommended that the discount rate be maintained within the range of 3% to a maximum of 6%.

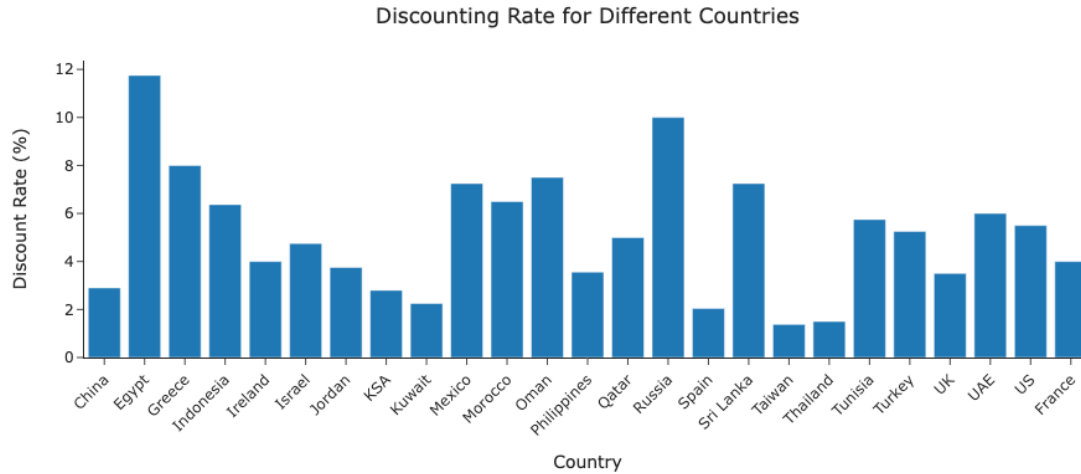


Figure 6–4: Discount rate for different countries according to central bank [362]

6.5.3 Sensitivity Analysis

Sensitivity analysis is a method employed to evaluate the degree of sensitivity exhibited by the outcome of a capital budgeting decision in response to alterations in a single critical input variable, while maintaining all other variables at a fixed level. One can do sensitivity analysis to examine the impact of altering the discount rate, growth rate, initial investment, or running expenses on the NPV or IRR of a project. This approach is a valuable tool for discerning the key factors that exert the most influence on decision-making processes. Additionally, it aids in determining the range of values within which a choice remains viable or becomes untenable.

6.6 Life Cycle Costing and SWRO

6.6.1 System Lifetime and Availability

The determination of the plant lifespan (L_p), which refers to the duration for which future cash flows are considered, is a fundamental requirement in all approaches used to assess the viability of desalination plants. The determination of the time period for calculating the return on investment is often established by the individuals responsible for making decisions. These decision makers must consider the technical limitations of the plant and its components when setting the duration. Typically, it is common to select a time span ranging from 15 to 25 years, with a preference for a 20-year duration in the majority of instances. Figure 6–5 presents a histogram showing the age of 1640 SWRO facilities currently in operation. The data was acquired through the DesalData platform [344]. The histogram indicates that there has been limited implementation of desalination plants since 1978 (40 years), with the majority of these plants having an operational lifespan

of 20 to 27 years. When considering the anticipated continuous operation of the technology over an extended duration, it is advisable to consider its potential for reducing water costs on average. However, it is crucial to acknowledge the maintenance and equipment replacement obligations that will arise periodically throughout the 30-year lifespan.

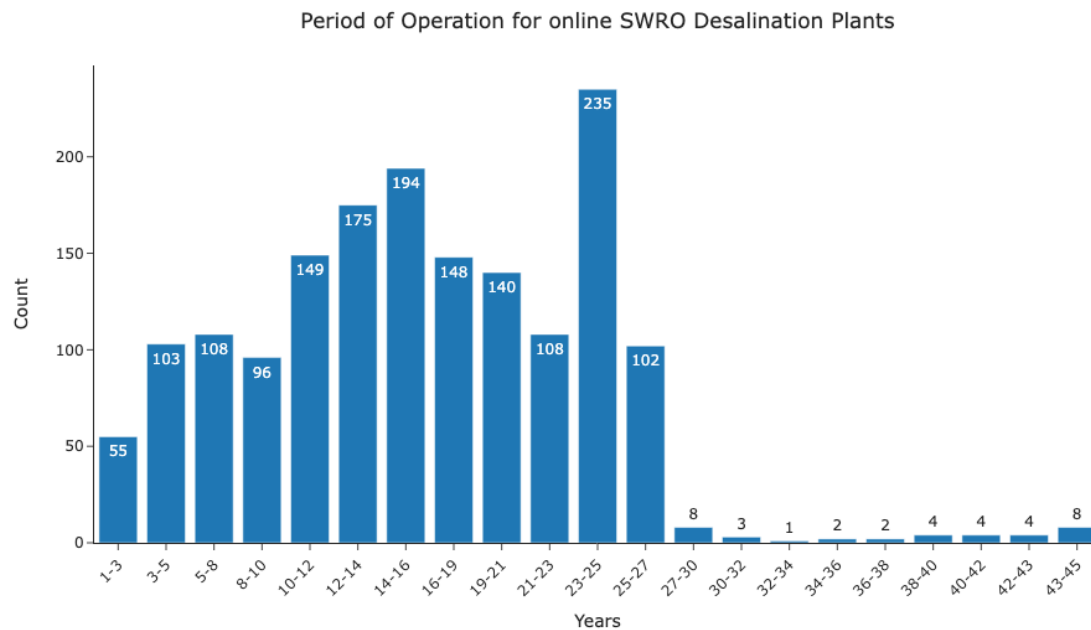


Figure 6–5: Histogram representation of lifetime of 1640 SWRO desalination that still operating

6.6.2 Capital Expenditure

Capital costs are considered a primary cost when designing or implementing a SWRO desalination plant. Capital costs include all costs associated with the plant construction, including land, equipment, materials, etc. A plant’s size, complexity, as well as its location, can have significant impact on the capital cost. For example, plants built in remote areas may have higher capital costs due to the need for additional infrastructure and transportation expenses [363]. In 2014, Loutatidou *et al.* [364] stated that CAPEX will fall by 2.25% every year in the Gulf Cooperation Council (GCC) from 2013 to 2030. Voutchkov [28] estimated that the unit cost of RO desalination plant would decrease by 20% due to the potential improvement in the RO and desalination technology. According to the estimation by Voutchkov, the CAPEX of SWRO plants would be around \$1,032–\$1,717 per cubic metre per day (m³/d) in 2015 and expected to drop further to \$528–\$924 for every m³/d by 2030. However, in 2017 a learning curve was applied to predict the CAPEX of a SWRO desalination plant [365]. Over the study period of 1977-2015, 4,237 SWRO plants were analysed. As worldwide SWRO plant capacity doubled, the average capital cost decreased by 15%.

Although this decline in capital expenditures is encouraging, it is difficult to predict whether this trend will continue in the future. It is essential to keep in mind that initial performance enhancements frequently involve relatively simple and cost-effective measures. Nonetheless, as these initial gains are realised, the subsequent pursuit of additional improvements may encounter the law of diminishing returns, wherein attaining additional advancements requires larger economic investments and becomes increasingly difficult to implement. Based on a 10% annual growth rate, the average CAPEX would drop to \$1,580 USD/m³/d and to \$1,340 USD/m³/d at a 20% annual growth rate [365].

6.6.3 Operational Expenditure

Expenses involved in operating and maintaining a desalination plant throughout its life cycle are commonly referred to using the term operational expenditure. The main factors that contribute to total OPEX are energy, chemical, labour, maintenance and membrane replacement, comprising 80 % of total OPEX. Energy is the single most crucial factor in OPEX costs. It is estimated that electrical energy expenditures account for at least 45% of overall operating costs on average [366]. This varies depending on the region due to the variability in the cost of electricity.

Table 6-1 summarises the current and forecasted energy usage and water cost values for medium and large RO desalination plants. According to Table 6-1, the cost of electricity is expected to fall in the coming years; however, according to Eurostat [367], as of January 2022, energy inflation in the EU has reached 27%, continuing a pattern of steady increase. Other energy sources costs increased for fuel by +26% and electricity by +24% while gas reached an all-time high of approximately 41%, a gain of 13.5 percentage points (pp) compared to that of the earlier month as shown in Figure 6–6. The significance and urgency of exploring how desalination plants can manage the increasing energy costs in the future cannot be overstated. This may prompt a shift in the focus of future research endeavours.

Table 6-1 : Forecast of energy use and cost for medium and large RO desalination plant [243]

Parameter for Desalination Plants		2018	2022	2030
Total Electrical Energy Use	(kWh/m ³)	3.5 – 4.0	2.8 – 3.2	2.1 – 2.4
Cost of Water	(US\$/m ³)	0.8 – 1.2	0.6 – 1.0	0.3 – 0.5
Construction Cost	(US\$/MLD)	1.2 – 2.2	1.0 – 1.8	0.5 – 0.9
Membrane Productivity	(m ³ /membrane)	28 – 48	55 – 75	95 – 120

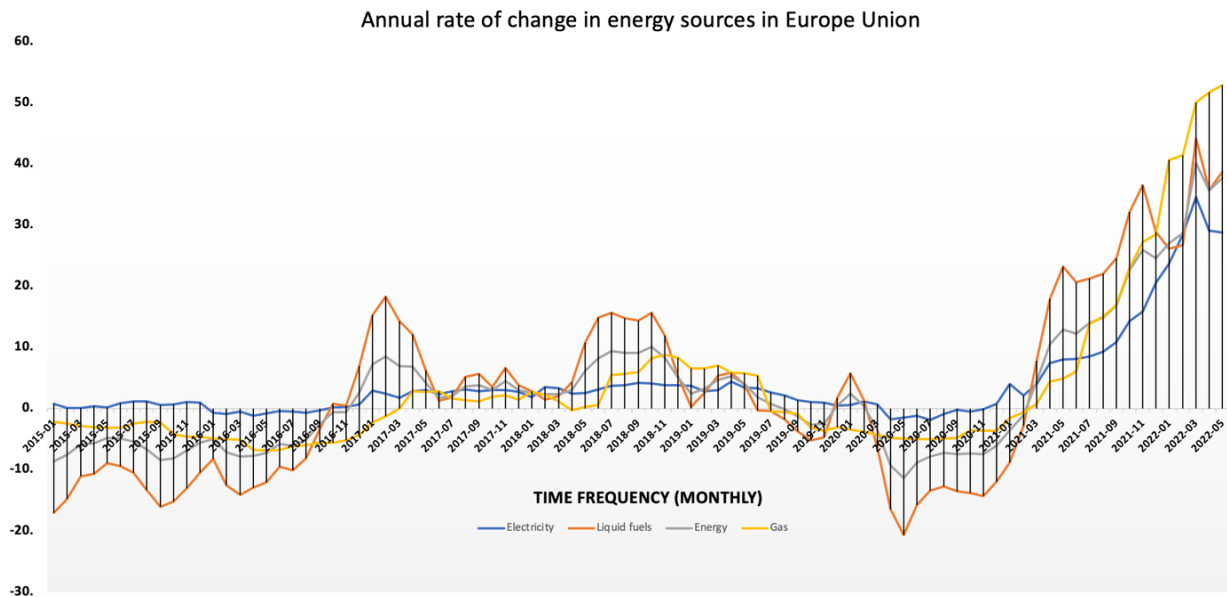


Figure 6–6: Inflation analysis of energy sources in EU [367]

It is essential for the desalination sector to research and explore techniques to raise the usage of renewable energy in powering desalination plants. In 2021, it was reported by the International Renewable Energy Agency [368] that over the past number of years there has been a steady decrease in renewable energy cost with an approximate 62% of the renewable energy added in 2020 coming at a cost lower than that of the cheapest fossil fuel options. Using renewable energy resources will lead to a reduction in energy costs as well as carbon footprints in powering desalination plants. At the moment, renewable energy has been deemed feasible in small to medium scale desalination applications [369], [370], [371], yet it is still absent in large scale desalination plants [372], [373]. There is no cost analysis for batch RO in the literature currently, therefore it is uncertain if the predicted energy savings would be sufficient to offset any potential increase in capital costs.

6.6.4 Factors Influencing Desalination Cost

6.6.4.1 Water Quality for Feeding

The quality of water used in desalination affects the necessary pretreatment and energy requirements, which are directly influenced by the multivalent TDS level and water impurities. Therefore, the presence of these solids in feed water necessitates extensive pretreatment measures, leading to higher operating expenses [292]. Additionally, this increases the susceptibility of the RO membrane to scaling and fouling.

6.6.4.2 Determination of Plant Capacity

The quantification of the desalination plant's capacity is determined by the quantity of water, defined in gallons or cubic metres, that is treated during a specific duration. The capacity of a desalination plant is determined by several elements, including the feed water system, pretreatment capacity, membrane processing size, and distillation capacity, among others. Plants with a smaller capacity need a reduced level of initial CAPEX in comparison to their larger capacity counterparts. The unit cost of a bigger facility is expected to be cheaper due to the concept of economies of scale. As an illustration, it can be observed that a plant with a capacity below 1000 m³/day would generate water at a unit cost varying from \$2.62 to \$13.23 (estimated conversion) per m³, but in plants with a capacity above 60,000 m³/day, the unit cost ranges from \$0.5 to \$1.0 per m³ [67].

6.6.4.3 Characteristics of the Site

The selection of the desalination plant's site should be carefully evaluated, taking into account the presence of intake structures and the pre-treatment medium [31]. The criteria that are influenced by the location include the quality of the feed water, the capacity of the water, the chemistry of the water, and the environmental conditions. The aforementioned factors exert an impact on the overall desalination process. It is advisable for the plant to be situated in proximity to a dependable power source derived from a stable grid system, or alternatively, include its own autonomous power generation facility [277]. Furthermore, it is imperative that the geometry and size of the space are designed in a manner that allows for the efficient installation and maintenance of the supporting systems for both the feed water and power supply [277]. The optimal placement of the desalination plant necessitates proximity to either the source of the feed water or a reservoir with an ample supply. The consideration of waste disposal appropriateness is an essential aspect in the development of the plant design, particularly with regards to the waste generated by the desalination process. When considering the selection of site features, it is important to adopt a meticulous and efficient methodology [277]. Figure 6–7 depicts the sequential process involved in the selection of a suitable location for the construction of a desalination plant.

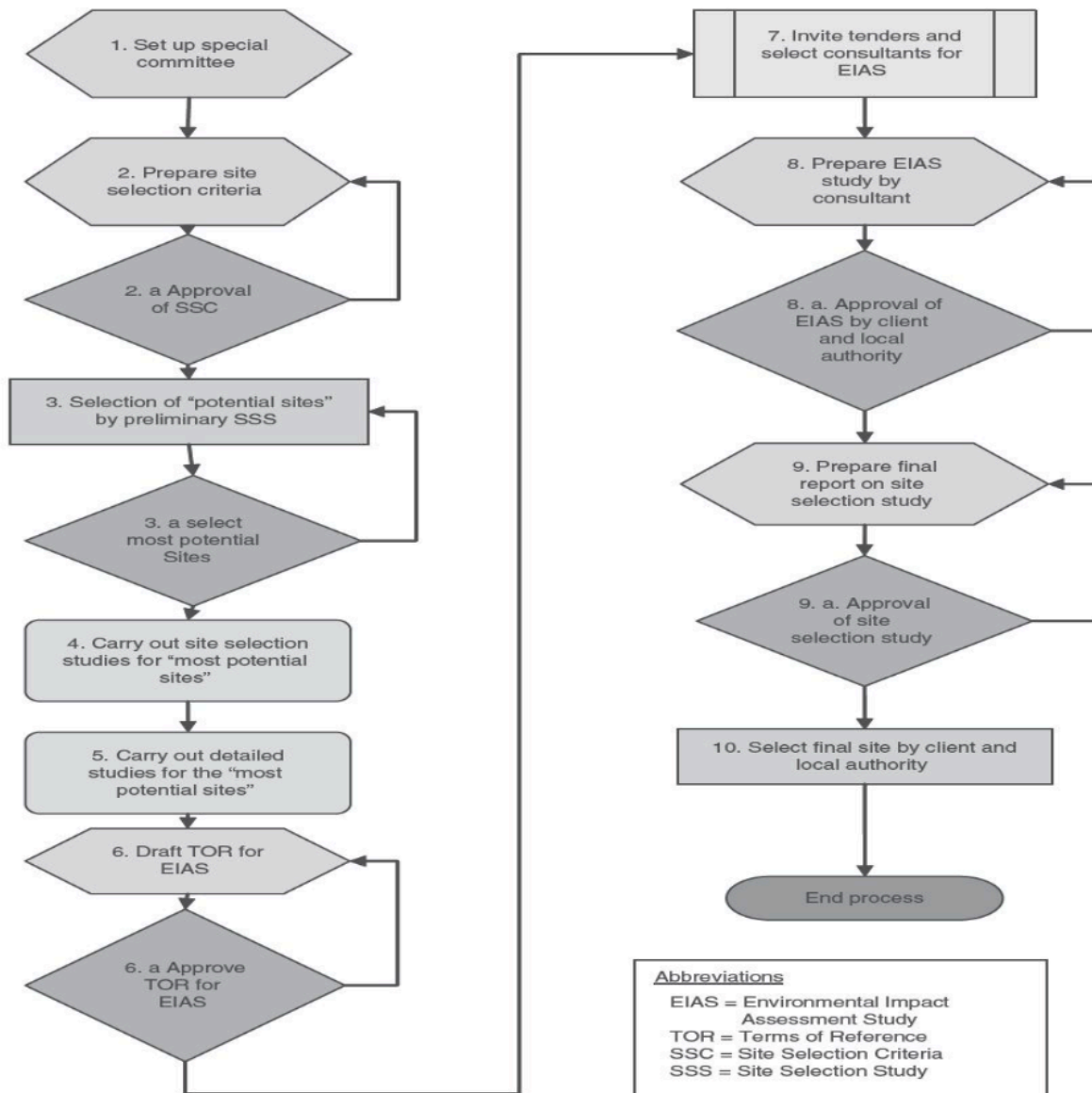


Figure 6–7: Flow chart for the process of selecting site [277]

6.6.4.4 Regulatory Requirement

Regulatory Requirements refer to the set of rules and regulations that an entity must comply with in order to operate within a certain industry or jurisdiction. This includes the permissions and regulations imposed by the state, as well as the related costs required to comply with these stipulations [17].

6.6.5 Life Cycle Cost Model

6.6.5.1 Empirical Model

Several researchers [364], [374], [375] have disseminated capital cost data for seawater desalination facilities, accompanied by corresponding empirical cost models. These numerical

values are commonly employed to formulate practical cost approximations that are frequently utilised in the initial phase of a project's planning process. Typically, regression analysis in these models involves the use of either a polynomial equation, log-log model, or semi-log model. For instance, Wittholz et al. [374] established a basic linear regression equation (Eq 6.4) employing a power law model. This equation was utilised to establish the correlation between capital cost and plant capacity, based on a dataset comprising 331 desalination plants employing various technologies. The values of the constant and m vary across different desalination technologies. One potential constraint of this study is that the reported margin of error for both the capital and unit manufacturing cost is around 50%. However, in accordance with the commonly accepted guideline for approximating capital costs, a margin of error of around $\pm 30\%$ is often considered [23]. This error can be attributed to the fact that, during the analysis of the data, it was noted that there frequently existed a significant disparity in capital cost data across facilities of identical size and utilising identical technology, often differing by an order of magnitude. The quality of the data had a significant role in contributing to this outcome. The inclusion of pertinent information, such as the incorporation of land and civil works into the capital cost, was not consistently documented.

$$\ln(\text{CAPEX}) = m \times \ln(\text{capacity}) + \text{constant} \quad \text{Eq 6.4}$$

Park et al. [376] proposed a stochastic cost estimation methodology for the construction and operation of a SWRO desalination plant. This approach aims to enhance the decision-making process by accounting for the growing uncertainty in future energy costs, specifically electricity prices, as well as finance costs such as interest rates and inflation rates.

The implementation of empirical models has various challenges, principally arising from the inherent vulnerability to errors linked to statistical computations. The aforementioned challenges are exacerbated by the utilisation of empirical data, hence introducing a degree of reliance on the quality and accuracy of the data that is available. As a result, the data utilised in these models may not comprehensively capture the complex and diverse characteristics of CAPEX estimates. Upon examining previous academic studies, it was noted that empirical models frequently provide rough estimates of CAPEX without offering a comprehensive explanation of the specific cost elements involved.

6.6.5.2 Water Treatment Cost Estimation Program (WTCost)

The WTCost model is a flexible framework for estimating costs associated with the construction, capital investment, operation and maintenance of desalination plants that use seawater and brackish water. This includes additional different desalination methods like MVC, MED, MSF, NF and EDR. WTCost is a visual basic programme developed by the Bureau of Reclamation in collaboration with I. Moch & Associates and Boulder Research Enterprises [377]. This computer model is built upon cost curves created by the US Environmental Protection Agency (USEPA) in 1979 and revised in 2001 [378]. The system allows consumers to choose various characteristics, including the type of pretreatment system, pretreatment chemicals, and the method of salt separation (RO, ion exchange, or electrodialysis). The programme allows users to consider various factors, such as the input and output system, post-treatment technology, and the quality of the source and product water. Users have the ability to modify default input data settings. This involves the capacity to modify various factors, such as the quality of the source water, expenses related to electricity and chemicals, charges for labour, indexes for construction, and capital costs. However, it is important to note that the software's unit cost assumptions are based on data from 2008 and have not been updated since then [377].

6.6.5.3 Desalination Economic Evaluation Programme (DEEP)

The Desalination Economic Evaluation Programme (DEEP) is a software tool developed by the International Atomic Energy Agency (IAEA) for estimating costs in desalination projects. The DEEP software, developed in 1989, allows users to evaluate the performance and costs of different power and seawater desalination co-generation configurations. DEEP utilises a hybrid approach that combines Microsoft Excel spreadsheets with Visual Basic methodology. DEEP 5.1, released in late 2014, introduces various improvements such as a comprehensive cash flow analysis feature for “bankable” feasibility studies, a scenario manager screen for comparing scenarios and data import/export, and an enhanced user-friendly interface. DEEP facilitates comparative analysis of various power generation plants, fuels, and desalination methods, including MED, MSF, RO, and hybrid approaches. However, it does not encompass the entire process of constructing a desalination plant from start to finish. Users have the ability to model different configurations, backup heat sources, intermediate loops, water transport costs, and carbon tax implications.

In 2016, a research study was undertaken to assess the water production cost of RO desalination plants with varying capacities (1000, 50,000, and 100,000 m³/day) [379]. Various cost analysis methods, including DEEP, WTCost, and empirical models, were employed to estimate these costs. Subsequently, these models were validated and compared against three existing desalination plants to evaluate their accuracy and reliability. Figure 6–8 illustrates the observed discrepancies between the generated results and the actual performance of the desalination plant. Specifically, in the case of smaller scenarios, the DEEP estimation closely approximated the real cost. However, for medium capacity scenarios, the DEEP estimation fell below the actual cost. Among the considered approaches, DEEP was found to be the closest in terms of its ability to estimate the CAPEX of large capacity desalination plants, while the remaining options were more than 43% higher than the actual value. When considering the estimation of unit water production cost, both DEEP and WTCost exhibited a similar level of proximity. It is important to consider that validating the capital cost in comparison to other costs can be challenging due to the numerous aspects involved in capital spending, some of which may not be adequately recorded in the publication. Various factors, including regulations, testing protocols, interest rates, and taxes, significantly influence the design of desalination plants. It is important to note that these factors vary among countries, resulting in differing cost structures for such projects.

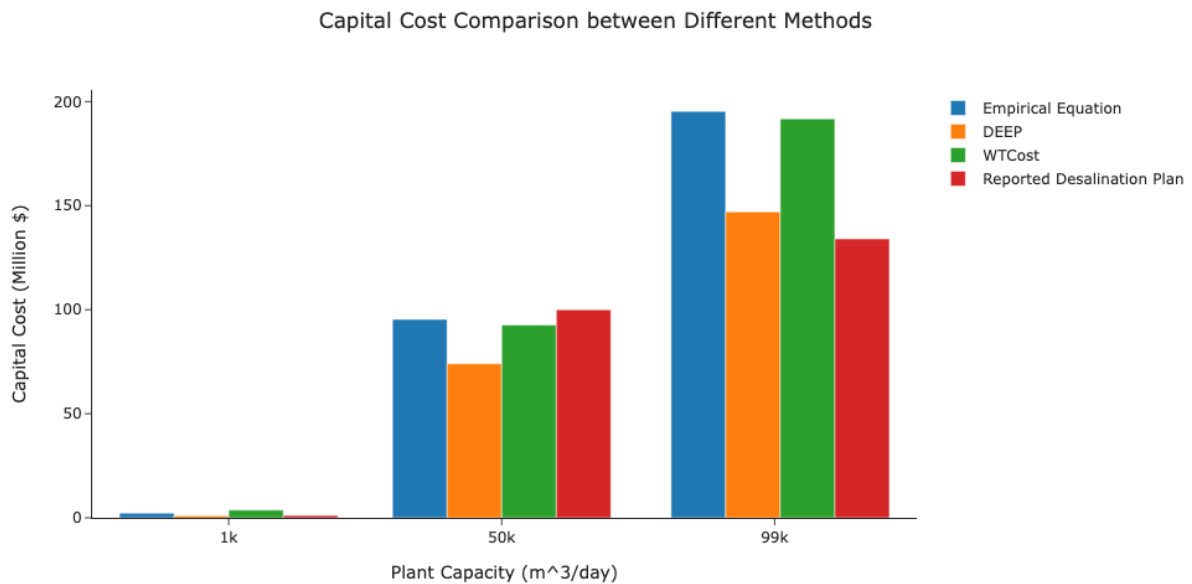


Figure 6–8: Capital cost comparison between real cases and obtained results by the empirical model, DEEP, and WTCost [379]

6.6.5.4 Water Application Value Engine (WAVE)

The Water Application Value Engine (WAVE) is a freely available software programme designed to combine several technologies created by DuPont, including UF, RO, IX, and the recently included DesaliTec™ SOAR CCRO. This comprehensive tool aims to provide a unified platform for modelling and analysis in the field of water applications [380]. The tool provided is a user-friendly application that enables users to construct various configurations of pretreatment and RO systems tailored to diverse water sources. This programme also offers users with an estimated cost for chemical and energy usage based on their design. One restriction of this strategy is its restricted capability to exclusively pick products developed by the corporation, hence limiting the building of alternative desalination processes inside the programme. Additionally, it is exclusively compatible with Windows operating systems.

6.7 Methodology

In this study, more detailed calculations for CAPEX and OPEX will be considered. Figure 6–9 below shows the structure of capital and operational expenditure that is followed in this research.

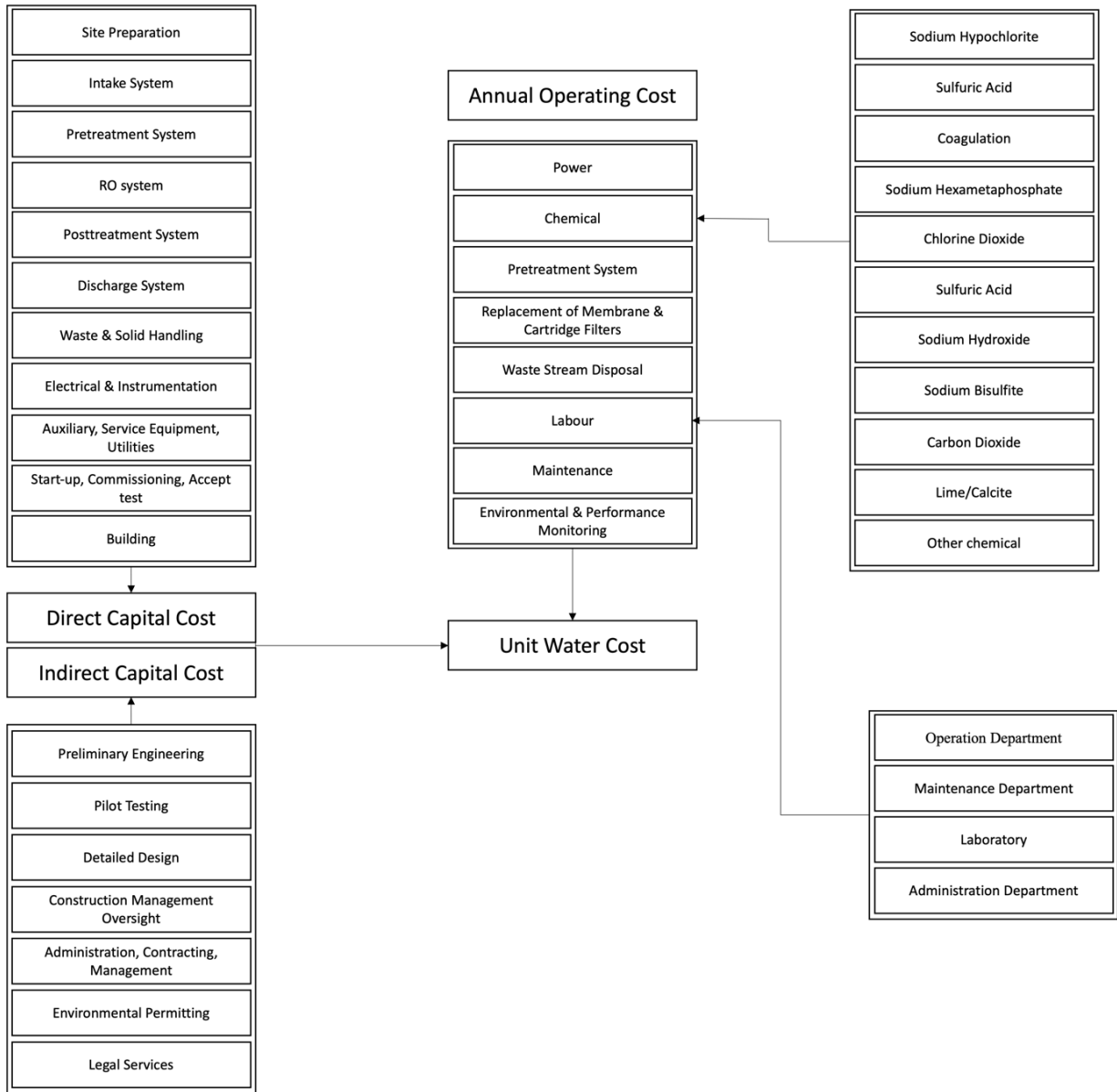


Figure 6–9: Structure of CAPEX and OPEX used in this research

6.7.1 Capital Expenditure

The total CAPEX is the sum of indirect and direct capital expenses as expressed in Eq 6.5.

$$C_{CAPEX} = \sum_j^{n=11} C_{CAPEX_{direct}} + \sum_j^{n=7} C_{CAPEX_{indirect}} \quad \text{Eq 6.5}$$

In the evaluation of direct and indirect capital expenses in the context of constructing a desalination plant, the standard approach is multiplying the individual cost elements by the plant's production capacity. This approach facilitates the assessment of expenses related to different components of a plant, while accounting for the magnitude of production. However,

in this research, there are exceptions for certain components encompassed by the construction framework, specifically the intake, pretreatment, RO, posttreatment, and discharge systems employed in the plant. The justification for these exceptions is based on the distinct complexity of each system's design, as well as the possible requirement to incorporate supplementary steps to the process, which may subsequently influence the total cost framework.

In 2018, Nikolay [381] devised a construction cost graph to represent the expenses associated with these systems, as well as the many types of technology that can be employed. The building cost graphs are conceptualised within the framework of functions, where the independent variable is represented by the plant's intake flow rate. Significantly, the depicted cost graphs cover the entire system, including the entire process from the intake system to the RO unit. In addition, the expenses associated with posttreatment are dependent on the rate at which permeate flows, whereas the costs of the discharge system are dependent on its capacity to handle brine. The utilisation of these tools facilitates a detailed examination that encompasses the financial consequences of diverse intake rates and alternative technological choices. In order to enhance practical implementation, the cost graphs were afterwards converted into a data format using PlotDigitizer [382]. This conversion was performed to ensure that the information may be easily accessed and applied in the wider context of desalination project planning and cost evaluation. Utilising data instead of a graphical representation enables seamless incorporation of future modifications, such as substituting an actual desalination plant or adjusting the present value according to the relevant year. All construction costs for these systems are available in APPENDIX E.

The costs connected with intake construction encompass the financial outlays for many components, such as plant saline water intake structures (including intake towers, wells, onshore forebays, etc.), pipeline infrastructure, intake pump station, and the necessary coarse and fine screening facilities. The expenses associated with source seawater intake can differ based on the specific type of intake method employed; the following equation (Eq 6.6) is used:

$$\begin{aligned}
 C_{\text{offshore intake}} &= L_{\text{pipe}} \times C_{\text{intake/m}} \\
 C_{\text{onshore intake}} &= C_{\text{intake}} \\
 C_{\text{subsurface intake}} &= N_{\text{well}} \times C_{\text{well}}
 \end{aligned}
 \tag{Eq 6.6}$$

Where L_{pipe} is the length of pipe in metres, $C_{\text{intake/m}}$ is the cost of intake structure per metre, C_{intake} is the cost of intake structure, N_{well} is number of wells and C_{well} is cost of an

individual well. Note that, C_{intake} for offshore intake represent the cost for the whole structure. The cost of screening can be calculated by adding the cost of the fine screen to the cost of the mechanical screen, as shown in Eq 6.7

$$C_{screening} = C_{fine} + C_{mechanical} \quad \text{Eq 6.7}$$

The total cost of the intake system is the sum of the intake structure, pumping station and screening. Within the domain of pretreatment, the building phase encompasses the establishment of clarifiers, along with the implementation of granular or membrane filtering and cartridge filters. It is imperative to acknowledge that, within the context of the RO system, there is an absence of distinct graphical cost allocation for different components. In contrast, the entirety of a single-pass RO system is subject to a single graphical construction cost for two salinities only at 35,000 mg/L and 46,000 mg/L. The building of the RO system follows a methodical approach (Eq 6.9), involving multiple steps, each of which contributes to the final expenditure and their corresponding cost ranges:

$$\begin{aligned} C_e &= C_u \times N_e \\ C_{pv} &= C_u \times N_{pv} \\ C_{RO\ Train\ Pipin} &= C_u \times N_{train} \\ C_{RO\ train\ support\ frame} &= C_u \times N_{train} \\ C_{RO\ train\ I\&C} &= C_u \times N_{train} \\ C_{HP\ pump} &= C_u \times N_{train} \\ C_{ERD} &= C_u \times N_{ERD} \end{aligned} \quad \text{Eq 6.8}$$

Where, C_u is the cost rate per auxiliary equipment. The expenses related to posttreatment construction (Eq 6.9) involve the integration of two essential subprocess: remineralisation system and disinfection system. In the field of permeate remineralisation, two often employed approaches may be identified: the combination of lime and carbon dioxide, and the use of calcite (limestone) and carbon dioxide. The calculation of the construction costs for each project is based on graphical representations of cost data. Further, the cost analysis encompasses the expenditures associated with the building and installation of the feed and storage facilities of the disinfection system, namely bulk sodium hypochlorite and chlorine dioxide.

$$C_{Posttreatment\ System} = C_{remineralisation} + C_{disinfection\ system} \quad \text{Eq 6.9}$$

Table 6-2 presents an in-depth breakdown of both direct and indirect CAPEXs, including cost ranges and associated parameters for each factor. Obtaining cost information pertaining to specific factors such as indirect cost, start-up, commissioning, building and utilities, in CAPEX from actual examples of SWRO desalination in practise is challenging, as there is limited documentation available on numerous factors. Hence, the cost ranges presented in the Table will be utilised for the computation of the remaining element in the CAPEX analysis. The following equation is a general one and which would be used to calculate the other factors in CAPEX:

$$C_f = C \times Q_p \quad \text{Eq 6.10}$$

6.7.2 Operational Expenditure

Table 6-3 provides a comprehensive overview on the components of operational expenditure, encompassing both fixed and variable aspects. The subsequent section will examine the approach in which these parameters will be taken into account and computed within the scope of this research. The total OPEX is calculated by adding up the factors outlined in Eq 6.11

$$C_{OPEX} = \sum_j^{n=4} C_{OPEX_{variable}} + \sum_j^{n=7} C_{OPEX_{fixed}} \quad \text{Eq 6.11}$$

Table 6-2: Breakdown for the factors included in direct and Indirect CAPEX in terms cost ranges and associated parameters for each factor [49], [366], [383], [384]

Cost item	Parameter & facilities included in the construction cost		Percentage	Cost range (\$/m ³ /day)
Direct cost			70.0 – 85.0	
Site preparation	Land cost	Fill		
	Clearing site	Fencing	1.5 – 2.0	10.0 – 30
	Grubbing	Road construction inside and outside		
Intake system	Intake structure	Pumping system	4.0 – 6.5	90.0 – 120.0
	Screening			
Pretreatment system	Clarifiers filtration	Granular media or membrane	8.5 – 9.5	150.0 – 230.0
	Chemical conditions			
RO system	Cartridge filters	RO pressure membrane vessels and racks		
	High-pressure			
	Pumps and motors to feed the RO system	SWRO membrane elements	38.0 – 40.0	450.0 – 520.0
	Energy recovery system	Membrane cleaning system		
Posttreatment	Interconnecting piping	Membrane flush system		
	Chemical conditioning system for permeate remineralisation	Disinfection system		
		Facilities for product water quality polishing	1.5 – 2.5	30.0 – 70.0
Concentrate disposal	Conveyance and disposal of the concentrate	Other waste streams generated at the desalination plan	2.5 – 3.5	

Cost item	Parameter & facilities included in the construction cost		Percentage	Cost range (\$/m ³ /day)
Waste and solid handling	Collection Storage tank and equipment for the waste membrane cleaning chemicals and flush water	Solids handling system for treatment and disposal of residuals generated during the pretreatment process Disposal of solid waste from cartridge & membrane	1.5 – 2.5	20.0 – 40.0
Electrical and instrumentation	Desalination plant's electrical supply system (electrical substation; equipment and conduits connecting the desalination plant to the electrical grid or to a power generation facility)	Transformers equipment Motor control centres Emergency power generation equipment	3.5 – 8.5	40.0 – 110.0
Auxiliary service equipment utilities	Plant chemical storage and feed systems Process air and water supply facilities The plant fire protection system	Sanitary wastewater collection system Storm water management system All utilities needed for the normal plant operation (potable and utility water telephone, gas, etc.)	2.5 – 3.0	15.0 - 35.0

Cost item	Parameter & facilities included in the construction cost	Percentage	Cost range (\$/m ³ /day)
Start-up, commissioning & accept test	Labour Consumable Equipment used during this phase Initial training of the permanent desalination plant O&M staff	Permitting and insurance Preparation of plant operation and maintenance manuals 1.5 – 2.5	10.0 – 30.0
Building	Plant administration & management Operator locker & shower facility	Laboratory Maintenance shop Equipment & chemical storage Key equipment of SWRO system 4.5 – 5.5	40.0 – 80.0
Indirect cost			
Preliminary engineering	Initial assessment of project feasibility Studies required to determine plant location	Define project scope and size Type of intake and equipment configuration 0.5 – 1.0	15.0 – 35.0
Pilot testing	Build pilot plant to assess the location water quality and compare performance between technologies	0.0 – 0.5	5.0 – 15.0 10,000–20,000*
Detailed design	Development of detailed project drawings and specifications	Document deviations from the original design during construction 3.5 – 4.5	80.0 – 100.0
Construction management oversight	Engineering activities associated with project construction Management of construction contractors	Management of equipment and material suppliers involved in project implementation 1.0–2.0	30.0 - 60

Cost item	Parameter & facilities included in the construction cost		Percentage	Cost range (\$/m ³ /day)
Environmental permitting	Fees for preparation of environmental studies and engineering analysis needed to obtain environmental permits	Fees associated with environmental permit filing and processing	0.5 – 3.5	30.0 – 65.0
Administration, contracting, management	It is owner responsibility which involves : In-house expenditures for owner staff and overhead associated with project	Implementation costs for contracting of outside engineering consultants Other advisers to provide specialized support services to project owner as needed	1.0 – 1.5	20.0 – 60.0
Legal services	Legal review processing of environmental permits, Reviewing and processing desalination plant land acquisition contracts Negotiate power supply contracts Preparation and negotiation of contracts for water supply	Engineering, construction, and O&M services Obtain easements for source and product water pipelines and electrical supply lines Prepare contracts for services, equipment, and goods for desalination plant construction and operation	0.5 – 1.0	15.0 – 35.0

*per month of expenditures for pilot operations and maintenance

Table 6-3: Breakdown for Operational Expenditure [49], [384], [385], [386]

Cost item	Parameter included	Percentage	Cost range (US\$/m ³)
Variable cost		45.0 – 75.0	0.30
Power	Annual desalination plant power costs	35.0 – 55.0	0.22
Chemical	Annual chemical usage	3.0 – 7.5	0.03 – 0.07
Replacement of membrane & cartridge filters	Cost for membrane replacement Cost for cartridge replacement	5.0 – 8.0	0.02 – 0.06
Waste stream disposal	Operation and maintenance of the outfall facilities Disposal generated during the filter backwash treatment	2.0 – 4.5	0.01 – 0.02
Fixed Cost		25.0 – 55.0	0.42
Labour	Annual labour cost	10.0 – 15.0	0.015 – 0.045
Maintenance	Routine operation Preventive and emergency maintenance of plant equipment, structures, buildings, and piping	9.5 – 22.0	0.025 – 0.07
Environmental & performance monitoring	Plant discharge monitoring Plant performance and product water quality monitoring	0.5 – 3.0	0.002 – 0.005 0.004 – 0.008
Indirect O&M costs	Staff training Professional development and certification Consumables and maintenance of plant service vehicles Administrative and utility/service (water, sewer, telephone, etc.) expenses Operations insurance	5.0 – 15.0	0.02 – 0.06
Capital recovery cost	Capital recovery cost is assumed at 25 years payment term at 5 percent interest rate	44	0.32

6.7.2.1 Labour

The operation of desalination plants necessitates the engagement of a wide range of experts. In order to ensure optimal performance and adherence to rigorous standards, it is imperative that the administration, operation, laboratory, and maintenance departments possess the necessary expertise to effectively manage a desalination plant. The allocation of labour costs across various regions constitutes approximately 11-12% of the overall operational expenditure. The labour costs associated with treating water vary from \$ 0.05 to 0.10 /m³ [49], [358], [387].

This research developed a tailored labour methodology due to the significant variability in worldwide labour costs, which may be a 30-fold difference, potentially leading to an increase in overall expenses. For example, the water tariff at Bahrain's Al Dur SWRO facility, with a capacity of 218 million litres per day, is priced at US\$0.89 per cubic metre. The construction cost of this facility amounted to US\$236 million, while the operational expenses reached US\$27.2 million. The aforementioned turnkey contractor was responsible for the design and construction of a 200 MLD SWRO plant in Barcelona, Spain, at a total cost of US\$380 million. Additionally, an annual expenditure of US\$52 million was allocated for capital, operation and maintenance (O&M) purposes. Consequently, the cost of water production amounted to US\$1.42 per cubic metre. The allocation of labour costs for the development of the Al Dur plant amounted to 11 percent of the total operational costs, whereas the creation of the Barcelona Plant incurred a higher labour cost of 32 percent [49].

There is no clear correlation between the number of staff in a desalination plant and its production capacity in the literature. However, the staffing level at a desalination plant may exhibit slight variations depending on factors such as the plant's dimensions, design, location and operational schedule. According to the literature, the number of staff of different skill levels varies according to the plant capacity as seen in Table 6-4. In the field of desalination plants, staff required for operations can display notable fluctuations, which are impacted by several factors such as the size of the plant and its geographical location. An example of empirical evidence is derived from the Campo de Cartagena desalination plant in Spain. This facility, known for its daily capacity of 140,000 cubic metres, demonstrates that it can effectively operate with a workforce consisting of only 18 employees [384]. In contrast, the Carlsbad Desalination facility located in the United States, having a daily capacity of 190,000 cubic metres, employs 36 individuals to ensure continuous operation throughout the day [388].

An important factor to take into account when assessing staffing needs is the specific geographical location of a desalination facility. The MENA region has a significant presence of desalination facilities, which has resulted in a great deal of knowledge and expertise in the operation of these plants. As a result, the ratio of employees to output in these areas tends to be more optimised. On the other hand, in areas where RO plants have had less historical implementation, such as the United States, attaining operational efficiency may require increased employee levels to offset the lack of institutional familiarity.

Table 6-4: The staffing requirements for a SWRO desalination plant, categorised by plant capacity and skill level [381]

Plant capacity (m ³ /day)	High Skill	Low Skill
1000	2 - 3	4 - 6
5000	4 - 6	8 - 10
10,000	7 - 10	12 - 14
20,000	9 - 12	16 - 18
40,000	12 - 16	18 - 20
100,000	14 - 18	20 - 25
200,000	18 - 28	30 - 40
300,000	35 - 50	60 - 80

Figure 6–10 shows the employee structure that is proposed in this research; the number of employees are selected from Table 6-4 and are then distributed among these roles. Working hours and number of shifts depend on the level and type of plant automation and the capacity of the plant. Eq 6.12 refers to the the yearly total costs of labour (C_{EE}) in SWRO desalination plant.

$$C_{EE} = N_{EE} \times C_{\$/h} \times HPD \times PO_{days} \quad \text{Eq 6.12}$$

Where N_{EE} is number of employees, $C_{\$/h}$ is hourly wage rate, HPD is working hours per day and PO_{days} is the total duration of plant operation in days.

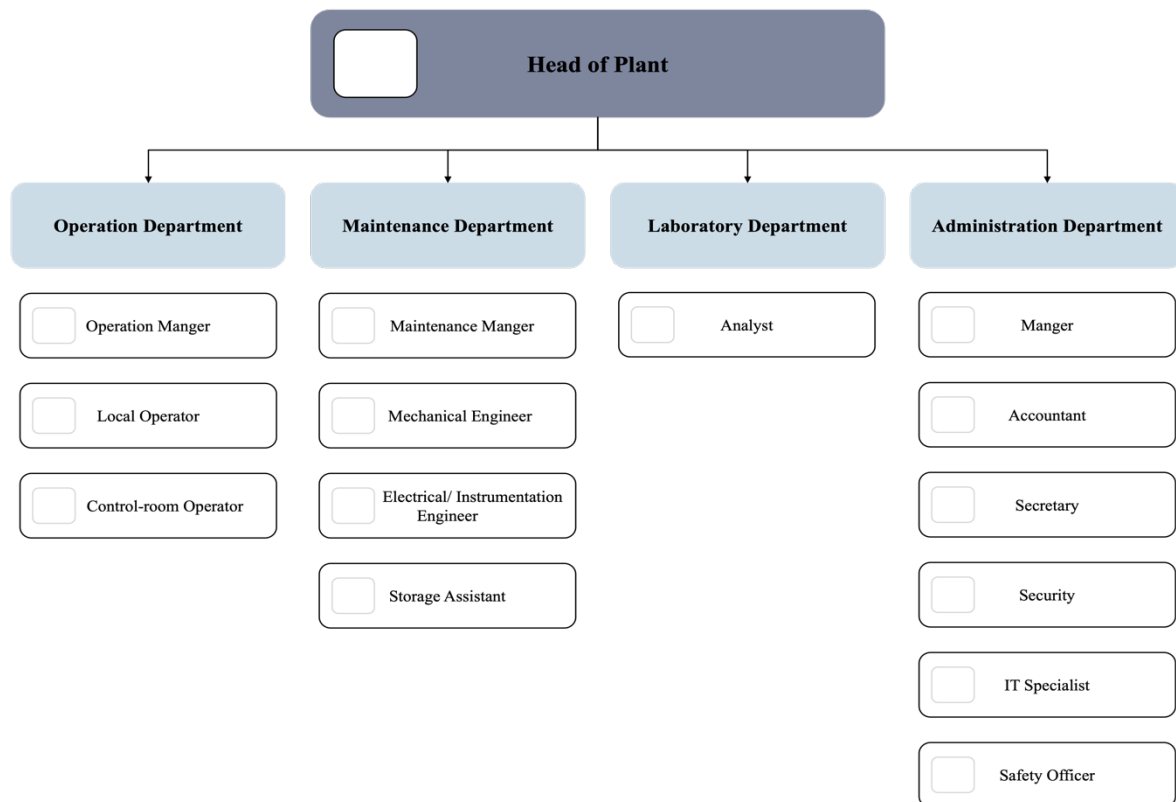


Figure 6–10: Recommended labour structure for SWRO desalination plant

Empirical labour costs for systems, in terms of hours, level of expertise, or individual wages, were not available. The majority of studies present an aggregate labour cost without providing detailed costs for individual categories. Therefore, the values utilised in this study are derived from a survey conducted based on estimate pay scale in Ireland from various websites [389], [390], [391] that provide information on job and salary scales which may not reflect actual figures across different regions. These values have the potential to be modified easily upon the specific geographical context. To simplify the process of estimating costs in the study, the labour type has been categorised into five distinct categories: head of plant, managers, engineers, operators, additional and others. The corresponding costs associated with each category are presented in Table 6-5.

Table 6-5: Labour categories, roles, and associated costs

Labour category	Roles	Cost per hour (\$/h)
Head of plant	Head of plant	40.0
Mangers	Operation manger, maintenance manager, administration manger, accountant	30.0
Engineers	Mechanical engineer, electrical/instrumentation engineer, IT engineer, and safety engineer	25.0
Operators	Local control room operator, local operator, and laboratory	20.0

Labour category	Roles	Cost per hour (\$/h)
Other	Storage assistant, secretary	18.0
Additional	Cleaner, security	13.0

6.7.2.2 Chemical

Determining the specific consumption of chemical dosing in a SWRO desalination plant is quite difficult due to many factors including the quality and type of water, water source and the method used to operate the desalination technology. These factors affect the level and dosage that should be used in the process. The increase in installation of desalination plants in the world results in a great demand on the chemical market. The President and chief operating officer in the US based BWA Water Additives estimated that \$500 million is the total cost of consumption of chemicals in desalination plants around the globally [392]. The IHS chemical company estimated that the overall global chemical consumption in the water treatment sector increased by approximately 3.2% per year between 2010 and 2015 [392], [393]. According to Almar Water Solution, the cost of chemical dosing is 11% of the total cost of OPEX in MENA region as unit cost is ranging from \$0.025 - \$0.075 /m³ [394][395]. Chapter 5 discussed the approach that would be used to calculate the chemical requirement per process (and subprocesses) and their associated cost.

$$C_{Chem} = \sum_{j=1}^n \text{chemical dosage } C_{\$/kg} PO_{days} \quad \text{Eq 6.13}$$

6.7.2.3 Energy

The most significant aspect of variable OPEX in the operation of a SWRO plant is its annual energy expenditure. The values are derived from Eq 6.14 which calculates the SEC cost ($C_{SEC_{total}}$) by summing the product of the volume of water processed at each process (Q_i), the specific energy consumption at that process (SEC_j), the cost of energy ($C_{\$/kwh}$), and the total duration of plant operation in days.

$$C_{SEC_{total}} = \sum_{j=0}^{n=5} Q_j SEC_j C_{\$/kwh} PO_{days} \quad \text{Eq 6.14}$$

Determining the precise cost of electrical power presents difficulties owing to its inherent fluctuations, as illustrated in Figure 6–11, which displays the 2023 businesses' electricity rates in several counties. In this research, the electricity rate can be determined by user input and is not predetermined. However, any figure from the graph can be utilised if it aligns with the user's specific scenario.

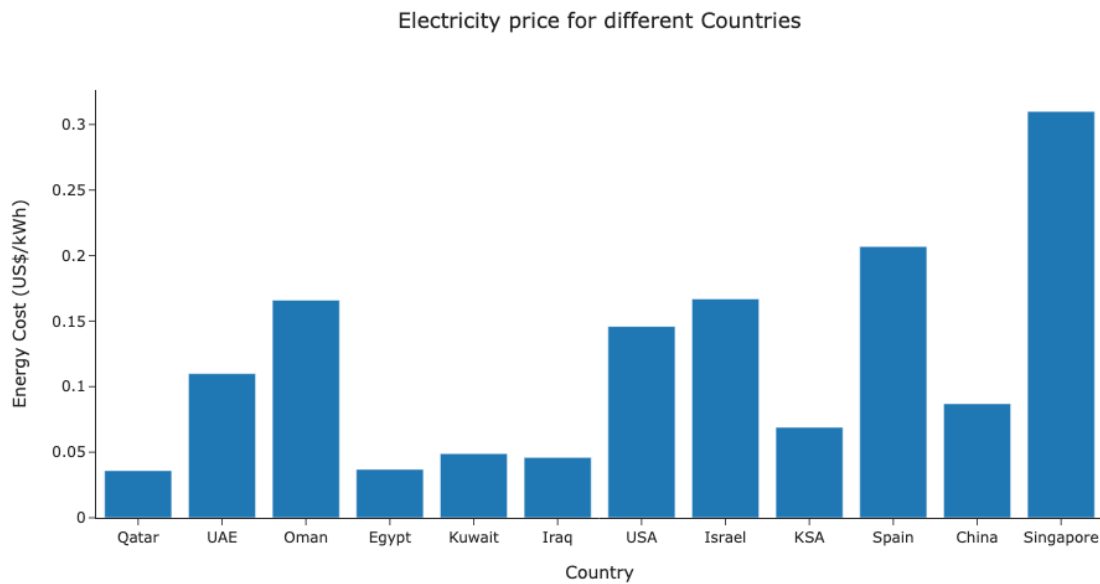


Figure 6–11: Electricity prices across a selection of countries utilising SWRO desalination

6.7.2.4 Maintenance and Repairs

Maintenance and repair are essential aspects of desalination plant operations. A well-structured scheduling system is necessary for this practise. A prudent method for estimating maintenance costs is to calculate the average annual expenses based on the projected lifespan of the equipment. Typically, the lifespan of equipment in desalination plants ranges from 25 to 50 years [45]. Maintenance costs are usually allocated between 2% [358] and 4% [396] of the total capital cost of the installed equipment only (C_{CAPEX}). In addition, the yearly expenses for maintaining structural components and piping infrastructure usually range from 1% to 2% of their initial construction expenses [397][45]. In this study, a 2% rate was used to calculate maintenance expenses (C_{maint}) as shown in Eq 6.15.

$$C_{maint} = 0.02C_{CAPEX} \quad \text{Eq 6.15}$$

6.7.2.5 Equipment Replacement

The lifespan of certain components in SWRO systems, such as cartridge filters, UF and RO membranes, as well as granular media filtration, is relatively shorter compared to that of other equipment. Cartridge filters typically have a lifespan ($L_{cartridge}$) ranging from two to three months [398], with a maximum potential lifespan of six months. The cost of cartridge filters ($C_{\$/cartridge}$) can range from \$8 to \$30 per filter. In the case of RO membranes, their life spans (L_e) from five to seven years [399]. However, with recent advancements in maintenance and improved pretreatment, the useful life of RO membranes can be extended up to ten years [397][40]. The replacement cost for cartridge filters ($C_{RPL_{cartridge}}$) and RO elements or UF elements (C_{RPL_e}) can be calculated using Eq 6.16 and Eq 6.17 respectively.

$$C_{repl_{cartridge}} = N_{cartridge} \frac{12 \text{ months}}{L_{cartridge}} C_{\$/cartridge} \quad \text{Eq 6.16}$$

$$C_{repl_e} = N_e \frac{L_{SWRO}}{L_e} C_{\$/e} \quad \text{Eq 6.17}$$

Where, L_j is the expected useful life of equipment (j) which can be in months or years, $C_{\$/e}$ is cost in dollars per element. There are two methods of maintaining granular media filtration, either cleaning or replacement. The cost associated with replacing any filter media is determined by three factors: the volume of the filter material used in the filtration plant, the annual replacement rate, and the cost of the specific filter medium. The granular filter media infill is typically replaced entirely every 10-20 years [271][301], resulting in an annual replacement rate of approximately 5-10% [40]. Eq 6.18 and Eq 6.19 are used to determine the variables $C_{repl_{filter_i}}$ and $C_{repl_{filter}}$ which represent the cost of the filter media layer and the total replacement cost of the media filter, respectively:

$$C_{repl_{filter_j}} = V_j f_{filter} C_{repl_j} \quad \text{Eq 6.18}$$

$$C_{repl_{filter}} = \sum_j^n C_{repl_{filter_j}} N_{filters} \frac{L_{SWRO}}{EUL_{filter}} \quad \text{Eq 6.19}$$

Where V_j is the volume of the layer; f_{filter} represents the number of replacements (ranging from 0.05 to 0.1); and n indicates the number of layers in the filter media. To perform the cleaning process, Eq 6.20 is used, with the additional step of multiplying it by V_j .

$$C_{cleaning_{filter}} = \sum_j^n C_{cleaning_{filter-j}} V_j N_{filters} \frac{L_{SWRO}}{L_{filter}} \quad \text{Eq 6.20}$$

Table 6-6 presents the expenses associated with the cleaning and replacement of a media filter per unit volume of 0.028 m³. The cost associated with cleaning encompasses the average expenses for labour and shipping, whilst the replacement cost comprises the expenses for catalyst, neutralisation process, and average shipping.

Table 6-6: Cost comparison of media cleaning and full media replacement [400]

Filter type	Cleaning (\$/0.028m ³)	Replacement (\$/0.028m ³)
Filter sand	48	40
Anthracite	18	55
Greensand	20	65
GAC	28	80

6.7.2.6 Disposal and Waste Management

In relation to cost, the expense associated with brine disposal ranges from 5% to 33% of the overall cost of the operations [401]. This cost fluctuates based on factors such as the properties and quantity of the brine, the extent of pretreatment, the method of disposal, and the environmental conditions in which the disposal takes place. However, it has been reported in other research[402] that the disposal of brine only constitutes a maximum of 5% of the overall operational costs. The values provided in Table 6-3 is for general estimation of disposal and waste management; however, these values might differ based on the technology used in disposal discharge. For instance, surface discharge costs ($C_{\$/m^3}$) between US \$0.05 – 0.3 per m³ of brine rejected while sewer discharge ($C_{\$/m^3}$) \$0.32–0.66/m³ of brine rejected [403][401]. The annual disposal and waste management cost is determined using Eq 6.21.

$$C_{Disposal} = Q_{disposal} C_{\$/m^3} P O_{days} \quad \text{Eq 6.21}$$

6.7.2.7 NPV and Sensitivity analysis

The interest rate is assumed to be 6% according to the literature. The cost estimates for CAPEX and OPEX pertaining to the desalination plant can be formulated as a basic design cost estimate, with an approximate accuracy of $\pm 15\%$. Therefore, a sensitivity analysis should be conducted to assess the impact of varying OPEX. Thus, to determine the influence of fluctuating energy costs on OPEX, this study implemented a sensitivity analysis using a variation range of $\pm 5\%$, $\pm 10\%$, and 20% .

6.7.3 Unit Product Cost

The cost of water production comprises of all expenditures related to the implementation, operation, maintenance, finance, and consists of both fixed and variable components. The calculation of the specific water production costs (WPC) during the cost accounting period (t) involves determining the expenses associated with producing a certain quantity of water [301]. This cost is computed using Eq 6.22

$$WPC_t = \frac{C_{CAPEX} + C_{OPEX}}{Q_{p_t}} \quad \text{Eq 6.22}$$

Where WPC_t is the cost of water produced by the desalination plant in ($\$/m^3$) and Q_{p_t} is the total permeate water that produced by the plant during a period (t).

6.8 Summary

This chapter provided a comprehensive analysis of the CAPEX and OPEX associated with SWRO desalination plants. The CAPEX analysis was based on an adaptable cost database covering various processes and subprocesses, allowing for easy updates to reflect current market prices. Detailed cost ranges for both direct and indirect CAPEX components were also established, providing a flexible framework for future adjustments based on specific project needs.

Furthermore, the chapter developed systematic steps for calculating OPEX, offering suggested cost ranges for these expenses. This approach provides a dual utility, serving both as a guideline and as a customizable input model, where users can substitute their own values as necessary.

The contributions of this chapter extend to the development of a robust cost database for SWRO desalination. This includes detailed calculations of CAPEX and OPEX, which have been integrated into a Life Cycle Cost Analysis (LCCA) tool. This tool is designed to enhance

decision-making processes by providing a comprehensive economic assessment platform, which will be further explained in the subsequent chapter.

Chapter 7

Evaluation of OntoSWRO and LCCA TOOL

This chapter outlines the development of a SWRO design and LCCA tool, based on the domain knowledge assimilated and aggregated in Chapter 5 and Chapter 6. The main objective is to validate the methodology and outcomes derived from analysis of the three use cases presented in Chapter 4. The outputs obtained from this tool will be analysed, and a thorough examination of the integrated results from these three chapters will be presented here.

To effectively assess the utility of the knowledge modelling performed here for the purpose of designing improved SWRO systems, three complex use cases were outlined in section 4.5. To exploit the knowledge modelling (Chapter 4) and the data gathered (Chapter 5 and Chapter 6), a SWRO design and LCCA tool was implemented that provided a graphical user interface to define and explore configurations and produces. Section 7.1 outlines the development and implementation of the prototype SWRO design and LCCA tool while section 7.2 performs an evaluation of the outcomes using the three cases studies. Section 7.3 discusses the consequences of integrating an ontology for SWRO with life cost analysis in this way.

7.1 Model Development and Implementation

The tool was built on the Dash Plotly platform (v2.17.0), a freely available Python web framework developed by Plotly, that allows for the production of interactive, web-based data visualisations. It emphasises simplicity and flexibility. Dash applications are commonly organised as a composition of layout components and callback methods.

The layout components determine the structure of the interface and visual presentation of the data, defining how graphs, charts, and other HTML elements are positioned and displayed. Callback methods in Python are functions that are activated in response to changes in the layout components, such as button clicks or slider adjustments. These functions have the ability to dynamically update the content of the application, resulting in a user experience that is both responsive and interactive. Dash facilitates the seamless exchange of information between the frontend (web browser) and the backend (Python server) and was chosen as the prototyping framework here due to the ability to generate interactive data visualisations without significant

web development. Figure 7–1 gives a visual overview of the SWRO design and LCCA tool as implemented in Dash.

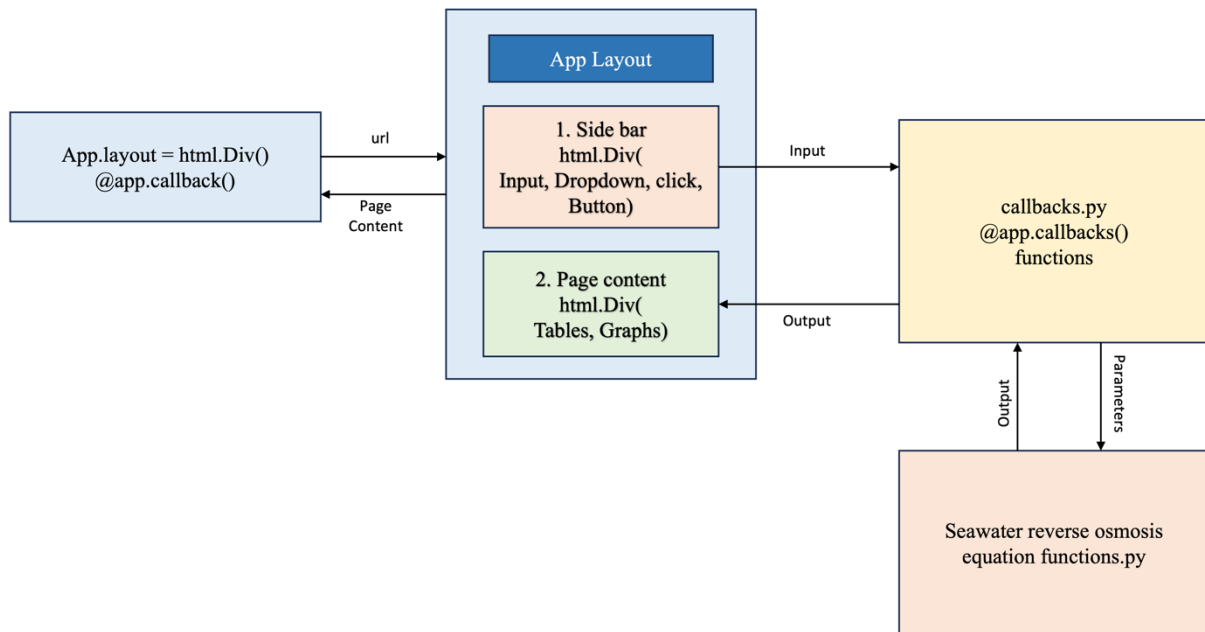


Figure 7–1: Dash plotly frameworks for SWRO design and LCCA tool

- ▶ Water Quality
- ▶ Intake System design
- ▶ Pretreatment System
- ▶ Reverse Osmosis System Design
- ▶ Discharge System
- ▶ Life Cycle Cost Analysis

Desalination Plant Design Tool

Reverse Osmosis System Design

Permeate Flowrate (m3/h)

Feed Salinity (mg/L)

Recovery Rate

Design Temperature (°C)

Flux (LMH)

Membrane Element properties at Test Conditions

Total Area of Element

Salt Rejection

Element Per Pressure Vessel

	Element Properties	SW30XLE-440i	SW30HRE-400i	SW30HR-380	SW30XFR-400	unit
<input checked="" type="checkbox"/>	Manufacture	DOW	DOW	DOW	DOW	
<input checked="" type="checkbox"/>	Purpose of Element	Low Energy	Low Energy & High Rejection	High Rejection	High Fouling	
<input checked="" type="checkbox"/>	Total Membrane Area	40.9	40.9	35	40.9	m2
<input checked="" type="checkbox"/>	Salt Rejection	0.998	0.998	0.997	0.9975	%
<input checked="" type="checkbox"/>	Qfmax	17.7	14.58	12.81	14.58	m3/h
<input checked="" type="checkbox"/>	Temperature at Testing	25	25	25	25	oC
<input checked="" type="checkbox"/>	Applied Feed Pressure	55	55	55	55	bar
<input checked="" type="checkbox"/>	Feed Salinity	32000	32000	32000	32000	mg/L
<input checked="" type="checkbox"/>	Element Recovery	0.08	0.08	0.08	0.08	
<input checked="" type="checkbox"/>	Nominal Capacity for Permeate (Qws)	1.416	1.167	1.025	1.167	m3/h

index	feed_flow	concentrate_flow	concentrate_concentration	average_concentration	permeate_concentration
0	11111	6111	63579	49289.5	99

index	flow_per_element	number_of_elements	number_of_pressure_vessels	number_of_elements1	flux	flow
0	0.573	8726	1454	8724	14.01	

index	pressure_loss_per_element	concentrate_concentration_test	average_concentration_test	permeate_concentr
0	0.15	34777.043	33388.522	

index	osmotic_feed_pressure	osmotic_concentrate_pressure	osmotic_permeate_pressure	applied_feed_pressure
0	29.692	53.936	0.084	53

Figure 7–2: Screenshot from the model interface

Figure 7–2 presents a screenshot of the model interface, illustrating how the responsive design of the dashboard dynamically populates the results in accordance with user input. The following process flowcharts (Figure 7–3 - Figure 7–11) illustrate a sophisticated approach designed to calculate various aspects of SWRO desalination plant that was developed based on the knowledge from Chapter 5 and Chapter 6. It presents a structured approach where the user can navigate through different components and parameters to define and evaluate the system.

The elements in blue represent dropdown menus that provide predefined options for the user to select from, thereby simplifying the choice of components such as surface or subsurface intake types etc. The orange elements signify the input fields where the user must enter specific data, such as the volume of intake pipes or the permeability of wells etc. These inputs are crucial as they directly affect the calculations and the outcomes of the model. The outputs of the model are highlighted in green and are the result of the calculations based on the selected options and entered inputs. They offer valuable information such as number of elements pressure vessels, intake capacity, diffuser design, enabling the user to gauge the viability of the SWRO systems. The red lines indicate the flow of the process, guiding the user from one step to the next.

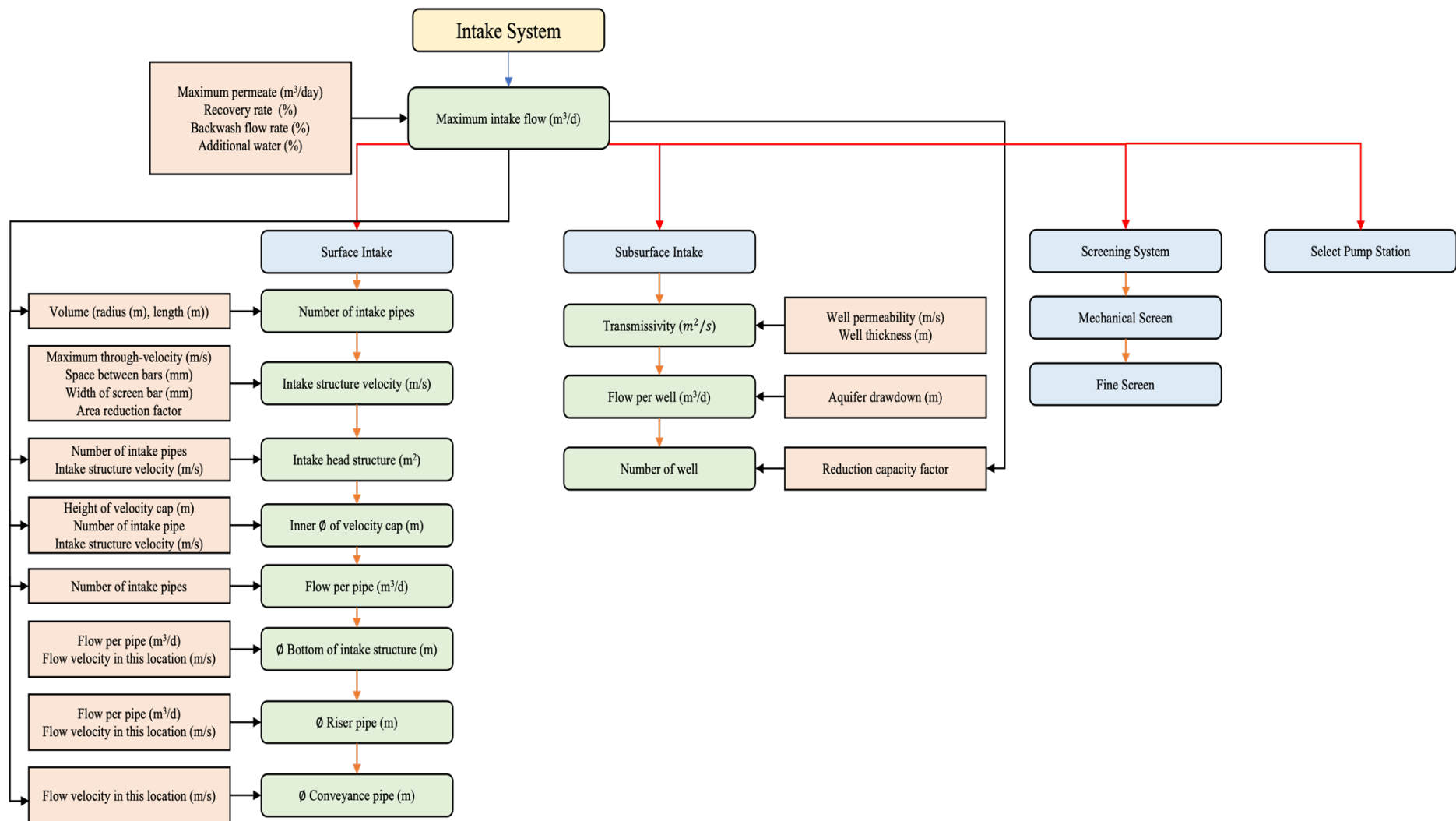


Figure 7–3: Intake system framework for support decision tool

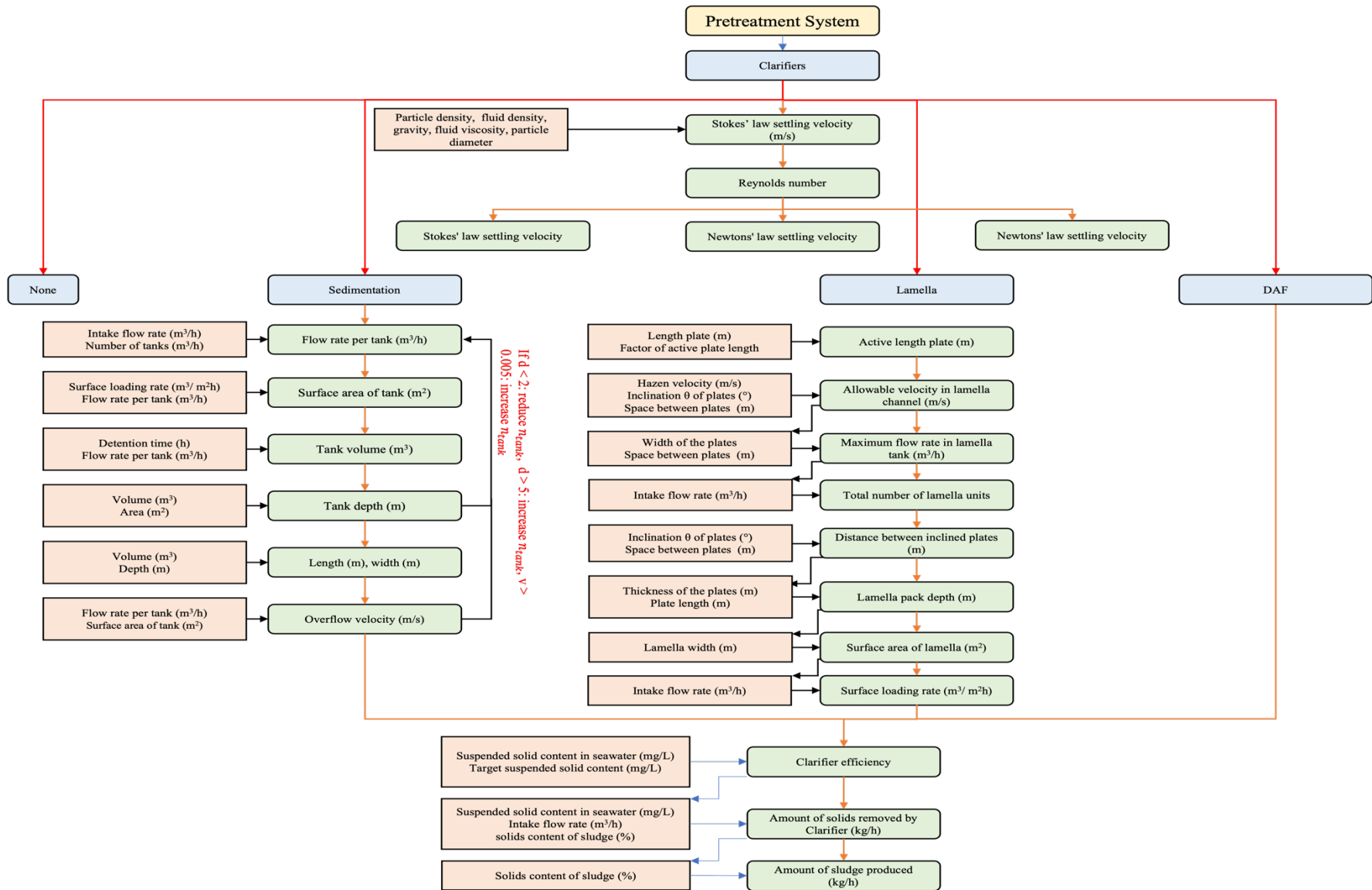


Figure 7-4: pretreatment system framework for support decision tool

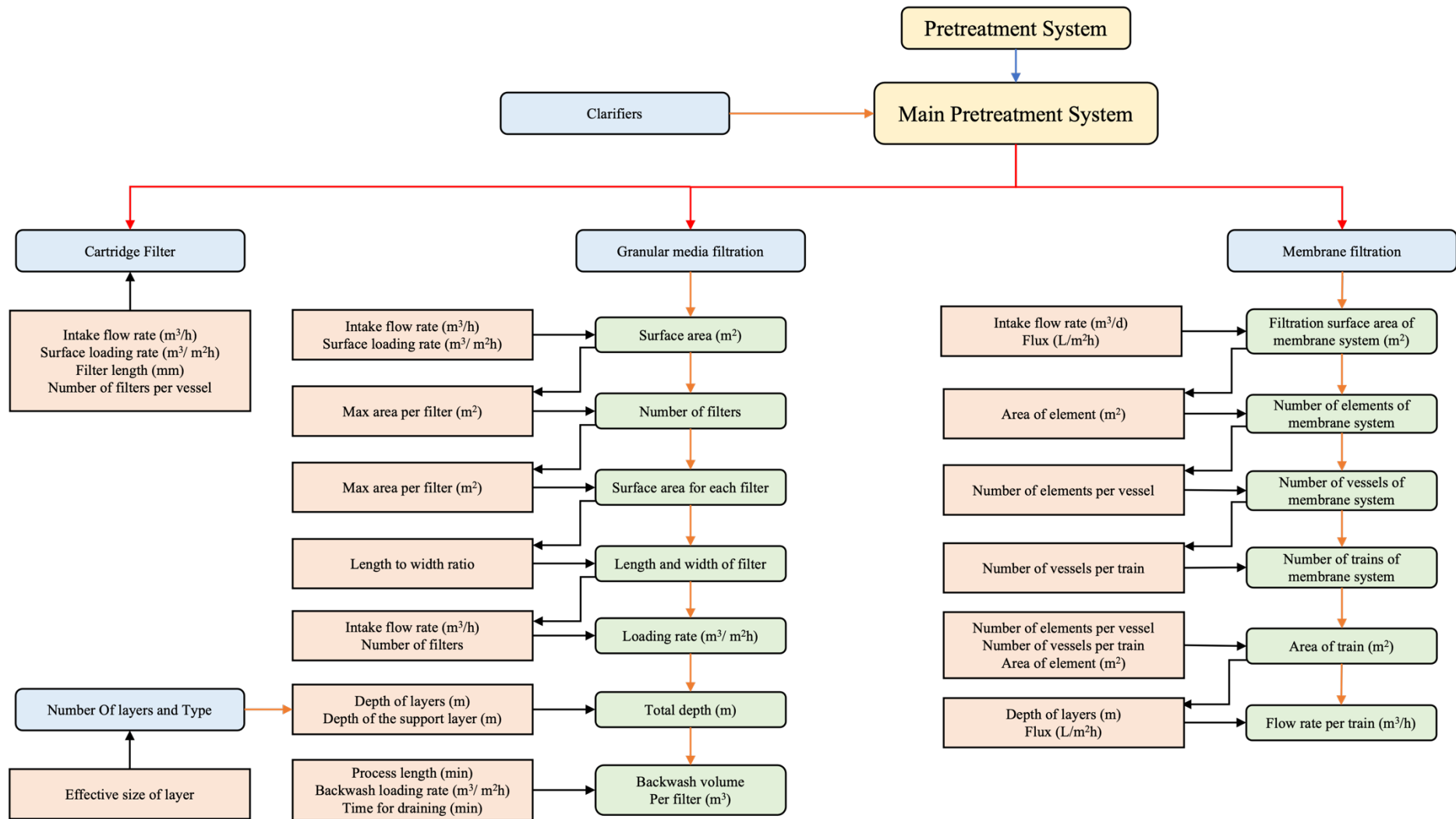


Figure 7-5: Pretreatment system framework for support decision tool

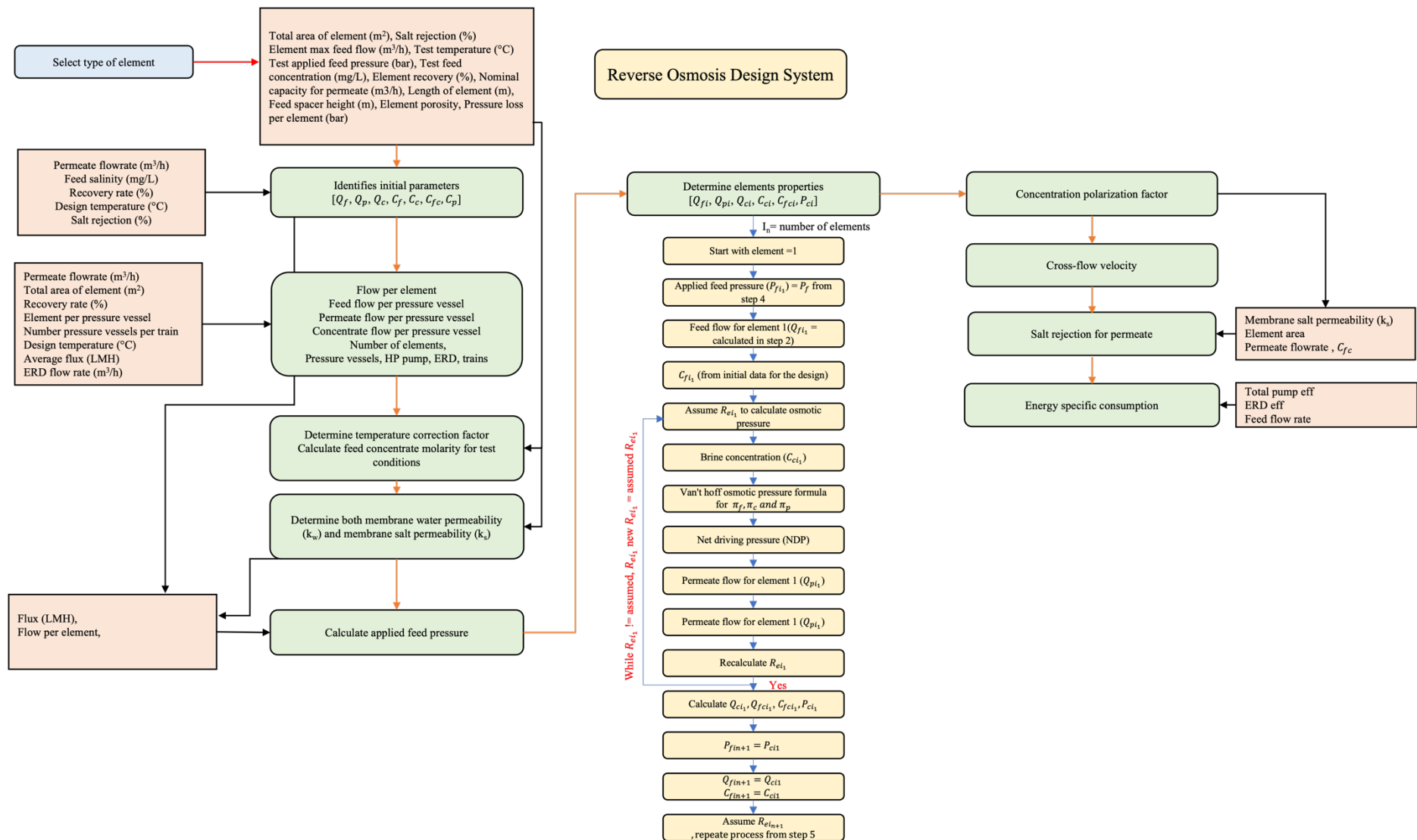


Figure 7–6: RO system framework for support decision tool

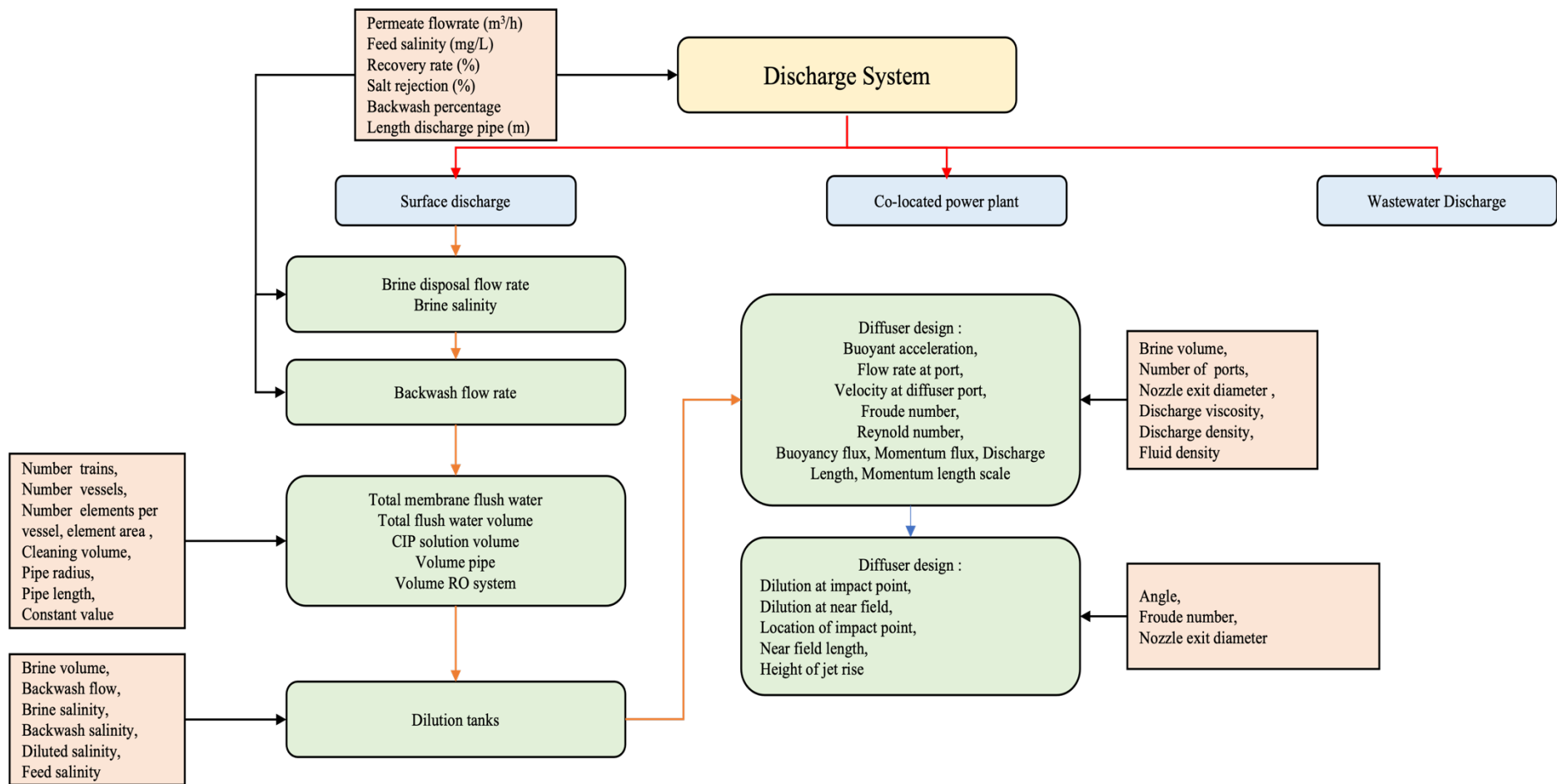


Figure 7–7: Discharge system framework for support decision tool

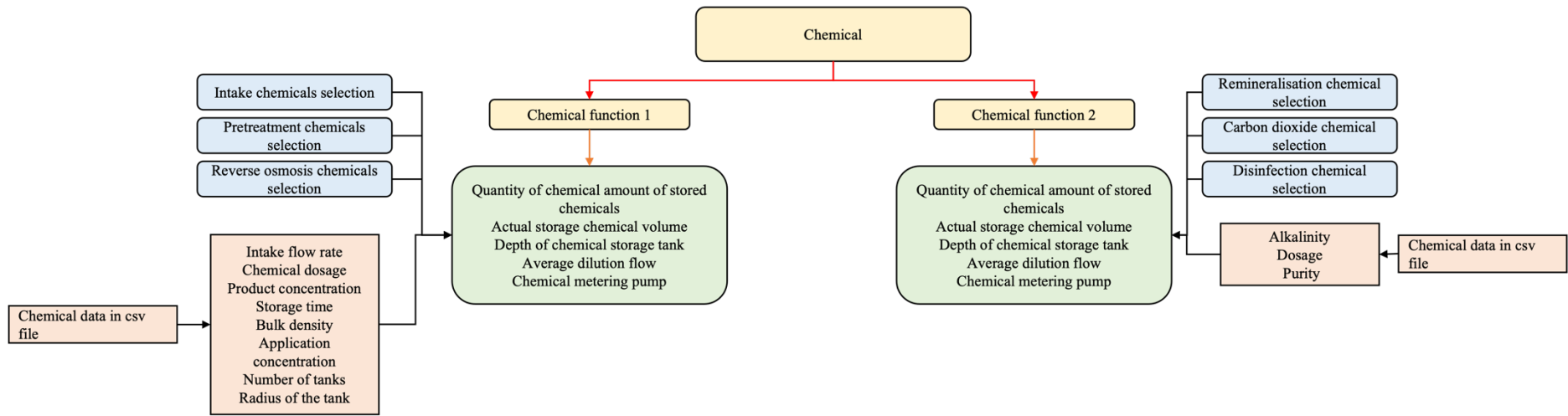


Figure 7–8: Chemical calculation framework for support decision tool.

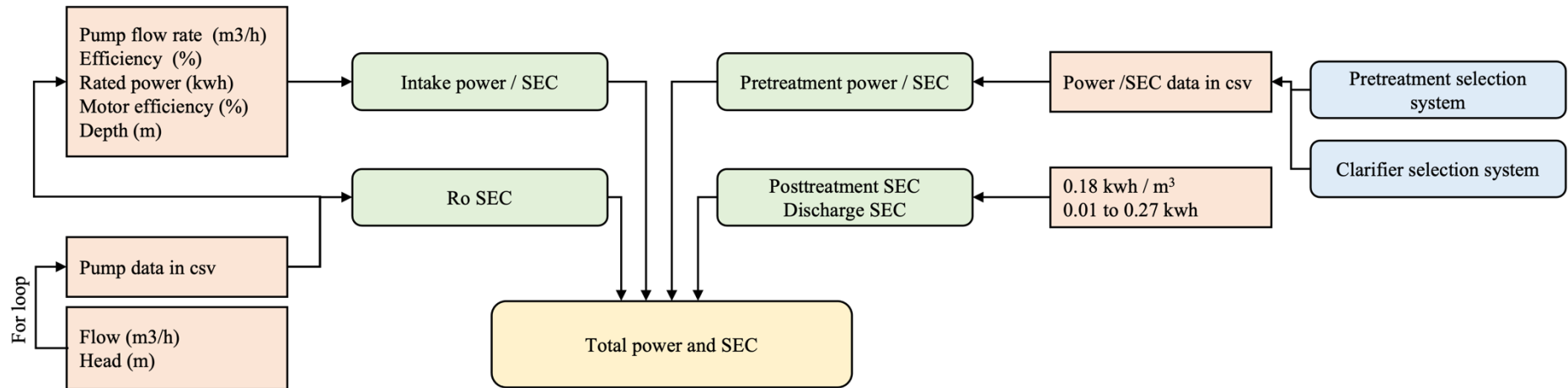


Figure 7–9: SEC framework for support decision tool

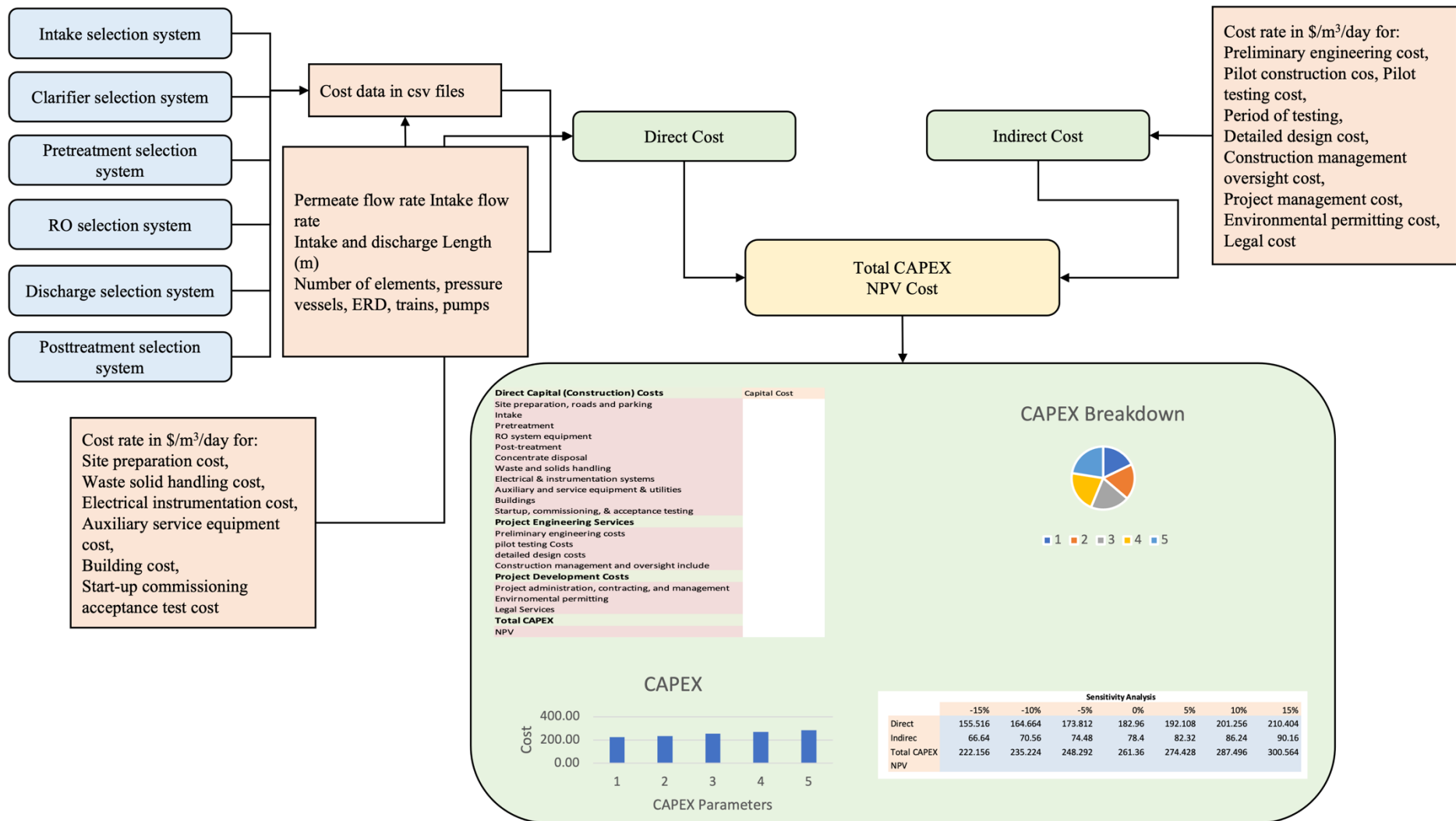


Figure 7–10: CAPEX framework for support decision tool

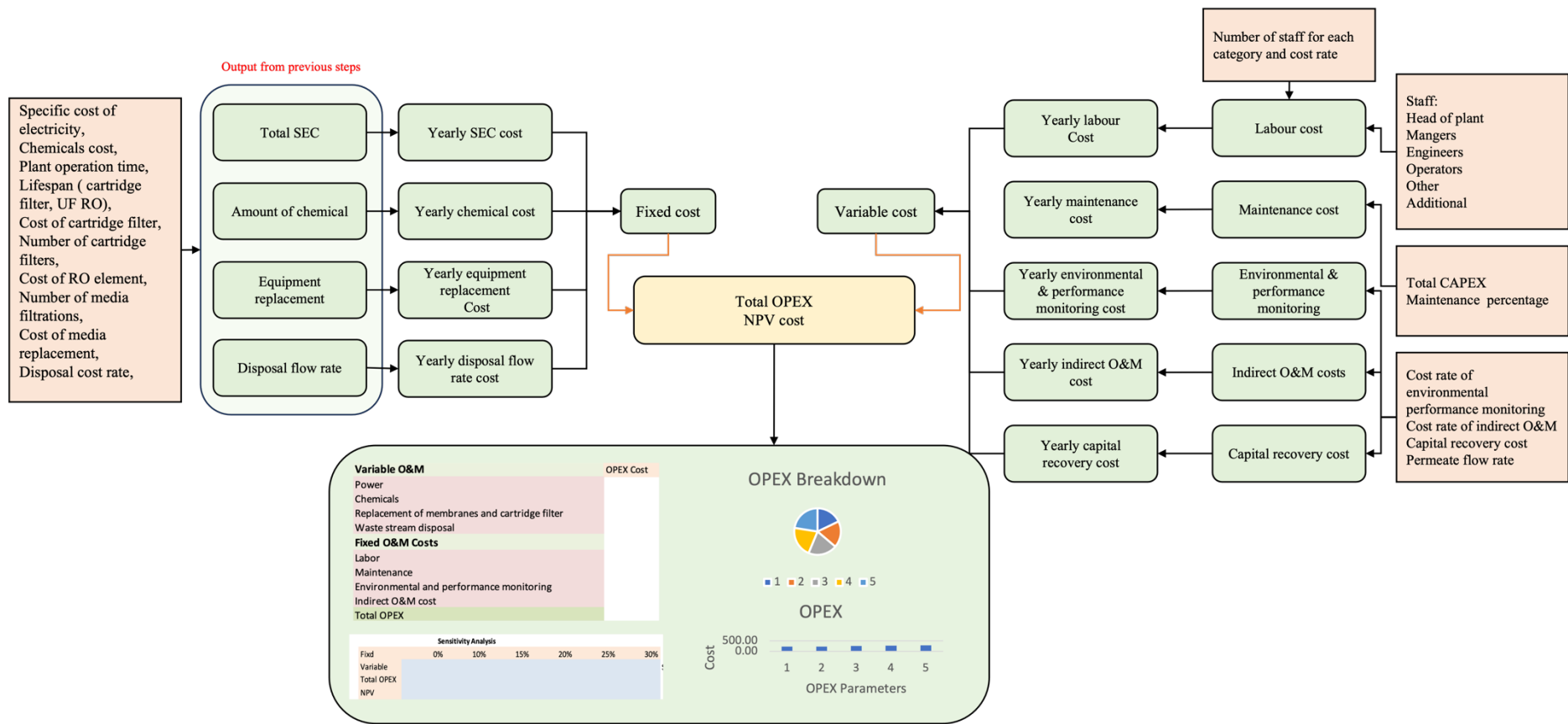


Figure 7–11: OPEX framework for support decision tool

The model has been developed in accordance with the layouts provided in the previous diagrams, as depicted in the figure illustrating the model's interface. This model is intended for the evaluation of three cases from Chapter 4

7.2 Model Analysis and Evaluation

This section details the outcomes derived from the model, along with an analysis and assessment of these findings. The following tables are color-coded for ease of interpretation: blue indicates values that are linked to the scenarios outlined in Chapter 4, yellow indicates assumed values selected from OntoSWRO, and green denotes outputs generated by the decision support tool. All tables related to the following evaluation are provided in APPENDIX F.

7.2.1 Analysis and Evaluation for Case 1

Table 7-1 outlined the design parameters for case one of the SWRO desalination, as generated by the SWRO design tool. For a detailed breakdown of each process, refer to APPENDIX F.

Table 7-1: Summary of SWRO design specifications for Case 1

Plant design Summary	Value	Unit
Product	25,000.00	m ³ /day
Recovery	45.00	%
Salinity	35,000.00	mg/L
Temperature	25.00	°C
Intake capacity	57,805.56	m ³ /day
Ro feed flow	55,556.00	m ³ /day
Brine flow rate	30,556.00	m ³ /day
Total discharge flow rate	32,778.96	m ³ /day
Brine salinity	63,579.00	mg/L
Permeate salinity	99.00	
Capacity per well	5,223.27	m ³ /day
Number of wells	16.00	
Required surface area of filters	161.00	m ²
Number of filters + standby	4.00	
Number of cartridges	659.00	
Number of cartridges per PV	82.00	
Number of pressure vessels	228.000	
Number of elements	1,824.000	
Number of trains	3.000	

Plant design Summary	Value	Unit
Number of ERD	14.000	
Water permeability coefficient at design	1.431	L/m ² .bar.h
Salt permeability coefficient at design	0.076	L/m ² h
Applied feed pressure	52.000	bar
Brine pressure	50.320	bar
Intake system SEC	0.13	kWh/m ³
Pretreatment system SEC	0.100	kWh/m ³
RO system SEC	2.390	kWh/m ³
Discharge SEC	0.270	kWh/m ³
Posttreatment SEC	0.170	kWh/m ³
Total SEC	3.01	kWh/m ³

According to the suggested design from OntoSWRO, it is determined that to meet the intake capacity outlined in Table - 17, the plant will need 16 beach wells, with each expected to produce 5,233.27 m³/day (Table - 18). This calculation is predicated on the anticipation of a 3% loss in production efficiency for the beach wells. Nonetheless, deploying 16 wells would slightly exceed the plant's maximum intake capacity, while 15 wells would not suffice to meet the required capacity. Table - 16, found in the APPENDIX F, illustrates that a plant with a daily capacity ranging from 54,600 to 60,000 m³ would typically operate with 11 to 12 wells [303]. The reported literature values, however, must be tempered with the understanding that variations in ground permeability and transmissivity, which are crucial to these calculations, are not fully documented, nor is it clear if the potential production losses have been fully accounted for.

Table - 19 and Table - 20 detail the recommended pretreatment system options, highlighting the design specifications for single media pressure filtration and cartridge filters, respectively. The design calls for 659 cartridge filters, based on the stipulation that each pressure vessel houses 8 cartridges, aligning with the number of elements in the RO system.

The RO system is calculated to require 1,824 elements across 228 pressure vessels (Table - 21) to achieve a production of 25,000 m³/day. The design's water and salt permeability coefficients are documented as 1.431 L/m².bar.h and 0.076 L/m².h, respectively, as indicated in Table - 22. An applied pressure of 52 bar is required to separate a solution with a salinity of 35,000 mg/L and produce permeate with a salinity of 106.32 mg/L, as indicated in Table - 23.

Table - 24 provides the performance of individual elements within the pressure vessels, noting that the first element achieves a recovery rate of 11.7%, while the final element has a recovery rate of 1.6%. The reasons for the decline in membrane recovery across the pressure vessels are explained in Sections 2.3.1 and 5.9. Ultimately, the decision to utilise 8 elements per pressure vessel is left to the discretion of the user.

The discharge system is engineered to accept a flow rate of 33,045.23 m³/day, a figure that exceeds the one presented in Table - 25(row 12). This value accounts for the inclusion of both backwash and CIP water. This figure represents the upper threshold of discharge that the desalination plant is capable of handling which happens once or twice per year. Otherwise, the daily discharge capacity is 32,778.22 m³/day; it is integral to the calculations for both OPEX and CAPEX. Additionally, Table - 25 outlines the specifications for the jet diffuser design, which ensures effective dilution of brine with seawater to mitigate the environmental footprint of the brine discharge.

The detailed SEC breakdown (Table - 26) shows that the RO system is the most energy-intensive process of the overall desalination system, consuming 2.39 kWh/m³, which is expected due to the high pressures required for reverse osmosis. The intake system SEC and pretreatment system SEC are comparatively lower at 0.13 kWh/m³ and 0.1 kWh/m³, while the posttreatment and discharge SECs are 0.17 kWh/m³ and 0.27 kWh/m³ respectively. Collectively, these components yield a total SEC of 3.01 kWh/m³. This total SEC that is computed by the model is in alignment with the values discussed in the literature review. The rated power for the intake system's pumps, sourced from the pump dataset, aligns with the design requirements of the intake system. The selected pump possesses a rated power of 314 kW, and is capable of delivering a flow rate of 2,423 m³/h at a head of 40.6 metres.

Table 7-2 provided a comprehensive summary of the CAPEX and OPEX for Case 1. For a more detailed analysis and breakdown of these financial metrics, APPENDIX F contains extensive supplementary data and specifics obtained from LCCA tool.

Table 7-2: Summary of CAPEX and OPEX for Case 1

Parameters	OPEX cost (\$millions/year)	Cost (\$M/20 years)	Note
Discounting rate	5%		
Power	4.58	91.69	Cost rate = \$0.15
Chemicals	0.50	9.97	

Parameters	OPEX cost (\$millions/year)	Cost (\$M/20 years)	Note
Replacement of membranes and cartridge filter	0.19	4.12	Cost rate = \$30.0*, \$40.0**, \$500.0***
Waste stream disposal	1.77	35.40	Cost rate = \$0.15
Labour	1.16	23.27	No of staff = 18
Maintenance	0.84	16.76	
Environmental and performance monitoring	0.04	0.72	Cost rate = \$0.004
Indirect O&M cost	0.36	7.20	Cost rate = \$0.04
Total OPEX (\$M/20 years)	9.45	189.14	
Total CAPEX (\$)		48.56	

*cartridge replacement price, ** pretreatment replacement price, *** RO replacement price

Table - 27 presents a breakdown of CAPEX for a desalination project for Case 1, including direct CAPEX and indirect CAPEX, along with the NPV of the investment.

The Direct CAPEX, amounting to \$41.91 million, encompasses the primary costs directly associated with the construction and installation of the desalination plant. For instance, the RO system and discharge system are the most expensive components, due to their complex technology and energy requirements, and these account for a significant portion of the budget at \$13.95 million and \$13.11 million respectively. Similar to Table 6-2, the RO system has the highest CAPEX contribution. However, contrary to Table 6-2, the contribution of the discharge system in Case 1 is relatively more significant.

The Indirect CAPEX, totalling \$6.65 million, accounts for the supportive and additional expenses such as project management, detailed design, construction management oversight, and environmental permitting. The NPV calculated at \$32.87 million is a measure of the profitability of the project. A positive NPV, such as the one presented, indicates that the projected earnings, discounted for the time value of money at a discount rate of 5%, exceed the initial investment outlays. This suggests that the project is financially viable given the parameters and assumptions used in the NPV calculation.

This desalination plant requires 18 employees (Table - 28); their expertise level was selected, and salary calculated, according to the approach in the methodology presented in Chapter 6. Regarding chemical alkalinity, most desalination plants are specifically built to generate finished water with a total hardness (calcium and magnesium) ranging from 80 to 120 mg/L as CaCO₃ [404], therefore, 80 mg/L of CaCO₃ was used for these cases.

Labour and maintenance costs are relatively moderate. Environmental and performance monitoring, along with indirect O&M costs, are comparatively low (Table - 29). Energy costs, often the most significant portion of OPEX in desalination plants due to the energy-intensive nature of the process, are listed at \$4.58 million/year. Chemical costs, at \$0.50 million/year, and the replacement of membranes, media filter and cartridge filters, at \$0.19 million/year, are also significant recurring costs. Waste stream disposal is another notable expense at \$1.77 million/year, highlighting the environmental management aspect of desalination operations, which often involves the handling of brine and other waste by products. The Total OPEX, summing up to \$9.45 million/year, and \$189.14 million over 20 years of operation. This design will lead to water production cost of \$1.32

Table - 32 illustrates the results of a sensitivity analysis. This sensitivity analysis was conducted by altering the cost of energy, both increases and decreases, with electricity prices being identified as the major factor that would vary over years. The energy prices were assessed at $\pm 5\%$; $\pm 10\%$ and $+20\%$. The total operational expenditure, when subjected to a -10% sensitivity analysis, dropped to \$198.3 million, which represents an increase of approximately \$207.47 million over the period of 20 years, reflecting a 20% increase.

Figure 7–12 and Figure 7–13 presents the breakdown for CAPEX and OPEX for the Case 1 desalination plant, respectively. The most substantial portion of OPEX is energy, reflecting the high energy requirements for the reverse osmosis process, which in turn is the most expensive system in the CAPEX, especially at such a scale. These findings are consistent across the literature.

Capital Expenditure Breakdown

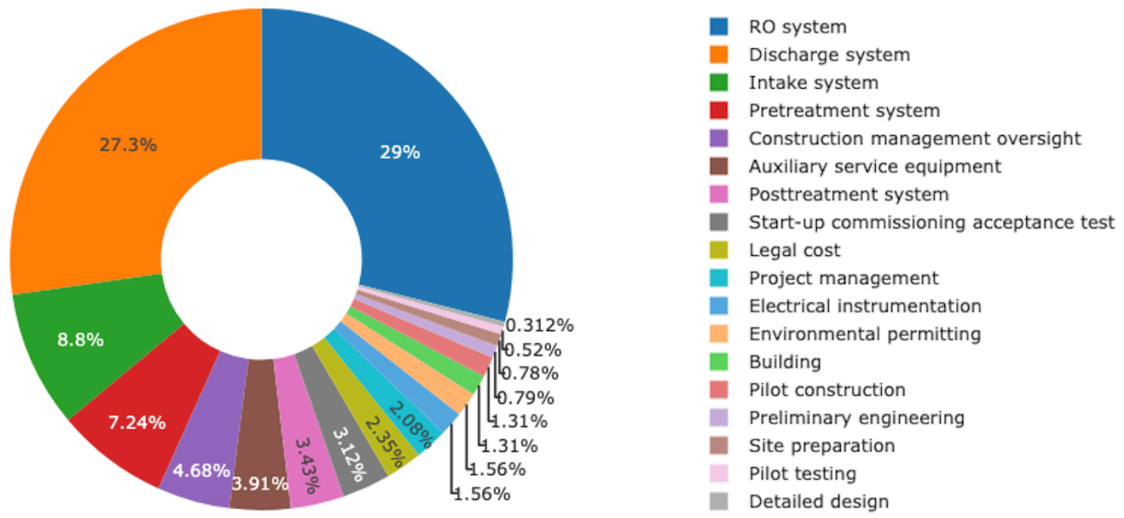


Figure 7-12: CAPEX breakdown for Case 1

Operational Expenditure Breakdown

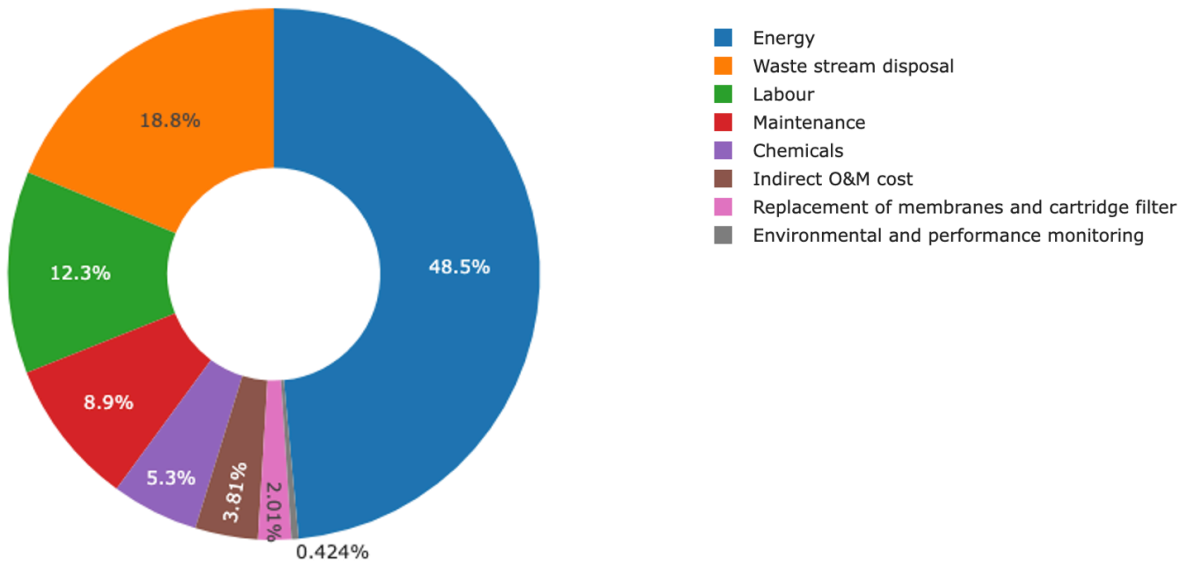


Figure 7-13: OPEX breakdown for Case 1

7.2.2 Analysis and Evaluation for Case 2

In this scenario, OntoSWRO has presented two potential solutions that are identical in all aspects except for the pretreatment system. The first approach recommends using gravity dual media filtration, while the second recommends UF. These two options are now analysed and compared to assess their respective impacts on design and cost. Table 7-3 presented a summary of the SWRO desalination design parameters for case 2, summarised from the SWRO design tool. Detailed designs for each process can be found in APPENDIX F.

Table 7-3: Summary of SWRO design specifications for Case 2

Plant water design	Solution 1	Solution 2	Unit
Product	120,000.00	120,000.00	m ³ /day
Recovery	40.00	40.00	%
Salinity	38,000.00	38,000.00	mg/L
Temperature	28-32	28-32	°C
Intake capacity	318,000.00	330,000.00	m ³ /day
Ro feed flow	300,000.00	300,000.00	m ³ /day
Brine flow rate	180,000.00	180,000.00	m ³ /day
Brine salinity	63,283.00	63,283.00	mg/L
Permeate salinity	101.00	101.00	
Feed water density	1023.62	1023.62	kg/m ³
Number of intake pipes	2.00	2.00	
Lamella settling velocity	0.015	0.015	m/s
Number of media filters + standby	16.00		
Media filter depth	5.15	-	m
Number of Cartridges	3,418.00	-	
Number of UF Element	-	5,980.00	
Number of UF Vessel	-	1,495.00	
Number of UF Train	-	31	
Number of RO elements	9,653.000	8,449.000	
Number of RO pressure vessels	1,379.000	1,207.000	
Number of ERD	80.000	80.000	
Number of RO trains	14.000	12.000	
Water permeability coefficient	1.369	1.372	L/m ² .bar.h
Salt permeability coefficient	0.073	0.073	L/m ² h
Applied feed pressure	54.000	56.000	bar
Brine pressure	52.88	54.53	bar
Salinity in permeate water	200.07	200.03	mg/L
Total discharge flow rate	195,003.35	208,041.69	m ³ /day

Plant water design	Solution 1	Solution 2	Unit
Intake system SEC	0.042	0.042	kWh/m ³
Pretreatment system SEC	0.150	0.202	kWh/m ³
RO system SEC	2.530	2.630	kWh/m ³
Discharge SEC	0.270	0.270	kWh/m ³
Posttreatment SEC	0.180	0.180	kWh/m ³
Other facilities	0.1	0.1	kWh/m ³
Total SEC	3.27	3.424	kWh/m ³

According to Case 2:

Table - 33, the UF-equipped plant requires a higher intake capacity than its media filtration counterpart by 12,000 m³/day, attributed to the UF system's need for more frequent backwashing [245], [405]. Consequently, costs related to the intake and discharge systems are higher for the UF solution, as reflected in Table - 34 and Table - 43. Moreover, the lamella in the UF solution (Table - 35) removes more solids due to the increased intake capacity which results in a higher sludge disposal. The gravity filtration solution requires 16 gravity filters, whereas the UF system necessitates 5,980 elements across 31 trains.

The media filtration solution entails an additional pretreatment step using 3,418 cartridge filters to eliminate finer particles, thus protecting the RO system, a step that the UF solution does not require. Furthermore, the media filtration will consume more chemicals than UF, as indicated in Table - 49 and Table - 50. However, since the UF solution process requires a larger volume of intake water, the expected cost advantage is negated, resulting in higher overall costs for the UF system.

In the RO system design, the UF solution calls for fewer membrane elements, pressure vessels, and trains due to its ability to operate at a higher flux, as seen in Table - 38, resulting from a higher water permeability coefficient (Table - 39) compared to the media filtration solution. Nonetheless, the UF system experiences greater pressure loss per element, necessitating a feed pressure that is 2 bar higher than that of the media filtration solution (54 bar).

The salinity in permeate for both solution is approximately 200 mg/L which is clearly higher than Table - 33 because this value takes into account the RO transport equations.

Table - 44 illustrates that both solutions report the same SEC for intake system, which is a contradiction given the higher capacity of the UF system. This arises because there was no available pump in the dataset that met the necessary capacity and head criteria; therefore, Eq

5.110 was employed to estimate the power, neglecting pipe losses and considering only capacity and depth. Research [387] has noted that offshore intake has an SEC of 0.05 kWh/m³ of desalinated water, suggesting the model's calculated values are not significantly divergent from those documented. Overall, the UF solution acquires a higher SEC at 3.424 kWh/m³, with the media filtration solution being more energy-efficient by 0.154 kWh/m³.

Table 7-4: Summary of CAPEX and OPEX for Case 2

	Cost solution 1 (\$M/year)	Cost solution 2 (\$M/year)	Note
Discounting rate	4%		
Power	12.60	13.64	Cost rate = \$0.08
Chemicals	2.88	4.1	
Replacement of membranes and cartridge filter	1.83	1.2	
Waste stream disposal	14.04	14.90	Cost rate = \$0.2
Labour	1.59	1.77	No of staff = 25, 28
Maintenance	5.82	5.84	
Environmental and performance monitoring	0.22	0.22	Cost rate = \$0.005
Indirect O&M cost	2.16	2.16	Cost rate = \$0.05
Total OPEX (\$M/20 years)	41.13	43.82	
Total CAPEX (\$)	322.13	328.3	

Table 7-4 showcases a summarised view of both the CAPEX and OPEX associated with Case 2. To explore the detailed components and individual calculations that underpin these figures, refer to APPENDIX F, where these elements are explored in greater depth. For instance, Table - 45 outlines the CAPEX for two distinct desalination plant scenarios which are summarised as follows:

1. In both scenarios, the intake system, discharge system followed by RO system represent significant portions of the initial investment as seen in Figure 7–14, reflective of their vital role in the desalination process. The UF scenario shows a slightly higher investment in these systems, but not in the RO system.
2. The posttreatment system, auxiliary service equipment, and waste solid handling costs are comparable across both scenarios, suggesting that these processes are not heavily influenced by the choice of pretreatment technology. However, building construction expenses as well as preliminary engineering, construction management oversight, and

project management are notably higher in the UF scenario due to the additional infrastructure required to support the more complex UF system. Therefore, the cost rate for Case 2, scenario 2 was lower than scenario 1.

Comparing the OPEX tables (Table - 53 and Table - 54) for the two desalination plants, several conclusions were drawn about the cost implications of each pretreatment method on overall operational expenses:

1. The UF pretreatment plant incurs slightly higher energy costs (\$13.64 million/year) compared to the media filtration plant (\$12.6 million/year) as shown in Table - 48 and Table - 48. This is due to the higher energy requirements of UF systems, which require electricity to maintain transmembrane pressure [406].
2. The UF plant also has higher chemical costs (\$4.10 million/year) relative to the media filtration plant (\$2.88 million/year) (Table - 50 and Table - 49).
3. Table - 52 shows a lower expense (\$1.20 million/year) in replacing equipment than the media filtration plant (\$1.83 million/year), see Table - 51, even though UF membranes may be more costly or need to be replaced more frequently due to the fine pore size and susceptibility to clogging [271]. However, in recent years the life span of RO and UF membrane has extended up to 10 years [40] with proper maintenance while cartridge filters still have a relatively short life span requiring more frequent replacement [398].
4. Waste stream disposal costs are notably higher for the UF plant (\$14.9 million/year) compared to the media filtration plant (\$14.04 million/year). The UF process typically generates a more concentrated waste stream, which can increase disposal costs [292]
5. Labour costs are higher in the UF plant (\$1.77 million/year) than in the media filtration plant (\$1.59 million/year), suggesting that UF operations require more specialised skills or intensive labour; therefore, the number of staff was higher in UF (Table - 46).
6. Maintenance costs are significantly higher in scenario 2 (\$5.52 million/year) than in scenario 1 (\$5.39 million/year) due to the complexity and sensitivity of the membrane components.
7. Both plants have similar costs for environmental and performance monitoring, suggesting that this expense is not heavily influenced by the type of pretreatment used. Additionally, this parameter is determined by multiplying the cost rate by the plant's production capacity, which remains consistent in both scenarios.

8. Overall, the total OPEX for the UF plant (\$43.82 million/year) is higher than the media filtration plant (\$41.13 million/year), reflecting the cumulative effect of the higher costs associated with the UF process.

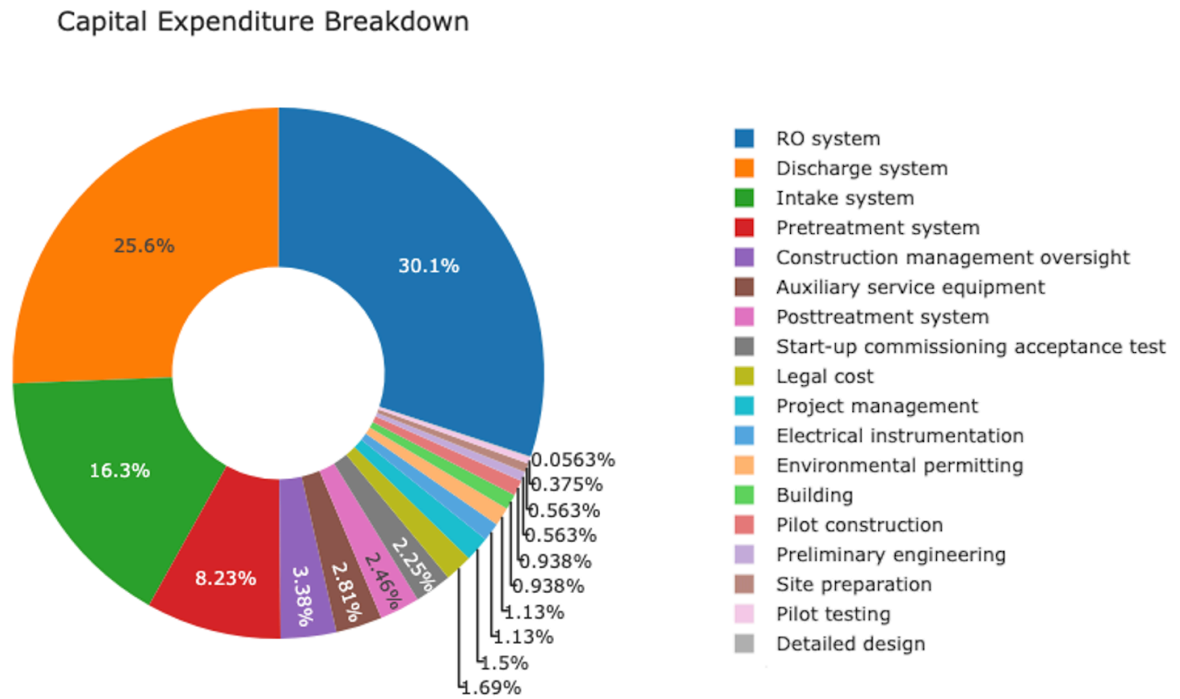


Figure 7-14: CAPEX breakdown for solution 1

Operational Expenditure Breakdown

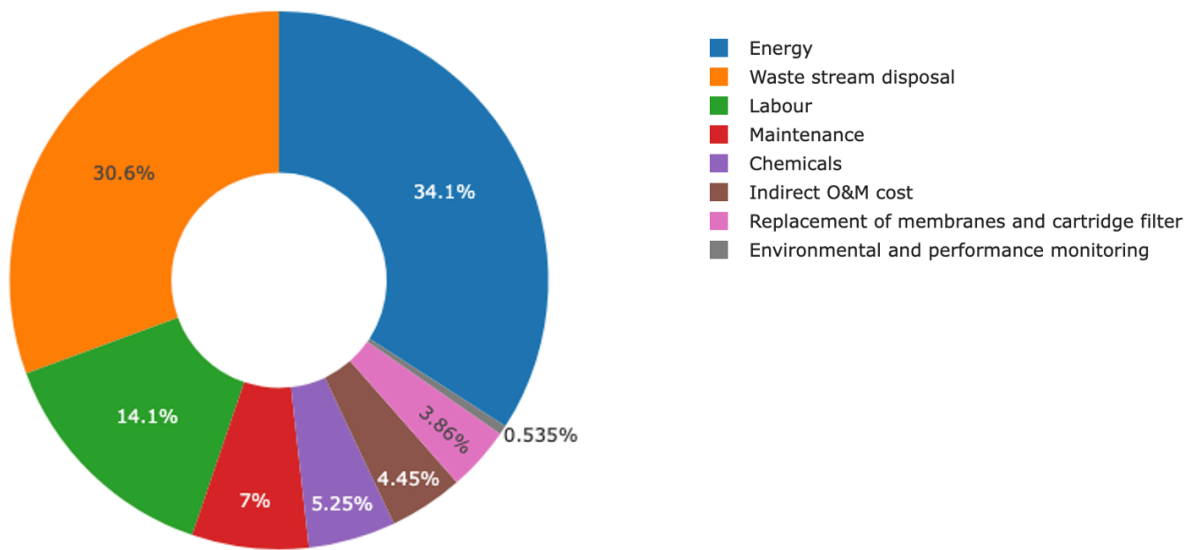


Figure 7-15: OPEX breakdown for solution 1.

Capital Expenditure Breakdown

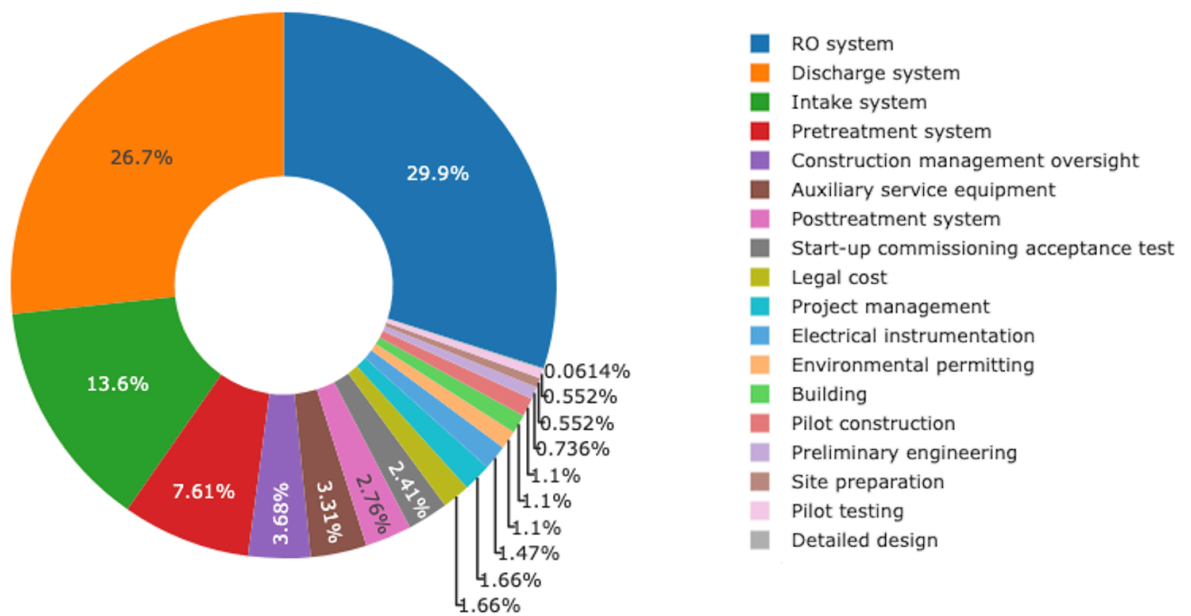


Figure 7-16: CAPEX breakdown for solution 2

Operational Expenditure Breakdown

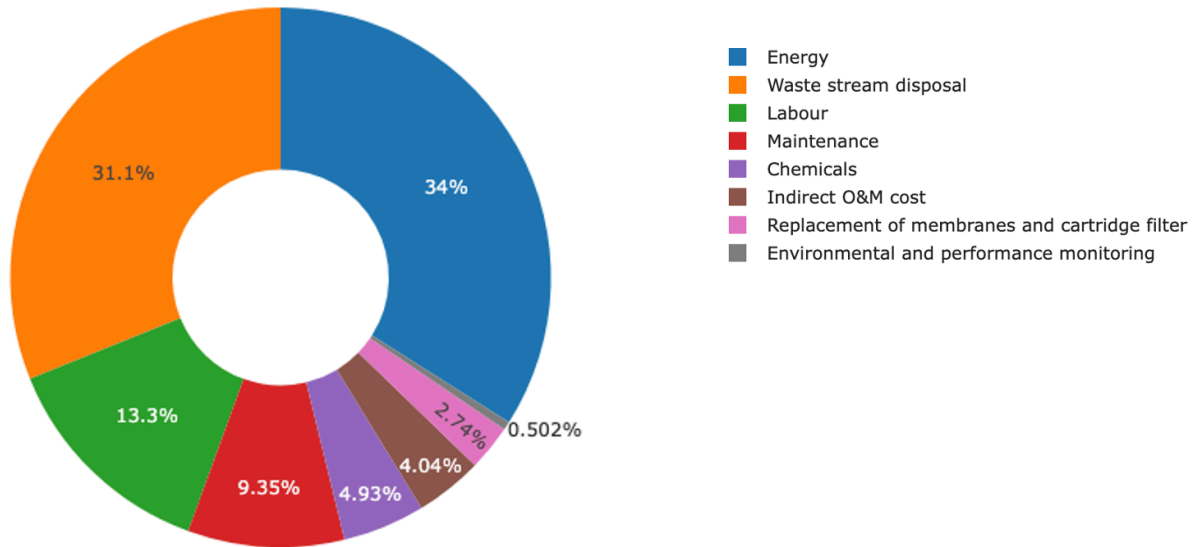


Figure 7–17: OPEX breakdown for solution 2

In conclusion, the UF system requires a slightly higher initial investment, both in direct and indirect CAPEX (\$328.3 million). The media filtration scenario is expensive by almost \$6.164 million. The comparison suggests that while UF pretreatment can offer higher water quality and possibly reduce downstream costs, it results in higher OPEX costs due to increased energy, chemical, and maintenance requirements. Conversely, media filtration has lower OPEX by almost \$2.69 million/year but may not provide the same level of water quality or might result in higher costs in other areas of the plant operation not reflected in the OPEX [407].

Figure 7–14 to Figure 7–17 reveal that intake and discharge systems, as well as waste stream management, play a substantial role in both CAPEX and OPEX. This finding contradicts the generally held opinion that the RO system and energy costs are the main contributing cost factors. This anomaly is mainly noticed in plants with large capacities. Contrary to the typical findings presented in the literature review, which estimate the costs of the discharge system by considering the volume of brine produced from the RO process, this study uses an additional method. By factoring in the additional volume produced by backwash activities, the expenses related to the discharge and intake systems in this study surpass those usually documented, leading to a higher overall cost.

When examining production costs, there is a slight difference between the two scenarios. The cost of producing desalinated water in the second scenario is \$1.36 per unit, whereas the first

scenario incurs a substantially lower production cost of \$1.28 per unit. This notable difference highlights the impact that the chosen pretreatment technology has on the operational economics of desalination which was also observed in this research [408].

7.2.3 Analysis and Evaluation for Case 3

In the third case, which features a smaller-capacity plant, the operating costs are inherently higher relative to larger plants, as supported by the referenced literature. This is consistent with the industry understanding that smaller plants often lack the economies of scale that contribute to cost efficiency [409]. A similar analytical approach to those used in the previous cases was applied to the smaller plant and Table 7-5 provided a summary report for design specification for case 3.

Table 7-5: Summary of SWRO design specifications for Case 3

Plant design Summary	Value	Unit
Product	5,000.00	m ³ /day
Recovery	47.00	%
Salinity	35,000.00	mg/L
Temperature	25.00	°C
Intake capacity	11,595.75	m ³ /day
Ro feed flow	10,638.00	m ³ /day
Brine flow rate	5,638.00	m ³ /day
Total discharge flow rate		m ³ /day
Brine salinity	65,976.00	mg/L
Permeate salinity	99.00	
Number of Intake pipes	1.00	
Eff DAF suspended solid	84.615	%
Removal of DAF suspended solid	10.629	kg/h
sludge produced from DAF	3	kg/h
Number of UF Element	189.00	
Number of Vessel	47.00	
Number of Train	1	
Number of pressure vessels	47.000	
Number of RO elements	342.000	
Number of trains	2.000	
Number of ERD	7.000	
Water permeability coefficient at design	1.431	L/m ² .bar.h
Salt permeability coefficient at design	0.075	L/m ² h
Applied feed pressure	54.000	bar

Plant design Summary	Value	Unit
Brine pressure	53.40	bar
Intake system SEC	0.032	kWh/m ³
Pretreatment system SEC	0.250	kWh/m ³
RO system SEC	2.340	kWh/m ³
Discharge SEC	0.010	kWh/m ³
Posttreatment SEC	0.100	kWh/m ³
Total SEC	2.732	kWh/m ³

A key finding for Case 3 is the slightly higher recovery rate in the desalination process, which consequently requires an increase in the feed pressure for the RO system. This is a direct consequence of the smaller volume throughput, which necessitates higher efficiency in the recovery of fresh water to make the process economically viable.

The recommended pretreatment system in this third case, which consists of DAF and UF, exhibits a high SEC, as detailed in Table - 64. High SEC is a characteristic concern for such technologies, especially in plants with smaller scales, where the energy costs per unit of produced water tend to be higher. In terms of CAPEX and OPEX, Table 7-6 summarises the main parameters for Case 3, derived from the detailed breakdown obtained from the LCCA tool. This information can be found in APPENDIX F.

Table 7-6: Summary of CAPEX and OPEX for Case 3

	OPEX cost (\$millions/year)	Cost (\$M/22 years)	Note
Discounting rate	5%		
Power	0.73	14.66	Cost rate = \$0.13
Chemicals	0.15	3.09	
Replacement of membranes and UF filter	0.04	0.75	Cost rate = \$400.0, \$1000.0
Waste stream disposal	1.17	23.46	Cost rate = \$0.49
Labour	0.62	12.33	No of staff = 10
Maintenance	0.00	0.04	
Environmental and performance monitoring	0.01	0.18	Cost rate = \$0.005
Indirect O&M cost	0.09	1.82	Cost rate = \$0.05
Total OPEX (\$M/20 years)	2.82	56.33	
Total CAPEX (\$)		18.49	

Interestingly, the discharge system's impact on CAPEX is minor due to the plant's utilisation of sewer discharge. While this might be seen as a cost-saving measure in terms of initial investment, it has led to disproportionately high OPEX, accounting for nearly 42% of the total. In most desalination operations, energy consumption is the dominant OPEX cost. However, in this small-scale case, the required integration with sewer discharge systems seems to have shifted the cost burden.

The unit product cost for Case 3 stands at \$2.06, marking it as the most expensive among the reviewed scenarios. Finding unit product cost data for desalination facilities with a capacity of 5000 m³/day was difficult to find in the literature. However, this value exceeds the world average unit product cost, which ranges between \$0.5 – 0.66/m³ [408] and the data documented in the literature review which reports a range of \$0.75 to \$2 per cubic metre [67]. Furthermore, a recent LCA of two SWRO desalination plants with differing configurations in Kuwait reported unit costs ranging from \$1.26 to \$1.46/m³ [408]. This highlights the challenge of operating smaller-scale desalination plants efficiently and raises questions about the long-term economic sustainability of such models without strategic measures to control and mitigate operational costs [410]. Additionally, the variance in unit production costs across the three distinct cases underscores the significant influence that system configurations, location and cost rate selection have on economic outcomes. Figure 7–18 and Figure 7–19 present the breakdown for CAPEX and OPEX for Case 3.

Capital Expenditure Breakdown

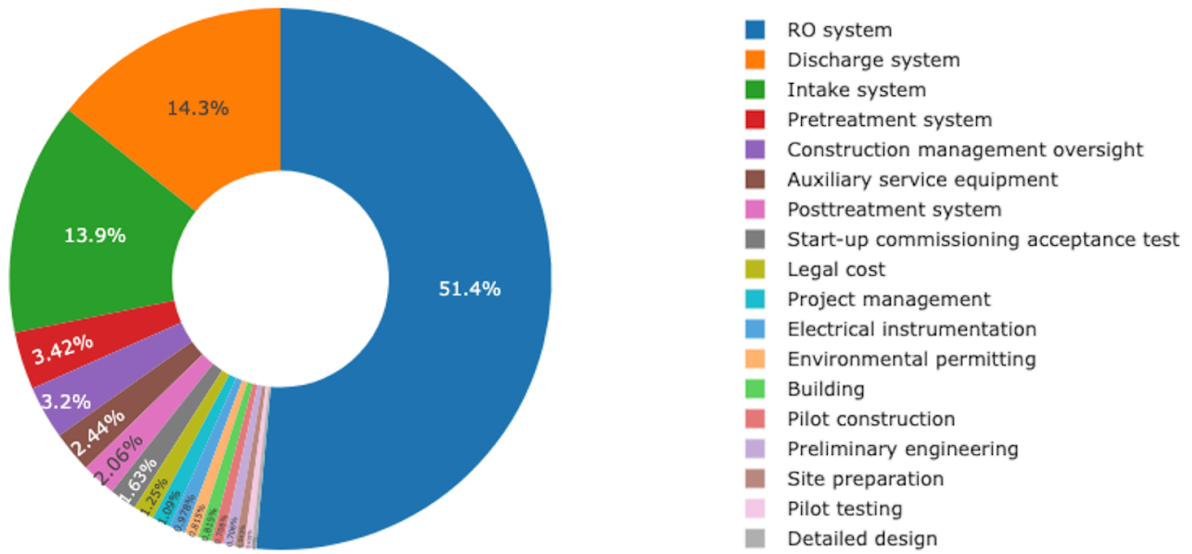


Figure 7–18: CAPEX breakdown for Case 3.

Operational Expenditure Breakdown

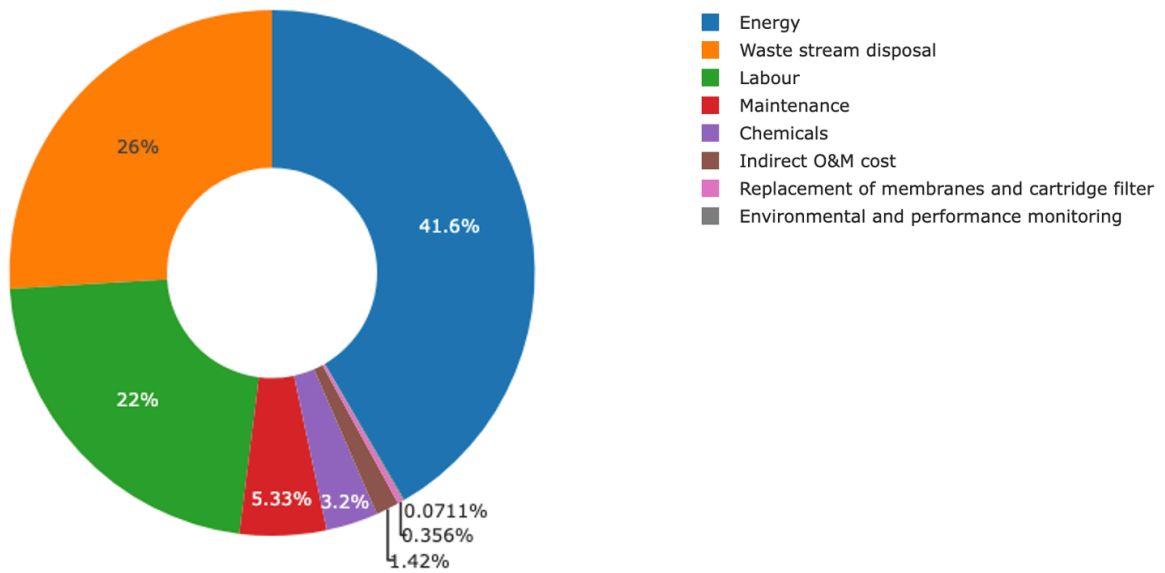


Figure 7–19: OPEX breakdown for Case 3

7.2.4 Benefit of SWRO Design and LCCA TOOL

The analysed cases highlight the crucial need of life cost analysis in evaluating and deciding the worth of various methods for SWRO desalination plants. An examination of this nature is essential for making well-informed decisions regarding the practicality and economic sustainability of different desalination processes.

Specifically, the Wave programme is limited to the design and analysis of equipment created by the DuPont firm [380], indicating that it does not provide a comprehensive solution for the entire design of an SWRO desalination plant. This constraint confines users to DuPont's selection of items, hence prohibiting them from integrating products from alternative manufacturers into their designs for reverse osmosis systems.

Conversely, the decision assistance tool created in this study provides users with increased adaptability. Users are given the option to either utilise predefined values from the ontology or integrate their own design data. This capability sets the tool apart from other options in the industry, such as WTCost and DEEP, which are exclusively LCCA tools and do not include design requirements. For example, reviewing the CAPEX obtained from current literature with the three scenarios described in this thesis, it became clear that these studies underestimate the capital expenses especially for small and large desalination capacity (Table 7-7). This difference highlights the constraints of regression cost estimation models or cost ranges reported in the literature, which may not comprehensively encompass all the factors that influence the outcome. Furthermore, the absence of clear access to the original data supporting these estimates adds complexity to the task of assessing their accuracy, raising doubts about the accuracy of these statistics for predicting cost. Hence, a SWRO design and LCCA tool that allows for individual factor customisation in accordance with each specific scenario and user is highly advantageous.

Table 7-7: Comparison between the literature and result obtained from the thesis

	Ref	5000 (m ³ /day)	25,000 (m ³ /day)	120,000 (m ³ /day)
CAPEX (\$million)	[39]	5.16 - 8.585	25.8 - 42.93	123.84 - 206.04
		2.64 - 4.62	13.2 - 23.1	63.36 - 110.88
	[365]	7.9 - 6.7	39.5 - 33.5	189.6- 160.8
	Thesis	18.49	27.59	322.13 and 328.3

An evident benefit of this developed model is its integration of current cost data and pump data, which not only accurately represents present market conditions but can also be easily modified to adapt to future changes. This characteristic provides a substantial advantage in comparison to other techniques examined in the literature study.

Moreover, the model's thoroughness enables a detailed assessment of every element involved in the desalination process, guaranteeing that no part is disregarded when calculating the overall cost during the lifespan. The model incorporates a flexible platform that can adjust to changes in technology design and cost considerations, such as fluctuations in energy prices, developments in membrane technology, or modifications in environmental legislation affecting waste disposal methods.

The research tool's adaptability allows users to perform comprehensive cost evaluations and customise design parameters according to their individual requirements, hence promoting a more personalised and potentially more streamlined design process. The high degree of customisation guarantees that the SWRO design and LCCA tool can adapt to various design circumstances, rendering it a valuable resource for engineers and decision-makers in the desalination business. For instance, the following review [411] demonstrated the existence of two desalination plants with almost comparable output capacities, although they differ in terms of CAPEX, OPEX and unit production cost. This demonstrates that various factors contribute to these differences, and it is imperative to utilise a technology that can accurately record them.

However, the developed model has some limitations in terms of designing some common technologies such as DAF, and would benefit from more accurate specific energy consumption values for the pretreatment system. When it comes to the cost, the developed dataset has cost for specific equipment and not all equipment is included. For instance, Case 1 features the choice of single media filtration for pretreatment, yet the cost dataset developed only has data for dual media filtration. Consequently, it was assumed that the costs for both filtration types would be comparable. However, this assumption may introduce a degree of inaccuracy. Additionally, the model is developed to design solely single-pass RO systems and does not accommodate second-pass RO systems. However, this is standard operation in SWRO desalination. As a result, it may not be appropriate for treating feedwater with lower or higher salinity levels.

7.3 Integration between OntoSWRO, SWRO Design and LCCA Tool

Integrating an ontology for SWRO with life cost analysis offers a potent tool to improve decision-making in the desalination business. The ontology functions as a systematic framework that contains organised information on SWRO, encompassing its constituents, operations, and factors. The integration of life cost analysis with a desalination plant's financial perspective yields a comprehensive decision support system that can yield substantial advantages.

Discussion Points for the Integration of Ontology and Life Cost Analysis:

1. **Enhanced Decision-Making:** The ontology facilitates a methodical comprehension of the SWRO processes, guaranteeing the inclusion of all relevant factors which clearly how captured the integration between the process and the parameters related about these sub-processes in the desalination plant which was very useful when the three cases were applied. The data highlighted in yellow in the preceding table were all sourced through a unified approach facilitated by the ontology. Furthermore, the SWRO design and LCCA tool is capable of computing parameters that can subsequently be assessed against the acceptable ranges established in the literature review, ranges that have also been integrated into the ontology. When combined with life cost analysis, it facilitates the process of making well-informed decisions by taking into account not only the technical feasibility but also the long-term financial consequences.
2. **Holistic Approach:** The ontology's structured knowledge base, coupled with the economic insights from life cost analysis, provides a holistic view. This combination ensures that decisions are not made in silos but consider the interplay between technical performance and cost-efficiency over the entire lifecycle of the plant.
3. **Predictive analysis** involves utilising a well-defined framework and established cost criteria to employ an integrated technology that can accurately simulate different situations and forecast potential results. By utilising this predictive capability, stakeholders are able to anticipate the long-term impact of their original design decisions, operational strategies, and maintenance schedules on the economic performance of the plant.
4. **Enhanced Communication:** the ontology facilitates effective communication by establishing a shared vocabulary among all participants engaged in the SWRO process.

When combined with life cost analysis, it guarantees that the financial team and the technical team are in agreement, promoting improved communication and mutual comprehension.

5. **Dynamic Optimisation:** As new data become available or conditions change, the ontology can be updated to reflect the most current knowledge, which can then be used to recalibrate the life cost analysis. This dynamic adaptability ensures that the SWRO design and LCCA tool remains relevant and accurate throughout the plant's operational life.
6. **Cost-Benefit Analysis:** The plant can do thorough cost-benefit assessments by evaluating the expenses linked to various configurations or operational modifications using the ontology as a framework. This can result in optimisations that decrease expenses without impacting the integrity or efficiency of the SWRO process.
7. **Knowledge Sharing and Transfer:** the ontology tool can be utilised for training or teaching purpose or shared with new plants. This promotes the exchange of knowledge and the sharing of best practices within the sector with more simplified language and can visualise the interconnection between the process and subprocess.

In conclusion, the symbiotic relationship between the SWRO ontology and life cost analysis can significantly enhance the capability to plan, execute, and manage desalination projects effectively. It embodies a comprehensive approach that considers the fine differences of SWRO systems and their financial aspects, thereby leading to more sustainable and economically viable desalination practices.

Chapter 8

Conclusion and Future Work

8.1 Conclusion

The objective of this research was to review innovations in reverse osmosis desalination and AI and ML, in an effort to integrate relevant learnings from both research disciplines to improve and optimise seawater desalination plants from a systems perspective. It was evident that although a variety of achievements had been made, there remain several, current challenges facing the implementation of AI and ML in the area of SWRO desalination. The review in Chapter 2 showed that RO has rapidly evolved into a well-developed and optimised desalination process, despite being commercialised only 50 years ago. Its relatively low specific energy and high reliability have made it the preferred method over thermal desalination techniques. This remarkable achievement is the result of significant improvements in the technology, including enhanced membrane characteristics and performance, high equipment efficiency, and the use of energy recovery devices. The technology has been developed to the extent that the thermodynamic limit of the lowest possible energy consumption is now almost within reach, albeit under specific, controlled operating conditions.

In addition to these advancements, a new configuration of the RO process, called batch reverse osmosis, has been developed. This process aims to recycle the brine until the desired recovery level is attained, gradually increasing the pressure to reduce energy usage. However, further research and real-world implementation are necessary to determine whether the technology can deliver the anticipated benefits over a continuous RO process and overcome specific challenges. This includes investigating optimal design configurations, addressing variations in water quality, and determining the appropriate duration of the flushing phase to achieve desired water quality and minimise scaling. Furthermore, a cost analysis would be valuable to quantify the potential savings of this approach.

It was found that AI and ML holds transformative potential across water industry sectors, offering insights in fouling prediction, water quality, efficiency, cost optimization, and performance issue resolution. A key challenge is the availability of accurate data with critical operating parameters over a representative duration. In current RO research, the focus is mainly on AI's applicability, particularly in membrane design. While engineering models provide information and facilitate numerous observations similar to AI, the integration of AI and membrane design shows particular promise by evaluating diverse designs and novel materials, reducing the need for trial-and-error experimentation.

AI and ML also demonstrate success in fault detection, algae detection, failure prediction, and maintenance scheduling. Challenges of applying AI and ML include limited data availability in the RO and energy fields, hindering comprehensive model training, especially considering the inherent dynamic water quality variations. Collaboration between researchers and desalination plants is crucial for model validation across diverse cases. Publicly inaccessible data on water technology and desalination poses a significant barrier to researching alternative AI methodologies and estimating computational resources for practical testing. Increased collaboration and data sharing are essential for advancing AI integration in water treatment technologies.

It was postulated that variation in site-specific and water quality conditions would influence the design, operation, and economic performance of SWRO desalination systems in different ways, and that each system should be evaluated under these conditions to assess their implementation and performance suitability. The development of a SWRO desalination plant is a complex and extensive design process that involves selecting the most suitable system configuration, given the environmental and economic conditions, to deliver both a sufficient and a sustainable supply of clean water. To address this complexity and to evaluate SWRO desalination design in terms of multiple factors such as water quality, geographical factors, geological factors, operation and design features and challenges, the research was carried out in two stages.

A data-driven approach using an ontology was undertaken to identify, evaluate, test and analyse the interrelationships among various processes and subprocesses within the SWRO desalination process. The objective of this approach was to produce a standard knowledge base within the SWRO desalination domain that could be reused for other cases within this domain. Using the developed approach, system analysis was carried out on a range of predetermined

scenarios to assess the utility and effectiveness methodology and the effect of parameter variation. The main findings from the preliminary study were that:

1. OntoSWRO is a detailed framework that encompasses the complex knowledge related to the SWRO desalination process, offering a thorough understanding of the entire system.
2. Through OntoSWRO, the interconnected nature of the SWRO process and its various subprocesses has been meticulously documented, revealing the constraints and advantages of each, as well as elucidating their mutual influences. Beyond merely cataloguing terminology, OntoSWRO possesses the capability to illustrate the interrelations among processes and, furthermore, to graphically represent the entire architectural layout of an SWRO desalination facility.
3. OntoSWRO has established a uniform vocabulary for SWRO, facilitating the organisation of data in an efficient manner that can be easily understood and processed by both humans and computational systems.

A preliminary LCCA study was conducted then to assess the design and operation parameters based on engineering first principles and empirical data. Following the preliminary LCCA study, it was postulated that the variation in design options obtained from the OntoSWRO should be evaluated in terms of economic costs over systems lifetime to understand the true cost of system ownership. Life cost analysis and LCCA approaches were determined as being the most appropriate economic assessment tool for system evaluation. The tool was then combined into a methodological framework and integrated into a SWRO design and LCCA tool designed to assess the performance and economic evaluation of SWRO desalination plants.

The SWRO design and LCCA tool provides a platform to assess the performance of a selection of SWRO desalination plants under a set of user-defined, site-specific conditions. Economic costs are presented also with the aim of providing a more holistic overview of system performance, but without aggregation of weighted indicators into a single result or score. This allows the user to identify any economic trade-offs that may exist. It provides a detailed breakdown of several categories of design parameters. It also outputs cost distributions associated with a given system in a given scenario, and facilitates comparisons of systems' CAPEX and OPEX. The SWRO design and LCCA tool captures the engineering principles of RO systems and other related processes, as well as providing a life cycle cost analysis for the three cases with different scenarios, however, the programme does have some limitations. The

CAPEX estimations provided in the toolkit are based on data from 2018 and different years which are prone to some level of uncertainty. Life cycle cost estimations provided by the SWRO design and LCCA tool would benefit from a more comprehensive, region-specific, CAPEX estimation methodology. Furthermore, the cost of replacement parts can only be assessed with an itemised bill of quantities, and details of a parts replacement regime. However, this approach involves a significant data collection exercise that may not produce a much higher level of accuracy to warrant such an undertaking.

8.2 Thesis Contribution

This thesis has made contribution to the seawater reverse osmosis desalination knowledge.

1. This thesis makes notable contributions by summarising recent advancements and current challenges in the field of RO systems. Additionally, it investigates into various applications of AI and ML across different aspects of water treatment and desalination, evaluating both the advantages and drawbacks of these tools. The comprehensive review sheds light on specific challenges identified across multiple research endeavours and explain how these challenges may hinder progress in this field.
2. The creation of the SWRO desalination plant ontology (OntoSWRO) represents a significant contribution to the field of desalination and water treatment. This ontology function as a systematic and comprehensive knowledge framework, capturing the interaction between SWRO processes and subprocess, design factors, features, limitations and operational issues. The formalisation of relationships and classifications within the area of SWRO desalination enables a more sophisticated understanding of the diverse factors associated with this process. This ontology serves as a basis for enhancing decision-making procedures. In addition, the utilisation of ontology contributes to the establishment of consistent terminology and concepts, hence promoting enhanced precision and logical consistency in communication among the desalination community.
3. The creation of the SWRO design and LCCA tool for SWRO desalination plant represents an important step forward in this field, as it combines many processes into a single, user-friendly interface. This tool not only includes the design elements of diverse desalination processes within a single platform, but also integrates a comprehensive LCCA component. The incorporation of this feature enables users to enhance the design and also evaluate the financial consequences throughout the whole

lifecycle of the project. The tool is notable in its user-friendliness, providing a seamless experience for users to modify values and input data effortlessly. The integrated OntoSWRO and LCCA model presented here offers enhanced accessibility and versatility, making it a valuable resource for professionals and researchers in the field of desalination who is looking for designing and economic evaluation.

8.3 Limitation

While conducting this research, a notable limitation emerged concerning the challenge of obtaining values for numerous parameters associated with the design of SWRO desalination processes and subprocesses. The aim was to create a comprehensive tool that not only relied on cost estimation but also incorporated design calculations. Developing a robust energy model based on engineering first principles posed a significant challenge due to the multitude of factors. The unavailability of these data, compounded by factors such as the scale of desalination plants and the proprietary nature of information held by private companies, hindered accessibility.

Additionally, the tool was tailored to design SWRO desalination facilities up to a specific scale of 400,000 m³/day. Limitations arose in addressing mega-scale desalination plants, as acquiring relevant cost analysis for this scale proved to be challenging.

Furthermore, the SWRO design and LCCA tool is designed with the specific adaptation of the RO design to match DOW equipment. While the tool allows users to easily modify values and input data, it is important to note that certain equations are specifically suitable for DOW equipment. If alternative membranes are employed, these equations may need to be adjusted accordingly.

.

8.4 Future Work

Potential areas for future research lie in enhancing the precision of the OntoSWRO and decision tool:

1. Enhance and expand the data contained in OntoSWRO by integrating knowledge acquired from real-world desalination plant cases and integrate further desalination technologies. The documentation of practical experiences and decision-making

processes in the construction and operation of complex structures holds significant value, as it is beyond the simple capture of theoretical insights from literature.

2. Establish a direct link between OntoSWRO and life cycle cost analysis SWRO design and LCCA tool to provide easy accessibility and enhance the comprehensive understanding of the economic implications associated with desalination plant operations and the integration and knowledge gained from OntoSWRO in one tool.
3. Adopt a more robust first principles power calculation for other process in SWRO desalination plant such as pretreatment and posttreatment, moving beyond reliance on empirical values. This approach ensures a more accurate assessment of energy efficiency.
4. Expand the design approach for desalination processes for other subprocesses such as DAF and backwash system. The design process for DAF is complicated, requiring consideration of multiple factors and graphs, such as Henry solubility, air bubble size, particle size, and functions relating air solubility changes with temperature and salinity.
5. Expand the dataset pertaining to the costs associated with SWRO desalination plants by incorporating real-world case studies as well as expanding the pump dataset. This augmentation aims to provide a more realistic and comprehensive perspective on the financial aspects of implementing and maintaining such facilities.
6. Integrate environmental assessments, offering a holistic evaluation of design selections. Additionally, refine the calculation of chemical treatment requirements by utilising actual water quality specifications, thereby moving away from rough estimations for a more precise evaluation.

Reference

- [1] S. Combs, “Texas Water Report: Going deeper for the solution,” 2012. Accessed: Oct. 01, 2020. [Online]. Available: <https://lrl.texas.gov/scanned/archive/2013/22698.pdf>
- [2] Population Action International, “Why population matters to water resources,” *Population Action International*, 2011.
- [3] M. Kummu *et al.*, “The world’s road to water scarcity: Shortage and stress in the 20th century and pathways towards sustainability,” *Scientific Reports*, vol. 6, no. 1, Dec. 2016.
- [4] M. M. Mekonnen and A. Y. Hoekstra, “Sustainability: Four billion people facing severe water scarcity,” *Science Advances*, vol. 2, no. 2, Feb. 2016.
- [5] O. Cann, “Top 10 global risks 2015,” World Economic Forum. Accessed: Sep. 01, 2020. [Online]. Available: <https://www.weforum.org/agenda/2015/01/top-10-global-risks-2015/>
- [6] World Economic Forum, *Global Risk Report 2024*. 2024.
- [7] United Nations Development Programme, “Human Development report 2006 beyond scarcity: power, poverty and the global water crisis,” 2006.
- [8] M. Abu-Zeid and I. A. Shiklomanov, “Water resources as a challenge of the twenty-first century world,” 2004.
- [9] European Environment Agency, “Climate change impacts in Europe’s regions Related,” 2018.
- [10] Food and Agriculture Organization of the United Nations, “Drought Fact,” Food and Agriculture Organization of the United Nations. Accessed: Jul. 23, 2020. [Online]. Available: <http://www.fao.org/3/aq191e/aq191e.pdf>
- [11] T. Smedley, “Is the world running out of fresh water? ,” BBC- Future Now. Accessed: Sep. 15, 2020. [Online]. Available: <https://www.bbc.com/future/article/20170412-is-the-world-running-out-of-fresh-water>
- [12] R. Lindsey and L. Dahlman, “Climate Change: Global Temperature,” Climate.gov science & information for a climate-smart nation. Accessed: Sep. 15, 2020. [Online].

- Available: <https://www.climate.gov/news-features/understanding-climate/climate-change-global-temperature>
- [13] NOAA National Centers for Environmental, “State of the Climate : Wildfires for annual 2019.” Accessed: Sep. 15, 2020. [Online]. Available: <https://www.ncdc.noaa.gov/sotc/fire/201913>
- [14] NASA, “Effects | Facts – Climate Change: Vital Signs of the Planet.” Accessed: Sep. 15, 2020. [Online]. Available: <https://climate.nasa.gov/effects/>
- [15] Max Roser, “Future population growth,” OurWorldInData.org. Accessed: Sep. 02, 2020. [Online]. Available: <https://ourworldindata.org/future-population-growth#citation>
- [16] K. van Leeuwen, J. Hofman, P. Driessen, and J. Frijns, “The Challenges of Water Management and Governance in Cities,” *Water*, vol. 11, no. 6, p. 1180, Jun. 2019.
- [17] H. Ritchie, “Water use and stress,” OurWorldInData.org. Accessed: Sep. 10, 2020. [Online]. Available: <https://ourworldindata.org/water-use-stress#citation>
- [18] CDP Global Water, “A Wave of Change (The Role of Companies in Building a Water-Secure World),” 2020.
- [19] D. J. Rodriguez and M. Madrigal, “4 Ways Water Shortages Are Harming Energy Production.” Accessed: Nov. 03, 2021. [Online]. Available: <https://blogs.worldbank.org/water/4-ways-water-shortages-are-harming-energy-production>
- [20] Y. Lian, “A Measurement of Population’s Driving effects on Water Resources Consumption in the Progress of Urbanization:A Case Study of Taihu basin,” 2014.
- [21] X. Weimin and R. Hong, “An empirical study on the impact of urbanization on housing sale in China,” *Proceedings of CRIOCM 2008 International Research Symposium on Advancement of Construction Management and Real Estate*, pp. 419–424, 2008.
- [22] S. J. McGrane, “Impacts of urbanisation on hydrological and water quality dynamics, and urban water management: a review,” *Hydrological Sciences Journal*, vol. 61, no. 13, pp. 2295–2311, Oct. 2016.

- [23] T. C. Cerqueira, R. L. Mendonça, R. L. Gomes, R. M. de Jesus, and D. M. L. da Silva, “Effects of urbanization on water quality in a watershed in northeastern Brazil,” *Environmental Monitoring and Assessment*, vol. 192, no. 1, pp. 1–17, Dec. 2019.
- [24] L. A. Freeman, D. R. Corbett, A. M. Fitzgerald, D. A. Lemley, A. Quigg, and C. N. Steppe, “Impacts of Urbanization and Development on Estuarine Ecosystems and Water Quality,” *Estuaries and Coasts*, vol. 42, no. 7, pp. 1821–1838, 2019.
- [25] European Environment Agency, “The European environment-state and outlook 2020. Knowledge for transition to a sustainable Europe,” Accessed: Sep. 10, 2020. [Online]. Available: <https://www.eea.europa.eu/soer/2020>
- [26] “Use of freshwater resources in Europe,” European Environment Agency. Accessed: Sep. 10, 2020. [Online]. Available: <https://www.eea.europa.eu/data-and-maps/indicators/use-of-freshwater-resources-3/assessment-4>
- [27] A. Makarigakis and B. Jimenez-Cisneros, “UNESCO’s contribution to face global water challenges,” *Water*, vol. 11, no. 2, p. 388, 2019.
- [28] N. Voutchkov, “Energy use for membrane seawater desalination – current status and trends,” *Desalination*, vol. 431, no. November, pp. 2–14, 2018.
- [29] WHO, “Total dissolved solids in Drinking-water Background document for development of WHO Guidelines for Drinking-water Quality,” 2003.
- [30] N. Voutchkov, *Desalination Engineering Planning And Design*. McGraw-Hill, 2013.
- [31] P. Fahmida and A. Sultana, “Desalination Technologies for Developing Countries : A Review,” *Journal of Scientific Research*, vol. 10, no. 1, pp. 77–97, 2018.
- [32] E. Jones, M. Qadir, M. T. H. Van Vliet, V. Smakhtin, and S. Kang, “The state of desalination and brine production: A global outlook,” *Science of The Total Environment*, vol. 657, pp. 1343–1356, 2019.
- [33] International Desalination Association, “Dynamic growth for desalination and water reuse in 2019,” 2019.
- [34] D. Curto, V. Franzitta, and A. Guercio, “A review of the water desalination technologies,” *Applied Sciences*, vol. 11, no. 2, pp. 1–36, 2021.

- [35] Y. C. Woo, S. H. Kim, H. K. Shon, and L. D. Tijing, "Introduction: Membrane Desalination Today, Past, and Future," in *Current Trends and Future Developments on (Bio-) Membranes*, Elsevier, 2019, pp. xxv-xlvi.
- [36] J. Kucera, *Desalination water from water*, 2nd ed. Scrivener Publishing LLC, John Wiley & Sons, 2019.
- [37] J. Eke, A. Yusuf, A. Giwa, and A. Sodiq, "The global status of desalination: An assessment of current desalination technologies, plants and capacity," *Desalination*, vol. 495, p. 114633, 2020.
- [38] A. Saavedra, H. Valdés, A. Mahn, and O. Acosta, "Comparative analysis of conventional and emerging technologies for seawater desalination: Northern Chile as a case study," *Membranes*, vol. 11, no. 3, p.180, 2021.
- [39] H. Mashhadi Meighani, A. Dehghani, F. Rekabdar, M. Hemmati, and I. Goodarznia, "Artificial intelligence vs. Classical approaches: A new look at the prediction of flux decline in wastewater treatment," *Desalination Water Treatment*, vol. 51, no. 40–42, pp. 7476–7489, 2013.
- [40] M. Badruzzaman, N. Voutchkov, L. Weinrich, and J. G. Jacangelo, "Selection of pretreatment technologies for seawater reverse osmosis plants: A review," *Desalination*, vol. 449, pp. 78–91, 2019.
- [41] X. Liu, S. Shanbhag, T. V. Bartholomew, J. F. Whitacre, and M. S. Mauter, "Cost Comparison of Capacitive Deionization and Reverse Osmosis for Brackish Water Desalination," *ACS ES&T Engineering*, vol. 1, no. 2, pp. 261–273, Feb. 2020.
- [42] A. Al-Karaghoul and L. L. Kazmerski, "Energy consumption and water production cost of conventional and renewable-energy-powered desalination processes," *Renewable and Sustainable Energy Reviews*, vol. 24, pp. 343–356, Aug. 2013.
- [43] R. Saidur, E. T. Elcevvadi, S. Mekhilef, A. Safari, and H. A. Mohammed, "An overview of different distillation methods for small scale applications," *Renewable and Sustainable Energy Reviews*, vol. 15, no. 9, pp. 4756–4764, 2011.
- [44] desalination, "Dubai prepares to add desalination capacity at Jebel Ali power station | desalination," <https://www.desalination.biz/>. Accessed: Aug. 22, 2021. [Online]. Available: <https://www.desalination.biz/desalination/dubai-prepares-to-add-desalination-capacity-at-jebel-ali-power-station/>

- [45] C. Fritzmann, J. Löwenberg, T. Wintgens, and T. Melin, “State of the art of reverse osmosis desalination,” *Desalination*, vol. 216, no. 1–3, pp. 1–76, 2007.
- [46] J. Kucera, *Reverse osmosis: design, processes, and applications for engineers*. Canada: John Wiley & Sons, 2010.
- [47] H. N. Lazarides and E. Katsanidis, “MEMBRANE TECHNIQUES | Principles of Reverse Osmosis,” *Encyclopedia of Food Sciences and Nutrition*, pp. 3827–3833, 2003.
- [48] J. Kim, K. Park, D. R. Yang, and S. Hong, “A comprehensive review of energy consumption of seawater reverse osmosis desalination plants,” *Applied Energy*, vol. 254, p. 113652, Nov. 2019.
- [49] World Bank, “The Role of Desalination in an Increasingly Water-Scarce World,” Washington, DC., 2019.
- [50] J. Glater, “The early history of reverse osmosis membrane development,” *Desalination*, vol. 117, no. 1–3, pp. 297–309, Sep. 1998.
- [51] J. Kucera, *Reverse Osmosis Industrial Processes and Applications*. Scrivener Publishing LLC, John Wiley & Sons, 2015.
- [52] S. Burn and S. Gray, *Efficient Desalination by Reverse Osmosis: A guide to RO practice*. IWA Publishing, 2015.
- [53] J. Swaminathan, E. W. Tow, R. L. Stover, and J. H. Lienhard, “Practical aspects of batch RO design for energy-efficient seawater desalination,” *Desalination*, vol. 470, p. 114097, Nov. 2019.
- [54] L. Wang, T. Cao, J. E. Dykstra, S. Porada, P. M. Biesheuvel, and M. Elimelech, “Salt and Water Transport in Reverse Osmosis Membranes: Beyond the Solution-Diffusion Model,” *Environmental Science & Technology*, vol. 55, no. 24, pp. 16665–16675, 2021.
- [55] C. Wang, M. J. Park, D. H. Seo, E. Drioli, H. Matsuyama, and H. Shon, “Recent advances in nanomaterial-incorporated nanocomposite membranes for organic solvent nanofiltration,” *Separation and purification technolog*, vol. 268, p. 118657, 2021.
- [56] S. Xiao, X. Huo, Y. Tong, C. Cheng, S. Yu, and X. Tan, “Improvement of thin-film nanocomposite (TFN) membrane performance by CAU-1 with low charge and small size,” *Separation and purification technolog*, vol. 274, pp. 118467–118467, 2021.

- [57] I. Wan Azelee *et al.*, “Enhanced desalination of polyamide thin film nanocomposite incorporated with acid treated multiwalled carbon nanotube-titania nanotube hybrid,” *Desalination*, vol. 409, pp. 163–170, May 2017.
- [58] A. Zirehpour, A. Rahimpour, and M. Ulbricht, “Nano-sized metal organic framework to improve the structural properties and desalination performance of thin film composite forward osmosis membrane,” *Journal of Membrane Science*, vol. 531, pp. 59–67, Jun. 2017.
- [59] H. Dong, L. Zhao, L. Zhang, H. Chen, C. Gao, and W. S. Winston Ho, “High-flux reverse osmosis membranes incorporated with NaY zeolite nanoparticles for brackish water desalination,” *Journal of Membrane Science*, vol. 476, pp. 373–383, Feb. 2015.
- [60] A. Giwa, N. Akther, V. Dufour, and S. W. Hasan, “A critical review on recent polymeric and nano-enhanced membranes for reverse osmosis,” *RSC Advances*, vol. 6, no. 10, pp. 8134–8163, Jan. 19, 2016.
- [61] Y. J. Lim, K. Goh, M. Kurihara, and R. Wang, “Seawater desalination by reverse osmosis: Current development and future challenges in membrane fabrication – A review,” *Journal of Membrane Science*, vol. 629, p. 119292, Jul. 2021.
- [62] A. Figoli, J. Hoinkis, and J. Bundschuh, *Membrane technologies for water treatment: Removal of toxic trace elements with emphasis on arsenic, fluoride and uranium*. CRC Press, 2016.
- [63] S. Senthilmurugan and S. K. Gupta, “Separation of inorganic and organic compounds by using a radial flow hollow-fiber reverse osmosis module,” *Desalination*, vol. 196, no. 1–3, pp. 221–236, Sep. 2006.
- [64] M. Qasim, M. Badrelzaman, N. N. Darwish, N. A. Darwish, and N. Hilal, “Reverse osmosis desalination: A state-of-the-art review,” *Desalination*, vol. 459, pp. 59–104, Jun. 2019.
- [65] Singh Rajindar, *Hybrid Membrane Systems for Water Purification: Technology, Systems Design and Operation*, 1st ed. Amsterdam: Elsevier, 2006.
- [66] Y. Okamoto and J. H. Lienhard, “How RO membrane permeability and other performance factors affect process cost and energy use: A review,” *Desalination*, vol. 470, p. 114064, Nov. 2019.

- [67] I. C. Karagiannis and P. G. Soldatos, “Water desalination cost literature: review and assessment,” *Desalination*, vol. 223, no. 1–3, pp. 448–456, 2008.
- [68] A. Shrivastava, S. Rosenberg, and M. Peery, “Energy efficiency breakdown of reverse osmosis and its implications on future innovation roadmap for desalination,” *Desalination*, vol. 368, pp. 181–192, Aug. 2015.
- [69] M. Elimelech and W. A. Phillip, “The future of seawater desalination: Energy, technology, and the environment,” *Science*, vol. 333, no. 6043, pp. 712–717, 2011.
- [70] M. Li, “Reducing specific energy consumption in Reverse Osmosis (RO) water desalination: An analysis from first principles,” *Desalination*, vol. 276, no. 1–3, pp. 128–135, Aug. 2011.
- [71] R. K. McGovern and J. H. Lienhard V, “On the potential of forward osmosis to energetically outperform reverse osmosis desalination,” *Journal of Membrane Science*, vol. 469, pp. 245–250, Nov. 01, 2014.
- [72] M. W. Shahzad, M. Burhan, L. Ang, and K. C. Ng, “Energy-water-environment nexus underpinning future desalination sustainability,” *Desalination*, vol. 413, pp. 52–64, Jul. 2017.
- [73] S. Li, K. Duran, S. Delagah, J. Mouawad, X. Jia, and M. Sharbatmaleki, “Energy efficiency of staged reverse osmosis (RO) and closed-circuit reverse osmosis (CCRO) desalination: A model-based comparison,” *Water Supply*, vol. 20, no. 8, pp. 3096–3106, 2020.
- [74] B. Huang, K. Pu, P. Wu, D. Wu, and J. Leng, “Design, selection and application of energy recovery device in seawater desalination: a review,” *Energies*, vol. 13, no. 6, p. 4150, 2020.
- [75] V. G. Gude, *Renewable Energy Powered Desalination Handbook: Application and Thermodynamics*. Elsevier Inc., 2018.
- [76] A. M. Farooque *et al.*, “Comparative study of various energy recovery devices used in SWRO process,” *Saline Water Desalination Research Institute, Saline Water Conversion Corporation (SWCC)*, pp. 1–44, 2004.
- [77] M. J. Guirguis, “Energy Recovery Devices in Seawater Reverse Osmosis Desalination Plants with Emphasis on Efficiency and Economical Analysis of Isobaric Versus Centrifugal Devices,” 2011.

- [78] D. Michas, “Design of an Energy Recovery Concept for a Small-scale Renewable-driven Reverse Osmosis Desalination System,” 2013.
- [79] C. R. Bartels and K. Andes, “Consideration of energy savings in SWRO,” *Desalination Water Treatment*, vol. 51, no. 4–6, pp. 717–725, 2013.
- [80] Energy Recovery Inc, “PX Pressure Exchanger - Energy Recovery.” Accessed: Apr. 07, 2021. [Online]. Available: <https://energyrecovery.com/water/px-pressure-exchanger/>
- [81] R. Stover, “Isobaric Energy Recovery Devices - Past , Present and Future,” no. December, 2016.
- [82] E. Kadaj and R. Bosleman, “Energy Recovery Devices in Membrane Desalination Processes,” in *Renewable Energy Powered Desalination Handbook: Application and Thermodynamics*, Elsevier Inc., 2018, pp. 415–444.
- [83] J. Kim, K. Park, D. R. Yang, and S. Hong, “A comprehensive review of energy consumption of seawater reverse osmosis desalination plants,” *Applied Energy*, vol. 254, p. 113652, 2019.
- [84] R. Stover, M. Angel Sanz, and R. L. Stover, “Energy efficiency in Perth’s desalination plant Low Energy Consumption in the Perth Seawater Desalination Plant,” 2007.
- [85] C. Wang *et al.*, “Comparison of two types of energy recovery devices: Pressure exchanger and turbine in an island desalination project case,” *Desalination*, vol. 533, Jul. 2022.
- [86] N. M. Eshoul, B. Agnew, M. A. Al-Weshahi, and M. S. Atab, “Exergy Analysis of a Two-Pass Reverse Osmosis (RO) Desalination Unit with and without an Energy Recovery Turbine (ERT) and Pressure Exchanger (PX),” *Energies*, vol. 8, no. 7, pp. 6910–6925, Jul. 2015.
- [87] A. Hermony, I. Sutzkover-Gutman, Y. Talmi, and O. Fine, “Palmachim Seawater desalination plant—seven years of expansions with uninterrupted operation together with process improvements,” *Desalination Water Treatment*, vol. 55, no. 9, pp. 2526–2535, Aug. 2015.
- [88] A. Hermony and J. M. Pinto, “New concept of upgrade energy recovery systems within an operating desalination plant,” in *EuroMed 2010 - Desalination for Clean Water and Energy Cooperation among Mediterranean Countries*, Tel Aviv, Israel, 2010.

- [89] C. Camero and R. Bosleman, “5 Top Reasons Carlsbad Swro Plant Chose Pressure Exchanger Technology,” in *American Water Works Association*, 2014.
- [90] M. H. Vyas, P. Mili, A. T. Sci, and S. D. Patil, “A Review on the Mixing Behavior of Pressure Exchanger in SWRO System,” *International Journal for Scientific Research & Development*, vol. 5, no. 09, pp. 249–250, 2017.
- [91] M. H. Vyas, P. Hitesh, R. R. Sci, and S. D. Patil, “Performance evaluation of mixing behavior of two different TDS liquids in pressure exchanger using CFD analysis,” *International Research Journal of Engineering and Technology*, vol. 05, no. 02, pp. 735–739, 2018.
- [92] F. Grondhuis, “Examining Isobaric Energy Recovery Systems at SWRO Plants,” Water technology solutions for industrial water management. Accessed: Aug. 07, 2022. [Online]. Available: <https://www.watertechonline.com/wastewater/article/16211602/examining-isobaric-energy-recovery-systems-at-swro-plants>
- [93] A. Valbjørn, “ERD for small SWRO plants,” *Desalination*, vol. 248, no. 1–3, pp. 636–641, Nov. 2009.
- [94] S. Arenas Urrea, F. Díaz Reyes, B. Peñate Suárez, and J. A. de la Fuente Bencomo, “Technical review, evaluation and efficiency of energy recovery devices installed in the Canary Islands desalination plants,” *Desalination*, vol. 450, pp. 54–63, Jan. 2019.
- [95] J. Song, T. Li, L. Wright-Contreras, and A. W. K. Law, “A review of the current status of small-scale seawater reverse osmosis desalination,” *Water International*, vol. 42, no. 5, pp. 618–631, Jul. 2017,
- [96] “Compact high energy system for RO plant,” *World Pumps*, vol. 2013, no. 9, pp. 27–28, 2013.
- [97] Danfoss, “Sea Water Pump with Energy Recovery.” Accessed: Apr. 28, 2022. [Online]. Available: <https://www.danfoss.com/en/products/hpp/energy-recovery-devices/energy-recovery-device-for-small-to-medium-swro-applications/>.
- [98] A. M. Bilton and S. Dubowsky, “A computer architecture for the automatic design of modular systems with application to photovoltaic reverse osmosis,” *Journal of Mechanical Design, Transactions of the ASME*, vol. 136, no. 10, Oct. 2014,

- [99] B. Contreras, “An energy recovery device for small-scale seawater reverse osmosis desalination,” 2009, Ph.D. thesis, Loughborough Univ, UK, 2009.
- [100] D. M. Warsinger, E. W. Tow, L. A. Maswadeh, G. B. Connors, J. Swaminathan, and J. H. Lienhard V, “Inorganic fouling mitigation by salinity cycling in batch reverse osmosis,” *Water Research*, vol. 137, pp. 384–394, 2018.
- [101] S. Jiang and N. Voutchkov, “Investigation of Desalination Membrane Biofouling Final Project Report and User Guidance,” *WateReuse Research Foundation*, 2010.
- [102] S. R. Pandey, V. Jegatheesan, K. Baskaran, and L. Shu, “Fouling in reverse osmosis (RO) membrane in water recovery from secondary effluent: a review,” *Reviews in Environmental Science and Bio/Technology*, vol. 11, no. 2, pp. 125–145, Feb. 2012.
- [103] Y. Chun, K. Jeong, and K. H. Cho, “Influences of combined organic fouling and inorganic scaling on flux and fouling behaviors in forward osmosis,” *Membranes*, vol. 10, no. 6, pp. 1–10, 2020.
- [104] Lenntech, “Foulants and Cleaning Procedures for composite polyamide RO Membrane Elements (ESPA, ESNA, CPA, LFC, NANO and SWC),” 2011.
- [105] C. Piyadasa *et al.*, “The application of electromagnetic fields to the control of the scaling and biofouling of reverse osmosis membranes - A review,” *Desalination*, vol. 418, pp. 19–34, Sep. 15, 2017.
- [106] A. Antony, J. H. Low, S. Gray, A. E. Childress, P. Le-Clech, and G. Leslie, “Scale formation and control in high pressure membrane water treatment systems: A review,” *Journal of Membrane Science*, vol. 383, no. 1, pp. 1–16, 2011.
- [107] N. Candoni, R. Grossier, M. Lagaize, and S. Veessler, “Advances in the Use of Microfluidics to Study Crystallization Fundamentals,” *Annual Review of Chemical and Biomolecular Engineering*, vol. 10, no. 1, pp. 59–83, Jun. 2019.
- [108] S. Shirazi, C. J. Lin, and D. Chen, “Inorganic fouling of pressure-driven membrane processes - A critical review,” *Desalination*, vol. 250, no. 1, pp. 236–248, Jan. 2010.
- [109] C. H. Koo, A. W. Mohammad, and F. Suja’, “Effect of cross-flow velocity on membrane filtration performance in relation to membrane properties,” *Desalination and Water Treatment*, vol. 55, no. 3, pp. 678–692, Jul. 2014.

- [110] H. Gu, M. H. Plumlee, M. Boyd, M. Hwang, and J. C. Lozier, “Operational optimization of closed-circuit reverse osmosis (CCRO) pilot to recover concentrate at an advanced water purification facility for potable reuse,” *Desalination*, vol. 518, p. 115300, Dec. 2021.
- [111] M. Li, Y. Heng, and J. Luo, “Batch reverse osmosis: a new research direction in water desalination,” *Science Bulletin*, vol. 65, no. 20, pp. 1705–1708, Oct. 30, 2020.
- [112] D. M. Warsinger, E. W. Tow, K. G. Nayar, L. A. Maswadeh, and J. H. Lienhard V, “Energy efficiency of batch and semi-batch (CCRO) reverse osmosis desalination,” *Water Research*, vol. 106, pp. 272–282, 2016.
- [113] S. Mirza, “Reduction of energy consumption in process plants using nanofiltration and reverse osmosis,” *Desalination*, vol. 224, no. 1–3, pp. 132–142, Apr. 2008.
- [114] E. Hosseini-pour, K. Park, L. Burlace, T. Naughton, and P. A. Davies, “A free-piston batch reverse osmosis (RO) system for brackish water desalination: Experimental study and model validation,” *Desalination*, vol. 527, p. 115524, Apr. 2022.
- [115] R. L. Stover and N. Efraty, “Low-Energy Consumption With Closed-Circuit Desalination,” *IDA Journal of Desalination and Water Reuse*, vol. 4, no. 3, pp. 12–19, 2012.
- [116] A. Efraty, “CCD series no-13: illustrating low-energy SWRO-CCD of 60% recovery and BWRO-CCD of 92% recovery with single element modules without energy recovery means—a theoretical extreme case study,” *Desalination Water Treatment*, vol. 57, no. 20, pp. 9148–9165, Apr. 2016.
- [117] D. M. Warsinger, J. H. Lienhard, E. Tow, and R. K. McGovern, “Batch Pressure - Driven Membrane Separation With Closed - Flow Loop and Reservoir,” US, Patent US10166510B2, 2019.
- [118] V. Sonera, J. Septon, and A. Efraty, “CCD series no-21: illustration of high recovery (93.8%) of a silica containing (57 ppm) source by a powerful technology of volume reduction prospects,” *Desalination Water Treatment*, vol. 57, no. 43, pp. 20228–20236, Sep. 2016.
- [119] Z. Gal, J. Septon, A. Efraty, and A. M. Lee, “CCD series no-20: high-flux low-energy upgrade of municipal water supplies with 96% recovery for boiler-feed and related applications,” *Desalination Water Treatment*, vol. 57, no. 43, pp. 20219–20227, 2016.

- [120] M. Uchymiak, E. Lyster, J. Glater, and Y. Cohen, “Kinetics of gypsum crystal growth on a reverse osmosis membrane,” *Journal of Membrane Science*, vol. 314, no. 1–2, pp. 163–172, Apr. 2008.
- [121] W. Y. Shih, A. Rahardianto, R. W. Lee, and Y. Cohen, “Morphometric characterization of calcium sulfate dihydrate (gypsum) scale on reverse osmosis membranes,” *Journal of Membrane Science*, vol. 252, no. 1–2, pp. 253–263, Apr. 2005.
- [122] T. Lee, J. Y. Choi, and Y. Cohen, “Gypsum scaling propensity in semi-batch RO (SBRO) and steady-state RO with partial recycle (SSRO-PR),” *Journal of Membrane Science*, vol. 588, p. 117106, 2019.
- [123] DOW, “FILMTEC Membranes - Steps to Design a Reverse Osmosis System.” Accessed: Feb. 20, 2019. [Online]. Available: https://water.custhelp.com/app/answers/detail/a_id/2209
- [124] A. Efraty, “CCD Series No-15: simple design batch SWRO-CCD units of high recovery and low energy without ERD for wide range flux operation of high cost-effectiveness,” *Desalination Water Treatment*, vol. 57, no. 20, pp. 9166–9179, 2016.
- [125] A. Efraty, R. N. Barak, and Z. Gal, “Closed circuit desalination series no-2: New affordable technology for sea water desalination of low energy and high flux using short modules without need of energy recovery,” *Desalination Water Treatment*, vol. 42, no. 1–3, pp. 189–196, 2012.
- [126] R. Stover, “CCD starts a new generation for RO,” *Desalination & Water Reuse*, 2011.
- [127] M. Barello, D. Manca, R. Patel, and I. M. Mujtaba, “Operation and modeling of RO desalination process in batch mode,” *Computers & Chemical Engineering*, vol. 83, pp. 139–156, Dec. 2015.
- [128] T. Y. Qiu and P. A. Davies, “Concentration polarization model of spiral-wound membrane modules with application to batch-mode RO desalination of brackish water,” *Desalination*, vol. 368, pp. 36–47, Jul. 2015.
- [129] S. Sourirajan, *Reverse Osmosis*. London: Logos Press, 1970.
- [130] J. R. Werber, A. Deshmukh, and M. Elimelech, “Can batch or semi-batch processes save energy in reverse-osmosis desalination?,” *Desalination*, vol. 402, pp. 109–122, Jan. 2016.

- [131] T. Y. Qiu and P. A. Davies, “Longitudinal dispersion in spiral wound RO modules and its effect on the performance of batch mode RO operations,” *Desalination*, vol. 288, pp. 1–7, Mar. 2012.
- [132] Q. J. Wei, C. I. Tucker, P. J. Wu, A. M. Trueworthy, E. W. Tow, and J. H. Lienhard, “Impact of salt retention on true batch reverse osmosis energy consumption: Experiments and model validation,” *Desalination*, vol. 479, Apr. 2020.
- [133] M. Li, “Effects of finite flux and flushing efficacy on specific energy consumption in semi-batch and batch reverse osmosis processes,” *Desalination*, vol. 496, p. 114646, 2020.
- [134] L. F. Greenlee, D. F. Lawler, B. D. Freeman, B. Marrot, and P. Moulin, “Reverse osmosis desalination: Water sources, technology, and today’s challenges,” *Water Research*, vol. 43, no. 9, pp. 2317–2348, 2009.
- [135] A. Efraty, R. N. Barak, and Z. Gal, “Closed circuit desalination - A new low energy high recovery technology without energy recovery,” *Desalination Water Treatment*, vol. 31, no. 1–3, pp. 95–101, 2011.
- [136] K. G. Nayar, N. C. Wright, G. P. Thiel, A. G. Winter, and J. H. Lienhard, “Energy requirements of alternative technologies for desalinating groundwater for irrigation,” 2015.
- [137] R. L. Stover, “Permeate recovery and flux maximization in semi-batch reverse osmosis,” in *AMTA/AWWA Membrane Technology Conference and Exposition 2013*, Taylor & Francis, 2013, pp. 1063–1070.
- [138] R. L. Stover, “Industrial and brackish water treatment with closed circuit reverse osmosis,” *Desalination Water Treatment*, vol. 51, no. 4–6, pp. 1124–1130, 2013.
- [139] P. A. Davies, J. Wayman, C. Alatta, K. Nguyen, and J. Orfi, “A desalination system with efficiency approaching the theoretical limits,” *Desalination Water Treat*, vol. 57, no. 48–49, pp. 23206–23216, 2016.
- [140] J. D. Kelleher, B. MacNamee, and A. D’Arcy, *Fundamentals of machine learning for predictive data analytics : algorithms, worked examples, and case studies*. MIT Press, 2016.
- [141] Y. Zhang, *New Advances in Machine Learning* . Books on Demand, 2010.

- [142] T. M. Mitchell and M. I. Jordan, “Machine learning: Trends, perspectives, and prospect,” *Science*, vol. 349, no. 6245, pp. 255–260, 2020.
- [143] R. S. Sutton and A. G. Barto, *Reinforcement learning : an introduction*. MIT Press.
- [144] M. Wang, Y. Cui, X. Wang, S. Xiao, and J. Jiang, “Machine Learning for Networking: Workflow, Advances and Opportunities,” *IEEE Network*, vol. 32, no. 2, pp. 92–99, Mar. 2018.
- [145] P. Malakar, S. Sarkar, A. Mukherjee, S. Bhanja, and A. Y. Sun, “Use of machine learning and deep learning methods in groundwater,” *Elsevier eBooks*, pp. 545–557, Jan. 2021 *Global Groundwater*, pp. 545–557, Jan. 2021.
- [146] G. Alam, I. Ihsanullah, M. Naushad, and M. Sillanpää, “Applications of artificial intelligence in water treatment for optimization and automation of adsorption processes: Recent advances and prospects,” *Chemical Engineering Journal*, vol. 427, p. 130011, Jan. 2021.
- [147] L. Li, S. Rong, R. Wang, and S. Yu, “Recent advances in artificial intelligence and machine learning for nonlinear relationship analysis and process control in drinking water treatment: A review,” *Chemical Engineering Journal*, vol. 405, p. 126673, Feb. 2021.
- [148] L. Corominas, M. Garrido-Baserba, K. Villez, G. Olsson, U. Cortés, and M. Poch, “Transforming data into knowledge for improved wastewater treatment operation: A critical review of techniques,” *Environmental Modelling & Software*, vol. 106, pp. 89–103, Aug. 2018.
- [149] L. Zhao, T. Dai, Z. Qiao, P. Sun, J. Hao, and Y. Yang, “Application of artificial intelligence to wastewater treatment: A bibliometric analysis and systematic review of technology, economy, management, and wastewater reuse,” *Process Safety and Environmental Protection*, vol. 133, pp. 169–182, Jan. 2020.
- [150] J. Jawad, A. H. Hawari, and S. Javaid Zaidi, “Artificial neural network modeling of wastewater treatment and desalination using membrane processes: A review,” *Chemical Engineering Journal*, vol. 419, p. 129540, Sep. 2021.
- [151] Y. Wang, Z. Cao, and A. Barati Farimani, “Efficient water desalination with graphene nanopores obtained using artificial intelligence,” *npj 2D Materials and Applications*, vol. 5, no. 1, pp. 1–9, Jul. 2021.

- [152] P. Cabrera, J. A. Carta, J. González, and G. Melián, “Artificial neural networks applied to manage the variable operation of a simple seawater reverse osmosis plant,” *Desalination*, vol. 416, pp. 140–156, 2017.
- [153] F. Dargam *et al.*, “Supporting Operational Decisions on Desalination Plants from Process Modelling and Simulation to Monitoring and Automated Control with Machine Learning,” *Lecture Notes in Business Information Processing*, pp. 150–164, May 2020.
- [154] S. Aani, Al, T. Bonny, S. W. Hasan, and N. Hilal, “Can machine language and artificial intelligence revolutionize process automation for water treatment and desalination?,” *Desalination*, vol. 458, no. January, pp. 84–96, 2019.
- [155] H. M. Benway *et al.*, “Ocean time series observations of changing marine ecosystems: An era of integration, synthesis, and societal applications,” *Frontiers in Marine Science*, vol. 6, 2019.
- [156] “Oxygen concentrations in coastal and marine waters surrounding Europe,” European Environmental Agency. Accessed: Oct. 29, 2022. [Online]. Available: <https://www.eea.europa.eu/ims/oxygen-concentrations-in-coastal-and>
- [157] A. Wulff *et al.*, “Ocean acidification and desalination: climate-driven change in a Baltic Sea summer microplanktonic community,” *Marine Biology*, vol. 165, p. 63, 2018.
- [158] Y. Choi, Y. Lee, K. Shin, Y. Park, and S. Lee, “Analysis of long-term performance of full-scale reverse osmosis desalination plant using artificial neural network and tree model,” *Environmental Engineering Research*, vol. 25, no. 5, pp. 763–770, 2020.
- [159] A. Srivastava *et al.*, “Response surface methodology and artificial neural network modelling for the performance evaluation of pilot-scale hybrid nanofiltration (NF) & reverse osmosis (RO) membrane system for the treatment of brackish ground water,” *Journal of Environmental Management*, vol. 278, p. 111497, Jan. 2021.
- [160] G. Jing, W. Du, and Y. Guo, “Studies on prediction of separation percent in electro dialysis process via BP neural networks and improved BP algorithms,” *Desalination*, vol. 291, pp. 78–93, 2012.
- [161] A. M. Aish, H. A. Zaqoot, and S. M. Abdeljawad, “Artificial neural network approach for predicting reverse osmosis desalination plants performance in the Gaza Strip,” *Desalination*, vol. 367, pp. 240–247, 2015.

- [162] S. K. Bhagat, T. Tiyasha, S. M. Awadh, T. M. Tung, A. H. Jawad, and Z. M. Yaseen, "Prediction of sediment heavy metal at the Australian Bays using newly developed hybrid artificial intelligence models," *Environmental Pollution*, vol. 268, p. 115663, Jan. 2021.
- [163] P. Dhal and C. Azad, "A comprehensive survey on feature selection in the various fields of machine learning," *Applied Intelligence*, vol. 52, no. 4, pp. 4543–4581, Mar. 2022.
- [164] S. B. Kotsiantis, "Feature selection for machine learning classification problems: a recent overview," *Artificial Intelligence Review*, vol. 42, no. 1, pp. 157–157, 2011.
- [165] S. Curcio, V. Calabrò, and G. Iorio, "Reduction and control of flux decline in cross-flow membrane processes modeled by artificial neural networks," *Journal of Membrane Science*, vol. 286, no. 1–2, pp. 125–132, Dec. 2006.
- [166] H. Chen and A. S. Kim, "Prediction of permeate flux decline in crossflow membrane filtration of colloidal suspension: a radial basis function neural network approach," *Desalination*, vol. 192, no. 1–3, pp. 415–428, May 2006.
- [167] J. Sargolzaei, M. Haghghi Asl, and A. Hedayati Moghaddam, "Membrane permeate flux and rejection factor prediction using intelligent systems," *Desalination*, vol. 284, pp. 92–99, Jan. 2012.
- [168] H. Shokrkar, A. Salahi, N. Kasiri, and T. Mohammadi, "Prediction of permeation flux decline during MF of oily wastewater using genetic programming," *Chemical Engineering Research and Design*, vol. 90, no. 6, pp. 846–853, Jun. 2012.
- [169] S. Park, S. S. Baek, J. C. Pyo, Y. Pachepsky, J. Park, and K. H. Cho, "Deep neural networks for modeling fouling growth and flux decline during NF/RO membrane filtration," *Journal of Membrane Science*, vol. 587, pp. 117164–117164, Oct. 2019.
- [170] J. Jawad, A. H. Hawari, and S. Zaidi, "Modeling of forward osmosis process using artificial neural networks (ANN) to predict the permeate flux," *Desalination*, vol. 484, p. 114427, Jun. 2020.
- [171] J. Jawad, A. H. Hawari, and S. J. Zaidi, "Modeling and Sensitivity Analysis of the Forward Osmosis Process to Predict Membrane Flux Using a Novel Combination of Neural Network and Response Surface Methodology Techniques," *Membranes*, vol. 11, no. 1, p. 70, Jan. 2021.

- [172] M. H. Khoshgoftar Manesh, H. Ghalami, M. Amidpour, and M. H. Hamed, "Optimal coupling of site utility steam network with MED-RO desalination through total site analysis and exergoeconomic optimization," *Desalination*, vol. 316, pp. 42–52, May 2013.
- [173] A. Stillwell and M. Webber, "Predicting the Specific Energy Consumption of Reverse Osmosis Desalination," *Water*, vol. 8, no. 12, p. 601, Dec. 2016.
- [174] A. Adda, S. Hanini, S. Bezari, H. Ameer, and R. Maouedj, "Managing and control of nanofiltration / reverse osmosis desalination system: Application of artificial neural network," *International Journal of Design and Nature and Ecodynamics*, vol. 15, no. 6, pp. 843–853, 2020.
- [175] C. Yang *et al.*, "Prediction model to analyze the performance of VMD desalination process," *Computers & chemical engineering*, vol. 132, p. 106619, Jan. 2020.
- [176] W. R. Bowen, M. G. Jones, J. S. Welfoot, and H. N. S. Yousef, "Predicting salt rejections at nanofiltration membranes using artificial neural networks," 2000.
- [177] A. T. Mohammad, M. A. Al-Obaidi, E. M. Hameed, B. N. Basheer, and I. M. Mujtaba, "Modelling the chlorophenol removal from wastewater via reverse osmosis process using a multilayer artificial neural network with genetic algorithm," *Journal of Water Process Engineering*, vol. 33, p. 100993, Feb. 2020.
- [178] S. Ghandehari, M. Mehdi Montazer-Rahmati, and M. Asghari, "A comparison between semi-theoretical and empirical modeling of cross-flow microfiltration using ANN," *Desalination*, vol. 277, no. 1–3, pp. 348–355, 2011.
- [179] C. Suh, B. Choi, S. Lee, D. Kim, and J. Cho, "Application of genetic programming to develop the model for estimating membrane damage in the membrane integrity test using fluorescent nanoparticle," *Desalination*, vol. 281, no. 1, pp. 80–87, Oct. 2011.
- [180] K. Park, J. Kim, D. R. Yang, and S. Hong, "Towards a low-energy seawater reverse osmosis desalination plant: A review and theoretical analysis for future directions," *Journal of Membrane Science*, vol. 595, p. 117607, 2020.
- [181] D. Torregrossa, U. Leopold, F. Hernández-Sancho, and J. Hansen, "Machine learning for energy cost modelling in wastewater treatment plants," *Journal of Environmental Management*, vol. 223, pp. 1061–1067, Oct. 2018.

- [182] N. D. Viet, D. Jang, Y. Yoon, and A. Jang, “Enhancement of membrane system performance using artificial intelligence technologies for sustainable water and wastewater treatment: A critical review,” *Critical Reviews in Environmental Science and Technology*, pp. 1–31, Jun. 2021.
- [183] C. Niu, X. Li, R. Dai, and Z. Wang, “Artificial intelligence-incorporated membrane fouling prediction for membrane-based processes in the past 20 years: A critical review,” *Water Research*, vol. 216, p. 118299, Jun. 2022.
- [184] M. Bagheri, A. Akbari, and S. A. Mirbagheri, “Advanced control of membrane fouling in filtration systems using artificial intelligence and machine learning techniques: A critical review,” *Process Safety and Environmental Protection*, vol. 123, pp. 229–252, Mar. 2019.
- [185] S. A. Aya, T. Ormanci Acar, and N. Tufekci, “Modeling of membrane fouling in a submerged membrane reactor using support vector regression,” *Desalination Water Treatment*, vol. 57, no. 51, pp. 24132–24145, Nov. 2016.
- [186] T. M. Lee *et al.*, “Prediction of membrane fouling in the pilot-scale microfiltration system using genetic programming,” *Desalination*, vol. 247, no. 1–3, pp. 285–294, Oct. 2009.
- [187] B. Teychene, A. Touffet, J. Baron, B. Welte, M. Joyeux, and H. Gallard, “Predicting of ultrafiltration performances by advanced data analysis,” *Water Research*, vol. 129, pp. 365–374, Feb. 2018.
- [188] S. J. Im, N. D. Viet, and A. Jang, “Real-time monitoring of forward osmosis membrane fouling in wastewater reuse process performed with a deep learning model,” *Chemosphere*, vol. 275, p. 130047, Jul. 2021.
- [189] H. Gao *et al.*, “Revolutionizing Membrane Design Using Machine Learning-Bayesian Optimization,” *Environmental science & technology*, vol. 56, no. 4, pp. 2572–258, 2021.
- [190] S. Kamrava, P. Tahmasebi, and M. Sahimi, “Physics- and image-based prediction of fluid flow and transport in complex porous membranes and materials by deep learning,” *Journal of Membrane Science*, vol. 622, pp. 119050–119050, 2021.
- [191] A. Anand, B. Unnikrishnan, J. Y. Mao, H. J. Lin, and C. C. Huang, “Graphene-based nanofiltration membranes for improving salt rejection, water flux and antifouling—A review,” *Desalination*, vol. 429, pp. 119–133, Mar. 2018.

- [192] P. Priya, T. C. Nguyen, A. Saxena, and N. R. Aluru, “Machine Learning Assisted Screening of Two-Dimensional Materials for Water Desalination,” *ACS Nano*, vol. 16, no. 2, pp. 1929–1939, Feb. 2022.
- [193] N. Jeong, R. Epsztein, R. Wang, S. Park, S. Lin, and T. Tong, “Exploring the Knowledge Attained by Machine Learning on Ion Transport across Polyamide Membranes Using Explainable Artificial Intelligence,” *Environmental science & technology*, vol. 57, no. 46, pp. 17851–17862, 2023.
- [194] Y. Nohara, K. Matsumoto, H. Soejima, and N. Nakashima, “Explanation of machine learning models using shapley additive explanation and application for real data in hospital,” *Computer Methods and Programs in Biomedicine*, vol. 214, p. 106584, 2022.
- [195] J. Yang, L. Tao, J. He, J. R. McCutcheon, and Y. Li, “Machine learning enables interpretable discovery of innovative polymers for gas separation membranes,” *Science Advances*, vol. 8, no. 29, p. 9545, Jul. 2022.
- [196] H. Yin *et al.*, “Machine learning for membrane design and discovery,” *Green Energy & Environment*, 2022.
- [197] EurEau, “Europe’s water in figures - 2017 Edition,” 2017.
- [198] Z. Hu, B. Chen, W. Chen, D. Tan, and D. Shen, “Review of model-based and data-driven approaches for leak detection and location in water distribution systems,” *Water Supply*, Apr. 2021.
- [199] S. Yazdekhashti, G. Vladeanu, and C. Daly, “Evaluation of Artificial Intelligence Tool Performance for Predicting Water Pipe Failures,” *Pipelines 2020: Utility Engineering, Surveying, and Multidisciplinary Topics - Proceedings of Sessions of the Pipelines 2020 Conference*, pp. 203–211, 2020.
- [200] D. Winkler, M. Haltmeier, M. Kleidorfer, W. Rauch, and F. Tscheikner-Gratl, “Pipe failure modelling for water distribution networks using boosted decision trees,” *Structure and Infrastructure Engineering*, vol. 14, no. 10, pp. 1402–1411, Oct. 2018.
- [201] F. Shi, Z. Liu, and E. Li, “Prediction of Pipe Performance with Ensemble Machine Learning Based Approaches,” *Proceedings - 2017 International Conference on Sensing, Diagnostics, Prognostics, and Control, SDPC 2017*, vol. 2017-Decem, pp. 408–414, Dec. 2017,

- [202] A. Robles-Velasco, C. Ramos-Salgado, J. Muñuzuri, and P. Cortés, “Artificial Neural Networks to Forecast Failures in Water Supply Pipes,” *Sustainability*, vol. 13, no. 15, p. 8226, Jul. 2021.
- [203] M. M. Giraldo-González and J. P. Rodríguez, “Comparison of Statistical and Machine Learning Models for Pipe Failure Modeling in Water Distribution Networks,” *Water*, vol. 12, no. 4, p. 1153, Apr. 2020.
- [204] E. D. Mackey, N. Pozos, W. James, T. Seacord, H. Hunt, and D. L. Mayer, “Assessing Seawater Intake Systems for Desalination Plants,” Water Research Foundation, 2011.
- [205] H. Sanawar, L. H. Kim, N. M. Farhat, M. C. M. van Loosdrecht, and J. S. Vrouwenvelder, “Periodic chemical cleaning with urea: disintegration of biofilms and reduction of key biofilm-forming bacteria from reverse osmosis membranes,” *Water Research*, vol. 13, p. 100117, Dec. 2021.
- [206] L. O. Villacorte, S. A. A. Tabatabai, N. Dhakal, G. Amy Cd, J. C. Schippers, and M. D. Kennedy, “Algal blooms: an emerging threat to seawater reverse osmosis desalination,” *Desalination Water Treatment*, vol. 55, no. 10, pp. 2601–2611, 2015.
- [207] B. Z. Rousso, E. Bertone, R. Stewart, and D. P. Hamilton, “A systematic literature review of forecasting and predictive models for cyanobacteria blooms in freshwater lakes,” *Water Research*, vol. 182, p. 115959, Sep. 2020.
- [208] H. M. Al Gheilani, K. Matsuoka, A. Y. AlKindi, S. Amer, and C. Waring, “Fish Kill Incidents and Harmful Algal Blooms in Omani Waters,” *Journal of Agricultural and Marine Sciences [JAMS]*, vol. 16, p. 23, Jan. 2011.
- [209] T. Deng, K. W. Chau, and H. F. Duan, “Machine learning based marine water quality prediction for coastal hydro-environment management,” *Journal of Environmental Management*, vol. 284, p. 112051, Apr. 2021.
- [210] H. S. Yi, B. Lee, S. Park, K. C. Kwak, and K. G. An, “Prediction of short-term algal bloom using the M5P model-tree and extreme learning machine,” *Environmental Engineering Research*, vol. 24, no. 3, pp. 404–411, 2019.
- [211] Y. Park *et al.*, “A machine learning approach for early warning of cyanobacterial bloom outbreaks in a freshwater reservoir,” *Journal of Environmental Management*, vol. 288, p. 112415, Jun. 2021.

- [212] J. H. Kim *et al.*, “Improving the performance of machine learning models for early warning of harmful algal blooms using an adaptive synthetic sampling method,” *Water Research*, vol. 207, p. 117821, Dec. 2021.
- [213] T. Deng, K. W. Chau, and H. F. Duan, “Machine learning based marine water quality prediction for coastal hydro-environment management,” *Journal of Environmental Management*, vol. 284, p. 112051, Apr. 2021.
- [214] X. Xiao *et al.*, “A novel single-parameter approach for forecasting algal blooms,” *Water Research*, vol. 108, pp. 222–231, Jan. 2017.
- [215] M. Mamun, J.-J. Kim, M. A. Alam, and K.-G. An, “Prediction of Algal Chlorophyll-a and Water Clarity in Monsoon-Region Reservoir Using Machine Learning Approaches,” *Water*, vol. 12, no. 1, p. 30, Dec. 2019.
- [216] L. Ye, Q. Cai, M. Zhang, and L. Tan, “Real-time observation, early warning and forecasting phytoplankton blooms by integrating in situ automated online sondes and hybrid evolutionary algorithms,” *Ecological Informatics*, vol. 22, pp. 44–51, Jul. 2014.
- [217] J. Wen, J. Yang, Y. Li, and L. Gao, “Harmful algal bloom warning based on machine learning in maritime site monitoring,” *Knowledge-Based Systems*, vol. 245, p. 108569, Jun. 2022.
- [218] X. Li, R. Liao, J. Zhou, P. T. Y. Leung, M. Yan, and H. Ma, “Classification of morphologically similar algae and cyanobacteria using Mueller matrix imaging and convolutional neural networks,” *Applied Optics*, vol. 56, no. 23, pp. 6520–6530, 2017.
- [219] P. Qian *et al.*, “Multi-Target Deep Learning for Algal Detection and Classification,” *Proceedings of the Annual International Conference of the IEEE Engineering in Medicine and Biology Society, EMBS*, pp. 1954–1957, Jul. 2020.
- [220] J. L. Deglint, C. Jin, A. Chao, and A. Wong, “The Feasibility of Automated Identification of Six Algae Types Using Feed-Forward Neural Networks and Fluorescence-Based Spectral-Morphological Features,” *IEEE Access*, vol. 7, pp. 7041–7053, 2019.
- [221] D. P. Yadav, A. S. Jalal, D. Garlapati, K. Hossain, A. Goyal, and G. Pant, “Deep learning-based ResNeXt model in phycological studies for future,” *Algal Research*, vol. 50, p. 102018, Sep. 2020.

- [222] J. Park, H. Lee, C. Y. Park, S. Hasan, T.-Y. Heo, and W. H. Lee, “Algal Morphological Identification in Watersheds for Drinking Water Supply Using Neural Architecture Search for Convolutional Neural Network,” *Water*, no. 7, p. 1338, Jun. 2019.
- [223] M. E. Sonmez, N. Eczacıoğlu, N. E. Gümüş, M. F. Aslan, K. Sabancı, and B. Aşikkutlu, “Convolutional neural network - Support vector machine based approach for classification of cyanobacteria and chlorophyta microalgae groups,” *Algal Research*, vol. 61, p. 102568, 2021.
- [224] S. B. Maind and P. Wankar, “Research Paper on Basic of Artificial Neural Network,” *International Journal on Recent and Innovation Trends in Computing and Communication*, vol. 2, no. 1, pp. 96–100, 2014.
- [225] M. Khayet, C. Cojocar, and M. Essalhi, “Artificial neural network modeling and response surface methodology of desalination by reverse osmosis,” *Journal of Membrane Science*, vol. 368, no. 1–2, pp. 202–214, Feb. 2010.
- [226] M. Stewart, “The Limitations of Machine Learning ,” Towards data science. Accessed: Nov. 22, 2021. [Online]. Available: <https://towardsdatascience.com/the-limitations-of-machine-learning-a00e0c3040c6>
- [227] D. Ghernaout, M. Aichouni, A. S. Alghamdi, and A. Alghamdi, “Applying big data in water treatment industry: A new era of advance,” *International Journal of ADVANCED AND APPLIED SCIENCES*, vol. 5, no. 3, pp. 89–97, 2018.
- [228] D. C. Montgomery and G. C. Runger, “The Role of Statistics in Engineering,” in *Applied Statistics and Probability for Engineers*, 5th ed., John Wiley & Sons, 2011, pp. 1–18.
- [229] Imranali, “5 major sensor data analytics challenges: deadly or curable? - Data Science Central,” Data Science Central . Accessed: Sep. 01, 2021. [Online]. Available: <https://www.datasciencecentral.com/profiles/blogs/5-major-sensor-data-analytics-challenges-deadly-or-curable>
- [230] N. Camin and O. Betancourt, “Variety of Sensors Needed to Monitor Membrane Treatment Systems,” Water technology solutions for industrial water management. Accessed: Jun. 27, 2022. [Online]. Available: <https://www.watertechonline.com/home/article/14171731/variety-of-sensors-needed-to-monitor-membrane-treatment-systems>

- [231] W. Eckerson, "Dsts Warehouse Institute Survey On Data Quality," in *Proceedings of the Seventh International Conference on Information Quality*, 2002, pp. 16–16.
- [232] T. C. Redman, "Bad Data Costs the U.S. \$3 Trillion Per Year," *Harvard Business Review*, Sep. 22, 2016. Accessed: Jun. 28, 2022. [Online]. Available: <https://hbr.org/2016/09/bad-data-costs-the-u-s-3-trillion-per-year>
- [233] C. Riverol and M. V. Pilipovik, "Assessing the seasonal influence on the quality of seawater using fuzzy linear programming," *Desalination*, vol. 230, pp. 175–182, 2008.
- [234] C. Riverol-Cañizares and V. Pilipovik, "The use of radial basis function networks (RBFN) to predict critical water parameters in desalination plants," *Expert Systems With Applications*, vol. 37, pp. 7285–7287, 2010.
- [235] C. Riverol and M. V. Pilipovik, "Prediction of the behaviour of the Silt Density Index (SDI) in the Caribbean Seawater and its impact on RO desalination plants," *Desalination*, vol. 268, no. 1–3, pp. 262–265, Mar. 2011.
- [236] J. K. Mahato and S. K. Gupta, "Exploring applicability of artificial intelligence and multivariate linear regression model for prediction of trihalomethanes in drinking water," *International Journal of Environmental Science and Technology 2021*, pp. 1–14, May 2021.
- [237] M. D. Guiry, "HOW MANY SPECIES OF ALGAE ARE THERE?," *Journal of Phycology*, vol. 48, no. 5, pp. 1057–1063, Oct. 2012.
- [238] Y. Zhang *et al.*, "Integrating water quality and operation into prediction of water production in drinking water treatment plants by genetic algorithm enhanced artificial neural network," *Water Research*, vol. 164, Nov. 2019.
- [239] S. M. A. Zaidi *et al.*, "Machine learning for energy-water nexus: challenges and opportunities," *Big Earth Data*, vol. 2, no. 3, pp. 228–267, Jul. 2018.
- [240] N. A. Barton, T. S. Farewell, S. H. Hallett, and T. F. Acland, "Improving pipe failure predictions: Factors affecting pipe failure in drinking water networks," *Water Research*, vol. 164, p. 114926, Nov. 2019.
- [241] H. J. Jun, J. K. Park, and C. H. Bae, "Factors Affecting Steel Water-Transmission Pipe Failure and Pipe-Failure Mechanisms," *Journal of Environmental Engineering*, vol. 146, no. 6, p. 04020034, Mar. 2020.

- [242] “ACCIONA’s decarbonization fund includes Maestro AI platform at the Umm Al Houl desalination plant in Qatar,” Acciona. Accessed: Aug. 20, 2022. [Online]. Available: https://www.acciona.com/updates/articles/acciona-decarbonization-fund-maestro-ai-platform-umm-al-houl-desalination-plant-qatar/?_adin=02021864894
- [243] G. T. Daigger, N. Voutchkov, U. Lall, and W. Sarni, “The Future of Water,” 2020.
- [244] N. Delion, G. Mauguin, and P. Corsin, “Importance and impact of post treatments on design and operation of SWRO plants,” *Desalination*, vol. 165, pp. 323–334, Aug. 2004.
- [245] N. Voutchkov, *Pretreatment for Reverse Osmosis Desalination*. Elsevier, 2017.
- [246] D. D. Ratnayaka, M. J. Brandt, K. Michael. Johnson, and A. C. Twort, *Twort’s water supply*. Butterworth-Heinemann is An Imprint Of Elsevier, 2009.
- [247] S. Miller, H. Shemer, and R. Semiat, “Energy and environmental issues in desalination,” *Desalination*, vol. 366, pp. 2–8, 2014.
- [248] G. Antoniou and F. van Harmelen, *A Semantic Web Primer*, vol. 24, no. 4. 2009.
- [249] H. Guillermo and N. Oscar, *The Furniture of the World: Essays in Ontology and Metaphysics*, 1st ed. Rodopi, 2012.
- [250] F. Baader, D. Calvanese, D. McGuinness, D. Nardi, and P. Patel-Schneider, *The Description Logic Handbook: Theory, Implementation and Applications*. Cambridge University Press, 2003.
- [251] B. McBride, *The Resource Description Framework (RDF) and its Vocabulary Description Language RDFS*. 2004.
- [252] W3, “SPARQL Protocol for RDF.” Accessed: Oct. 07, 2023. [Online]. Available: <https://www.w3.org/TR/rdf-sparql-protocol/>
- [253] L. Jean-Baptiste, *Ontologies with Python*. 2021.
- [254] L. Branquinho, R. A. Baracho, M. B. Almeida, and R. R. Souza, “Using Ontologies and Inference Engines in Association Rules of Data Mining : An Application in a Medical Laboratory Diagnostic Company,” *Knowledge Discovery use Ontologies in Data Mining*, pp. 1–7, 2015.
- [255] N. Kaewboonma, K. Tuamsuk, and M. Buranarach, “Ontology Modeling for a Drought Management Information System Nattapong,” *Libres*, vol. 24, no. 1, pp. 21–33, 2014.

- [256] K. W. Chau, “An ontology-based knowledge management system for flow and water quality modeling,” *Advances in Engineering Software*, vol. 38, no. 3, pp. 172–181, Mar. 2007.
- [257] S. Howell, Y. Rezgui, and T. Beach, “Water utility decision support through the semantic web of things,” *Environmental Modelling & Software*, vol. 102, pp. 94–114, Apr. 2018.
- [258] T. Koegst, J. Tränckner, F. Blumensaat, J. Eichhorn, and V. Mayer-Eichberger, “On the use of an ontology for the identification of degree of freedom in urban wastewater systems,” *Water Science and Technology*, vol. 55, no. 4, pp. 155–163, 2007.
- [259] L. R. Chernyakhovskaya, J. A. Muelle, R. A. Shkundina, and M. S. Ugryumov, “Ontological Knowledge Base Development for the Business Process Control in a Wastewater Treatment Plant,” in *International Workshop on Computer Science and Information Technologies CSIT*, 2006.
- [260] J. Wölle, H. Steinmetz, J. Hansen, K. Einsfeld, and A. Ebert, “An intelligent visualisation and decision support system for decentralised wastewater treatment plants,” *Water Science and Technology*, vol. 56, no. 5, pp. 183–191, 2007.
- [261] L. Ceccaroni, U. Cortés, and M. Sánchez-Marrè, “OntoWEDSS: augmenting environmental decision-support systems with ontologies,” *Environmental Modelling & Software*, vol. 19, no. 9, pp. 785–797, Sep. 2004.
- [262] M. Oprea, “A knowledge modelling framework for intelligent environmental decision support systems and its application to some environmental problems,” *Environmental Modelling & Software*, pp. 72–97, 2018.
- [263] J. Garrido and I. Requena, “Proposal of ontology for environmental impact assessment: An application with knowledge mobilization,” *Expert Systems with Applications*, vol. 38, no. 3, pp. 2462–2472, Mar. 2011.
- [264] O. Cabezut-Boo and A. Sánchez-Aguilar, “Towards an ontology of waste water treatment plants: the identification phase,” *Environmental Modelling & Software*, vol. 14, pp. 401–408, 1999.
- [265] D. Sottara *et al.*, “An ontology-based approach for the instrumentation, control and automation infrastructure of a WWTP,” *International Congress on Environmental Modelling and Software*, vol. 3, pp. 1222–1228, 2014.

- [266] L. Ahmedi, E. Jajaga, and F. Alunedi, “An ontology framework for water quality management,” *CEUR Workshop Proc*, vol. 1063, pp. 35–50, 2013.
- [267] Z. Xiaomin, Y. Jianjun, H. Xiaoci, and C. Shaoli, “An Ontology-based Knowledge Modelling Approach for River Water Quality Monitoring and Assessment,” *Procedia Computer Science*, vol. 96, pp. 335–344, 2016.
- [268] M. Grimaldi, M. Sebillio, G. Vitiello, and V. Pellicchia, “An Ontology Based Approach for Data Model Construction Supporting the Management and Planning of the Integrated Water Service,” in *Computational Science and Its Applications – ICCSA*, Springer International Publishing, 2019, pp. 243–252.
- [269] M. A. Musen, “The protégé project,” *AI Matters*, vol. 1, no. 4, pp. 4–12, 2015.
- [270] H. Zhao, S. Zhang, and J. Zhao, “Research of using protégé to build ontology,” *International Conference on Computer and Information Science*, pp. 697–700, 2012.
- [271] N. Voutchkov, “Considerations for selection of seawater filtration pretreatment system,” *Desalination*, vol. 261, no. 3, pp. 354–364, 2010.
- [272] N. Voutchkov, “SWRO desalination process: On the beach - Seawater intakes,” *Filtration and Separation*, vol. 42, no. 8, pp. 24–27, 2005.
- [273] A. H. A. Dehwah and T. M. Missimer, “Subsurface intake systems: Green choice for improving feed water quality at SWRO desalination plants, Jeddah, Saudi Arabia,” *Water Research*, vol. 88, pp. 216–224, 2016.
- [274] A. Panagopoulos, K.-J. Haralambous, and M. Loizidou, “Desalination brine disposal methods and treatment technologies-A review,” *Science of The Total Environment*, vol. 693, p. 133545, 2019.
- [275] D. R. Mohamed, M. M. Shahien, and H. H. Hafez, “Influence of Well Location on Drawdown in Area Surrounded By Vertical Cutoff Walls,” in *Advances in Structural and Geotechnical Engineering*, 2015, pp. 15–25.
- [276] T. M. Missimer, B. Jones, and R. G. Maliva Editors, *Environmental Science Intakes and Outfalls for Seawater Reverse-Osmosis Desalination Facilities Innovations and Environmental Impacts*. Springer International Publishing, 2015.
- [277] N. X. Tsiourtis, “Criteria and procedure for selecting a site for a desalination plant,” *Desalination*, vol. 221, no. 1–3, pp. 114–125, 2008.

- [278] T. M. Missimer, B. Jones, and R. G. Maliva, *Intakes and Outfalls for Seawater Reverse-Osmosis Desalination Facilities*. Springer Cham, 2015.
- [279] D. E. Williams, “Slant Well Intake Systems: Design and Construction,” in *Intakes and Outfalls for Seawater Reverse-Osmosis Desalination Facilities*, Springer Cham, 2015.
- [280] Kennedy/Jenks Consultants, “scwd Seawater desalination Intake Technical Feasibility Study,” Santa Cruz, California, 2011.
- [281] M. J. Brandt, K. Michael. Johnson, A. J. Elphinston, and D. D. Ratnayaka, *Twort’s water supply*. Butterworth-Heinemann, 2016.
- [282] N. O’Keeffe and a. W. H. Turnpenny, “Screening for Intake and Outfalls : a best practice guide,” 2005.
- [283] T. M. Pankratz, *Screening Equipment Handbook*, 2nd ed. CRC Press, 2017.
- [284] EIMCO Water Technology, “Water Intake Screens: Passive Screens offer advantages not found in other types of screens,” 2008.
- [285] University of California - Santa Cruz, “Study of brine discharge from desalination plant finds good news and bad news,” PHYS ORG. Accessed: Apr. 03, 2019. [Online]. Available: <https://phys.org/news/2019-01-brine-discharge-desalination-good-news.html>
- [286] T. Bleninger *et al.*, “Environmental hydraulics framework of the design of discharges from desalination plants,” *Environmental Hydraulics - Proceedings of the 6th International Symposium on Environmental Hydraulics*, 2010, pp. 571–576, 2010.
- [287] S. Al Aani, C. J. Wright, and N. Hilal, “Investigation of UF membranes fouling and potentials as pre-treatment step in desalination and surface water applications,” *Desalination*, vol. 432, pp. 115–127, Apr. 2018.
- [288] S. Kawamura, “Design and operation of high-rate filters,” *Journal of the American Water Works Association*, vol. 91, no. 12, pp. 77–90, Dec. 1999.
- [289] N. Voutchkov, “Conventional and membrane filtration: Selecting a SWRO pre-treatment system,” *Filtration Separation*. Accessed: Mar. 13, 2019. [Online]. Available: <https://www.filtsep.com/water-and-wastewater/features/conventional-and-membrane-filtration-selecting-a/>

- [290] S. M. Hossein Fayaz, R. Mafigholami, F. Razavian, and K. Ghasemipanah, “Correlations between silt density index, turbidity and oxidation-reduction potential parameters in seawater reverse osmosis desalination,” *Water Science and Engineering*, vol. 12, no. 2, pp. 115–120, Jun. 2019.
- [291] R. Tarpagkou and A. Pantokratoras, “The influence of lamellar settler in sedimentation tanks for potable water treatment - A computational fluid dynamic study,” *Powder Technology*, vol. 268, pp. 139–149, 2014.
- [292] J. Kavitha, M. Rajalakshmi, A. R. Phani, and M. Padaki, “Pretreatment processes for seawater reverse osmosis desalination systems—A review,” *Journal of Water Process Engineering*, vol. 32, p. 100926, Dec. 2019.
- [293] S. J. Duranceau, R. J. Wilder, and S. S. Douglas, “Guidance and recommendations for posttreatment of desalinated water,” *Journal of the American Water Works Association*, vol. 104, no. 9, 2012.
- [294] A. Lesimple, F. E. Ahmed, and N. Hilal, “Remineralization of desalinated water: Methods and environmental impact,” *Desalination*, vol. 496, p. 114692, 2020.
- [295] M. Horridge *et al.*, “A Practical Guide To Building OWL Ontologies Using Protege 4 and CO-ODE Tools,” 2011.
- [296] J.-B. Lamy, “Owlready: Ontology-oriented programming in Python with automatic classification and high level constructs for biomedical ontologies,” *Artificial intelligence in medicine*, vol. 80, pp. 11–28, 2017.
- [297] T. M. Missimer and R. G. Maliva, “Environmental issues in seawater reverse osmosis desalination: Intakes and outfalls,” *Desalination*, vol. 434, pp. 198–215, 2018.
- [298] L. R. Lujan and T. M. Missimer, “Technical feasibility of a seabed gallery system for SWRO facilities at Shoaiba, Saudi Arabia, and regions with similar geology,” *Desalination Water Treatment*, vol. 52, no. 40–42, pp. 7431–7442, 2014.
- [299] A. H. A. Dehwah, S. Al-Mashharawi, K. C. Ng, and T. M. Missimer, “Aquifer Treatment of Sea Water to Remove Natural Organic Matter Before Desalination,” *Groundwater*, vol. 55, no. 3, pp. 316–326, 2016.
- [300] H. Ludwig, *Reverse Osmosis Seawater Desalination Volume 1*, Springer Nature, 2022.
- [301] H. Ludwig, *Reverse Osmosis Seawater Desalination Volume 2*, Springer Nature, 2022.

- [302] H. T. El-Dessouky and Hisham Mohamed Ettouney, *Fundamentals of salt water desalination*. Amsterdam ; New York: Elsevier, 2002.
- [303] T. M. Missimer, N. Ghaffour, A. H. A. Dehwah, R. Rachman, R. G. Maliva, and G. Amy, “Subsurface intakes for seawater reverse osmosis facilities: Capacity limitation, water quality improvement, and economics,” *Desalination*, vol. 322, pp. 37–51, Aug. 2013.
- [304] T. W. Bennett, “On the Design and Construction of Infiltration Galleries,” *Groundwater*, vol. 8, no. 3, pp. 16–24, 1970.
- [305] T. Grischek, R. Batrak, S. Paufler, and R. A. Wahaab, “Beach wells as pre-treatment for sea water desalination,” 2019.
- [306] R. Valavala, J. Sohn, J. Han, N. Her, and Y. Yoon, “Pretreatment in Reverse Osmosis Seawater Desalination: A Short Review,” *Environmental Engineering Research*, vol. 16, no. 4, pp. 205–212, 2011.
- [307] M. Aslam, H. Kainz, and G. Gruber, “Settling of Solids in Primary Clarifiers / Storm Water Tanks,” 2011.
- [308] A. Koohestanian, M. Hosseini, and Z. Abbasian, “The Separation Method for Removing of Colloidal Particles from Raw Water,” *IDOSI*, 2008.
- [309] M. S. Shankar, M. Pandey, and A. K. Shukla, “Analysis of existing equations for calculating the settling velocity,” *Water*, vol. 13, no. 14, pp. 1–12, 2021.
- [310] G. Tchobanoglous, H. D. Stensel, R. Tsuchihashi, F. Burton, M. Abu-Orf, and W. Pfrang, *Wastewater Engineering Treatment and Resources Recovery*, Fifth. McGraw-Hill Education, 2014.
- [311] J. R. Mihelcic and J. B. Zimmerman, *Environmental engineering : fundamentals, sustainability, design*, 3rd ed. Hoboken: Wiley, 2021.
- [312] F. A. & Engineers, “Water Treatment Plant Operator Program Manual,” 2003.
- [313] K. Vidya and M. Ramachandran, “Design of Water Treatment Plant for Musiri Town (Tiruchirapalli),” *International journal of scientific research in science, engineering and technology*, vol. 2, no. 1, pp. 201–206, 2016.

- [314] M. J. Brandt, K. M. Johnson, A. J. Elphinston, and D. D. Ratnayaka, “Storage, Clarification and Chemical Treatment,” in *Twort’s Water Supply*, 7th ed., Butterworth-Heinemann, 2017, pp. 323–366.
- [315] M. Lytra, “Hydraulics of sedimentation. A study of the lamella settlers at Ringsjö water treatment plant, Sweden,” 2019.
- [316] G. Tchobanoglous, F. L. Burton, D. H. Stensel, and R. Tsuchihashi, *Wastewater Engineering Treatment and Resource Recovery*, Boston: Mcgraw-Hill, 2014.
- [317] H. Boulahfa, S. Belhamidi, F. Elhannouni, M. Taky, M. Hafsi, and A. Elmidaoui, “Pretreatment process optimization and reverse osmosis performances of a brackish surface water demineralization plant, Morocco,” *Desalination and Water Treatment*, vol. 206, pp. 189–201, 2020.
- [318] A. F. Corral *et al.*, “Comparison of slow sand filtration and microfiltration as pretreatments for inland desalination via reverse osmosis,” *Desalination*, vol. 334, no. 1, pp. 1–9, Feb. 2014.
- [319] D. D. Ratnayaka, M. J. Brandt, and K. M. Johnson, “CHAPTER 8 – Water Filtration Granular Media Filtration,” *Water Supply*, pp. 315–350, 2009.
- [320] M. F. Hamoda, I. Al-Ghusain, and D. M. Al-Jasem, “Application of Granular Media Filtration in Wastewater Reclamation and Reuse,” *Journal of Environmental Science and Health*, vol. 39, no. 2, pp. 385–395, 2004.
- [321] Dow Filmtec, “Dow Water Solutions FILMTEC™ Membranes Product Information Catalog,” 2009.
- [322] DuPont, “FilmTec™ SW30XFR-400/34i,” 2022.
- [323] S. G. Salinas-Rodriguez, J. C. Schippers, G. L. Amy, I. S. Kim, and M. D. Kennedy, “Seawater Reverse Osmosis Desalination: Assessment and Pre-treatment of Fouling and Scaling,” *IWA*, 2021.
- [324] Y. Y. Lu, Y. D. Hu, X. L. Zhang, L. Y. Wu, and Q. Z. Liu, “Optimum design of reverse osmosis system under different feed concentration and product specification,” *Journal of Membrane Science*, vol. 287, no. 2, pp. 219–229, Jan. 2007.
- [325] DuPont, “Troubleshooting Symptoms of Trouble, Causes, and Corrective Measures,” 2022.

- [326] DuPont, “System Design System Performance Projection Design Equations and Parameters,” 2023.
- [327] G. E. Dévora-Isiordia *et al.*, “Evaluation of Concentration Polarization Due to the Effect of Feed Water Temperature Change on Reverse Osmosis Membranes,” *Membranes*, vol. 13, no. 1, 2022.
- [328] A. Siddiqui *et al.*, “Porosity of spacer-filled channels in spiral-wound membrane systems: Quantification methods and impact on hydraulic characterization,” *Water Research*, vol. 119, pp. 304–311, 2017.
- [329] J. S. Vrouwenvelder, D. A. Graf von der Schulenburg, J. C. Kruithof, M. L. Johns, and M. C. M. van Loosdrecht, “Biofouling of spiral-wound nanofiltration and reverse osmosis membranes: A feed spacer problem,” *Water Research*, vol. 43, no. 3, pp. 583–594, 2009.
- [330] T. Bleninger, A. Niepelt, and G. Jirka, “Desalination plant discharge calculator,” *Desalination and Water Treatment*, vol. 13, no. 1–3, pp. 156–173, 2010.
- [331] O. Abessi and P. J. W. Roberts, “Rosette Diffusers for Dense Effluents in Flowing Currents,” *Journal of Hydraulic Engineering*, vol. 144, no. 1, 2018.
- [332] C. C. K. Lai and J. H. W. Lee, “Mixing of inclined dense jets in stationary ambient,” *Journal of Hydro-Environment Research*, vol. 6, no. 1, pp. 9–28, 2012.
- [333] B. J. Philip W Roberts, A. Ferrier, and G. Daviero, “Mixing in Inclined Dense Jets,” *Journal of Hydraulic Engineering*, vol. 123, no. 8, pp. 693–699, 1997.
- [334] O. Abessi and P. J. W. Roberts, “Dense Jet Discharges in Shallow Water,” *Journal of Hydraulic Engineering*, vol. 142, no. 1, pp. 1–13, 2016.
- [335] O. Abessi and P. J. W. Roberts, “Effect of Nozzle Orientation on Dense Jets in Stagnant Environments,” *Journal of Hydraulic Engineering*, vol. 141, no. 8, pp. 1–8, 2015.
- [336] B. R. Munson, H. O. Theodore, F. Y. Donald, and W. Huebsch, *A Brief Introduction to Fluid Mechanics*. Wiley, 2011.
- [337] R. Navarro, J. L. Sánchez Lizaso, and I. Sola, “Assessment of Energy Consumption of Brine Discharge from SWRO Plants,” *Water (Switzerland)*, vol. 15, no. 4, p.786, 2023.
- [338] The European Commission, “Eu Regulation 2019/1781,” 2019.

- [339] C. P. Koutsou, E. M. Kritikos, A. J. Karabelas, and M. Kostoglou, “Analysis of temperature effects on the specific energy consumption in reverse osmosis desalination processes,” *Desalination*, vol. 476, pp. 114213, 2019.
- [340] Z. Yang, X. H. Ma, and C. Y. Tang, “Recent development of novel membranes for desalination,” *Desalination*, vol. 434, no. May 2017, pp. 37–59, 2018.
- [341] J. R. Werber, A. Deshmukh, and M. Elimelech, “The Critical Need for Increased Selectivity, Not Increased Water Permeability, for Desalination Membranes,” *Environmental Science & Technology Letters*, vol. 3, no. 4, pp. 112–120, 2016.
- [342] B. Shi, P. Marchetti, D. Peshev, S. Zhang, and A. G. Livingston, “Will ultra-high permeance membranes lead to ultra-efficient processes? Challenges for molecular separations in liquid systems,” *Journal of Membrane Science*, vol. 525, no. October 2016, pp. 35–47, 2017.
- [343] R. K. McGovern and J. H. Lienhard V, “On the asymptotic flux of ultrapermeable seawater reverse osmosis membranes due to concentration polarisation,” *Journal of Membrane Science*, vol. 520, pp. 560–565, 2016.
- [344] Global Water Intelligence, “DesalData.” Accessed: Nov. 11, 2022. [Online]. Available: <https://www.desaldata.com/>
- [345] International Standard Organization, “ISO 15686-5 Buildings and constructed assets - Service life planning; Part 5 - life Cost Analysis,” 2017.
- [346] S. Kara, “Life Cycle cost,” in *CIRP Encyclopedia of Production Engineering*, Berlin, Heidelberg: Springer, 2014.
- [347] G. Norman, “Life cycle costing,” *Property Management*, vol. 8, no. 4, pp. 344-356, 1990.
- [348] L. E. Greene and B. L. Shaw, “The steps for successful life cycle cost analysis,” *IEEE Proceedings of the National Aerospace and Electronics Conference*, vol. 3, pp. 1209–1216, 1990.
- [349] D. Kehily, A. Hore, F. McDonnell, E. McAuley, K. Dempsey, and C. Mitchell, “Guide to Life Cycle Costing,” 2022.
- [350] D. Kehily *et al.*, “Society of Chartered Surveyors Ireland Guide to Life Cycle Costing,” 2011.

- [351] M. Samis, D. Laughton, and R. Poulin, “Risk Discounting: The Fundamental Difference between the Real Option and Discounted Cash Flow Project Valuation Methods,” 2003.
- [352] Davis Langdon Management Consulting, “Literature review of life cycle costing (LCC) and life cycle assessment (LCA),” 2006.
- [353] “The Public Spending Code D . Standard Analytical Procedures Guide to economic appraisal : Carrying out a cost benefit analysis,” Department of Public, 2012.
- [354] “Project discount & inflation rates,” National Development Plan. [Online]. Available: <https://www.per.gov.ie/en/project-discount-inflation-rates/>
- [355] M. Bindels, J. Carvalho, C. Bayona Gonzalez, N. Brand, and B. Nelemans, “Techno-economic assessment of seawater reverse osmosis (SWRO) brine treatment with air gap membrane distillation (AGMD),” *Desalination*, vol. 489, p. 114532, 2020.
- [356] M. Gökçek and Ö. B. Gökçek, “Technical and economic evaluation of freshwater production from a wind-powered small-scale seawater reverse osmosis system (WP-SWRO),” *Desalination*, vol. 381, pp. 47–57, Mar. 2016.
- [357] C. Morgante *et al.*, “Valorisation of SWRO brines in a remote island through a circular approach: Techno-economic analysis and perspectives,” *Desalination*, vol. 542, p. 116005, Nov. 2022.
- [358] U. K. Kesieme, N. Milne, H. Aral, C. Y. Cheng, and M. Duke, “Economic analysis of desalination technologies in the context of carbon pricing, and opportunities for membrane distillation,” *Desalination*, vol. 323, pp. 66–74, 2013.
- [359] T. Altmann and R. Das, “Process improvement of sea water reverse osmosis (SWRO) and subsequent decarbonization,” *Desalination*, vol. 499, p. 114791, Feb. 2021.
- [360] F. Giacalone, M. Papapetrou, G. Kosmadakis, A. Tamburini, G. Micale, and A. Cipollina, “Application of reverse electrodialysis to site-specific types of saline solutions: A techno-economic assessment,” *Energy*, vol. 181, pp. 532–547, Aug. 2019.
- [361] A. Hermelink and D. de Jager, “Evaluating our future - The crucial role of discount rates in,” 2015.
- [362] Relief central, “Central bank discount rate.” Accessed: Oct. 07, 2022. [Online]. Available: https://relief.unboundmedicine.com/relief/view/The-World-Factbook/563791/all/Central_bank_discount_rate

- [363] T. Younos, “The economics of desalination,” *IEEE Spectrum*, vol. 3, no. 132, pp. 39–45, 2005.
- [364] S. Loutatidou, B. Chalermthai, P. R. Marpu, and H. A. Arafat, “Capital cost estimation of RO plants: GCC countries versus southern Europe,” *Desalination*, vol. 347, pp. 103–111, 2014.
- [365] C. Upeksha and Christian Breyer, “Learning Curve for Seawater Reverse Osmosis Desalination Plants: Capital Cost Trend of the Past, Present, and Future,” *Water Resources Research*, vol. 53, no. 12, pp. 10523–10538, 2017.
- [366] Danfoss, “Understanding the cost drivers of SWRO,” 2021.
- [367] Eurostat, “Energy inflation rate continues upward hike, hits 27%.” Accessed: Jun. 22, 2022. [Online]. Available: <https://ec.europa.eu/eurostat/web/products-eurostat-news/-/ddn-20220225-2>
- [368] “Majority of New Renewables Undercut Cheapest Fossil Fuel on Cost,” International Renewable Energy Agency. Accessed: Jun. 30, 2022. [Online]. Available: <https://www.irena.org/newsroom/pressreleases/2021/Jun/Majority-of-New-Renewables-Undercut-Cheapest-Fossil-Fuel-on-Cost>
- [369] A. Alkaisi, R. Mossad, and A. Sharifian-Barforoush, “A Review of the Water Desalination Systems Integrated with Renewable Energy,” *Energy Procedia*, vol. 110, pp. 268–274, 2017.
- [370] K. Elmaadawy *et al.*, “Optimal sizing and techno-enviro-economic feasibility assessment of large-scale reverse osmosis desalination powered with hybrid renewable energy sources,” *Energy Conversion and Management*, vol. 224, p. 113377, 2020.
- [371] G. Kyriakarakos, G. Papadakis, F. Calise, and E. Poursmaeil, “Is Small Scale Desalination Coupled with Renewable Energy a Cost-Effective Solution?,” *Applied Sciences 2021, Vol. 11, Page 5419*, vol. 11, no. 12, p. 5419, 2021.
- [372] E. T. Sayed, A. G. Olabi, K. Elsaid, M. Al Radi, R. Alqadi, and M. Ali Abdelkareem, “Recent progress in renewable energy based-desalination in the Middle East and North Africa MENA region,” *Journal of Advanced Research*, 2022.
- [373] M. T. Mito, X. Ma, H. Albuflasa, and P. A. Davies, “Reverse osmosis (RO) membrane desalination driven by wind and solar photovoltaic (PV) energy: State of the art and

- challenges for large-scale implementation,” *Renewable and Sustainable Energy Reviews*, vol. 112, pp. 669–685, Sep. 2019.
- [374] M. K. Wittholz, B. K. O’Neill, C. B. Colby, and D. Lewis, “Estimating the cost of desalination plants using a cost database,” *Desalination*, vol. 229, no. 1–3, pp. 10–20, Sep. 2008.
- [375] R. Huehmer, D. Water, J. Gomez, J. M. Curl, J. Curl, and K. Moore, “Cost Modelling of Desalination Systems,” *IDA World Congress*, 2011.
- [376] C. Park *et al.*, “Stochastic cost estimation approach for full-scale reverse osmosis desalination plants,” *Journal of Membrane Science*, vol. 364, no. 1–2, pp. 52–64, 2010.
- [377] I. Moch, W. R. Querns, and D. Steward, “WT Cost II Modeling the Capital and Operating Costs of Thermal Desalination Processes Utilizing a Recently Developed Computer Program that Evaluates Membrane Desalting , Electrodialysis , and Ion Exchange Plants,” 2008.
- [378] United States Environmental Protection Agency, “Estimation of cost curves applicable to 2500 gpd to 1 mgd Treatment Plant,” 1979.
- [379] G. Ahmed, A. Bazedi, M. M. Elsayed, and M. Amin, “Comparison between Reverse Osmosis Desalination Cost Estimation Trends,” *Scientific and Engineering Research*, vol. 3, no. October, pp. 56–62, 2016.
- [380] DuPont, “WAVE Design Software UF,” 2021.
- [381] N. Voutchkov, *Desalination Project Cost Estimating and Management*. CRC Press, 2018.
- [382] A. Rohatgi, “WebPlotDigitizer.” Accessed: Mar. 02, 2022. [Online]. Available: <https://automeris.io/WebPlotDigitizer>
- [383] M. Papapetrou, A. Cipollina, U. La Commare, G. Micale, G. Zaragoza, and G. Kosmadakis, “Assessment of methodologies and data used to calculate desalination costs,” *Desalination*, vol. 419, no. June, pp. 8–19, 2017.
- [384] J. Díaz-Caneja and M. Fariñas, “Cost estimation briefing for large seawater reverse osmosis facilities in Spain,” *International Conference on Desalination Costing, MiddleEast Research Center, Lemosos, Cyprus*, pp. 6–8, 2004.

- [385] Y. Dreizin, “Ashkelon seawater desalination project — off-taker’s self costs, supplied water costs, total costs and benefits,” *Desalination*, vol. 190, no. 1–3, pp. 104–116, Apr. 2006.
- [386] R. V. Linares *et al.*, “Life cycle cost of a hybrid forward osmosis e low pressure reverse osmosis system for seawater desalination and wastewater recovery,” *Water Research*, vol. 88, pp. 225–234, 2015.
- [387] M. P. Shahabi, A. McHugh, and G. Ho, “Environmental and economic assessment of beach well intake versus open intake for seawater reverse osmosis desalination,” *Desalination*, vol. 357, pp. 259–266, Feb. 2015.
- [388] Carlsbad Desal Plant, “How We Do It - Carlsbad Desal Plant.” Accessed: Sep. 26, 2023. [Online]. Available: <https://www.carlsbaddesal.com/how-we-do-it.html>
- [389] Payscale EU, “Compensation data and software solutions | Payscale EU.” Accessed: Jun. 28, 2023. [Online]. Available: <https://www.payscale.com/en-eu/>
- [390] Salary.com, “Salary Calculator, Salary Comparison, Compensation Data.” Accessed: Jun. 28, 2023. [Online]. Available: <https://www.salary.com/>
- [391] Glassdoor, “Company Salaries | Glassdoor.” Accessed: Jun. 28, 2023. [Online]. Available: <https://www.glassdoor.ie/Salaries/index.htm>
- [392] ECN, “Desalination presents growing chemical opportunity.” [Online]. Available: <https://www.icis.com/explore/resources/news/2010/06/28/9371401/desalination-presents-growing-chemical-opportunity/>
- [393] A. Williams, “Desalination: Chemical Use in Water Treatment,” *WaterWorld*. Accessed: Sep. 28, 2023. [Online]. Available: <https://www.waterworld.com/home/article/16202099/desalination-chemical-use-in-water-treatment>
- [394] B. Rahimi, J. May, A. Christ, K. Regenauer-Lieb, and H. Tong Chua, “Thermo-economic analysis of two novel low grade sensible heat driven desalination processes,” *Desalination*, vol. 365, pp. 316–328, 2015.
- [395] MEDRC, “Toolbox of Graphic and Numeric Models for Estimating Costs of Seawater Reverse Osmosis Desalination Projects,” 2013.

- [396] U. Caldera, D. Bogdanov, and C. Breyer, “Local cost of seawater RO desalination based on solar PV and wind energy: A global estimate,” *Desalination*, vol. 385, pp. 207–216, 2016.
- [397] M. M. Generous, N. A. A. Qasem, U. A. Akbar, and S. M. Zubair, “Techno-economic assessment of electrodialysis and reverse osmosis desalination plants,” *Separation and Purification Technology*, vol. 272, p. 118875, Oct. 2021.
- [398] N. M. Farhat, C. Christodoulou, P. Placotas, B. Blankert, O. Sallangos, and J. S. Vrouwenvelder, “Cartridge filter selection and replacement: Optimization of produced water quantity, quality, and cost,” *Desalination*, vol. 473, pp. 114172–114172, 2020.
- [399] S. A. Avlonitis, K. Kouroumbas, and N. Vlachakis, “Energy consumption and membrane replacement cost for seawater RO desalination plants,” *Desalination*, vol. 157, no. 1–3, pp. 151–158, 2003.
- [400] blueearthproducts, “Media Cleaning versus Media Replacement.” Accessed: Oct. 17, 2022. [Online]. Available: <https://blueearthproducts.com/media-cleaning-versus-media-replacement-a-cost-comparison/>
- [401] A. Panagopoulos, K. J. Haralambous, and M. Loizidou, “Desalination brine disposal methods and treatment technologies - A review,” *Science of The Total Environment*, vol. 693, p. 133545, Nov. 2019.
- [402] V. B. Jensen and J. L. Darby, “Brine Disposal Options for Small Systems in California’s Central Valley,” *Journal - American Water Works Association*, vol. 108, no. 5, pp. E276–E289, 2016.
- [403] J. R. Ziolkowska and R. Reyes, “Prospects for Desalination in the United States- Experiences From California, Florida, and Texas,” in *Competition for Water Resources: Experiences and Management Approaches in the US and Europe*, no. 2013, Elsevier Inc., 2017, pp. 298–316.
- [404] L. Birnhack and O. Lahav, “Post-Treatment of Desalinated Water-Chemistry, Design, Engineering, and Implementation,” in *Sustainable Desalination Handbook: Plant Selection, Design and Implementation*, Elsevier Inc., 2018, pp. 305–350.
- [405] “The Selection of UF as Pretreatment for Seawater Desalination.” Accessed: Feb. 01, 2022. [Online]. Available: <https://www.amtaorg.com/the-selection-of-uf-as-pretreatment-for-seawater-desalination>

- [406] F. Knops, S. van Hoof, H. Futselaar, and L. Broens, "Economic evaluation of a new ultrafiltration membrane for pretreatment of seawater reverse osmosis," *Desalination*, vol. 203, no. 1–3, pp. 300–306, 2007.
- [407] A. Al-Kaabi, H. Al-Sulaiti, T. Al-Ansari, and H. R. Mackey, "Assessment of water quality variations on pretreatment and environmental impacts of SWRO desalination," *Desalination*, vol. 500, p. 114831, Mar. 2021.
- [408] A. Aljuwaisseri, E. Aleisa, and K. Alshayji, "Environmental and economic analysis for desalinating seawater of high salinity using reverse osmosis: a life cycle assessment approach," *Environ Dev Sustain*, vol. 25, pp. 4539–4574, 2023.
- [409] A. Hafez and S. El-Manharawy, "Economics of seawater RO desalination in the Red Sea region, Egypt. Part 1. A case study," *Desalination*, vol. 153, no. 1–3, pp. 335–347, Feb. 2003.
- [410] F. Mohammadi, M. Sahraei-Ardakani, Y. Al-Abdullah, and G. T. Heydt, "Cost-Benefit Analysis of Desalination: A Power Market Opportunity," *Electric Power Components and Systems*, vol. 48, no. 11, pp. 1091–1101, 2020.
- [411] R. A. Mohammed and R. J. M. Alkhafaja, "Review: Water Desalination Cost," *Engineering sciences*, vol. 1, 2023.

APPENDIX

APPENDIX A : ONTOSWRO DESCRIPTION

Table - 1: An overview of object properties utilised in OntoSWRO, focusing on their definitions, classes, and subclasses

Object Properties	definition	Class	Subclasses
hasScale	“Plant Scale Relation” is utilised to establish the quantitative scale of a desalination facility, specifically pertaining to its capacity.	Scale	Small, Medium, Large
hasGeographicalFeature	The “Geographical Relation” aims to build the spatial context surrounding a desalination plant, taking into account different geographical elements that may have an influence on its operation or impact.	GeographicalFeature	BeachErosion, HighSandDepth, Limestone Muddy, NaturalWaveFlushing, PermeableSand, Shallow, SpaciousLand, StableSandBeach
hasIssueOf	The “Issue Association Relation” is a relationship that links classes in the desalination ontology with probable obstacles or problems that may occur during the desalination process	issue	HardInspection, HighDisposableSolid, Hypersaline HighLongTermMaintenance, HighToxic, LowQuality , HighNoise, HighEnergyConsumption, HighConstructionCost, AnaerobicBacteria, HighMaintenance, ComplexToOperate, LargeFootprint, LowChlorineResistance, Leakage, LowDurability, LowFlexibility, LowPermeability, LowPressureSurgeHandling, Medium- HighFoulingPotential, None-LowFoulingPotential, OverFlush, PlantShutDown, ReduceCartridgeLifespan, ReduceROLifespan, SeashoreBedContamination, VariableWaterQuality, Vegetation,
hasLocation	The class “Location relation” refers to the precise physical or position of a class within the infrastructure of a desalination plant.	Location	IndustrialSites, OilLeaks, SeasonalRain SandyCoastWithLowGradient, OffSeaShore, RockyCoast, AdditionalLayer, AboveSeaFloor, Forebay, PowerPlant, Port, SecondLayer, River, NearshoreOilStorageTank, MENA, ParkingLots, Seashore, ThirdLayer, ShipChannel. TopLayer, UnderSea, UnderSeaFloor, WasteDischarge, WastewaterTreatmentPlant

Object Properties	definition	Class	Subclasses
hasEnvironmentalImpact	Relation of “Environmental Impact” specification provides clarification on the category or type of environmental consequences that can be caused by other classes inside the ontology	EnvironmentalImpact	ExposeJellyfish, High, Low, LowEntrainment, LowImpingement, MarineLife, Moderate, ModerateEntrainment, ModerateImpingement
hasPump	This Relation outline type of pump that suitable for specific classes	Pump	HorizontalCentrifugal, HorizontalTurbine, ReciprocatingHP, SegmentedRingMultistage, SplitCaseMultistageCentrifugal, Submersible, VerticalTurbine
hasFeatureOf	The “Feature Relation” refers to the integration of special features or unique attributes that are related with a specific class.	Feature	LowToxic, HighPurity, LowMaintenance, EasyToOperate, HighCorrosion, NoConstructionCost, HighChlorineResistance, HighPermeability, EasyInspection, HighStrength, MediumStrength, MediumFlexibility, HighRejection, LowDisposableSolid, LowEnergyConsumption, LowConstructionCost, HighDurability HighQuality, HighPressureSurgeHandling, LowFouling, LowCorrosion, LowPurity, ReduceBiogrowth, ReducepH, SeparateStructure, SmallFootprint
hasComponent	The “Component” relation serves to construct connections between classes related to desalination and their individual parts or components	Component	CaissonScreen, CollectorPipe, Diffuser, FilterPack, InletAndSuctionWell, Lateral, OilSpillLeakDetection, PumpRoom, RefrigerationUnit, SuctionBellVelocity, PumpHead1, PumpHead2, PumpHead3, SurfaceSeal, VaporHeater, Vaporiser, WellScreen, WellCasing, WellSeal
IsCausedby	This relation elucidates the various aspects and sources that contribute to the presence of fouling agents in the desalination process.	FoulantType	Colloidal, NaturalOrganicMatter, Organic, Particulate, Scaling

Object Properties	definition	Class	Subclasses
hasMaterialOf	Relation pertains to the explicit material composition of specified categories, providing an account of the components utilised in their construction..	Material	HDPE, Polypropylene, Polyethersulfone, Metal, GlassReinforcedPlastic, PolyvinylideneDifluoride, Concrete, JettiesStoneRock, Steel
hasSedimentOf	The Sedimentation relation refers to the specific sedimentation approach utilised in the design and operation of certain equipment within the context of desalination.	SedimentType	Anthracite, Clay, CoarseSand, Garnet, GranularActivatedCarbon, Gravel, Sand, Pumice
hasImpactOn	This relation is utilised to explicate the effect or implications that one class may exert on another inside the ontology.		
IsAppliedWith	Relation is established to delineate the classes that need be concurrently applied or utilised together to ensure the effectiveness of desalination operations		
isNotSuitableFor	Relation outlines cases in which certain classes are not suited for particular settings, places, material types, or owing to specific concerns	ParticlesType	Algae, Bacteria, Detritus, FineDebris, Fungi, Plankton, Silt
isSuitableFor	Refers to the limited the suitability of some classes, which restricts their relevance to specific and specialised scenarios or circumstances.		

APPENDIX B : OntoSWRO Matrix

Table - 2: Matrix for Case 2.

120000 m ³ /d				
River, valley				
Seasonal rain				
High algal bloom, Chlorophyll-a = 4.8 µg,				
Algal count 48,000			Sodium Hypochlorite, Sulfuric Acid = reduce biogrowth	
32000 m ²				
Temp = 28 - 32				
Turbidity = 32 - 100				
TDS = 38000				
SDI = 13				
TOC = 4				
Transmissivity = 800				
Depth = 12				
Distance = 800 m				
	Offshore	Screening	Chemical treatment	Pump station

Coagulation															
Mixing system															
Lamella															
DAF															
Dual media gravity															
Tri media - gravity															

Total point		
Additional auxiliary		Velocity cap, coarse-band screen
Corrosion-resistant		
Environmental impact		
MENA		
High rejection		
Low energy		
Easy to operate		
Easy to maintain		
	Offshore	Screening

Posttreatment	Surface discharge

6	6	6		
Two stage, dual media, cartridge filter	Two stage, Tri media, cartridge filter	Submerged system, microscreen must be used		Sodium Hexameta phosphate
Need clarifier in this case		Submerged system		
			With media filtration only	
			With media filtration only	
Dual media gravity	Tri media - gravity	Membrane	Cartridge filter	Chemical treatment

Reverse osmosis			SW30HRLE400, SW30HRLE400	SW30HRLE400						
Centrifugated (Pelton wheel)										Up to the user
PXERD										
Posttreatment					chlorine gas is commonly applied for disinfection					
Surface discharge										

Guideline

Has an issue

Meet the criteria



Opposite to the requirement

Meet criteria if the followed equipment used only



APPENDIX C : EQUATION EXPLANATION

The determination of brine salinity in membrane processes can be achieved through the application of mass balance principles. Assuming that the feed flow rate is the sum of the permeate flow rate and brine flow rate, and assuming also that salt is not deposited within the RO system. Therefore, the mass balance equation is expressed as follows:

$$Q_f C_f = Q_p C_p + Q_c C_c \quad \text{Eq 0.1}$$

However, in practical RO systems, some salt deposition occurs, and the membrane rejection is not 100%. Therefore, an alternate formula is employed. Introducing parameters that are known, for instance, the recovery rate relationship is established as follows:

$$R = \frac{Q_p}{Q_f} = \frac{Q_f - Q_c}{Q_f} \quad \text{Eq 0.2}$$

In the context of membrane separation, salt rejection (SR) refers to a membrane's capacity to restrict the passage of dissolved salts and other solutes while permitting the passage of the solvent. It is a measurement of the membrane's efficiency in producing desalinated or purified water by retaining salts on one side of the membrane while allowing the pure solvent to pass through. The proportion of salt rejected is determined by finding the difference between the salt concentrations in the feed solution and the permeate solution over feed concentration as presented below.

$$SR = 1 - SP \quad \text{Eq 0.3}$$

Salt passage (SP) is the opposite of salt rejection which known as the proportion of salt or dissolved ions that pass through the membrane during a separation process that can be calculated using Equation 0.4

$$SP = \frac{C_p}{C_f} \quad \text{Eq 0.4}$$

By dividing both sides of the mass balance equation by Q_f , the obtained equation is represented as follows:

$$C_f = \frac{Q_p}{Q_f} C_p + \frac{Q_c}{Q_f} C_c \quad \text{Eq 0.5}$$

Utilising Equation 0.2 and substituting Equation 0.4 into Equation 0.3 to eliminate C_p , Equation 0.5 can be rearranged as follows: To rearrange the equation to include more known parameters, equation 0.2 would be utilised and equation 0.4 would be substituted in equation 0.3, which will be employed to replace the parameter C_p .

$$C_f - C_f R(1 - SR) = \frac{Q_c}{Q_f} C_c \quad \text{Eq 0.6}$$

Furthermore, the recovery is also equal to $R = 1 - \frac{Q_c}{Q_f}$, therefore:

$$C_f - C_f R(1 - SR) = (1 - R) C_c \quad \text{Eq 0.7}$$

Finally, the equation for brine concentration can be derived as follows:

$$C_c = \frac{C_f(1 - R(1 - SR))}{(1 - R)} \quad \text{Eq 0.8}$$

APPENDIX D : RO MODEL EVALUATION

Table - 3: Obtained result from WAVE model for different temperature

WAVE Model								
Temp	Salinity	SEC (kWh/m ³)	B	A	C _p (mg/L)	Applied pressure	concentration pressure	pressure drop
15	36045.	4.1	-	0.8187	124.0	52.9	51.5	1.4
18	36043	4.06	-	0.8696	147.8	52.5	51.0	1.5
20	36041	4.03	-	0.8974	165.8	52.2	50.7	1.5
22	36041	4.01	-	0.9272	185.7	51.9	50.5	1.4
24	36039	4	-	0.9589	207.6	51.7	50.4	1.3
25	36039	3.99	-	0.9722	219.4	51.6	50.3	1.3
28	36039	3.98	-	1.0000	257.9	51.6	50.3	1.3
30	36039	3.98	-	1.0219	286.6	51.5	50.3	1.2
32	36037	3.98	-	1.0448	318.0	51.5	50.3	1.2
34	36037	3.98	-	1.0606	353.3	51.5	50.4	1.1

Table - 4: Obtained result from research model for different temperature

Research Model									
Temp	Salinity	SEC (kWh/m ³)	B	A	C _p (mg/L)	Applied pressure	concentration pressure	pressure drop	CPF
15.00	36045.00	4.29	0.0560	1.00	171.87	55.99	54.937	1.05	1.055
18.00	36043.00	4.21	0.0655	1.12	188.68	54.99	53.941	1.05	1.053
20.00	36041.00	4.17	0.0655	1.20	200.55	54.42	53.372	1.05	1.055
22.00	36041.00	4.13	0.0696	1.29	212.99	53.93	52.874	1.06	1.054
24.00	36039.00	4.10	0.0740	1.38	226.01	53.49	52.437	1.05	1.051
25.00	36039.00	4.08	0.0762	1.43	232.74	53.29	52.241	1.05	1.051
28.00	36039.00	4.05	0.0832	1.56	253.90	52.90	51.846	1.05	1.051
30.00	36039.00	4.03	0.0882	1.65	268.79	52.68	51.630	1.05	1.050
32.00	36037.00	4.02	0.0934	1.75	284.66	52.50	51.446	1.05	1.049
34.00	36037.00	4.01	0.0988	1.85	300.55	52.35	51.296	1.05	1.049

Table - 5: Obtained result from Salini-Rodriguez et al model for different temperature

Salini-Rodriguez et al Model								
Temp	Salinity	Energy	B	A	C _p (mg/L)	Applied pressure	Brine pressure	CPF
15.00	36045	3.97	0.0762	1.39	304.4	51.83	50.779	1.055
18.00	36043	3.97	0.0762	1.39	304.4	51.83	50.779	1.055
20.00	36039	3.97	0.0762	1.39	304.4	51.83	50.773	1.055
22.00	36041	3.97	0.0762	1.39	304.4	51.83	50.779	1.055
24.00	36039	3.97	0.0762	1.39	304.4	51.83	50.779	1.055
25.00	36039	3.97	0.0762	1.39	304.4	51.83	50.773	1.055
28.00	36039	3.97	0.0762	1.39	304.4	51.83	50.779	1.055
30.00	36039	3.97	0.0762	1.39	304.4	51.83	50.779	1.055
32.00	36039	3.97	0.0762	1.39	304.4	51.83	50.773	1.055
34.00	36039	3.97	0.0762	1.39	304.4	51.83	50.773	1.055

Table - 6: Obtained result from WAVE and this research model for different salinities

Temp	Salinity	Energy	B	A	C _p (mg/L)	Applied pressure	Brine pressure	pressure drop
Research model								
25.00	32,945	3.71	0.0762	1.43	206.94	48.48	47.425	1.055
25.00	36039.00	4.08	0.0762	1.43	232.74	53.29	52.241	1.05
25.00	41,199	4.55	0.0762	1.43	265.61	59.45	58.394	1.06
Wave								
25.00	32,945	3.66	-	1.045	199.8	47.3	46	1.3
25.00	36039	3.99	-	0.972	219.4	51.6	50.3	1.3
25.00	41,199	4.57	-	0.854	252.1	59.1	57.8	1.3

APPENDIX E COST DATABASE

Table - 7: CAPEX for surface intake system

Desalination plant intake flow (m ³ /day)	Onshore intake (\$)	Offshore intake concrete (\$/meter)	Offshore intake HDPE (\$/metre)
1000	142,033.86	1,120.34	386.49
2000	243,890.73	1,934.61	600.41
5000	498,412.00	3,983.00	1,074.86
7000	647,990.09	5,192.46	1,331.12
8,000	719,121.18	5,768.69	1,449.02
10,000	855,838.64	6,877.83	1,669.79
12,000	986,627.60	7,940.62	1,874.92
14,000	1,112,683.78	8,966.34	2,067.90
16,000	1,234,825.18	9,961.36	2,251.05
18,000	1,353,643.94	10,930.30	2,426.02
20,000	1,469,586.95	11,876.64	2,594.02
22,000	1,583,002.43	12,803.10	2,756.00
24,000	1,694,168.72	13,711.85	2,912.70
26,000	1,803,312.95	14,604.68	3,064.69
28,000	1,910,623.67	15,483.06	3,212.49
30,000	2,016,259.70	16,348.24	3,356.48
32,000	2,120,356.44	17,201.27	3,497.01
34,000	2,223,030.62	18,043.06	3,634.37
36,000	2,324,383.81	18,874.42	3,768.82
38,000	2,424,505.06	19,696.05	3,900.57
40,000	2,523,473.12	20,508.56	4,029.82
42,000	2,621,358.00	21,312.50	4,156.73
44,000	2,718,222.34	22,108.37	4,281.45
46,000	2,814,122.50	22,896.61	4,404.13
48,000	2,909,109.41	23,677.61	4,524.88
50,000	3,003,229.31	24,451.75	4,643.80
52,000	3,096,524.34	25,219.35	4,761.01
54,000	3,189,033.07	25,980.72	4,876.58
56,000	3,280,790.90	26,736.14	4,990.60
58,000	3,371,830.43	27,485.86	5,103.15
60,000	3,462,181.77	28,230.12	5,214.29
62,000	3,551,872.83	28,969.14	5,324.09
64,000	3,640,929.50	29,703.12	5,432.61
66,000	3,729,375.90	30,432.26	5,539.89

Desalination plant intake flow (m ³ /day)	Onshore intake (\$)	Offshore intake concrete (\$/meter)	Offshore intake HDPE (\$/metre)
68,000	3,817,234.52	31,156.74	5,646.00
70,000	3,904,526.38	31,876.71	5,750.98
72,000	3,991,271.19	32,592.33	5,854.87
74,000	4,077,487.44	33,303.76	5,957.71
76,000	4,163,192.50	34,011.12	6,059.54
78,000	4,248,402.74	34,714.54	6,160.40
80,000	4,333,133.61	35,414.16	6,260.33
82,000	4,417,399.68	36,110.07	6,359.34
84,000	4,501,214.75	36,802.40	6,457.48
86,000	4,584,591.90	37,491.25	6,554.77
88,000	4,667,543.51	38,176.71	6,651.25
90,000	4,750,081.35	38,858.87	6,746.92
92,000	4,832,216.63	39,537.83	6,841.82
94,000	4,913,959.99	40,213.67	6,935.98
96,000	4,995,321.58	40,886.47	7,029.40
98,000	5,076,311.09	41,556.31	7,122.12
100,000	5,156,937.77	42,223.25	7,214.16
102,000	5,237,210.43	42,887.38	7,305.52
104,000	5,317,137.55	43,548.75	7,396.23
106,000	5,396,727.20	44,207.43	7,486.31
108,000	5,475,987.14	44,863.48	7,575.78
110,000	5,554,924.81	45,516.96	7,664.64
112,000	5,633,547.34	46,167.93	7,752.91
114,000	5,711,861.58	46,816.44	7,840.61
116,000	5,789,874.12	47,462.55	7,927.75
118,000	5,867,591.30	48,106.29	8,014.35
120,000	5,945,019.21	48,747.73	8,100.41
122,000	6,022,163.72	49,386.91	8,185.95
124,000	6,099,030.49	50,023.87	8,270.99
126,000	6,175,624.98	50,658.66	8,355.52
128,000	6,251,952.46	51,291.32	8,439.56
130,000	6,328,017.99	51,921.88	8,523.13
132,000	6,403,826.50	52,550.40	8,606.23
134,000	6,479,382.72	53,176.90	8,688.88
136,000	6,554,691.24	53,801.42	8,771.07
138,000	6,629,756.50	54,423.99	8,852.83
140,000	6,704,582.79	55,044.66	8,934.15
142,000	6,779,174.28	55,663.45	9,015.06

Desalination plant intake flow (m ³ /day)	Onshore intake (\$)	Offshore intake concrete (\$/meter)	Offshore intake HDPE (\$/metre)
144,000	6,853,534.99	56,280.40	9,095.54
146,000	6,927,668.82	56,895.53	9,175.63
148,000	7,001,579.56	57,508.89	9,255.31
150,000	7,075,270.89	58,120.48	9,334.60
152,000	7,148,746.37	58,730.35	9,413.51
154,000	7,222,009.45	59,338.53	9,492.04
156,000	7,295,063.51	59,945.03	9,570.20
158,000	7,367,911.80	60,549.89	9,647.99
160,000	7,440,557.49	61,153.12	9,725.43
162,000	7,513,003.68	61,754.77	9,802.51
164,000	7,585,253.36	62,354.83	9,879.25
166,000	7,657,309.46	62,953.35	9,955.65
168,000	7,729,174.81	63,550.35	10,031.71
170,000	7,800,852.19	64,145.84	10,107.44
172,000	7,872,344.28	64,739.85	10,182.85
174,000	7,943,653.72	65,332.39	10,257.94
176,000	8,014,783.05	65,923.50	10,332.72
178,000	8,085,734.78	66,513.18	10,407.19
180,000	8,156,511.34	67,101.46	10,481.35
182,000	8,227,115.09	67,688.35	10,555.22
184,000	8,297,548.36	68,273.89	10,628.78
186,000	8,367,813.40	68,858.07	10,702.06
188,000	8,437,912.41	69,440.92	10,775.05
190,000	8,507,847.55	70,022.47	10,847.76
192,000	8,577,620.91	70,602.71	10,920.19
194,000	8,647,234.56	71,181.68	10,992.35
196,000	8,716,690.50	71,759.38	11,064.23
198,000	8,785,990.69	72,335.84	11,135.85
200,000	8,855,137.05	72,911.06	11,207.20
202,000	8,924,131.45	73,485.07	11,278.30
204,000	8,992,975.72	74,057.87	11,349.14
206,000	9,061,671.67	74,629.49	11,419.73
208,000	9,130,221.04	75,199.92	11,490.06
210,000	9,198,625.55	75,769.20	11,560.15
212,000	9,266,886.88	76,337.33	11,630.00
214,000	9,335,006.69	76,904.33	11,699.61
216,000	9,402,986.58	77,470.20	11,768.98
218,000	9,470,828.13	78,034.97	11,838.12

Desalination plant intake flow (m ³ /day)	Onshore intake (\$)	Offshore intake concrete (\$/meter)	Offshore intake HDPE (\$/metre)
220,000	9,538,532.89	78,598.64	11,907.03
222,000	9,606,102.37	79,161.22	11,975.71
224,000	9,673,538.06	79,722.73	12,044.16
226,000	9,740,841.41	80,283.18	12,112.39
228,000	9,808,013.86	80,842.58	12,180.40
230,000	9,875,056.80	81,400.94	12,248.20
232,000	9,941,971.61	81,958.27	12,315.78
234,000	10,008,759.62	82,514.58	12,383.15
236,000	10,075,422.17	83,069.89	12,450.31
238,000	10,141,960.55	83,624.20	12,517.26
240,000	10,208,376.02	84,177.53	12,584.00
242,000	10,274,669.85	84,729.88	12,650.55
244,000	10,340,843.25	85,281.26	12,716.89
246,000	10,406,897.42	85,831.69	12,783.04
248,000	10,472,833.56	86,381.17	12,848.99
250,000	10,538,652.81	86,929.71	12,914.75
252,000	10,604,356.32	87,477.32	12,980.31
254,000	10,669,945.21	88,024.01	13,045.69
256,000	10,735,420.58	88,569.79	13,110.88
258,000	10,800,783.50	89,114.67	13,175.88
260,000	10,866,035.05	89,658.65	13,240.70
262,000	10,931,176.27	90,201.75	13,305.34
264,000	10,996,208.18	90,743.96	13,369.80
266,000	11,061,131.79	91,285.31	13,434.08
268,000	11,125,948.10	91,825.80	13,498.19
270,000	11,190,658.08	92,365.43	13,562.12
272,000	11,255,262.69	92,904.22	13,625.88
274,000	11,319,762.87	93,442.17	13,689.47
276,000	11,384,159.56	93,979.29	13,752.88
278,000	11,448,453.67	94,515.58	13,816.14
280,000	11,512,646.10	95,051.05	13,879.22
282,000	11,576,737.74	95,585.72	13,942.15
284,000	11,640,729.45	96,119.58	14,004.91
286,000	11,704,622.09	96,652.65	14,067.50
288,000	11,768,416.51	97,184.93	14,129.94
290,000	11,832,113.55	97,716.42	14,192.23
292,000	11,895,714.01	98,247.14	14,254.35
294,000	11,959,218.70	98,777.09	14,316.32

Desalination plant intake flow (m ³ /day)	Onshore intake (\$)	Offshore intake concrete (\$/meter)	Offshore intake HDPE (\$/metre)
296,000	12,022,628.43	99,306.27	14,378.14
298,000	12,085,943.96	99,834.70	14,439.80
300,000	12,149,166.08	100,362.38	14,501.32
302,000	12,212,295.54	100,889.31	14,562.68
304,000	12,275,333.09	101,415.51	14,623.90
306,000	12,338,279.47	101,940.97	14,684.97
308,000	12,401,135.40	102,465.70	14,745.90
310,000	12,463,901.60	102,989.71	14,806.68
312,000	12,526,578.77	103,513.01	14,867.32
314,000	12,589,167.61	104,035.59	14,927.81
316,000	12,651,668.81	104,557.47	14,988.17
318,000	12,714,083.05	105,078.66	15,048.39
320,000	12,776,410.98	105,599.14	15,108.47
322,000	12,838,653.27	106,118.94	15,168.41
324,000	12,900,810.57	106,638.05	15,228.22
326,000	12,962,883.51	107,156.49	15,287.89
328,000	13,024,872.73	107,674.25	15,347.43
330,000	13,086,778.85	108,191.35	15,406.84
332,000	13,148,602.48	108,707.78	15,466.12
334,000	13,210,344.23	109,223.55	15,525.26
336,000	13,272,004.70	109,738.67	15,584.28
338,000	13,333,584.47	110,253.13	15,643.17
340,000	13,395,084.13	110,766.96	15,701.93
342,000	13,456,504.25	111,280.14	15,760.57
344,000	13,517,845.41	111,792.69	15,819.08
346,000	13,579,108.15	112,304.61	15,877.47
348,000	13,640,293.04	112,815.90	15,935.73
350,000	13,701,400.62	113,326.56	15,993.88
352,000	13,762,431.42	113,836.61	16,051.90
354,000	13,823,385.98	114,346.05	16,109.80
356,000	13,884,264.83	114,854.88	16,167.59
358,000	13,945,068.47	115,363.10	16,225.25
360,000	14,005,797.44	115,870.72	16,282.80
362,000	14,066,452.22	116,377.74	16,340.23
364,000	14,127,033.32	116,884.17	16,397.55
366,000	14,187,541.24	117,390.01	16,454.75
368,000	14,247,976.46	117,895.26	16,511.84
370,000	14,308,339.46	118,399.94	16,568.81

Desalination plant intake flow (m ³ /day)	Onshore intake (\$)	Offshore intake concrete (\$/meter)	Offshore intake HDPE (\$/metre)
372,000	14,368,630.72	118,904.03	16,625.67
374,000	14,428,850.71	119,407.55	16,682.42
376,000	14,488,999.90	119,910.51	16,739.06
378,000	14,549,078.74	120,412.89	16,795.59
380,000	14,609,087.68	120,914.71	16,852.02
382,000	14,669,027.18	121,415.97	16,908.33
384,000	14,728,897.68	121,916.68	16,964.54
386,000	14,788,699.62	122,416.84	17,020.64
388,000	14,848,433.43	122,916.44	17,076.63
390,000	14,908,099.54	123,415.50	17,132.52
392,000	14,967,698.37	123,914.02	17,188.30
394,000	15,027,230.34	124,412.00	17,243.98
396,000	15,086,695.86	124,909.44	17,299.56
398,000	15,146,095.35	125,406.35	17,355.04
400,000	15,205,429.21	125,902.74	17,410.41

Table - 8: CAPEX for subsurface intake system

Well type	Typical production capacity of individual well (m ³ /day)	Cost of individual well (\$ million)
Vertical	100.0 - 8640	0.2 - 1.5
Horizontal radial collector	500 - 38,880	1.3 - 6.0
Slant	500 - 12,960	0.8 - 2.8
HDD	100 - 5000	0.4 - 2.0
Infiltration galleries	100 - 50,000	0.5 - 27.0

Table - 9: CAPEX for pump station

Desalination plant intake flow (m ³ /day)	Dry well pump (\$)	Wet well pump (\$)
1000	29,535.44	14,051.34
2000	54,040.72	26,579.39
5000	120,106.26	61,729.20
7000	161,038.91	84,114.33
8,000	180,915.85	95,104.13
10,000	219,757.34	116,766.39
12,000	257,607.06	138,080.68
14,000	294,651.45	159,109.89
16,000	331,020.10	179,898.10

Desalination plant intake flow (m ³ /day)	Dry well pump (\$)	Wet well pump (\$)
18,000	366,808.08	200,477.87
20,000	402,088.01	220,874.22
22,000	436,917.05	241,106.96
24,000	471,341.31	261,192.14
26,000	505,398.74	281,143.04
28,000	539,121.09	300,970.81
30,000	572,535.30	320,684.93
32,000	605,664.48	340,293.59
34,000	638,528.68	359,803.89
36,000	671,145.44	379,222.09
38,000	703,530.23	398,553.70
40,000	735,696.81	417,803.63
42,000	767,657.44	436,976.31
44,000	799,423.18	456,075.69
46,000	831,003.99	475,105.38
48,000	862,408.93	494,068.64
50,000	893,646.25	512,968.46
52,000	924,723.51	531,807.58
54,000	955,647.62	550,588.51
56,000	986,424.99	569,313.60
58,000	1,017,061.52	587,984.97
60,000	1,047,562.67	606,604.65
62,000	1,077,933.53	625,174.48
64,000	1,108,178.83	643,696.21
66,000	1,138,302.99	662,171.44
68,000	1,168,310.16	680,601.72
70,000	1,198,204.19	698,988.46
72,000	1,227,988.75	717,333.00
74,000	1,257,667.25	735,636.61
76,000	1,287,242.92	753,900.49
78,000	1,316,718.81	772,125.76
80,000	1,346,097.81	790,313.49
82,000	1,375,382.64	808,464.70
84,000	1,404,575.89	826,580.35
86,000	1,433,680.02	844,661.35
88,000	1,462,697.37	862,708.57
90,000	1,491,630.16	880,722.84
92,000	1,520,480.50	898,704.94
94,000	1,549,250.41	916,655.65

Desalination plant intake flow (m ³ /day)	Dry well pump (\$)	Wet well pump (\$)
96,000	1,577,941.83	934,575.67
98,000	1,606,556.60	952,465.70
100,000	1,635,096.48	970,326.39
102,000	1,663,563.16	988,158.39
104,000	1,691,958.25	1,005,962.30
106,000	1,720,283.31	1,023,738.69
108,000	1,748,539.83	1,041,488.14
110,000	1,776,729.23	1,059,211.19
112,000	1,804,852.90	1,076,908.34
114,000	1,832,912.16	1,094,580.10
116,000	1,860,908.27	1,112,226.94
118,000	1,888,842.48	1,129,849.35
120,000	1,916,715.95	1,147,447.75
122,000	1,944,529.84	1,165,022.59
124,000	1,972,285.24	1,182,574.27
126,000	1,999,983.21	1,200,103.21
128,000	2,027,624.79	1,217,609.80
130,000	2,055,210.97	1,235,094.40
132,000	2,082,742.70	1,252,557.39
134,000	2,110,220.93	1,269,999.11
136,000	2,137,646.54	1,287,419.92
138,000	2,165,020.41	1,304,820.14
140,000	2,192,343.39	1,322,200.10
142,000	2,219,616.29	1,339,560.11
144,000	2,246,839.92	1,356,900.47
146,000	2,274,015.04	1,374,221.48
148,000	2,301,142.40	1,391,523.42
150,000	2,328,222.73	1,408,806.57
152,000	2,355,256.74	1,426,071.20
154,000	2,382,245.11	1,443,317.58
156,000	2,409,188.51	1,460,545.95
158,000	2,436,087.60	1,477,756.58
160,000	2,462,943.00	1,494,949.70
162,000	2,489,755.33	1,512,125.55
164,000	2,516,525.19	1,529,284.36
166,000	2,543,253.16	1,546,426.36
168,000	2,569,939.82	1,563,551.75
170,000	2,596,585.71	1,580,660.76
172,000	2,623,191.39	1,597,753.60

Desalination plant intake flow (m ³ /day)	Dry well pump (\$)	Wet well pump (\$)
174,000	2,649,757.37	1,614,830.46
176,000	2,676,284.17	1,631,891.55
178,000	2,702,772.29	1,648,937.06
180,000	2,729,222.22	1,665,967.18
182,000	2,755,634.45	1,682,982.09
184,000	2,782,009.43	1,699,981.97
186,000	2,808,347.63	1,716,967.00
188,000	2,834,649.49	1,733,937.36
190,000	2,860,915.44	1,750,893.20
192,000	2,887,145.92	1,767,834.70
194,000	2,913,341.34	1,784,762.02
196,000	2,939,502.10	1,801,675.32
198,000	2,965,628.61	1,818,574.74
200,000	2,991,721.26	1,835,460.44
202,000	3,017,780.42	1,852,332.58
204,000	3,043,806.48	1,869,191.28
206,000	3,069,799.79	1,886,036.71
208,000	3,095,760.72	1,902,868.99
210,000	3,121,689.62	1,919,688.26
212,000	3,147,586.83	1,936,494.66
214,000	3,173,452.69	1,953,288.31
216,000	3,199,287.53	1,970,069.35
218,000	3,225,091.67	1,986,837.90
220,000	3,250,865.43	2,003,594.09
222,000	3,276,609.12	2,020,338.04
224,000	3,302,323.05	2,037,069.86
226,000	3,328,007.52	2,053,789.67
228,000	3,353,662.82	2,070,497.60
230,000	3,379,289.24	2,087,193.74
232,000	3,404,887.06	2,103,878.21
234,000	3,430,456.56	2,120,551.13
236,000	3,455,998.02	2,137,212.59
238,000	3,481,511.70	2,153,862.70
240,000	3,506,997.87	2,170,501.56
242,000	3,532,456.78	2,187,129.29
244,000	3,557,888.68	2,203,745.96
246,000	3,583,293.84	2,220,351.69
248,000	3,608,672.49	2,236,946.57
250,000	3,634,024.87	2,253,530.69

Desalination plant intake flow (m ³ /day)	Dry well pump (\$)	Wet well pump (\$)
252,000	3,659,351.22	2,270,104.15
254,000	3,684,651.78	2,286,667.04
256,000	3,709,926.77	2,303,219.44
258,000	3,735,176.42	2,319,761.45
260,000	3,760,400.95	2,336,293.15
262,000	3,785,600.58	2,352,814.63
264,000	3,810,775.51	2,369,325.98
266,000	3,835,925.98	2,385,827.27
268,000	3,861,052.17	2,402,318.59
270,000	3,886,154.30	2,418,800.02
272,000	3,911,232.56	2,435,271.63
274,000	3,936,287.16	2,451,733.51
276,000	3,961,318.29	2,468,185.73
278,000	3,986,326.14	2,484,628.37
280,000	4,011,310.90	2,501,061.50
282,000	4,036,272.75	2,517,485.19
284,000	4,061,211.89	2,533,899.53
286,000	4,086,128.48	2,550,304.57
288,000	4,111,022.71	2,566,700.39
290,000	4,135,894.75	2,583,087.06
292,000	4,160,744.78	2,599,464.65
294,000	4,185,572.96	2,615,833.22
296,000	4,210,379.46	2,632,192.84
298,000	4,235,164.46	2,648,543.57
300,000	4,259,928.10	2,664,885.48
302,000	4,284,670.55	2,681,218.64
304,000	4,309,391.98	2,697,543.10
306,000	4,334,092.53	2,713,858.93
308,000	4,358,772.36	2,730,166.19
310,000	4,383,431.62	2,746,464.94
312,000	4,408,070.46	2,762,755.23
314,000	4,432,689.03	2,779,037.13
316,000	4,457,287.47	2,795,310.70
318,000	4,481,865.93	2,811,575.98
320,000	4,506,424.55	2,827,833.05
322,000	4,530,963.47	2,844,081.94
324,000	4,555,482.83	2,860,322.72
326,000	4,579,982.76	2,876,555.45
328,000	4,604,463.40	2,892,780.17

Desalination plant intake flow (m ³ /day)	Dry well pump (\$)	Wet well pump (\$)
330,000	4,628,924.89	2,908,996.94
332,000	4,653,367.34	2,925,205.81
334,000	4,677,790.89	2,941,406.83
336,000	4,702,195.67	2,957,600.05
338,000	4,726,581.81	2,973,785.52
340,000	4,750,949.43	2,989,963.30
342,000	4,775,298.65	3,006,133.42
344,000	4,799,629.59	3,022,295.95
346,000	4,823,942.37	3,038,450.92
348,000	4,848,237.12	3,054,598.39
350,000	4,872,513.95	3,070,738.39
352,000	4,896,772.97	3,086,870.98
354,000	4,921,014.29	3,102,996.21
356,000	4,945,238.04	3,119,114.11
358,000	4,969,444.33	3,135,224.73
360,000	4,993,633.25	3,151,328.12
362,000	5,017,804.93	3,167,424.32
364,000	5,041,959.46	3,183,513.37
366,000	5,066,096.96	3,199,595.31
368,000	5,090,217.53	3,215,670.19
370,000	5,114,321.27	3,231,738.04
372,000	5,138,408.29	3,247,798.92
374,000	5,162,478.69	3,263,852.85
376,000	5,186,532.56	3,279,899.88
378,000	5,210,570.02	3,295,940.05
380,000	5,234,591.15	3,311,973.40
382,000	5,258,596.05	3,327,999.97
384,000	5,282,584.81	3,344,019.79
386,000	5,306,557.55	3,360,032.91
388,000	5,330,514.33	3,376,039.35
390,000	5,354,455.27	3,392,039.16
392,000	5,378,380.45	3,408,032.38
394,000	5,402,289.96	3,424,019.04
396,000	5,426,183.89	3,439,999.17
398,000	5,450,062.33	3,455,972.82
400,000	5,473,925.37	3,471,940.01

Table - 10: CAPEX for screening equipments

Desalination plant intake flow (m ³ /day)	Drum screen (\$)	Band screen (\$)	Wedgewire (\$)	Microscreen (\$)
1000	12,148.37	4,248.97	14,391.80	20,456.80
2000	24,521.77	9,527.60	22,400.60	31,212.80
5000	62,056.10	27,706.61	46,367.00	63,408.80
7000	87,268.19	41,003.66	62,294.60	84,812.80
8,000	99,912.36	47,905.26	70,243.40	95,496.80
10,000	125,261.66	62,127.43	86,111.00	116,828.80
12,000	150,678.92	76,829.77	101,938.60	138,112.80
14,000	176,152.85	91,943.82	117,726.20	159,348.80
16,000	201,675.40	107,419.50	133,473.80	180,536.80
18,000	227,240.52	123,218.48	149,181.40	201,676.80
20,000	252,843.53	139,310.33	164,849.00	222,768.80
22,000	278,480.67	155,670.31	180,476.60	243,812.80
24,000	304,148.86	172,277.86	196,064.20	264,808.80
26,000	329,845.56	189,115.58	211,611.80	285,756.80
28,000	355,568.58	206,168.58	227,119.40	306,656.80
30,000	381,316.07	223,423.90	242,587.00	327,508.80
32,000	407,086.42	240,870.21	258,014.60	348,312.80
34,000	432,878.22	258,497.47	273,402.20	369,068.80
36,000	458,690.21	276,296.75	288,749.80	389,776.80
38,000	484,521.29	294,260.02	304,057.40	410,436.80
40,000	510,370.47	312,380.03	319,325.00	431,048.80
42,000	536,236.85	330,650.20	334,552.60	451,612.80
44,000	562,119.62	349,064.54	349,740.20	472,128.80
46,000	588,018.05	367,617.55	364,887.80	492,596.80
48,000	613,931.46	386,304.18	379,995.40	513,016.80
50,000	639,859.25	405,119.75	395,063.00	533,388.80
52,000	665,800.83	424,059.95	410,090.60	553,712.80
54,000	691,755.69	443,120.76	425,078.20	573,988.80
56,000	717,723.35	462,298.43	440,025.80	594,216.80
58,000	743,703.34	481,589.47	454,933.40	614,396.80
60,000	769,695.25	500,990.59	469,801.00	634,528.80
62,000	795,698.69	520,498.74	484,628.60	654,612.80
64,000	821,713.29	540,111.02	499,416.20	674,648.80
66,000	847,738.71	559,824.69	514,163.80	694,636.80
68,000	873,774.62	579,637.20	528,871.40	714,576.80
70,000	899,820.72	599,546.10	543,539.00	734,468.80
72,000	925,876.72	619,549.09	558,166.60	754,312.80
74,000	951,942.35	639,643.98	572,754.20	774,108.80
76,000	978,017.35	659,828.70	587,301.80	793,856.80
78,000	1,004,101.48	680,101.26	601,809.40	813,556.80
80,000	1,030,194.51	700,459.78	616,277.00	833,208.80
82,000	1,056,296.21	720,902.45	630,704.60	852,812.80

Desalination plant intake flow (m ³ /day)	Drum screen (\$)	Band screen (\$)	Wedgewire (\$)	Microscreen (\$)
84,000	1,082,406.39	741,427.57	645,092.20	872,368.80
86,000	1,108,524.83	762,033.50	659,439.80	891,876.80
88,000	1,134,651.36	782,718.64	673,747.40	911,336.80
90,000	1,160,785.78	803,481.51	688,015.00	930,748.80
92,000	1,186,927.93	824,320.66	702,242.60	950,112.80
94,000	1,213,077.65	845,234.69	716,430.20	969,428.80
96,000	1,239,234.76	866,222.28	730,577.80	988,696.80
98,000	1,265,399.12	887,282.15	744,685.40	1,007,916.80
100,000	1,291,570.59	908,413.05	758,753.00	1,027,088.80
102,000	1,317,749.01	929,613.81	772,780.60	1,046,212.80
104,000	1,343,934.27	950,883.27	786,768.20	1,065,288.80
106,000	1,370,126.23	972,220.33	800,715.80	1,084,316.80
108,000	1,396,324.75	993,623.93	814,623.40	1,103,296.80
110,000	1,422,529.74	1,015,093.03	828,491.00	1,122,228.80
112,000	1,448,741.06	1,036,626.63	842,318.60	1,141,112.80
114,000	1,474,958.60	1,058,223.78	856,106.20	1,159,948.80
116,000	1,501,182.27	1,079,883.54	869,853.80	1,178,736.80
118,000	1,527,411.95	1,101,605.02	883,561.40	1,197,476.80
120,000	1,553,647.54	1,123,387.32	897,229.00	1,216,168.80
122,000	1,579,888.95	1,145,229.61	910,856.60	1,234,812.80
124,000	1,606,136.08	1,167,131.07	924,444.20	1,253,408.80
126,000	1,632,388.85	1,189,090.89	937,991.80	1,271,956.80
128,000	1,658,647.15	1,211,108.30	951,499.40	1,290,456.80
130,000	1,684,910.92	1,233,182.55	964,967.00	1,308,908.80
132,000	1,711,180.06	1,255,312.91	978,394.60	1,327,312.80
134,000	1,737,454.49	1,277,498.67	991,782.20	1,345,668.80
136,000	1,763,734.14	1,299,739.13	1,005,129.80	1,363,976.80
138,000	1,790,018.93	1,322,033.63	1,018,437.40	1,382,236.80
140,000	1,816,308.79	1,344,381.50	1,031,705.00	1,400,448.80
142,000	1,842,603.64	1,366,782.11	1,044,932.60	1,418,612.80
144,000	1,868,903.42	1,389,234.85	1,058,120.20	1,436,728.80
146,000	1,895,208.06	1,411,739.10	1,071,267.80	1,454,796.80
148,000	1,921,517.49	1,434,294.27	1,084,375.40	1,472,816.80
150,000	1,947,831.65	1,456,899.80	1,097,443.00	1,490,788.80
152,000	1,974,150.48	1,479,555.11	1,110,470.60	1,508,712.80
154,000	2,000,473.91	1,502,259.66	1,123,458.20	1,526,588.80
156,000	2,026,801.89	1,525,012.92	1,136,405.80	1,544,416.80
158,000	2,053,134.36	1,547,814.36	1,149,313.40	1,562,196.80
160,000	2,079,471.27	1,570,663.48	1,162,181.00	1,579,928.80
162,000	2,105,812.55	1,593,559.77	1,175,008.60	1,597,612.80
164,000	2,132,158.16	1,616,502.75	1,187,796.20	1,615,248.80
166,000	2,158,508.04	1,639,491.95	1,200,543.80	1,632,836.80
168,000	2,184,862.15	1,662,526.89	1,213,251.40	1,650,376.80
170,000	2,211,220.43	1,685,607.13	1,225,919.00	1,667,868.80

Desalination plant intake flow (m ³ /day)	Drum screen (\$)	Band screen (\$)	Wedgewire (\$)	Microscreen (\$)
172,000	2,237,582.83	1,708,732.21	1,238,546.60	1,685,312.80
174,000	2,263,949.31	1,731,901.71	1,251,134.20	1,702,708.80
176,000	2,290,319.82	1,755,115.19	1,263,681.80	1,720,056.80
178,000	2,316,694.32	1,778,372.23	1,276,189.40	1,737,356.80
180,000	2,343,072.76	1,801,672.44	1,288,657.00	1,754,608.80
182,000	2,369,455.10	1,825,015.40	1,301,084.60	1,771,812.80
184,000	2,395,841.29	1,848,400.72	1,313,472.20	1,788,968.80
186,000	2,422,231.30	1,871,828.03	1,325,819.80	1,806,076.80
188,000	2,448,625.09	1,895,296.93	1,338,127.40	1,823,136.80
190,000	2,475,022.60	1,918,807.07	1,350,395.00	1,840,148.80
192,000	2,501,423.82	1,942,358.08	1,362,622.60	1,857,112.80
194,000	2,527,828.69	1,965,949.61	1,374,810.20	1,874,028.80
196,000	2,554,237.18	1,989,581.29	1,386,957.80	1,890,896.80
198,000	2,580,649.26	2,013,252.80	1,399,065.40	1,907,716.80
200,000	2,607,064.89	2,036,963.80	1,411,133.00	1,924,488.80
202,000	2,633,484.03	2,060,713.95	1,423,160.60	1,941,212.80
204,000	2,659,906.65	2,084,502.93	1,435,148.20	1,957,888.80
206,000	2,686,332.71	2,108,330.43	1,447,095.80	1,974,516.80
208,000	2,712,762.19	2,132,196.13	1,459,003.40	1,991,096.80
210,000	2,739,195.04	2,156,099.73	1,470,871.00	2,007,628.80
212,000	2,765,631.25	2,180,040.91	1,482,698.60	2,024,112.80
214,000	2,792,070.77	2,204,019.39	1,494,486.20	2,040,548.80
216,000	2,818,513.58	2,228,034.88	1,506,233.80	2,056,936.80
218,000	2,844,959.65	2,252,087.09	1,517,941.40	2,073,276.80
220,000	2,871,408.94	2,276,175.73	1,529,609.00	2,089,568.80
222,000	2,897,861.43	2,300,300.54	1,541,236.60	2,105,812.80
224,000	2,924,317.09	2,324,461.23	1,552,824.20	2,122,008.80
226,000	2,950,775.90	2,348,657.55	1,564,371.80	2,138,156.80
228,000	2,977,237.81	2,372,889.22	1,575,879.40	2,154,256.80
230,000	3,003,702.82	2,397,155.98	1,587,347.00	2,170,308.80
232,000	3,030,170.88	2,421,457.60	1,598,774.60	2,186,312.80
234,000	3,056,641.98	2,445,793.80	1,610,162.20	2,202,268.80
236,000	3,083,116.10	2,470,164.35	1,621,509.80	2,218,176.80
238,000	3,109,593.19	2,494,569.00	1,632,817.40	2,234,036.80
240,000	3,136,073.24	2,519,007.51	1,644,085.00	2,249,848.80
242,000	3,162,556.23	2,543,479.65	1,655,312.60	2,265,612.80
244,000	3,189,042.13	2,567,985.18	1,666,500.20	2,281,328.80
246,000	3,215,530.92	2,592,523.88	1,677,647.80	2,296,996.80
248,000	3,242,022.57	2,617,095.52	1,688,755.40	2,312,616.80
250,000	3,268,517.06	2,641,699.88	1,699,823.00	2,328,188.80
252,000	3,295,014.38	2,666,336.73	1,710,850.60	2,343,712.80
254,000	3,321,514.49	2,691,005.87	1,721,838.20	2,359,188.80
256,000	3,348,017.37	2,715,707.09	1,732,785.80	2,374,616.80
258,000	3,374,523.01	2,740,440.16	1,743,693.40	2,389,996.80

Desalination plant intake flow (m ³ /day)	Drum screen (\$)	Band screen (\$)	Wedgewire (\$)	Microscreen (\$)
260,000	3,401,031.38	2,765,204.89	1,754,561.00	2,405,328.80
262,000	3,427,542.47	2,790,001.07	1,765,388.60	2,420,612.80
264,000	3,454,056.24	2,814,828.51	1,776,176.20	2,435,848.80
266,000	3,480,572.69	2,839,687.00	1,786,923.80	2,451,036.80
268,000	3,507,091.79	2,864,576.34	1,797,631.40	2,466,176.80
270,000	3,533,613.52	2,889,496.36	1,808,299.00	2,481,268.80
272,000	3,560,137.87	2,914,446.85	1,818,926.60	2,496,312.80
274,000	3,586,664.80	2,939,427.63	1,829,514.20	2,511,308.80
276,000	3,613,194.32	2,964,438.51	1,840,061.80	2,526,256.80
278,000	3,639,726.39	2,989,479.32	1,850,569.40	2,541,156.80
280,000	3,666,261.00	3,014,549.87	1,861,037.00	2,556,008.80
282,000	3,692,798.13	3,039,649.98	1,871,464.60	2,570,812.80
284,000	3,719,337.76	3,064,779.49	1,881,852.20	2,585,568.80
286,000	3,745,879.88	3,089,938.21	1,892,199.80	2,600,276.80
288,000	3,772,424.47	3,115,125.97	1,902,507.40	2,614,936.80
290,000	3,798,971.51	3,140,342.62	1,912,775.00	2,629,548.80
292,000	3,825,520.99	3,165,587.98	1,923,002.60	2,644,112.80
294,000	3,852,072.88	3,190,861.88	1,933,190.20	2,658,628.80
296,000	3,878,627.18	3,216,164.17	1,943,337.80	2,673,096.80
298,000	3,905,183.86	3,241,494.68	1,953,445.40	2,687,516.80
300,000	3,931,742.92	3,266,853.26	1,963,513.00	2,701,888.80
302,000	3,958,304.33	3,292,239.75	1,973,540.60	2,716,212.80
304,000	3,984,868.08	3,317,654.00	1,983,528.20	2,730,488.80
306,000	4,011,434.15	3,343,095.84	1,993,475.80	2,744,716.80
308,000	4,038,002.53	3,368,565.14	2,003,383.40	2,758,896.80
310,000	4,064,573.21	3,394,061.75	2,013,251.00	2,773,028.80
312,000	4,091,146.17	3,419,585.51	2,023,078.60	2,787,112.80
314,000	4,117,721.39	3,445,136.28	2,032,866.20	2,801,148.80
316,000	4,144,298.86	3,470,713.92	2,042,613.80	2,815,136.80
318,000	4,170,878.57	3,496,318.28	2,052,321.40	2,829,076.80
320,000	4,197,460.51	3,521,949.23	2,061,989.00	2,842,968.80
322,000	4,224,044.65	3,547,606.62	2,071,616.60	2,856,812.80
324,000	4,250,630.99	3,573,290.32	2,081,204.20	2,870,608.80
326,000	4,277,219.52	3,599,000.19	2,090,751.80	2,884,356.80
328,000	4,303,810.21	3,624,736.11	2,100,259.40	2,898,056.80
330,000	4,330,403.06	3,650,497.92	2,109,727.00	2,911,708.80
332,000	4,356,998.05	3,676,285.52	2,119,154.60	2,925,312.80
334,000	4,383,595.18	3,702,098.76	2,128,542.20	2,938,868.80
336,000	4,410,194.42	3,727,937.51	2,137,889.80	2,952,376.80
338,000	4,436,795.77	3,753,801.66	2,147,197.40	2,965,836.80
340,000	4,463,399.21	3,779,691.07	2,156,465.00	2,979,248.80
342,000	4,490,004.74	3,805,605.62	2,165,692.60	2,992,612.80
344,000	4,516,612.33	3,831,545.18	2,174,880.20	3,005,928.80
346,000	4,543,221.98	3,857,509.65	2,184,027.80	3,019,196.80

Desalination plant intake flow (m ³ /day)	Drum screen (\$)	Band screen (\$)	Wedgewire (\$)	Microscreen (\$)
348,000	4,569,833.68	3,883,498.89	2,193,135.40	3,032,416.80
350,000	4,596,447.41	3,909,512.78	2,202,203.00	3,045,588.80
352,000	4,623,063.16	3,935,551.22	2,211,230.60	3,058,712.80
354,000	4,649,680.92	3,961,614.08	2,220,218.20	3,071,788.80
356,000	4,676,300.69	3,987,701.24	2,229,165.80	3,084,816.80
358,000	4,702,922.44	4,013,812.60	2,238,073.40	3,097,796.80
360,000	4,729,546.17	4,039,948.04	2,246,941.00	3,110,728.80
362,000	4,756,171.87	4,066,107.45	2,255,768.60	3,123,612.80
364,000	4,782,799.53	4,092,290.71	2,264,556.20	3,136,448.80
366,000	4,809,429.13	4,118,497.72	2,273,303.80	3,149,236.80
368,000	4,836,060.67	4,144,728.38	2,282,011.40	3,161,976.80
370,000	4,862,694.13	4,170,982.56	2,290,679.00	3,174,668.80
372,000	4,889,329.51	4,197,260.18	2,299,306.60	3,187,312.80
374,000	4,915,966.79	4,223,561.11	2,307,894.20	3,199,908.80
376,000	4,942,605.97	4,249,885.26	2,316,441.80	3,212,456.80
378,000	4,969,247.03	4,276,232.53	2,324,949.40	3,224,956.80
380,000	4,995,889.96	4,302,602.80	2,333,417.00	3,237,408.80
382,000	5,022,534.76	4,328,995.99	2,341,844.60	3,249,812.80
384,000	5,049,181.42	4,355,411.99	2,350,232.20	3,262,168.80
386,000	5,075,829.92	4,381,850.70	2,358,579.80	3,274,476.80
388,000	5,102,480.26	4,408,312.02	2,366,887.40	3,286,736.80
390,000	5,129,132.43	4,434,795.86	2,375,155.00	3,298,948.80
392,000	5,155,786.41	4,461,302.11	2,383,382.60	3,311,112.80
394,000	5,182,442.20	4,487,830.69	2,391,570.20	3,323,228.80
396,000	5,209,099.80	4,514,381.50	2,399,717.80	3,335,296.80
398,000	5,235,759.18	4,540,954.44	2,407,825.40	3,347,316.80
400,000	5,262,420.34	4,567,549.43	2,415,893.00	3,359,288.80

Table - 11: CAPEX for pretreatment subprocesses

Desalination plant intake flow (m ³ /day)	DAF clarifier (\$)	Lamella settlers (\$)	Gravity granular dual media filters (\$)	Pressure granular dual media filters (\$)	Membrane pretreatment (upper cost bracket) (\$)	Membrane pretreatment (lower cost bracket) (\$)	Cartridge filter (\$)
1000	63,228.69	53,171.46	477,201.00	76,196.61	255,551.92	163,991.68	41,417.43
2000	115,536.70	95,278.58	546,764.00	138,654.91	454,637.41	287,153.59	70,544.72
5000	256,335.28	205,997.44	755,093.00	305,939.84	973,628.13	602,184.22	142,627.02
7000	343,475.64	273,418.92	893,679.00	409,116.34	1,287,775.39	790,369.27	184,702.17
8,000	385,772.74	305,934.73	962,882.00	459,128.73	1,438,921.92	880,438.73	204,657.28
10,000	468,397.07	369,129.33	1,101,108.00	556,718.49	1,732,124.65	1,054,439.85	242,931.13
12,000	548,880.88	430,337.88	1,239,094.00	651,665.14	2,015,517.97	1,221,844.94	279,459.01
14,000	627,627.15	489,942.71	1,376,840.00	744,468.68	2,291,005.61	1,383,956.66	314,596.10
16,000	704,915.92	548,208.19	1,514,346.00	835,476.19	2,559,901.53	1,541,670.56	348,584.88
18,000	780,952.59	605,327.45	1,651,612.00	924,942.02	2,823,164.09	1,695,637.64	381,600.58
20,000	855,893.96	661,447.38	1,788,638.00	1,013,060.20	3,081,521.28	1,846,350.94	413,775.25
22,000	929,863.45	716,683.23	1,925,424.00	1,099,983.36	3,335,543.68	1,994,195.91	445,211.64
24,000	1,002,960.64	771,127.72	2,061,970.00	1,185,834.54	3,585,689.71	2,139,481.50	475,991.79
26,000	1,075,267.43	824,856.93	2,198,276.00	1,270,714.91	3,832,335.23	2,282,460.50	506,182.57
28,000	1,146,852.36	877,934.35	2,334,342.00	1,354,709.07	4,075,793.59	2,423,343.24	535,839.45
30,000	1,217,773.52	930,413.69	2,470,168.00	1,437,888.71	4,316,329.76	2,562,307.27	565,009.08
32,000	1,288,080.80	982,340.98	2,605,754.00	1,520,315.36	4,554,170.53	2,699,504.29	593,731.23
34,000	1,357,817.45	1,033,756.05	2,741,100.00	1,602,042.33	4,789,512.04	2,835,065.33	622,040.15
36,000	1,427,021.30	1,084,693.68	2,876,206.00	1,683,116.26	5,022,525.50	2,969,104.56	649,965.61
38,000	1,495,725.73	1,135,184.50	3,011,072.00	1,763,578.27	5,253,361.52	3,101,722.30	677,533.70
40,000	1,563,960.38	1,185,255.66	3,145,698.00	1,843,464.85	5,482,153.61	3,233,007.37	704,767.48
42,000	1,631,751.72	1,234,931.40	3,280,084.00	1,922,808.61	5,709,020.82	3,363,038.87	731,687.43
44,000	1,699,123.57	1,284,233.47	3,414,230.00	2,001,638.86	5,934,069.95	3,491,887.66	758,311.88

Desalination plant intake flow (m ³ /day)	DAF clarifier (\$)	Lamella settlers (\$)	Gravity granular dual media filters (\$)	Pressure granular dual media filters (\$)	Membrane pretreatment (upper cost bracket) (\$)	Membrane pretreatment (lower cost bracket) (\$)	Cartridge filter (\$)
46,000	1,766,097.43	1,333,181.48	3,548,136.00	2,079,982.04	6,157,397.28	3,619,617.59	784,657.28
48,000	1,832,692.81	1,381,793.22	3,681,802.00	2,157,862.18	6,379,090.07	3,746,286.42	810,738.52
50,000	1,898,927.50	1,430,084.88	3,815,228.00	2,235,301.14	6,599,227.68	3,871,946.68	836,569.10
52,000	1,964,817.78	1,478,071.25	3,948,414.00	2,312,318.93	6,817,882.63	3,996,646.27	862,161.32
54,000	2,030,378.59	1,525,765.90	4,081,360.00	2,388,933.92	7,035,121.39	4,120,429.11	887,526.42
56,000	2,095,623.69	1,573,181.32	4,214,066.00	2,465,163.03	7,251,005.10	4,243,335.53	912,674.73
58,000	2,160,565.80	1,620,329.03	4,346,532.00	2,541,021.88	7,465,590.20	4,365,402.72	937,615.75
60,000	2,225,216.72	1,667,219.70	4,478,758.00	2,616,524.96	7,678,928.89	4,486,665.07	962,358.24
62,000	2,289,587.39	1,713,863.24	4,610,744.00	2,691,685.71	7,891,069.62	4,607,154.47	986,910.34
64,000	2,353,688.01	1,760,268.85	4,742,490.00	2,766,516.66	8,102,057.44	4,726,900.55	1,011,279.58
66,000	2,417,528.11	1,806,445.14	4,873,996.00	2,841,029.50	8,311,934.39	4,845,930.92	1,035,472.98
68,000	2,481,116.59	1,852,400.15	5,005,262.00	2,915,235.17	8,520,739.71	4,964,271.36	1,059,497.08
70,000	2,544,461.81	1,898,141.38	5,136,288.00	2,989,143.91	8,728,510.18	5,081,946.00	1,083,357.99
72,000	2,607,571.61	1,943,675.91	5,267,074.00	3,062,765.34	8,935,280.27	5,198,977.45	1,107,061.44
74,000	2,670,453.37	1,989,010.38	5,397,620.00	3,136,108.52	9,141,082.40	5,315,386.95	1,130,612.80
76,000	2,733,114.04	2,034,151.03	5,527,926.00	3,209,181.99	9,345,947.09	5,431,194.49	1,154,017.11
78,000	2,795,560.19	2,079,103.76	5,657,992.00	3,281,993.79	9,549,903.12	5,546,418.91	1,177,279.14
80,000	2,857,798.04	2,123,874.16	5,787,818.00	3,354,551.54	9,752,977.67	5,661,077.99	1,200,403.36
82,000	2,919,833.45	2,168,467.48	5,917,404.00	3,426,862.44	9,955,196.45	5,775,188.52	1,223,394.01
84,000	2,981,672.00	2,212,888.72	6,046,750.00	3,498,933.32	10,156,583.80	5,888,766.43	1,246,255.08
86,000	3,043,318.98	2,257,142.63	6,175,856.00	3,570,770.67	10,357,162.84	6,001,826.80	1,268,990.37
88,000	3,104,779.43	2,301,233.70	6,304,722.00	3,642,380.65	10,556,955.49	6,114,383.94	1,291,603.47
90,000	3,166,058.12	2,345,166.21	6,433,348.00	3,713,769.13	10,755,982.61	6,226,451.45	1,314,097.79
92,000	3,227,159.61	2,388,944.24	6,561,734.00	3,784,941.69	10,954,264.04	6,338,042.28	1,336,476.58
94,000	3,288,088.26	2,432,571.67	6,689,880.00	3,855,903.65	11,151,818.71	6,449,168.76	1,358,742.92
96,000	3,348,848.21	2,476,052.22	6,817,786.00	3,926,660.11	11,348,664.66	6,559,842.63	1,380,899.76
98,000	3,409,443.44	2,519,389.41	6,945,452.00	3,997,215.92	11,544,819.13	6,670,075.11	1,402,949.89

Desalination plant intake flow (m ³ /day)	DAF clarifier (\$)	Lamella settlers (\$)	Gravity granular dual media filters (\$)	Pressure granular dual media filters (\$)	Membrane pretreatment (upper cost bracket) (\$)	Membrane pretreatment (lower cost bracket) (\$)	Cartridge filter (\$)
100,000	3,469,877.73	2,562,586.63	7,072,878.00	4,067,575.72	11,740,298.57	6,779,876.92	1,424,896.00
102,000	3,530,154.73	2,605,647.13	7,200,064.00	4,137,743.97	11,935,118.75	6,889,258.31	1,446,740.63
104,000	3,590,277.91	2,648,574.00	7,327,010.00	4,207,724.94	12,129,294.75	6,998,229.09	1,468,486.24
106,000	3,650,250.62	2,691,370.22	7,453,716.00	4,277,522.70	12,322,841.04	7,106,798.64	1,490,135.16
108,000	3,710,076.05	2,734,038.63	7,580,182.00	4,347,141.17	12,515,771.48	7,214,975.98	1,511,689.64
110,000	3,769,757.29	2,776,581.98	7,706,408.00	4,416,584.14	12,708,099.37	7,322,769.74	1,533,151.83
112,000	3,829,297.31	2,819,002.90	7,832,394.00	4,485,855.22	12,899,837.52	7,430,188.23	1,554,523.79
114,000	3,888,698.94	2,861,303.91	7,958,140.00	4,554,957.89	13,090,998.21	7,537,239.42	1,575,807.50
116,000	3,947,964.92	2,903,487.46	8,083,646.00	4,623,895.52	13,281,593.27	7,643,930.98	1,597,004.86
118,000	4,007,097.91	2,945,555.88	8,208,912.00	4,692,671.31	13,471,634.08	7,750,270.28	1,618,117.71
120,000	4,066,100.43	2,987,511.43	8,333,938.00	4,761,288.41	13,661,131.61	7,856,264.44	1,639,147.81
122,000	4,124,974.96	3,029,356.28	8,458,724.00	4,829,749.79	13,850,096.42	7,961,920.29	1,660,096.84
124,000	4,183,723.86	3,071,092.55	8,583,270.00	4,898,058.37	14,038,538.72	8,067,244.43	1,680,966.45
126,000	4,242,349.41	3,112,722.25	8,707,576.00	4,966,216.93	14,226,468.34	8,172,243.24	1,701,758.21
128,000	4,300,853.83	3,154,247.34	8,831,642.00	5,034,228.19	14,413,894.78	8,276,922.86	1,722,473.64
130,000	4,359,239.25	3,195,669.72	8,955,468.00	5,102,094.76	14,600,827.22	8,381,289.22	1,743,114.21
132,000	4,417,507.75	3,236,991.21	9,079,054.00	5,169,819.15	14,787,274.53	8,485,348.06	1,763,681.33
134,000	4,475,661.32	3,278,213.57	9,202,400.00	5,237,403.82	14,973,245.30	8,589,104.93	1,784,176.37
136,000	4,533,701.90	3,319,338.53	9,325,506.00	5,304,851.14	15,158,747.83	8,692,565.18	1,804,600.65
138,000	4,591,631.36	3,360,367.75	9,448,372.00	5,372,163.40	15,343,790.15	8,795,734.02	1,824,955.45
140,000	4,649,451.53	3,401,302.81	9,570,998.00	5,439,342.81	15,528,380.06	8,898,616.46	1,845,242.02
142,000	4,707,164.17	3,442,145.29	9,693,384.00	5,506,391.54	15,712,525.11	9,001,217.38	1,865,461.54
144,000	4,764,770.98	3,482,896.70	9,815,530.00	5,573,311.68	15,896,232.60	9,103,541.50	1,885,615.19
146,000	4,822,273.64	3,523,558.49	9,937,436.00	5,640,105.25	16,079,509.63	9,205,593.39	1,905,704.08
148,000	4,879,673.74	3,564,132.08	10,059,102.00	5,706,774.21	16,262,363.09	9,307,377.49	1,925,729.32
150,000	4,936,972.86	3,604,618.86	10,180,528.00	5,773,320.49	16,444,799.66	9,408,898.11	1,945,691.94
152,000	4,994,172.52	3,645,020.17	10,301,714.00	5,839,745.94	16,626,825.83	9,510,159.44	1,965,592.99

Desalination plant intake flow (m ³ /day)	DAF clarifier (\$)	Lamella settlers (\$)	Gravity granular dual media filters (\$)	Pressure granular dual media filters (\$)	Membrane pretreatment (upper cost bracket) (\$)	Membrane pretreatment (lower cost bracket) (\$)	Cartridge filter (\$)
154,000	5,051,274.19	3,685,337.30	10,422,660.00	5,906,052.36	16,808,447.92	9,611,165.52	1,985,433.46
156,000	5,108,279.31	3,725,571.53	10,543,366.00	5,972,241.52	16,989,672.03	9,711,920.32	2,005,214.31
158,000	5,165,189.27	3,765,724.08	10,663,832.00	6,038,315.10	17,170,504.14	9,812,427.66	2,024,936.49
160,000	5,222,005.45	3,805,796.14	10,784,058.00	6,104,274.79	17,350,950.04	9,912,691.27	2,044,600.90
162,000	5,278,729.16	3,845,788.90	10,904,044.00	6,170,122.19	17,531,015.36	10,012,714.77	2,064,208.45
164,000	5,335,361.70	3,885,703.46	11,023,790.00	6,235,858.88	17,710,705.59	10,112,501.71	2,083,759.99
166,000	5,391,904.31	3,925,540.95	11,143,296.00	6,301,486.38	17,890,026.08	10,212,055.51	2,103,256.36
168,000	5,448,358.22	3,965,302.44	11,262,562.00	6,367,006.21	18,068,982.02	10,311,379.52	2,122,698.37
170,000	5,504,724.63	4,004,988.96	11,381,588.00	6,432,419.80	18,247,578.48	10,410,476.99	2,142,086.83
172,000	5,561,004.70	4,044,601.55	11,500,374.00	6,497,728.58	18,425,820.41	10,509,351.09	2,161,422.52
174,000	5,617,199.56	4,084,141.20	11,618,920.00	6,562,933.93	18,603,712.61	10,608,004.92	2,180,706.17
176,000	5,673,310.32	4,123,608.88	11,737,226.00	6,628,037.21	18,781,259.78	10,706,441.50	2,199,938.54
178,000	5,729,338.05	4,163,005.54	11,855,292.00	6,693,039.72	18,958,466.50	10,804,663.75	2,219,120.34
180,000	5,785,283.82	4,202,332.09	11,973,118.00	6,757,942.76	19,135,337.24	10,902,674.56	2,238,252.26
182,000	5,841,148.64	4,241,589.44	12,090,704.00	6,822,747.59	19,311,876.36	11,000,476.71	2,257,334.99
184,000	5,896,933.53	4,280,778.48	12,208,050.00	6,887,455.41	19,488,088.10	11,098,072.94	2,276,369.19
186,000	5,952,639.47	4,319,900.05	12,325,156.00	6,952,067.44	19,663,976.64	11,195,465.90	2,295,355.52
188,000	6,008,267.41	4,358,955.01	12,442,022.00	7,016,584.84	19,839,546.02	11,292,658.21	2,314,294.60
190,000	6,063,818.29	4,397,944.17	12,558,648.00	7,081,008.76	20,014,800.21	11,389,652.41	2,333,187.05
192,000	6,119,293.03	4,436,868.33	12,675,034.00	7,145,340.31	20,189,743.10	11,486,450.97	2,352,033.48
194,000	6,174,692.53	4,475,728.27	12,791,180.00	7,209,580.59	20,364,378.45	11,583,056.33	2,370,834.48
196,000	6,230,017.65	4,514,524.77	12,907,086.00	7,273,730.66	20,538,709.99	11,679,470.85	2,389,590.62
198,000	6,285,269.27	4,553,258.57	13,022,752.00	7,337,791.57	20,712,741.32	11,775,696.85	2,408,302.47
200,000	6,340,448.21	4,591,930.41	13,138,178.00	7,401,764.34	20,886,475.99	11,871,736.61	2,426,970.58
202,000	6,395,555.29	4,630,541.00	13,253,364.00	7,465,649.98	21,059,917.46	11,967,592.33	2,445,595.48
204,000	6,450,591.33	4,669,091.04	13,368,310.00	7,529,449.45	21,233,069.13	12,063,266.20	2,464,177.70
206,000	6,505,557.11	4,707,581.23	13,483,016.00	7,593,163.73	21,405,934.32	12,158,760.32	2,482,717.76

Desalination plant intake flow (m ³ /day)	DAF clarifier (\$)	Lamella settlers (\$)	Gravity granular dual media filters (\$)	Pressure granular dual media filters (\$)	Membrane pretreatment (upper cost bracket) (\$)	Membrane pretreatment (lower cost bracket) (\$)	Cartridge filter (\$)
208,000	6,560,453.39	4,746,012.23	13,597,482.00	7,656,793.76	21,578,516.26	12,254,076.79	2,501,216.16
210,000	6,615,280.94	4,784,384.70	13,711,708.00	7,720,340.44	21,750,818.15	12,349,217.63	2,519,673.39
212,000	6,670,040.49	4,822,699.29	13,825,694.00	7,783,804.68	21,922,843.10	12,444,184.83	2,538,089.94
214,000	6,724,732.77	4,860,956.63	13,939,440.00	7,847,187.37	22,094,594.16	12,538,980.35	2,556,466.27
216,000	6,779,358.48	4,899,157.35	14,052,946.00	7,910,489.37	22,266,074.31	12,633,606.09	2,574,802.86
218,000	6,833,918.33	4,937,302.04	14,166,212.00	7,973,711.53	22,437,286.50	12,728,063.94	2,593,100.15
220,000	6,888,413.00	4,975,391.30	14,279,238.00	8,036,854.69	22,608,233.59	12,822,355.71	2,611,358.58
222,000	6,942,843.15	5,013,425.72	14,392,024.00	8,099,919.65	22,778,918.39	12,916,483.22	2,629,578.60
224,000	6,997,209.44	5,051,405.86	14,504,570.00	8,162,907.21	22,949,343.67	13,010,448.22	2,647,760.62
226,000	7,051,512.52	5,089,332.29	14,616,876.00	8,225,818.17	23,119,512.13	13,104,252.44	2,665,905.06
228,000	7,105,753.02	5,127,205.57	14,728,942.00	8,288,653.29	23,289,426.43	13,197,897.57	2,684,012.34
230,000	7,159,931.56	5,165,026.22	14,840,768.00	8,351,413.33	23,459,089.18	13,291,385.28	2,702,082.86
232,000	7,214,048.74	5,202,794.78	14,952,354.00	8,414,099.03	23,628,502.91	13,384,717.20	2,720,117.00
234,000	7,268,105.17	5,240,511.77	15,063,700.00	8,476,711.11	23,797,670.15	13,477,894.92	2,738,115.16
236,000	7,322,101.43	5,278,177.69	15,174,806.00	8,539,250.30	23,966,593.36	13,570,920.02	2,756,077.70
238,000	7,376,038.10	5,315,793.06	15,285,672.00	8,601,717.29	24,135,274.95	13,663,794.03	2,774,005.02
240,000	7,429,915.75	5,353,358.36	15,396,298.00	8,664,112.76	24,303,717.29	13,756,518.47	2,791,897.45
242,000	7,483,734.92	5,390,874.07	15,506,684.00	8,726,437.41	24,471,922.71	13,849,094.83	2,809,755.38
244,000	7,537,496.16	5,428,340.67	15,616,830.00	8,788,691.89	24,639,893.50	13,941,524.55	2,827,579.14
246,000	7,591,200.02	5,465,758.63	15,726,736.00	8,850,876.86	24,807,631.90	14,033,809.07	2,845,369.08
248,000	7,644,847.01	5,503,128.40	15,836,402.00	8,912,992.96	24,975,140.13	14,125,949.80	2,863,125.55
250,000	7,698,437.66	5,540,450.43	15,945,828.00	8,975,040.81	25,142,420.34	14,217,948.12	2,880,848.86
252,000	7,751,972.48	5,577,725.17	16,055,014.00	9,037,021.05	25,309,474.68	14,309,805.38	2,898,539.35
254,000	7,805,451.96	5,614,953.05	16,163,960.00	9,098,934.27	25,476,305.23	14,401,522.92	2,916,197.35
256,000	7,858,876.61	5,652,134.49	16,272,666.00	9,160,781.08	25,642,914.06	14,493,102.05	2,933,823.15
258,000	7,912,246.89	5,689,269.92	16,381,132.00	9,222,562.07	25,809,303.18	14,584,544.05	2,951,417.08
260,000	7,965,563.29	5,726,359.75	16,489,358.00	9,284,277.81	25,975,474.59	14,675,850.19	2,968,979.43

Desalination plant intake flow (m ³ /day)	DAF clarifier (\$)	Lamella settlers (\$)	Gravity granular dual media filters (\$)	Pressure granular dual media filters (\$)	Membrane pretreatment (upper cost bracket) (\$)	Membrane pretreatment (lower cost bracket) (\$)	Cartridge filter (\$)
262,000	8,018,826.28	5,763,404.39	16,597,344.00	9,345,928.88	26,141,430.24	14,767,021.72	2,986,510.51
264,000	8,072,036.32	5,800,404.23	16,705,090.00	9,407,515.84	26,307,172.06	14,858,059.86	3,004,010.61
266,000	8,125,193.85	5,837,359.67	16,812,596.00	9,469,039.24	26,472,701.94	14,948,965.82	3,021,480.02
268,000	8,178,299.34	5,874,271.10	16,919,862.00	9,530,499.62	26,638,021.74	15,039,740.77	3,038,919.03
270,000	8,231,353.21	5,911,138.89	17,026,888.00	9,591,897.51	26,803,133.29	15,130,385.88	3,056,327.90
272,000	8,284,355.89	5,947,963.42	17,133,674.00	9,653,233.45	26,968,038.39	15,220,902.30	3,073,706.92
274,000	8,337,307.82	5,984,745.06	17,240,220.00	9,714,507.94	27,132,738.82	15,311,291.16	3,091,056.36
276,000	8,390,209.41	6,021,484.17	17,346,526.00	9,775,721.51	27,297,236.33	15,401,553.55	3,108,376.48
278,000	8,443,061.08	6,058,181.11	17,452,592.00	9,836,874.64	27,461,532.63	15,491,690.58	3,125,667.54
280,000	8,495,863.22	6,094,836.22	17,558,418.00	9,897,967.84	27,625,629.40	15,581,703.32	3,142,929.80
282,000	8,548,616.24	6,131,449.86	17,664,004.00	9,959,001.58	27,789,528.33	15,671,592.83	3,160,163.52
284,000	8,601,320.54	6,168,022.36	17,769,350.00	10,019,976.36	27,953,231.04	15,761,360.14	3,177,368.94
286,000	8,653,976.49	6,204,554.07	17,874,456.00	10,080,892.64	28,116,739.15	15,851,006.28	3,194,546.32
288,000	8,706,584.49	6,241,045.30	17,979,322.00	10,141,750.88	28,280,054.25	15,940,532.27	3,211,695.88
290,000	8,759,144.90	6,277,496.39	18,083,948.00	10,202,551.54	28,443,177.90	16,029,939.09	3,228,817.87
292,000	8,811,658.10	6,313,907.66	18,188,334.00	10,263,295.08	28,606,111.66	16,119,227.72	3,245,912.52
294,000	8,864,124.46	6,350,279.42	18,292,480.00	10,323,981.93	28,768,857.03	16,208,399.13	3,262,980.06
296,000	8,916,544.33	6,386,611.98	18,396,386.00	10,384,612.55	28,931,415.51	16,297,454.27	3,280,020.72
298,000	8,968,918.07	6,422,905.65	18,500,052.00	10,445,187.34	29,093,788.59	16,386,394.07	3,297,034.73
300,000	9,021,246.03	6,459,160.74	18,603,478.00	10,505,706.76	29,255,977.71	16,475,219.45	3,314,022.29
302,000	9,073,528.55	6,495,377.53	18,706,664.00	10,566,171.20	29,417,984.30	16,563,931.33	3,330,983.64
304,000	9,125,765.98	6,531,556.33	18,809,610.00	10,626,581.09	29,579,809.79	16,652,530.60	3,347,918.98
306,000	9,177,958.65	6,567,697.43	18,912,316.00	10,686,936.84	29,741,455.55	16,741,018.14	3,364,828.53
308,000	9,230,106.88	6,603,801.10	19,014,782.00	10,747,238.84	29,902,922.97	16,829,394.82	3,381,712.49
310,000	9,282,211.01	6,639,867.63	19,117,008.00	10,807,487.49	30,064,213.40	16,917,661.50	3,398,571.06
312,000	9,334,271.36	6,675,897.30	19,218,994.00	10,867,683.19	30,225,328.16	17,005,819.02	3,415,404.45
314,000	9,386,288.25	6,711,890.39	19,320,740.00	10,927,826.31	30,386,268.58	17,093,868.23	3,432,212.86

Desalination plant intake flow (m ³ /day)	DAF clarifier (\$)	Lamella settlers (\$)	Gravity granular dual media filters (\$)	Pressure granular dual media filters (\$)	Membrane pretreatment (upper cost bracket) (\$)	Membrane pretreatment (lower cost bracket) (\$)	Cartridge filter (\$)
316,000	9,438,261.97	6,747,847.15	19,422,246.00	10,987,917.24	30,547,035.95	17,181,809.92	3,448,996.48
318,000	9,490,192.86	6,783,767.86	19,523,512.00	11,047,956.36	30,707,631.55	17,269,644.93	3,465,755.51
320,000	9,542,081.20	6,819,652.78	19,624,538.00	11,107,944.03	30,868,056.65	17,357,374.05	3,482,490.13
322,000	9,593,927.31	6,855,502.17	19,725,324.00	11,167,880.62	31,028,312.49	17,444,998.07	3,499,200.53
324,000	9,645,731.47	6,891,316.28	19,825,870.00	11,227,766.49	31,188,400.29	17,532,517.76	3,515,886.91
326,000	9,697,493.98	6,927,095.37	19,926,176.00	11,287,602.00	31,348,321.28	17,619,933.89	3,532,549.43
328,000	9,749,215.13	6,962,839.68	20,026,242.00	11,347,387.49	31,508,076.64	17,707,247.22	3,549,188.29
330,000	9,800,895.20	6,998,549.47	20,126,068.00	11,407,123.32	31,667,667.55	17,794,458.49	3,565,803.65
332,000	9,852,534.48	7,034,224.97	20,225,654.00	11,466,809.82	31,827,095.19	17,881,568.45	3,582,395.70
334,000	9,904,133.24	7,069,866.42	20,325,000.00	11,526,447.33	31,986,360.69	17,968,577.81	3,598,964.61
336,000	9,955,691.75	7,105,474.06	20,424,106.00	11,586,036.18	32,145,465.20	18,055,487.30	3,615,510.55
338,000	10,007,210.29	7,141,048.12	20,522,972.00	11,645,576.71	32,304,409.82	18,142,297.63	3,632,033.68
340,000	10,058,689.13	7,176,588.83	20,621,598.00	11,705,069.25	32,463,195.68	18,229,009.48	3,648,534.17
342,000	10,110,128.52	7,212,096.43	20,719,984.00	11,764,514.10	32,621,823.86	18,315,623.57	3,665,012.19
344,000	10,161,528.73	7,247,571.12	20,818,130.00	11,823,911.58	32,780,295.43	18,402,140.55	3,681,467.89
346,000	10,212,890.02	7,283,013.14	20,916,036.00	11,883,262.02	32,938,611.46	18,488,561.11	3,697,901.45
348,000	10,264,212.64	7,318,422.70	21,013,702.00	11,942,565.71	33,096,773.00	18,574,885.92	3,714,313.00
350,000	10,315,496.84	7,353,800.02	21,111,128.00	12,001,822.97	33,254,781.09	18,661,115.62	3,730,702.72
352,000	10,366,742.86	7,389,145.32	21,208,314.00	12,061,034.09	33,412,636.75	18,747,250.86	3,747,070.76
354,000	10,417,950.97	7,424,458.80	21,305,260.00	12,120,199.38	33,570,341.00	18,833,292.28	3,763,417.26
356,000	10,469,121.38	7,459,740.67	21,401,966.00	12,179,319.12	33,727,894.83	18,919,240.52	3,779,742.37
358,000	10,520,254.36	7,494,991.13	21,498,432.00	12,238,393.61	33,885,299.23	19,005,096.20	3,796,046.25
360,000	10,571,350.12	7,530,210.40	21,594,658.00	12,297,423.13	34,042,555.17	19,090,859.93	3,812,329.04
362,000	10,622,408.92	7,565,398.67	21,690,644.00	12,356,407.97	34,199,663.63	19,176,532.32	3,828,590.88
364,000	10,673,430.96	7,600,556.13	21,786,390.00	12,415,348.41	34,356,625.55	19,262,113.98	3,844,831.92
366,000	10,724,416.50	7,635,682.99	21,881,896.00	12,474,244.73	34,513,441.87	19,347,605.49	3,861,052.29
368,000	10,775,365.74	7,670,779.44	21,977,162.00	12,533,097.19	34,670,113.53	19,433,007.45	3,877,252.14

Desalination plant intake flow (m ³ /day)	DAF clarifier (\$)	Lamella settlers (\$)	Gravity granular dual media filters (\$)	Pressure granular dual media filters (\$)	Membrane pretreatment (upper cost bracket) (\$)	Membrane pretreatment (lower cost bracket) (\$)	Cartridge filter (\$)
370,000	10,826,278.91	7,705,845.68	22,072,188.00	12,591,906.08	34,826,641.43	19,518,320.43	3,893,431.61
372,000	10,877,156.24	7,740,881.88	22,166,974.00	12,650,671.65	34,983,026.49	19,603,545.01	3,909,590.82
374,000	10,927,997.94	7,775,888.23	22,261,520.00	12,709,394.18	35,139,269.61	19,688,681.75	3,925,729.92
376,000	10,978,804.22	7,810,864.93	22,355,826.00	12,768,073.92	35,295,371.67	19,773,731.21	3,941,849.03
378,000	11,029,575.31	7,845,812.15	22,449,892.00	12,826,711.13	35,451,333.56	19,858,693.95	3,957,948.29
380,000	11,080,311.40	7,880,730.08	22,543,718.00	12,885,306.07	35,607,156.12	19,943,570.51	3,974,027.82
382,000	11,131,012.71	7,915,618.89	22,637,304.00	12,943,858.99	35,762,840.23	20,028,361.43	3,990,087.76
384,000	11,181,679.45	7,950,478.76	22,730,650.00	13,002,370.14	35,918,386.73	20,113,067.25	4,006,128.22
386,000	11,232,311.81	7,985,309.86	22,823,756.00	13,060,839.77	36,073,796.46	20,197,688.49	4,022,149.34
388,000	11,282,910.00	8,020,112.37	22,916,622.00	13,119,268.12	36,229,070.24	20,282,225.68	4,038,151.24
390,000	11,333,474.21	8,054,886.46	23,009,248.00	13,177,655.44	36,384,208.90	20,366,679.33	4,054,134.04
392,000	11,384,004.65	8,089,632.30	23,101,634.00	13,236,001.96	36,539,213.24	20,451,049.95	4,070,097.86
394,000	11,434,501.51	8,124,350.04	23,193,780.00	13,294,307.91	36,694,084.07	20,535,338.05	4,086,042.82
396,000	11,484,964.98	8,159,039.87	23,285,686.00	13,352,573.54	36,848,822.17	20,619,544.13	4,101,969.03
398,000	11,535,395.25	8,193,701.94	23,377,352.00	13,410,799.08	37,003,428.33	20,703,668.68	4,117,876.62
400,000	11,585,792.51	8,228,336.41	23,468,778.00	13,468,984.75	37,157,903.32	20,787,712.18	4,133,765.70

Table - 12: CAPEX for RO system equipment

Item	Construction cost (US\$/item or as indicated)		
8-inch SWRO membrane elements	400.00	600.00	Per element
16-inch SWRO membrane elements	2,900.00	3,400.00	Per element
SWRO pressure vessels for 8-inch elements	1,400.00	1,800.00	Per vessel
SWRO pressure vessels for 16-inch elements	3,700.00	5,200.00	Per vessel
RO train piping	260,000.00	620,000.00	Per train
RO train support frame	160,000.00	360,000.00	Per train
RO train instrumentation and controls	32,000.00	110,000.00	Per train
High-pressure pumps	160,000.00	2,500,000.00	Per train
UF element		1000.0	Per element
Energy recovery devices (PX-Q300)		25,625.0	Per PX

Table - 13: CAPEX for discharge subprocesses

Type of post treatment	Disposal construction cost - low price (\$/m ³ /day)	Disposal construction cost - high price (\$/m ³ /day)
New surface water discharge (new outfall with diffusers)	40.0	800.0
Collocation of desalination plant and power plant discharge	20.0	40.0
Co-disposal with wastewater treatment plant discharge	30.0	160.0

Table - 14: CAPEX for posttreatment subprocesses

Permeate (m ³ /day)	Lime and carbon dioxide (\$)	Calcite and carbon dioxide (\$)	Chlorine dioxide disinfection (\$)	Sodium hypochlorite disinfection (\$)
5,000.00	1,006,434.10	546,178.57	126,111.94	82,175.11
10,000.00	1,535,653.48	828,713.10	191,906.68	124,752.91
15,000.00	1,966,248.75	1,057,604.02	245,328.81	159,261.37
20,000.00	2,343,155.51	1,257,400.83	292,027.63	189,391.75
25,000.00	2,684,586.84	1,438,020.63	334,289.20	216,635.66
30,000.00	3,000,173.32	1,604,695.51	373,321.00	241,780.25
35,000.00	3,295,771.60	1,760,601.76	409,856.75	265,303.43
40,000.00	3,575,271.26	1,907,845.87	444,383.39	287,522.22
45,000.00	3,841,418.08	2,047,913.12	477,244.47	308,660.16
50,000.00	4,096,239.51	2,181,899.08	508,693.53	328,882.16
55,000.00	4,341,285.25	2,310,640.39	538,924.30	348,314.16
60,000.00	4,577,772.75	2,434,793.75	568,088.89	367,055.03

Permeate (m ³ /day)	Lime and carbon dioxide (\$)	Calcite and carbon dioxide (\$)	Chlorine dioxide disinfection (\$)	Sodium hypochlorite disinfection (\$)
65,000.00	4,806,679.99	2,554,886.35	596,309.46	385,184.14
70,000.00	5,028,807.28	2,671,349.26	623,685.96	402,766.40
75,000.00	5,244,819.82	2,784,540.58	650,301.40	419,855.73
80,000.00	5,455,277.95	2,894,761.77	676,225.72	436,497.52
85,000.00	5,660,659.14	3,002,269.58	701,518.49	452,730.45
90,000.00	5,861,374.37	3,107,284.88	726,230.98	468,587.77
95,000.00	6,057,780.56	3,209,999.39	750,407.68	484,098.36
100,000.00	6,250,190.11	3,310,580.88	774,087.55	499,287.49
105,000.00	6,438,878.41	3,409,177.12	797,304.91	514,177.42
110,000.00	6,624,089.75	3,505,919.19	820,090.22	528,787.89
115,000.00	6,806,042.09	3,600,923.98	842,470.62	543,136.50
120,000.00	6,984,930.91	3,694,296.27	864,470.47	557,239.06
125,000.00	7,160,932.35	3,786,130.46	886,111.71	571,109.76
130,000.00	7,334,205.84	3,876,511.96	907,414.20	584,761.49
135,000.00	7,504,896.24	3,965,518.35	928,395.97	598,205.93
140,000.00	7,673,135.68	4,053,220.36	949,073.47	611,453.73
145,000.00	7,839,045.07	4,139,682.71	969,461.75	624,514.65
150,000.00	8,002,735.42	4,224,964.79	989,574.64	637,397.64
155,000.00	8,164,308.94	4,309,121.29	1,009,424.85	650,110.93
160,000.00	8,323,860.03	4,392,202.67	1,029,024.12	662,662.12
165,000.00	8,481,476.04	4,474,255.64	1,048,383.33	675,058.27
170,000.00	8,637,238.06	4,555,323.54	1,067,512.56	687,305.89
175,000.00	8,791,221.48	4,635,446.66	1,086,421.19	699,411.07
180,000.00	8,943,496.60	4,714,662.55	1,105,117.96	711,379.45
185,000.00	9,094,129.05	4,793,006.26	1,123,611.04	723,216.31
190,000.00	9,243,180.25	4,870,510.60	1,141,908.06	734,926.62
195,000.00	9,390,707.78	4,947,206.30	1,160,016.18	746,514.98
200,000.00	9,536,765.69	5,023,122.21	1,177,942.12	757,985.76

Table - 15: Chemical cost

Chemical	Cost (US\$/kg)
Sodium Hypochlorite	2.2 - 3.5
Sulfuric Acid (93% H ₂ so ₄)	0.06 - 0.1
Ferric Sulfate	0.4 - 1.2
Ferric Chloride	1.67
Sodium Hexametaphosphate	1.6 - 4.0

Chemical	Cost (US\$/kg)
Chlorine Dioxide	3.0 - 5.5
Sodium Hydroxide	0.65 - 0.85
Sodium Bisulfite	0.35 - 0.55
Hydrated Lime	0.3 - 0.4
Calcite	0.05 - 0.08
Carbon Dioxide	0.08 - 0.12
Other Cleaning Chemicals (US\$/M ³ Of Permeate)	0.005 - 0.008

APPENDIX F LIFE COST ANALYSIS EVALUATION

Case 1:

Table - 16: Selected seawater RO facilities using well intake systems [303]

Facility name	Location	Capacity (m ³ /d)	No. of wells
Sur	Oman	160,000	28
Alicante (combined for two facilities)	Spain	130,000	30
Tordera	Blanes, Spain	128,000	10
Bajo Almanzora	Almeria, Spain	120,000	14
Bay of Palma	Mallorca, Spain	89,600	16
WEB	Aruba	80,000	10
Lanzarote IV	Canary Islands, Spain	60,000	11
Blue Hills	New Providence I., Bahamas	54,600	12
Santa Cruz de Tenerife	Canary Islands, Spain	50,000	8
Ghar Lapsi	Malta	45,000	18
SAWACO	Jeddah, Saudi Arabia	31,250	10
Dahab	Red Sea, Egypt	25,000	15
Turks & Caicos Water	Providenciales, Turks	23,260	6
Ibiza	Spain	15,000	8
Al-Birk	Saudi Arabia	5100-8700	3
Lower Valley	Grand Cayman	8000	3
Britannia	Grand Cayman	5400	4
Morro Bay	California, USA	4500	5

Table - 17: Design specification of Plant intake and brine specifications for Case 1

Plant water design	Value	Unit
Product	25,000.00	m ³ /day
Recovery	45.00	%
Salinity	35,000.00	mg/L
Temperature	25.00	°C
Backwash	4.00	%
Additional water	0.50	%
Life scale	20.00	Year
Operation days	360	Days
Intake capacity	57,805.56	m ³ /day
Ro feed flow	55,556.00	m ³ /day

Brine flow rate	30,556.00	m ³ /day
Brine salinity	63,579.00	mg/L
Brine average salinity	49,289.50	
Permeate salinity	99.00	
Feed water density	1023.03	kg/m ³
Sweater dynamic viscosity	0.00096	kg/ms
Seawater kinematic viscosity	9.37×10^{-7}	m ² /s

Table - 18: Design specification of Vertical well for Case 1

Intake design	Vertical well value	Unit
Ground permeability	0.0005	m/s
Depth	38.00	m
Aquifer drawdown	14.00	m
Reduction capacity loss	0.30	
Transmissivity	0.019	m ² /s
Capacity per well	5,223.27	m ³ /day
Number of wells	16.00	

Table - 19: Design specification of Pressure granular media filtration for Case 1

Pretreatment system	Single pressure granular media filtration	Unit
Loading rate	15.00	m ³ /m ² /h
Length to width ratio	4.00	
Max surface area per filter	50.00	m ²
Backwash loading rate	40.00	m ³ /m ² /h
Duration	10.00	min
Downflow rinse	5.00	min
Sediment type	Sand	
Effective size	1.6	
Required surface area	161.00	m ²
Number of filters + standby	4.00	
Surface area per filter	40.00	m ²
Length	9.03	m
Width/diameter	2.26	m
Media loading rate	29.55	m ³ /m ² h
Backwash flow rate	128.80	m ³ /min
Volume per filter	1,932.00	m ³

Table - 20: Design specification of Cartridge filter for Case 1

Pretreatment system	Cartridge filter	Unit
Loading rate	0.25	m ³ /m ² h
Length	1,016.00	mm
N cartridge per PV	8.00	
Number of cartridges	659.00	
Number of cartridges per PV	82.00	
Actual loading rate per 250 mm	0.25	

Table - 21: Design specification of RO system for Case 1

Ro system	SW30XL400	Unit
Flux	14.00	Lmh
Element type	SW30XLE-440i	
Number pressure vessel per train	80.000	
Flow rate ERD	93.500	m ³ /h
Flow per element	0.573	m ³ /h
Number of elements	1,819.000	
Number of pressure vessels	228.000	
Number of elements	1,824.000	
Flux	14.000	
Flow per element	0.573	m ³ /h
Feed flow per pressure vessel	10.153	m ³ /h
Permeate flow per pressure vessel	4.569	m ³ /h
Concentrate flow per pressure vessel	5.584	m ³ /h
Number of trains	3.000	
Number of ERD	14.000	

Table - 22: Water and salt permeability coefficient for Case 1

RO system	Membrane permeability coefficient for water	Unit
Pressure loss per element	0.210	bar
Concentrate concentration test	34,777.043	mg/L
Average concentration test	33,388.522	mg/L
Permeate concentration test	66.777	mg/L

RO system	Membrane permeability coefficient for water	Unit
Osmotic feed pressure test	27.147	bar
Osmotic concentrate pressure test	29.502	bar
Average osmotic pressure test	28.325	bar
Osmotic permeate pressure test	0.057	bar
Osmotic pressure difference test	28.268	bar
Permeate pressure test	-	bar
NDPs test	26.657	bar
Water flux test	38.093	Lmh
Water permeability coefficient test	1.431	L/m ² .bar.h
Permeability productivity test	0.059	m ³ /bar.h
Salt permeability coefficient test	0.076	L/m ² h
Water permeability coefficient at design	1.431	L/m ² .bar.h
Salt permeability coefficient at design	0.076	L/m ² h

Table - 23: RO feed pressure for Case 1

RO system	Feed pressure	Unit
Osmotic feed pressure	29.692	bar
Osmotic concentrate pressure	53.936	bar
Osmotic permeate pressure	0.084	bar
Applied feed pressure	52.000	bar
Salinity of permeate water	106.32	mg/L

Table - 24: Elements performance analysis in PV for Case 1

RO system	Calculation for RO element performance							
Parameters	1	2	3	4	5	6	7	8
P_{f_i}	52.000	51.790	51.580	51.370	51.160	50.950	50.740	50.530
ΔP_e	0.210	0.210	0.210	0.210	0.210	0.210	0.210	0.210
Q_{f_i}	10.153	8.965	8.020	7.075	6.388	5.925	5.636	5.469
C_{f_i}	35,000.000	39,628.324	44,317.587	44,317.587	49,068.648	52,868.084	55,586.649	57,302.385
C_{p_i}	74.628	83.946	83.946	93.386	101.937	108.455	112.889	115.535
C_{c_i}	39,628.324	44,317.587	44,317.587	49,068.648	52,868.084	55,586.649	57,302.385	58,232.268
$C_{f_{c_i}}$	37,314.162	41,972.955	44,317.587	46,693.118	50,968.366	54,227.367	56,444.517	57,767.326
π_{f_i}	29.692	33.618	33.618	37.596	41.626	44.850	47.156	48.611
π_{c_i}	33.618	37.596	37.596	41.626	44.850	47.156	48.611	49.400
$\pi_{f_{c_i}}$	31.655	35.607	35.607	39.611	43.238	46.003	47.883	49.005
π_{p_i}	0.063	0.071	0.071	0.079	0.086	0.092	0.096	0.098
$\Delta\pi_{fcs-fps}$	31.592	35.536	35.536	39.532	43.152	45.911	47.787	48.907
NDP_i	20.303	16.149	16.149	11.733	7.903	4.934	2.848	1.518
Q_{c_i}	8.965	8.020	7.075	6.388	5.925	5.636	5.469	5.380
Q_{p_i}	1.188	0.945	0.945	0.687	0.463	0.289	0.167	0.089
R_i	0.117	0.106	0.106	0.097	0.072	0.049	0.030	0.016
P_{c_i}	51.790	51.580	51.370	51.160	50.950	50.740	50.530	50.320
CPF _i	1.085	1.077	1.077	1.070	1.052	1.035	1.021	1.011
CPF _i < 1.2	TRUE	TRUE	TRUE	TRUE	TRUE	TRUE	TRUE	TRUE
v_i	0.220	0.190	0.170	0.150	0.140	0.130	0.130	0.120

Table - 25: Design specification of Discharge system for Case 1

Discharge System	Surface Discharge	Unit
Cleaning volume	1.40	L/m ²
Ro pipe radius	0.10	m
Ro pipe length	1,500.00	m
C value	5.00	
Volume RO system	109,939.20	L/day
Volume of Pipe	47,123.89	L/day
CIP solution volume	157,063.09	L/day
Total flush water volume	109,945.20	L/day
Total membrane flush water	0.74	m ³ /day
Backwash volume	2,222.22	m ³ /day
Total discharge flow rate	32,778.96	m ³ /day
Diffuser design		
Number of diffuser port	2.00	
Discharge angle	45.00	degree
Diameter of Diffuser	0.23	m
Viscosity discharge	9.71E-07	m ² /s
Brine density	1,044.65	kg/m ³
Seawater density	1,023.03	kg/m ³
Buoyant acceleration	0.197	m ² /s
Flow per port	0.190	m ³ /s
Velocity at diffuser port	4.573	m/s
Froude number	21.483	
Reynold's number	1.08E+06	
Buoyancy flux	0.04	m ⁴ /s ³
Momentum flux	0.87	m ⁴ /s ³
Discharge length	0.20	m
Momentum length scale	4.68	m
Dilution at Impact Point	34.37	
Dilution at Near Field	53.71	
Location of Impact Point	17.79	m
Near – field length	54.35	m
Height of Jet Rise	8.89	m

Table - 26: SEC breakdown for Case 1

System	Value	Unit
ERD efficiency	0.97	%
Intake system pump efficiency	0.83	%
RO system pump efficiency	0.8	%
Intake system SEC	0.13	kWh/m ³
Pretreatment system SEC	0.100	kWh/m ³
RO system SEC	2.390	kWh/m ³
Discharge SEC	0.270	kWh/m ³
Posttreatment SEC	0.170	kWh/m ³
Total SEC	3.01	kWh/m ³

Table - 27: CAPEX breakdown for Case 1

CAPEX parameters	Cost rate (\$)	Cost (\$)
n	8	
Discounting rate	5%	
Site preparation	15.00	375,000.00
Intake system	2000	4,217,061.52
Pretreatment system		3,478,637.63
RO system (Element , PV, train piping, train support frame, train instrument and control, HP pump, ERD)	500, 1600, 440,000, 260,000, 71,000, 2,500,000, 25,625,	13,948,550.00
Discharge system	300	13,111,584.68
Posttreatment system		1,654,656.29
Waste solid handling	30.00	750,000.00
Electrical instrumentation	75.00	1,875,000.00
Auxiliary service equipment	25.00	625,000.00
Building	60.00	1,500,000.00
Start-up commissioning acceptance test	15.00	375,000.00
Preliminary engineering	25.00	625,000.00
Pilot construction	10.00	250,000.00
Pilot testing	15,000.00	150,000.00
Period of testing	10.00	
Detailed design	90.00	2,250,000.00
Construction management oversight	40.00	1,000,000.00
Project management	30.00	750,000.00

CAPEX parameters	Cost rate (\$)	Cost (\$)
Environmental permitting	45.00	1,125,000.00
Legal cost	20.00	500,000.00
Direct CAPEX		41,910,490.12
Indirect CAPEX		6,650,000.00
Total CAPEX		48,560,490.12
NPV		32,867,651.15

Table - 28: Staff breakdown and yearly salary for Case 1

Staff	Number of staff	Cost (\$US/year)
Head of plant	1	115,200.00
Mangers	2	172,800.00
Engineers	3	216,000.00
Operators	9	518,400.00
Other staff	2	103,680.00
Additional staff	1	37,440.00
Total	18	1,163,520.00
Total for 20 years		23,270,400.00

Table - 29: SEC and cost breakdown for Case 1

		Total energy (kWh/day)	Total energy (kWh/year)	Cost (\$ /day)	Cost (\$ /year)	Cost (\$/20 year)
SEC cost rate	0.15					
Intake	0.130	7514.72	2,705,300.00	1,127.21	405,795.00	8,115,900.00
Pretreatment	0.100	5780.56	2,081,000.00	867.08	312,150.00	6,243,000.00
RO	2.390	59750	21,510,000.00	8,962.50	3,226,500.00	64,530,000.00
Discharge	0.270	8850.32	3,186,115.08	1,327.55	477,917.26	9,558,345.23
Posttreatment	0.120	3000	1,080,000.00	450.00	162,000.00	3,240,000.00
Total	3.01	84,895.60	30,562,415.08	12,734.34	4,584,362.26	91,687,245.23

Table - 30: Chemical cost breakdown for Case 1

Chemical	Chemical dosage (mg/L)	Chemical use (kg/day)	Amount of chemical (kg)	Actual storage volume (m ³)	Average dilution flow (m ³ /h)	Chemical metering pump (m ³ /h)	Cost (\$/day)	Cost (\$/year)	Cost(\$/20year)
Sodium hypochlorite	4.00	231.22	53358.923	49.888	0.017	0.0078	658.983	68,534.23	1,370,684.64
Ferric sulfate	5.00	289.03	21677.1	16.083	0.089	0.0078	231.222	83,239.92	1,664,798.40
Sodium hexametaphosphate	2.13	122.84	3722.333	4.28	0.02	0.0051	343.944	123,819.84	2,476,396.80
Chlorine dioxide	0.19	10.98	332.818	0.255	0.001	0.0003	46.678	16,804.08	336,081.60
Sodium hydroxide	6.00	346.83	20809.98	15.693	0.027	0.0095	260.125	93,645.00	1,872,900.00
Sodium bisulfite	3.00	173.42	5255.061	4.084	0.031	0.0049	78.038	28,093.68	561,873.60
Sulfuric acid	1.02	58.96	1804.959	1.134	0.011	0.0013	4.717	1,698.12	33,962.40
Calcite	80.81	2,020.20	-	-	-	-	141.414	50,909.09	1,018,181.82
Carbon dioxide	35.20	880.00	-	-	-	-	88.00	31,680.00	633,600.00
Total		4,133.48					1,853.12	498,423.96	9,968,479.26

Table - 31: Equipment replacement cost breakdown for Case 1

Equipment replacement	Selected life span	Cost (\$/filter)	Cost (\$/year)	Cost (\$/ 20 year)
Cartridge filter	4.00 months	30	49,425.00	988,500.00
Media filtration *	10.00 year	40	31,360.90	627,217.98
RO membrane	8.00 year	500	114,000.00	2,508,000.00
Total			194,785.90	4,123,717.98

* Replacement price = 40 / 0.028 m³

Table - 32: OPEX breakdown for Case 1

	OPEX cost (\$millions/year)	Cost (\$M/20 years)	Sensitivity Analysis					
			-10	-5	5	10	20	
Variable O&M								
Power	4.58	91.69	82.52	87.10	96.27	100.86	110.02	
Chemicals	0.50	9.97	9.97	9.97	9.97	9.97	9.97	
Replacement of membranes and cartridge filter	0.19	4.12	4.12	4.12	4.12	4.12	4.12	
Waste stream disposal	1.77	35.40	35.40	35.40	35.40	35.40	35.40	
Fixed O&M costs					-	-	-	
Labour	1.16	23.27	23.27	23.27	23.27	23.27	23.27	
Maintenance	0.84	16.76	16.76	16.76	16.76	16.76	16.76	
Environmental and performance monitoring	0.04	0.72	0.72	0.72	0.72	0.72	0.72	

	OPEX cost (\$millions/year)	Cost (\$M/20 years)	Sensitivity Analysis				
Indirect O&M cost	0.36	7.20	7.20	7.20	7.20	7.20	7.20
Total OPEX	9.45	189.14	179.97	184.55	193.72	198.30	207.47
NPV	9.00	71.28	67.83	69.56	73.01	74.74	78.19

Case 2:

Table - 33: Design specification for Plant intake and brine specification for Case 2

Plant water design	Solution 1	Solution 2	Unit
Product	120,000.00		m ³ /day
Recovery	40.00		%
Salinity	38,000.00		mg/L
Temperature	28-32		°C
Backwash	4.00	8.00	%
Additional water	1.00	1.00	%
Life scale	22.00	22.00	Year
Intake capacity	318,000.00	330,000.00	m ³ /day
Ro feed flow	300,000.00	300,000.00	m ³ /day
Brine flow rate	180,000.00	180,000.00	m ³ /day
Brine salinity	63,283.00	63,283.00	mg/L
Brine average salinity	50,641.50	50,641.50	
Permeate salinity	101.00	101.00	
Feed water density	1023.62	1023.62	kg/m ³
Sweater dynamic viscosity	0.00087	0.00087	kg/ms
Seawater kinematic viscosity	8.47×10^{-7}	8.47×10^{-7}	m ² /s

Table - 34: Design specification of Offshore intake for Case 2

Intake Design	Solution 1	Solution 2	Unit
Number of pipes	2.00	2.00	
Approached velocity	0.15	0.15	m/s
Width of screen bars	25.00	25.00	mm
Space between the bars	100.00	100.00	mm
Reduction of area factor	0.40	0.40	
Velocity in the bottom structure	0.80	0.80	m/s
Velocity in intake riser pipe	2.00	2.00	m/s
Velocity in conveyance pipe	2.00	2.00	m/s
Height of velocity cap	2	2	m
Area of velocity cap	30.67	31.83	m ²
Through velocity	0.06	0.06	m/s
Inner diameter of velocity cap	4.88	5.07	m/s

Internal diameter of the bottom of intake structure	1.71	1.74	m
Internal diameter of the riser pipe	1.08	1.10	m
Internal diameter of the conveyance pipe	1.53	1.56	m

Table - 35: Design specification of Lamella sedimentation for Case 2

Pretreatment System	Solution 1	Solution 2	Unit
Particle density	2650	2650	kg/m ³
Particle diameter	9.0E-05	9.00E-05	μm
Length of plate	2.50	2.50	m
Factor active plate	0.80	0.80	
Hazen velocity	0.80	0.80	m/s
Angle	60.00	60.00	Degree
Space between plates	0.06	0.06	m
Plate width	1.25	1.25	m
Thickness of plates	0.01	0.01	m
Suspended solid in seawater	29.90	29.90	mg/L
Suspended solid lam	5.00	5.00	mg/L
Detention time	0.20	0.20	h
Solid content sludge	2.00	2.00	%
Settling velocity	0.015	0.015	m/s
Reynolds number	3.49	3.49	
Active length	2	2	m
Velocity in lamella channel	0.0037	0.0037	m/s
Q lam	1	1	m ³ /h
Number lam	13250	13750	
Distance between inclined plates	0.069	0.069	m
Pack depth lam	981.75	1018.75	m
Area of lam package	1227.188	1273.438	m ²
Loading rate lam	10.797	10.798	m ³ /m ² h
Eff lam suspended solid	83.278	83.278	%
Eff lam bod	5.263	5.263	
Removal of suspended solid	329.927	342.377	kg/h
Sludge produced	16496.35	17118.85	kg/h

Table - 36: Design specification of Pretreatment system for solution 1 in Case 2

Pretreatment System	Dual gravity granular media	Unit
Loading rate	12.00	m ³ /m ² /h
Length to width ratio	3.00	
Max surface area per filter	70.00	m ²
Backwash loading rate	50.00	m ³ /m ² /h
Duration	15.00	min
Downflow rinse	8.00	min
Sediment type (effective size)	Sand (0.6), Anthracite (1.5)	
Required surface area	1,104.00	m ²
Number of filters + standby	16.00	
Surface area per filter	70.00	m ²
Length	14.40	m
Width/diameter	4.80	m
Media loading rate	11.98	m ³ /m ² /h
Backwash flow rate	1,104.00	m ³ /h
Volume per filter	25,392.00	m ³
Depth	5.15	m
Pretreatment System	Cartridge filter	Unit
Loading rate	0.25	m ³ /m ² /h
Length	1,016.00	mm
N cartridge per PV	7.00	
Number of Cartridges	3,418.00	
Number of Cartridges per PV	488.00	
Actual loading rate per 250 mm	0.25	m ³ /m ² /h

Table - 37: Design specification of UF for solution 2 in Case 2

Pretreatment System	Membrane Filtration	Unit
Element type	ZeeWeed 1500 Module	
Average flux	45.00	Lmh
Element area	51.10	m ²
Number of Element Per Module	4.00	
Number module per train	48.00	
Temperature	30.00	°C
Flux at Design Temperature	38.88	Lmh
Filtration area membrane system	305,555.56	m ²
Number of Element	5,980.00	

Number of Vessel	1,495.00	
Number of Train	31	
Area train	9811.2	
Flow rate per train	441.504	m ³ /h

Table - 38: Design specification of RO system for Case 2

RO system	Solution 1	Solution 2	Unit
Element type	SW30XL400	SW30XL400	
Flux	14	16.00	Lmh
Number pressure vessel per train	100	100.00	
Flow rate ERD	93.5	93.500	m ³ /h
Flow per element	0.518	0.592	m ³ /h
Number of elements	9,653.000	8,446.000	
Number of pressure vessels	1,379.000	1,207.000	
Number of elements	9,653.000	8,449.000	
Flux	14.000	16.000	
Flow per element	0.518	0.592	m ³ /h
Feed flow per pressure vessel	9.065	10.356	m ³ /h
Permeate flow per pressure vessel	3.626	4.142	m ³ /h
Concentrate flow per pressure vessel	5.439	6.214	m ³ /h
Number of trains	14.000	12.000	
Number of ERD	80.000	80.000	

Table - 39: Water and salt permeability for Case 2

RO system	Solution 1	Solution 2	Unit
Pressure loss per element	0.160	0.210	bar
Concentrate concentration test	34,777.043	34,777.043	mg/L
Average concentration test	33,388.522	33,388.522	mg/L
Permeate concentration test	66.777	66.777	mg/L
Osmotic feed pressure test	27.147	27.147	bar
Osmotic concentrate pressure test	29.502	29.502	bar
Average osmotic pressure test	28.325	28.325	bar
Osmotic permeate pressure test	0.057	0.057	bar
Osmotic pressure difference test	28.268	28.268	bar
Permeate pressure test	-	-	bar

RO system	Solution 1	Solution 2	Unit
NDP test	26.652	26.657	bar
Water flux test	31.541	31.541	Lmh
Water permeability coefficient test	1.183	1.185	L/m ² .bar.h
Permeability productivity test	0.044	0.044	m ³ /bar.h
Salt permeability coefficient test	0.063	0.063	L/m ² h
Water permeability coefficient at design	1.369	1.372	L/m ² .bar.h
Salt permeability coefficient at design	0.073	0.073	L/m ² h

Table - 40: Applied feed pressure for Case 2

RO System	Solution 1	Solution 2	Unit
Osmotic feed pressure	32.777	32.777	bar
Osmotic concentrate pressure	54.585	54.585	bar
Osmotic permeate pressure	0.087	0.087	bar
Applied feed pressure	54.000	56.000	bar
Salinity in permeate water	200.07	200.03	mg/L

Table - 41: Elements performance analysis in PV for solution 1

RO system	Calculation for RO element performance						
Parameters	1	2	3	4	5	6	7
P_{f_i}	54	53.84	53.68	53.52	53.36	53.2	53.04
ΔP_e	0.16	0.16	0.16	0.16	0.16	0.16	0.16
Q_{f_i}	9.065	8.091	7.322	6.746	6.339	6.065	5.889
C_{f_i}	38000	42591.695	47053.705	51081.727	54393.498	56832.623	58526.598
C_{p_i}	80.592	89.645	98.135	105.475	111.226	115.359	118.124
C_{c_i}	42591.695	47053.705	51081.727	54393.498	56832.623	58526.598	59597.241
C_{fc_i}	40295.848	44822.7	49067.716	52737.613	55613.06	57679.61	59061.92
π_{f_i}	32.777	36.738	40.586	44.061	46.917	49.021	50.482
π_{c_i}	36.738	40.586	44.061	46.917	49.021	50.482	51.406
π_{fc_i}	34.758	38.662	42.323	45.489	47.969	49.752	50.944
π_{p_i}	0.07	0.077	0.085	0.091	0.096	0.1	0.102
$\Delta\pi_{fcs-fps}$	34.688	38.585	42.238	45.398	47.873	49.652	50.842
NDP_i	19.232	15.175	11.362	8.042	5.407	3.468	2.118
Q_{c_i}	8.091	7.322	6.746	6.339	6.065	5.889	5.782
Q_{p_i}	0.974	0.769	0.576	0.407	0.274	0.176	0.107
R_i	0.108	0.095	0.079	0.061	0.043	0.029	0.018
P_{c_i}	53.84	53.68	53.52	53.36	53.2	53.04	52.88
CPF_i	1.0785	1.0688	1.0569	1.0436	1.0306	1.0205	1.0127
$CPF_i < 1.2$	TRUE	TRUE	TRUE	TRUE	TRUE	TRUE	TRUE
v_i	0.22	0.19	0.18	0.17	0.16	0.15	0.15

Table - 42: Elements performance analysis in PV for solution 2

RO System	Calculation for RO Element Performance						
Parameters	1	2	3	4	5	6	7
P_{f_i}	56	55.79	55.58	55.37	55.16	54.95	54.74
ΔP_e	0.21	0.21	0.21	0.21	0.21	0.21	0.21
Q_{f_i}	10.356	9.275	8.398	7.719	7.218	6.866	6.63
C_{f_i}	38000	42401.893	46844.018	50964.559	54500.464	57302.968	59315.809
C_{p_i}	80.402	89.246	97.809	105.465	111.803	116.619	120.025
C_{c_i}	42401.893	46844.018	50964.559	54500.464	57302.968	59315.809	60709.397
C_{fc_i}	40200.946	44622.955	48904.288	52732.512	55901.716	58309.389	60012.603
π_{f_i}	32.777	36.574	40.406	43.96	47.01	49.427	51.163
π_{c_i}	36.574	40.406	43.96	47.01	49.427	51.163	52.365
π_{fc_i}	34.675	38.49	42.183	45.485	48.218	50.295	51.764
π_{p_i}	0.069	0.077	0.084	0.091	0.096	0.101	0.104
$\Delta \pi_{fcs-fps}$	34.606	38.413	42.099	45.394	48.122	50.194	51.66
NDP_i	21.289	17.272	13.376	9.871	6.933	4.651	2.975
Q_{c_i}	9.275	8.398	7.719	7.218	6.866	6.63	6.478
Q_{p_i}	1.081	0.877	0.679	0.501	0.352	0.236	0.151
R_i	0.104	0.095	0.081	0.065	0.049	0.034	0.023
P_{c_i}	55.79	55.58	55.37	55.16	54.95	54.74	54.53
CPF_i	1.0755	1.0688	1.0583	1.0466	1.0349	1.0241	1.0162
$CPF_i < 1.2$	TRUE	TRUE	TRUE	TRUE	TRUE	TRUE	TRUE
v_i	0.25	0.22	0.2	0.19	0.18	0.17	0.17

Table - 43: Design specification of Discharge system for Case 2

Discharge System	Solution 1	Solution 2	Unit
Cleaning volume	1.50	1.60	L/m ²
Ro pipe radius	0.10	0.10	m
Ro pipe length	1,500.00	1,500.00	m
C value	5.00	5.00	
Volume RO system	580,160.00	497,280.00	L/day
Volume of Pipe	47,123.89	47,123.89	L/day
CIP solution volume	627,283.89	544,403.89	L/day
Total flush water volume	580,166.00	497,286.00	L/day
Total membrane flush water	3.35	1,041.69	m ³ /day
Backwash volume	15,000.00	27,000.00	m ³ /day
Total discharge flow rate	195,003.35	208,041.69	m ³ /day
Diffuser Design			
Number of diffuser port	10.00	10.00	
Discharge angle	50.00	50.00	degree
Diameter of Diffuser	0.25	0.25	m
Viscosity discharge	8.85E-07	8.85E-07	m ² /s
Brine density	1,042.68	1,042.68	kg/m ³
Seawater density	1,023.62	1,023.62	kg/m ³
Buoyant acceleration	0.179	0.179	m ² /s
Flow per port	0.226	0.241	m ³ /s
Velocity at diffuser port	4.604	4.910	m/s
Froude number	21.764	23.211	
Reynold's number	1.30E+06	1.39E+06	
Buoyancy flux	0.04	0.04	m ⁴ /s ³
Momentum flux	1.04	1.18	m ⁴ /s ³
Discharge length	0.22	0.22	m
Momentum length scale	5.15	5.47	m
Dilution at Impact Point	35.37	37.72	
Dilution at Near Field	55.50	59.19	
Location of Impact Point	17.28	18.42	m
Near – field length	55.77	59.48	m
Height of Jet Rise	11.02	11.75	m

Table - 44: SEC breakdown for Case 2

System	Solution 1	Solution 2	Unit
ERD efficiency	0.97	0.97	%
Intake System pump efficiency	0.8	0.8	%
RO System pump efficiency	0.8	0.8	%
Intake system SEC	0.042	0.042	kWh/m ³
Pretreatment system SEC	0.150	0.202	kWh/m ³
RO system SEC	2.530	2.630	kWh/m ³
Discharge SEC	0.270	0.270	kWh/m ³
Posttreatment SEC	0.180	0.180	kWh/m ³
Other facilities	0.1	0.1	kWh/m ³
Total SEC	3.27	3.424	kWh/m ³

Table - 45: CAPEX breakdown for Case 2

CAPEX Parameters	Cost Rate (\$)	Cost solution 1 (\$)	Cost solution 2 (\$)
n	8		
Discounting rate	4%		
Site preparation	15, 20	1,800,000.00	2,400,000.00
Intake system		96,211,990.78	97,521,291.97
Pretreatment system		26,307,279.86	24,793,007.96
RO system		52,083,300.00	44,388,900.00
Posttreatment system		7,849,401.38	7,849,401.38
Discharge system		81,901,408.69	86,941,215.31
Waste solid handling	30, 40	3,600,000.00	4,800,000.00
Electrical instrumentation	75, 90	9,000,000.00	10,800,000.00
Auxiliary service equipment	25, 30	3,000,000.00	3,600,000.00
Building	60, 75	7,200,000.00	9,000,000.00
Start-up commissioning acceptance test	15, 15	1,800,000.00	1,800,000.00
Preliminary engineering	25, 30	3,000,000.00	3,600,000.00
Pilot construction	10, 15	1,200,000.00	1,800,000.00
Pilot testing	15,000, 17000		
Period of testing	12.00	180,000.00	204,000.00
Detailed design	90, 100	10,800,000.00	12,000,000.00
Construction management oversight	40, 45	4,800,000.00	5,400,000.00
Project management	30	3,600,000.00	3,600,000.00
Environmental permitting	45	5,400,000.00	5,400,000.00

CAPEX Parameters	Cost Rate (\$)	Cost solution 1 (\$)	Cost solution 2 (\$)
Legal cost	20	2,400,000.00	2,400,000.00
Direct capex		290,753,380.71	292,093,816.62
Indirect capex		31,380,000.00	36,204,000.00
Total capex		322,133,380.71	328,297,816.62
NPV		235,379,705.99	239,883,998.92

Table - 46: Staff breakdown and yearly salary for Case 2

Staff	Solution 1		Solution 2	
	NO of staff	Cost (\$US/year)	NO of staff	Cost (\$US/year)
Head of plant	1	115,200.00	1	115,200.00
Mangers	4	345,600.00	4	345,600.00
Engineers	4	288,000.00	4	288,000.00
Operators	10	576,000.00	13	748,800.00
Other staff	3	155,520.00	3	155,520.00
Additional staff	3	112,320.00	2	112,320.00
Total	25	1,592,640.00	28	1,765,440.00
Total for 20 years		35,038,080.00		38,839,680.00

Table - 47: SEC and cost breakdown for solution 1

		Total energy (kWh/day)	Total energy (kWh/year)	Cost (\$ /day)	Cost (\$ /year)	Cost (\$ for/22 year)
SEC cost rate	0.08					
Intake	0.042	13,292.40	4,785,264.00	1,063.39	382,821.12	8,422,064.64
Pretreatment	0.150	47,700.00	17,172,000.00	3,816.00	1,373,760.00	30,222,720.00
RO	2.530	303,600.00	109,296,000.00	24,288.00	8,743,680.00	192,360,960.00
Discharge	0.270	52,650.91	18,954,326.01	4,212.07	1,516,346.08	33,359,613.78
Posttreatment	0.170	20,400.00	7,344,000.00	1,632.00	587,520.00	12,925,440.00
Total	3.162	437,643.31	157,551,590.01	35,011.46	12,604,127.20	277,290,798.42

Table - 48: SEC and cost breakdown for solution 2

		Total energy (kWh/day)	Total energy (kWh/year)	Cost (\$ /day)	Cost (\$/year)	Cost (\$ /22 year)
SEC cost rate	0.08					
Intake	0.042	13794	4,965,840.00	1,103.52	397,267.20	8,739,878.40
Pretreatment	0.202	66561	23,961,960.00	5,324.88	1,916,956.80	42,173,049.60
RO	2.630	315600	113,616,000.00	25,248.00	9,089,280.00	199,964,160.00
Discharge	0.270	55890.78	20,120,681.26	4,471.26	1,609,654.50	35,412,399.01
Posttreatment	0.180	21600	7,776,000.00	1,728.00	622,080.00	13,685,760.00
Total	3.324	473,445.78	170,440,481.26	37,875.66	13,635,238.50	299,975,247.01

Table - 49: Chemical cost breakdown for solution 1

Chemical	Chemical dosage (mg/L)	Chemical use (kg/day)	Amount of chemical (kg)	Actual storage volume (m ³)	Average dilution flow (m ³ /h)	Chemical metering pump (m ³ /h)	Cost (\$/day)	Cost (\$/year)	Cost(\$/22year)
Sodium hypochlorite	4.00	1,272.00	293,538.46	274.45	0.10	0.04	3,625.20	377,020.80	8,294,457.60
Sulfuric Acid (93% h ₂ so ₄)	120.00	38,160.00	1,168,163.27	734.09	6.92	0.87	3,052.80	122,112.00	2,686,464.00
Ferric sulfate	10.00	3,180.00	238,500.00	176.95	0.98	0.09	2,544.00	915,840.00	20,148,480.00
Sodium hexametaphosphate	2.13	675.75	20,477.27	23.55	0.11	0.03	1,892.10	681,156.00	14,985,432.00
Chlorine dioxide	0.19	60.42	1,830.91	1.40	0.01	0.00	256.79	92,442.60	2,033,737.20
Sodium hydroxide	6.00	1,908.00	114,480.00	86.33	0.15	0.05	1,431.00	515,160.00	11,333,520.00
Sodium bisulfite	3.00	954.00	28,909.09	22.46	0.17	0.03	429.30	154,548.00	3,400,056.00
Sulfuric acid	1.02	324.36	9,929.39	6.24	0.06	0.01	25.95	9,341.64	205,516.08
Hydrated lime	62.98	7,557.45					18.89	6,801.70	149,637.45
Carbon dioxide	70.40	8,448.00					7.04	2,534.40	55,756.80
Total		62,539.98					13,283.07	2,876,957.14	63,293,057.13

Table - 50: Chemical cost breakdown for solution 2

Chemical	Chemical dosage (mg/L)	Chemical use (kg/day)	Amount of chemical (kg)	Actual storage volume (m ³)	Average dilution flow (m ³ /h)	Chemical metering pump (m ³ /h)	Cost (\$/day)	Cost (\$kg/year)	Cost(\$/22 year)
Sodium hypochlorite	4	1,320.00	304,615.39	284.80	0.10	0.04	3,762.00	391,248.00	8,607,456.00
Sulfuric Acid (93% h ₂ so ₄)	120	39,600.00	1,212,244.90	761.79	7.18	0.90	3,168.00	126,720.00	2,787,840.00
Ferric sulfate	5	3,300.00	247,500.00	183.63	1.01	0.09	2,640.00	950,400.00	20,908,800.00
Sodium hexametaphosphate	2.125	701.25	21,250.00	24.44	0.12	0.03	1,963.50	706,860.00	15,550,920.00
Chlorine dioxide	0.19	62.70	1,900.00	1.46	0.01	0.00	266.48	95,931.00	2,110,482.00
Sodium hydroxide	6	1,980.00	118,800.00	89.59	0.15	0.05	1,485.00	534,600.00	11,761,200.00
Sodium bisulfite	3	990.00	30,000.00	23.31	0.18	0.03	445.50	160,380.00	3,528,360.00
Sulfuric acid	1.02	336.60	10,304.08	6.48	0.06	0.01	26.93	9,694.08	213,269.76
Hydrated lime		7,557.45					2,267.23	816,204.26	17,956,493.62
Carbon dioxide		8,448.00					844.80	304,128.00	6,690,816.00
total		64,296.00					16,869.44	4,096,165.34	90,115,637.38

Table - 51: Equipment replacement cost breakdown for solution 1

Equipment replacement	Selected life span	Cost (\$/filter)	Cost (\$/year)	Cost (\$/ 22 year)
Cartridge filter	5.00	30	256,350.00	5,639,700.00
Media filtration *	10.00	40	879,471.82	8,794,718.21
RO membrane	7.00	500	689,500.00	15,169,000.00
Total			1,825,321.82	29,603,418.21

* Replacement price = 40 / 0.028 m³

Table - 52: Equipment replacement cost breakdown for solution 2

Equipment replacement	Selected life span	Cost (\$/filter)	Cost (\$/year)	Cost (\$/ 22 year)
UF	10.00	1000	598,000.00	13,156,000.00
RO membrane	7.00	500	603,500.00	13,277,000.00
Total			1,201,500.00	26,433,000.00

* Replacement price = 40 / 0.028 m³

Table - 53: OPEX breakdown for solution 1

Variable O&M	OPEX Cost	Cost (\$M/22 years)	Sensitivity Analysis				
	(\$M/year)		-10	-5	5	10	20
Power	12.60	277.29	249.56	263.43	291.16	305.02	332.75
Chemicals	2.88	63.29	63.29	63.29	63.29	63.29	63.29
Replacement of membranes and cartridge filter	1.83	29.60	29.60	29.60	29.60	29.60	29.60
Waste stream disposal	14.04	308.89	308.89	308.89	308.89	308.89	308.89

Fixed O&M costs								-
Labour	1.59	35.04	35.04	35.04	35.04	35.04	35.04	35.04
Maintenance	5.82	127.93	127.93	127.93	127.93	127.93	127.93	127.93
Environmental and performance monitoring	0.22	4.75	4.75	4.75	4.75	4.75	4.75	4.75
Indirect O&M cost	2.16	47.52	47.52	47.52	47.52	47.52	47.52	47.52
Total OPEX	41.13	894.31	866.59	880.45	908.18	922.04	949.77	
NPV	39.17	305.72	326.61	331.83	342.28	389.06	400.76	

Table - 54: OPEX breakdown for solution 2

	OPEX Cost (\$M/year)	Cost (\$M/22 years)	Sensitivity Analysis				
			-10	-5	5	10	20
Variable O&M			-10	-5	5	10	20
Power	13.64	299.98	269.98	284.98	314.97	329.97	359.97
Chemicals	4.10	90.12	90.12	90.12	90.12	90.12	90.12
Replacement of membranes and cartridge filter	1.20	26.43	26.43	26.43	26.43	26.43	26.43
Waste stream disposal	14.90	327.89	327.89	327.89	327.89	327.89	327.89
Fixed O&M costs							
Labour	1.77	38.84	38.84	38.84	38.84	38.84	38.84
Maintenance	5.84	128.52	128.52	128.52	128.52	128.52	128.52
Environmental and performance monitoring	0.22	4.75	4.75	4.75	4.75	4.75	4.75
Indirect O&M cost	2.16	47.52	47.52	47.52	47.52	47.52	47.52
Total OPEX	43.82	964.05	934.05	949.05	979.05	994.05	1,024.04
NPV	41.73	329.56	352.03	357.69	368.99	419.44	432.10

Case 3:

Table - 55: Plant water quality specification for Case 3

Plant water design	Value	Unit
Product	5,000.00	m ³ /day
Recovery	47.00	%
Salinity	35,000.00	mg/L
Temperature	25.00	°C
Backwash	6.00	%
Additional water	1.00	%
Life scale	20.00	Year
Intake capacity	11,595.75	m ³ /day
Ro feed flow	10,638.00	m ³ /day
Brine flow rate	5,638.00	m ³ /day
Brine salinity	65,976.00	mg/L
Brine average salinity	50,488.00	
Permeate salinity	101.00	
Feed water density	1023.03	kg/m ³
Sweater dynamic viscosity	0.00096	kg/ms
Seawater kinematic viscosity	9.37×10^{-7}	m ² /s

Table - 56: Design specification of Offshore Intake system for Case 3

Intake Design	Value	Unit
Number of pipes	1.00	
Approached velocity	0.15	m/s
Width of screen bars	25.00	mm
Space between the bars	100.00	mm
Reduction of area factor	0.40	
Velocity in the bottom structure	0.80	m/s
Velocity in intake riser pipe	2.00	m/s
Velocity in conveyance pipe	2.00	m/s
Height of velocity cap	2	m
Area of velocity cap	2.24	m ²
Through velocity	0.06	m/s
Inner diameter of velocity cap	0.36	m/s
Internal diameter of the bottom of intake structure	0.46	m
Internal diameter of the riser pipe	0.29	m
Internal diameter of the conveyance pipe	0.29	m

Table - 57: Design specification of DAF for Case 3

DAF	Parameters		unit
Mixer or Coagulation Chamber	Velocity gradient	900	
Flocculation Chamber	Contact time	15	min
	Number of flocculation chamber	2	
	Water depth	3.5	m
	Blade area as percentage of tank	0.1	%
	Shaft speed	50	r/min
DAF Chamber	Min number of tank	2	
	Tank width	6	m
	Tank length	10	m
	Tank depth	3	m
	Surface loading rate	25	m ³ /m ² h
	Hydraulic detention time	15	min
	Area	180	m ²
Treated water Recycle System	Recycle rate	9	%
	Maximum air loading	10	g/m ³
	Saturator loading rate	62	m ³ /m ² h
	Operating pressure	7	bar
DAF sludge performance	Suspended solid SW	26	mg/L
	Suspended solid DAF	4	mg/L
	Solid content sludge	3	
	Eff DAF suspended solid	84.615	%
	Removal of suspended solid	10.629	kg/h
	sludge produced	3	kg/h

Table - 58: Design specification of UF for Case 3

Pretreatment System	Membrane Filtration	Unit
Element type	ZeeWeed 1500 Module	
Average flux	50.00	Lmh
Element area	51.10	m ²
Number of Element Per Module	4.00	

Pretreatment System	Membrane Filtration	Unit
Number module per train	48.00	
Temperature	25.00	°C
Flux at Design Temperature	50.00	Lmh
Filtration area membrane system	9,663.13	m ²
Number of Element	189.00	
Number of Vessel	47.00	
Number of Train	1	
Area train	9811.2	
Flow rate per train	490.56	m ³ /h

Table - 59: Design specification of RO system for Case 3

RO System	SW30XL400	Unit
Flux	15.00	Lmh
Element Type	SW30XLE-440i	
Number pressure vessel per train	25.000	
Flow rate ERD	93.500	m ³ /h
Flow per element	0.614	m ³ /h
Number of elements	340.000	
Number of pressure vessels	47.000	
Number of elements	342.000	
Flux	15.000	
Flow per element	0.614	m ³ /h
Feed flow per pressure vessel	7.776	m ³ /h
Permeate flow per pressure vessel	3.655	m ³ /h
Concentrate flow per pressure vessel	4.121	m ³ /h
Number of trains	2.000	
Number of ERD	7.000	

Table - 60: RO membrane permeability coefficients for Case 3

RO system	Membrane permeability coefficients	Unit
Pressure loss per element	0.100	bar
Concentrate concentration test	34,777.043	mg/L
Average concentration test	33,388.522	mg/L
Permeate concentration test	66.777	mg/L
Osmotic feed pressure test	27.147	bar

RO system	Membrane permeability coefficients	Unit
Osmotic concentrate pressure test	29.502	bar
Average osmotic pressure test	28.325	bar
Osmotic permeate pressure test	0.057	bar
Osmotic pressure difference test	28.268	bar
Permeate pressure test	-	bar
NDP test	28.682	bar
Water flux test	37.702	Lmh
Water permeability coefficient test	1.431	L/m ² .bar.h
Permeability productivity test	0.058	m ³ /bar.h
Salt permeability coefficient test	0.075	L/m ² h
Water permeability coefficient at design	1.431	L/m ² .bar.h
Salt permeability coefficient at design	0.075	L/m ² h

Table - 61: Applied feed pressure for Case 3

RO System	Feed Pressure	Unit
Osmotic feed pressure	29.692	bar
Osmotic concentrate pressure	55.969	bar
Osmotic permeate pressure	0.086	bar
Applied feed pressure	54.000	bar

Table - 62: RO Elements Performance for Case 3

RO System	Calculation for RO Element Performance					
Parameters	1	2	3	4	5	6
P_{f_i}	54	53.9	53.8	53.7	53.6	53.5
ΔP_e	0.1	0.1	0.1	0.1	0.1	0.1
Q_{f_i}	7.776	6.52	5.605	5.008	4.66	4.476
C_{f_i}	35000	41752.578	48535.915	54339.897	58359.182	60722.82
C_{p_i}	76.753	90.288	102.876	112.699	119.082	122.682
C_{c_i}	41752.578	48535.915	54339.897	58359.182	60722.82	61959.583
C_{fc_i}	38376.289	45144.247	51437.906	56349.539	59541.001	61341.201
π_{f_i}	29.692	35.42	41.174	46.098	49.508	51.513
π_{c_i}	35.42	41.174	46.098	49.508	51.513	52.562
π_{fc_i}	32.556	38.297	43.636	47.803	50.511	52.037
π_{p_i}	0.065	0.077	0.087	0.096	0.101	0.104
$\Delta\pi_{fcs-fps}$	32.491	38.22	43.549	47.707	50.41	51.933
NDP_i	21.459	15.63	10.201	5.943	3.14	1.517
Q_{c_i}	6.52	5.605	5.008	4.66	4.476	4.387
Q_{p_i}	1.256	0.915	0.597	0.348	0.184	0.089
R_i	0.162	0.14	0.107	0.069	0.039	0.02
P_{c_i}	53.9	53.8	53.7	53.6	53.5	53.4
CPF _i	1.1201	1.103	1.0778	1.0495	1.0277	1.0141
CPF _i < 1.2	TRUE	TRUE	TRUE	TRUE	TRUE	TRUE
v_i	0.16	0.14	0.12	0.11	0.1	0.1

Table - 63: Design specification of Dilution tank for Case 3

Dilution tank	Value	Unit
Backwash TDS	25000	mg/L
Diluted TDS	3000	mg/L
Required diluted water	9713.19	m ³ /day

Table - 64: SEC breakdown for Case 3

System	Value	Unit
ERD efficiency	0.97	%
Intake system pump efficiency	0.7	%
RO system pump efficiency	0.8	%
Intake system SEC	0.032	kWh/m ³
Pretreatment system SEC	0.250	kWh/m ³
RO system SEC	2.340	kWh/m ³
Discharge SEC	0.010	kWh/m ³
Posttreatment SEC	0.100	kWh/m ³
Total SEC	2.732	kWh/m ³

Table - 65: CAPEX breakdown for Case 3

CAPEX Parameters	Cost rate (\$)	Cost (\$)
n	8	
Discounting rate	3%	
Site preparation	20.00	100,000.00
Intake system	2,628,036.08	2,628,036.08
Pretreatment system	2,564,398.85	2,564,398.85
RO system	6,978,103.00	9,467,575.00
Discharge system	63,000.00	628,353.69
Posttreatment system	628,353.69	593,617.05
Waste solid handling	30.00	150,000.00
Electrical instrumentation	75.00	375,000.00
Auxiliary service equipment	25.00	125,000.00
Building	60.00	300,000.00
Start-up commissioning acceptance test	15.00	75,000.00
Preliminary engineering	25.00	125,000.00
Pilot construction	10.00	50,000.00
Pilot testing	15,000.00	
Period of testing	12.00	180,000.00

CAPEX Parameters	Cost rate (\$)	Cost (\$)
Detailed design	90.00	450,000.00
Construction management oversight	40.00	200,000.00
Project management	30.00	150,000.00
Environmental permitting	45.00	225,000.00
Legal cost	20.00	100,000.00
Direct capex		17,006,980.67
Indirect capex		1,480,000.00
Total capex		18,486,980.67
NPV		14,593,793.25

Table - 66: Staff breakdown and yearly salary for Case 3

Staff	Number of staff	Cost (\$US/year)
Head of plant	1	115,200.00
Mangers	0	0
Engineers	2	144,000.00
Operators	4	230,400.00
Other staff	1	51,840.00
Additional staff	2	74,880.00
Total	10	616,320.00
Total for 20 years		12,326,400.00

Table - 67: SEC breakdown for Case 3

		Total energy (kwh/day)	Total energy (kwh/year)	Cost (\$/day)	Cost (\$ /year)	Cost (\$/20 year)
SEC cost rate	0.13					
Intake	0.032	369.90	134,275.25	48.09	17,455.78	349,115.65
Pretreatment	0.250	2,898.94	289.89	376.86	136,800.80	2,736,016.03
RO	2.340	11,700.00	1,170.00	1,521.00	552,123.00	11,042,460.00
Discharge	0.010	65.96	6.60	8.57	3,112.53	62,250.64
Posttreatment	0.100	500.00	50.00	65.00	23,595.00	471,900.00
Total	2.732	15,534.80	135,791.74	2,019.52	733,087.12	14,661,742.32

Table - 68: Chemical cost breakdown for Case 3

Chemical	Chemical dosage (mg/L)	Chemical use (kg/day)	Amount of chemical (kg)	Actual storage volume (m ³)	Average dilution flow (m ³ /h)	Chemical metering pump (m ³ /h)	Cost (\$/day)	Cost (\$/year)	Cost(\$/20year)
Sodium hypochlorite	4.00	46.38	10,703.77	10.01	0.00	0.00	132.19	13,747.97	274,959.36
Sulfuric Acid (93% h2so4)	100.00	1,391.49	42,596.63	26.77	0.25	0.03	111.32	4,452.76	89,055.20
Ferric sulfate	5.00	115.96	8,696.78	6.45	0.04	0.00	92.77	33,395.76	667,915.20
Sodium hexametaphosphate	1.00	24.64	746.70	0.86	0.00	0.00	69.00	24,838.20	496,764.00

Chemical	Chemical dosage (mg/L)	Chemical use (kg/day)	Amount of chemical (kg)	Actual storage volume (m ³)	Average dilution flow (m ³ /h)	Chemical metering pump (m ³ /h)	Cost (\$/day)	Cost (\$/year)	Cost(\$/20year)
Chlorine dioxide	0.18	2.20	66.76	0.05	0.00	0.00	9.36	3,370.68	67,413.60
Sodium hydroxide	5.00	69.58	4,174.50	3.15	0.01	0.00	52.18	18,785.16	375,703.20
Sodium bisulfite	3.00	34.79	1,054.15	0.82	0.01	0.00	15.65	5,635.44	112,708.80
Sulfuric acid	1.02	11.83	362.08	0.23	0.00	0.00	0.95	340.56	6,811.20
Calcite	80.81	404.04					121.21	43,636.36	872,727.27
Carbon dioxide	35.20	176.00					17.60	6,336.00	126,720.00
total							622.23	154,538.89	3,090,777.83

Table - 69: Equipment replacement cost breakdown for Case 3

Equipment replacement	Selected life span	Cost (\$/filter)	Cost (\$/year)	Cost (\$/ 20 year)
UF	8.00	1000	23,625.00	472,500.00
RO membrane	10.00	400	13680	273,600.00
Total			37,305.00	746,100.00

* Replacement price = 40 / 0.028 m³

Table - 70: OPEX breakdown for solution 2

	OPEX Cost (\$M/year)	Cost (\$M/20 years)	Sensitivity Analysis				
Variable O&M			-10	-5	5	10	20
Power	0.73	14.66	13.20	13.93	15.39	16.13	17.59
Chemicals	0.15	3.09	3.09	3.09	3.09	3.09	3.09
Replacement of membranes and cartridge filter	0.04	0.75	0.75	0.75	0.75	0.75	0.75
Waste stream disposal	1.17	23.46	23.46	23.46	23.46	23.46	23.46
Fixed O&M costs			-	-	-	-	-
Labour	0.62	12.33	12.33	12.33	12.33	12.33	12.33
Maintenance	0.00	0.04	0.04	0.04	0.04	0.04	0.04
Environmental and performance monitoring	0.01	0.18	0.18	0.18	0.18	0.18	0.18
Indirect O&M cost	0.09	1.82	1.82	1.82	1.82	1.82	1.82
Total OPEX	2.82	56.33	54.86	55.59	57.06	57.79	59.26
NPV	2.73	29.40	20.68	20.95	21.50	30.16	30.93

